DOCTOR OF PHILOSOPHY

Clogging in horizontal subsurface flow constructed wetlands

Paul Knowles

2012

Aston University

CLOGGING IN HORIZONTAL SUBSURFACE FLOW CONSTRUCTED WETLANDS

PAUL ROBERT KNOWLES

Doctor of Philosophy

ASTON UNIVERSITY

September 2010

Aston University

Clogging in Horizontal Subsurface Flow Constructed Wetlands

Paul Robert Knowles

Doctor of Philosophy

2010

Summary

Horizontal Subsurface Flow Treatment Wetlands (HSSF TWs) are used by Severn Trent Water as a low-cost tertiary wastewater treatment for rural locations. Experience has shown that clogging is a major operational problem that reduces HSSF TW lifetime. Clogging is caused by an accumulation of secondary wastewater solids from upstream processes and decomposing leaf litter. Clogging occurs as a sludge layer where wastewater is loaded on the surface of the bed at the inlet. Severn Trent systems receive relatively high hydraulic loading rates, which causes overland flow and reduces the ability to mineralise surface sludge accumulations. A novel apparatus and method, the Aston Permeameter, was created to measure hydraulic conductivity *in situ*. Accuracy is ±30 %, which was considered adequate given that conductivity in clogged systems varies by several orders of magnitude. The Aston Permeameter was used to perform 20 separate tests on 13 different HSSF TWs in the UK and the US. The minimum conductivity measured was 0.03 m/d at Fenny Compton (compared with 5,000 m/d clean conductivity), which was caused by an accumulation of construction fines in one part of the bed. Most systems displayed a 2 to 3 order of magnitude variation in conductivity in each dimension. Statistically significant transverse variations in conductivity were found in 70% of the systems. Clogging at the inlet and outlet was generally highest where flow enters the influent distribution and exits the effluent collection system, respectively. Surface conductivity was lower in systems with dense vegetation because plant canopies reduce surface evapotranspiration and decelerate sludge mineralisation. An equation was derived to describe how the water table profile is influenced by overland flow, spatial variations in conductivity and clogging. The equation is calibrated using a single parameter, the Clog Factor (CF), which represents the equivalent loss of porosity that would reproduce measured conductivity according to the Kozeny-Carman Equation. The CF varies from 0 for ideal conditions to 1 for completely clogged conditions. Minimum CF was 0.54 for a system that had recently been refurbished, which represents the deviation from ideal conditions due to characteristics of non-ideal media such as particle size distribution and morphology. Maximum CF was 0.90 for a 15 year old system that exhibited sludge accumulation and overland flow across the majority of the bed. A Finite Element Model of a 15 m long HSSF TW was used to indicate how hydraulics and hydrodynamics vary as CF increases. It was found that as CF increases from 0.55 to 0.65 the subsurface wetted area increases, which causes mean hydraulic residence time to increase from 0.16 days to 0.18 days. As CF increases from 0.65 to 0.90, the extent of overland flow increases from 1.8 m to 13.1 m, which reduces hydraulic efficiency from 37 % to 12 % and reduces mean residence time to 0.08 days.

Keywords: clogging, wastewater treatment, horizontal subsurface flow treatment wetland, operations and maintenance, finite element analysis

Acknowledgements

The research described in this thesis was made possible thanks to joint funding from Severn Trent Water Plc. and a CASE studentship granted by the Engineering and Physical Science Research Council of the United Kingdom (ref. CASE/CNA/06/28).

Over the duration of this project I have consulted the advice, wisdom and expertise of many, and many more have provided indispensable assistance in the form of data, technical expertise and constructive criticism. Without their crucial support this project would never have materialised and I give to them my eternal gratitude. I will give recognition to as many of them as I can, although I am sure that there are many more to whom my thanks is owed.

First and foremost; thanks to Philip Davies for his exemplary supervision and guidance of this project. Never once did he curtail my ambitions for this project and I hope that I have done justice to the trust he placed in me. Secondly, thanks to Paul Griffin at Severn Trent Water for instilling within me a passion for this research topic. He has tolerated me with equally large measures of good humour and patience. Thirdly, thanks to Jaime Nivala for her unrelenting faith in my research and her incredible kindness. She always managed to inspire me during the difficult moments.

Special thanks go to Scott Wallace for supporting my investigations in the USA and providing me with his expert counsel. Few are so privileged as to have had access to such a knowledgeable mentor. My kindest sentiments go to Joan Garcia and Anna Pedescoll from Universidad Politecnica de Catalunya for their commitment to this research area, their incredibly constructive feedback on my work and the fun they always create during our interactions. The superb generosity of Clodagh Murphy and David Cooper from ARM Ltd. deserves a special mention, as they provided data which has greatly enriched the analysis achieved during this work. Other notable mentions go to the staff at Severn Trent Water, such as Clifford Corbey, Ian Gray, Lee Wilson and Gabriela Dotro, who helped me tremendously in my endeavours.

At Aston University, my warmest gratitude goes to George for his friendship, empathy and culinary wizardry. Without his psychological support I may well have succumbed to madness long ago. At Nottingham Trent University, thanks go to Rob Morris for his enthusiasm and willingness to soundboard my crazier ideas. At the Indian Institute of Technology, Delhi my sincere thanks extends to Professor Pradeep Sen, Professor Padman Vesudevan and Mr Seghal for a memorable stay. My deepest thanks to the Hewitts for making me feel so at home during my stay in the USA.

Finally, thanks and love to my parents for supporting me always, and enabling me to explore my intellectual curiosities.

Paul Knowles – September 2010

Table of Contents

List of Tables

List of Figures

List of Symbols

Symbol	Unit	Description
A	-	A geometrical factor related to turbulent energy dissipation in porous media
a		A factor to represent the magnitude reduction from clean hydraulic conductivity at the inlet due to clogging
A_{CELL}	m^2	Cross-sectional area of the permeameter cell (circular)
A_w	m^2	wetted cross section of the system
B		Empirical coefficient that describes the relationship between accumulation of specific deposit and clogged hydraulic conductivity
b		An empirical coefficient that governs the impact of clogging downstream of the inlet
C		Empirical coefficient that describes the relationship between accumulation of specific deposit and clogged hydraulic conductivity
CF		Clog Factor
CF_X		Longitudinal component of Clog Factor at a point
CF_T		Bulk system Clog Factor
CF_Z		Vertical component of Clog Factor at a point
c_{in}	mg/L	Solute concentration in the influent
c_{out}	mg/L	Solute concentration in the effluent
c_S	mg/L	Concentration of solids in the wastewater
C_u	-	The coefficient of uniformity for a porous media, equal to the quotient of d_{60} over d_{10}
D	m	Fluid elevation in reference to a vertical datum
D		Empirical coefficient that describes the relationship between accumulation of specific deposit and clogged hydraulic conductivity
D	m2/s	Dispersion Coefficient for solute mixing in a flow system
d	mm	Media particle diameter
d_{10}	mm	The diameter of sieve-spacing that allows only 10% by mass of a sample of gravel to pass through
d_{50}	mm	The diameter of sieve-spacing that allows only 50% by mass of a sample of gravel to pass through
d_{60}	mm	The diameter of sieve-spacing that allows only 60% by mass of a sample of gravel to pass through
d_φ	m	Clogged media diameter
E		An empirical coefficient that describes the suspended solid removal efficiency of the bulk reactor
e_M		Mixing efficiency of the reactor
ET	m/d	Evapotranspiration from the system
e_V		Volumetric efficiency of the reactor
f	m	The length that overland flow extends along the length of the bed

g	m/s^2	Gravitational acceleration equal to 9.81
h	m	The depth of water in the system
H	m	System height (including surface layer) at the influent
h_f	m	Water table depth at f
h_{in}	m	Hydraulic head at the influent of the system
h_n		Head loss across the nth section of the gravel core measured by the Aston Permeameter
h_{out}	m	Hydraulic head at the outlet of the system
h_T		Head loss across the entire gravel core measured by the Aston Permeameter
J		A bulk parameter describing the influence of accumulated solids on system hydraulic conductivity
k	m/d	The hydraulic conductivity of the media
k_i	m^2	Intrinsic permeability of the gravel media
k_n		Hydraulic conductivity of the n^{th} section of the gravel core measured by the Aston Permeameter
k_T		Hydraulic conductivity of the entire gravel core measured by the Aston Permeameter
k_v	m/d	variably saturated hydraulic conductivity
k_φ	m/d	Clogged media hydraulic conductivity
L	m	The length of the system
L_{CELL}	m	Length of the permeameter cell
M_{in}	kg	Mass of solute added to system as a unit impulse
n		Number of tanks in series
n		Total number of equally spaced take-off points along the permeameter cell in the Aston Permeameter experiment
P	m/d	Precipitation into the system
P_M	J/m^3	pressure associated with matrix potential
Q		Discharge through Aston Permeameter
Q_{in}	m^2/d	Width-averaged influent flow-rate
Q_{out}	m^2/d	Width-averaged effluent flow-rate
Re	-	The porous media Reynolds number
s		The operator in the Laplace Transform Function
s	kg/m2	Cumulative applied solids load since system startup per meter squared of wetland footprint
$\dot{s}$	kg/d	Wastewater solids loading rate
t	d	Time given in days or seconds
t_c	d	Time to clogging
u	m/d	Longitudinal component of velocity
$\bar{U}$	m/s	Multi-dimensional velocity vector
$\overline{u}$	m/s	Depth averaged longitudinal velocity
v	m/d	Transverse component of velocity
w	m/d	Vertical component of velocity
W	m	System width

w_r	m/d	Vertical recharge rate
x	m	Longitudinal ordinate in the system space
$\bar{x}$		Dimensionless longitudinal length
y	m	Transverse ordinate in the system space
z	m	Vertical ordinate in the system space
$\bar{z}$		Dimensionless vertical depth
β	1/m	Filter coefficient describing the ability of a porous media to physically remove suspended particles from flow
β_c	1/m	Clean filter coefficient
Γ		The gamma distribution function
ε	-	Media porosity
ε_ϕ	-	Clogged media porosity
θ	-	Media saturation
λ		Hydraulic efficiency of the reactor
μ	$kg/m.s^2$	Dynamic viscosity of the porous media-flow system
ϖ	-	An empirical coefficient that governs the relationship between specific deposit and filter coefficient
ρ	kg/m^3	The density of wastewater
ρ_B	kg/m3	Density of biofilm accumulation
ρ_s	kg/m3	Density of wastewater solids
σ^2	d2	Variance of the residence time distribution
σ_L	m	Longitudinal dispersivity
σ_T	m	Transverse dispersivity
σ_θ^2	-	Dimensionless variance of the residence time distribution
τ	d	Mean residence time of solute in the reactor
τ_P	d	The residence time at which solute peak concentration is detected at the effluent
τ_T	d	Design residence time of solute in the reactor
ϕ	-	Specific volume of clog matter deposit
ϕ_B		Specific volume of the biological component of the clog matter deposit
ϕ_C		Specific volume of the chemical component of the clog matter deposit
ϕ_P		Specific volume of the physical component of the clog matter deposit
ψ	m	Pressure-head

List of Acronyms and Abbreviations

Acronym	Definition
BOD	Biological Oxygen Demand – a water quality parameter
CF	Clog Factor
COD	Chemical Oxygen Demand - a water quality parameter
CSTR	Continually Stirred Tank Reactor – a type of ideal hydrodynamic reactor
HLR	Hydraulic Loading Rate – of flow into the TW
HRT	Hydraulic Retentional Time – of flow in the TW
HSSF	Horizontal Subsurface Flow – a type of TW
IWA	International Water Association
NH_3	Ammonia-Nitrogen – a water quality parater
PE	Population Equivalent – a unit of flow-rate
PF	Plug Flow – a type of ideal hydrodynamic reactor
POR	Period-of-Record – of sampling at a system
RBC	Rotating Biological Contactor – a secondary treatment technology
RTD	Residence Time Distribution - of flow within the TW
TIS	Tanks in Series – a hydrodynamic performance parameter
TSS	Total Suspended Solids – a water quality parameter
TW	Treatment Wetland
UK	United Kingdom
US	United States of America
VF	Vertical Flow – a type of TW
W:L	Width-to-length ratio – of a HSSF TW footprint

1. Introduction

PREMISE FOR RESEARCH

Horizontal Subsurface Flow Treatment Wetlands (HSSF TWs) are the preferred technology choice of Severn Trent Water Ltd. (Severn Trent), a United Kingdom (UK) water utility, for providing tertiary municipal wastewater treatment to decentralised communities with populations up-to 2,000 (Green and Upton, 1995). These natural systems typically employ common reeds (Phragmites australis) planted in basins of 3-12 mm gravels, which provide suitable biological, physical and chemical conditions for final purification (Kadlec and Wallace, 2010). Severn Trent has over two decades of experience operating HSSF TWs, in which time it has become apparent that clogging is a major operational and maintenance issue (Cooper et al., 2005, Cooper et al., 2008). Experience with clogging has seen estimates of lifetime reduced from 20 years (Cooper et al., 1996) to 8 years (Griffin et al., 2008), which compromises the economic advantage offered by using HSSF TWs over conventional tertiary wastewater treatment technologies. The need to understand clogging and improve asset longevity resulted in this Doctoral Research collaboration between Severn Trent Water and Aston University.

The main aim of this study can be concisely stated:

"To help designers and operators make informed decisions that result in improved asset longevity, by improving the knowledge and understanding of clogging in Severn Trent HSSF TWs"

The remainder of this chapter gives the essential information required to appreciate the nature of the study – namely: the reasons why HSSF TWs are increasingly being used for decentralised communities; the way that Severn Trent implements the technology including details of the standard design approach; and the magnitude of the HSSF TW clogging problem facing Severn Trent. Subsequently, the research approach and report structure will be explained.

1.1. Horizontal Subsurface Flow Treatment Wetlands: an overview

Horizontal Subsurface Flow Treatment Wetlands (HSSF TWs) have been used to treat many types of urban, industrial and agricultural wastewaters around the world (Kadlec, 2009). Many thousands of HSSF TWs have been constructed over the last two decades (Vymazal and Kropfelova, 2008) and the technology has become an established technology In the UK, particularly for the tertiary treatment (polishing) of municipal wastewaters for small, decentralised communities. Cooper (2007) reported that by 2006 the UK Constructed Wetland Association database contained records for 736 HSSF TW systems.

The growing popularity of HSSF TWs can be attributed to a list of technical and fiscal advantages for operators, and ecological benefits that have led to a positive public perception. These reasons are elaborated in **Table 1-1**, which is mainly adapted from opinions presented in the International Water Association (IWA) Specialist Group Technical Report on Constructed Wetlands for Pollution Control (IWA, 2000).

Table 1-1 Some of the major technological and ancillary benefits offered by treating wastewater using HSSF TWs. Adapted from IWA (2000) with additional references where indicated.

Technological Benefits	Wider Benefits
TWs can be less expensive to build than other treatment options	They are an environmentally sensitive approach that is viewed with favour by the general public
Operation and maintenance expenses (energy and chemicals) are low	They provide habitat conservation and biodiversity for plant, bird, animal, insect and aquatic life (Worrall et al., 1997)
Operation and maintenance requires little expertise and periodic, rather than continuous, on-site labour	They can be built to fit harmoniously into the landscape
TWs are able to tolerate fluctuations in flow and pollutant loading	Value added crop cultivation, such as ornamental plants (Zurita et al., 2008) or manufacturing materials for e.g. roofing, fencing, insulation (Löffler, 1990)
TWs are able to treat wastewater with low organic load (too low for conventional activated sludge methods)	Plant biomass can be harvested for use as an energy crop (Ciria et al., 2005)
They facilitate water reuse and recycling (Rousseau et al., 2008)	Aesthetic enhancement of open spaces (Burka and Lawrence, 1990)
They can treat a wide range of pollutants, often simultaneously	Social benefits such as education and recreation (nature watching, exercise, hunting) (Knight et al., 2000)

Water purification by HSSF TWs is achieved through a combination of physical, biological and chemical mechanisms, that occur due to interactions between the wastewater, the porous media, the atmosphere, and microbial entities that assimilate wastewater constituents for survival (Vymazal et al., 1998). The mechanisms by which HSSF TWs remove the major constituents of wastewater are detailed in **Table 1-2** (Wallace and Knight, 2006).

Table 1-2 Removal mechanisms in HSSF TWs - significant processes are italicised. Table reproduced from Wallace and Knight (2006).

Water Quality Parameter	Physical	Chemical	Biological
Suspended solids	*Filtration*		Microbial degradation
Biological oxygen demand (BOD)	*Filtration*		Microbial degradation
Chemical oxygen demand (COD)	*Filtration*		Microbial degradation
Metals (Ag, As, Cd, Cr, Cu, Hg, Ni, Pb, Se, Zn)	*Filtration*	*Precipitation;* adsorption; ion exchange	Microbial uptake; plant uptake
Petroleum hydrocarbons (fuel, oil and grease, alcohols, BTEX, TPH)	Volatilisation	Adsorption	Microbial degradation; plant uptake
Synthetic hydrocarbons (PAHs, chlorinated and non-chlorinated solvents, pesticides, herbicides, insecticides)	Filtration; volatilisation	Adsorption; volatilisation (ammonia)	Microbial degradation; plant uptake
Nitrogenous compounds (organic N, NH_3, NH_4^+, NO_3^-, NO_2^-)	Filtration	*Precipitation; adsorption*	Microbial uptake and transformation; plant uptake
Inorganic and organic P	Filtration		Microbial uptake; plant uptake
Pathogens (bacteria, viruses, protozoa, helminths)	*Filtration*		Die-off; microbial predation

1.2. Severn Trent Water and the use of HSSF TWs

The privatisation of the UK water industry in 1989 led to the formation of Severn Trent Water, serving 8 million users across the Midlands (Green and Upton, 1995). **Figure 1-1** is a map illustrating the Severn Trent service area. At the time Severn Trent had 1,048 wastewater treatment plants with 70% of these serving populations of less than 2,000 people (Griffin and Pamplin, 1998): those defined as 'small works' under the European Commission Urban Wastewater Treatment Directive (Commission, 1999). Small works were

highlighted as those most susceptible to failing permit compliance, as they often discharge straight into rivers and are generally subject to more stringent consents by the UK Environment Agency (i.e. allowable levels of pollutants in the discharge) than other works (Green et al., 1998). In 1985, Severn Trent commissioned a rolling programme to upgrade small works in order to ensure compliance; however, this required minimal cost as these 700 works only constitute 3% of the utility's customer base (Green and Upton, 1994).

Figure 1-1 Map illustrating the Severn Trent Water service area for water and sewer services. Map provided by Severn Trent Water South Staffs. division. Image kindly provided by P. Griffin.

The concept of using HSSF TWs to provide municipal wastewater treatment was introduced to the UK in 1985 after the UK Water Research Council visited a German researcher named Kickuth, who was an early proponent of the technology (Boon, 1985, Kickuth, 1977). The UK Water Services Association (of which Severn Trent is a member) and the Water Research Council founded the Reed Bed Treatment Systems Coordinating Group, which pooled the results of initial technology trials performed by water utilities with the aim of accelerating progress (Cooper and Green, 1998, Murphy and Cooper, 2010).

Using two pilot systems, Severn Trent proved the ability of HSSF TWs to provide secondary treatment for populations of less than 50 people (Little Stretton, Leics.) and tertiary treatment for populations of less than 2,000 people (Leek Wooton, Warks.) (Green and Upton, 1993). In 1990 Severn Trent began the use of HSSF TWs for treatment of storm water overflow (Green and Martin, 1996). Installation of HSSF TWs became part of the Small Works maintenance programme, and between 1987 and 2009 systems were installed at 419 sites across the Severn Trent jurisdiction (Griffin and Pamplin, 1998, Griffin et al., 2008) (**Figure 1-2**). **Figure 1-3** illustrates the various ways that Severn Trent integrate HSSF TWs into process flow sheets for rural treatment works (Griffin and Pamplin, 1998). According to **Figure 1-2**, the greatest application is for tertiary municipal wastewater treatment (approximately 75 %).

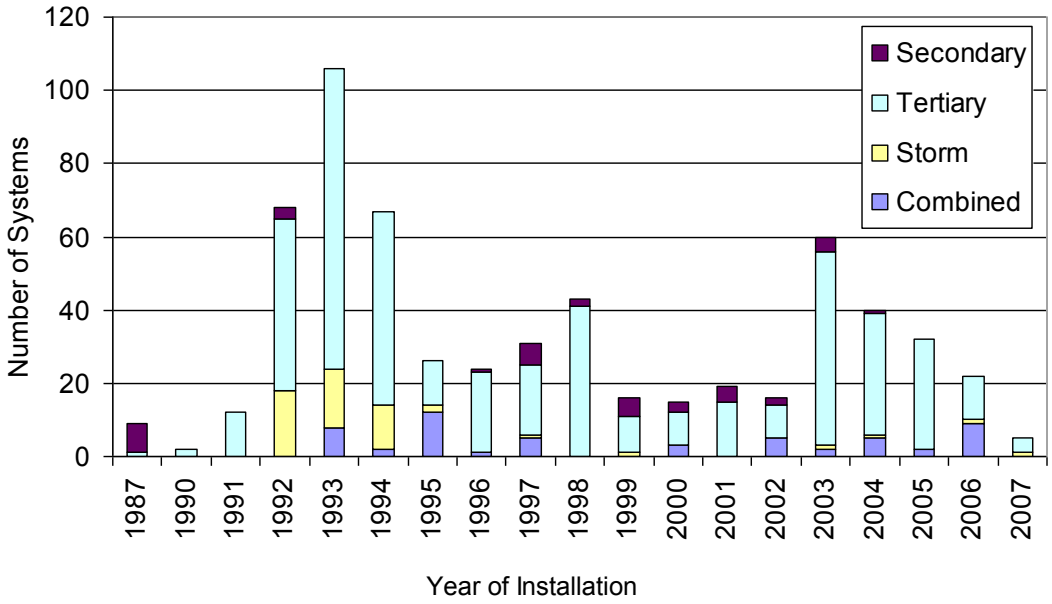

Figure 1-2 History of HSSF TW system installation at decentralised wastewater treatment plants operated by Severn Trent, between 1987 and 2007. Applications are A) *Secondary* Treatment, B) *Tertiary* Treatment C) *Separate* tertiary and stormwater treatment, D) *Combined* tertiary and stormwater treatment. Records for 582 HSSF TWs kindly provided by C.Murphy.

Systems that provide secondary treatment and separate tertiary and storm-water treatment have since been dropped from the Severn Trent selection matrix. This is because experience has shown that HSSF TWs are inefficient for provision of secondary treatment, and combined tertiary and storm-water TWs can achieve similar treatment performance as systems that use separate components, but with reduced cost and land requirements (Griffin *et al.*, 2008).

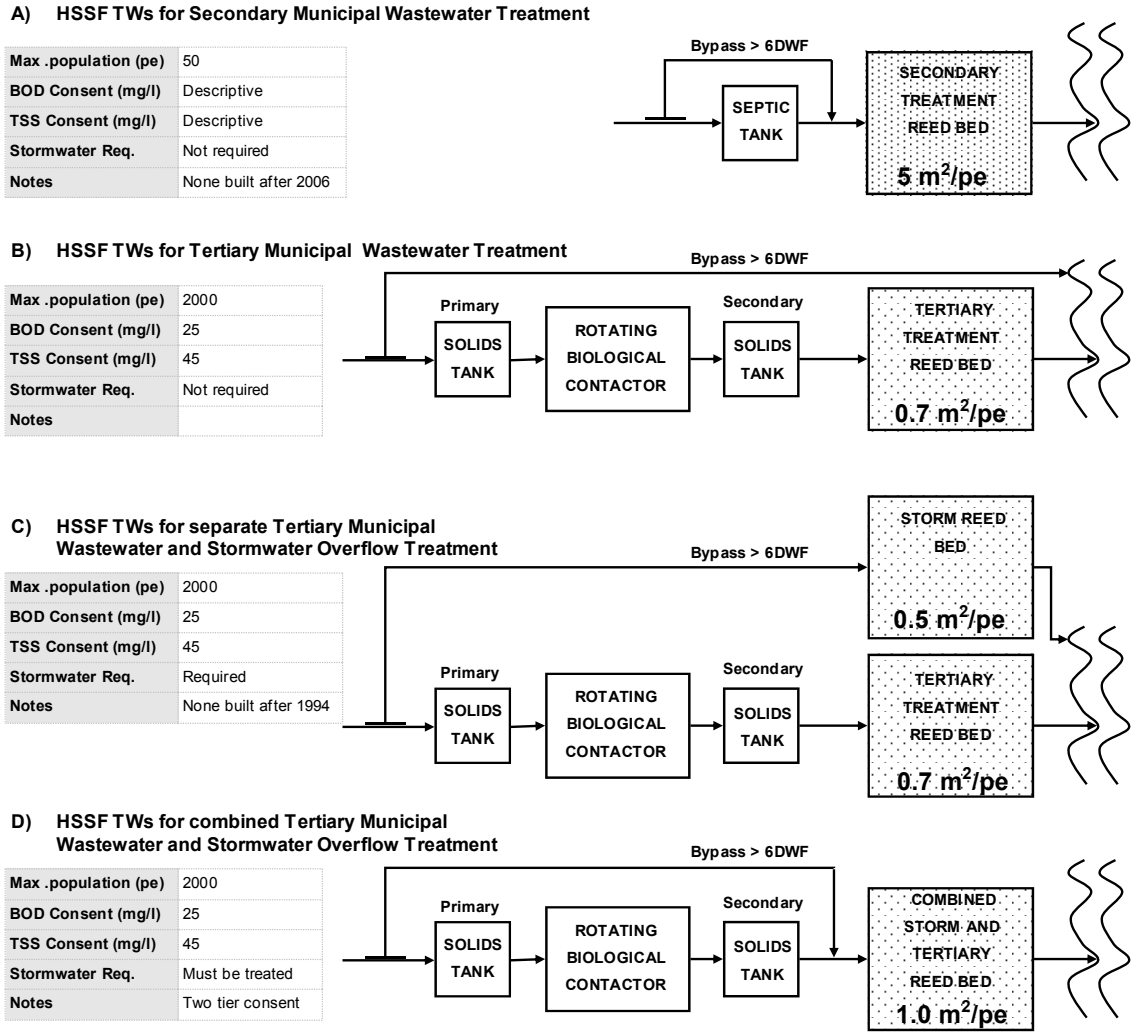

Figure 1-3 The manner in which HSSF TWs are typically incorporated into process flow sheets by Severn Trent, for various treatment requirements, including bypasses for storm-water above six-times dry weather flow (DWF). Information adapted from Griffin and Pamplin (1998) and Griffin (2003). Rotating Biological Contactor may be replaced by an equivalent secondary treatment process.

The ability of HSSF TWs to successfully achieve tertiary treatment of municipal wastewater is demonstrated in **Table 1-3**, which shows Periods or Record (PORs) for 17 systems operated by Severn Trent, based on the removal performance of three common water quality indicators: Biological Oxygen Demand (BOD), Total Suspended Solids (TSS) and Ammonia-Nitrogen (NH_3). As evident in **Table 1-3**, these systems can further purify secondary treated wastewaters which already have relatively low contaminant concentrations, achieving an average removal performance of 69% BOD, 73% TSS and 60% NH_3, for the cases illustrated.

Table 1-3 Treatment performance of 15 HSSF TWs operated by Severn Trent, based on average influent and effluent concentrations across the Period of Record for each system, for Biological Oxygen Demand (BOD), Total Suspended Solids (TSS) and Ammonia (NH_3). A total of 2,323 data records are considered altogether. Data summarised from the Constructed Wetland Association performance database (CWA, 2006).

System Name	Number of Records	Area (m^2)	Flow (m^3/d)	BOD in (mg/L)	BOD out (mg/L)	BOD % Removal	TSS in (mg/L)	TSS out (mg/L)	TSS % Removal	NH_3 in (mg/L)	NH_3 out (mg/L)	NH_3 % Removal
Ashby Folville	149	825	164	9.82	1.87	81%	24.50	4.21	83%	3.78	2.02	47%
Claverley	70	292	115	13.24	4.86	63%	20.16	5.07	75%	5.28	1.66	69%
Earlswood	134	1,196	618	9.01	2.33	74%	19.07	4.91	74%	0.83	0.37	55%
Forton	10	165	22	78.33	36.86	53%	49.67	19.14	61%	17.27	7.06	59%
Gailey	19	23	25	3.00	1.83	39%	22.00	6.00	73%	1.53	0.61	60%
Hognaston	153	936	132	3.03	1.95	36%	8.59	2.58	70%	1.45	0.57	61%
Knowbury	62	330	43	8.21	1.63	80%	22.25	3.76	83%	0.87	0.24	73%
Leek Wootton	269	825	206	12.61	2.34	81%	20.31	5.24	74%	6.83	2.65	61%
Lighthorne Heath	150	321	300	5.04	1.43	72%	8.93	3.87	57%	3.33	1.28	61%
Little Wenlock	95	53	80	18.17	7.34	60%	24.35	8.92	63%	7.42	4.36	41%
Lydbury North (Old)	45	334	55	10.96	1.11	90%	20.67	1.95	91%	7.32	3.97	46%
Middleton (Shropshire)	57	168	10	322.11	28.83	91%	113.61	19.74	83%	65.11	34.31	47%
Middleton (Warwickshire)	635	450	70	8.97	2.24	75%	22.32	7.94	64%	2.70	0.64	76%
Naseby	415	1,003	90	6.62	1.31	80%	17.87	6.62	63%	1.89	0.44	77%
Norton Lindsey	60	257	110	5.78	1.91	67%	20.64	3.64	82%	1.78	0.71	60%
AVERAGE		**479**	**136**	**34**	**7**	**69%**	**28**	**7**	**73%**	**8**	**4**	**60%**

1.3. Typical Design of Severn Trent HSSF TWs for tertiary treatment

The main visual feature of HSSF TWs in the UK is aquatic macrophytes, such as Phragmites australis (common wetland reed), planted in a porous gravel bed; thus TWs are colloquially referred to as 'reed beds'. Under normal operation wastewater flows under the surface of the gravel where the correct conditions are encountered for final purification (Cooper et al., 1996). The HSSF TWs employed by Severn Trent are built according to the European Design and Operation Guidelines for Reed Bed Treatment Systems (EC/EWPCA, 1990), and a typical design is shown in **Figure 1-4**, which details a transverse cross-section.

In **Figure 1-4** the wastewater flows from left to right through gravel with recommended media size distributions of 3-6 mm or 6-12 mm. The gravel is filled to a 0.6 m depth to accommodate the typical root penetration of Phragmites australis (Nuttall et al., 1997) and the gravel surface is levelled. The basin is lined with a 1 mm thick high density polyethylene plastic liner to prevent any infiltration of wastewater to the ground and is built with a bottom slope of about 1% to facilitate complete drainage of the bed if required. The depth of water in the bed is established using an outlet level control device such as a swivelling elbow or sluice gate. The wastewater is continuously fed through surface-based inlet distributors which span the width of the bed. Distributor designs vary and include pipes with multiple risers and troughs with numerous distribution weirs. The coarse rock berm around the perimeter of the bed incorporates media with sizes 50-200 mm and improves flow distribution at the inlet and outlet regions. The berms are constructed with a freeboard of 50-100 cm to accommodate bed expansion from root growth, and leaf litter accumulation (IWA, 2000). A photograph of a HSSF TW at a Severn Trent wastewater treatment plant is given in **Figure 1-5**.

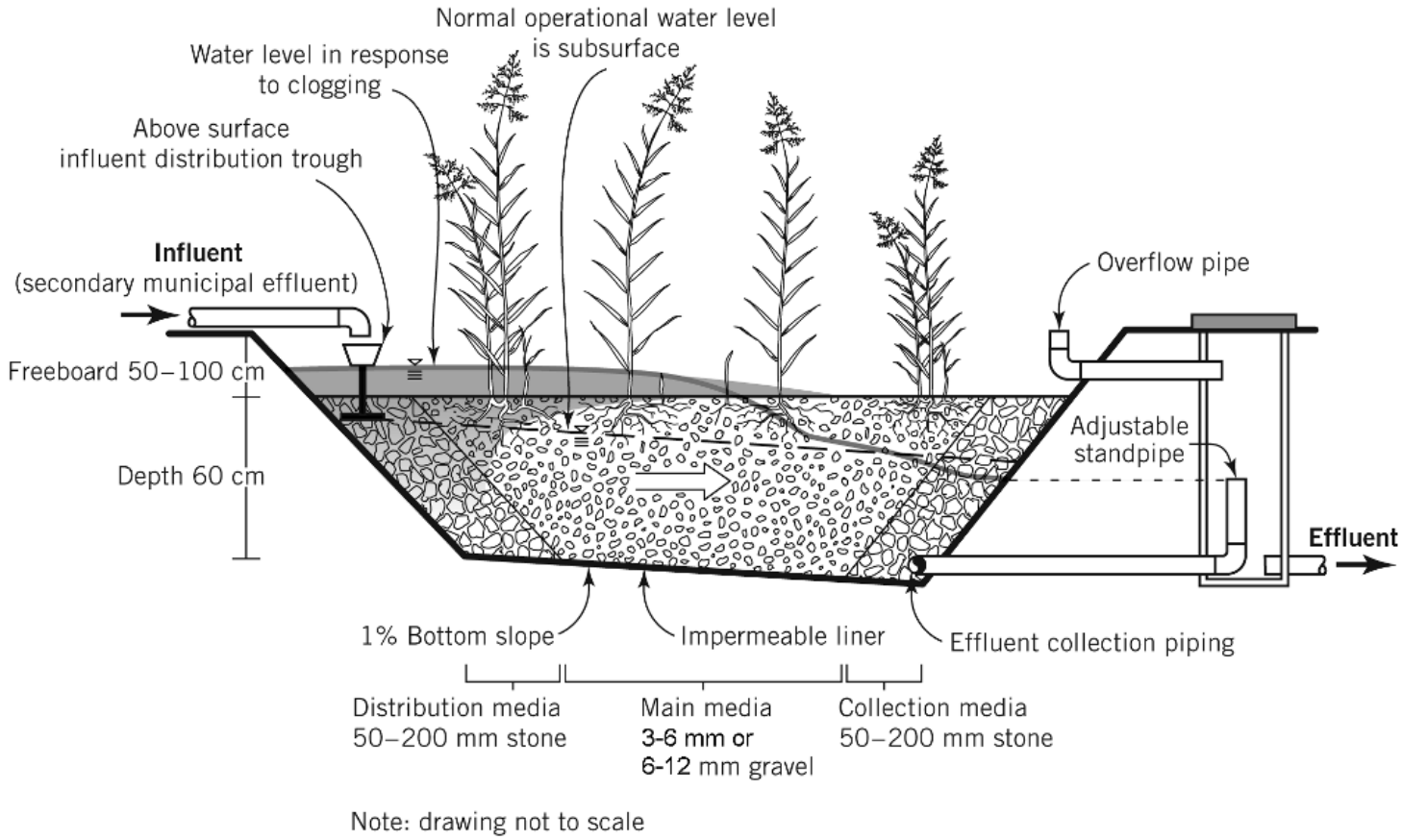

Figure 1-4 The typical design of Horizontal Subsurface Flow Treatment Wetlands as used by Severn Trent Water for the tertiary treatment of municipal wastewater in the UK. The figure illustrates both normal and clogged hydraulic operation, where the grey matter indicates the zone where clogging typically occurs. Figure reproduced from Knowles et al. (2011).

Figure 1-5 Two tertiary HSSF TW cells at Severn Trent, Snitterfield wastewater treatment plant. The cells are 12.5 m long by 28 m wide and are showing a full growth of Phragmites australis.

Severn Trent have determined that the footprint of HSSF TW required to provide tertiary treatment is 0.7 m^2 per population equivalent (PE), where one PE is the typical quantity and quality of domestic wastewater produced by one individual (Green and Upton, 1995). The average system has a footprint of 318 m^2 with a length-to-width aspect ratio of 0.83-to-1 (Murphy and Cooper, 2010), although there is a large variation in reported system dimensions. Similarly, the cost of systems can be highly variable. Green and Upton (1995) report that economies of scale reduce capital costs for Severn Trent systems from £180/PE to £75/PE (inflated to 2009 price index) as the population requirement increases from 100 to 1,000. As such, at 2009 prices a 300 m^2 system would cost in the region of £75,000 to construct (Murphy and Cooper, 2010). These prices are specific to the UK and do not include land costs as the systems are installed on existing Severn Trent sites.

1.4. Clogging in Severn Trent Water HSSF TWs

Generally speaking HSSF tertiary TWs have proven very successful for Severn Trent and have been met with considerable enthusiasm from operators, who appreciate the security to compliance and low maintenance requirements (Griffin and Pamplin, 1998). However, problems with clogging prevent these systems from being 'fit-and-forget' solutions.

Clogging is commonly qualified by undesirable ponding of wastewater on the surface of the system. This occurs because clog matter with low hydraulic conductivity accumulates both within the pore space of the gravel and on the surface of the bed, and disrupts the intended subsurface flow operation (Cooper et al., 2005). Clogging occurs first at the inlet, within the upper layers of the gravel and on the surface of the bed. In their survey of 255 HSSF TWs in the UK, Cooper et al. (2005, 2008) frequently encountered systems with surface sludge accumulations in excess of 150 mm at the inlet and 40 mm at the outlet **(Table 1-4)**. Rousseau et al. (2005b) made similar observations in their survey of 12 UK based HSSF stormwater treatment wetlands, reporting that the vast majority of them had experienced sludge build-up over the entire surface of the bed. These authors also speculated that symptoms such as poor reed growth and weed infestation may be connected to clogging (Rousseau et al., 2005b, Cooper et al., 2005, Cooper et al., 2008).

Table 1-4 Frequency of operational problems encountered from a survey of 255 HSSF TWs operated by Severn Trent. Data reproduced from Cooper et al. (2008).

Operational Problem	Frequency	% of 255
Sludge depth greater than 150 mm at inlet	111	44
Sludge depth greater than 40 mm at outlet	48	19
Bed flooded at inlet on 1st visit	132	52
Bed flooded at outlet on 1st visit	76	30
Inlet distributor problems	34	13
Outlet collector problems	21	8
Weed infestation (greater than 25% cover)	130	51
Poor growth of reeds	34	13

In ponded systems, overland flow will extend across the surface layer until the cumulative infiltration through the surface layer can adequately transmit the applied wastewater load. In 30% of the 255 systems surveyed by Cooper et al. (2008), overland flow was present over the majority of the HSSF TW surface. The contrast between initial and clogged conditions can be seen by comparing **Figure 1-6**, which shows the surfaces of a 1 year old unclogged system, and **Figure 1-7**, which shows the surface of a 7 year old clogged system.

In excessively clogged systems the subsurface may be unable to convey the intended hydraulic load, in which case the influent wastewater will pool on top of the bed to the point that virtually untreated wastewater bypasses the system through the overflow pipe (as illustrated in **Figure 1-4**). As a pre-emptive measure clogged systems are usually refurbished before they reach this stage. Refurbishment has historically involved replacing the fouled gravel with clean media. As reported by Murphy and Cooper (2010), the refurbishment of a 300 m^2 system in 2009 incurred an approximate cost of £50,000, 50% of which was associated with disposal of the fouled media to landfill (£64/tonne). The cost of £50,000 is substantial given that a new system of the same size may cost £75,000 (Murphy and Cooper, 2010).

When the first systems were installed it was expected that HSSF TWs would last 15-20 years between refurbishments. In fact refurbishments have been required much more frequently. Only 24 % of systems have operated longer than 15 years without requiring refurbishment, with the oldest two systems currently running for 18 years.

Figure 1-6 The surface of a refurbished, 1 year old tertiary treatment HSSF TW operated by Severn Trent at Fenny Compton wastewater treatment plant. The photograph shows rock berms, gravel media and early Phragmites australis establishment. Wastewater is flowing 10 cm below the surface of the gravel.

Figure 1-7 The surface of a clogged, 7 year old tertiary treatment HSSF TW operated by Severn Trent at Gaydon wastewater treatment plant. The photograph shows a 'v-notch trough' style influent distributor which spans the width of the system at the inlet, and a significant surface sludge accumulation which has obscured the gravel surface and rock berms and results in overland flow of the wastewater. The difference in Phragmites australis health between **Figure 1-6** and **Figure 1-7** is related to winter die-off rather than the impact of clogging.

Refurbishment of HSSF TWs has become a common practice for Severn Trent, with an average of 17 beds per year refurbished since 1998. Overall, Severn Trent has refurbished 175 out of 491 tertiary systems (some of these multiple times). **Figure 1-8** illustrates the distribution of system ages at the time of refurbishment. The minimum and maximum ages at refurbishment are 1 and 19 years, with a median age of 11 years. These findings have recently caused Severn Trent to redefine asset longevity to 8 years (Griffin et al., 2008), which practically doubles HSSF TW capital replacement costs for Severn Trent. If the HSSF TW inventory is to be maintained against a depreciation age of 8 years, then the number of refurbishments per year could be as high as 61. Based on an average system size of 318 m^2 and a unit refurbishment cost of 167 £/m^2, refurbishing 61 systems per year would cost Severn Trent approximately £ 3.2 million per year – all for 3 % of the service population.

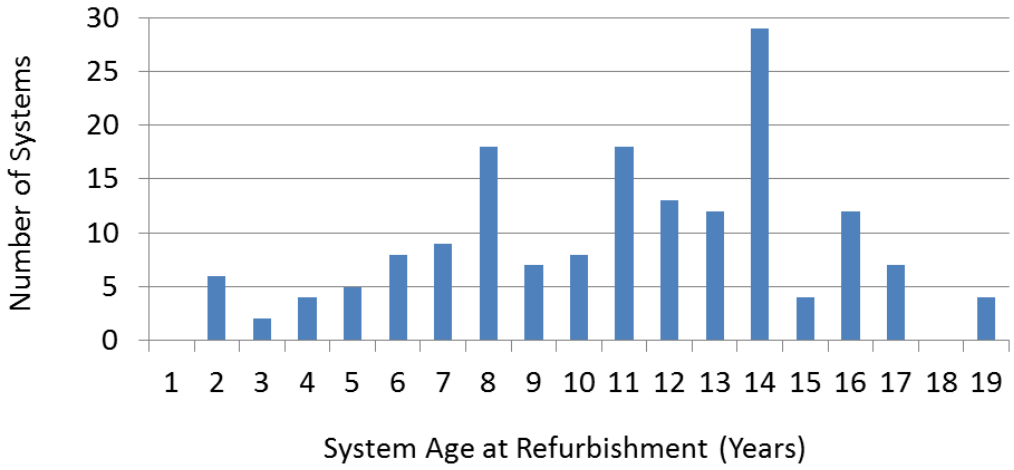

Figure 1-8 Distribution of system age at the time of refurbishment for 166 tertiary HSSF TW systems. Records kindly provided by C.Murphy.

The substantially higher than expected refurbishment costs threaten to make HSSF TW technology an unviable tertiary treatment option for Severn Trent, unless the clogging issue can be addressed. Despite these economics concerns and the numerous accounts of clogging in Severn Trent HSSF TWs, the factors responsible for clogging are still not well understood (Kadlec and Wallace, 2010). Systems are still considered as black boxes (Rousseau et al., 2004) with little insight into the symbiotic relationship between hydraulics, treatment and clogging, and how this relationship changes as clogging develops. Limited knowledge exists about the magnitude and distribution of hydraulic conductivity in clogged

HSSF TWs. This lack of understanding means that clogging is not properly addressed and prevented, and the development of a robust treatment performance prediction tool for HSSF TWs is not possible (Langergraber, 2003). If this information were available then HSSF TWs could be designed for better reliability and control, and to achieve more ambitious treatment objectives.

1.5. Aims and Thesis Structure

A series of research obstacles have been identified that must be overcome to achieve the major study aim: improving the knowledge and understanding of clogging in Severn Trent HSSF TWs. Corresponding objectives are stipulated that address these obstacles and thus provide the basis for the overall research approach adopted by this study.

Problem	**The factors that cause clogging are not well understood.**
Obstacle	Numerous sources exist proffering various observations, hypotheses and conclusions regarding clogging; however, a comparative review of the literature which identifies trends and salient factors does not exist.
Objective	**Summarise the relevant literature on HSSF TW clogging.**
Output	Determination of current best practice design guidelines for mitigation of clogging, and identification of where more research is required.

Problem	**Little is known about the relationship between clogging, hydraulics and treatment and how this develops over time.**
Obstacle	Current design tools for HSSF TW hydrology are too simple to be representative, and computational models are too complicated to be useful. Not enough information exists to allow better tools to be derived.
Objective	**Derive design tools that are representative and practical to apply, and validate them through experimentation and dynamic modelling.**
Output	Design tools that relate the changing hydrology of HSSF TWs to changes in clogging, calibrated using experimentally derived data.

Problem	**Not enough information is available on the magnitude and distribution of hydraulic conductivity to make conclusions about design or allow models to be developed.**
Obstacle	Many conventional methods for *in situ* measurement of hydraulic conductivity are not suitable for HSSF TWs, and as such no simple method exists to obtain data.
Objective	**Design an *in situ* method to obtain this information.**
Output	Hydraulic conductivity profiles for several tertiary HSSF TWs of various ages that can then be used to calibrate hydraulic models. This will also allow the influence of design and operational parameters on clogging to be studied.

The above objectives will be achieved through several stages that are reflected by the structure of this thesis. It should be pointed out that the thesis structure does not represent the chronological manner in which the study was executed, as interrelation between the study objectives means that understanding, theory and methodology were developed simultaneously. Rather, the thesis structure represents the most logical way to convey the outcomes of this research to the reader. The thesis chapters are structured as follows:

Chapter 2 A review of the relevant literature on HSSF TW clogging will be presented to inform the remainder of the thesis. This will draw on international experience and consider other varieties of subsurface flow treatment wetland technology. The review will discuss the salient factors associated with clogging and current best practices to prevent and manage clogging.

Chapter 3 The hydrological theory underlying HSSF TWs will be presented and used to illustrate the inadequacy of current simplified design tools. A novel one-dimensional analytical expression is derived that better represents the hydrology of HSSF TWs. The expression relates the state of clogging in a system to the wetted volume by considering practicalities of operation, such as overland flow and varying hydraulic conductivity profiles. A new metric, the Clog Factor, will be presented, which allows different systems to be objectively compared with regard to the severity of clogging. The Clog Factor will be used as a parameter that describes the severity of clogging in the analytical expression; thus creating the opportunity for calibration via experimentation and dynamic simulation. A dynamic simulation tool based

on Finite Element Analysis (FEA) will be used to explore the relationship between Clog Factor, hydraulics and hydrodynamics.

Chapter 4 Existing methods for measuring hydraulic parameters in porous media flow systems are reviewed with regard to their appropriateness for HSSF TWs. A novel *in situ* method is developed that measures the spatial hydraulic conductivity profile in HSSF TWs. The method uses custom made apparatus called The Aston Permeameter. Validation and quantification of error are provided for the method.

Chapter 5 The experimental results obtained by the method of **Chapter 4** are reported for numerous HSSF TWs operated by Severn Trent. During the course of this study, the chance was taken to perform the method of **Chapter 4** on three HSSF TWs operated by EcoCheck LLC in the vicinity of Stillwater, Minnesota, USA. This provided a point of comparison for how clogging can develop differently in HSSF TWs depending on local variations in design and operation.

Chapter 6 The results of **Chapter 5** for Severn Trent HSSF TWs are analysed in more detail, to show how design and operational variables affect the development of clogging, the spatial development of clogging over time, and how clogging influences flow. The theory of **Chapter 3** is applied to these results to yield Clog Factors for each system. The Clog Factor is used to derive expressions that link the spatial variation of clogging in the system to the overall severity of clogging. These expressions allow the analytical relationship between clogging and system hydrology to be calibrated for Severn Trent tertiary HSSF TWs. The FEA tool is validated using experimentally obtained hydrodynamic and hydraulic data from a real HSSF TW. Subsequently, an empirical expression is deduced that indicates how hydrodynamics respond to clogging in Severn Trent tertiary HSSF TWs. This relationship could then be used by wetland practitioners to calculate how treatment performance would vary as the system clogs.

Chapter 7 The salient conclusions from the study are presented, along with priorities and possibilities for future research.

1.6. Scope of Research

This study was funded through a CASE studentship awarded to Aston University (an academic higher education and research institution located within the Severn Trent Water service area) by the UK Engineering and Physical Science Research Council and Severn Trent Water. The funds were awarded with the specific intention of investigating clogging in Severn Trent HSSF TWs. As such, the scope of research will be limited to investigation of HSSF TWs owned and operated by Severn Trent, with the exception of the three HSSF TWs operated by EcoCheck in Minnesota. The investigations performed on the three HSSF TWs operated by EcoCheck provide a point of comparison regarding international experiences with clogging in HSSF TWs; however the EcoCheck systems are not subject to the same rigor of analysis as the Severn Trent systems. Other varieties of subsurface flow Treatment Wetlands are not investigated. The approach described by this thesis can be used as a framework to investigate clogging in other varieties of subsurface flow Treatment Wetland; however, the theory, analysis and results presented by this thesis are specific to Severn Trent HSSF TWs.

The scope of research is limited to investigations into the hydrology of HSSF TWs, which encompasses the relationship between hydraulics, hydrodynamics and clogging. The influence of hydrology on treatment performance is not explored; however the results provided can be used as a basis for others to investigate the impact of clogging on treatment performance.

1.7. Conclusions

Severn Trent has commissioned this doctoral research study to better understand clogging in their Horizontal Subsurface Flow Treatment Wetland systems so that methods to increase asset longevity can be identified. Experience with these systems has shown that clogging is a major operational problem that limits asset longevity to almost half of the anticipated longevity.

The major advantage of HSSF TWs over conventional treatment technologies is low upfront capital cost and low operating requirements. This advantage has encouraged Severn Trent to install 419 HSSF TW systems throughout their service area since the introduction of the technology to the UK in 1985. The typical cost to install a HSSF TW to provide tertiary

wastewater treatment for communities of up to 2,000 PE is £250/m^2 of HSSF TW footprint, or £175/PE served.

Over time, the cumulative biological, physical and chemical treatment processes that occur between HSSF TWs and the wastewater stream may cause clogging of the filter media. This occurs because clog matter with low hydraulic conductivity accumulates both within the media pore spaces and on the surface of the bed. Severn Trent periodically replace the filter media in systems where excessive clogging causes a decrease in treatment performance or undesirable hydraulic malfunctions, such as ponding of wastewater on the surface of the system and bypass of untreated wastewater.

Between 1998 and 2009 Severn Trent refurbished 166 clogged HSSF TWs. A typical cost to refurbish a HSSF TW is £166/m^2 of HSSF TW footprint, which is two-thirds of the cost to construct a new system. It was originally anticipated that typical asset lifetime would be on the order of 15 years; however, experience has shown that the median age for refurbishment of clogged systems is 11 years. Severn Trent have recently redefined the longevity of HSSF TWs to 8 years, which would imply refurbishing an average of 61 systems per year (based on a current inventory of 419 systems) at an associated annual cost of £ 3.2 million per year (based on an average system size of 318 m^2).

The major research objective of this study is: *"To help designers and operators make informed decisions that result in improved asset longevity, by improving the knowledge and understanding of clogging in Severn Trent Water HSSF TWs".*

It is proposed to achieve the major objective by completing three aims that correspond to gaps in the current breadth of knowledge on HSSF TWs:

1. **Summarise the relevant literature on HSSF TW clogging**
2. **Derive practical design tools that adequately represent the relationship between clogging, hydraulics and hydrodynamics, and validate the tools through experimentation and dynamic modelling**
3. **Design an *in situ* method to measure the magnitude and distribution of clogging in HSSF TWs**

The remainder of this thesis will document the execution of the above three tasks and discuss how the work performed achieves the major study objective.

2. Background

This Chapter will review background material regarding clogging in Horizontal Subsurface Flow Treatment Wetlands (HSSF TWs). **Sections 2.2, 2.3** and **2.5** of this chapter were written in collaboration with Dr. Gabriela Dotro, Ms. Jaime Nivala and Prof. Joan Garcia, and have been published as a manuscript (Knowles et al., 2011), entitled "Clogging in subsurface-flow treatment wetlands: Occurrence and contributing factors" in Ecological Engineering, volume 37 (2), pages 99-112.

Section 2.1 of this chapter will identify those characteristics that distinguish the HSSF TWs used by Severn Trent from similarly named technology variants around the world. The history behind the beginnings and international adoption of HSSF TW technology will be presented to elucidate how these regional variations in HSSF TW design have evolved. This introduction will allow the reader to appreciate the subsequent literature review on how clogging develops in different varieties of Subsurface Flow TWs. This demarcation has not previously been made in the literature and is required to identify information relevant to clogging in Severn Trent HSSF TWs.

Section 2.2 summarises the factors that are responsible for clogging and **Section 2.3** explores the influence of different design and operational variables on clogging. Making reference to these factors, **Section 2.4** explains the typical development of clogging in Severn Trent HSSF TWs specifically and analyses the longevity of the Severn Trent system stock with regard to typical design and operational parameters. **Section 2.5** considers the typical development of clogging in variants of subsurface flow treatment wetland, and explores why some systems are more prone to clogging than others. Based on international and Severn Trent experience, conclusions are drawn regarding which design and operations strategies will result in robust performance for Severn Trent HSSF TWs.

2.1. Treatment Wetland Technology

Several terms combine to provide the name Horizontal Subsurface Flow Treatment Wetlands. Firstly, HSSF TWs are constructed replications of natural wetland environments. They are colloquially referred to in the UK as 'reed beds' and are one example of HSSF TW design that exists around the world. HSSF TWs are a subgroup of Subsurface Flow TWs,

which are a further subgroup of Treatment Wetland technology. The classification system for HSSF TWs will be explained in stages and the standard nomenclature used within the remainder of this document will be defined.

2.1.1. Major characteristics of Wetland Environments

Natural wetlands are often known through colloquialisms such as fens, bogs, swamps, marshes and ditches (Vymazal et al., 1998) and occur in coastal regions or topographical depressions where the water-table is close to the land surface (Kadlec, 2009). Vymazal and Kropfelova (2008) explain that natural wetlands are often temporary ecosystems that will eventually become fully aquatic or terrestrial depending on water-table fluctuations caused by season, drought, flood or sea-level rise. According to Mitsch and Gosselink (2007) the typical characteristics of wetlands that differentiate them from completely terrestrial or aquatic natural wastewater treatment systems are:

1 **Saturated hydrology** – standing water, either above the soil surface or within the rootzone, which supports a habitat of aquatic flora and fauna, and biota responsible for biological treatment.

2 **Hydric soils** – soils with variable oxidation states such that a variety of anaerobic, anoxic and aerobic reduction-oxidation reactions can be achieved.

3 **Hydrophytic plants** – plants that can root in saturated conditions, and have high productivity in comparison to terrestrial plants. Plant growth can be emergent or submergent.

These three properties makes wetlands ideally suited for wastewater treatment in comparison to other natural treatment technologies. The saturated conditions and large surface area provided by plants and soil promote a high rate of biological activity (Wallace and Knight, 2006), and the gradient of redox conditions facilitates numerous contaminant removal mechanisms. Wetlands have popularly been dubbed ‘the kidneys of the earth’ due to their proficiency for natural water purification (Brix, 1994b, Mitsch and Gosselink, 2007). Wastewater has been discharged to natural wetlands for as long as it has been collected, albeit more through convenience than intentional means of treatment (Kadlec and Wallace, 2010). The potential for wetlands to provide wastewater treatment, as well as other significant social and ecological benefits, was not realised by researchers until the 1950s

(Mitsch and Gosselink, 2007). Prior to this many countries (particularly low lying regions of Europe) historically drained wetland regions to enable use for other purposes like urbanisation or agriculture. These countries are now restoring wetland areas as the crucial role of wetlands for providing inland nutrient retention and buffering of flood waters has become apparent (Gopal, 1999, Kjellin et al., 2007). Other benefits, as summarised by Vymazal and Kropfelova (2008), include:

- Providing a unique habitat for numerous species of wildlife, birdlife, aquatic life, flora and fauna.
- Producing high-growth-rate plant biomass with numerous applications such as biofuels, paper production, staple foods (rice), fertilisers, fodder, matting and roofing materials.
- Water supply for irrigation, groundwater recharge and drinking water, and water treatment.
- Amenity and recreation (e.g. boating, fishing).

2.1.2. Treatment Wetland Classification Systems

The use of wetland systems for water treatment is now widely established, resulting in the terminology "Treatment Wetland" (TW). Treatment Wetlands lay on the gradient between land-based and aquatic-based wastewater treatment systems, which include slow-rate land application, rapid infiltration systems, overland flow systems, Treatment Wetlands and waste stabilisation ponds or lagoons (Crites and Tchobanoglous, 1998; IWA, 2000). Using a hydrological generalisation, the ratio of hydraulic loading rate to soil hydraulic conductivity increases along this gradient, such that subsurface flow is predominant in land based systems and surface flow is prevalent in aquatic systems.

The major difference between natural and conventional wastewater treatment technologies is the trade-off between land and operational costs. In natural systems, processes occur at natural rates and often require more land and/or time to achieve a given treatment requirement. Conventional technologies typically incorporate augmentations such as mechanical agitation and forced aeration, such that treatment can be achieved in a smaller footprint but with higher energy consumption and operational costs (Crites and Tchobanoglous, 1998, IWA, 2000, Reed et al., 1995).

Natural wetland environments are often replicated to optimise treatment capability and the resulting manmade systems are referred to as Constructed Wetlands. The HSSF systems of Severn Trent are examples of Constructed Treatment Wetland systems. The two major subdivisions of TW technology are defined according to hydrology as Surface Flow and Subsurface Flow systems. Within each of these subdivisions exist further technology variations, as indicated in the classification system of Fonder and Headley (2011), (**Figure 2-1**). According to the classification system of Fonder and Headley (2011), the systems of Severn Trent are TW Type 4: horizontal subsurface flow systems with emergent non-woody vegetation.

Surface Flow Systems

Surface Flow TWs do not suffer operational problems related to clogging to the same extent as subsurface flow TWs, and this discussion will be limited to a brief description of Surface Flow TWs for the purpose of distinction. Surface Flow wetlands are also referred to as Free Water Surface Wetlands. This is because the water surface is above the level of the soil and the vast majority of the flow is overland, such that the water surface is always visible. Wetland surface waters are often shallow in comparison to lagoons or ponds, and this promotes soil-water interaction (IWA, 2000). High biological productivity produces large communities of macrophytes, which distinguish surface flow TWs from lagoon and pond systems (IWA, 2000, Vymazal and Kropfelova, 2008).

Subsurface Flow Systems

Subsurface Flow Treatment Wetlands differ from surface flow systems because water flows through a porous medium, such as sand or gravel, through which the wastewater is passed for purification (Cooper et al., 1996). Typically the water level is kept below the surface of the porous media so that the free water surface is not visible. The system can be designed so flow can occur either in the vertical (VF) or horizontal direction (HSSF). In VF systems the wastewater is usually dosed so that the subsurface goes through cycles of saturation and desaturation (Cooper et al., 1996), whereas generally, HSSF TWs are operated with constant saturation (Brix, 1987). The use of porous media makes subsurface flow systems similar to other filter-bed technologies, but they differ from trickling filters and sand filters due to the presence of macrophytes (Nuttall et al., 1997).

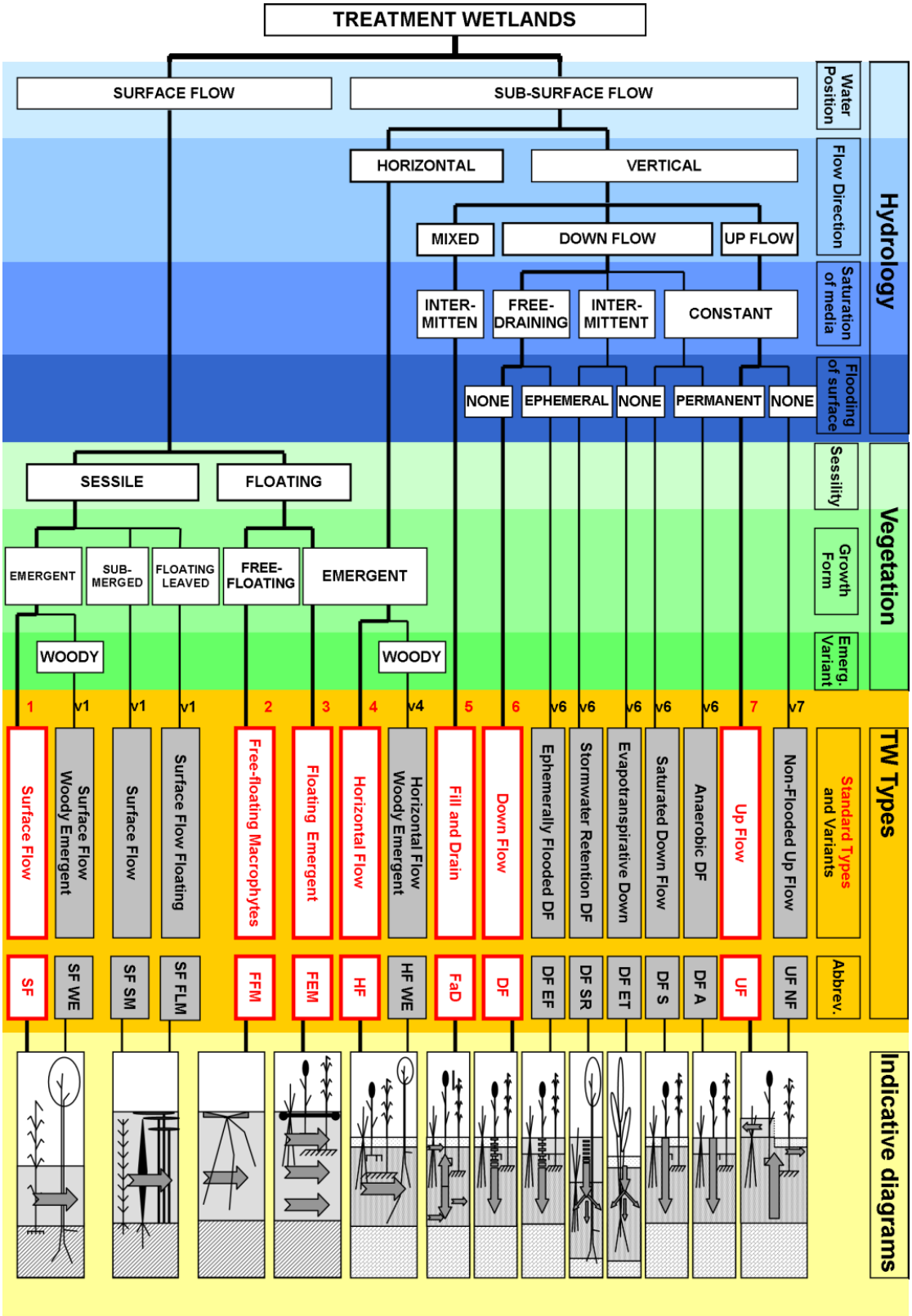

Figure 2-1 Treatment Wetland classification system showing the numerous design variants that have evolved over the last three decades. Reproduced from Fonder and Headley (2011).

Subsurface Flow systems can only accommodate emergent macrophytes, and in early wetland classification systems they were often listed as a subset of emergent systems (**Figure 2-2**) (Brix, 1993, Vymazal et al., 1998, Vymazal, 2003, Vymazal, 2001). The organisational structure of **Figure 2-2** is based around the significant role of plants in enabling treatment processes within Surface Flow TWs. However, the role of plants in Subsurface Flow TWs is mainly structural, i.e. supporting biomass (Wallace and Knight, 2006) and providing insulation in cold climates through accumulation of plant litter (Mander and Jenssen, 2003). Any treatment provided by plants is confined to the immediacy of the rhizosphere (Bezbaruah and Zhang, 2004, Brix, 1997) and is negligible in comparison to the treatment processes supported by the porous medium (Brix, 1994a). The necessity for subsurface flow TWs to include plants has been questioned, however, Wallace and Knight (2006) reason that public acceptance of wetland technologies is partly attributed to the aesthetic enhancement and biodiversity provided by plants.

Figure 2-2 Early classification system for Treatment Wetland technology that is based on the role of the plants. Reproduced from Vymazal (2003).

Subsurface systems offer greater scope for engineering, and the last decade has witnessed numerous adaptations for achieving advanced treatment performance, smaller system footprints or application for specialist wastewaters. Examples include HSSF systems augmented with forced-bed aeration (Wallace, 2001), and fill-and-drain VF systems which operate with successive upward and downward flow regime to achieve a series of redox potentials over a loading cycle (Behrends et al., 2001, Cooper and Cooper, 2005). It should

be noted that these intensifications require an increase in energy consumption and operational costs in comparison to natural systems

The subsurface technology boom, and realisation that hydrology is more significant to treatment than planting, is reflected in the revised TW classification tree presented in **Figure 2-1** (Fonder and Headley, 2011), which elucidates the variety of Subsurface Flow systems that have evolved.

2.1.3. Historical Development of Subsurface Flow Treatment Wetlands

All variants of Subsurface Flow TW are prone to clogging problems if operated incorrectly. However, numerous regional variations of Subsurface Flow TW have evolved and the manner in which they clog is directly related to the typical design and operation of the system. This design evolution will be introduced to allow the subsequent discussion on clogging in different systems to be better appreciated.

A German botanist named Kathe Seidel pioneered research on early VF and HSSF TW concepts during the 1950s. Seidel's research focus was the phytoremediation of wastewaters using aquatic plants for the removal of organic and inorganic pollutants from wastewater (Brix, 1994b). To appear more akin to conventional filter-type treatment technologies, planting was done in trays and ditches of high-hydraulic conductivity sand and gravels (Vymazal and Kropfelova, 2008). The initial concept had horizontal flow and was used as a secondary treatment stage for decentralised septic tank wastewater treatment systems (Börner et al., 1998). Seidel later realised that a modification of the technology which used vertical flow could achieve solids filtration and maintain aerobic conditions, thus providing a superior alternative to the septic tank. The vertical flow and horizontal flow stages were referred to as 'filtration' and 'elimination' stages respectively and Seidel arranged multiple cells in cascading networks to promote oxygenation between stages (Brix, 1994b).

Uptake of this technique, which became known as the Max Planck Institute Process or Krefeld System, was not immediate. According to Vymazal and Kropfelova (2008) early publications which focussed on nutrient removal (Seidel, 1966) were met with criticism that may have hindered adoption of Seidel's ideas. International dissemination of the concept was delayed until publication in English (Rousseau, 2005) in 1976 (Seidel, 1976).

Seidel collaborated with a German soil scientist called Roland Kickuth, in the hope that comparative tests against conventional soil based treatment systems would encourage acceptance of the technology. However, disagreement between the scientists led to the formation of two rival schools of thought, which further hampered the overall adoption of the technology by sewage engineers and authorities (Börner et al., 1998). Kickuth believed a single HSSF TW stage could replace the Krefeld System if a soil or clay medium was used as opposed to sand or gravel. The idea was that the high sorption capacity of the soil and root-zone aeration provided by the plants would provide sufficient treatment, and the plants would additionally maintain hydraulic conductivity through the soil via root network expansion (Kickuth and Konemann, 1988). The practicality of a single system rather than a network, and the publication of a simple design equation (Kickuth, 1977) made the Root Zone Method popular with engineers, local authorities and utility providers.

During the 1980s and 1990s the two techniques began to spread through Europe. Whether a country aligned with the Krefeld System or Root Zone Method depended on exposure, and has resulted in numerous regional technology variations and design guidelines (ATV, 1998, Brix and Arias, 2005, EC/EWPCA, 1990, García and Corzo, 2008, Iwema et al., 2005, ÖNORM-B-2505, 1997).

Examples of Krefeld Systems exist in the UK (Burka and Lawrence, 1990), Austria (Brix, 1994b) and North America (Lakshman, 1979, Wolverton, 1982) and the potential of hybrid systems for achieving treatment beyond the capabilities of the single stage Root Zone Method has caused a resurgence of the Krefeld System, especially in France (Lienard et al., 1990, Lienard et al., 1998, Molle et al., 2005) where it is the TW methodology advised by national guidelines (Iwema et al., 2005). A VF system analogous to the 1st stage of the Krefeld System has become the preferred choice for decentralised secondary wastewater treatment in European countries such as Denmark (Brix and Arias, 2005), Austria (ÖNORM-B-2505, 1997) and Germany (ATV, 1998).

Early experience with the Root Zone Method in Germany, Denmark, Austria and the UK indicated that initial methodological claims did not translate well to field experience (Brix, 1994b) and the following conclusions were drawn:

- The role of plants for aeration is secondary and HSSF environments are predominantly anoxic or anaerobic (Brix and Schierup, 1990).

- The hydraulic conductivity of the soil filter did not improve due to root network expansion, and numerous reports of clogging and overland flow were reported (Brix and Schierup, 1989, Coombes, 1990, Haberl and Perfler, 1990, Netter and Bischofsberger, 1990, Pauly, 1990).

European design guidelines were published in 1990 (EC/EWPCA, 1990) to reflect these findings and encourage designs that reduced the occurrence of overland flow. The two major changes were: a) modifications to the aspect ratio suggested by the Root Zone Method, which transformed the typical design from having greater length than width to having greater width than length (Brix and Schierup, 1989); and b) the use of coarse media such as sand or gravel, which are less prone to clogging than soil (Cooper et al., 1996). These guidelines made the technology more akin to the original systems of Seidel and the term Root Zone Method was superseded by the colloquialism 'reed beds'. However, the Kickuth equation is still widely used for sizing the beds and the dissemination of HSSF TW technology is often attributed to Kickuth.

A similar HSSF TW concept was developed in the US during the early 1970s (Fetter et al., 1976, Spangler et al., 1976) and 1980s (Gersberg et al., 1983, Gersberg et al., 1984), although pilot systems incorporated much larger media sizes than the systems of Seidel and Kickuth, and flow occurred simultaneously over the surface and through the subsurface (Wallace and Knight, 2006). Development of these systems, which were colloquially referred to as 'rock-reed-filters' or 'vegetated submerged beds', culminated in the publication of design guidelines by the US Environmental Protection Agency (USEPA, 1993), which differed to those outlined by European specifications (Wallace and Knight, 2006).

In an attempt to standardise reporting in the literature, it has been suggested that the terminologies Horizontal Subsurface Flow Treatment Wetland and Vertical Flow Treatment Wetland fully replace all colloquialisms such as 'reed beds' or 'Krefeld filtration stage' (Fonder and Headley, 2011). However, standardised nomenclature conceals the specific variations in design and operation that result in different clogging modes in different systems.

2.2. Factors Attributing to Clogging

This section addresses the various physical, chemical and biological factors that are responsible for clogging. Clogging occurs due to the accumulation of materials associated with treatment (e.g., intentional or external loads) and other operational factors (e.g., incidental or internal loads) that reduce the free volume available for flow through porous media. The quantity and composition of accumulated material, often referred to as *biosolids* (Kadlec and Wallace, 2010) but hereafter referred to as *clog matter* (because it does not have to contain biological constituents), will vary depending on internal and external loads. Clog matter typically consists of highly hydrated gels and sludge (often more than 70 % water by volume) that are formed of inorganic and organic solids (IWA, 2000). Clog matter often has a lower density than its constituents such that it can effectively reduce pore space in the granular medium (Baveye et al., 1998). The typical components of clog matter are categorised in **Table 2-1**, which includes biofilm, plant detritus, chemical precipitates, and wastewater solids.

Table 2-1 Non-hydrous components of clog matter categorised into intentional accumulations (part of the wastewater treatment process), or incidental accumulations (a result of the wastewater treatment process). Incidental accumulations include accidental operations, which are italicised. Reproduced from Knowles et al. (2011).

Component	**Intentional accumulation (external loads)**	**Incidental accumulation (internal loads)**
Organic solids	• Wastewater solids	• Biomass growth • Plant roots • Biofilm and plant detritus • *Solids introduced during construction*
Inorganic solids	• Wastewater solids • Chemical precipitates	• Solids from chemical erosion of gravel • *Solids introduced during construction*

Figure 2-3 depicts some of the clog matter components listed in **Table 2-1** and how they accumulate within the TW at the macroscopic system-scale and at the microscopic pore-scale. The net accumulation rate of clog matter is a balance between intentional (application of wastewater) and incidental accumulations (such as biofilm and plant matter), and loss due to export and decomposition (Tanner et al., 1998). At the pore scale clog

matter will accumulate in pore spaces with varying morphology, such as coatings on the surface of the media or dendrite formations. Clog matter accumulations may be formed of a single phase (i.e. biofilm on media surfaces) or a complex of phases, such as biofilm forming around entrapped wastewater solids. Accumulations that occur within pore spaces reduce subsurface hydraulic conductivity and accumulations that occur on the bed surface reduce surface infiltration rates. The combination of surface and subsurface clogging will determine whether or not hydraulic issues occur at the macroscopic scale.

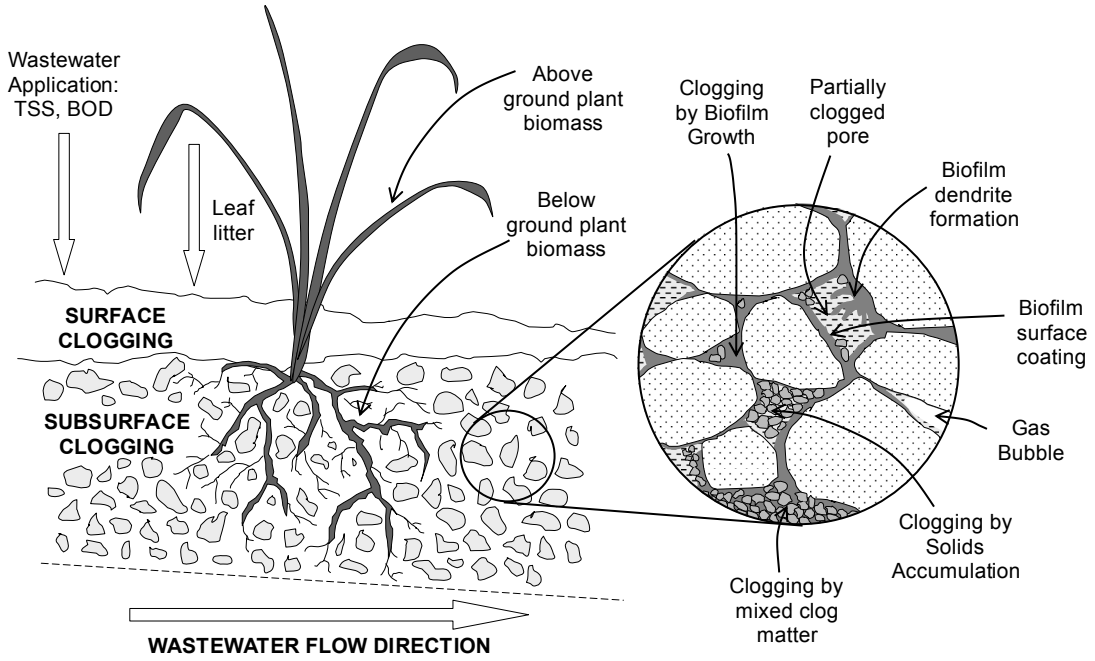

Figure 2-3 Clogging processes that occur at the surface and in the subsurface of Horizontal Subsurface Flow Treatment Wetlands. The diagram may not be applicable to other varieties of Subsurface Flow Treatment Wetland. The inset gives detail of clogging processes at the pore level. Adapted from Kadlec and Knight (1996).

The subsequent parts of this section discuss the factors that are responsible for clogging in greater detail. The discussion will consider filtration of particulate matter and additional solids contributions from microorganisms (biofilms), vegetal growth and chemical precipitation. The composition and biodegradability of typical clog matter accumulations is also discussed.

2.2.1. Solids Entrapment

Suspended solids are filtered and retained by subsurface flow treatment wetlands via the mechanisms of transport and attachment (Yao et al., 1971). These mechanisms are the same as those responsible for flocculation, whereby transport mechanisms create collisions between particles, and attachment mechanisms cause these particles to adhere upon impact (Swift and Friedlander, 1964).

Wastewater contains solids with a variety of sizes and compositions. A variety of physico-chemical mechanisms are responsible for TSS reduction, depending on the size of the particle, as explained in **Table 2-2** and depicted in **Figure 2-4**. The balance of the forces listed in **Table 2-2** leads to a range of removal efficiencies for different particle sizes. Kadlec and Wallace (2010) explain that sedimentation of large particles is the major mechanism of solids removal in HSSF TWs, which predominantly takes place in the first few meters of the wetland. It has frequently been observed that the nadir in removal efficiency occurs for particles that are approximately 1 – 2 μm in diameter, because they are too small to be removed by inertial and other physical effects, but too large to be affected by electrostatic and Brownian forces (Yao et al., 1971, Logan et al., 1995, Zamani and Maini, 2009). A large number of wastewater particles fall into this size range (Levine et al., 1991, Tchobanoglous, 1993) and Puigagut et al. (2008) observed that particles in the 0.7 – 2 μm range were the most abundant in the influent and effluent of a HSSF TW in Spain.

As particles accumulate within the media, the efficacy of subsequent removal is often enhanced due to the reduction in pore space. For example, particles that are electrostatically attracted to each other are capable of stacking and form dendrites that protrude into the pore space and increase the likelihood of particle interception (Hubbe et al., 2009).

Particle retention on media surfaces is due to the electro-chemical effect of adsorption (summation of electrical double-layer interactions and the dipole interactions known as van der Waals' forces). The strength of attachment depends on the relative charge of particles, media surfaces and bulk fluid (Hermansson, 1999). Detachment of particles can occur for several reasons. A change in the ionic strength of the wastewater may neutralise or overcome the attractive force between particles and surfaces, such that they are released back into solution (an effect known as peptisation). Hydrodynamic shear forces can lead to sloughing of particles, especially if interstitial velocities increase as a consequence of pore

constriction (Zamani and Maini, 2009). However, this effect is generally confined to closed pressurised reactors, and in gravitational flow systems such as Subsurface TWs flow will find an alternative path (such as overland) once faced with hydraulic resistance (Maloszewski et al., 2006).

Table 2-2 The physico-chemical mechanisms responsible for solids removal in Subsurface Flow TWs. The emboldened numbers in brackets refer to the removal mechanisms illustrated in **Figure 2-4**. Reproduced from Knowles et al. (2011).

Large Particle Filtration Mechanisms	
Sedimentation and bouyancy	According to Stoke's Law, particles with a different density to wastewater will move vertically across the flow-field under the effect of gravity, until they impact a surface **(2).**
Hydrodynamic effects	Non-uniform hydrodynamic forces across the body of a particle will cause it to drift across the flow-field **(1).**
Inertial divergence	Particles with significant inertia may deviate from streamlines and impact a surface as flow diverges around obstacles **(3).**
Interception	If the streamline conveying a particle is closer than the radius of the particle interception of the media surface will occur **(4)**. The chance of interception increases as pore diameters are reduced by prior accumulation **(13).**
Straining and trapping	Particles that are larger than pore spaces will be strained **(7)**. Particles may be trapped by media morphological irregularities **(9)**. Filamentous/fibrous particles are particularly susceptible to these modes of removal **(8)**. Filamentous biofim growth enhances the likelihood of straining by reducing the diameter of flowpaths **(12)**.

Small Particle Filtration Mechanisms	
Brownian motion	Colloidal particles are influenced by the thermal forces responsible for Brownian motion, which induce random trajectory through the flow field **(5)**.
Electrostatic forces	Repulsive or attractive forces between particles in suspension, and other particles or media surfaces will influence particle trajectory and cause particles to adhere to media surfaces **(6)**. Monolayer accumulations will occur **(14)** if attraction to media surfaces is greater than repulsion between particles. Dendrite accumulations can occur if particles are attracted to other particles and media surfaces **(11)**.
Bridging	Small particles can be removed within relatively large pores if numerous particles arrive simultaneously and block the pore by bridging **(10).**
Coagulation	The coagulation of smaller colloids into larger particles promotes their removal through the previously outlined mechanisms **(15)**.

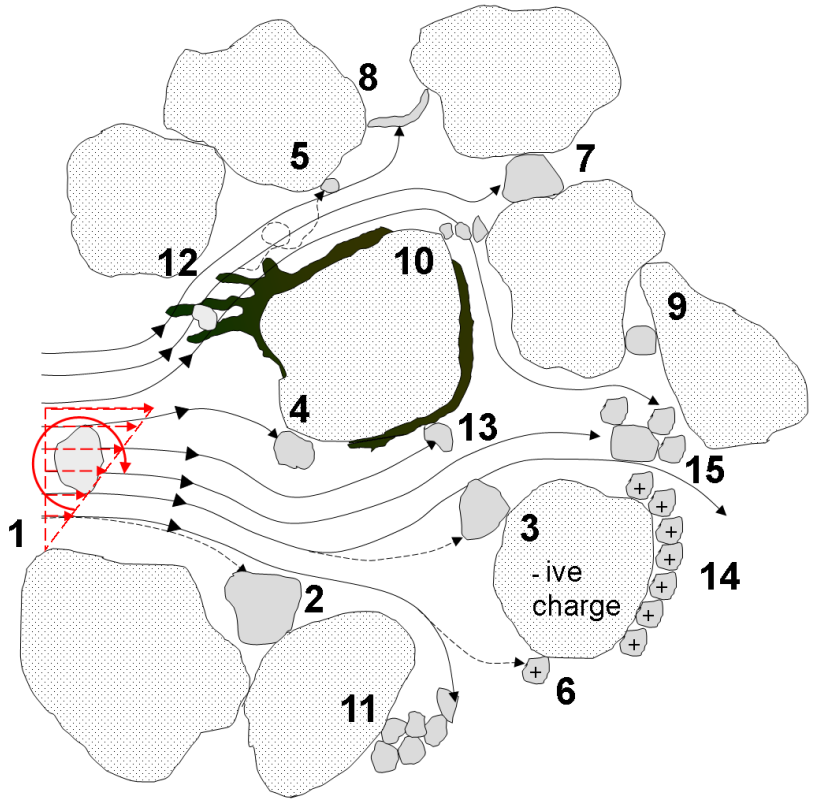

1. Hydrodynamic forces
2. Sedimentation
3. Inertial impaction
4. Interception
5. Brownian motion
6. Electrostatic forces
7. Diameter straining
8. Fibre straining
9. Trapping
10. Bridging
11. Electrostatic dendrite formation
12. Straining by filamentous biofilms
13. Interception by surface biofilms
14. Electrostatic monolayer accumulation
15. Particle coagulation

Figure 2-4 Particle removal processes in a porous medium, such as gravel in HSSF TWs. Based on information from Hubbe *et al.* (2009), Thullner (2009) and Zamani and Maini (2009). The numbered removal mechanisms illustrated above are described in **Table 2-2**.

2.2.2. Biofilm Clogging

Transport and attachment of microbes through porous media can be described using the same set of principles as outlined for solids (Hermansson, 1999, Tufenkji, 2007). Once microbes have colonised media surfaces, further biomass can proliferate. Resultantly, in Subsurface Flow TWs most biomass forms as biofilms on the surfaces of the medium, with very little matter suspended in the wastewater (Khatiwada and Polprasert, 1999). Several studies conclude that greater biofilm development occurs at the inlet region where the concentration of organic matter in the wastewater is greatest (Ragusa et al., 2004, Tietz et

al., 2007). García et al. (2007) performed dynamic simulations of an experimental HSSF TW and predicted that the concentration of Heterotrophs would be 45% greater at the inlet than at the outlet. Caselles-Osorio and García (2006) observed that the inlet hydraulic conductivity in an experimental HSSF TW fed with soluble carbon was reduced to 64 % of outlet hydraulic conductivity; an effect they attributed to biofilm establishment at the inlet.

Biomass morphology, density and hydraulic conductivity will vary between accumulations depending on composition and microbial community. (Thullner, 2010). The majority of biofilms secrete extracellular polymeric slime (mainly for enzymatic and structural purposes) (Madigan et al., 2006) that are highly hydrated (typically 99% water) (Rittmann and McCarty, 1980, Tanner and Sukias, 1995). deBeer and Stoodley (1995) expound that these slimes are analogous to gel networks with pore diameters on the nanometric scale, thus making them relatively impermeable (Taylor et al., 1990, Vandevivere and Baveye, 1992c) and proficient at forming associations with other inorganic and organic materials (Baveye et al., 1998, Thullner, 2010). Some biofilms develop as filamentous colonies or aggregates (Vandevivere and Baveye, 1992a, Vandevivere and Baveye, 1992b, Vandevivere and Baveye, 1992c, Dupin and McCarty, 1999, Dupin et al., 2001) that form webs across pore spaces and trap particulate matter more proficiently than uniform biofilm coatings (Mays and Hunt, 2005). If biofilms on separate gravel particles bridge, then pore plugging will occur and the hydraulic conductivity of the bulk porous media will tend towards the hydraulic conductivity of the biofilm (Wallace and Knight, 2006).

2.2.3. Vegetal Contributions

The role of plants in Subsurface Flow TW clogging is an evolving debate. One of the original assumptions of the Root Zone Method was that root growth would counteract media clogging (Kickuth and Konemann, 1988), and the tubular structure of the roots would provide a macro-porous network for flow. However, there is very little data in the literature to support this claim. Fisher (1990) observed that root expansion in an Australian field-scale HSSF TW increased the depth of the reactor at the inlet zone by 60 mm over three years, which would serve to counteract clogging. However, early experience with soil-based HSSF TWs in Northern Europe proved that root growth did not prevent hydraulic malfunctions such as overland flow (Netter and Bischofsberger, 1990, Pauly, 1990, Brix, 1994b). According to IWA (2000), subsurface roots and rhizomes below a dense macrophyte stand

will have a dry weight of 500 – 5,000 g per m^2 of footprint. This root mass provides additional surface area for accumulation and occludes one quarter to one third of pore volume in the root-zone. The root mat of *Phragmites australis* has been reported to have hydraulic conductivity on the order of 1 – 20 m/d (Baird et al., 2004), which is approximately two orders of magnitude smaller than the hydraulic conductivity of clean gravels typically used in Subsurface Flow TWs (USEPA, 2000).

Plant detritus (dead matter) decomposition and accumulation rates will vary geographically and will provide a net contribution to clog matter over time if the accumulation rate of detritus exceeds decomposition rates (Kirschner et al., 2001, Asaeda et al., 2002, Rybczyk et al., 2002, Chimney and Pietro, 2006). Kadlec and Wallace (2010) state that typically 5 – 15% of plant detritus is recalcitrant. Root detritus contributes to subsurface clogging and leaf litter-fall contributes to surface clogging. Kadlec and Watson (1993) measured an average leaf-litter accumulation of 2,410 g of dry matter per m^2 of footprint after three years of operation in a HSSF TW in Kentucky (US). Above ground, up to half of the standing plant biomass (stems) may be dead, but remain relatively stable due to esters in the plant tissue that resist degradation (Tanner et al., 1998).

Tanner et al. (1998) illustrated the potential for clogging by plant detritus whilst studying dairy wastewater treatment HSSF TWs in New Zealand. Organic matter accumulation rates of 1,300 to 3,000 g /m^2·yr were recorded but only 400 to 1,600 g /m^2·yr could be directly attributed to wastewater loading, and only 4% of pore blockage was due to live root penetration (Tanner, 1994). Moreover, during the same study Tanner and Sukias (1995) compared organic matter accumulation rates in equivalent planted and unplanted beds and found that accumulation rates were 1,200 – 2,000 g /m^2·yr higher in the planted systems. Accumulations of humic substances were two to eight times higher in the top 100 mm of gravel than they were at lower gravel depths, and only 50% greater in the inlet region than at the outlet. Therefore, the authors concluded that the humic contributions from plants, rather than accumulation of wastewater organic matter, controlled clogging.

In addition to Tanner and Sukias (1995), several other authors have reported that more plant matter accumulates near the surface of the TW than towards the base of the TW (USEPA, 1993, Reed et al., 1993). For example, Parr (1990) surveyed 12 gravel bed HSSF TWs in the UK and found that 70 – 100% of root growth occurred in the top 20 cm of the media. It is believed that the higher hydraulic resistance in the vegetated upper gravel layer causes flow to short-circuit along the less resistive bottom layer and numerous researchers have

performed internal hydrodynamic visualizations using water tracers that report similar observations of preferential flow along the bottom of the bed (Spangler et al., 1976, Gersberg et al., 1984, Bowmer, 1987, Fisher, 1990, Waters et al., 1993, Breen and Chick, 1995, García et al., 2003, Knowles et al., 2010).

Several authors have reported that certain plant functions can mitigate the effects of clogging. For example, when studying planted and unplanted HSSF TW mesocosms in Canada, Chazarenc et al. (2007) found that planted systems had consistently longer hydraulic residence times than unplanted systems. The authors suggested that water retention in the leaf litter layer and plant evapotranspiration counteracted any discernible loss of hydraulic residence time associated with clogging. Other authors suggest that, by creating macro-pores through clog matter accumulations on the surface of the bed, the wind-induced sway of emergent shoots and stems maintains infiltration rates through to the subsurface (Brix, 1994a, Molle et al., 2006).

2.2.4. Chemical Effects

Chemical treatment processes, such as adsorption and precipitation, can also contribute to clogging. Physico-chemical adsorption is associated with the removal of metals, petroleum, and synthetic hydrocarbons, ammonia-nitrogen, and phosphorous (Wallace and Knight, 2006). For instance, it is common practice for HSSF TWs in Norway to incorporate lightweight expanded clay aggregates with high sorption capacity, for the purposes of phosphorous removal (Zhu et al., 1997). However, adsorbate films do not generally become thick enough to create clogging problems because adsorption is limited by the sorption capacity of the media.

Chemical precipitation of metal hydroxides and sulphides (Sheoran and Sheoran, 2006), calcium carbonate (Fleming et al., 1999) and elemental sulphur (Kadlec and Wallace, 2010) are more likely to cause clogging problems as these precipitants accumulate as film-like coatings on media surfaces. Kadlec and Wallace (2010) summarise that precipitation of these compounds is encouraged through biological interactions, and systems that treat industrial wastewaters may clog rapidly if both the rate of biological activity and concentration of these compounds is high. Such a phenomenon was described by Nivala et al. (2007), who observed severe iron fouling of the gravel in an aerated HSSF TW for the treatment of landfill leachate. Nivala et al. (2007) attributed this to ferric hydroxide

precipitation under highly oxidizing conditions, which adsorbed to media surfaces and became associated with interstitial biological matter such that porosity was heavily reduced and media particles became welded together.

2.2.5. Clog Matter Composition

The biodegradability of accumulated clog matter dictates its impact on clogging. Initially it was assumed that organic matter would decompose sufficiently such that only inorganic solids would contribute to Subsurface Flow TW clogging. Based on an influent inorganic solids loading of 8 kg/m^3 over 18 months, USEPA (1993) predicted that only 1% of interstitial volume would be lost from a HSSF TW. Similar calculations based on the assumption of clogging solely by inorganic matter were responsible for early over-estimations regarding system longevity (Conley et al., 1991, Bavor and Schulz, 1993, Blazejewski and Murat-Blazejewska, 1997). However, the literature confirms that clogging is caused by accumulation of both organic and inorganic matter.

Regarding predominantly organic clog matter; Tanner et al. (1998) state that 80% of accumulations in a dairy wastewater HSSF TW were volatile, although subsequent investigation found that 63 – 96% of these organic matter fractions were relatively refractory (Nguyen, 2000, Nguyen, 2001). Accumulations were predominantly composed of refractory humic, humin and fulvic acids, derived from lignocellulosic and humic compounds in the dairy wastewater and plant detritus. Nguyen (2000) discussed that variable decomposition rates leads to a mixture of macro-morphological plant residues and morphologically unstructured humic compounds with a range of molecular weights and packing densities. Furthermore, humic compounds are highly colloidal and amorphous with great hydrophilic potential and physical binding properties (Christensen et al., 1998, Nguyen, 2000). For example, Tanner and Sukias (1995) point out that clog matter accumulations in this HSSF TW were approximately 80 % water by volume. These properties give humic organic matter great potential to block pores.

Regarding predominantly inorganic clog matter accumulations; Platzer and Mauch (1997) reported that less than 3% of the deposits in a soil-based VF TW in Merzdorf, Germany were organic. Kadlec and Watson (1993) described that over 80 % of the clog matter accumulated in a HSSF TW that polishes lagoon effluent was inorganic in composition, explaining that biological matter was being satisfactorily degraded. Similarly, Caselles-Osorio et al. (2007),

Llorens et al. (2009) and Pedescoll et al. (2009) also reported clog matter accumulations with inorganic content greater than 75 % in six secondary treatment HSSF TWs in Catalonia, Spain. From the information presented in Llorens et al. (2009) and Kadlec and Watson (1993) it is possible to calculate that the porosity loss attributable to accumulation of inorganic solids in each of these studies is very small, and in agreement with earlier calculations mentioned above (1 % – 3 % pore occlusion based on an inorganic solids density of 2,650 kg/m^3). However, association with small quantities of present biological material can form low-density gelatinous sludge with very high water retention capacity (Kadlec and Watson, 1993, Tanner et al., 1998, IWA, 2000). The composite clog matter in the studies of Llorens et al. (2009) and Kadlec and Watson (1993) had resulting densities between 33 kg/m^3 and 371 kg/m^3 which increased effective pore occlusion to between 27 % and 77 %. In the case of Kadlec and Watson (1993) the authors postulate that this occurred due to silica algae combining with calcium and aluminium at low redox values. In the case of Llorens et al. (2009), the sludge density in the inlet region was on average four times lower than that at the outlet region (60 kg/m^3 versus 240 kg/m^3) but was doubly effective at reducing porosity (66 % occlusion versus 28 %). This corresponded to lower values of hydraulic conductivity at the front end of the bed in comparison to the back end of the bed (20 m/d versus 45 m/d) (Pedescoll et al., 2009).

2.3. Design and Operational Influences

The distribution of clogging through the system and the speed with which it develops depends on numerous design and operational factors, such as the wastewater loading rate and pollutant characteristics, the physical properties of the porous media, inlet arrangement and system dimensions, and whether the system is operated with periods of resting. This section elaborates on the influence of these parameters.

2.3.1. Wastewater characteristics

Knowledge of wastewater characteristics, such as flow rates, solids content and pollutant characteristics, are vital for understanding clogging processes in Subsurface Flow TWs. Regarding the influence of hydraulic loading rate; hydraulic overloading may lead to periods of overland flow in both HSSF TWs and VF TWs. Overland flow reduces the transfer of

atmospheric oxygen to microorganisms responsible for degrading accumulated organic matter, and increases the likelihood that surface layer accumulation rates will exceed mineralization rates (Platzer and Mauch, 1997, Langergraber et al., 2003, Zhao et al., 2004). For example, Molle et al. (2006) established that French VF treatment wetlands will work reliably as long as they are not consistently hydraulically overloaded. Systems that had been consistently overloaded were found to have poorly mineralised surface sludge deposits with infiltration rates as low as 2.5 m/d, thus providing a bottleneck to flow.

Regarding pollutant characteristics; both the physical form and biodegradability of wastewater constituents will effect clogging. Low TSS does not necessarily preclude clogging, as demonstrated by Caselles-Osorio and García (2006) who performed side-by-side tests on experimental HSSF TWs system fed with different forms of organic matter (glucose vs. starch). Their results suggest that the system fed with dissolved glucose had lower inlet hydraulic conductivities than a system fed with particulate starch, leading them to conclude that glucose stimulated greater biofilm clogging due to its readily-biodegradable nature.

Generally speaking, most authors report a positive correlation between system clogging and both TSS and COD (Chemical Oxygen Demand) loading rates (Tanner and Sukias, 1995). Winter and Goetz (2003) found that loading rates of TSS and COD correlated positively with severity of clogging in a survey of 21 VF TWs in Germany. Clogging problems were not apparent in systems that received less than 20 $g/m^2 \cdot d$ COD and 5 $g/m^2 \cdot d$ TSS. Caselles-Osorio et al. (2007) compared the COD loading rate versus solids accumulation rates for six HSSF TWs in Catalonia, Spain (Caselles-Osorio et al., 2007), versus a VF TW in France (Chazarenc and Merlin, 2005). Over two years, the secondary HSSF TW systems in Catalonia received average influent COD loading rates of 12 $g/m^2 \cdot d$ respectively with a resulting average solids accumulation rate of 11 $kg/m^2 \cdot yr$. The primary VF TW of Chazarenc and Merlin (2005) received a larger COD loading rate (67 $g/m^2 \cdot d$ on average) which resulted in a higher solids accumulation rate (51 $kg/m^2 \cdot yr$ on average). Despite this, the French systems reportedly operated without clogging whereas evidence of surface ponding existed in several of the Catalonian HSSF TWs. This is attributed to a lower hydraulic loading rate in the French VF TW than in the Catalonian HSSF TW (see **Section 2.5**).

2.3.2. Intermittent Operation

Intermittent operation involves discharging of wastewater in a manner such that subsurface aeration will occur, which restores aerobic conditions and accelerates clog matter mineralization. This principle is fundamental to the operation of VF TWs. The periodicity of loading to resting will determine the ability of the system to operate without clogging (Cooper, 2004). The required recovery period for a particular cell will depend on climatic conditions. Systems in cold and wet climates will require a longer recovery period than those in hot and arid climates. Resting periods on the order of days to weeks are suggested for VF TWs in Northern Europe (Platzer and Mauch, 1997, Langergraber et al., 2003, Green et al., 2006), with different cells rested in rotation so that plant operation will not be interrupted.

Variants of VF TWs such as fill-and-drain wetlands (Zoeller and Byers, 1999, Lahav et al., 2001), tidal flow wetlands (Zhao et al., 2004, Austin, 2005) and reciprocating wetlands (Behrends et al., 2001) incorporate operating strategies that promote increased subsurface oxygen availability, such as water level fluctuation, intermittent dosing, and alternate operation. Additionally, these systems operate without the typical application of wastewater over the surface of the bed, which in principle reduces the tendency of the system to clog on the surface. Zhao et al. (2004) showed that clogging of a tidal flow wetland could be mitigated by arranging gravel fractions with increasing diameter from top to bottom, so that accumulated solids were better distributed throughout the reactor depth. However, studies indicate that these systems may still clog in the upper surface despite their operation mode (Cooper and Cooper, 2005, Sun et al., 2007).

Studies also suggest that intermittent operation may be beneficial for reversing clogging in HSSF TWs (Nguyen, 2000, Corzo et al., 2008). Batchelor and Loots (1997) rested a field-scale HSSF TW to allow for surface sludge layer mineralization, and successfully restored infiltration to the subsurface.

2.3.3. Media Characteristics

To maintain subsurface flow through porous media it is advisable to utilise media with high hydraulic conductivity (Cooper et al., 1996). Large diameter media has a higher hydraulic conductivity than small diameter media, as explained in **Section 3.2**. Despite this, smaller

media, such as soil and sands, were originally used (Brix and Schierup, 1989, Coombes, 1990, Haberl and Perfler, 1990, Netter and Bischofsberger, 1990) as they were believed to offer superior treatment performance to larger media. Indeed, the smaller the particle size, the higher specific surface area available for biofilm establishment, and surface chemistry; and the greater the likelihood of suspended solids interception due to narrower pore diameters. However, this makes fine media prone to rapid clogging by filtration and the bridging of biofilm on adjacent media particles (Blazejewski and Murat-Blazejewska, 1997, Platzer and Mauch, 1997, Langergraber et al., 2003, Wallace and Knight, 2006).

Subsequent work by Griffin et al. (2008) on the performance of 25 Severn Trent HSSF TWs showed that larger media with median diameters between 6 mm and 11 mm did not impair the ability of the system to achieve treatment requirements. All medium sizes achieved effluent BOD levels below 5 mg/L and the 11 mm medium theoretically has a clean hydraulic conductivity over three times greater than the 6 mm medium. Resultantly, the desire to maximise asset longevity has led to a gradual increase in the media sizes employed in HSSF TWs, towards coarser media such as gravels (Cooper et al., 1996, USEPA, 2000, Iwema et al., 2005, ÖNORM-B-2505, 1997, García and Corzo, 2008). This evolution is reflected in **Table 2-3** which summarises recommended media specifications from different countries that have been published since 1988.

Table 2-3 Examples of media size distributions recommended by various national and international design guidelines and publications. Based on information presented in Wallace and Knight (2006) and Kadlec and Wallace (2010).

Country	Gravel size distribution	Source
Austria	0-4 mm (gray water) 1-4 mm (tertiary treatment) 4-8 mm (primary treatment)	ÖNORM-B-2505 (1997)
Czech Republic	d < 20 mm	Vymazal (1996)
Germany	0.2-1.0 mm (sand)	ATV (1998)
United Kingdom	10-12 mm	Griffin et al. (2008)
United States	1-8 mm 3-6 mm 12-25 mm 2-28 mm 20-30 mm d >4 mm	USEPA (1988) TVA (1993) USEPA (1993) Reed et al. (1995) USEPA (2000) Wallace and Knight (2006)
European Design Guidelines	3-6 mm 6-12 mm	EC/EWPCA (1990)
International Water Association	8-16 mm	IWA (2000)

Particle size distribution and particle shape also influence media hydraulic conductivity. An extreme example of this is when the medium contains a large quantity of fines. Excessive fines will reduce pore space and promote clogging (USEPA, 1993, Tanner and Sukias, 1995). Media that is relatively non-spherical or angular will exacerbate clogging as it reduces porosity and increases the specific surface area available for biofilm growth (Kadlec and Knight, 1996, Hyánková et al., 2006).

The significant benefit to asset lifetime offered by controlling media specification was emphasised by Griffin et al. (2008), who announced that Severn Trent HSSF TWs built after 2008 would only incorporate washed round gravels with particle diameters between 10 mm and 12 mm.

2.3.4. Upstream Treatment Processes

Accidental spill-over of solids and sludge from upstream treatment processes, such as septic tanks and rotating biological contactors, creates shock loads of solids to downstream Subsurface Flow TWs (Cooper et al., 2005, Caselles-Osorio et al., 2007). Good design and maintenance of upstream processes can mitigate the likelihood of this occurrence; however, it is recommended that effluent filters or clarifiers are used between the upstream process and the Subsurface Flow TW to reduce solids carry-over (Tchobanoglous, 2003).

Alternative pre-treatment technologies are under investigation for use in conjunction with Subsurface Flow TWs, with the aim of maximizing system lifetime by minimizing solids loading. Caselles-Osorio and García (2007) estimate that when compared with primary-settled effluent (e.g., septic tank effluent), physicochemical pre-treatment could extend the life of a HSSF TW by approximately ten years. They note, however, that the operations and maintenance cost of coagulant, energy usage and sludge handling will prevent this option from being suitable in every situation. Other possible pre-treatments include Up-flow Anaerobic Sludge Blanket reactors, (Green et al., 2006, Barros et al., 2008, Dornelas et al., 2009) Hydrolytic Up-flow Sludge Bed reactors (Álvarez et al., 2008, Corzo et al., 2008) and Surface Flow TWs with planted rafts (Gray, 2008). All of the aforementioned technologies are reported to produce a primary effluent relatively low in COD and TSS in comparison to septic tank effluent; however, technologies such as UASB are best suited to warm climates.

Gray (2008) performed pilot experiments to establish the effective operating cost associated with refurbishing a clogged HSSF TWs when compared to sludge extraction as routine maintenance for Surface Flow TWs with planted rafts. The author found that refurbishing a clogged HSSF TWs imposed an expense equivalent to 0.06 £/m^3 of treated wastewater; whereas extracting sludge from Surface Flow TWs with planted rafts imposed an expense of less than 0.0001 £/m^3 of treated wastewater. Gray (2008) concluded that Surface Flow TWs with planted rafts could be a cost-effective means of pre-treatment for existing Severn Trent HSSF TWs.

2.3.5. System Aspect Ratio and Inlet Distribution

As explained in **Section 2.2**, the factors responsible for clogging lead to preferential clogging at the inlet where the wastewater is most concentrated. The extent of preferential clogging can be mitigated by uniformly loading wastewater over the greatest possible area and is, therefore, controlled by the system dimensions and the influent distribution arrangement. Early HSSF TW designs had aspect ratios with greater lengths than widths, which resulted in good width distribution but high cross-sectional wastewater loading rates at the inlet (Watson et al., 1990). Resulting experience of extensive clogging and overland flow in the inlet region of these systems (Netter and Bischofsberger, 1990) prompted the Danish to modify the aspect ratio, so that the width exceeded the length (Brix and Schierup, 1989). Wider systems reportedly suffered less overland flow issues and became recommended by most HSSF TW design guidelines (EC/EWPCA, 1990).

Regarding influent distributor design; the operation of typical VF TWs necessitates distributors that are located on or near the surface of the bed so that vertical percolation through the media will occur. Uniform loading over the bed surface is achieved using a network of perforated pipes that cover the majority of the surface, or by using concrete splash pads (ATV, 1998, Brix and Arias, 2005, Molle et al., 2005, ÖNORM-B-2505, 1997).

In HSSF TWs, whether clogging initially develops on the surface or within the subsurface corresponds to whether a surface or subsurface-based influent distributor is used. Experience in the UK has shown that poorly designed, incorrectly installed or ill-maintained inlet distributors will encourage uneven flow distribution (Rousseau et al., 2005b, Griffin et al., 2008) and uneven clogging of the bed media (Knowles et al., 2010). Early inlet distributor designs in Severn Trent HSSF TWs exacerbated this situation, as they were

generally comprised of discrete point sources distributed at multiple points along the width of the bed, such that flow was not loaded uniformly across the width of the bed (Murphy and Cooper, 2010). Cooper et al. (2008) found inlet distribution problems that required intervention at 34 from a survey of 255 HSSF TWs operated by Severn Trent. The design of surface based distributors for these TWs has evolved to achieve better width distribution, for instance by using troughs that span the width of the bed (Murphy and Cooper, 2010). Troughs are still susceptible to solids accumulation but are preferred by operators because of their ease of maintenance (Griffin et al., 2008).

Some early US HSSF TWs also utilised surface distributors with multiple adjustable outlet ports (Steiner and Freeman Jr., 1989, Watson and Hobson, 1989), however, the design of these systems eventually shifted towards the use of subsurface manifolds (TVA, 1993). Initial subsurface distributors for HSSF TWs comprised a pipe distributor located a few centimetres below the gravel surface. Designs of this type are still prevalent in mainland Europe (Vymazal et al., 1998, Vymazal and Kropfelova, 2008), but they have been superseded in the US by subsurface infiltration chambers perpendicular to the flow direction (Campbell and Ogden, 1999, Wallace and Knight, 2006), due to the opinion that simple pipe distributors resulted in clogging in the vicinity of the pipe. The use of subsurface infiltration chambers is intended to maximise the cross-sectional area over which wastewater solids are loaded. To further minimise cross-sectional loading rates, some US authors have utilised extended influent distributors that load wastewater along the width of the bed, but also include distribution manifolds that protrude longitudinally into the bed (Muñoz et al., 2006, Wallace and Knight, 2006).

Another method for achieving uniform width distribution has been to incorporate an open trench at the inlet that precedes subsurface flow. This also serves as a pre-treatment for solids settling, thus reducing accumulation within the subsurface (USEPA, 1993, King et al., 1997, Murphy and Cooper, 2010).

2.4. Clogging in Severn Trent Water HSSF TWs

Using the previous discussion it is possible to put into context the development of clogging in Severn Trent HSSF TWs. The typical design of these systems was outlined in **Section 1.3**. As described in **Section 1.4**, clogging in these systems is characterised by accumulation of clog matter on the surface of the bed and a corresponding region of overland flow. This

section will describe how typical design and operational parameters influence the development of the surface layer. Subsequently, the longevities of 465 Severn Trent HSSF TWs are statistically analysed in relation to design and operational parameters with the aim of identifying trends in asset longevity.

2.4.1. The influence of design and operational parameters

The nature and distribution of surface layer formation in Severn Trent HSSF TWs can be largely attributed to design and operational factors, such as upstream processes, influent distributor designs, and wastewater solids loading. This will be explained with supporting photographic evidence.

Upstream processes for Severn Trent HSSF TWs are typically rotating biological contactors or trickling filters (Griffin and Pamplin, 1998). **Figure 2-5** shows large biomass flocs in a post-secondary treatment clarification tank, which have been sloughed from an upstream rotating biological contactors. The HSSF TW is directly downstream from the clarification tank and receives any solids carryover from the secondary clarifier.

Figure 2-5 The secondary clarifier that directly follows a rotating biological contactor and precedes a HSSF TW. Large biomass flocs can be seen that have not settled. Photograph taken at Severn Trent, Moreton Morrell wastewater treatment plant, August 2008.

The wastewater is continuously fed through surface-based inlet distributors that span the width of the bed. Distributor designs vary and include pipes with multiple risers and troughs with numerous distribution weirs. These are highly prone to clogging with solids from upstream processes, as shown in **Figure 2-6**.

The nature of wastewater loading onto these systems results in preferential clogging at the inlet, within the upper layers of gravel and on the surface. The photographic example in **Figure 2-7** illustrates the typical horizontal gradient of sludge layer thickness observed on the surface of the beds, where the depth of accumulation at the inlet is greater than at the outlet. Transverse gradients in surface layer accumulations are also common at the inlet region due to uneven width distribution. Such phenomenon was reported by Horton (2003) in a survey of several Severn Trent HSSF TWs. Overland flow results across the surface layer unto the point where the cumulative infiltration through the surface layer equals the hydraulic loading rate.

Analysis of data collected by Wilson (2007) from 21 Severn Trent HSSF TWs indicates that the relationship between sludge layer thickness at the inlet and cumulative solids load to the bed is approximately linear (**Figure 2-8**). By this relationship (R^2 fit of 0.78), for every kilogram of solids loaded per m^2 of system footprint, the sludge layer at the inlet increases by 16 mm. However, without knowing the solids density and sludge porosity it is not possible to estimate the mineralisation rate of the sludge layer. **Figure 2-9** is a photograph of a core of clog matter that was extracted from the top layers of an eight-year-old HSSF TW. Three distinct layers are visible: a) a layer of clog matter that has accumulated above the surface of the gravel and is a composite of wastewater solids and patchy masses of leaf litter in various stages of decomposition; b) the top layer of gravel particles that are held together by clog matter; and c) a transition layer between the upper layers of clogged cohesive gravel and unclogged non-cohesive gravel at lower depths. Overland flow has prevented the clog matter from adequately mineralizing. The nature of clog matter formation illustrated by **Figure 2-9** is similar to that described by Tanner et al. (1998) whom identified that clog matter in a dairy wastewater HSSF TWs formed as a 50 mm-deep sludge layer on the surface of the bed and clogging in the top 100 mm of media.

Figure 2-6 Surface influent distributors in Severn Trent HSSF TWs, all showing the effects of accumulated clog matter: (A) vertical riser pipe blocked with solids (Photo taken at Moreton Morrell wastewater treatment plant, March 2009), (B) horizontal pipe partially submersed in clog matter (Photo by J. Nivala at Fenny Compton wastewater treatment plant, March 2009), (C) V-notch trough showing accumulation of solids (Photo by C. Murphy at Gaydon wastewater treatment plant, March 2009).

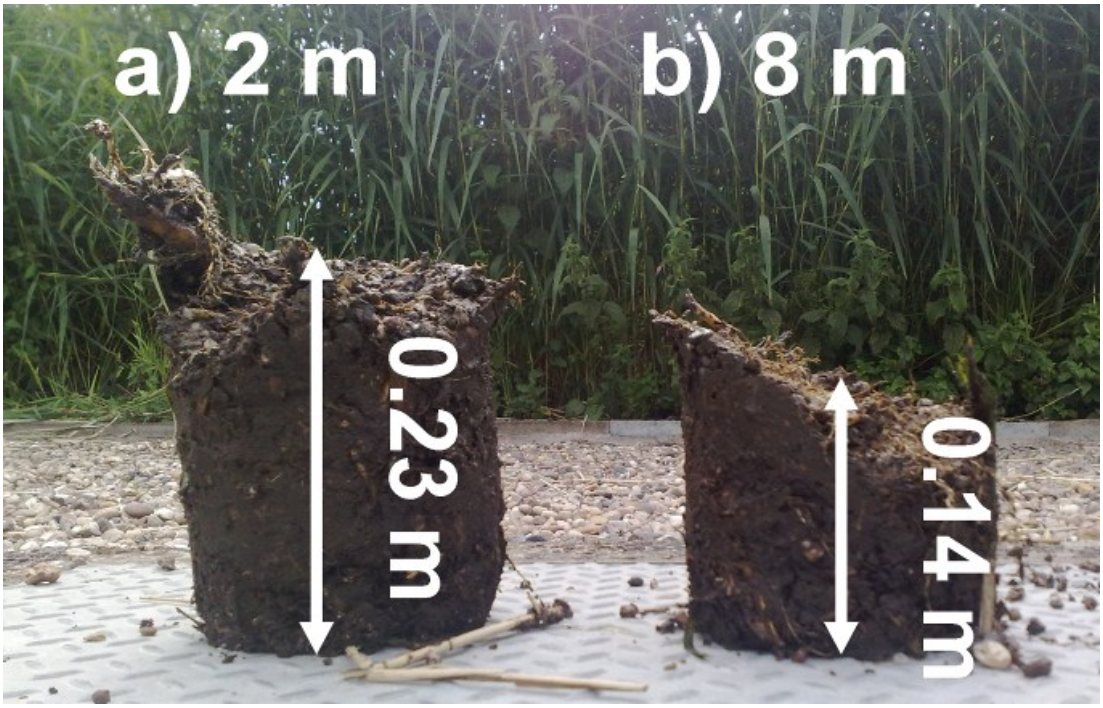

Figure 2-7 A horizontal gradient of solids accumulation is observed in surface-loaded HSSF treatment wetlands. These cores were extracted from an eight-year-old Severn Trent HSSF TW at longitudinal points (a) 2 m and (b) 8 m from the inlet. Photo taken at Rowington wastewater treatment plant, July 2009.

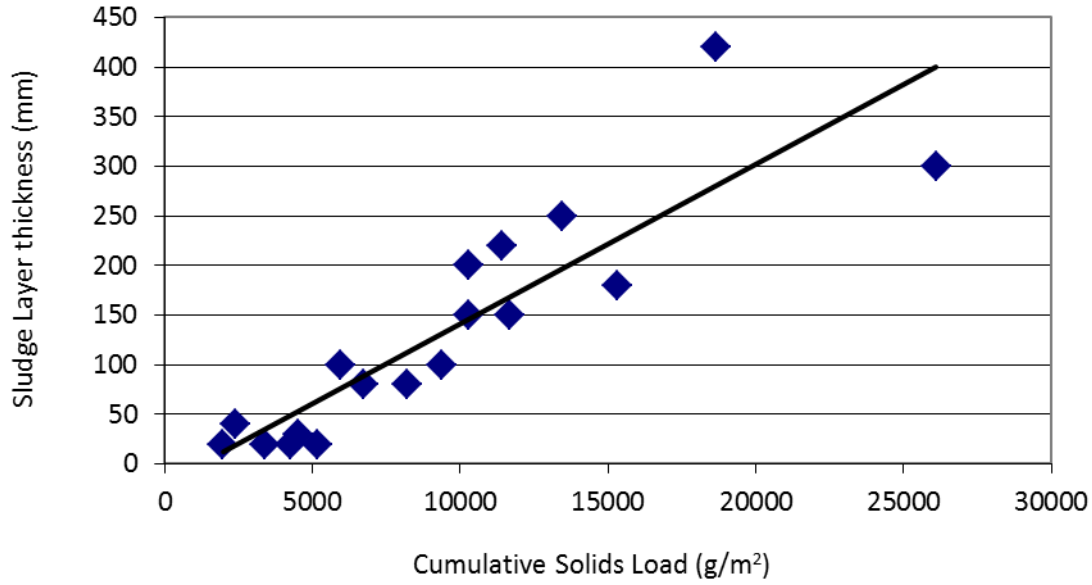

Figure 2-8 The relationship between cumulative solids loading and sludge layer thickness at the inlet, derived from data for 21 Severn Trent HSSF TWs as surveyed by Wilson (2007).

Figure 2-9 A core taken from the top layers of an eight-year-old HSSF TW. Three distinct layers are visible: (Top) A layer of clog matter that has accumulated above the surface of the gravel, (Middle) a top layer of gravel that is held together by clog matter, (Bottom) the transition between upper layers of clogged cohesive gravel and unclogged non-cohesive gravel at lower depth. Photo taken at Severn Trent, Rowington wastewater treatment plant, July 2009.

2.4.2. The relationship between design, operation and longevity

The influence of various design and operational parameters on the longevity of Severn Trent HSSF TWs will be statistically analysed. The analysis will consider upstream processes, influent distributor design, aspect ratio, specific surface area per unit population, and hydraulic loading rate. The data used for the statistical analysis is kindly provided by ARM Ltd., Rugeley, UK, and it has been agreed not to publish the dataset as part of this thesis. From a total of 491 Severn Trent tertiary HSSF TWs, there have been 226 refurbishments on

175 systems (i.e. some systems have been refurbished multiple times). The analysis will be used to identify characteristics of design and operation that maximise longevity.

Figure 2-10 uses box-and-whisker plots to demonstrate the distribution of asset lifetime at refurbishment versus: a) upstream processes (data available for 85 % of refurbishments); and b) influent distributor type (data available for 94 % of refurbishments). For each box-and-whisker plot the five horizontal lines proceeding from top to bottom represent the sample maximum value, upper quartile, median, lower quartile and minimum value.

Of those systems for which data was available, the vast majority of refurbishments (88 %) were performed on beds that have rotating biological contactors or trickling filters upstream. Respectively, 37% and 48% of systems with rotating biological contactors and trickling filters have been refurbished at least once, suggesting that systems with trickling filters are more prone to clogging. **Figure 2-10** illustrates that the median longevity of refurbished systems is 4 years longer when rotating biological contactors are upstream compared with trickling filters (12 years versus 8 years).

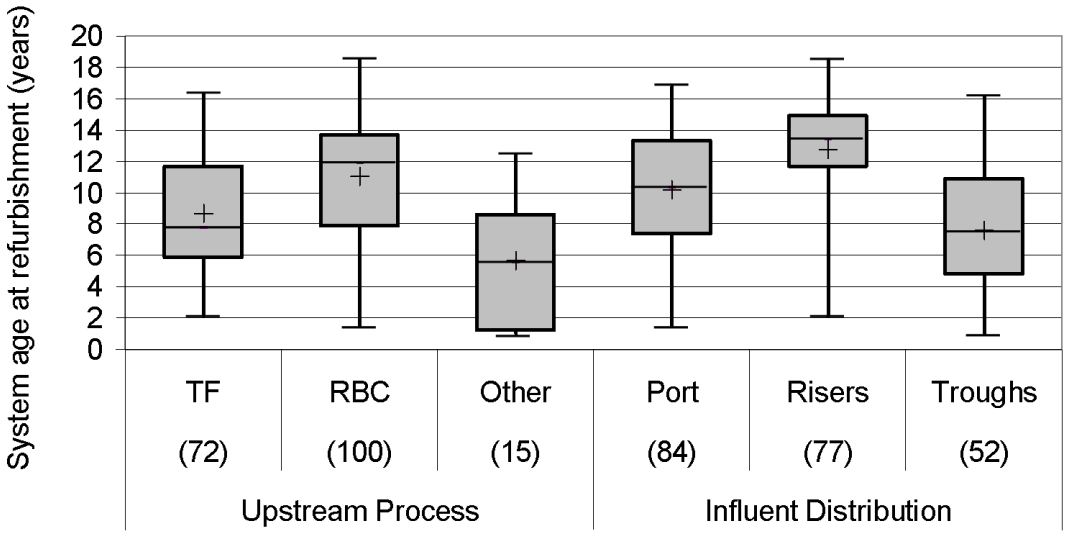

Figure 2-10 Box-and-Whisker plots showing the age at refurbishment for Severn Trent HSSF TWs versus: a) the upstream secondary treatment process (RBC = rotating biological contactor and TF = Trickling Filter); and b) influent distribution system. Brackets indicate the number of records for each case. For each box-and-whisker plot the five horizontal lines proceeding from top to bottom represent the sample maximum value, upper quartile, median, lower quartile and minimum value.

Regarding influent distribution; 70% of all systems with horizontal ports have been refurbished, followed by 44% of systems with vertical risers and 29% of systems with troughs. However, according to **Figure 2-10** the median asset age at refurbishment is highest for systems with risers (13 years) and lowest for systems with troughs (7 years). This apparent paradox regarding the influence of troughs is explained by bias introduced into the data by design evolution. Early designs were mainly fitted with risers, although experience with clogging caused an evolution towards use of ports and trough based distributors. Newer designs predominantly incorporate troughs, which has coincided with an increased awareness over the last decade regarding the need to refurbish.

The period 1992-1997 witnessed the commission of almost 50% of the current Severn Trent tertiary HSSF TW systems, and a period of overlap regarding inclusion of different distributor designs. Using this data as a fairer ground for comparison, 37% of 126 systems with risers, 65% of 51 systems with ports, and 40% of 53 systems with troughs, have been refurbished. This suggests that ports may be the least reliable distributor and troughs are the most robust distributor.

It is speculated that verticals risers are more robust because they are vertically aligned which encourages larger solids to settle inside the distributor, thus preventing them from being loaded onto the surface of the bed. During maintenance the accumulated solids in the risers are pumped out by sludge tanker. Troughs may also act like settlement vessels but, rather than being removed from the system, the accumulated solids are drained back on to the bed during maintenance. Severn Trent operators prefer troughs over risers because troughs are easier to maintain. Photographic evidence (**Figure 2-6**) suggests that ports are not effective at intercepting solids, perhaps due to their horizontal alignment, which results in more solids being discharged onto the gravel media.

Figure 2-11 illustrates two cumulative distribution plots representing the distribution of width-to-length (W:L) ratios for 270 beds that have not been refurbished and 213 beds that either have been refurbished or are pending refurbishment. The W:L ratios for these 483 systems range from 0.3 : 1 to 5.6 : 1, with the majority of W:L ratios being relatively equally distributed between 0.3 : 1 and 3.2 : 1. The profiles of the two cumulative distribution plots are similar suggesting that the ratio of refurbished to non-refurbished beds is relatively equal across the spectrum of W:L ratios. The distribution of beds that have been refurbished is slightly more inclined towards lower W:L ratios than beds that have not been

refurbished, however, the difference is not considered significant enough to suggest that beds with larger W:L ratios are less likely to have been refurbished.

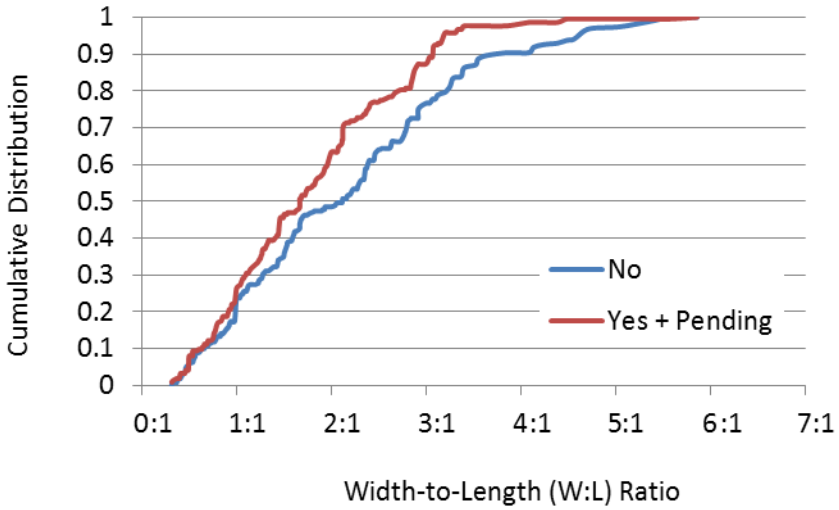

Figure 2-11 Cumulative distribution plots showing the distribution of width-to-length ratios (W:L) for 270 beds that have not been refurbished, and 213 that either have been refurbished or are pending refurbishment.

Figure 2-12 illustrates two cumulative distribution plots representing the distribution of specific system footprint (m^2/PE) for 206 beds which have not been refurbished and 184 beds which either have been refurbished or are pending refurbishment. The specific footprints for these 390 systems range from 0.02 m^2/PE to 6.2 m^2/PE, with the majority of footprints being relatively equally distributed between 0.4 m^2/PE and 2.2 m^2/PE. The profiles of the two cumulative distribution plots are similar suggesting that the ratio of refurbished to non-refurbished beds is relatively equal across the spectrum of specific footprints. The distribution of beds that have been refurbished is slightly more inclined towards lower specific footprints than beds that have not been refurbished, however, the difference is not considered significant enough to suggest that beds with larger specific footprints are less likely to have been refurbished.

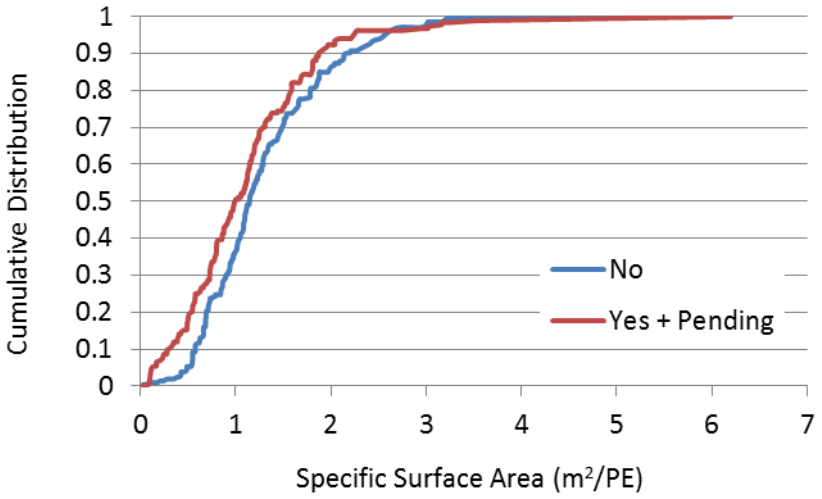

Figure 2-12 Cumulative distribution plots showing the distribution of specific footprints (m^2/PE) for 206 beds that have not been refurbished, and 184 that either have been refurbished or are pending refurbishment.

2.5. Clogging in other common variants of Subsurface Flow Treatment Wetlands

The previous example demonstrated how the consolidated literature could be used to explain the development of clogging in Severn Trent HSSF TWs. The same principle can be applied to explain the system specific development of clogging in three other common variants of Subsurface Flow TW. In this section, a distinction is made between HSSF TWs with subsurface influent distribution (**Section 2.5.1**), VF TWs with sand media (**Section 2.5.2**) and VF TWs with gravel media (**Section 2.5.3**). The development of clogging in each type of system is discussed with regard to flow configuration, design features, and operational parameters; however, data sets for system longevity were not available for statistical analysis (as was the case for Severn Trent systems). **Section 2.5.4** discusses the reason why some Subsurface Flow TWs appear more susceptible to clogging related problems than others. This is done by comparing data-sets representing the typical wastewater loading rates of these systems, as obtained from countries where they are commonplace.

2.5.1. Horizontal subsurface flow with subsurface loading

Systems of this nature are popular in the US, Australia and parts of continental Europe, where they are predominantly used for the secondary treatment of domestic wastewater. The wastewater is continuously fed directly into the subsurface through slotted pipes that are located a few centimetres below the gravel surface (**Figure 2-13**) (Knowles et al., 2011). Design guidelines in Europe recommend gravel sizes of 3-16 mm whilst those in the US have suggested inclusion of media as large as 30 mm. Design guidelines relevant to these systems can be found in IWA (2000), USEPA (2000), and Wallace and Knight (2006).

The subsurface loading results in a preferential accumulation of solids in the proximity of the influent distributor. The primary-treated wastewaters received at the inlet often create anaerobic conditions, as typified by the development of black biological coatings on the gravel surface (Bowmer, 1987, Kadlec and Watson, 1993, Suliman et al., 2006a, Wallace and Knight, 2006, Vymazal and Kropfelova, 2008).

In advanced stages of clogging, the loss of conductivity at the inlet forces the flow to surface and take an overland flow path until is it is able to sufficiently infiltrate through the surface layer and back into the subsurface. Reports describing clogging of this nature have originated from the US (Watson et al., 1990, Kadlec and Watson, 1993, USEPA, 1993, Zachritz and Fuller, 1993), Australia (Fisher, 1990), Canada (Chazarenc et al., 2007), Czech Republic (Vymazal, 1996) and Poland (Maloszewski et al., 2006). Once flow has surfaced, clogging dynamics similar to those described for surface loaded HSSF TWs may develop.

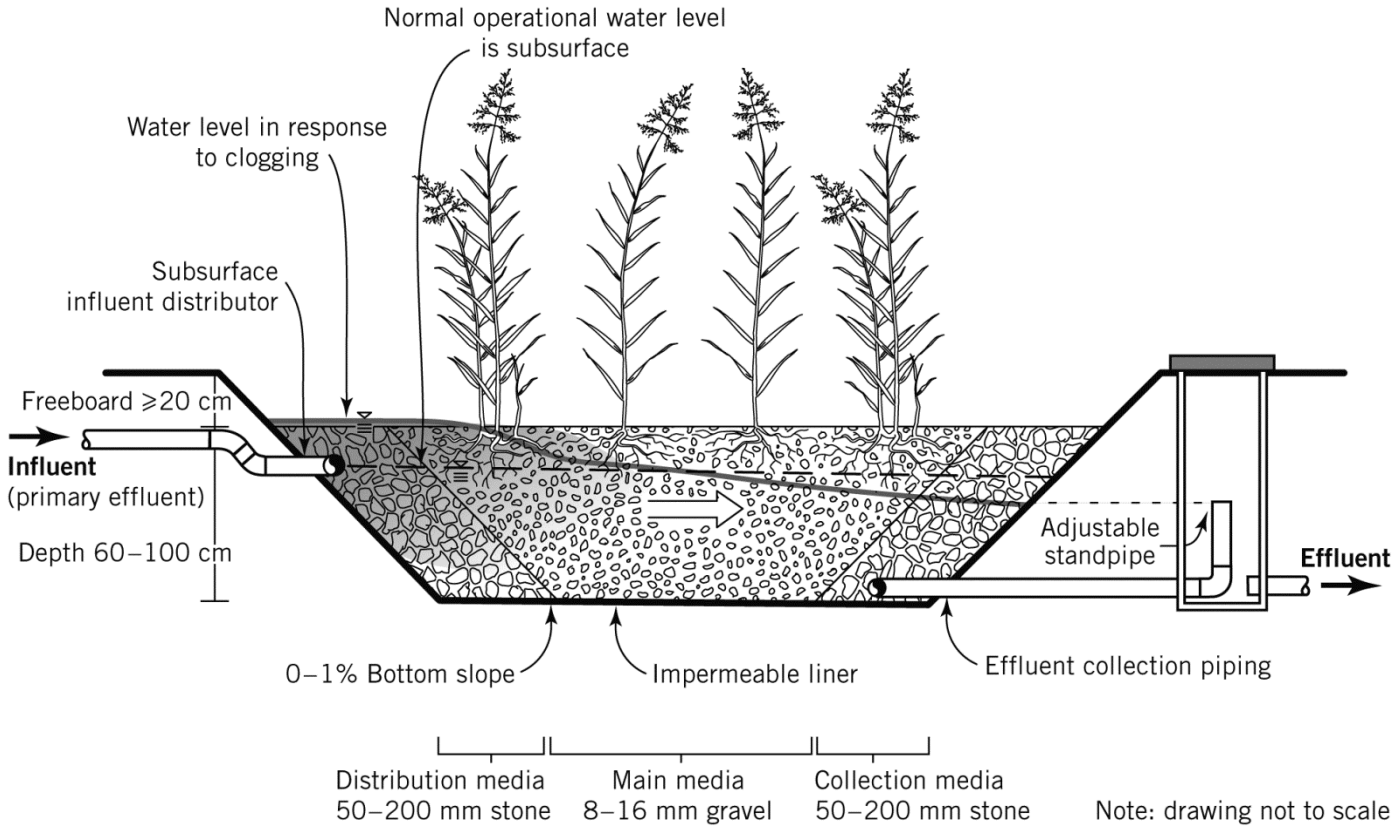

Figure 2-13 Clogging profile for a typical HSSF wetland with subsurface influent distribution. Design details are adapted from Vymazal et al. (1998) and IWA (2000); clogging profile is adapted from Kadlec and Wallace (2010). Figure reproduced from Knowles et al. (2011).

2.5.2. Vertical flow with sand media

The original vertical flow systems of Seidel (1976) incorporated sand or soil media, after which these systems became popular in countries such as Germany, Austria, and Denmark where they are commonly used for the secondary treatment of domestic wastewater. A schematic of a typical VF TW with a sand medium is shown in **Figure 2-14** (Knowles et al., 2011). The most common influent distribution system consists of perforated piping, equally distributed to cover the surface area of the bed. The first layer of media generally consists of 8–16 mm gravel to enhance flow percolation throughout the bed. The main treatment media is a mixture of sand and fine gravel with an average grain size smaller than 4 mm. Below the main treatment layer, a transition layer and a drainage layer of increasingly coarser gravels is used to facilitate final effluent collection. Wastewater dosing is typically intermittent as this allows greater oxygen transfer within the wetland bed and promotes aerobic degradation processes. Further details regarding the specification of these systems are given in ATV (1998), Brix and Johansen (1999) and ÖNORM-B-2505 (1997).

The use of sand and soil as opposed to gravel means that these VF TW systems are highly prone to clogging if they are operated incorrectly (Cooper and Green, 1995). For example, Winter and Goetz (2003) reported that six from a survey of 21 VF filters in Germany had clogged and found that this was mainly linked to overloading of wastewater. Clogging preferentially develops in the top part of the main layer, where the greatest biological growth occurs due to contact between the fine medium and organic matter in the influent wastewater. Indeed, Tietz et al. (2007) found, through an average of four different methods, that 85% of biofilm mass by dry matter was present in the top 10% of a VF TW filter. The microbial population was mainly heterotrophic due to the aerobic operating conditions of the system.

Clogging can be extremely rapid if the period between doses does not allow sufficient time for wastewater percolation (Langergraber et al., 2003), because sealing of the surface by wastewater reduces organic matter mineralisation rates (Platzer and Mauch, 1997). Kayser and Kunst (2005) observed that the oxygen content of air in a “healthy” filter consistently returned to the atmospheric level of 21% between doses. However, the oxygen content of air in a clogged filter was below 5% and was relatively unaffected by dosing cycles.

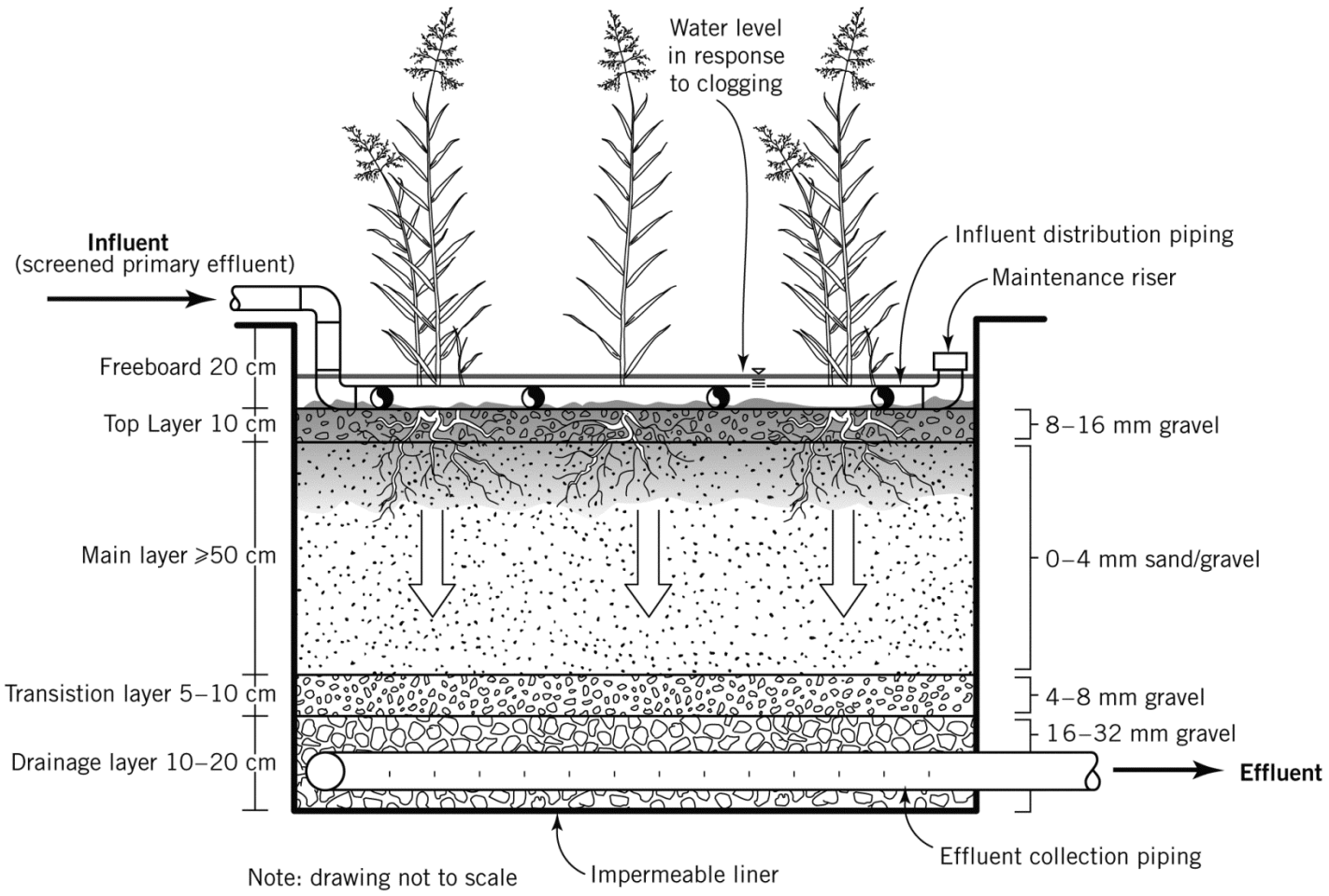

Figure 2-14 Clogging profile for a typical VF treatment wetland with sand media. Design details are adapted from ÖNORM-B-2505 (1997); clogging profile is based on information given in Langergraber et al. (2003). Figure reproduced from Knowles et al. (2011).

2.5.3. Vertical flow with gravel media

The gravel media VF TWs commonly employed in France are used to treat raw, screened primary municipal wastewaters, and form the first stage of a multiple cell wetland network. A schematic of the French VF treatment wetland system is shown in **Figure 2-15** (Knowles et al., 2011). Wastewater is loaded at numerous points over the surface of the bed onto concrete splash pads that aid surface distribution. The main filter layer is small gravel with a size distribution of 2-8 mm. This layer is followed by a transition layer and a drainage layer with respective gravel sizes of 3-20 mm and 20-40 mm. Further details regarding the design of these systems can be found in Iwema et al. (2005).

The French-type of VF treatment wetlands are designed to accumulate a solids layer on the surface of the bed, through which the applied wastewater must percolate (Iwema et al., 2005, Molle et al., 2005); i.e. they are designed to clog (Kadlec and Wallace, 2010). However, the French wetlands are operated in a manner such that the surface layer is beneficial to treatment performance without becoming detrimental to hydraulic performance (Chazarenc and Merlin, 2005). The wastewater is dosed intermittently, which provides time for the surface layer to dewater and mineralise so that hydraulic conductivity is maintained.

It is believed this mode of operation effectively prevents significant ponding, with Chazarenc and Merlin (2005) citing this as the reason that several gravel-based VF systems in France of ages varying up to eight years showed no signs of clogging. Molle et al. (2005) further support the effectiveness of the French design by reporting that only one out of 71 VF systems reviewed had ever required intervention due to clogging. Generally, mineralisation ratios of 60% have prevented this phenomenon from occurring in other systems (Boutin et al., 1997).

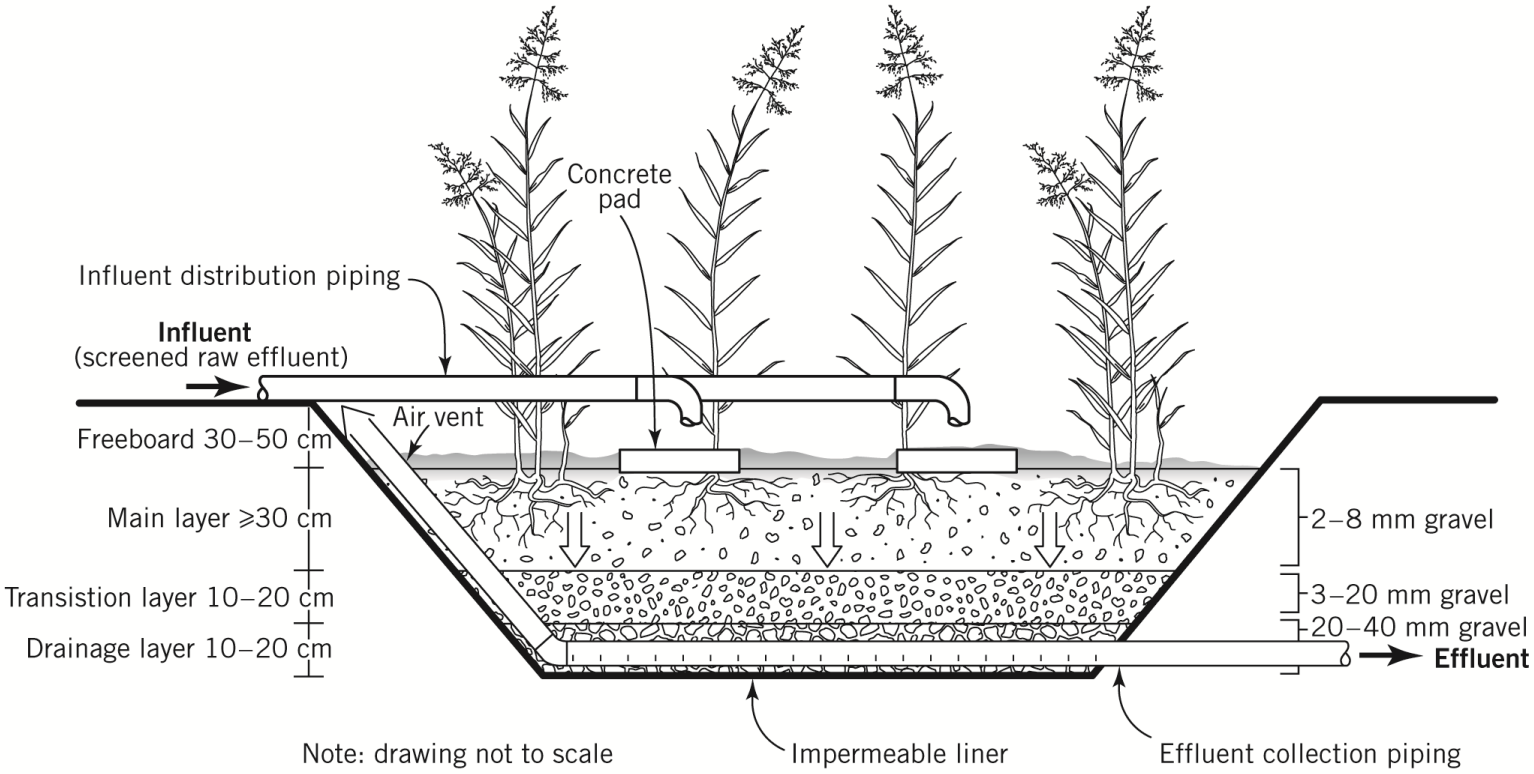

Figure 2-15 Clogging profile for a typical VF (French-type) treatment wetland with gravel media. These systems are generally designed with several beds in series; the first bed in the series (shown) is constructed with larger gravel and retains most of the solids. Design details are adapted from Lienard et al. (1998); clogging profile is based on information from Molle et al. (2005). Figure reproduced from Knowles et al. (2011).

2.5.4. Why clogging impacts some systems more than others

From the literature reviewed thus far it appears that some Subsurface Flow TW variants are more prone to problematic clogging than others. For example, more reports of clogging have originated regarding tertiary Severn Trent HSSF TWs than from the primary VF TWs of France, although this seems counterintuitive. This section will compare the typical wastewater loading characteristics of the four Subsurface Flow TW variants previously discussed, to elucidate why some systems appear more prone to clogging than others. Prior to this, however, discussion will be given to regional differences in the qualification of clogging problems and how this may influence how clogging is reported.

The extent of ponding that qualifies as "undesirable" varies regionally and depends on operator expectations and regulatory requirements. In the US, clogging usually presents hydraulic rather than treatment performance issues in HSSF TWs. This is because US regulatory agencies generally prohibit the surface exposure of wastewater to protect public health (USEPA, 2002) and therefore HSSF TWs exhibiting even a small degree of surface flow will necessitate restorative action (Kadlec and Wallace, 2010). A much greater degree of ponding is often tolerated in Severn Trent (UK) HSSF TWs before the problem is addressed (Cooper et al., 2005), as these systems are typically confined from public access. Furthermore, it has generally been observed that even those Severn Trent HSSF TWs that exhibit advanced symptoms of clogging consistently achieve treatment requirements (Rousseau et al., 2005b, Wilson, 2007). Resultantly, the motivation to intervene in Severn Trent HSSF TWs is to prevent surface flow (induced by clogging) from eventually ponding to the depth where untreated wastewater can bypass the system through the overflow pipe. In German secondary VF TWs the infiltration time for each dose will increase as clogging develops, until the wastewater no longer completely infiltrates between doses. However, it is the associated reduction in aerobic treatment conditions, rather than the hydraulic issues, which necessitate intervention (Kayser and Kunst, 2005, Langergraber et al., 2003). French primary VF TWs are designed to operate with some degree of ponding between doses, which may explain why clogging problems are reported less frequently for these systems.

Irrespective of the degree to which clogging is tolerated, the typical operation of the previously discussed systems will control the speed at which clogging develops, and whether clogging becomes a problem that requires intervention. **Figure 2-16** compares datasets of influent wastewater characteristics typically applied to the four Subsurface Flow TW variants, to highlight the differences in their operation. The datasets representing each of

the four system types are: 1) the Constructed Wetland Association Wetland Database (CWA, 2006) from which operational records were taken for 71 Severn Trent HSSF Tertiary TWs with surface influent distribution; 2) the Water Environment Research Federation Wetland Database (WERF, 2006), from which operational records were taken for 24 different US HSSF Secondary TWs with subsurface influent distribution; 3) data adapted from Winter and Goetz (2003), from which records were taken for 21 different German VF TWs with sand media; and 4) data adapted from Boutin et al. (1997), from which operational records were taken for 53 different French VF TWs with gravel media. Over the Period of Operational Record (POR) for each system, the average Hydraulic Loading Rate (HLR) in m/d (normalised based on system footprint) and average Total Suspended Solids (TSS) loadings in $g/m^2 \cdot d$, were taken. **Figure 2-16** compares the distributions of average HLR and TSS values for the PORs in each dataset using box-and-whisker plots.

What is evident from **Figure 2-16** is that Severn Trent HSSF TWs receive a combination of relatively high HLR and TSS loadings (median HLR = 0.12 m/d and median TSS = 7 $g/m^2.d$) in comparison to the other data sets, where either one or both measures are relatively low in comparison to the Severn Trent systems. The US HSSF TWs receive the lowest TSS and HLR (median HLR = 0.02 m/d and median TSS = 2 $g/m^2.d$). The German VF TWs receive a high HLR (median = 0.3 m/d) but a relatively low TSS load (median = 3 $g/m^2.d$). Statistically, the French VF TWs receive the highest TSS load (17 $g/m^2.d$) but a comparatively low HLR (0.06 m/d).

As discussed in **Section 2.3.1**, the extent of undesirable surface ponding does not always correspond to the extent of accumulation in a system. French primary VF TWs accumulate clog matter almost five times faster than secondary HSSF TWs in Spain; however, the low HLRs for French systems prevent this from presenting a problem. In contrast, Severn Trent tertiary systems receive a smaller TSS load than French systems but the HLR in Severn Trent systems is higher, which makes Severn Trent systems more prone to long-term ponding. Tertiary Severn Trent HSSF TWs are sized to be seven times smaller than secondary Severn Trent HSSF TWs (0.7 m^2/PE versus 5 m^2/PE, respectively) (Green and Upton, 1995) but they receive the same wastewater flow-rate. This means that the HLR to the tertiary systems is seven times greater than the HLR to the secondary systems. The combination of hydraulic overloading and relatively high solids loading (contributed by failing upstream processes and storm solids conveyed by combined sewers) results in ponding in many Severn Trent tertiary HSSF TWs.

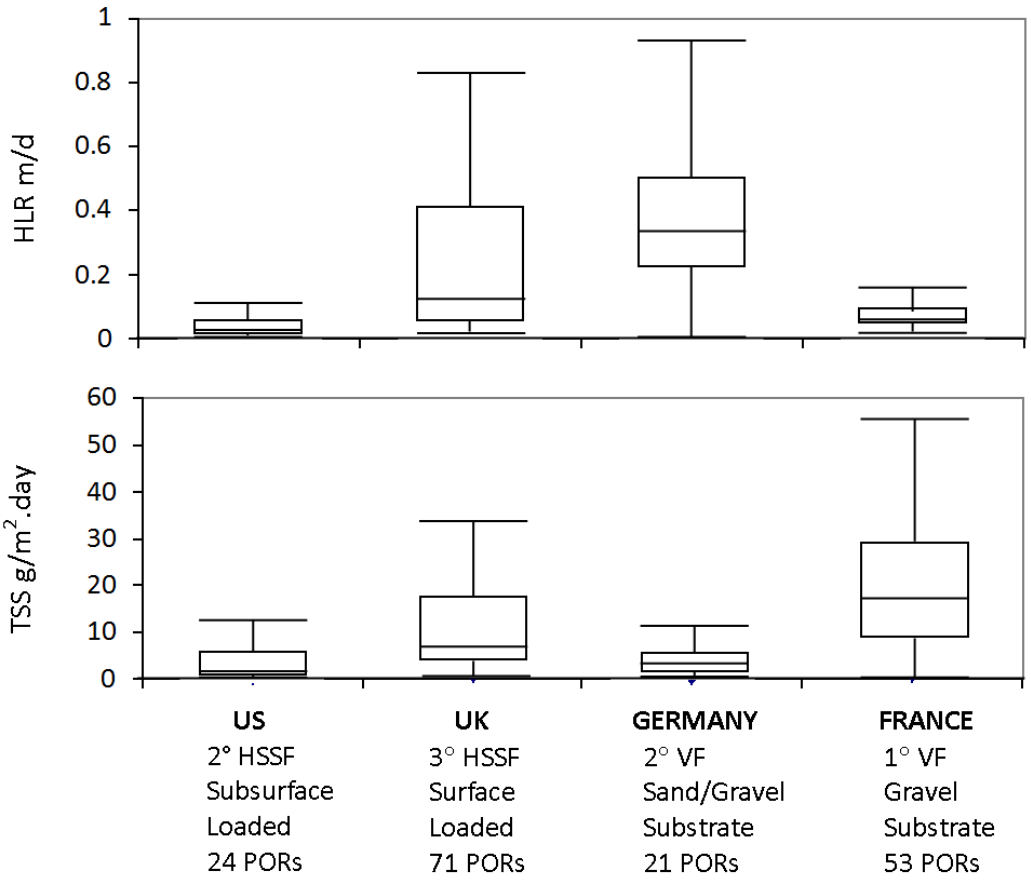

Figure 2-16 Box-and-whisker plots showing the distributions of average HLR and TSS loadings over the Period-of-Operational-Record (POR) for different systems. System data is obtained from four national treatment wetland databases: UK (CWA, 2006); US (WERF, 2006); Germany (data adapted from Winter and Goetz (2003)); France (data adapted from Boutin et al. (1997)). Figure reproduced from Knowles et al. (2011).

A similar discussion can be used to explain why clogging problems have been reported from Germany more frequently than from France. The German secondary VF TWs operate at lower TSS loads but higher HLR than the French systems. This increases the likelihood that clog matter accumulation in German systems will eventually cause hydraulic problems, whereas in French systems the low HLR means that organic solids are able to mineralise well enough to preclude clogging in most cases. This comparison serves as testament to the claims of clog-free operation in French VF TWs (Molle et al., 2005) and emphasises the need to prescribe design and operational limits for both HLR and wastewater pollutant loading rates, to produce Subsurface Flow TWs that are less prone to clogging problems.

2.6. Conclusions

There have been four major findings from this literature review that will be used to inform the remainder of this study:

1. Clog matter is a combination of inorganic and organic solids from wastewater treatment processes, and biomass and vegetation contribution from internal wetland functions. The components of clog matter combine as highly-hydrated, low-density gelatinous sludge that can occlude pore space and reduce hydraulic conductivity more effectively than the individual constituents of the clog matter. Resultantly, the dry mass of clog matter will not necessarily correlate closely with changes in hydraulic conductivity. In the case of Severn Trent HSSF TWs, clog matter is usually a composite of wastewater solids and patchy masses of leaf litter in various stages of decomposition that forms on the surface of the bed and in the upper gravel layers.
2. Severn Trent tertiary HSSF TWs clog in a specific manner that can be attributed to the way that they are designed and operated. Secondary HSSF TWs for Severn Trent are designed using a guideline footprint of 5 m^2/PE whereas tertiary systems have a footprint of 0.7 m^2/PE on the premise that pollutant loading to tertiary systems will be lower than secondary systems. However, Severn Trent use tertiary HSSF TWs to intercept solids carryover from upstream processes that occur during storm events in combined (storm water and municipal wastewater) sewer systems. The combined sewers subject Severn Trent HSSF TWs to a combination of high hydraulic loading rate and high solids loading rate. The solids combine with plant detritus to form a surface sludge layer, and the high storm flow results in overland flow which covers the surface sludge layer and prevents the sludge from mineralising. The result is that the sludge layer thickens in direct proportion to cumulative solids loading at a rate of approximately 16 mm for every kilogram of solids loaded per square metre of system. There is discussion about incorporating Surface Flow Treatment Wetlands with planted rafts as an additional stage between secondary treatment stages and tertiary HSSF TWs, as these would intercept sloughed solids before they reach the bed. Work by Gray (2008) showed that this could be a cost-effective strategy where space is available.
3. The typical operation of Severn Trent HSSF TWs was compared with other variants of Subsurface Flow TW used internationally, to elucidate the reason why some systems appear more prone to clogging than others, and highlight best practices. It is apparent

that the manner in which clogging develops can be attributed to the specific design and operation of the system. Primary and secondary Subsurface Flow TW systems elsewhere in the world (France, Germany and the US) typically operate with lower hydraulic loading rates and/or solids loading rates than Severn Trent tertiary Subsurface Flow TWs. Lower loading rates provide the conditions for adequate clog matter mineralisation such that clogging is less frequently reported from international experience. For example, French primary VF TWs are operated with low HLR such that high solids accumulation rates do not cause operational issues, and adequate mineralization of surface clog matter can occur between loadings. Consequently, it appears that separate limits must be considered for solids and hydraulic loading rates, rather than their combined quotient of wastewater solids concentration, when designing Subsurface Flow TWs for robust operation.

4. By statistically analysing the Severn Trent tertiary HSSF TW system-stock it was possible to identify several best practice and operational design guidelines to achieve good longevity. Trough and riser style influent distribution systems appear to be similarly robust (37-40 % refurbishment rate); however, the ease of maintenance and superiorly uniform width distribution offered by troughs justifies their increased use by Severn Trent. Systems downstream from trickling filters are more likely to have been refurbished than those downstream from rotating biological contactors. Statistical evidence suggests that the width-to-length aspect ratio and per capita footprint of a system has little influence on whether or not it is likely to have been refurbished.

Until now design guidelines for Severn Trent HSSF TWs have been unable to produce robust operating systems. Using the knowledge gained from the literature review, this study will proceed to address two objectives required to inform new and more robust design guidelines.

- A more refined theory of clogging in HSSF TWs is required to provide a foundation upon which to base new design guidelines (Chapter 3).
- New experimental techniques are required to measure empirical information about the form and magnitude of clogging in HSSF TWs so that the theory can be validated and calibrated (Chapter 4).

3. Theory and models

This chapter develops upon existing theory underlying the relationship between hydraulics, hydrodynamics and clogging in Horizontal Subsurface Flow Treatment Wetlands (HSSF TWs), as operated by Severn Trent Water (Severn Trent). The refined theory will be used to improve on the representativeness of existing simple 'rule-of-thumb' models that have previously been used to inform HSSF TW design, but without requiring the complexity of computational models.

Wetlands are dynamic flow systems with a symbiotic relationship between treatment, hydrodynamics, hydraulics and clogging. This relationship varies depending on system conditions and changes over time as the system clogs. However, comprehension of this symbiosis is hindered because theoretical modelling and empirical validation of hydraulics and clogging have been relatively neglected. Existing theoretical descriptions of HSSF TW clogging have tended to over-simplify system hydraulics by assuming, for example, that clogged hydraulics can be represented by a homogeneous 'equilibrium' hydraulic conductivity. These simple design approaches have not been successful at producing systems that operated without clogging problems.

Previous wetland modelling efforts have mainly been focussed upon simulating treatment kinetics by relating measurements of treatment performance to measurements of system hydrodynamics. Many authors have been able to calibrate their models to describe the performance that they measure; however, a calibrated model that can predict subsequent performances still eludes wetland science. This may be because existing hydrodynamic models do not account for the fact that hydrodynamics will change as the system clogs.

It has become apparent that the most accurate treatment performance models depend on a good description of system hydrology (Langergraber, 2008). The term 'hydrology' is used here and throughout this chapter to encompass the real hydraulic, hydrodynamic and clogging behaviour of the system. Resultantly, there is motivation to model better the hydrological relationship between hydrodynamics, hydraulics and clogging, so that the robustness of treatment models and design guidelines can be improved.

Firstly in this chapter, the fundamental and applied theory of HSSF TW hydrology is explored by giving individual consideration to wetland hydraulics, hydrodynamics and clogging.

Secondly, the previous work which has been performed to model these aspects is reviewed. Subsequently, a novel mathematical derivation is presented that better represents the influence of clogging on system hydraulics, and shows how this can be related to system hydrodynamics. The proposed mathematical relationship is calibrated using a simple, novel metric, The Clog Factor, which is also defined in this chapter. The combined theories will provide wetland practitioners with simple tools that can be used to predict how hydraulic and hydrodynamic conditions in HSSF TWs will vary over time as the system clogs. The theory is derived specifically for Severn Trent HSSF TWs but the approach is applicable for all HSSF TWs.

3.1. An Introduction to HSSF TW Hydrology

Severn Trent HSSF TWs are three-dimensional porous media flow systems that operate at atmospheric pressure and flow with an unconfined free-water surface under the influence of gravity. The overall system can be discretised into several hydrological components that are detailed in the exploded view presented in **Figure 3-1**. These components are:

- An influent distributor that distributes the wastewater above-surface, across the width of the bed at the inlet. The nature and uniformity of loading depends on the influent distributor design (e.g. trough or vertical riser), and differences in levelling, clogging and internal pressure losses of the plumbing components.
- A region of overland flow which infiltrates into the subsurface. The overland flow will extend from the inlet unto the point whereby the cumulative infiltration rate through the surface equals the influent flow rate. In unclogged systems the length of this overland flow front may be negligible.
- An accumulation of clog matter which forms a sludge layer on the surface of the bed. The overland flow must infiltrate through any surface layer to reach the subsurface.
- The subsurface flow wetland basin that constitutes a porous gravel medium, through which the wastewater flows for purification.
- Accumulation of clog matter in the subsurface that reduces the porosity of the gravel.
- A macrophyte root network that tends to be most dense in the upper region of the gravel.

- A horizontally flowing subsurface water table that is recharged by vertical infiltration through the surface layer, evapotranspiration from the plants (negative recharge) and precipitation.
- An effluent collector that in Severn Trent HSSF TWs is most typically a 6 inch diameter PVC slotted agricultural drainage pipe that is laid across the width on the base of the bed at the outlet. The uniformity of collection depends on clogging and internal pressure losses within the collector pipe. The effluent collector terminates at a swivelling elbow, which is a set at a height that controls the level of water in the bed at the outlet.

Figure 3-1 also shows how facets such as overland flow, subsurface water table geometry, surface clogging and subsurface clogging vary three-dimensionally. The way these spatial relationships develop depends on the interrelationship among **hydraulics**, **hydrodynamics** and **treatment** in the system. The spatial relationship will develop temporally according to changes in climatic conditions, hydraulic loading rate (HLR), treatment conditions and in response to the development of clogging.

A simple generalization is that: hydraulics describes the equilibrium volume of water in the system that corresponds to boundary and subdomain conditions; hydrodynamics represents the dynamic response of flow through the equilibrium volume; and clogging is the link that causes hydraulics to alter in response to hydrodynamics, and hydrodynamics to alter in response to hydraulics. For example, treatment leads to clogging in a specific part of the system. The hydraulic conductivity of the clogged gravel is now lower than the hydraulic conductivity of adjacent unclogged gravel, and the hydrodynamics of the system change to follows the path of least resistance through the unclogged gravel. Treatment begins to occur within the unclogged gravel, which resultantly begins to clog. This inter-relationship between hydraulics, hydrodynamics and clogging can result in the following problems.

- Excessive short-circuiting leads to insufficient residence time for adequate treatment of wastewater in the system.
- Excessive reduction in hydraulic conductivity can inhibit the ability to convey the influent flow rate and will result in hydraulic malfunctions such as system overspill.

The theory describing hydraulics, clogging and hydrodynamics in HSSF TWs will be introduced in the next three subsections, so that the inter-relationship can be elaborated.

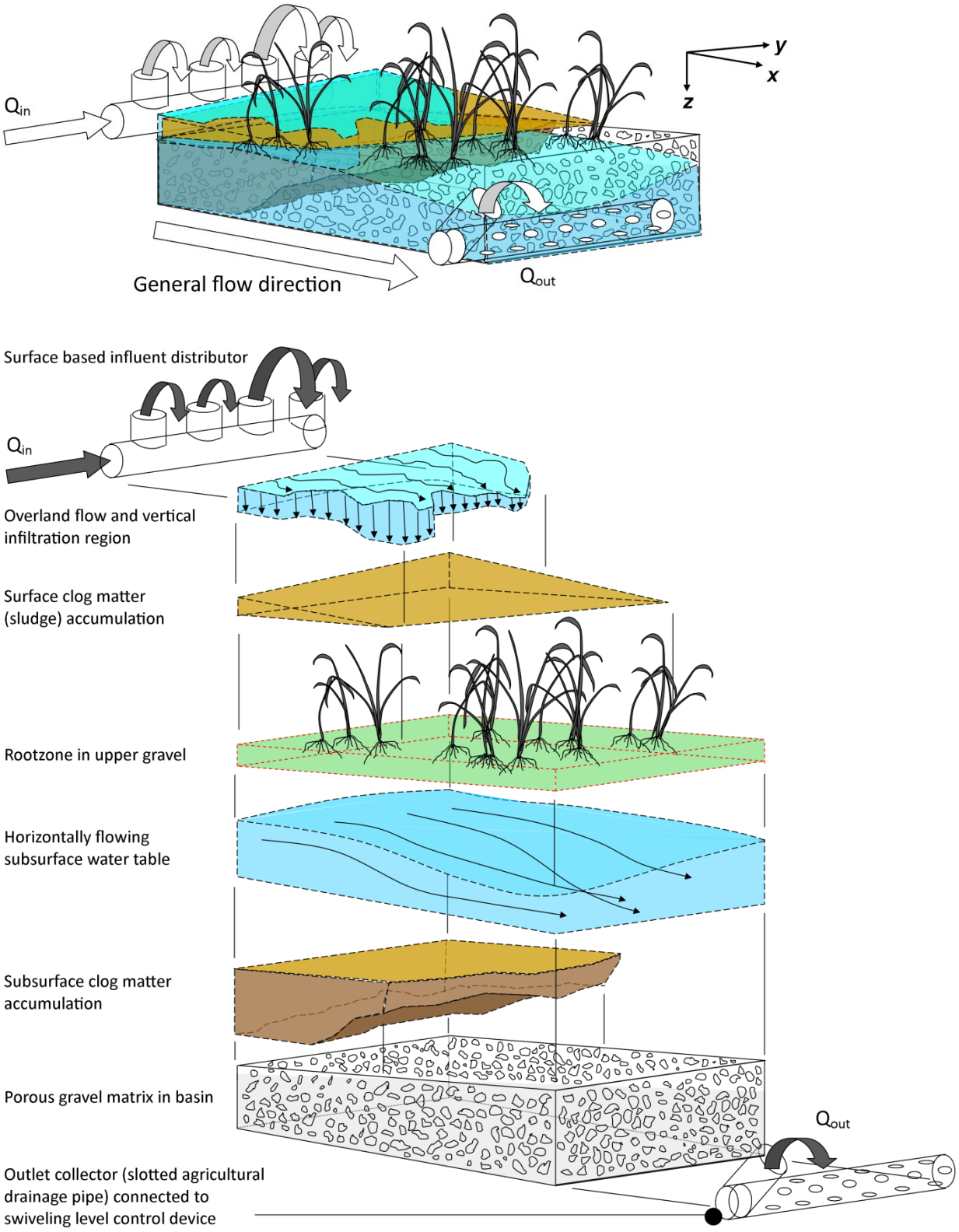

Figure 3-1 A schematic of a Severn Trent Water Horizontal Subsurface Flow Treatment Wetland with a corresponding exploded view that details major hydrological components.

3.2. Hydraulics

Hydraulically, HSSF TWs can be likened to unconfined aquifers with a phreatic water surface that is exposed to atmosphere. The flow of viscous fluid through resistive porous media dissipates energy, resulting in a pressure loss in the direction of flow. In unconfined systems this pressure loss is physically balanced by a variation in water depth, referred to as head-loss, i.e. an equilibrium between kinetic and potential energy (Bear, 1979).

The exact profile of the water table is governed by the intrinsic relationship between the three-dimensional physical properties of the porous media flow system (subdomain conditions), and the distribution of flow to the system (boundary conditions). This idea is illustrated in **Figure 3-2**, which uses a 2D simplification of the HSSF TW in the longitudinal-vertical ***x-z*** plane. It should be reiterated that variations will also occur in the transverse ***y*** plane. For the purposes of derivation, all parameters that are a function of width will be interpreted as being width averaged (e.g. m^3 becomes m^2).

The major fluxes of water into the system are the influent wastewater flow rate $\boldsymbol{Q_{in}}$ (m^2/d) and precipitation ***P*** (m/d), and the major fluxes out of the system are evapotranspiration ***ET*** (m/d) and effluent discharge $\boldsymbol{Q_{out}}$ (m^2/d). Generally speaking, ***P*** will be a uniform spatial load; however, ***ET*** may vary depending on spatial variations in plant establishment. $\boldsymbol{Q_{in}}$ is a distributed surface flux that represents overland flow, and that varies over the surface of the bed depending on the infiltration rate through the surface layer. The overland flow will extend to a length ***f*** (m) from the inlet which depends on the combination of boundary and subdomain conditions. Unlike in some wetland systems, there is zero flux between Severn Trent HSSF TWs and the surrounding land because an impermeable plastic lines the inside walls of the reactor (Kadlec, 1989).

The wastewater will have a dynamic viscosity $\boldsymbol{\mu}$ (kg/m.s) and a velocity with components ***u, v*** and ***w*** (m/s) in the longitudinal, transverse and vertical directions respectively. The gravel media in the system has intensive physical properties, such as porosity $\boldsymbol{\varepsilon}$ (-) and saturation $\boldsymbol{\theta}$ (-). The bulk $\boldsymbol{\varepsilon}$ and $\boldsymbol{\theta}$ of the reactor is the average of varying intensive media properties within the reactor. Generally speaking, the saturation of the wetted reactor volume can be taken as 1 whereas un-wetted reactor volume has a saturation of 0. The porosity of natural porous media is typically in the region of 0.35, and media porosity will tend to 0 as clogging occurs. The media will also consist of particles with a distribution of geometrical properties such as size and shape. The tenth-percentile diameter $\boldsymbol{d_{10}}$ (m) of the medium represents the

diameter of sieve-spacing that allows only 10% of the particles to pass through on a mass basis. Similar measures exist for the fiftieth-percentile diameter d_{50} (m) and sixtieth-percentile diameter d_{60} (m). The uniformity coefficient C_u (-) is the quotient of d_{60} over d_{10} and is often used to characterise the spread of particle size distributions in a bulk sample of gravel.

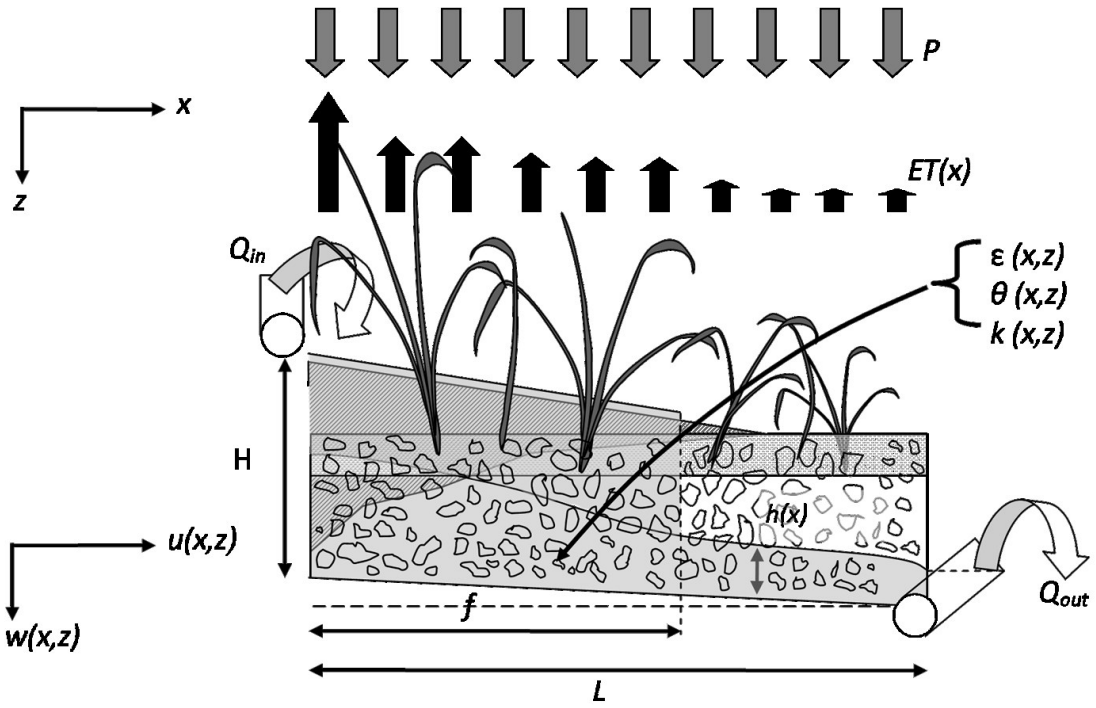

x	Longitudinal distance (m)	H	Depth of bed (including surface layer) (m)
z	Vertical distance (m)	f	Length of overland-flow (m)
u	Longitudinal component of velocity (m/d)	L	Length of bed (m)
w	Vertical component of velocity (m/d)	h	Water depth (m)
Q_{in}	Width-averaged influent flowrate (m^2/d)	ε	Media porosity
P	Precipitation (m/d)	θ	Media saturation
ET	Evapotranspiration (m/d)	k	Media hydraulic conductivity (m/d)
Q_{out}	Width-averaged effluent flowrate (m^2/d)		

Figure 3-2 A 2D simplification of the hydrology shown in **Figure 3-1**, with nomenclature for boundary conditions and subdomain hydraulic properties. Adapted from Kadlec and Knight (1996) and Knowles and Davies (2011).

The resistance against flow imposed by porous media is quantified using a physical property that is neither intensive nor extensive, the hydraulic conductivity k (m/d), which depends on particle dimensions, ε, and θ. The varying physical properties of the medium result in a heterogeneous hydraulic conductivity profile throughout the reactor. Dissipation of kinetic

energy due to viscous flow through the porous media equates to lateral and longitudinal variations in water depth throughout the system $\boldsymbol{h}$ (m). The minimum water depth in the system $\boldsymbol{h_{out}}$ (m) is controlled by the height of the outlet level control device. The water depth at the inlet $\boldsymbol{h_{in}}$ (m) depends on the combination of boundary and subdomain conditions. Integrating $\boldsymbol{h}$ over the length of the bed yields the wetted section, $\boldsymbol{A_w}$ (m^2). Multiplying $\boldsymbol{A_W}$ by the bulk reactor porosity provides the quantity of water in the system.

3.2.1. The relationship between longitudinal flow velocity and water depth

The relationship between the dissipation of fluid kinetic energy that results from viscous flow through porous media and head-loss is described using **Equation 3-1**, and is based upon the following assumptions:

- Simplification of the Navier-Stokes equations under the assumptions of steady-state, incompressible flow with zero pressure head (atmospheric pressure).
- Applying Bernoulli's Principle with conditions of constant elevation.
- The fluid is Newtonian and the relationship between head-loss and the ratio of viscous to inertial forces can be described using Reynolds number ***(Re)***.
- Using multiplication factors (as performed by Reynolds) to account for the combined resistance to flow created by internal fluid effects and the physical geometry of the porous media flow system.
- The porous media is fully saturated by the fluid.

$$-\nabla h = \frac{\mu}{k_i \rho g}\overline{U} + \frac{A}{g}\overline{U}^2 \qquad \textbf{Equation 3-1}$$

In **Equation 3-1**, $\boldsymbol{k_i}$ (m^2) is the intrinsic permeability of the media under laminar flow conditions, $\boldsymbol{A}$ is a geometrical factor related to turbulent energy dissipation, $\boldsymbol{\mu}$ (kg/m.s) is the dynamic viscosity of the fluid, $\boldsymbol{\rho}$ (kg/m^3) is the density of the fluid, $\boldsymbol{g}$ (m/s^2) is gravitational acceleration and $\boldsymbol{\bar{U}}$ (m/s) is the two dimensional velocity vector. Reynolds number for an ideal homogeneous media composed of spheres with identical diameter $\boldsymbol{d}$ (m) and face-centred cubic lattice packing is stated in **Equation 3-2**:

$$\boldsymbol{Re} = \frac{2}{3}\frac{\rho u d}{\mu(1-\varepsilon)} \qquad \textbf{Equation 3-2}$$

The empirical relationship between $\boldsymbol{k_i}$, $\boldsymbol{A}$ and the geometry of an ideal porous media composed of homogeneous spheres has been derived through the combined formulations of Kozeny (1927), Blake (1922), Carman (1937), Burke and Plummer (1928) and Ergun (1952):

$$k_i = \frac{\varepsilon^3 d^2}{150\,(1-\varepsilon)^2} \qquad \textbf{Equation 3-3}$$

$$A = 1.75\,\frac{(1-\varepsilon)}{\varepsilon^3 d} \qquad \textbf{Equation 3-4}$$

Combining **Equation 3-1** with the empirical formulations given in **Equation 3-3** and **Equation 3-4** yields the Ergun Equation (Ergun, 1952), which relates the laminar and turbulent components of head loss to the size and porosity of the medium and the viscosity of the fluid:

$$-\nabla h = 150\frac{(1-\varepsilon)^2}{\varepsilon^3 d^2}\frac{\mu}{\rho g}\overline{U} + 1.75\frac{(1-\varepsilon)}{\varepsilon^3 d}\frac{1}{g}\overline{U}^2 \qquad \textbf{Equation 3-5}$$

It should be noted that the theoretical derivation of the Ergun Equation relies on the assumption that the hydraulic conductivity of an ideal medium is isotropic. Real media may be anisotropic, such that the hydraulic conductivity varies in different flow directions and a three-dimensional hydraulic conductivity tensor is required to relate head-loss to flow velocity (Ingebritsen et al., 2006). The relationship described by **Equation 3-5** is illustrated by **Figure 3-3**. The Ergun Equation is a combination of the Kozeny-Carman Equation, which assumes that turbulent inertial forces (second term on the right-hand side of **Equation 3-5**) can be neglected when ***Re*** is less than 10, and the Burke-Plummer Equation, which assumes that laminar viscous forces (first term on the right-hand side of **Equation 3-5**) can be neglected when ***Re*** is more than 1,000. **Figure 3-3** illustrates that the Ergun Equation provides a good empirical fit to a large range of experimental data that describes the relationship between ***Re*** and drag force, as ***Re*** transitions from laminar to turbulent conditions.

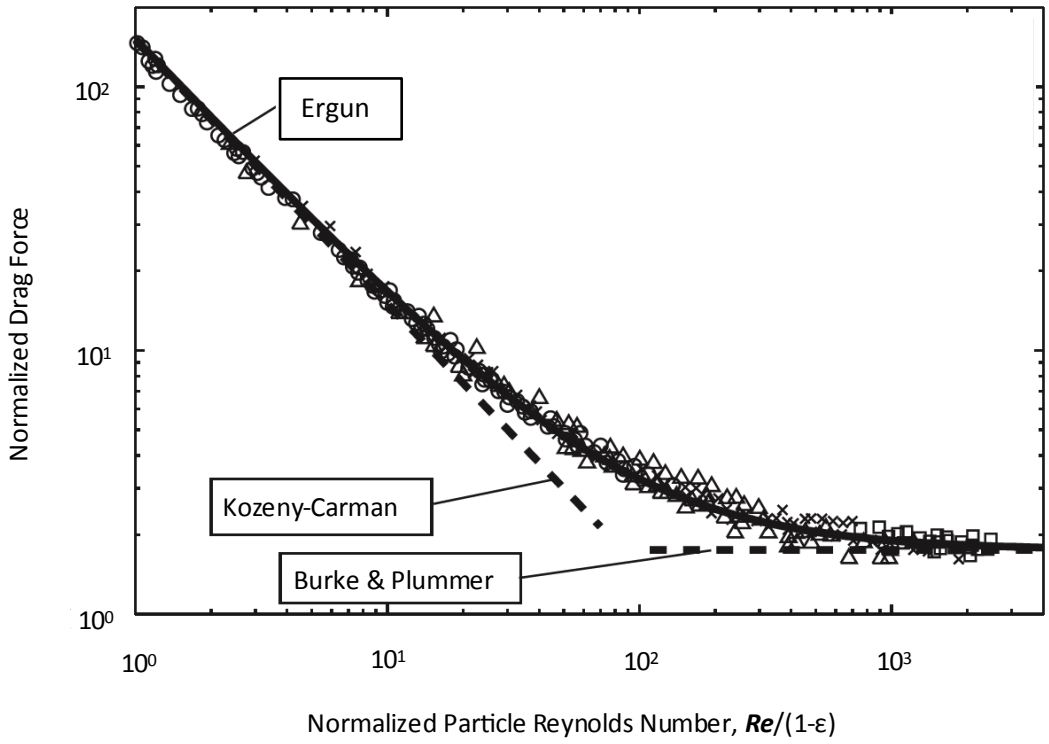

Figure 3-3 The relationship between porous media Reynolds number and drag force as described by the Ergun Equation. The relationship is compared to a large number of experimental results summarised in Ergun (1952). Graphic adapted from Shamy and Zeghal (2007).

Table 3-1 includes 21 operational records detailing the flow-rate and system dimensions for various HSSF TWs around the world, as summarised by Knowles et al. (2011). Based on these records, the ***Re*** number for each system was calculated and the range of ***Re*** is between 0.01 and 3.94. Kadlec and Wallace (2010) explain that the turbulent inertial component of head-loss (second term on the right-hand side) can be ignored with minimal error when Reynolds numbers in HSSF TWs is below 10. Under laminar flow conditions **Equation 3-5** reduces to the Kozeny-Carman equation (**Equation 3-6**), which states that head-loss has first-order linear proportionality to flow velocity.

$$-\nabla h = 150\frac{(1-\varepsilon)^2}{\varepsilon^3 d^2}\frac{\mu}{\rho g}\overline{U} \qquad \textbf{Equation 3-6}$$

Table 3-1 Length ***(L)***, width ***(W)***, height ***(H)***, flow-rate ***(Q_{in})***, gravel size ***(d)*** and computed range of Reynolds Number ***(Re)*** for 21 field-scale HSSF TWs. Adapted from Knowles et al. (2011).

Reference	**System Name**	***Q_{in}*** **(m^3/d)**	***L:W:H*** **(m)**	***d*** **(mm)**	***Re***
Caselles-Osorio et al. (2007)	Verdú 1	177	30:31:0.5	6 – 12	0.81 - 1.63
	Verdú 2	177	27:16:0.4	6 – 12	1.97 - 3.94
	Alfés	60	32:38:0.5	6 – 12	0.22 - 0.45
	Corbins	218	35:35:0.5	6 – 12	0.89 - 1.77
	Almatret N	25	23:20:0.5	6 – 12	0.18 - 0.36
	Almatret S	27	28:18:0.5	6 – 12	0.21 - 0.43
Kadlec and Watson (1993)	Benton Cell 3	254	333:44:0.8	14 – 23	1.20 - 1.97
Watson and Choate (2001)	Jones	0.40	13:3.1:0.5	3 – 6	0.01 - 0.02
	Gray	0.70	12:3:0.5	3 – 6	0.02 - 0.03
	Terrell	0.10	2.7:1.8:0.3	3 – 6	0.01 - 0.01
	Snelling	0.60	4.3:2.4:0.3	3 – 6	0.03 - 0.06
Fisher (1990)	*Scirpus*	20	100:4:0.5	3 – 10	0.36 - 1.19
	Typha	19	100:4:0.5	3 – 10	0.34 - 1.13
	Control	15	100:4:0.5	3 – 10	0.27 - 0.89
Sanford et al. (1995a)	Bed 4	1.40	33:3:0.6	5	0.05 - 0.05
Drury and Mainzhausen (2000)	Cell 1	45	33:33:0.7	6 – 20	0.14 - 0.46
	Cell 2	45	16:28:1.2	6 – 20	0.09 - 0.32
Pedescoll et al. (2009)	Verdú 1	72	30:31:0.6	6 – 12	0.27 - 0.55
	Corbins	72	35:35:0.5	6 – 12	0.29 - 0.59

The constants in **Equation 3-6** can be combined into a single constant ***k*** that represents the saturated hydraulic conductivity of the porous media-flow system (**Equation 3-8**). This enables **Equation 3-6** to be rewritten as Darcy's Law (Darcy, 1856), as shown in **Equation 3-8**:

$$k = \frac{1}{150}\frac{pg}{\mu}\frac{\varepsilon^3 d^2}{(1-\varepsilon)^2} \qquad \textbf{Equation 3-7}$$

$$-\nabla h = \frac{1}{k}\overline{U} \qquad \textbf{Equation 3-8}$$

Darcy's Law governs the relationship between fluid velocity and head-loss over a distance, dependent on the specific physical properties of the porous media and the fluid. The negative sign in front of $\nabla \boldsymbol{h}$ indicates that head is lost in the direction of flow. In HSSF TWs, where flow is along the longitudinal ordinate ***x*** with velocity ***u***, Darcy's Law results in a decrease of water depth ***h*** between the inlet and the outlet. If the water depth diminishes downstream then the flow velocity must increase if continuity is to be observed. The Dupuit-Forchheimer Assumption applies boundary conditions to Darcy's Law to describe the longitudinal profile of water depth in an ideal unconfined porous media flow-system that results from the relationship between continuity and head-loss (**Equation 3-9**);

$$h(x) = \sqrt{2\frac{Q_{in}}{k}(L-x) + h_{out}^2} \qquad \textbf{Equation 3-9}$$

,where $\boldsymbol{h_{out}}$ (m) is the outlet water depth controlled by the outlet level control device. Integrating **Equation 3-9** with respect to ***x*** over the length of the HSSF TW gives the wetted section $\boldsymbol{A_W}$ (m^2) of the HSSF TW (**Equation 3-10**).

$$A_W = \frac{k}{3\,Q_{in}}\left(\left(\frac{2\,Q_{in}\,L}{k} + h_{out}^2\right)^{\frac{3}{2}} - h_{0ut}^3\right) \qquad \textbf{Equation 3-10}$$

3.2.2. Spatial Variations in Hydraulic Conductivity

The previously presented theory is valid for a HSSF TW containing ideal media with homogeneous hydraulic conductivity, however, the typical operation of HSSF TWs results in variations in hydraulic conductivity in all three dimensions. Preferential development of clogging near the inlet results in a longitudinal gradient of hydraulic conductivity from inlet to outlet. Uneven influent distribution and effluent collection result in transverse variations in clogging. The preferential accumulation of clog matter on the surface of the bed, and the establishment of the root-zone in the upper layers of gravel leads to vertical variations in clogging. Variations in hydraulic conductivity throughout the system will reduce the accuracy of **Equation 3-9** and **Equation 3-10**, which are based on the assumption of a singular value for hydraulic conductivity.

The records included in **Table 3-1** are for systems that were the subject of previous research into longitudinal variations in hydraulic conductivity. **Table 3-2** provides the measured values of inlet and outlet hydraulic conductivities for these 21 studies, as obtained using the methods described in **Chapter 4**. As evident from **Table 3-2**, measured values of hydraulic conductivity in HSSF TWs vary considerably depending on media size and longitudinal position. The lowest value of hydraulic conductivity included in **Table 3-2** is 1 m/d and was recorded after 36 months of operation at the inlet of a Spanish secondary treatment HSSF TW with 6-12 mm gravel. The highest value of hydraulic conductivity included in **Table 3-2** is 27,500 m/d and was recorded after 41 months of operation at a US secondary treatment HSSF TW with 14-23 mm gravel. The results presented in **Table 3-2** generally suggest that systems with larger gravel sizes have higher hydraulic conductivities than systems with smaller gravel sizes, and values at the inlet are an order of magnitude lower than values at the outlet.

The results provided in **Table 3-2** emphasise that the assumption of homogeneous hydraulic conductivity in the longitudinal direction is invalid, however, the results are depth aggregated and do not illustrate vertical variations in hydraulic conductivity (no method exists to measure vertical variations of hydraulic conductivity within HSSF TWs - see **Chapter 4**). Vertical variations in hydraulic conductivity will influence the longitudinal profile of water depth at different flow-rates. **Figure 3-4** illustrates this principle using a vertical column of gravel media with decreasing hydraulic conductivity from base to surface. Different equilibrium water depths exist that depend on the flow-rate and the hydraulic conductivity of the corresponding wetted column depth.

Table 3-2 Reported values for media hydraulic conductivities in the inlet and outlet regions of 21 field-scale HSSF TWs. Information is also included regarding the age of the system at the time of study and the method used to measure hydraulic conductivity. Adapted from Knowles et al. (2011).

Reference	System Name	Treatment Type	Age at time of study (months)	Inlet Conductivity (m/d)*	Outlet Conductivity (m/d)*	Method of measurement
Caselles-Osorio et al. (2007)	Verdú 1	Secondary	48	2	12	Falling head
	Verdú 2	Tertiary	48	25	61	Falling head
	Alfés	Secondary	48	7	2	Falling head
	Corbins	Primary	48	2	200	Falling head
	Almatret N	Secondary	36	1	87	Falling head
	Almatret S	Secondary	36	1	82	Falling head
Kadlec and Watson (1993)	Benton Cell 3	Secondary	41	2,500	27,500	Survey
Watson and Choate (2001)	Jones	Secondary	72	1,000	5,400	Survey
	Gray	Secondary	72	10,200	8,100	Survey
	Terrell	Secondary	72	4,900	4,700	Survey
	Snelling	Secondary	72	85	325	Survey
Fisher (1990)	Scirpus	Secondary	33	1,800	25,000	Survey
	Typha	Secondary	33	2,500	25,000	Survey
	Control	Secondary	33	2,500	25,000	Survey
Sanford et al. (1995a)	Bed 4	Landfill leachate	26	4,150	3,370	Survey
Drury and Mainzhausen (2000)	Cell 1	Acid drainage	30	6	3,500	Survey
	Cell 2	Acid drainage	30	6	3,500	Survey
Pedescoll et al. (2009)	Verdú 1	Secondary	177	20	45	Falling head
	Corbins	Secondary	218	3	55	Falling head

* Denotes average value across the width of the bed

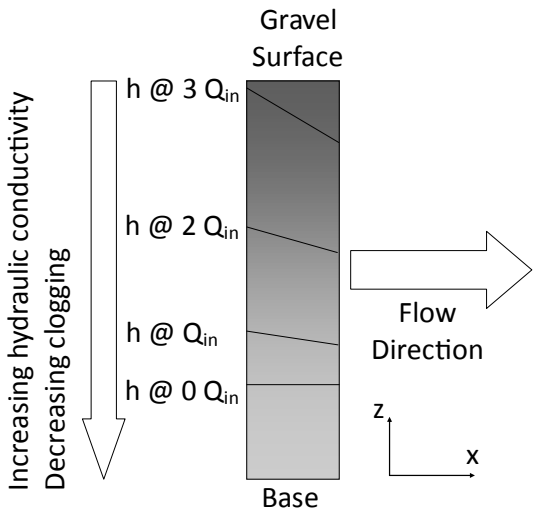

Figure 3-4 A conceptualisation of the relationship between flow-rate $\boldsymbol{Q_{in}}$, hydraulic conductivity ***k*** and resulting water depth ***h***. The diagram depicts a column of gravel with hydraulic conductivity that increases from surface to base, and black lines that represent the equilibrium water table profiles corresponding to multiples of $\boldsymbol{Q_{in}}$ and the hydraulic conductivity of the wetted column.

Figure 3-4 indicates that an increase in flow-rate will cause the water level in the column to increase, but the upper strata offers more resistance to flow than the lower layers, such that the effective hydraulic conductivity of the column in the longitudinal direction decreases and the head-loss across the column increases. The change in head-loss is not directly proportional to the increase in flow and instead the resulting water table profile is a function of flow-rate and the effective hydraulic conductivity of the wetted gravel depth.

3.2.3. The Influence of the Surface Layer

In clogged HSSF TWs a dual hydrological regime exists, whereby overland flow must first vertically infiltrate through any clog matter positioned above the water table before it can become part of the horizontal water table (**Figure 3-5**) (Knowles et al., 2010). Clog matter is generally similar to soils with regard to structure and particle size. It has much lower hydraulic conductivity ***k*** than gravels and often creates a 'bottle-neck' for flow through HSSF TWs. The overland flow extends a distance ***f*** across the surface of the bed until it is able to completely percolate through to the subsurface. The infiltration rates are slower near the inlet, where surface layer depth and hydraulic resistance to infiltration are greatest, and

increase with distance downstream. The relationship between vertical infiltration through the surface layer and longitudinal distance influences the water table profile shown in **Figure 3-5**, and the fraction of flow that longitudinally short-circuits downstream of the inlet.

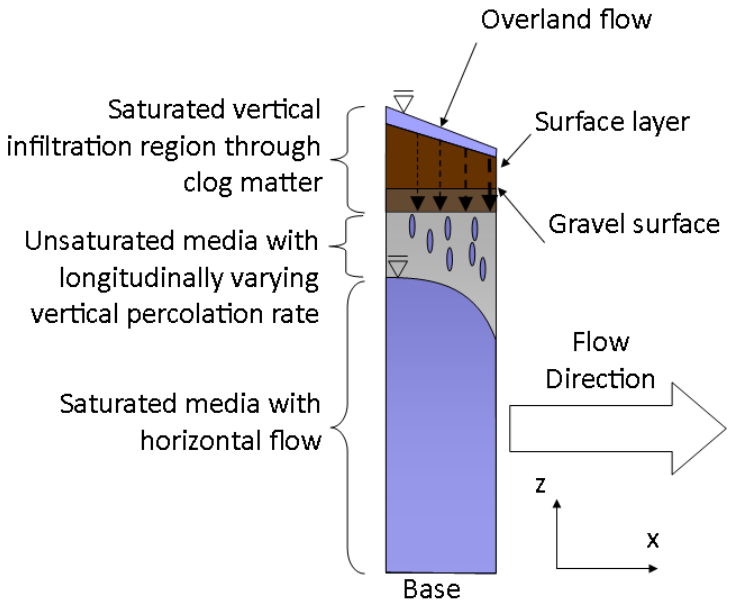

Figure 3-5 A depiction of the dual hydrological regime that can be attributed to infiltrating overland flow through the low hydraulic conductivity surface layer, providing distributed variable recharge to the phreatic subsurface water table.

The description of head-loss through the surface layer varies from the description of head-loss through the gravel because the assumption that pressure-head $\boldsymbol{\psi}$ (m) is zero is not valid for porous materials with small pore diameters. The influence of liquid surface tension on matrix potential is inversely proportional to pore-diameter (Ingebritsen et al., 2006). Matrix potential provides an additional resistance to flow through porous media, alongside the dynamic viscous and inertial effects discussed previously. Macro-porous structures such as gravels have negligible matrix potential; however, matrix potential can have a notable influence on flow through small-diameter porous media such as the surface layer.

Darcy's Law (**Equation 3-8**) can be rewritten in a form that describes the head-loss through the surface layer and accounts for the influence of pressure head on flow (Ingebritsen et al., 2006) (**Equation 3-13**).

$$\psi = \frac{P_M}{\rho\, g} \qquad \textbf{Equation 3-11}$$

$$h = \psi + D \qquad \textbf{Equation 3-12}$$

$$-\frac{\partial}{\partial\, z}\left(\frac{P_M}{\rho\, g} + D\right) = \frac{1}{k} w_r \qquad \textbf{Equation 3-13}$$

, where ***z*** is the vertical ordinate, ***D*** (m) is the fluid elevation in reference to a vertical datum, $\boldsymbol{w_r}$ (m/d) is the vertical infiltration rate, and $\boldsymbol{P_M}$ (J/m^3) is the pressure associated with matrix potential. Other components of water potential that contribute to pressure head include solute potential, mechanically applied pressure (pumping), and potential derived from humidity effects. However, consideration of pressure head by this study will be limited to matrix potential in clog matter.

If flow is free to extend longitudinally until it has completely infiltrated through the surface layer, then it can be assumed that the ponded water depth is small in comparison to the depth of the surface layer. It is assumed that once the surface layer is well saturated and infiltration rates through the surface layer reach steady state, that the entire surface layer depth is wetted and that the height of the capillary fringe at the end of the wetted front is negligible. According to the Green-Ampt equation for infiltration, under these conditions the vertical infiltration rate through the surface layer becomes the hydraulic conductivity of the surface layer (Bouwer, 2002) (**Equation 3-14**).

$$w_r = k \qquad \textbf{Equation 3-14}$$

Media saturation also influences hydraulic conductivity through clog matter. Pores that are variably saturated provide less pore space for flow and the variably saturated hydraulic conductivity of the media is some fraction of the saturated hydraulic conductivity ***k.*** The hydraulic conductivity of the media will tend to ***k*** as the media saturates, however, the ability of the media to saturate is inversely proportional to pore diameter (Brooks and Corey,

1964). Micro-porous media such as clog matter will saturate less easily than macro-porous media such as gravel. However, as stated above, it is assumed for modelling purposes that the hydrology of the system has reached steady-state and is saturated. No further consideration is given to variably saturated hydraulic conductivity by this study.

3.3. Clogging

Clogging in HSSF TWs occurs when the porosity of the clean gravel media $\boldsymbol{\varepsilon}$ is reduced by clog matter with a specific volume $\boldsymbol{\phi}$. The porosity of the clogged gravel media $\boldsymbol{\varepsilon_\phi}$ is calculated from **Equation 3-15**.

$$\varepsilon_\phi = \varepsilon - \phi \qquad \textbf{Equation 3-15}$$

Chapter 2 explains that clog matter is composed of organic and inorganic solids that accumulate through physical, chemical and biological mechanisms:

1. Physical filtration and retention of solids suspended in the flow
2. Biological assimilation of wastewater constituents into biofilms and plant roots
3. Chemical accumulation through precipitation and sorption of constituents

As such, the specific deposit can be considered to be formed of three constituent parts: physical $\boldsymbol{\phi_S}$, biological $\boldsymbol{\phi_B}$ and chemical $\boldsymbol{\phi_C}$ (**Equation 3-16**).

$$\phi = \phi_P + \phi_B + \phi_C \qquad \textbf{Equation 3-16}$$

It is assumed that the majority of clogging in Severn Trent HSSF TWs is caused by physical clogging and biological clogging, and the influence of clogging by chemical absorption and precipitation can be neglected.

3.3.1. Physical Deposition

The ability of filter media to accumulate a specific deposit by filtering suspended solids from flow can be described using the filter coefficient **β** (1/m). The filter coefficient lends itself to macroscopic or phenomenological derivations i.e. when variations in clogging at the pore scale can be neglected and the specific deposit per unit collector is sufficient to describe the clogging process.

Iwasaki (1937) suggested that the change in specific deposit over time can be related to the flux of solids through the media and the filter coefficient according to **Equation 3-17**, **Equation 3-18** and **Equation 3-19**.

$$\frac{\partial \phi_P}{\partial t} = \beta u \, \varepsilon_\phi \frac{c_s}{\rho_s} \qquad \textbf{Equation 3-17}$$

$$\frac{\partial \phi_P}{\partial t} = -u \frac{\varepsilon_\phi}{\rho_s} \frac{\partial c_s}{\partial x} \qquad \textbf{Equation 3-18}$$

$$\frac{1}{c_s} \frac{\partial c_s}{\partial x} = -\beta \qquad \textbf{Equation 3-19}$$

, where $\boldsymbol{u}$ (m/s) is the effective velocity through the media, $\boldsymbol{c_s}$ (mg/L) is the concentration of solids in the wastewater, $\boldsymbol{\varepsilon_\phi}$ is the clogged porosity and $\boldsymbol{\rho_s}$ is the density of the wastewater solids (kg/m^3). Parameter values for **β** specifically apply to the properties of the system under which they were derived. As the filter clogs the geometrical and ionic properties of the system will change such that the filter coefficient is a function of the deposit. Numerous functions have been published for the evolution of the filter coefficient based on the specific relationship between wastewater and media geometrical and ionic properties. It is assumed that clogging accelerates as the deposit accumulates in HSSF TWs, and a formulation presented by Cui et al. (2008) will be used to describe the maturation of the filter coefficient (**Equation 3-20**), where $\boldsymbol{\beta_c}$ (1/m) represents the initial filter coefficient and $\boldsymbol{\varpi}$ *i*s an empirical parameter that describes the significance of the specific deposit on the filter coefficient.

$$\beta = \beta_c \exp\left(\varpi \frac{\phi}{\varepsilon_\phi}\right) \qquad \textbf{Equation 3-20}$$

3.3.2. Biological Deposition

Accumulation by biological matter is a balance between rates of attachment, growth and detachment. Attachment can be described using similar principles as those that describe accumulation of suspended solids. Detachment may occur due to cell lysis or as a function of shear stress and transport. Descriptions of attachment and detachment will not be considered by this study and it is assumed that all biomass deposition is due to growth $\dot{X}_G$ (mg/L.d). Growth will occur due to substrate utilization, which depends on the concentration of substrate in the wastewater according to Monod type kinetics (Langergraber et al., 2009, Llorens et al., 2011a) (**Equation 3-21**);

$$\dot{X_G} = \mu_{MAX}\left(\frac{S}{K_S + S}\right)X \qquad \textbf{Equation 3-21}$$

, where X (mg/L) is the biomass concentration, S (mg/L) is the substrate concentration, K_S (mg/L) is the half saturation constant, and μ_{MAX} (1/d) is the growth rate coefficient. The substrate consumption rate $\dot{S}$ (mg/L.d) can be related to $\dot{X_G}$ by the biomass yield coefficient Y (-) (**Equation 3-22**).

$$\dot{X_G} = -Y\,\dot{S} \qquad \textbf{Equation 3-22}$$

The change in substrate concentration over the length of the bed can be related to the spatial concentrations of biomass and substrate though the following non-linear partial differential equation (Llorens et al., 2011b) (**Equation 3-23**):

$$\frac{\partial S}{\partial x} = \frac{\dot{X_G}}{u\ Y} \qquad \textbf{Equation 3-23}$$

, where the values of X, S and u vary along the length of the bed. The biological deposit volume ϕ_B can be calculated from **Equation 3-24** if the density of the biomass ρ_B (kg/m^3) and clogged porosity of the media ε_ϕ are known.

$$\phi_B = \frac{\varepsilon_\phi X}{\rho_B} \qquad \textbf{Equation 3-24}$$

3.3.3. Influence of Clog Matter Deposition on Hydraulic Conductivity

The clean hydraulic conductivity ***k*** (m/d) of bulk gravel will decrease as clog matter accumulates in the pores spaces between gravel particles. The clogged hydraulic conductivity k_ϕ is a function of the clogged porosity ε_ϕ. If the clog matter accumulations are simplified to mono-disperse emulsion layers on the surface of the gravel particles then the reduction in porosity leads to an increase in effective particle diameter d_ϕ (m). If the bed volume stays the same and the gravel is composed of ideal media then it can be shown that (**Equation 3-25**):

$$d_\phi = d\left(\frac{(1-\varepsilon_\phi)}{1-\varepsilon}\right)^{\frac{1}{3}} \qquad \textbf{Equation 3-25}$$

With ideal media it is possible to rewrite **Equation 3-25** using a ratio of Kozeny-Carmen equations (**Equation 3-7**) based on clean media with diameter ***d*** and clogged media with diameter d_ϕ (**Equation 3-26**):

$$\frac{k_\phi}{k} = \left(\frac{d}{d_\phi}\right)^2 \frac{\varepsilon^3(1-\varepsilon_\phi)^2}{\varepsilon_\phi^3(1-\varepsilon)^2} \qquad \textbf{Equation 3-26}$$

Substituting **Equation 3-25** and **Equation 3-15** into **Equation 3-26** and rearranging allows an expression for clogged hydraulic conductivity to be written in terms of clean media properties and the specific deposit **ϕ** (Zamani and Maini, 2009)***.***

$$k_\phi = k\left(1+\frac{\phi}{1-\varepsilon}\right)^{\frac{4}{3}}\left(1-\frac{\phi}{\varepsilon}\right)^{-3} \qquad \textbf{Equation 3-27}$$

It should be emphasised that the above expressions are based on geometrical relationships for one spherical collector particle. A more precise solution would require correction factors

for gravel inhomogeneity, clog matter that forms as aggregates and dendrites with random structure, and the convergence of films at contact points between particles for different lattice packing arrangements (Cooke and Rowe, 1999). However, analytical expressions to accurately describe these realities are generally intractable and resultantly there have been numerous semi-empirical relationships published similar to **Equation 3-27** (Zamani and Maini, 2009, Thullner, 2010, Ives and Pienvichitr, 1965), which take the general form presented in **Equation 3-28**.

$$k_\phi = k\left(1 + \frac{B\,\phi}{1-\varepsilon}\right)^C \left(1 - \frac{\phi}{\varepsilon}\right)^D \qquad \textbf{Equation 3-28}$$

, where ***B, C*** and ***D*** are empirical parameters to be derived.

As the pore becomes fully occluded with clog matter the value of k_ϕ tends towards the hydraulic conductivity of the clog matter. Clog matter has a highly hydrated micro-porous structure with small effective particle diameters and hydrophilic matric potential induced by the biological organisms. Resultantly the hydraulic conductivity of the clog matter is typically orders of magnitude smaller than the value of ***k***. It can therefore be approximated that the hydraulic conductivity of the gravel tends towards 0 as clog matter accumulates.

3.4. Hydrodynamics

The amount of time that wastewater is theoretically resident in the reactor τ_T (d) is given by **Equation 3-29**, which accounts for the fraction of the wetted section available for flow.

$$\tau_T = \frac{A_W}{Q_{in}}\varepsilon_\phi \qquad \textbf{Equation 3-29}$$

For a HSSF TW that hydrodynamically behaves as an ideal Plug Flow Reactor (PFR), zero mixing occurs and all flow will remain in the reactor for τ_T. However, deviations from PFR conditions occur due to mixing within the HSSF TW. An infinite amount of mixing (instantaneous distribution of the solute throughout the reactor volume) is represented by

the theoretical hydrodynamic behaviour of a Continually Stirred Tank Reactor (CSTR). The result of mixing is a distribution of residence times (RTD) about τ_T, for any parcel of water introduced at the inlet (Kadlec and Knight, 1996). In both situations the mean hydraulic residence time τ (d) (defined as the time elapsed between injection and passage of 50% of the injected flow out of the reactor) is equal to τ_T. The RTD associated with ideal PFR and CSTR conditions is illustrated in **Figure 3-7**.

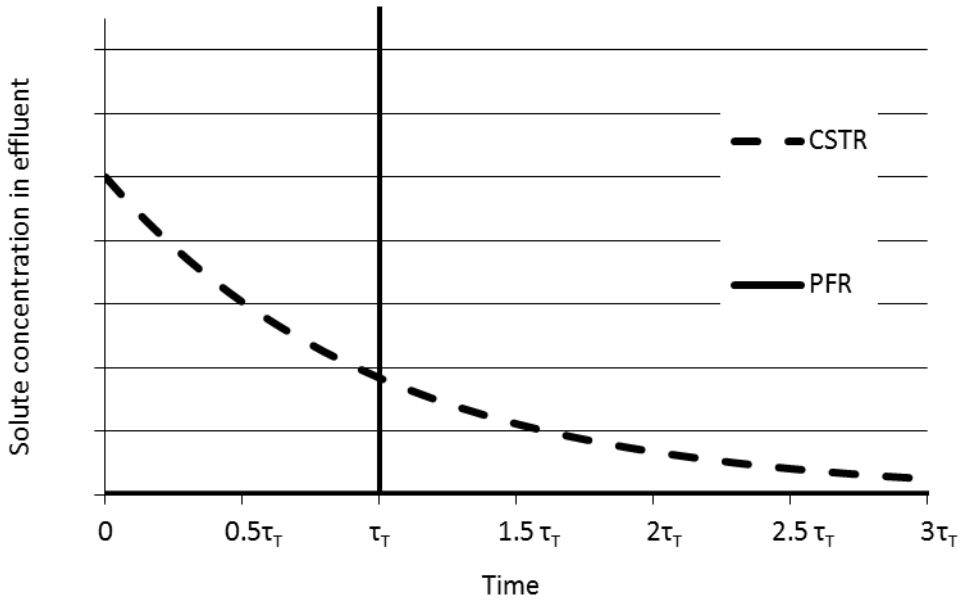

Figure 3-6 Theoretical Residence Time Distribution around the theoretical residence time (τ_T) of a packet of solute introduced into a Plug Flow Reactor (PFR) and a Continually Stirred Tank Reactor (CSTR).

Mixing inside a HSSF TW is between the hydrodynamic extremes of the PFR and CSTR. The Dispersion Coefficient ***D*** (m^2/s) represents the magnitude of solute mixing about a point, caused by the combined effects of molecular diffusion, turbulent diffusion, and shear dispersion. **Table 3-3** summarises the relative magnitude of each of these components in a fluid-flow system, and emphasises that differential advection has an impact on mixing four orders of magnitude larger than turbulent diffusion and 12 orders of magnitude larger than molecular diffusion. In a flowing fluid, the influence of mixing due to molecular diffusion can be neglected.

Table 3-3 The magnitude of various solute dispersion processes in fluid flow systems

Process	Cause	Magnitude of Dispersion Coefficient (m^2/s)
Molecular Diffusion	Random Brownian motion at the molecular scale	$D \sim \mathcal{O}(10^{-10})$
Turbulent Diffusion	Increased mixing between streamlines caused by turbulent flow	$D \sim \mathcal{O}(10^{-2})$
Shear Dispersion	The effect of differential advection imposed on a flowing fluid by the system	$D \sim \mathcal{O}(10^{2})$

Short-circuiting reduces the fraction of the porous volume that is involved in flow and causes the mean hydraulic residence time τ to occur before τ_T. The volumetric efficiency e_v (-) defines the fraction of the reactor volume that is actively involved in flow (**Equation 3-30**).

$$e_v = \frac{\tau}{\tau_T} \qquad \textbf{Equation 3-30}$$

It should be noted that τ will not necessarily correspond to the hydraulic residence time at which peak packet concentration is detected in the effluent τ_p. Short-circuiting occurs in the longitudinal flow direction because of transverse or vertical variations in the following factors:

- Uneven influent distribution
- Downward flow induced by the usual position of the outlet pipe along the bottom of the bed
- Overland flow across the surface of the bed
- Short-circuiting along areas of low hydraulic resistance, such as macro-pores created by gravel separation and tubular plant roots
- Short-circuiting around areas of high hydraulic resistance created by clogging, and plant establishment in the upper regions of the gravel bed
- Vertical density gradients between wastewater and rainwater that infiltrates through the surface of the system.

Table 3-4 summarises the work of authors who have monitored the propagation of tracer at internal points inside the system and observed vertical short-circuiting of tracer. The summary indicates the factor that was believed to be causing vertical short-circuiting and the measured volumetric efficiency, as derived from the tracer RTD. Volumetric efficiencies ranged between 22 % and 94 % for the ten systems studied, which emphasises the impact that vertical short-circuiting can have on hydrodynamic performance.

The real hydraulic behaviour of HSSF TWs exhibits aspects of mixing and short-circuiting. **Figure 3-7** illustrates a typical hydraulic residence time distribution (RTD) for a packet of flow emerging from a HSSF TW in Italy. This was obtained by adding a pulse of lithium tracer at the inlet and monitoring its emergence at the outlet. There are several features of the real RTD that stand out:

- Dye is detected at the outlet long before τ_T
- The peak concentration precedes τ_T
- The τ for the RTD is premature in comparison to τ_T
- Multiple peaks exist on the dye breakthrough curve
- Dye is detected exiting the system long after τ_T
- The dye concentration eventually decays exponentially to zero (referred to as the tail of the RTD).

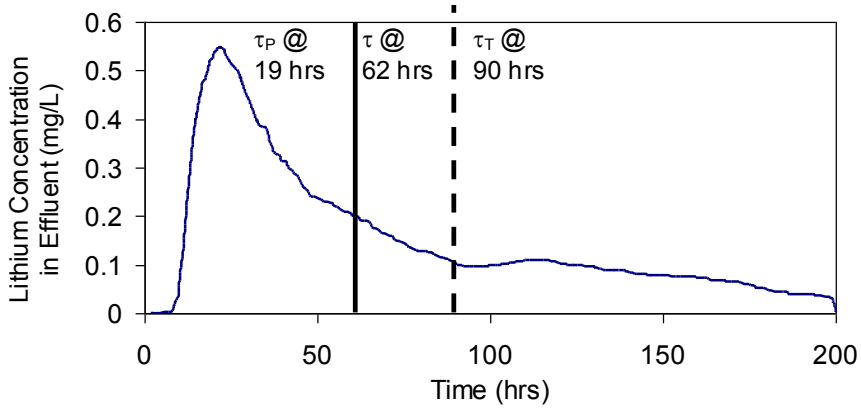

Figure 3-7 The Residence Time Distribution (RTD) for a lithium tracer experiment performed on a HSSF TW at Sieci, Italy. The HRT at peak concentration τ_p, mean HRT τ and theoretical HRT τ_T are given. If the HSSF TW behaved as an ideal Plug Flow Reactor then the RTD would be a single pulse at τ_T, which corresponds to the total amount of tracer injected (2.8 g). Data adapted from information presented in Marsili-Libelli and Checchi (2005).

Table 3-4 Results from 9 tracer studies into the effects of clogging in various HSSF TWs. Details include the system design, hydraulic operation, tracer selection and observed volumetric efficiency e_v. Authors observed vertical short circuiting which they attributed to the various factors; including vegetation (V), system design (S), precipitation effects (P) and tracer density differences (D). Reproduced from Nivala et al. (2012).

Reference	System Name	Treatment Type	Hydraulic Loading Rate (mm/d)	Dimensions L:W:H (m)	Age at time of study (months)	Tracer	V	S	P	D	e_v
Batchelor and Loots (1997)	Pilot Scale	Secondary	*360*	*9.3:4.2:1.1*	*120*	*Sodium Chloride*		X			77 %
Pilgrim et al. (1992), Waters et al. (1993)	Unit 2	Tertiary	*96*	*25:25:0.5*	*18*	*Rhodamine WT*	X			X	75 %
Sanford et al. (1995b)	Bed 4	Landfill leachate	*14*	*33:3:0.6*	*26*	*Fresh water*		X	X		22 – 49 %
Fisher (1990)	Scirpus	Secondary	*50*	*100:4:0.5*	*33*	*Fluorescein*	X				89 %
Rash and Liehr (1999)	SSF vegetated	Landfill leachate	*25*	*14.8:4.0:0.61*	*24*	*Lithium Chloride*	X		X	X	28 – 43 %
Breen and Chick (1995)	HSSF	Tertiary	*43*	*50:2:0.5*	*24*	*Erichrome acid red*	X				
Bowmer (1987)	Planted	Tertiary	*112*	*50:2:0.5*	*3*	*Erichrome acid red, Bromide*	X				87 %
García et al. (2003)	Pilot C1 (coarse media)	Secondary	*37*	*10.5:5.2:0.55*	*17*	*Potassium Bromide*				X	89 %
	Pilot C2 (fine media)	Secondary	*37*	*10.5:5.2:0.55*	*17*	*Potassium Bromide*				X	94 %
Grismer et al. (2001)	Old tank	Secondary Winery	*34*	*6.1:2.4:0.95*	*36*	*Potassium Bromide*		X			70 %

3.4.1. Physical description of mixing and short-circuiting

The transport of wastewater constituents in the flow of wastewater is fundamentally described using the advection-dispersion equation (ADE) (**Equation 3-31**).

$$\frac{\partial c}{\partial t} + \bar{U}\nabla c = D\nabla.\nabla c \qquad \textbf{Equation 3-31}$$

, where $\boldsymbol{D}$ (m^2/s) is the isotropic Dispersion Coefficient that assumes dispersion along the directions orthogonal and perpendicular to flow are similar, $\boldsymbol{c}$ (mg/L) represents the concentration of constituents in solution at a point in the system and $\boldsymbol{\bar{U}}$ (m/s) is the two-dimensional (2D) velocity vector. The ADE has no analytical solution, which prevents it from being directly used to simulate the hydrodynamics of HSSF TWs and recreate realistic RTDs for the system. This is because the specific boundary and subdomain conditions that produce the hydraulic behaviour typical to HSSF TWs cannot be represented using the ADE.

Persson *et al.* (1999) proposed a parameter, the Hydraulic Efficiency $\boldsymbol{\lambda}$ (-), which is based on the properties of the RTD, to account for the combined effects of mixing and short-circuiting. The Hydraulic Efficiency is defined according to **Equation 3-32**.

$$\lambda = e_v e_M \qquad \textbf{Equation 3-32}$$

, where $\boldsymbol{e_v}$ is the volumetric efficiency of the system and $\boldsymbol{e_M}$ is the mixing efficiency. The two parameters $\boldsymbol{e_v}$ and $\boldsymbol{e_M}$ can be derived from the RTD using **Equation 3-30** and **Equation 3-33**, respectively.

$$e_M = \left(1 - \sigma_\theta^2\right) \qquad \textbf{Equation 3-33}$$

, where $\boldsymbol{\sigma_\theta^2}$ is the dimensionless variance of the RTD about the mean HRT, τ, and can be derived from the real variance of the RTD $\boldsymbol{\sigma^2}$ accordingly (Kadlec and Wallace, 2010).

$$\sigma_\theta^2 = \frac{\sigma^2}{\tau^2} \qquad \textbf{Equation 3-34}$$

Typical values for HSSF TW volumetric efficiency are summarised in **Figure 3-8**, which shows that from a survey of tracer tests performed on 37 HSSF TWs, 29 underperformed with an average volumetric efficiency of 91% (Kadlec and Wallace, 2010). Evidently, non-ideal flow is a common facet of HSSF TW hydraulic performance.

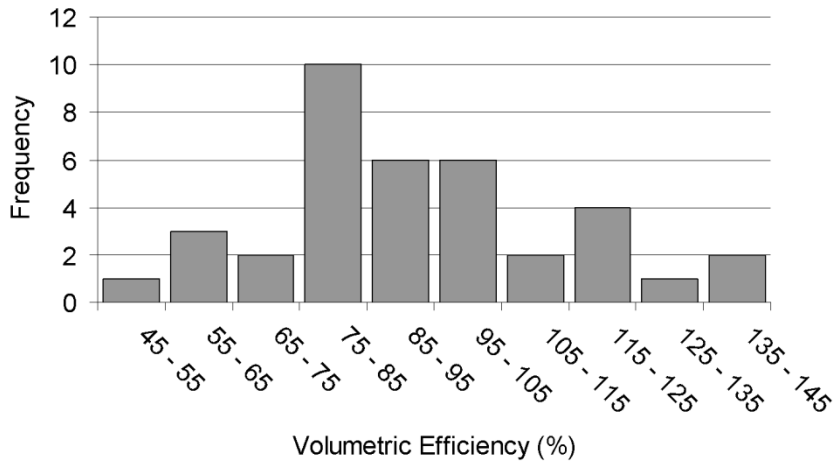

Figure 3-8 Frequency Distribution of the Volumetric Efficiency measured in 37 HSSF TWs, by comparison of observed and design Hydraulic Residence Times. Based on data provided in Kadlec and Wallace (2010). Reproduced from Knowles et al. (2010)

3.5. Modelling the hydrology of HSSF TWs

Generally speaking, good models are relatively simple to apply without neglecting important physical factors. The previously introduced nomenclature and fundamental theory will be used to analyse models of HSSF TW hydrology and their ability to simulate the true behaviour of the system. Firstly, the relationship among spatial variations in hydraulic conductivity that arise from clogging, flow-rate, the wetted volume of the reactor and resulting hydrodynamics will be discussed. This will then lead into a review of currently available models to describe hydraulics, hydrodynamics and clogging in these systems. The review will identify areas where current models cannot accurately represent the true hydrological performance of HSSF TWs and help to identify where simple but robust models are needed.

3.5.1. Models of HSSF TW Hydraulics

In pursuit of simple and widely adoptable design guidelines, the hydraulic behaviour of HSSF TWs has often been modelled using a single hydraulic conductivity value that represents the bulk response of the heterogeneous hydraulic conductivity profile. This approach is similar to common practice in hydrology where the bulk hydraulic response of a heterogeneous hydraulic conductivity profile is approximated using the geometrical mean of the dataset (Binley et al., 1989). In the case of HSSF TWs, these guidelines are based on the assumption that clogged hydraulic conductivity would eventually reach an equilibrium value determined by the balance between plant growth and clog matter accumulation (Cooper et al., 1996).

Several current design manuals (IWA, 2000, Wallace and Knight, 2006, EC/EWPCA, 1990) advocate the use of the equilibrium hydraulic conductivity in a 1D closed-form solution to Darcy's Law, to describe how the water level varies between inlet and outlet as a function of flow rate $\boldsymbol{Q_{in}}$ (m^2/d) (**Equation 3-35**).

$$h(x) = h_{out} + \frac{Q_{in}}{k\,H}(L - x) \qquad \textbf{Equation 3-35}$$

, where $\boldsymbol{h_{out}}$ (m) is the outlet water depth, $\boldsymbol{H}$ (m) is the reactor depth in the axial flow direction, $\boldsymbol{L}$ (m) is the bed length, and $\boldsymbol{h}$ (m) is the water depth at a distance $\boldsymbol{x}$ (m) downstream of the inlet. In other words, the water level gradient between inlet and outlet would be a straight line with gradient $\boldsymbol{Q_{in}/k.H}$. In this case the wetted section, $\mathbf{A_w}$ (m^2) would be (**Equation 3-36**):

$$A_W = h_{out}\,L + 0.5\,\frac{Q_{in}}{k\,H}L^2 \qquad \textbf{Equation 3-36}$$

To reflect the generally accepted observation that clogging is most severe towards the inlet, USEPA (2000) design guidelines propose a 'dual-zone' Darcy model that assumes hydraulic conductivity in the front third of the bed is an order of magnitude lower than in the back two-thirds of the bed. The resulting water table profile can be described using two

equations (**Equation 3-37** and **Equation 3-38**), where ***k*** would be the hydraulic conductivity of the downstream region:

$$\lim_{0.3L \to L} h(x) = h_{out} + \frac{Q_{in}}{k\,H}(L - x) \qquad \textbf{Equation 3-37}$$

$$\lim_{0 \to 0.3L} h(x) = h_{x=0.3L} + 10\frac{Q_{in}}{k\,H}(0.3L - x) \qquad \textbf{Equation 3-38}$$

The wetted section would therefore become (**Equation 3-39**):

$$A_W = h_{out}\,L + 0.9\frac{Q_{in}}{k\,H}L^2 \qquad \textbf{Equation 3-39}$$

This is slightly more representative of the situation reported by several authors, whereby the hydraulic gradient in the front end of the bed is more pronounced than in the back end (Watson and Choate, 2001, Sanford et al., 1995a). However, **Equation 3-36** and **Equation 3-39** are limited because in their formulation they neglect the relationship between continuity and the groundwater energy balance described by the Dupuit-Forchheimer assumption (**Equation 3-9**). If the water depth diminishes downstream then the flow velocity must increase if continuity is to be observed. **Figure 3-9** illustrates the water table profiles predicted by the **Equation 3-36** (Darcy), **Equation 3-39** (Dual Zone) and **Equation 3-9** (Dupuit) for a system with h_{out} equal to 0.2 m, ***L*** equal to 15 m, and $k.H/Q_{in}$ equal to 360. As emphasised by **Figure 3-9**, **Equation 3-36** and **Equation 3-39** underestimate A_W in comparison to **Equation 3-9**.

Guideline design values for equivalent hydraulic have been derived from field scale studies; by measuring the difference in water depths between inlet and outlet and inferring an effective hydraulic conductivity using **Equation 3-35**. **Table 3-5** lists published guidelines for equilibrium hydraulic conductivity values in HSSF TWs. According to **Table 3-5**, the applicable range of hydraulic conductivities for gravel with a median size of 5 mm could range from 86 m/d to 2600 m/d, depending on which guidelines are applied.

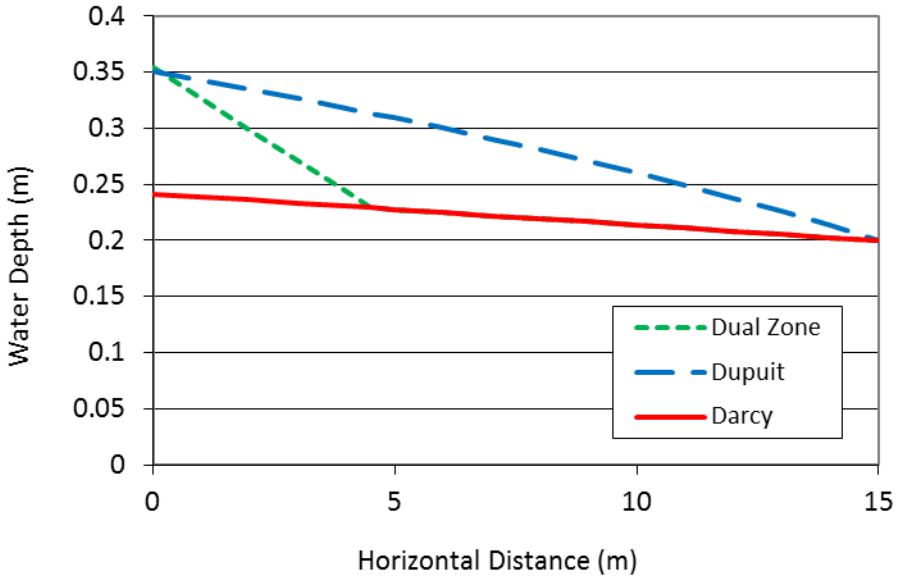

Figure 3-9 The water table profiles produced by the aforementioned equations for Darcy's Law, Dual Zone Darcy's Law, and the Dupuit-Forchheimer assumption, when $k.H/Q_{in}$ = 360, h_{out} = 0.2 m and L = 15 m.

Table 3-5 Suggested design guidelines applicable to 5-6 mm gravel media, for equilibrium hydraulic conductivity at the inlet zone. Reproduced from Knowles et al. (2010).

Source	Range of applicable media (mm)	Predicted Hydraulic Conductivity (m/d)
EC/EWPCA (1990)	5-10	86
TVA (1993)	3-6	2,600
ÖNORM B 2505(1997)	4-8	518
IWA (2000)	3 – 16	1,000

The problem with the guideline ***k*** values published in **Table 3-5** is that they represent a generalisation of hydraulic factors that are unique to the system from which they were derived, such as three-dimensionally varying hydraulic conductivity profile, overland flow, and variations in media size distribution and morphology. Differences in hydraulic factors among these systems mean that a single value representing the bulk hydraulic response of one system cannot be accurately applied to describe the bulk hydraulic response of another system. Additionally, the measurements reported in **Table 3-2** for 21 field-scale HSSF TWs indicate that hydraulic conductivity can increase by several orders of magnitude between the inlet and the outlet of the system. Consequently, it is difficult to derive representative

average values of bulk system hydraulic conductivity that can be used to model the theoretical hydraulic behaviour of the system. A single value approximation of a property such as hydraulic conductivity, that is neither intensive nor extensive, is not appropriate when the value varies by several orders of magnitude over a small scale (Binley et al., 1989).

3.5.2. Models of HSSF TW Hydrodynamics

The hydrodynamic behaviour of HSSF TWs is said to be somewhere between that of a Plug Flow Reactor (PFR) (whereby dispersion is zero and all flow is resident in the system for the design hydraulic residence time) and a Continually Stirred Tank Reactor (CSTR) (whereby dispersion is infinite and flow is instantaneously mixed throughout the reactor volume upon entering the system). Numerous hydrodynamic models have been used with varying success to try and simulate the true hydrodynamic performance of HSSF TWs. Many of these are summarised in **Table 3-6** which includes model variations such as closed form approximations to the advection-dispersion equation (ADE), coupling of the ADE with solute retardation and storage equations, multiple ADE flow-path models, Finite Element Analysis (FEA) solutions to the ADE, empirical data-fits and Tanks-In-Series (TIS) models.

The TIS model will be used in this study to allow data-fitting to RTDs. The TIS approach is considered state of the art due to the closeness of fit that it reportedly achieves (Kadlec and Wallace, 2010). Several authors have used parallel TIS models with two or more branches to improve the accuracy of fit to RTDs and emulate preferential flow-paths in the system (Marsili-Libelli and Checchi, 2005, Wang and Jawitz, 2006). Others have included pure plug-flow phases in series with TIS modules to recreate the delay often seen between injection and detection (Marsili-Libelli and Checchi, 2005, Chazarenc et al., 2003). A semi-infinite stage TW model that simulated dead zone storage was produced by Werner and Kadlec (2000). The model of Werner and Kadlec (2000) is based on Levenspiel's Model G (Levenspiel, 1999) and models the TW as 100 TIS, with each element able to exchange solute with an independent side-stream CSTRs.

Table 3-6 A summary of the various models which have been used to describe the hydrodynamic performance of Subsurface Flow TWs. The table indicates which models are Plug Flow (PF), Plug Flow with Dispersion (PFD), Tanks-in-Series (TIS), Advanced Plug Flow with Dispersion (PFD+) and Advanced Tanks-in-Series (TIS+), and also gives a brief description. Table continued overleaf.

Reference	PF	PFD	TIS	PFD+	TIS+	Notes
King *et al.* (1997)				X		One PFR followed by three PFDs in parallel
Chen *et al.* (1999)		X	X			Determines a number of TIS depending on length, flow-rate and dispersion obtained from tracer tests. Provides a semi-physical ascription for n TIS, and a semi-analytical solution to the ADE
Werner and Kadlec (2000)					X	100 TIS model with coupled equation for solute exchange/storage
Wynn and Liehr (2001)			X			1*CSTR, Darcy's Law and P-ET considerations to calculate water budget. No RTD support
Grismer *et al.* (2001)	X	X	X			Compared data-fits for a tracer RTD using all three models
Mashauri and Kayombo (2002)	X					Assume plug flow for the purposes of treatment model evaluation – not based on an actual RTD. Extra term for sedimentation
Martinez and Wise (2003)				X		PFD model with one and two storage zones
Chazarenc *et al.* (2003)		X	X		X	Compared data fits for classical PFD and TIS models, and then a modified TIS model with parameters for P-ET and a time lag
García *et al.* (2004)		XX	X			Two PFD models, open-open and closed-closed boundary conditions One TIS model with a delay
McGechan *et al.* (2005)		X				Assume PFD in a simple finite difference model, for purposes of treatment model evaluation – not based on an actual RTD. Plug flow hydraulics. 6 path model
Mayo and Bigambo (2005)	X					Assume plug flow for the purposes of treatment model evaluation – not based on an actual RTD

Table 3-6 A summary of the various models which have been used to describe the hydrodynamic performance of Subsurface Flow TWs. The table indicates which models are Plug Flow (PF), Plug Flow with Dispersion (PFD), Tanks-in-Series (TIS), Advanced Plug Flow with Dispersion (PFD+) and Advanced Tanks-in-Series (TIS+), and also gives a brief description.

Reference	PF	PFD	TIS	PFD+	TIS+	Notes
Marsili-Libelli and Checchi (2005)					X	One model with 3TIS + a PF phase One model with 3*TIS + 1 stage with 2 CSTRs in parallel + PF phase
Rousseau *et al.* (2005a)			X			2*CSTR, Darcy's Law, P-ET and overland flow via Manning's Equation (where flow backs up, it does not infiltrate). No RTD support
Maloszewski *et al.* (2006)		X		X		One model with single PFD plus storage One model with three to four PFDs in parallel
Suliman *et al.* (2006b)		X				PFD equations with retardation factor used to fit RTD from lab-scale HSSF TW
Wang and Jawitz (2006)		X	X	X	X	Compared four modelling techniques, PFD, PFD with storage, one and two path TIS
García et al. (2007)			X			CSTR network with four stages in series, each stage has two CSTR in parallel, with flow splitter and combiner for each stage.
Freire *et al.* (2009)					X	3 * CSTR, one of variable volume to simulate flooding, and one as a side storage exchange

The TIS model uses principles derived from Chemical Engineering to model the TW as a series of CSTRs by using Fourier Transforms. The RTD from a CSTR can be mathematically represented by introducing a differential operator into the conservation of mass equation for a reactor, and rearranging the equation into a Transfer Function (**Equation 3-40**).

$$c_{out}(t) = \frac{c_{in}(t)}{1 + \tau\, s} \qquad \textbf{Equation 3-40}$$

, where c_{in} (mg/L) is the solute concentration at the inlet, c_{out} (mg/L) is the solute concentration at the outlet, τ (d) is the mean Hydraulic Residence Time (HRT) in the reactor, and s is operator in the Laplace Transform Function. By modelling the input concentration as a unit impulse of mass M_{in} (kg) with Laplace Transform of 1, **Equation 3-40** can be rearranged to give **Equation 3-41**.

$$c_{out}(t) = \frac{M_{in}}{\tau}\left(\frac{1}{\frac{1}{\tau} + s}\right) \qquad \textbf{Equation 3-41}$$

The inverse Laplace Transform of the Transfer Function yields the theoretical RTD formulation for a CSTR, which is an exponential function of time t (d) (**Equation 3-42**).

$$c_{out}(t) = \frac{M_{in}}{\tau} exp \frac{-t}{\tau} \qquad \textbf{Equation 3-42}$$

In the same manner, the RTD response of several CSTRs in series can be shown to be (**Equation 3-43**):

$$c_{out}(t) = \frac{M_{in} n^n t^{n-1}}{\tau^n \Gamma(n)} exp\left(\frac{-n\, t}{\tau}\right) \qquad \textbf{Equation 3-43}$$

where n is the number of CSTRs in series and Γ is the gamma distribution of n. **Figure 3-10** illustrates the shape of the gamma distribution as n tends from 1 to infinity, from which it can be deduced that the RTD of a PFR is equivalent to an infinite number of CSTRs in series. The value of n that best fits the obtained RTD indicates whether the HSSF TW performance

tends more towards a PFR or a CSTR. According to data from Kadlec and Wallace (2010), HSSF TW RTDs can typically be modelled using 10 to 12 TIS.

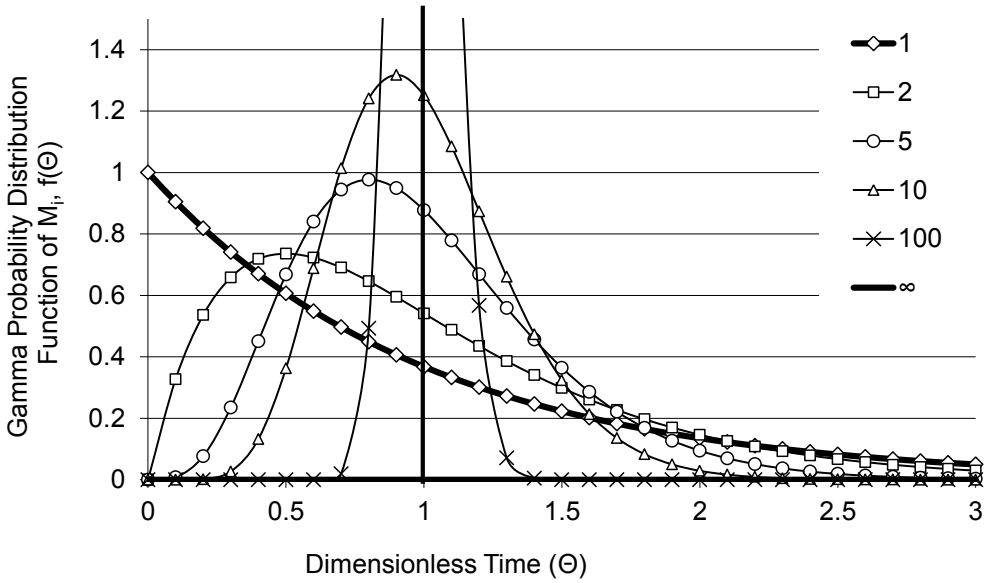

Figure 3-10 The variation of system response, for gamma probability distribution function of a unit impulse over dimensionless time, as the number of tanks-in-series varies from 1 (CSTR) to infinity (PF).

3.5.3. Models of HSSF TW Clogging

An early attempt to model clogging in Vertical Flow (VF) TWs assumed that porosity was diminished cumulatively by the volume of influent suspended solids loaded into the system over time, such that system longevity corresponded to zero porosity (Blazejewski and Murat-Blazejewska, 1997). Langergraber et al. (2003) and Zhao et al. (2004) extended the theory making it applicable to solids fractions with a biodegradable component. Hydraulic conductivity in the system was calculated according to the Kozeny-Carmen equation. Kadlec and Wallace (2010) summarise that the time to clogging t_c (d) calculable using this relationship is given by **Equation 3-39**, where A_W (m^2) is the reactor wetted section, $\dot{s}$ (kg/d) is the influent suspended solids loading rate, ρ_s (kg/m^2) is the density of the wastewater solids, ε is the clean porosity of the reactor, and E (-) is an empirical coefficient that represents the suspended solids removal efficiency for the system.

$$t_c = E\ A_W\ \varepsilon\ \frac{\rho_s}{\dot{s}} \qquad \textbf{Equation 3-44}$$

An alternative approach has been to model the clogging phenomenon using an exponential relationship between loss in hydraulic conductivity and the cumulative applied solids load (Platzer and Mauch, 1997, Hyánková et al., 2006). **Figure 3-11** illustrates the relationships between the hydraulic conductivity k_Φ of the wetland and the cumulative applied load since system start-up s (kg/m^2), for the five aforementioned models of clogging. The relationships can be described using the **Equation 3-45**:

$$k_\Phi = k \,.\exp(-J.s) \qquad \textbf{Equation 3-45}$$

, where k (m/d) is the initial hydraulic conductivity of the wetland media and J is a parameter describing the influence of s on k_Φ. The values of k and J reported for each of these studies are provided in **Table 3-7**. The value of J has a strong dependency on the diameter of the media particles.

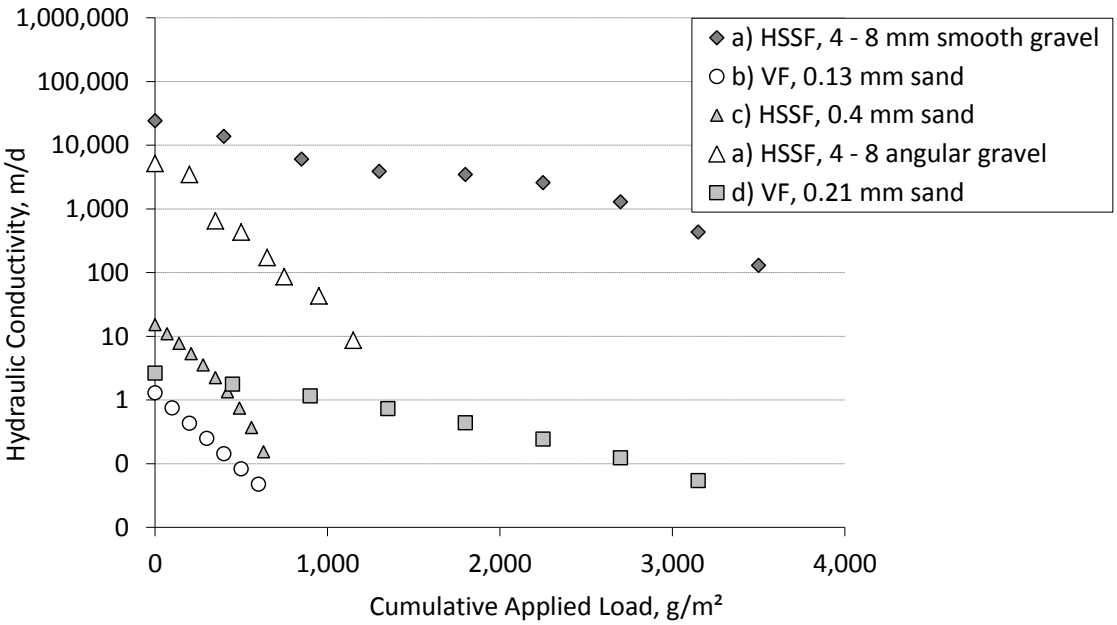

Figure 3-11 The relationship between hydraulic conductivity and cumulative applied load for five Subsurface Flow treatment wetlands with different media. Data from (a) Hyánková et al. (2006); (b) Langergraber et al. (2003) analysed according to Blazejewski and Murat-Blazejewska (1997) (c) Blazejewski and Murat-Blazejewska (1997) with data from Bavor and Schulz (1993); (d) Platzer and Mauch (1997). Reproduced from Nivala et al. (2012).

Table 3-7 The relationship between hydraulic conductivity ***k*** and cumulative applied load ***s*** for five Subsurface Flow treatment wetlands. All relationships are based on Total Suspended Solids (TSS) loading rate, apart from Platzer and Mauch (1997) which is based on Chemical Oxygen Demand (COD). Reproduced from Nivala et al. (2012).

Study	Media	d_{10} (mm)	Loading parameter	Loading rate ($g/m^2.d$)	*k* (m/d)	*J*
Hyánková *et al.*, (2006)	Crushed gravel	4	TSS		25,000	0.0013
	Sand	2	TSS		6,500	0.0056
Platzer and Mauch, (1997)	Sand/bentonite mixture	0.1	COD	6-15	1.3	0.0055
Blazejewski and Murat-Blazejewska (1997) with data from Bavor and Schulz (1993)	Sand	0.3	TSS	70	20.4	0.0071
Langergraber *et al.*(2003) analysed according to Blazejewski and Murat-Blazejewska (1997)	Sand and gravel	0.13	TSS	45	3.2	0.0012

It must be emphasised that the relationships in **Figure 3-11** represent the hydrology of the entire system and do not consider spatial variations within the subsurface or clogging due to biological or chemical factors. Consequently the extent of clogging was under-predicted when one of these models was applied to a pilot-scale VF TW in Austria (Langergraber et al., 2003).

García et al. (2007) adapted a dynamic HSSF TW process dynamics model (Rousseau, 2005) so that rules were included for particle transport, and biomass growth was linked to substrate utilisation. The model was used to explore the extent to which clogging could be mitigated by various physico-chemical pre-treatment options within two pilot-scale HSSF TWs, but was not used for comparison with the actual clogging present in those systems.

Giraldi et al. (2010) developed a 1D FEA model of a VF TW named FITROVERT, which coupled analytical expressions for flow, mass-transport of particulate and dissolved matter, and clogging by biofilm and particulate matter accumulation. The coupling between clogging and hydraulics was achieved using a modification of **Equation 3-27** by O'Melia and Ali (1978), which relates the accumulation of clog matter to loss of media porosity.

3.5.4. Coupled Models of HSSF TW Hydraulics, Hydrodynamics and Clogging

Advanced coupled models of HSSF TW hydrology have been used to represent the interrelationships between hydraulics, clogging and hydrodynamics. These models often use Finite Element Analysis (FEA) software to represent the non-linear realities of physical systems; realities that ordinarily prevent analytical solutions to specific problems from being ascertained. Briefly, FEA involves discretising a system into elemental subdomains and, according to the application of stimuli along the boundaries of the system, solving the mass and momentum balances over the network of elements. Through FEA, highly representative and flexible models can be achieved, although a certain degree of operator expertise is required to achieve meaningful results.

In terms of HSSF TWs, Grismer *et al.* (2001), Fan *et al.* (2008), Ojeda *et al.* (2008), Toscano *et al.* (2009), Wanko *et al.* (2009), Knowles and Davies (2011) and Llorens et al. (2011a) have all presented FEA models that incorporate spatial descriptions of hydrology. Langergraber and Šimůnek (2005) and Giraldi et al. (2010) have presented FEA models of VF TWs hydrology. **Table 3-8** summarises the nature of these FEA models and indicates whether they incorporated descriptions of Darcy's Law, the Richards Equation, clogging, and solute transport; and in how many dimensions the model is applicable. Most authors solve in 2 dimensions and incorporate a solute transport module coupled to Darcy's Law or perhaps a closed-form solution to the Richards Equation (Langergraber and Šimůnek, 2005, van Genuchten, 1980). Richards Equation is a modification of Darcy's Law that uses a transient-state general partial differential equation to describe flow in unsaturated non-swelling soils (Bear, 1979).

Good fit to experimental measurements is generally reported for FEA models; however, these models require expertise that extends beyond a good working knowledge of HSSF TWs and, therefore, do not lend themselves to the creation of widely useful design guidelines.

Table 3-8 A summary of subsurface flow wetland models that have used Finite Element Analysis. The table details which studies incorporated descriptions of Darcy's Law (DAR), Richards Equation (RIC), Solute Transport via the Advection Dispersion Equation (SOL), Clogging (CLO); and in how many dimensions the model was developed.

Reference	DAR	RIC	SOL	CLO	DIM	Notes
Grismer et al. (2001)	X				2	Used Hydrus 2D to determine the flow field through the TW. Assumed constant hydraulic conductivity and ET surface flux. Point source and sink in the top right and bottom left corners
Langergraber (2003), Langergraber and Ŝimůnek (2005)		X	X		2	Uses Hydrus 2D for VF TWs. Considers constant can Genucthen parameters in the Richard's Equation
Fan *et al.* (2008)	X		X		2	Used Fluent
Wanko *et al.* (2009)		X	X		2	Solves for heterogeneous flow fields using mixed hybrid finite element methods
Toscano *et al.* (2009)		X	X		2	Uses Hydrus 2D with HSSF TWs.
Ojeda *et al.* (2008)	X		X		2	Based on the flow and heat code CodeBright. Requires definition of initial water and gas pressure for each node, the wetland hydraulic conductivity, and water depths at inlet and outlet
Giraldi et al. (2010)		X	X	X	2	A VF TW model that considers clogging via the phenomenological model of Ives and Pienvichitr (1965) and Iwasaki (1937)
Llorens et al. (2011a), Llorens et al. (2011b)	X		X		2	A combination of a hydraulic and solute transport model called RetrasoCodeBright. The model also couples HSSF TW process dynamics using the terminology set-forth by Constructed Wetlands Model 1 (Langergraber et al., 2009)

3.6. Novel tools to represent the hydrology of HSSF TWs

The previous review of existing theory and models suggests that a new design tool is needed that more accurately captures the real hydraulic behaviour of HSSF TWs. The specification for the model is as such:

- It must not rely on complex FEA computational tools to achieve good accuracy.
- It must be more representative than simpler calculation methods that are available.
- It must be able to describe how the relationship between clogging and hydraulics varies over time.

With regard to this specification, it is proposed that the model be an algorithm with a closed form solution so that it can be solved using only basic calculation tools. The algorithm will incorporate a spatially varying description of hydraulic conductivity and overland flow, and relate this to how the water table varies longitudinally. The relationship will use parameters based on the overall state of clogging in the system. This will allow the water-table produced by the relationship to change in response to clogging. The derivation of this relationship is given in **Section 3.6.1**.

If the parameters in the relationship are to be based on the overall state of clogging in the system, then a single parameter value is required that adequately quantifies the state of clogging in the system. As discussed, a single value approximation of a property that is neither intensive nor extensive, such as hydraulic conductivity, is not appropriate when the value varies by several orders of magnitude over a relatively small scale. A single value parameter is derived in **Section 3.6.2** that is based on an extensive property - the bulk porosity lost to clog matter. The parameter is called The Clog Factor $\boldsymbol{CF_T}$ and values will be derived from measurements in field-scale HSSF TWs. Statistical analyses will be used to deduce a trend between values of $\boldsymbol{CF_T}$ and the hydraulic conductivity profiles from which they are derived. The trend will allow statistically representative two-dimensional hydraulic conductivity profiles to be recreated for Severn Trent HSSF TWs at particular values of $\boldsymbol{CF_T}$ (i.e. at different stages of clogging). The model will be developed in the two-dimensional vertical-longitudinal plane and neglect transverse variations on the premise that well-functioning HSSF TWs would not develop transverse variations in flow or clogging.

To complete calibration of the parameters in the algorithm, an FEA model of a Severn Trent HSSF TW will be developed in **Section 3.6.3**. The FEA model describes the relationship between the 2D hydraulic conductivity profiles produced by the $\boldsymbol{CF_T}$ values, the flow-rate $\boldsymbol{Q_{in}}$,

the length of overland flow ***f,*** and the water table-profile ***h(x)***. Based on the results, algorithms will be produced that describe how the water table profile varies depending on the value of CF_T. The model will be coupled to a solute transport module to monitor how the hydrodynamic behaviour of the system varies in response to clogging. The obtained RTDs will be fitted to a Tanks-In-Series hydrodynamic model and CF_T will be correlated to the number of tanks, ***n***. The overall deliverable will be an algorithm specifically calibrated to Severn Trent HSSF TWs that can model how the water table profile in the system changes as the Clog Factor varies.

3.6.1. An improved model of HSSF TW hydraulics

A novel model is now proposed with improved representation of HSSF TW hydraulics. Some simplifications are required to achieve an analytical solution, and therefore the expression will be derived for the one dimensional longitudinal plane, similar to models described in **Section 3.5**. Note that the effects of evapotranspiration and precipitation are neglected, but could be incorporated if desired.

To begin with, it is proposed that the relationship between longitudinal distance and bulk media hydraulic conductivity in HSSF TWs can be described using an exponential relationship. This is based on the fact that media clogging in Severn Trent HSSF TWs is primarily due to solids filtration, and solids filtration efficacy in linear filters can be described using an exponential relationship, according to the phenomenological formulations of Ives and Pienvichitr (1965), Einstein (1968) and Iwasaki (1937) (**Equation 3-46**).

$$k_{\Phi}(x) = k.a\, e^{bx} \qquad \textbf{Equation 3-46}$$

, where ***k*** is the clean hydraulic conductivity of the gravel and $k_{\Phi}(x)$ is the longitudinally varying clogged media hydraulic conductivity. Physically, ***a*** (-) represents the reduction from clean media hydraulic conductivity at the inlet of the bed, and ***b*** (-) describes the influence of clogging downstream of the inlet. The parameter values ***a*** and ***b*** will be calibrated to reproduce water table profiles observed in practice.

Secondly, the bed is divided into two theoretical subzones: an upstream and downstream region. Overland flow applies over the upstream region and extends from the inlet by distance ***f***, whereas no distributed fluxes influence the water table in the downstream region. The flow-rate into the upstream region can be described accordingly:

$$Q_{in} = \int_0^f w_r . dx \qquad \textbf{Equation 3-47}$$

where $\boldsymbol{w_r}$ is the vertical recharge into the water table at some distance from the inlet ***x***. It is assumed that a dual hydrological regime is present, as discussed earlier, such that there are two water levels in the system: the overland flow; and a subsurface water table with horizontal flow. According to the Green-Ampt Equation (**Equation 3-14**) the vertical recharge rate through the surface layer is equivalent to the hydraulic conductivity such that:

$$Q_{in} = \int_0^f k . a\, e^{bx} . dx \qquad \textbf{Equation 3-48}$$

and therefore the extent of overland flow would be:

$$f = \frac{1}{b} ln\left(\frac{Q_{in}\, b}{k\, a} + 1\right) \qquad \textbf{Equation 3-49}$$

The downstream water table profile is deduced first and is described using a formulation similar to the derivation of the Dupuit assumption, such that continuity and energy balance are observed, but modified to account for the longitudinal variation in hydraulic conductivity. Neglecting fluxes via precipitation and evapotranspiration, if mass is to be conserved then the cross-sectional flow rate at a longitudinal point in the system ***x*** must be equal to $\boldsymbol{Q_{in}}$:

$$Q_{in} = \bar{u}(x)h(x) \qquad \textbf{Equation 3-50}$$

, where $\bar{u}$ is the depth averaged longitudinal velocity and h is the water depth in the subsurface. Following the derivation of Dupuit, by substituting Darcy's Law (**Equation 3-8**) into **Equation 3-50**, but rewriting k using **Equation 3-46**; and substituting **Equation 3-49** into **Equation 3-50** by rearranging in terms of Q_{in}; it is possible to write the following expression (**Equation 3-51**):

$$\frac{2}{b}\left[e^{-bx} - e^{b(f-x)}\right] = \frac{\partial(h^2)}{\partial x} \qquad \textbf{Equation 3-51}$$

Integrating **Equation 3-51** with respect to x yields the following expression that describes the variation of the subsurface water table depth downstream of the overland flow region:

$$\lim_{f \to L} h^2(x) = \frac{2}{b^2}\left[e^{-bL} + e^{b(f-x)} - e^{-bx} - e^{b(f-L)}\right] + h_{out}^2 \qquad \textbf{Equation 3-52}$$

The water depth at the subzone transition, h_f can be calculated as:

$$h_f^2 = \frac{2}{b^2}\left[e^{-bL} + 1 - e^{-bf} - e^{b(f-L)}\right] + h_{out}^2 \qquad \textbf{Equation 3-53}$$

Next considering the upstream region: by applying the limitless version of **Equation 3-48** and performing a similar mathematical procedure as for the downstream region it can be shown that the flow rate up to a point x can be related to the hydraulic gradient according to:

$$\frac{2}{b}\left[e^{-bx} - 1\right] = \frac{\partial(h^2)}{\partial x} \qquad \textbf{Equation 3-54}$$

, such that the following expression can be derived to describe how the water table profile varies up to point ***f***:

$$\lim_{0\to f} h^2(x) = \frac{2}{b^2}\left[e^{-bf} - e^{-bx} + b(f-x)\right] + h_f^2 \qquad \textbf{Equation 3-55}$$

Therefore, an analytical solution for water height at the inlet can be published when a value for ***f*** is substituted into **Equation 3-56**, by using **Equation 3-49** and parameter values for $\boldsymbol{Q_{in}}$, ***k, a*** and ***b***. The resulting water table profile corresponds to the variable hydraulic conductivity field and overland flow region common to Severn Trent HSSF TWs.

$$h_{in} = \sqrt{\frac{2}{b^2}[e^{-bf} + bf - 1] + h_f^2} \qquad \textbf{Equation 3-56}$$

Further integration and addition of **Equation 3-52** and **Equation 3-55** with respect to ***x*** yields a closed form solution for $\boldsymbol{A_W}$. The resulting expression is unwieldy, however, and it is advisable to plot the water table profile at numerous ***x*** values using spread-sheet tools, and thus obtain the integral numerically.

3.6.2. A novel single metric to quantify clogging in HSSF TWs

A novel metric, the Clog Factor ***CF***, is proposed as a single value parameter that adequately represents the hydraulic behaviour of clogged HSSF TWs. The ***CF*** is a novel metric that converts hydraulic conductivity, a property that is neither intensive nor extensive, into an intensive bulk property that can be representatively averaged for subsequent analysis. It can be used to describe the state of clogging in any porous media flow system but has been derived intentionally to explore clogging dynamics in HSSF TWs. The ***CF*** is based on the Kozeny-Carman equation:

$$k = \frac{\rho g d^2 \varepsilon^3}{150\,\mu\,(1-\varepsilon)^2}$$ **Equation 3-57**

The Kozeny-Carman equation is applicable to porous media composed of spheres with homogeneous diameter. However, as discussed in **Section 2.3.3**, gravel particles used in HSSF TWs will generally be non-spherical and have a distribution of diameters around the sample mean particle diameter d_{50}. According to Kadlec and Knight (1996), Idelchik and Fried (1986) found that the hydraulic conductivity of crushed angular media is one third of the hydraulic conductivity of spherical media with equivalent size. Work by Masch and Denny (1966) found that media with a particle size variance of 50 % around d_{50} has half of the hydraulic conductivity of media with homogeneous particle diameter d_{50}. Kadlec and Knight (1996) provide a modification to **Equation 3-57** that accounts for the effects of media non-ideality, based on media with porosity 0.35 and particle size distribution variance of 50 % around d_{50}:

$$k = \frac{\rho g d_{50}^2 \varepsilon^{3.7}}{255\,\mu\,(1-\varepsilon)}$$ **Equation 3-58**

The clean media hydraulic conductivity predicted by **Equation 3-58** is 82 % lower than the clean media hydraulic conductivity predicted by **Equation 3-57**. The same result can be achieved by assuming that porosity in **Equation 3-57** is reduced from 0.35 to 0.225. In other words, based on the calculation of **Equation 3-57**, the effect of particle size distribution and particle angularity is to reduce hydraulic conductivity of the ideal sample with known d_{50} and ε to a hydraulic conductivity that corresponds to an effective porosity ε_Φ of 0.225. This principle is used to derive the Clog Factor ***CF***, which is defined as one less the ratio of clogged porosity to initial porosity ε (**Equation 3-59**), whereby a value of zero (0) indicates no clogging and a value of one (1) indicates complete clogging.

$$CF = 1 - \frac{\varepsilon_\Phi}{\varepsilon}$$ **Equation 3-59**

Due to non-ideal media characteristics it is not realistic to achieve Clog Factors close to 0. Based on **Equation 3-59,** if non-ideal media has ε_Φ of 0.225 but actual ε of 0.35 (as in the

example above), the sample has a ***CF*** of 0.36. The interpretation of this result is that the practical hydraulic conductivity of the media corresponds to a reduction of 36 % of available pore volume, as calculated using **Equation 3-57**. Any additional increase in the value of ***CF*** above 0.36 will be due to clogging. Using this theory, experimentally measured values of hydraulic conductivity and the median particle diameter of the clean gravel can be used to calculate effective clogged porosities ε_{Φ} in **Equation 3-57**.

It is important to emphasise that ***CF*** is a relative measure of clogging based on the idea that d_{50} is a constant but ε decreases as the media clogs, and the Kozeny-Carman equation can be used to indicate how the hydraulic conductivity of the media changes as the porosity is reduced. The limitation of this assumption is that the Kozeny-Carman equation is derived for clean media and **Equation 3-57** may not be appropriate for describing the relationship between hydraulic conductivity and media properties in clogged media. Practically, clogging will change the effective d_{50} of the media due to biofilm growth on the surface of media particles. However, it has been assumed that the majority of clogging in Severn Trent HSSF TWs is due to solids filtration and retention in pore spaces, and therefore, the generalisation that clogging can be represented by a change in ε is considered acceptable. Finally, the ***CF*** may not represent the practical clogged porosity, as it has been shown that reductions in hydraulic conductivity often do not correspond to reductions in porosity, and rather it is the form and nature of clogging that are important (Tanner et al., 1998, Caselles-Osorio et al., 2007, Platzer and Mauch, 1997). The ***CF*** should be considered a relative indication of the reduction of free-volume available for flow, as opposed to an accurate measure of porosity reduction.

By measuring ***CF*** values at numerous equally spaced points in the system, and taking the arithmetic mean, it is possible to approximate a bulk system Clog Factor value CF_T that indicates the total reduction of reactor volume effectively lost to clogging and media non-ideality (**Equation 3-60**). CF_T can be used as a benchmarking tool to compare relative states of clogging in different systems.

$$CF_T = \frac{1}{n}\sum_{i=0}^{n} CF \qquad \textbf{Equation 3-60}$$

To summarise, the advantages of ***CF*** are:

- Intensive bulk property that can be applied to any scale of porous media flow system
- Non-dimensionalises data so that comparisons can be performed between systems with different dimensions and media sizes
- Highlights deviations from theoretical clean conductivity due to both clogging and media non-ideality
- Allows reasonable statistical comparisons where orders of magnitude changes in hydraulic conductivity would skew a data set
- Allows single-parameter values to be published to indicate the health of bed at a point in time

Conversion of hydraulic conductivity data to Clog Factors and subsequent analysis via Analysis of Variance (ANOVA) will allow a more robust insight into the hydraulics of HSSF TWs. The ANOVA test compares means and distributions of data sets to see whether a significant difference (at the 95% confidence level) exists between data sets. Furthermore, the ANOVA test disaggregates the variance in a dataset into the relative contributions from different factor, such that the influence of each factor on the data can be delineated. The factors to be investigated include $\boldsymbol{CF_T}$, transverse position, longitudinal position and vertical position. This will allow longitudinal and vertical variations in ***CF*** to be related to bulk system $\boldsymbol{CF_T}$, such that the relationship can be used to recreate statistically representative two-dimensional hydraulic conductivity profiles of HSSF TWs that correspond to a particular value of $\boldsymbol{CF_T}$ (i.e. at a particular stage of clogging).

3.6.3. A Finite Element Analysis Model of HSSF TW Hydrology

Modelling is achieved using COMSOL Multiphysics 3.5 FEA software (COMSOL A.B., Sweden) by coupling several different physical sub-models. The hydraulic model is represented in **Figure 3-12** and depicts two subdomains and eight boundaries numbered according to the bold font. A full list of the boundary conditions is given in **Table 3-9** and the sources of modelling parameters are disclosed in **Table 3-10**. The upper subdomain represents vertical saturated flow through the surface layer up to a distance ***f*** from the inlet and is governed by Darcy's Law. It is assumed that the surface layer accumulates to a depth of 0.1 m above the 0.6 m depth of gravel in the system. It is assumed that the upper subdomain is unsaturated between ***f*** and the outlet. The lower subdomain represents the horizontal saturated flow

through the subsurface and is governed by Darcy's Law. It is assumed that the lower subdomain is unsaturated above the water table height.

The minimum depth of water in the system corresponds to the outlet height h_{out} and flux is only permitted through boundary 7. Wastewater is applied on boundary 3 over a region that extends from the inlet to a distance representative of the ponding length f. The infiltration rate through the upper sub-domain is dependent on the hydraulic conductivity of the upper sub-domain, as described by the Green-Ampt Equation (**Equation 3-14**). It is assumed that the longitudinal profile of outward flux from boundary 4 is identical to the longitudinal profile of inward flux into boundary 5. The pressure head is specified as 0 along boundary 4 and boundary 5. This creates vertical flow between boundary 3 and 4, through the region bounded by f, and allows the shape of boundary 3, 4 and 5 to change in order to find an equilibrium geometry that satisfies boundary conditions and subdomain conditions. This is achieved using an additional 'moving-mesh' model available in COMSOL 3.5, which allows mesh movement depending on certain physical criteria. Conditions exist to allow the height of boundary 5 to exceed the height of boundary 4, at which point the two hydraulic subdomains become one horizontally flowing subsurface water table. The height of boundary 5 can only exceed the height of boundary 3 when f is equal to L. An iterative solver is used to find the length of f that produces the flow-rate Q_{in} through the system.

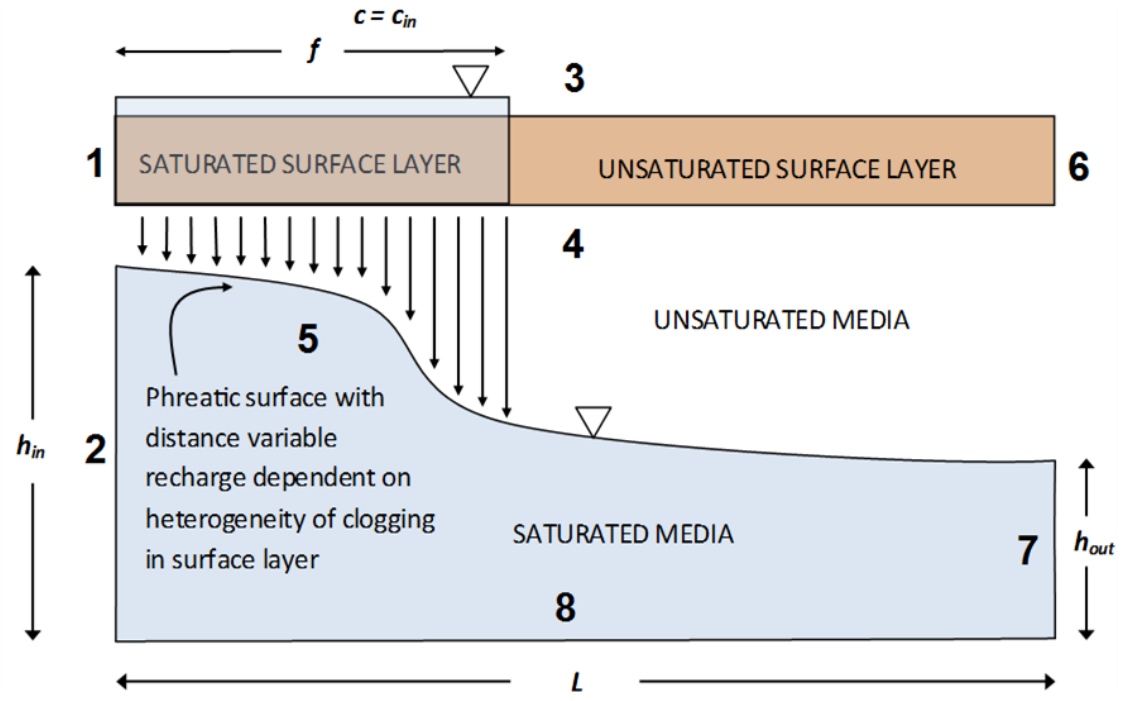

Figure 3-12 A schematic of the FEA model of a Severn Trent HSSF TW, detailing the boundary and subdomain conditions of the hydraulic modules. Adapted from Knowles and Davies (2011).

The hydrodynamic response to the hydraulic model is found using a reactive transport model that links the volumetric concentration of wastewater constituents with velocity using the advection-dispersion equation. The reactive transport model applies over both sub-domains. The boundary conditions for the reactive transport model specify the volumetric concentration of solids in the influent wastewater c_{in} across the ponding length f, and assume an advective flux condition exists at boundary 3 and boundary 7. It is assumed that the longitudinal inward flux profile to boundary 5 is identical to the longitudinal outward flux profile from boundary 4. All other boundaries have a zero-flux condition.

Table 3-9 A full list of boundary conditions prescribed in the model. The boundary numbers are consistent with labelling in **Figure 3-12**.

Darcy's Law Boundary Conditions – Lower Subdomain		
Boundary	**Condition**	**Description**
2,8	$\mathbf{n}.[k\nabla(h)] = 0$	Neumann – zero flux
5	$\mathbf{n}.[k\nabla(h)] = -v_{r_{(\partial\Omega_3)}}$	Neumann – inward flux
7	$h_{(x)} = h_{out}$	Dirichlet – outlet height
1,3,4,6		Does not apply
Darcy's Law Boundary Conditions – Upper Subdomain		
Boundary	**Condition**	**Description**
1,6	$\mathbf{n}.[k\nabla(h)] = 0$	Neumann – zero flux
3	$h_{(0<x<f)} = 0.7$ $h_{(x\geq f)} = h_{(\partial\Omega_4)}$	Dirichlet – overland flow
4	$h_{\left(0<x<f;\, h_{(\partial\Omega_5)}<0.6\right)} = 0.6$ $h_{\left(x\geq f;\, h_{(\partial\Omega_5)}\geq 0.6\right)} = h_{(\partial\Omega_5)}$	Dirichlet – capillary fringe
2,7,5,8		Does not apply
Advection Dispersion Equation Boundary Conditions		
Boundary	**Condition**	**Description**
1,2,6,8	$-\mathbf{n}.[-\varepsilon D\nabla c + \bar{\mathbf{U}}c] = 0$	Neumann – zero flux
3	$c_{(0<x\leq f;t\leq 1)} = c_{in}$	Dirichlet – influent solids concentration
4, 7	$-\mathbf{n}.[-\varepsilon D\nabla c] = 0$	Neumann –advective flux only
5	$-\mathbf{n}.[-\varepsilon D\nabla c + \bar{\mathbf{U}}c] = \bar{\mathbf{U}}c_{(\partial\Omega_4)}$	Neumann –inward flux
Deformed Mesh Boundary Conditions		
Boundary	**Condition**	**Description**
1,2,6	$dx = 0$	Horizontally constrained
3,7,8	$dx = 0$ $dy = 0$	Fully constrained
4	$dy = h - y$	Vertical displacement until ψ = 0
5	$dy_{(y<0.7)} = h - y$	Vertical displacement until ψ = 0 up to a maximum of 0.7 m

Table 3-10 A list of the parameters included in the model, along with the references from which the parameters were obtained and justifications for use. Adapted from Knowles and Davies (2011).

Description	Symbol	Units	Value	Reference and notes
Width-average flow-rate	Q_{in}	m^2/d	11.5	Knowles et al. (2010) – based on conditions in a typical HSSF TW with mature hydrology
Outlet Height	h_{out}	m	0.4	
Ponding Height	H	m	0.7	
Gravel surface		m	0.6	
Molecular diffusion coefficient	D	m^2/s	1e-9	Langergraber (2003)– based on sandy gravel media with d_{10} of 0.13 mm
Longitudinal dispersivity in upper subdomain	σ_L	m	0.0125	
Transverse dispersivity in upper subdomain	σ_T	m	0.01	
Longitudinal dispersivity in lower subdomain	σ_L	m	0.1	Cooke and Rowe (2008) – based on gravel diameter of 6 mm
Transverse dispersivity in lower subdomain	σ_T	m	0.1	

3.7. Conclusions

The aim of this Chapter was to enhance the theory that exists to describe the relationship between hydraulics, hydrodynamics and clogging. Through a review of existing theory and models it was identified that an algorithm was required that better describes the true hydraulic behaviour of HSSF TWs, including overland flow, spatial variations in hydraulic conductivity and changes in hydraulic properties over time due to clogging. The model should also be simple enough to be solved using simple calculation methods. Incorporation of this hydraulic model into wetland treatment models would improve the ability to predict how wetland treatment performance will change over time.

The derivation of the model required three separate components:

1. A 1D algorithm, as described in **Section 3.6.1**, with two parameters to be calibrated that describe how the water table profile varies in the longitudinal direction. The algorithm incorporates: a) an exponential relationship to describe the longitudinal hydraulic conductivity profile; and b) the influence of overland flow.

2. A single value parameter to describe the extent of clogging in the system, the Clog Factor CF_T as introduced in Section **3.6.2**, which is an intensive bulk property representing the effective porosity lost to clogging. The Clog Factor avoids problems that have previously been encountered trying to derive equilibrium hydraulic conductivity values to represent the bulk effect of spatially varying hydraulic conductivity profiles. The parameter calibration will be deduced from experimental measurements of Severn Trent HSSF TWs and will be specific to the performance of these systems.
3. A 2D FEA model, as introduced in **Section 3.6.3**, which describes the interaction between HSSF TW hydraulics and hydrodynamic behaviour. The model will be used to find the relationship between parameter values a and b and values of CF_T, so that these relationships can be used in the 1D algorithm of **Section 3.6.1**.

The approach to be taken can be summarised as follows:

1. Perform experimental surveys to measure the spatial variations of hydraulic conductivity in field-scale HSSF TWs.
2. Convert all hydraulic conductivity measurements to CF values and derive bulk CF_T values for each reactor.
3. Statistically analyse the obtained values of CF to find the relationship between CF_T and the longitudinal and vertical variation of CF.
4. Use the statistical relationship to recreate hydraulic conductivity profiles that correspond to values of CF_T. These profiles will be overlain onto the FEA model subdomain.
5. Apply boundary conditions on the FEA model for flow and solute concentration to determine the values of f, h_{in}, n and τ that correspond to the modelled hydraulic conductivity profiles.
6. Use **Equation 3-49** and **Equation 3-56** to calibrate parameter values for a and b that closely recreate the modelled water table profile for corresponding values of CF_T, Q_{in}, h_{out} and k.

A method is now required that enables the spatial variation of hydraulic conductivity in a field-scale HSSF TWs to be determined, and will hence allow Clog Factors to be derived.

4. Experimental method

The information reviewed unto now has emphasised the need to appreciate better the magnitude and distribution of clogging in Horizontal Subsurface Flow Treatment Wetlands (HSSF TWs). However, progress has been hampered because a simple technique to obtain this information has been unavailable. From the information detailed in **Chapter 2** it is possible to identify constraints that an appropriately designed method would take into account. **Chapter 3** emphasised the need for a method that can delineate horizontal and vertical variations in hydraulic conductivity. **Table 4-1** provides the desired specification for an experimental method that measures clogging in HSSF TWs, based on the technical requirements for the method and the project specific requirements of Severn Trent.

Table 4-1 Technical and project specific requirements for a field method to measure distribution of clogging in HSSF TWs

Technical Requirements
Tests will need to be performed *in situ* because the non-cohesive nature of gravel precludes tests that would disturb the sample during extraction and risk rendering the sample unrepresentative.
The method should be suitable for a large range of hydraulic conductivities. **Table 3-2** indicated that the range of hydraulic conductivities within a system may span several orders of magnitude (between 1 m/d and 25,700 m/d) and will vary between system depending on age, design and operation.
The tests must measure hydrological variations in all three dimensions as preferential clogging profiles develop longitudinally, transversely and vertically.
Project Requirements
Tests must not take more than 1 week and be low cost so that numerous beds can be profiled during the study period and with the available budget.
Tests must be portable and simple enough such that the test is performable by one operator under a range of site conditions.
The test must not interfere with normal system operation and must be executable in a safe fashion in accordance with Severn Trent policy.

The field of hydrology has provided numerous experimental techniques to assess clogging in natural porous media flow systems, such as groundwater aquifers. Three major groups of established experimental techniques are hydraulic conductivity tests, clogged media characterisation and hydrodynamic visualisation. **Section 4.1** will review the existing techniques within these categories, some of which have previously been applied to HSSF TWs, and will explain why they do not satisfy the entire specification stipulated in **Table 4-1**.

Section 4.2 will describe the development, principle of operation and experimental accuracy of The Aston Permeameter; a purpose made device that allows the three dimensional hydraulic conductivity profiles of HSSF TWs to be measured *in situ*.

4.1. Existing Techniques for Assessment of clogging in Subsurface Flow TWs

In general, there are three ways to measure the extent and impact of clogging in porous media and each approach provides information that the others cannot. All three approaches may be required to fully understand the behaviour of a clogged HSSF TW:

1. Measuring the hydraulic conductivity of the clogged media indicates the severity of clogging
2. Characterising the physical properties of the media and clog matter indicates what is causing clogging
3. Visualising flow hydrodynamics reveals the effect of clogging on flow.

4.1.1. Hydraulic Conductivity Measurements

Hydraulic conductivity methods include laboratory methods such as axial and anisotropic permeameters, and *in situ* methods such as water level surveys, pump tests, borehole tests, infiltration tests and slug tests.

Laboratory permeameters are either flexible or rigid wall and constant or falling head. Generally, rigid wall constant head permeameters are best suited for high hydraulic conductivity media like gravel (Daniel, 1994, BS-ISO-17313, 2004). These methods are only able to determine hydraulic conductivity in the axial direction of flow. However, recent laboratory methods have been developed to allow anisotropic hydraulic conductivity to be evaluated in extracted soil samples (Renard et al., 2001). One such method called the

Modified Cube Method has been applied to measure anisotropy in natural wetland peat samples (Beckwith et al., 2003, Kruse et al., 2008, Rosa and Larocque, 2008).

The non-cohesive nature of gravel makes it difficult to remove undisturbed samples from the field for representative laboratory testing (Ranieri, 2003). A few researchers have attempted to extract intact cores by freezing the media with liquid nitrogen (Kadlec and Watson, 1993), or by injecting temporary jellification agents that can subsequently be chemically or thermally liquefied. However, application of potentially polluting chemicals to final stage wastewater treatment reactors is prohibited by Severn Trent Water policy. Most wetland researchers have relied on *in situ* methods that were developed for cohesive unsaturated geological material, such as soils, with hydraulic conductivities far below those usually measured in gravel beds (ASTM-D5126, 2004). This may explain why direct measurements of HSSF TW gravel hydraulic conductivity are lacking.

Regarding *in-situ* methods, the hydraulic conductivity profile of HSSF TWs has predominantly been estimated from Darcy's Law, by measuring the corresponding water table height at different points in the bed. Often referred to as water table surveys, these methods were first suggested by Childs (1952) for evaluation of aquifer hydraulic conductivity under steady state conditions. Sanford et al. (1995b) question the accuracy of using hydraulic gradient measurements, stating that small variations in measured hydraulic levels can cause large discrepancies in reported results. Indeed, Kadlec and Watson (1993) only suggest accuracy of surveying techniques to 10 mm. Watson and Choate (2001) employed a dumpy level to try and improve accuracy, quoting an associated measuring error of ±1.52 mm. However, when surveying four field scale HSSF TWs, changes in the water table height as low as 1 mm per 1 m longitudinal interval were measured, thus calling into question the limiting accuracy of this method.

The theory introduced in **Chapter 3** explains that Darcy's Law cannot account for the varying thickness of the water table resulting from the groundwater energy balance (Bear, 1979, Oosterbaan et al., 1996). Therefore, calculations of hydraulic conductivity made using this form of Darcy's Law and data from water table surveys will never be accurate. Furthermore, hydraulic conductivity values derived from water table surveys can only provide an approximation of bulk hydraulic conductivity in the flow direction. It is not possible to resolve hydraulic conductivity variations in all three planes, thus shrouding potentially important vertical variation of hydraulic conductivity (Dittrich, 2006).

Well pumping tests are often used to assess the bulk hydraulic conductivity of large-scale aquifer materials (Theis, 1935). These tests typically contain simplifications that render them incapable of resolving hydraulic conductivity variations in all three planes. According to the solution of Theis (1935) it is convenient to simplify the flow field to 2D and neglect variations in the vertical direction: the aquifer depth usually being shallow in comparison to the radial influence of the well test (Bear, 1979). As discussed for water table surveys, such an assumption is unsuitable when considering HSSF TW hydrology. Furthermore, the high conductivity of gravel means that a large pumping rate is required to produce enough head-loss so that differences in water depth between sampling points can be measured to reasonable accuracy. This was achieved in three HSSF TWs by Sanford et al. (1995a), who dropped the water level control device so the bed rapidly emptied, and monitored the cone of depression inside the system over time. Values from the experiment compared well with a second method, the 'cumulative discharge technique', which calculates hydraulic conductivity from the varying discharge of the system over time (Sanford et al., 1995a). Both methods require interruption to normal operation as the bed must be emptied for data analysis, which makes the methods unsuitable for use on Severn Trent sites.

Borehole tests were the first *in situ* methods for localised measurement of hydraulic conductivity, and involve making an auger hole into the porous material, adding water above the water table and monitoring the discharge rate through the borehole walls (Diserens, 1934). This test requires that the media be cohesive so a borehole structure is maintained during saturation, which is not possible with clean gravels. Luthin and Kirkham (1949) explain that the measured hydraulic conductivity is the composite of the entire soil depth and significant vertical variation of hydraulic conductivity may be shrouded by the homogenised result. Ranieri (2003) used a soil borehole testing apparatus called the Guelph Permeameter (Reynolds and Elrick, 1986) to survey a gravel bed HSSF TW in Italy. Hydraulic conductivity values measured with the Guelph Permeameter ranged from 190 m/d to 610 m/d, which are relatively low hydraulic conductivity values for gravel and would typically be indicative of clogging. However, the measured values are above the practical measurement range of the device (1 m/d to 90 m/d), which calls into question whether the measured values actually represent the limitations of the Guelph Permeameter rather than the true hydraulic conductivity of the media. Langergraber et al. (2003) used the Guelph Permeameter to measure the hydraulic conductivity of a sand-gravel media in a Vertical Flow Treatment Wetland. The sand-gravel media had clean hydraulic conductivity that was within the suitable range for measurement by the Guelph Permeameter.

Disc permeameters used in infiltration tests are generally unsuitable for HSSF TWs as they only measure vertical infiltration rates through the media surface (ASTM-D3385, 2003). Perhaps in Severn Trent HSSF TWs that are susceptible to surface clogging and overland flow, double ring infiltrometry could be used to determine the ability of the surface to absorb surface flow. However, these tests will reveal nothing about the subsurface hydrology and are mainly for determining the ability of surface flow to infiltrate through unsaturated porous materials (Benson and Gribb, 1997).

Slug tests involve driving a piezometer tube into the media down to the depth where measurement is desired (Luthin and Kirkham, 1949). A 'slug' of water is then added through the piezometer to create either a falling or constant head of water above the water table (Bouwer and Rice, 1976). The discharge through the end of the tube into the media is monitored, and the hydraulic conductivity calculated according to piezometer shape factors (Hvorslev, 1951). As the test indicates hydraulic conductivity in the immediate vicinity of the tube, it is possible to detect hydraulic conductivity variations in all three planes by repeating the test at several depths across numerous locations (Surridge et al., 2005). However, the apertures on the piezometer need to be large in comparison to media diameter. For gravel, the required aperture size would necessitate an impractically large pipe.

By using an adaptation of the method proposed in the Naval Facilities Soil Mechanics Design Manual (NAVFAC, 1986) it has been possible to directly determine gravel conductivity in HSSF TWs in Catalonia (Caselles-Osorio and García, 2007, Caselles-Osorio et al., 2007, Pedescoll et al., 2009). An open ended tube is used such that the piezometer encases the sample to be tested. It is not possible to easily delineate variations in vertical conductivity because the method measures the vertical conductivity of the entire gravel core. However, the method introduced by Caselles-Osorio and García (2007) is the only existing successful method to directly measure the hydraulic conductivity of media used in HSSF TWs.

From the above review it is apparent that no *in situ* methods are available that allow the hydraulic conductivity profile of high conductivity non-cohesive media, such as gravel, to be measured in three dimensions.

4.1.2. Clog Matter Characterisation

Techniques that measure the properties of clog matter include assays of accumulated solids, direct porosity measurements, Time Domain Reflectometry, Capacitance Probes and Ground Penetrating Radar.

Several authors have directly measured the solids that have accumulated in the void spaces of the porous medium as a way of quantifying clogging (Tanner et al., 1998, Caselles-Osorio et al., 2007). This is achieved by measuring the dried mass of clog matter that can be washed from samples taken from the wetland. If desired, ignition tests above 550°C can then be used to calculate the volatile fraction of the sample (BS-EN-872, 2005). However, previous studies report that the relationship between mass of clog matter and media hydraulic conductivity is poorly correlated (Tanner et al., 1998, Caselles-Osorio et al., 2007). This may be because form, density and water retention properties will determine the hydrological influence of clog matter, as discussed in **Chapter 2**.

Certain studies have measured the specific yield (also known as drainage porosity) of media to reflect the hydraulic influence of water retention in clog matter. The specific yield is less than or equal to the medium porosity, depending on the saturation of the medium and the retention of water in interstitial matter. The specific yield is the ratio of the volume of water drained from the sample versus the total volume of the sample. When studying the inlet region of a secondary treatment HSSF system in the US, Kadlec and Watson (1993) found that the accumulation of highly hydrated gelatinous slime reduced void volume by 50%, compared with a void volume reduction of 10 – 20% in downstream media. Suliman et al. (2006a) measured a change in drainable porosity from 30% to 10.5% in their laboratory shell sand HSSF wetlands, before and after biological growth.

Capacitance probes (Langergraber et al., 2003) and Time Domain Reflectometry (Platzer and Mauch, 1997) have been used *in situ* to measure the ability of media in VF TWs to desaturate between loading cycles. These technologies rely on the fact that the dielectric constant of water is proportional to saturation, making them highly suitable for application in VF TWs. Based on broadly similar principles, it was proposed to use Ground Penetrating Radar to assess clog matter accumulations in Severn Trent HSSF TWs (Cooper et al., 2008, Fogg, 2007). The concept was that porosity occlusion by clog matter would lower the dielectric constant of the porous media in comparison to unclogged interstices. However, it was not possible to calibrate the obtained radiograms against corresponding clog matter

assays, such that the method could not be used for accurate determination of subsurface clog matter accumulation (Fogg, 2007). Application of Ground Penetrating Radar, Time Domain Reflectometry and Capacitance Probes for determining clog matter accumulation in saturated HSSF TW media would be difficult because clog matter is usually over 90% water by volume. This means resolution between clogged and unclogged regions would be very poor (Pedescoll, 2009). Ground Penetrating Radar has been used to delineate subsurface features along natural wetlands (Lapen et al., 1996), although these tended to be major geological transitions such as bedrock versus soil, or saturated versus unsaturated regions, rather than small differences in organic matter accumulation.

4.1.3. Hydrodynamic Visualisations

Information regarding the effect of clogging on flow dynamics can be gained using tracer tests. The passage of the tracer can either be monitored at the system outlet or at points within the subsurface. The choice of monitoring point provides different information about the wetland hydrology (Kadlec and Wallace, 2010).

Studying the outlet will indicate the aggregated affect that short-circuiting will have on flow through the wetland. The tracer Residence Time Distribution (RTD) for the system indicates hydraulic performance parameters such as hydraulic retention time (HRT), axial dispersion coefficients, equivalent number of Tanks In Series ***n***, emergence delay and volumetric and hydraulic efficiency (Headley and Kadlec, 2007, Kadlec and Wallace, 2010, Persson et al., 1999, Werner and Kadlec, 2000). The existence of multiple preferential paths through the wetland has been attributed to multiple-peak RTDs observed in some HSSF tracer breakthrough curves (Batchelor and Loots, 1997). Maloszewski et al. (2006) used Bromide tracer breakthrough curves to identify that a primary flow path accounted for over two-thirds of the flow they observed through three experimental gravel bed HSSF TWs in Poland. Successful data fits were achieved by assuming that three flow-paths existed that separately conveyed 70 %, 21 % and 9 % of the influent.

Internal tracer studies can be used to identify the location of preferential flow paths through the wetland (Nivala, 2005) and to study how flow is influenced by features such as uneven inlet distribution (Shilton and Prasad, 1996), short-circuiting below the root-zone (Bowmer, 1987, Fisher, 1990, Breen and Chick, 1995), and surface clogging (Christian, 1990, Batchelor and Loots, 1997). **Table 3-4** gave an overview of several studies that have used internal

tracer tests to identify vertical short circuiting in HSSF TWs, along with the major factors that were thought to be responsible for these observations: preferential establishment of vegetation in the top of the bed; the design of the influent distribution and effluent collection systems; density differences between precipitation and wastewater; and density differences between tracer and wastewater. Measurement of internal flow-rates would be needed if internal RTDs are to be used to indicate the flow-rates along different preferential flow-paths (Kadlec, 2000). This idea is often explained using the 'mixing cup' versus 'through the wall' analogy common to chemical engineering (Levenspiel, 1999).

It should be emphasised that a single tracer test on a subsurface flow TW may only be showing one, from a possible range of hydraulic behaviours (Kadlec and Wallace, 2010). The specific hydraulic performance of HSSF wetlands is probabilistic (Waters et al., 1993) and will depend on flow and seasonal effects such as evapotranspiration and freezing (He and Mankin, 2001, Hedges et al., 2008). For example, Waters et al. (1993) and Fonder and Xanthoulis (2008) found that the short-term repeatability of internal tracer studies on HSSF TWs was good at some locations and poor at others, obtaining fluctuations of the observed breakthrough curves under similar control conditions. HSSF TW flow profiles change over time according to changes in the subsurface hydrology, as indicated by the findings of Bowmer (1987). Erichrome Red tracer studies, performed two years apart in an Australian gravel bed HSSF system, indicated that an area that had once represented a substantial preferential flow path had changed into a large dead-zone.

The phenomenon of short-circuiting means that Hydraulic Retention Time should not be used to calculate system hydraulic conductivity because this does not represent the Darcy hydraulic conductivity of the media. For example, whilst investigating two soil-based HSSF TWs in Germany, Pauly (1990) found that Darcy hydraulic conductivity derived from measured hydraulic gradients returned values an order of magnitude lower than Tissou hydraulic conductivity derived from measured HRT. Hydraulic conductivity studies and tracer tests should be used complementarily to elucidate the complex hydrology of HSSF TWs (Knowles et al., 2010).

4.1.4. Other Measures of Clogging

Alternative clogging indicators often measure parameters that are not a property of the gravel medium. For example, Molle et al. (2006) and Sun et al. (2007) measured the depth

of ponding on the surface of VF TWs during dosing. The authors found that as the system clogged the residual depth of water and the percolation time through the system both increased. As discussed in **Chapter 2**, Cooper et al. (2005) and Rousseau et al. (2005b) measured the depth of sludge that had accumulated on the surface of Severn Trent HSSF TWs as an indication of the state of clogging. A novel clogging indicator was suggested by Nguyen (2000), who found that microbial biomass and microbial respiration correlated well with the stability and quantity of organic matter in a dairy wastewater treatment HSSF TW in New Zealand.

4.1.5. Discussion on the suitability of methods for this study

Table 4-2 rates the fourteen previously discussed methods according to their ability to meet the six requirements specified in **Table 4-1**:

1) Application is *in situ*
2) Operable by a single-user.
3) Rapid and inexpensive enough to allow multiple site surveys.
4) Applicable while the system is operating.
5) Suitable for media with high hydraulic conductivity.
6) Provides the ability to resolve variations in hydraulic conductivity in three dimensions.

Certain requirements are not applicable to all methods and scoring is adjusted accordingly. The scoring method used in **Table 4-2** implies that the slug test introduced by Caselles-Osorio and García (2007) is the most suitable for measuring the hydraulic conductivity of HSSF TW media; achieving 5 from 6 requirements. However, this method is unable to resolve hydraulic conductivity in 3D, which is critical to this study. The requirements that are most difficult to achieve with existing methods are: applicability across a wide range of media conductivities (only achievable by 4 methods); and the ability to measure variations in hydraulic conductivity in all three planes (only achievable by 8 methods).

The previous review has highlighted that no single method is available that completely meets the specification outlined in **Table 4-1**.

Table 4-2 Tests that are available to assess: media hydraulic conductivity (yellow); clog matter properties (green); and hydrodynamic behaviour (blue); and their ability to meet the following six requirements: 1) *In situ;* 2) Quick and inexpensive; 3) Portable and single-user-friendly; 4) Non-interruptive; 5) Appropriate for media with high hydraulic conductivity; 6) 3D resolution possible. N/A indicates that the requirement is not applicable to that method and scoring is adjusted accordingly. Table continued overleaf.

	Test	Description	1	2	3	4	5	6	√
Hydraulic Conductivity Tests	Slug Test	A piezometer tube (devoid of media) is inserted into the media and either a falling or constant head of water is applied above the water table. The discharge through the end of the tube into the media is monitored, and the hydraulic conductivity calculated according to shape factors.	√	√	√	√	X	√	**5/6**
	Pumping Test	Water is pumped at a constant rate into or out of a well, and the resulting cone of depression in the aquifer material is monitored over time according to the solution of Theis (1935).	√	√	X	X	X	X	**2/6**
	Water Level Survey	Flow through the aquifer material results in a hydraulic gradient. Differences in the height of the water table are observed in different wells.	√	√	√	√	X	X	**4/6**
	Borehole Test	A borehole is made into the media and water is either added of removed. The recharge rate or flow rate into the media is monitored.	√	√	√	√	X	X	**4/6**
	Infiltration Tests	A ring is impressed into the surface of the media and water is added to measure the infiltration rate through the surface.	√	√	√	√	X	X	**4/6**
	Laboratory Permeameter	A sample of the media is placed into a laboratory permeameter cell which may be rigid or flexible wall. A constant or variable head of water is then applied across the media. Manometer take off points allow the variation in resistivity across the sample to be determined.	X	√	NA	√	√	X	**3/5**
	Modified Cube Method	A cubic sample of the media is sealed in wax. By sequentially removing single sets of opposing faces, and passing flow through the media, the hydraulic conductivity in different planes (anisotropy) can be determined.	X	√	NA	√	√	√	**4/5**

Table 4-2 Tests that are available to assess: media hydraulic conductivity (yellow); clog matter properties (green); and hydrodynamic behaviour (blue); and their ability to meet the following six requirements: 1) *In situ;* 2) Quick and inexpensive; 3) Portable and single-user-friendly; 4) Non-interruptive; 5) Appropriate for media with high hydraulic conductivity; 6) 3D resolution possible. N/A indicates that the requirement is not applicable to that method and scoring is adjusted accordingly.

	Test	Description	1	2	3	4	5	6	√
Clog matter properties	Direct porosity measurements	Either saturated or drainable porosity of the extracted sample. This gives a good indication of free versus associated interstitial water	X	√	NA	√	NA	√	**3/4**
	Time Doman Reflectometry (TDR)	A family of methods that rely on the dielectric constant of water being proportional to saturation. Therefore the electrical capacitance of media depends on the water content. Each method measures this property in a different way. TDR and Capacitance Probes can be inserted at different points in the media and give readings in the immediate locality. GPR devices are swept over the surface of the system and provide an image of the subsurface.	√	√	√	√	X	√	**5/6**
	Capacitance Probe		√	√	√	√	X	√	**5/6**
	Ground Penetrating Radar (GPR)		√	X	√	√	X	√	**4/6**
	Solids Assays	Total solids and volatile solids content of the interstitial clog matter are measured. The interstitial water may also be analysed for suspended fractions	X	√	NA	√	NA	√	**3/4**
Tracer tests	Breakthrough Curve	The breakthrough of a pulse of tracer added to the inlet of the system is monitored at the outlet of the system.	√	√	√	√	NA	X	**4/5**
	Internal Tracing	The dynamics of the tracer within the system are monitored by measuring the tracer concentration at different points within the system.	√	X	√	√	NA	√	**4/5**

The majority of previous *in situ* hydraulic conductivity testing in HSSF TWs has been based on water table surveys that do not directly measure the media conductivity. It is questionable whether hydraulic conductivity values derived from water table surveys are representative because of the limiting accuracy of surveying techniques and inaccuracies caused by neglecting the groundwater energy balance during calculations. The method of Caselles-Osorio and García (2007) is the only successful method to directly measure media hydraulic conductivity in HSSF TWs; however, this method cannot measure vertical variations in hydraulic conductivity.

Although tracer tests have proven that vertical short-circuiting is common in HSSF TWs, this has never been supported with corresponding vertical hydraulic conductivity profiles. Variations in vertical hydraulic conductivity are neglected by HSSF TW design documents, which assume that hydraulic conductivity only varies longitudinally. A method is required that allows media hydraulic conductivity to be resolved in three dimensions. This is particularly significant for this study due to evidence that Severn Trent HSSF TWs are prone to excessive surface clogging in comparison to other HSSF TW variants.

Tracer tests will be employed to monitor outlet RTDs and validate the hydrodynamic performance of the FEA model proposed in **Chapter 3**. Lastly, previous attempts to explain hydraulic conductivity results by comparison with physical measures of clog matter (mass, density etc.) have been inconclusive and will not be employed during this research.

4.2. The Aston Permeameter

This section details the development of The Aston Permeameter: a novel *in situ* method and apparatus that can be used to measure three dimensional variations in the hydraulic conductivity of coarse media, such as gravels in HSSF TWs. After a brief introduction to the rationale behind the method, discussion is given to the principles of operation, materials used to make the apparatus, experimental procedure, accuracy, repeatability and sources of potential experimental error.

The hydraulic conductivity of media in HSSF TWs varies by several orders of magnitude according to media size and state of clogging (**Table 3-2**). For clean gravels of 10 mm diameter, hydraulic conductivities on the order of 10,000 m/d are typical (Wallace and Knight, 2006). A good way of achieving practical flow-rates through high conductivity media

is to use a Mariotte Siphon, which controls a small, constant head above the water table. The same principle underlies the design of the Guelph Permeameter method (Reynolds and Elrick, 1986), the Amoozemeter Permeameter (Amoozegar, 1989) and the Philip-Dunne Permeameter (Muñoz-Carpena et al., 2002). These borehole methods are not wholly appropriate for this study because measurements cannot be taken at specific depths. However, the principle of using a Mariotte Siphon to control the flow-rate through clean gravel is useful.

Enlarging typical Slug Test apparatus for use in large granular media such as gravel would make piezometer insertion impractical. The NAVFAC (1986) adaptation brings the media inside the piezometer tube and passes water through it (as opposed to water flowing through an empty tube and out of perforations in the tube wall to the surrounding media). Kadlec and Knight (1996) indicate that a tube diameter approximately 10 times larger than the media diameter is required to ensure that tube side-wall effects are minimised and the measured hydraulic conductivity is representative of the encased sample.

An obscure method for *in situ* infiltration measurements was developed by Schiff and Johnson (1958) whereby a disc permeameter was buried 1 ft. into aquifer material and a constant head applied to create a flow rate. The loss in hydraulic head through the aquifer material was monitored using manometer take off points at various depths. In this way it was possible to apply the theory underlying the laboratory constant head permeameter method to determine infiltration rates in the field.

The Aston Permeameter incorporates the above three principles to achieve 3D *in situ* determination of low and high hydraulic conductivity media in HSSF TWs:

1) A Mariotte Siphon to control a small, constant head.
2) A permeameter cell that encases the sample to be tested.
3) Subsurface manometric take-off points to recreate the laboratory constant head hydraulic conductivity test *in situ.*

4.2.1. Principle of Operation

The principles behind the operation of the Aston Permeameter are provided below. From this point on, all letters in square brackets refer to those labels indicated on **Figure 4-1**. As shown in **Figure 4-1**, a PVC tube with diameter at least equal to ten times the largest gravel

particle diameter is driven vertically into the bed. This constitutes the permeameter cell [h], entrapping a gravel core [p,r] with length L_{CELL} (m) and cross-sectional area A_{CELL} (m^2).

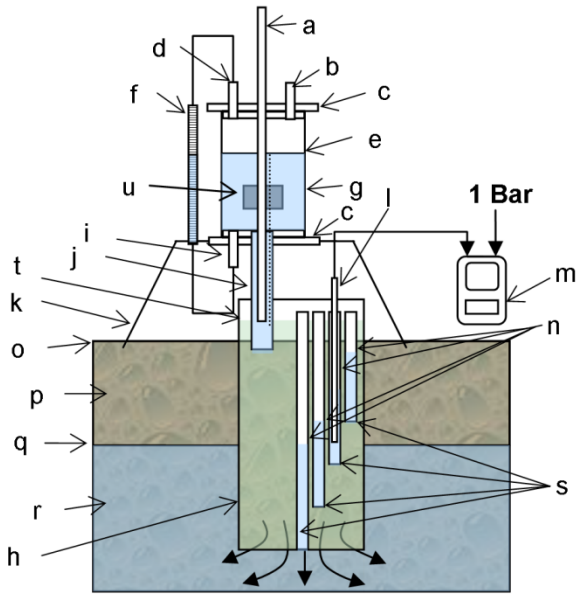

a. Air Inlet Pipe
b. Filling port
c. End cap
d. Air Port
e. Fluid Level in reservoir
f. Graduated measuring tube
g. Reservoir
h. 50cm long Permeameter Cell
i. Drain Port
j. Down pipe
k. Tripod
l. Graduated Depth Gauge
m. Digital Differential Manometer
n. Levels in manometer takeoff tubes
o. Gravel Surface
p. Unsaturated gravel
q. Free water surface
r. Saturated gravel
s. Manometer takeoff tubes
t. Mariotte Siphon Level
u. Stop cap

Figure 4-1 Experimental set-up for *in situ* measurement of the vertical hydraulic conductivity profile across media with high hydraulic conductivity. Figure is not to scale and is reproduced from Knowles and Davies (2009).

During the test, the water level inside the tube is raised to above the gravel surface and kept constant by using the Mariotte Siphon technique. This is achieved by using a reservoir device [g], similar to the Guelph Permeameter (Reynolds and Elrick, 1986), but enlarged to make it suitable for applications in higher conductivity media such as gravel as well as the lower conductivity media for which the Guelph Permeameter is intended.

Four manometer take-off tubes [s], ranging from 200 to 500 mm length in 100 mm increments, are inserted into the gravel core prior to the experiment commencing. This provides a number (in this case 4) of evenly distributed take-off points n at 100, 200, 300 and 400 mm depths into the gravel core. Using a digital differential manometer [m] with a 500 mm graduated depth gauge [l] it is possible to determine the static [q] and dynamic [n] water levels in each take-off tube, thus allowing the vertical head loss across each 100 mm section h_n (m) to be measured. By monitoring the discharge of water Q (m^3/d) from the reservoir [e,f], in keeping the permeameter head h_T (m) constant, it is possible to calculate

the hydraulic conductivity of the gravel core k_T (m/d) using Darcy's Law (**Equation 4-1**). Subsequently the hydraulic conductivity of each 100 mm section k_n (m/d) can be found (**Equation 4-2**). The test provides vertical conductivity profiles, although by interpolating between sample points it is possible to predict a horizontal conductivity profile. This is based on the assumption that media at the sampling point is isotropic and the vertical and horizontal hydraulic conductivities are analogous. If the water table is below the surface of the bed, the head is applied across a layer of media that is previously unsaturated. It is assumed that upon commencing the experiment the unsaturated layer becomes suitably saturated so that Darcy's Law, rather than Richard's Law, is the governing equation for flow. If only the hydraulic conductivity of the wetted gravel is of interest, the unsaturated layer should be removed from the permeameter cell before commencing the experiment, and the subsequent analysis modified to reflect the new test conditions.

$$k_T = \frac{Q\ L_{CELL}}{h_T\ A_{CELL}} \qquad \textbf{Equation 4-1}$$

$$k_n = \frac{1}{n\left(\frac{h_n}{h_T k_T}\right)} \qquad \textbf{Equation 4-2}$$

Figure 4-2 uses an electrical analogy to describe how Darcy's Law is applied to the Aston Permeameter. The analogy used is based on an electrically conducting wire of constant dimensions but varying electrical resistivity. The electrical resistance of the wire can be represented by ***n*** sections in series that have equal length but different resistances. **Figure 4-2** illustrates how the hydraulic conductivity of the media can be related to the electrical conductivity (reciprocal of electrical resistivity) of the wire. **Figure 4-2** also illustrates how the dynamic water levels in each take-off tube are expected to vary because of head loss across the length of the permeameter cell.

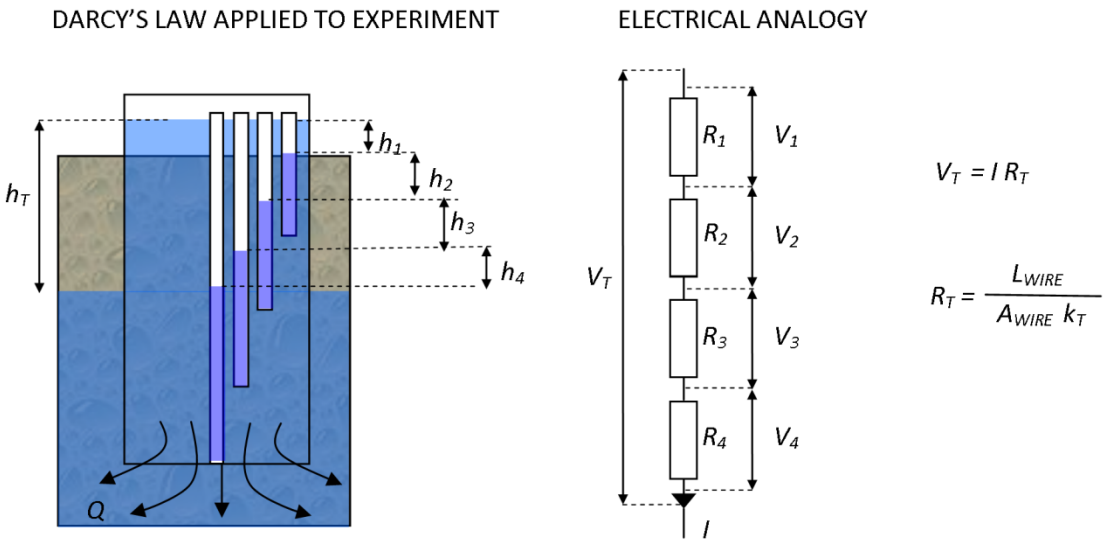

$$h_T = \frac{Q\,L_{CELL}}{k_T\,A_{CELL}} \qquad V_T = \frac{I\,L_{WIRE}}{k_T\,A_{WIRE}}$$

$$h_T = h_1 + h_2 + h_3 + h_4 \qquad V_T = V_1 + V_2 + V_3 + V_4$$

$$h_n = \frac{Q\,\frac{L_{CELL}}{n}}{k_n\,A_{CELL}} \qquad V_n = \frac{I\,\frac{L_{WIRE}}{n}}{k_n\,A_{WIRE}}$$

$$h_T = \frac{Q\,L_{CELL}}{n\,A_{CELL}}\left(\frac{1}{k_1} + \frac{1}{k_2} + \frac{1}{k_3} + \frac{1}{k_4}\right) \qquad V_T = \frac{I\,L_{WIRE}}{n\,A_{WIRE}}\left(\frac{1}{k_1} + \frac{1}{k_2} + \frac{1}{k_3} + \frac{1}{k_4}\right)$$

Figure 4-2 An electrical analogy of the Aston Permeameter, represented by the voltage ***V*** drop across a wire of constant dimensions but varying electrical conductivity, split into ***n*** lengths of equal section. Reproduced from Knowles and Davies (2009).

4.2.2. Apparatus

Figure 4-3 depicts the apparatus during an experiment at a Severn Trent HSSF TW, and **Figure 4-4** shows the apparatus laid-out so that the individual components can be identified. The corresponding list of components used to assemble the Mariotte Siphon activated reservoir, and other apparatus used in the experiment, is provided in **Table 4-3** with costs and supplier information. Total cost for all equipment was £1055 in 2008 and almost 90% of this was apportioned to the purchase of the four digital manometers used in the experiment.

Figure 4-3 Photograph of the experimental set-up at a Constructed Wetland in South Warwickshire, UK, depicting the Mariotte Siphon activated reservoir standing above the permeameter cell, which has been submersed into the gravel. Three digital manometers are in a blue toolbox at the forefront of the shot. The orange manometer lines are inserted into the white manometer take off tubes. The reservoir is empty in this shot.

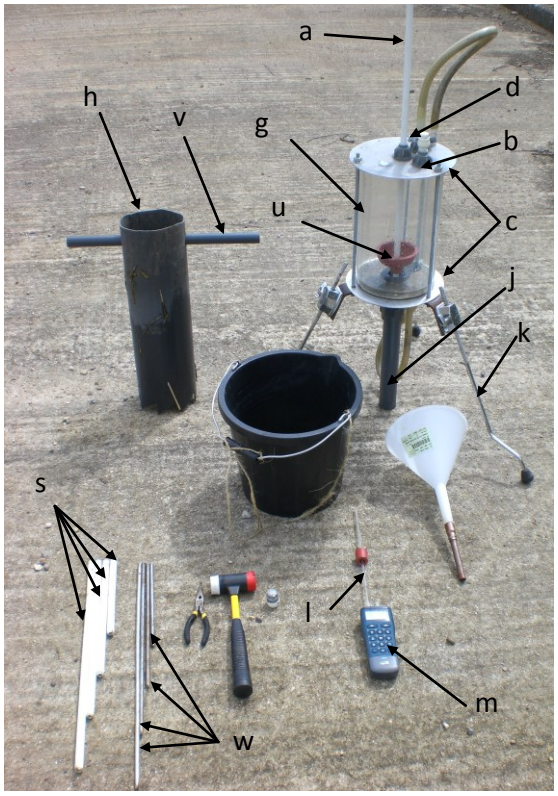

a. Air inlet pipe
b. Filling port
c. End cap
d. Air port
g. Reservoir
h. 50cm long permeameter cell
j. Down pipe
k. Tripod
l. Manometer lines
m. Digital differential manometer
s. Manometer take-off tubes
u. Stop cap
v. T-Bar accessory
w. Metal stakes

Figure 4-4 Photograph of the full inventory of apparatus used in the experiment (labels as per **Figure 4-1**). The method is designed to be highly portable so that it can be performed by one user, *in-situ*. Reproduced from Knowles and Davies (2009).

The maximum practical flow rate that can be sustained by the Aston Permeameter depends on the dimensions of the permeameter cell [h], reservoir cell [g] and down pipe [j]. **Figure 4-5** illustrates the maximum flow velocity that can be maintained in the permeameter cell at maximum discharge by the version of the Aston Permeameter designed and fabricated for this study. The profile shown in **Figure 4-5** is based on the application of Bernoulli's Equation across the reservoir device and the following assumptions:

- A reservoir with a diameter of 0.2 m and length of 0.5 m.
- A down pipe with a diameter of 0.075 m and length of 0.5 m.
- A permeameter cell with a diameter of 0.168 m.
- The volume of water exiting the down-pipe is equal to the volume of air that travels up the down-pipe and enables displacement to occur. Therefore, it is assumed that that only half of the cross-sectional area of the down-pipe is available for flow.
- Minor losses in the reservoir can be attributed to the sudden contraction between the reservoir cell and the down pipe, and the exit losses from the down pipe.
- A clean media porosity of 0.35.

Table 4-3 A list of the major components used to make the apparatus for the experiment. Costs are rounded to the nearest pound sterling and reflect 2008 UK prices. Only the components which are considered specialist or difficult to identify are listed. Reproduced from Knowles and Davies (2009).

Label	Part	Product	Supplier	Cost (£)
a,s	Air inlet pipe, Manometer take-off tubes	15 mm diameter speedfit barrier pipe	John Guest, Middlesex, UK	2
b,d,i	Filling port, Air port, Drain port	15 mm speedfit tank connector	John Guest, Middlesex, UK	4
c	End caps	Aluminium Plate	N/A Manufactured in house	25
f	Graduated measuring tube	25ml acrylic burette tube	Scilabware, Staffs., UK	22
g	Reservoir chamber	L0.5m D0.2m, wall 0.003m Polycarbonate tube	Wake Plastics, Middlesex, UK	50
h	Permeameter cell	L0.5m D0.168m wall 0.004m PVC ducting	N/A modified in house	4
j	Down tube	2” PVC tank connector with 3” PVC plain socket adaptor and 3” PVC pipe	George Fischer, Coventry, UK	20
k	Tripod legs	3* floor tom drum legs	N/A	20
l	Graduated depth probe	6 mm OD 1.5 mm wall acrylic tube	N/A modified in house	5
m	Digital Manometers	1 * Digitron 2080P	Sifam, Devon, UK	300
m	Digital Manometers	3 * Kane 3100-1	Kane International, Herts., UK	600
u	Stop cap	Rubber plunger head	N/A	1
v	T-Bar	1.25” PVC pipe	N/A	1
w	Metal stakes	10 mm OD CSS steel tube	N/A Manufactured in house	1
TOTAL COST				**£1055**

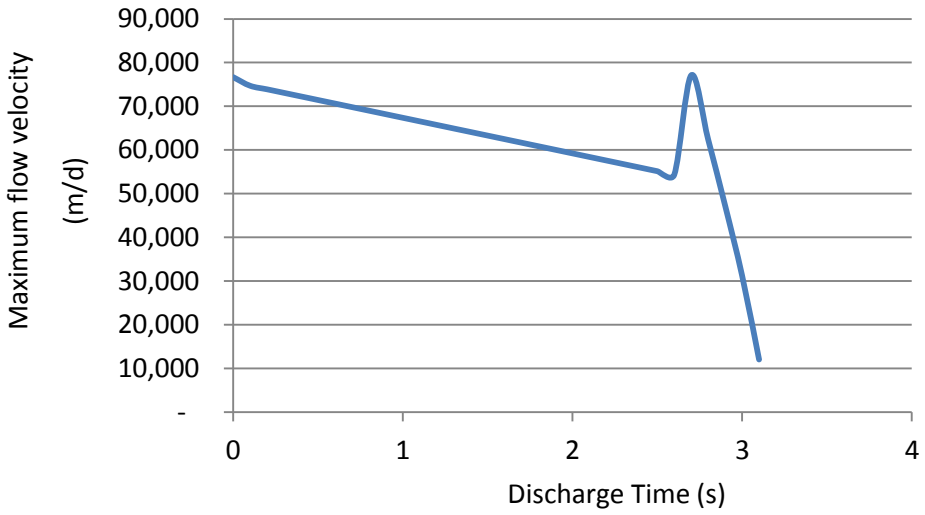

Figure 4-5 The maximum practical flow velocity that can be sustained in the permeameter cell at maximum discharge by the Aston Permeameter used in this study.

As shown in **Figure 4-5**, at maximum discharge the reservoir device takes 3.2 seconds to empty. The sudden peak shown in **Figure 4-5** represents the time at which the reservoir chamber is completely evacuated and only the down-pipe contains water. The maximum flow velocity that can be maintained in the permeameter cell during the period that the reservoir chamber contains water varies between 77,000 m/d and 54,000 m/d. According to **Equation 3-2**, the maximum flow-velocity that maintains porous media ***Re*** below 10 varies from 842 m/d for media with a 1 mm diameter, to 56 m/d for media with a 15 mm diameter. Therefore, the Aston Permeameter is appropriately sized to ensure that laminar flow hydraulic conductivity tests can be performed across a wide range of hydraulic conductivities in field-scale HSSF TWs. The Mariotte Siphon feature on the Aston Permeameter will be used to adjust the constant head across the sample for a wide range of media hydraulic conductivities and achieve a flow velocity that is below the maximum laminar flow velocity.

Kadlec and Knight (1996) propose that a cell with diameter at least ten times greater than the mean particle diameter is required to obtain a hydraulic conductivity measurement that is representative of the sample. A permeameter cell with diameter 0.168 m was deemed appropriate as this is 14 times larger than a 12 mm diameter gravel particle, which is the largest gravel typically employed in Severn Trent HSSF TWs. A larger diameter permeameter cell would further reduced side-wall effects, however, it was found that a 0.168 m diameter cell was the largest cell size that could be manually inserted into the gravel by a single operator.

4.2.3. Experimental Procedure

The instructions followed when performing the experiment are listed below, where the labels in square brackets refer to the components illustrated in **Figure 4-1** and **Figure 4-4**. To aid clarity, **Figure 4-6** illustrates how the measurements described in the subsequent procedure are obtained.

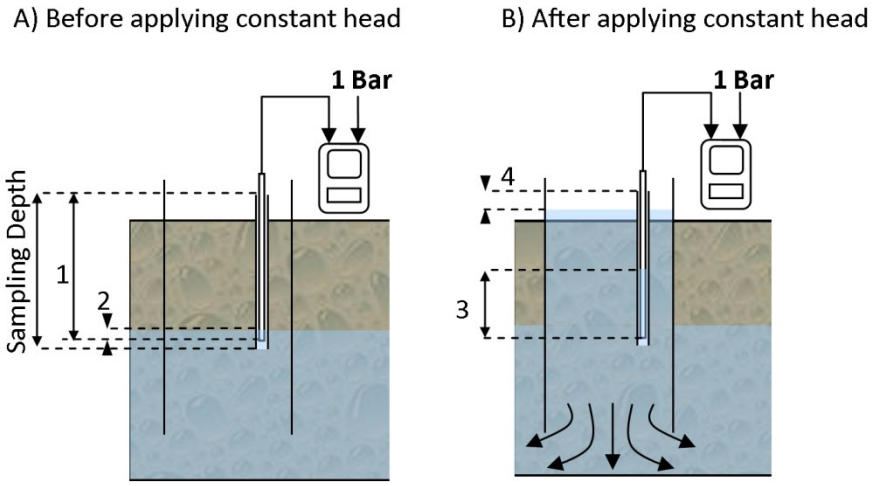

1. Probe depth inside manometer take-off tube (from depth probe graduations)
2. Static water level measured inside probe (from digital manometer readout)
3. Dynamic water level measured inside probe (from digital manometer readout)
4. Distance between top of manometer take-off tube and applied head level (from graduations along the emergent portion of the manometer take-off tube)

Figure 4-6 Measurements that are taken during the experiment, depicted for one take-off tube. Corresponding readings will need to be taken in each individual take-off tube. For clarity, the reservoir device which maintains the constant head has been omitted from graphic B): "After applying constant head". Reproduced from Knowles and Davies (2009).

1. Drive the permeameter cell [h] into the gravel until the top 100 mm is emergent from the gravel surface, thus creating a 400 mm gravel plug. Serrations were cut into the penetrating end of the permeameter cell to aid its insertion into the gravel, and there are two holes at the top of the tube to allow a T-Bar accessory [v] to be utilised during insertion. To minimise disturbance to the gravel core, a circular jigsaw cutting action should be used to submerge the tube into the gravel.
2. Insert the four manometer take-off tubes [s] to the required depths, so that the top of them is in line with the top of the permeameter cell. To aid insertion of the take-off tubes four metal stakes [w] with lengths just greater than, and ODs just smaller

than, the respective dimensions of the take-off tubes, can first be driven into the ground. The take-off tube is then sheathed over the top of the stake and driven into the gravel until the stake re-emerges from the top of the take-off tube. Once the stake has been removed, the inside of the take-off tube is left free from gravel blockages. This ensures the water level inside the take-off tube is free to fluctuate only according to the hydraulic conditions in the permeameter cell; this otherwise being a possible source of error in measurements.

3. Attach a graduated depth probe [l] to each manometer [m] and insert one probe into each take-off tube to locate the static water level. The distance the probe is immersed into the water should be small, to minimise errors caused by displacement. Record the digital manometer readings after they have stabilised, and the distance the probes have been inserted into the take-off tube. This may not be possible in all the tubes depending on the water level in the bed, but as a check, any readings obtained should be roughly equal. Any disparity between the readings will be caused by minor differences between the vertical alignments of the top of the take-off tubes, and therefore, recording the different static water level readings will allow these discrepancies to be accounted for.
4. Assemble the Mariotte Siphon activated reservoir by combining the parts as illustrated in **Figure 4-4**. Adjust the tripod legs [k] so that the down pipe [j] rests just above the surface of the gravel. Lower the air pipe [a] so that it is in line with the end of the down pipe and so the stop cap [u] inside the reservoir covers the down pipe inlet.
5. Open the filling [b] and air ports [d] on the reservoir and fill the reservoir with water. This was done using a bucket and long stem funnel although any method is applicable. Close the air and filling ports.
6. Pre fill the permeameter cell [h] with water until the water level rises to just above the gravel surface. This will maximise the amount of water inside the reservoir that can be used for steady measurements.
7. Raise the air pipe [a] so that the water level in the cell settles at a height above the gravel surface, but below the lip of the cell. The Mariotte Siphon will engage and the reservoir will begin to empty to maintain the constant head inside the cell. Measure the water level indicated by the graduated measuring tube [f] and begin timing. The emergent 100 mm of each take-off tubes is marked with a scale so that the distance between the top of the take-off tubes and the water level inside the permeameter

cell can be accurately recorded. This allows the total applied head across the permeameter cell, and corresponding head loss measured in each take-off tube, to be accurately calculated.

8. The value indicated by the manometers will change to reflect the dynamic water level inside the take-off tubes. Record the digital manometer readings after they have stabilised. This stage must be completed before the reservoir empties.
9. Record the water level in the graduated measuring tube against time.

4.2.4. Agreement of the Aston Permeameter with Standard Experimental Methods

Experimental accuracy was tested by comparing results from the Aston Permeameter with those measured using a laboratory standard constant head permeameter (ELE, Bedfordshire) according to BS-ISO-17313 (2004). When applied to samples from the same fine silica sand, the Aston Permeameter gave hydraulic conductivity values of 27.9 m/d and the laboratory constant head permeameter gave hydraulic conductivity values of 27.1 m/d. In addition to being in good agreement (within 3%), these values are within the range quoted in the literature for the hydraulic conductivity of silica sand: 8.6 m/d to 86 m/d (Barnes, 2000, Craig, 2004, Smith and Smith, 1990). **Figure 4-7** shows the head loss over the sand plug used in each experiment, as obtained from manometer take-off points. Silica sand is very homogeneous and the hydraulic gradient should be linear; which was achieved with both the standard and proposed methods, yielding R^2 fits of 0.990 and 0.989 respectively.

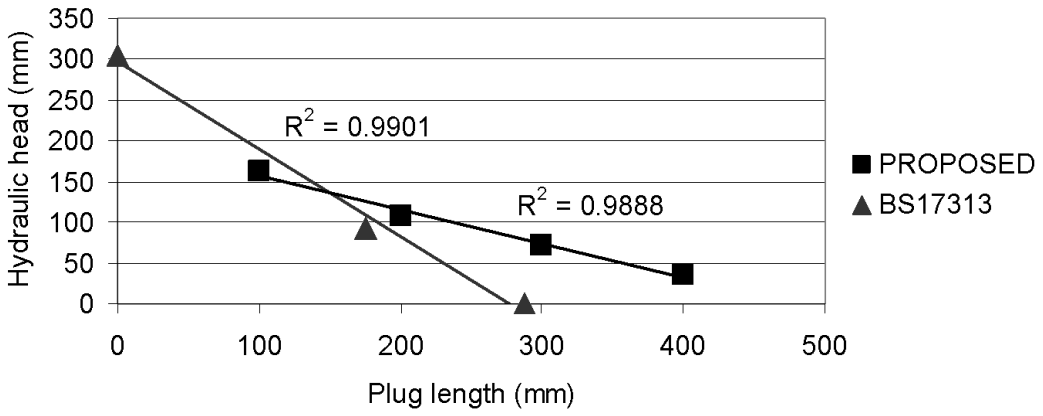

Figure 4-7 Head loss across homogeneous silica sand cores, tested using both BS-ISO-17313 (2004) and the proposed method. Good linearity was achieved with both methods. Reproduced from Knowles and Davies (2009).

4.2.5. Repeatability

An experiment was performed *in-situ* at a Severn Trent HSSF TW at Fenny Compton. The gravel media had a size distribution between 6 mm and 12 mm diameter. The permeameter cell was immersed at a point near the TW inlet and the experiment repeated five times at the same point to ensure the repeatability of the method. This is seen to be good in **Figure 4-8**, with standard deviations ranging from 1% to 4% of total normalised head loss, between 100 mm and 400 mm depth respectively. As evident from **Figure 4-8** the small residual head loss that remains at a 400 mm depth indicates that exit losses from gravel cores to the TW macrocosm are negligible in comparison to total head-loss within the permeameter cell.

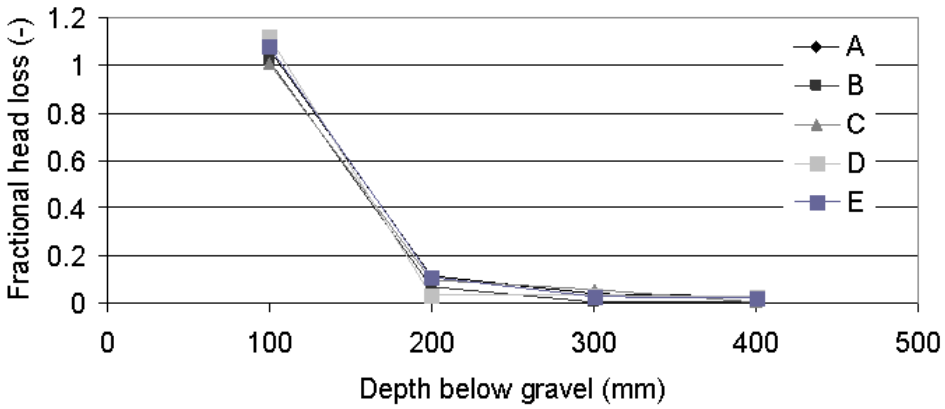

Figure 4-8 The head loss across a gravel core in a HSSF TW at Fenny Compton. The test was repeated five times (Runs A-E) to determine that the experimental repeatability was good; returning standard deviations of 1-4% of total normalised head loss. Reproduced from Knowles and Davies (2009)

A second experiment was performed to investigate the repeatability of results at different test points in close proximity. The assumption is that the hydraulic conductivities of samples in close proximity would be relatively similar and large disparities between readings would indicate that inserting the permeameter cell disturbs the sample to the degree that measurements are not representative. Small differences in hydraulic conductivity will naturally arise between proximal cores because of heterogeneity of particle size distributions and varying root growth (Bavor and Schulz, 1993), but it is expected that results will be within an order of magnitude. **Figure 4-9** shows the location of the sampling points for the homogeneity experiment that was performed at a HSSF TW at Moreton Morrell. Four points were chosen (A1, B2, C3 and D4) and matrices of three additional sampling points were closely installed around each of these points. The ranges of sample hydraulic

conductivity results for the four groups of holes, along with averages and standard deviations, are reported in **Table 4-4**. Hydraulic conductivity is 3 orders of magnitude lower at the inlet ($\boldsymbol{k} \sim \mathcal{O}(1\ m/d)$) than at the outlet ($\boldsymbol{k} \sim \mathcal{O}(1{,}000\ m/d)$), and generally increases with distance from the inlet.

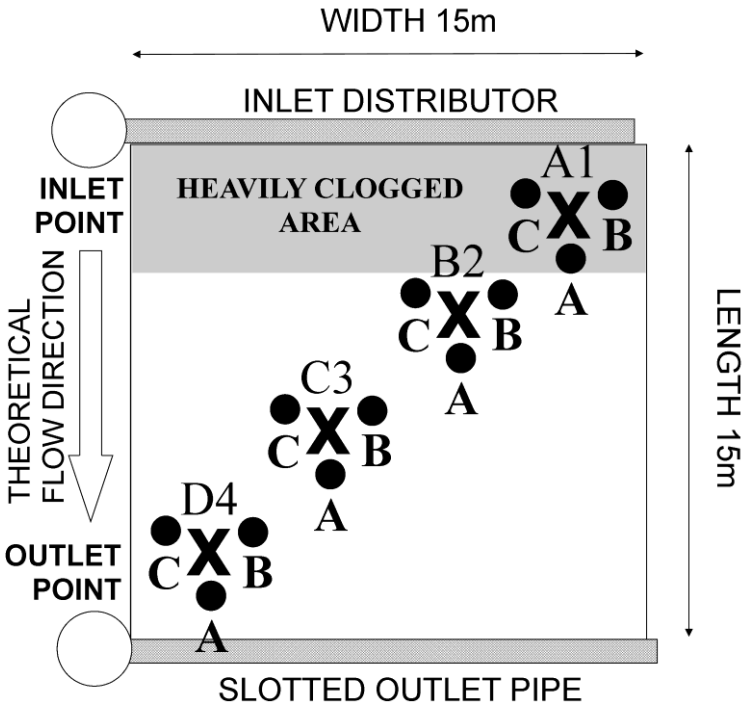

Figure 4-9 The locations of 16 sampling points installed to perform a homogeneity experiment at Moreton Morrell, to assess the possible errors introduced by inserting the permeameter cell into the gravel (not to scale: points marked **X** were set at a longitudinal and transverse pitch of 4 m. Points marked ● were arranged around the **X** points at a radius of 0.2m). Reproduced from Knowles and Davies (2009)

Regarding variance in each group of holes, standard deviation is always within the order of magnitude of the average hydraulic conductivity. Additionally, apart from near the inlet region where differences between results appear relatively large in comparison to the magnitude of the average hydraulic conductivity, the standard deviation was always within 30% of the average. It can therefore be stated that, when applied *in situ*, the method gives results representative of the order of magnitude of the hydraulic conductivity of the media in that area, and the practical reading recorded has a ±30 % associated degree of uncertainty associated with a combination of natural variations of media characteristics and sample disturbance during insertion of the permeameter cell. However, the uncertainty is small in comparison to the three order of magnitude variation in measured ***k*** values.

Table 4-4 The range of hydraulic conductivity values, averages and standard deviations recorded for each group of holes during the homogeneity experiment at Moreton Morrell. Reproduced from Knowles and Davies (2009).

	Hydraulic Conductivity m/d			
	Max.	Min.	Avg.	St. Dev.
A1	9	1	3	2
B2	344	181	261	72
C3	302	235	286	34
D4	1,231	399	802	295

4.2.6. Sources of Error

The potential errors when performing the experiment, and methods for minimising them, are detailed in **Table 4-5**. **Figure 4-10** shows the results from Run A of the Fenny Compton repeatability experiment, with associated maximum and minimum error bars. **Figure 4-10** (top) includes the +20% of manometer readout error associated with the displacement caused by depth probe insertion, whereas **Figure 4-10** (bottom) omits this error. It can be seen that taking the instantaneous reading off the manometer and reinserting the probe between static and dynamic readings increases the associated error, for example with the 400 mm depth measurement, from ±9 % to ± 40% of the total normalised head. Therefore, it should be ensured that the initial static reading is allowed to stabilise before being recorded, and that a different manometer is used within each take-off tube to negate the requirement to reinsert the probe between static and dynamic level readings.

Table 4-5 Sources of error associated with the method and ways to minimise them. Reproduced from Knowles and Davies (2009).

Error	Magnitude	Minimisation
Use of digital manometer	±0.15% reading ±0.15% fixed error ±0.2% display resolution	Unavoidable
Insertion of depth probe causing displacement	+20% of actual reading ±1 mm	Allow time for reading to stabilise
Misreading reservoir level	±1 mm	Use graduated scale
Stop watch error	±0.5s	Use large reservoir volume

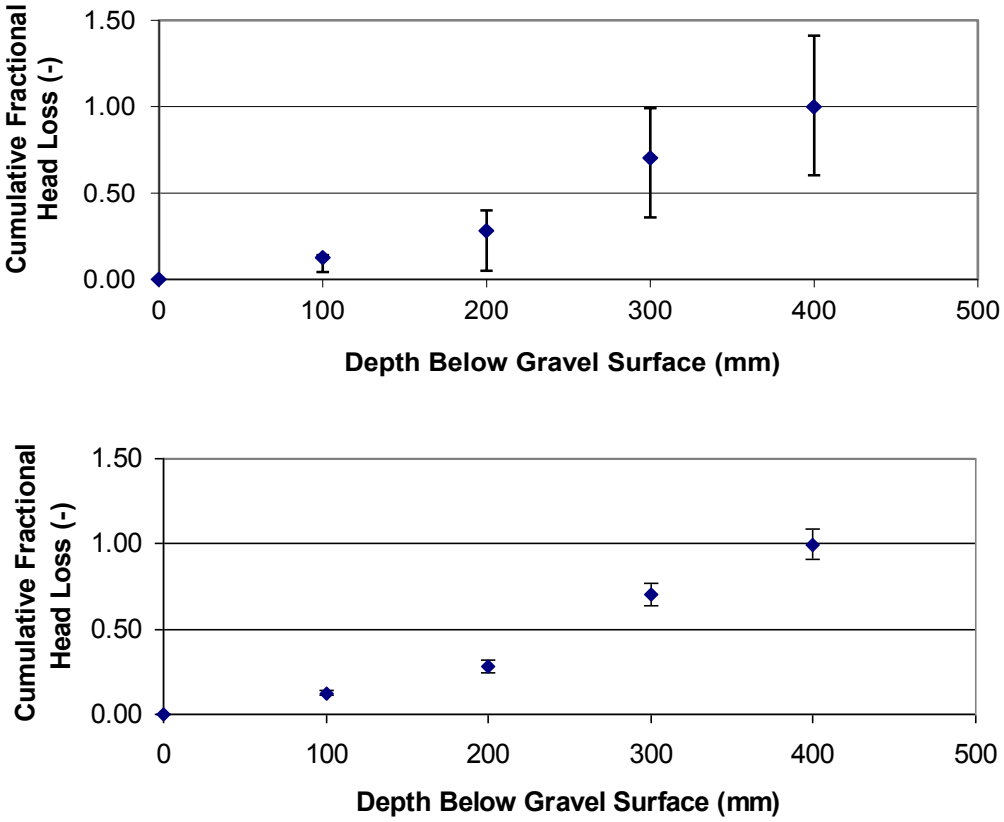

Figure 4-10 The errors associated with the results of Run A of the Fenny Compton repeatability experiment, both with (top) and without (bottom) inclusion of the error introduced by instantaneous reading of the manometer when reinserting the probe between readings. Reproduced from Knowles and Davies (2009).

A major source of error that does not appear in **Table 4-5**, because it is difficult to approximate, is the effect of inserting the permeameter cell into the media. Forcing the permeameter cell into the gravel requires mechanical agitation of the sample and may cause compaction, destroy bonds between interstitial solids and will consequently have an adverse effect on the representativeness of results. Regarding compaction, it should be ensured that after insertion of the permeameter cell the sample level on the inside of the tube is at a similar level to the media on the outside of the tube. Any discrepancy between these two levels suggests that sample compaction has occurred and the experiment would be better conducted at a new point close by.

4.3. Conclusions

A specification was developed for a method that would enable the three-dimensional spatial variation of hydraulic conductivity in a HSSF TW to be measured *in situ* and by a single operator. Several existing experimental methods were assessed on their ability to meet the specification, including: slug tests, pumping tests, water level surveying, borehole tests, infiltration tests, the laboratory permeameter, the modified cube method, direct porosity measurements, time domain reflectometry, capacitance probes, solids assays, tracer breakthrough curves and internal tracing. None of the existing methods were able to achieve the specification, which resulted in the development of a novel apparatus: the Aston Permeameter. The Aston Permeameter makes it possible, for the first time, to delineate vertical variations in hydraulic conductivity in HSSF TWs. The apparatus for the permeameter will enable measurements across a wide range of media hydraulic conductivities and can therefore be effectively utilised in both clean and clogged gravels. The apparatus is low cost, portable and robust, can be operated by one person with 10 litres of water or less, and most importantly complies with Severn Trent site safety policy.

The accuracy, repeatability and potential sources of error for the method were investigated, and it was concluded that measured hydraulic conductivity values are accurate to within ±30 %. This is because it is difficult to minimise or approximate the uncertainty associated with forcing the permeameter cell into the gravel and impacting the structural integrity of the sample. However, given the fact that hydraulic conductivity varies by several orders of magnitude in clogged systems, and most *in situ* hydraulic conductivity tests are invasive, it was deemed that The Aston Permeameter technique is adequate for the purpose of this study.

The apparatus will now be used to survey numerous HSSF TWs in the Severn Trent Water service area and three HSSF TWs operated by EcoCheck LLC in Minnesota, US.

5. Experimental Results

This Chapter provides the results obtained from experimental investigations into Horizontal Subsurface Flow Treatment Wetlands (HSSF TWs) using The Aston Permeameter (as introduced in **Chapter 4)**. The test explores spatial variations in media hydraulic conductivity in all three dimensions. By applying the test at numerous different sites it is hoped to improve understanding regarding how design and operational factors affect clogging, and provide data to calibrate the model derived in **Chapter 3**.

The test was applied at numerous HSSF TWs operated by Severn Trent, some several times to monitor how clogging develops over time. The test was also applied at three HSSF TWs in Minnesota, USA. An inventory of the systems surveyed is given in **Table 5-1** which provides the details for each system.

In early tests, vertical variations in hydraulic conductivity were not measured; only 2D clogging profiles were obtained. For these 2D experiments, the obtained results represent bulk hydraulic conductivity of the media in the vertical direction. Subsequent evolution of the Aston Permeameter allowed vertical variations in clogging to be identified, and 3D clogging profiles to be measured.

For each site visit a narrative and general observations are provided to help explain the results. Photographs are provided to relate the obtained results to the specific findings at a particular site. Each set of results includes:

a) A plan view figure that shows the location of experimental sampling points and major architectural features of the system. In these figures the hatched border around the white central region represents the rock berms. Grey shaded area indicates the presence of overland flow.
b) A plan view figure that includes a contour plot to show how the bulk hydraulic conductivity in the vertical direction varies over the surface of the bed.
c) Where 3D hydraulic conductivity profiling was performed, a figure that includes four or five contour plots (depending on how many longitudinal transects were measured). The contour plots detail the longitudinal and vertical variations of hydraulic conductivity for each transect.

Table 5-1 Inventory of the systems surveyed during this study, including salient features: system age at the test date; latitude (Lat.); longitude (Long.); length (L); width (W); upstream process (Upst. Proc.); influent distributor type (Infl. Dist); the d_{50} of the media; Hydraulic Loading Rate (HLR); and whether a 2D or 3D survey was performed. Table continued overleaf.

	Name	UK US	Test Date	Lat.	Long	Age yrs	L, m	W, m	Upst. Proc.	Influent Distributor	d_{50}, mm	HLR, m^3/d	2D 3D	Notes
1	Ashorne	UK	Jun 09	52.215	-1.553	16	15	18	RBC	Backwards trough	5	96	3D	Poor reed growth, some surface flow
2	Fenny Compton	UK	Mar 07	52.175	-1.386	0	12	40	RBC	Ports * 7	7	208	2D	Top 0.2 m has partial refurb. Equal influent dist.
3	Fenny Compton	UK	Feb 08	52.175	-1.386	1	12	40	RBC	Ports * 7	7	208	3D	No reed take up by year 1
4	Fenny Compton	UK	Feb 09	52.175	-1.386	2	12	40	RBC	Ports * 7	7	208	3D	Sporadic reed take up by year 2
5	Fenny Compton	UK	Mar 10	52.175	-1.386	2	12	40	RBC	Ports * 7	7	208	3D	Better reed establishment, some surface flow at inlet
6	Gaydon	UK	Apr 07	52.177	-1.464	5	15	30	RBC	Trough	5	208	2D	Overland flow over 60 % of bed
7	Greens of Dellwood	US	Jul 09	45.106	-92.981	12	20	15	Septic Tank	Subsurface Ports	10	9.5	3D	Some flooding, 6" clay mulch layer, small gravel
8	Jackson Meadows	US	Aug 09	45.193	-92.785	12	20	30	Septic Tank	Infiltration Chamber	12	20	3D	Aerated, dosing at inlet and outlet, geomembrane, reoriented header
9	Knightcote	UK	Mar 07	52.187	-1.411	0.5	12	20	RBC	Risers * 6	10	67	2D	Combined system, surface sludge formation
10	Leek Wooton	UK	Jun 09	52.315	-1.569	3	16	28	Filter	Risers * 5	6	180	3D	Good system

Table 5-1 Inventory of the systems surveyed during this study, including salient features: system age at the test date; latitude (Lat.); longitude (Long.); length (L); width (W); upstream process (Upst. Proc.); influent distributor type (Infl. Dist); the d_{50} of the media; Hydraulic Loading Rate (HLR); and whether a 2D or 3D survey was performed.

	Name	UK US	Test Date	Lat.	Long	Age yrs	L, m	W, m	Upst. Proc.	Influent Distributor	d_{50}, mm	HLR, m^3/d	2D 3D	Notes
11	Moreton Morrell A	UK	Jun 08	52.204	-1.556	16	15	15	RBC	Risers * 4	5	185	3D	Some surface flow
12	Moreton Morrell A	UK	Feb 09	52.204	-1.556	16.5	15	15	RBC	Risers * 4	5	185	3D	Lots of surface flow
13	Moreton Morrell A	UK	Sep 09	52.204	-1.556	17	15	15	RBC	Risers * 4	5	185	3D	Lots of surface flow
14	Moreton Morrell B	UK	Oct 09	52.204	-1.556	17	15	15	RBC	Risers * 4	5	0	3D	Receiving NO flow
15	Northend	UK	Jun 09	52.174	-1.431	17	14	40	RBC	Risers * 8	5	190	3D	Reeds trimmed and removed, 10% surface flow
16	Northend	UK	Apr 07	52.174	-1.431	15	14	40	RBC	Risers * 8	5	196	2D	20% surface flow, bad regrowth
17	Rowington	UK	Jul 09	52.325	-1.726	8	13	53	Filter	Ports * 6	6	280	3D	40% surface flow, good growth
18	Snitterfield	UK	Aug 09	52.241	-1.677	15	16	30	RBC	Risers * 6	5	275	3D	80% surface flow, good growth
19	Tamarack Farms	US	Jul 09	45.018	-92.865	8	33	18	Septic Tank	Subsurface Ports	10	10	3D	Hydrogen peroxide, been running at low level
20	Weston Under Wetherley	UK	May 09	52.315	-1.457	6	16	46	Filter	Trough	6	154	3D	Poor reed growth, operating with flooded surface, surface clog layer

The contour plots are produced using COMSOL Multiphysics 3.5 FEA software (COMSOL A.B., Sweden), which automatically performs linear extrapolations between measured values at each sampling point to produce surface plots. The contour levels represent order of magnitude changes in hydraulic conductivity. Each one of these plots uses the same colour palette for contours, which are expressed logarithmically:

- Black: -2 to -1 (0.01 m/d to 0.1 m/d)
- Brown: -1 to 0 (0.1 m/d to 1 m/d)
- Red: 0 to 1 (1 m/d to 10 m/d)
- Orange: 1 to 2 (10 m/d to 100 m/d)
- Yellow: 2 to 3 (100 m/d to 1,000 m/d)
- White: 3 to 4 (1,000 m/d to 10,000 m/d)

For tests in the UK, the surface clogging layer was not removed and therefore the vertical hydraulic conductivity profile also includes the hydraulic conductivity of the surface layer. This is done because in Severn Trent HSSF TWs the flow must infiltrate through the surface layer and therefore the hydraulic conductivity of the surface is an important hydrological component. Regarding UK beds, a 1 m clearance from where the gravel meets the rock berm was generally used to define the perimeter of the sampling net. In Minnesota, wastewater is loaded directly into the subsurface, and therefore the 0.3 m thick insulating mulch layer on the surface of the gravel plays no hydrological role in the system. The surface layer was removed at sampling locations in US systems so that the test was only performed on the subsurface gravel media.

Generally speaking sampling matrices consisted of 12-20 points, arranged in 3X4, 4X4 or 5X4 patterns depending on the geometry of the bed, and were distributed to evenly cover as much of the bed surface as possible. Hydraulic conductivities were measured down to a 0.4 m depth, which provided a 0.2 m safety clearance between the serrated end of the permeameter cell and the plastic liner. In 3D tests, four vertical measurements at 0.1 m intervals from the surface of the bed were recorded at each sampling point, to provide measurements down to a 0.4 m depth.

Results are reported according to the chronology of the tests, although sites where multiple investigations were performed over time have their results grouped together. Copies of the measurements taken during each test are included in **Appendix A**.

5.1. Northend (February 2007)

By April 2007 the HSSF TW at Northend had been providing tertiary support to a pair of RBCs for 15 years. Just prior to the survey the reeds had been harvested to allow GPR based clogging detection to be trialled. As such, the only visible aboveground vegetation was the cut stems of the reeds, although their relatively high density suggested a well-developed root mat. Northend is a 14 m long by 40 m wide system with influent distribution via six vertical risers that are width distributed along the inlet width (**Figure 5-1**). The influent entry point is situated in the centre of the influent distributor and the effluent exit point is located at one end of the effluent collector. **Figure 5-1** also details the 4X3 matrix of sampling points used in the experiment, which covered the central 20 m of the gravel media and most of the length. In subsequent tests the matrix was assigned to cover a larger fraction of the bed volume. At the time of the test a small region of overland flow was identified at the inlet in the vicinity of Transect A, as indicated by the grey shaded area in **Figure 5-1**.

The 2D vertical hydraulic conductivity profile obtained from the results is portrayed in **Figure 5-2**. For the region of the system that was surveyed, the vertical hydraulic conductivities of the different cores varied by three orders of magnitude. The lowest conductivity of 8 m/d was detected at Point A1 in the vicinity of the overland flow, which was the only value below 10 m/d. The vast majority of the bed had hydraulic conductivity between 10 and 100 m/d, although the three points adjacent to the outlet pipe displayed hydraulic conductivities above 100 m/d. The highest conductivity recorded was 590 m/d at Point B4.

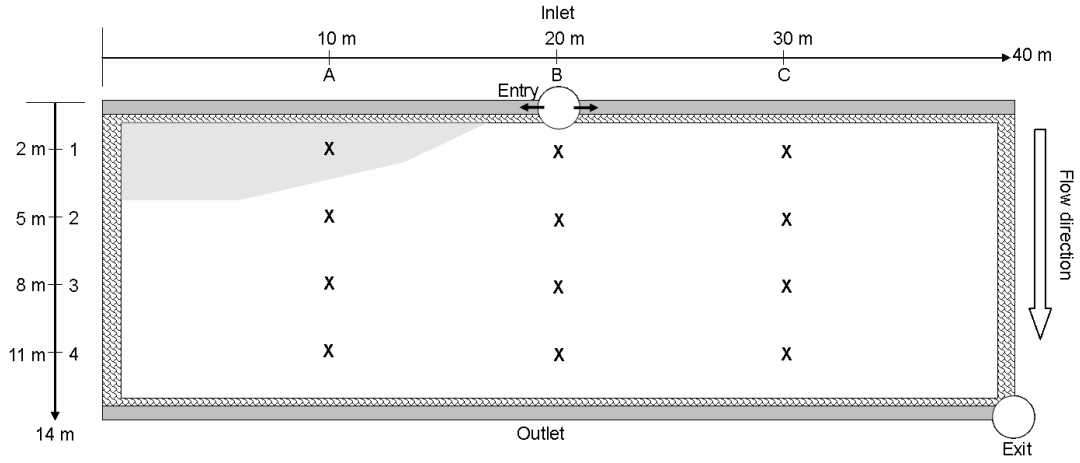

Figure 5-1 Plan view of Northend HSSF TW showing major architectural features and locations of sampling points for the February 2007 test. The influent distributor comprises 6 horizontal ports equally distributed along the length of the inlet pipe between Transects A and C. The hatched border around the white central region represents the rock berms. The grey shaded area indicates the occurrence of overland flow.

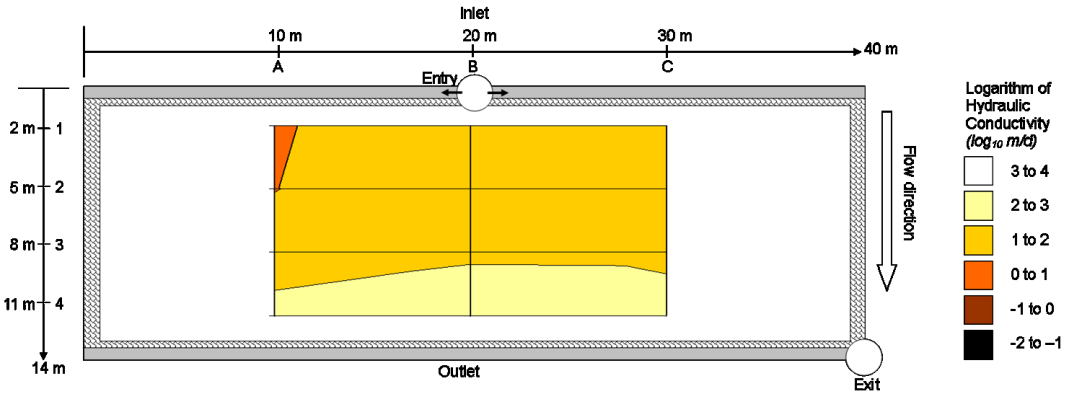

Figure 5-2 Northend 2D hydraulic conductivity profile at February 2007. The coloured contours represent the bulk vertical hydraulic conductivity profile in the top 0.4 m of media, which is based on a linear interpolation between the results obtained from each sampling point.

5.2. Gaydon (March 2007)

The wastewater treatment plant at Gaydon uses a 15 m long by 30 m wide HSSF TW to provide tertiary treatment for a combined humus tank/RBC. By March 2007 this wetland was 5 years old and showing good plant growth, with reeds generally greater than 2 m in height. **Figure 5-3** illustrates the system and the distribution of sampling points. The inlet distributor is a forward facing 'v-notch trough', which receives load from the secondary stage at an entry point located roughly halfway between Transect A and B. Conversely, the effluent exit point is located on the end of the effluent collector closest to Transect C. At the time of the test, large areas of the surface at Gaydon were affected by overland flow, as illustrated by the grey shaded area in **Figure 5-3**.

The 2D vertical hydraulic conductivity profile is shown in **Figure 5-4**. Up to 5.5 m from the inlet the entire width of the bed has hydraulic conductivity below 10 m/d. For Transect A and B this phenomenon extends up to 9.5 m from the inlet, although the corresponding location for Transect C was comparatively less clogged with a hydraulic conductivity value two orders of magnitude higher than Points A3 and B3. Hydraulic conductivities for those cores adjacent to the effluent collector were typically two orders of magnitude higher than elsewhere in the bed, with values between 67 and 109 m/d. The lowest hydraulic conductivity measured in the system was 0.34 m/d at Point C1, whilst the highest value was 109 m/d measured at Point B4.

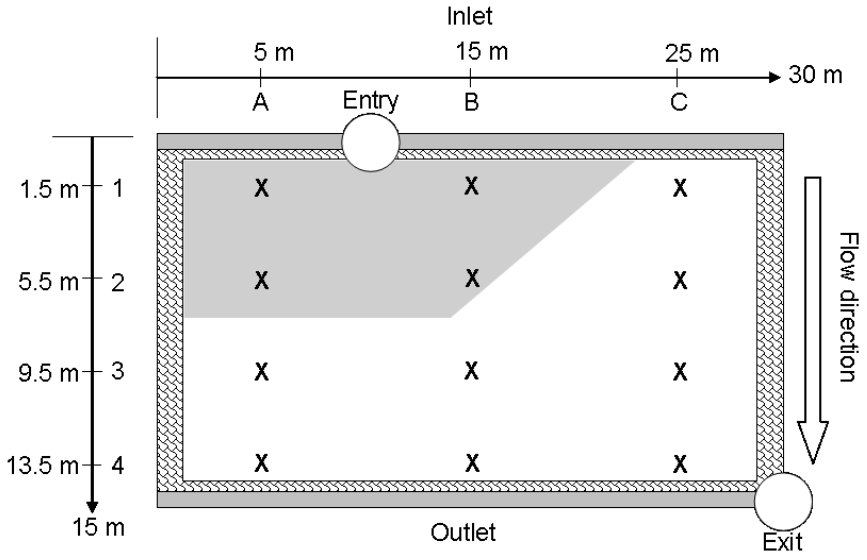

Figure 5-3 Plan view of Gaydon HSSF TW showing major architectural features and locations of sampling points for the February 2007 test. The influent distributor comprises a forward facing trough with v-notches at numerous points along the bed width.

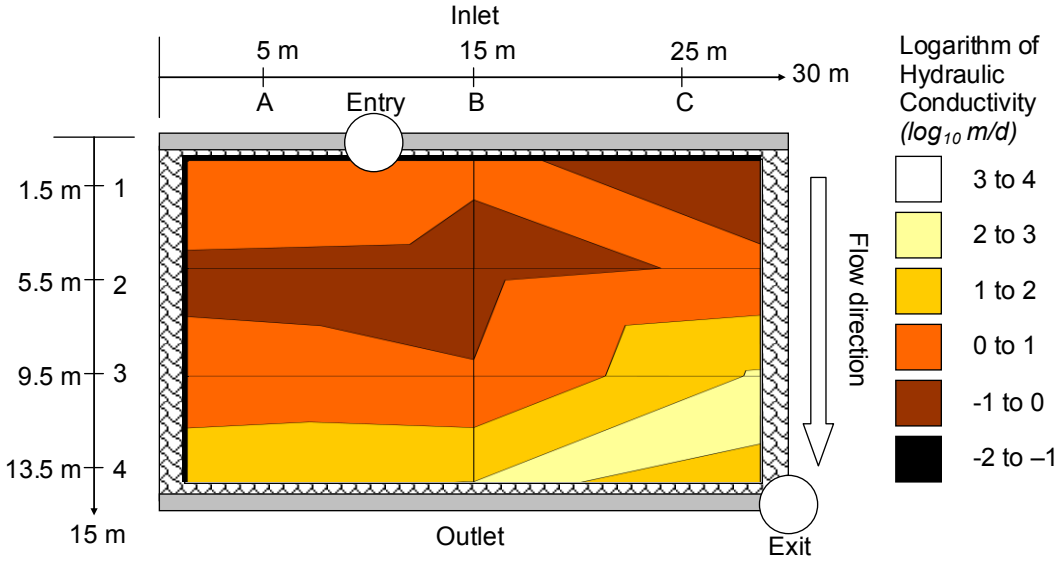

Figure 5-4 The 2D vertical hydraulic conductivity profile measured at Gaydon.

5.3. Knightcote (March 2007)

Knightcote is the only combined tertiary and storm wastewater treatment HSSF TW to be considered during this study, all the rest being tertiary only. Knightcote is 12 m long by 20 m wide, and the inlet comprises six vertical risers equally distributed along the width at the inlet. This information, along with the sample point layout is summarised in **Figure 5-5**. The influent entry point and effluent exit point are both located on the same side of the bed, adjacent to Transect A. The wetland was surveyed five months after it was fully refurbished and was already displaying symptoms of clogging caused by stormwater solids and uneven influent distribution. The vast majority of the flow was emanating from the two vertical risers closest to the influent entry point, near Transect A. This had resulted in a region of overland flow that stretched from inlet to outlet along Transect A and across most of the inlet region (**Figure 5-6**).

Figure 5-7 illustrates the 2D vertical hydraulic conductivity profile for Knightcote. The lowest hydraulic conductivity in the bed is 0.7 m/d and was measured for Point A2. Generally speaking, hydraulically conductivity down Transect A was below 100 m/d, which coincided with the occurrence of overland flow. In contrast, large areas of Transects B and C downstream from the inlet had hydraulic conductivity above 1,000 m/d. The highest hydraulic conductivity is 1,928 m/d and was measured at point B2. Adjacent to the inlet, conductivity values were on the order of 10 to 100 m/d.

A revisit to the system a few weeks after the survey showed that the surface sludge layer had largely mineralised (**Figure 5-8**), reducing in volume and resulting in the disappearance of overland flow. This occurred because the weather had been predominantly sunny and the bed surface was able to adequately mineralise in the absence of plant shading. The site was not resurveyed but the hydraulic benefit is clear by comparing **Figure 5-6** with **Figure 5-8**.

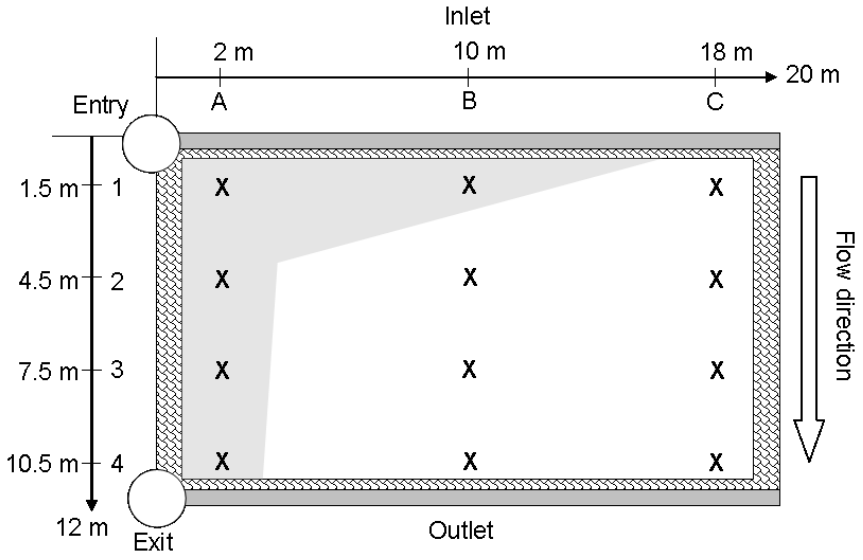

Figure 5-5 Plan view of Knightcote HSSF TW showing major architectural features and locations of sampling points. The influent distributor comprises six vertical risers evenly distributed along the inlet pipe. The grey shaded area indicates the occurrence of overland flow.

Figure 5-6 (Left) Sludge accumulation on the surface of Knightcote just five months after refurbishment, which has resulted in surface flow. This picture is taken looking down Transect A from inlet to outlet. A vertical riser can be seen in the forefront. The poor reed growth is a symptom of planting just prior to winter. (Right) Sludge accumulations within the upper layer of the gravel media at Point A2.

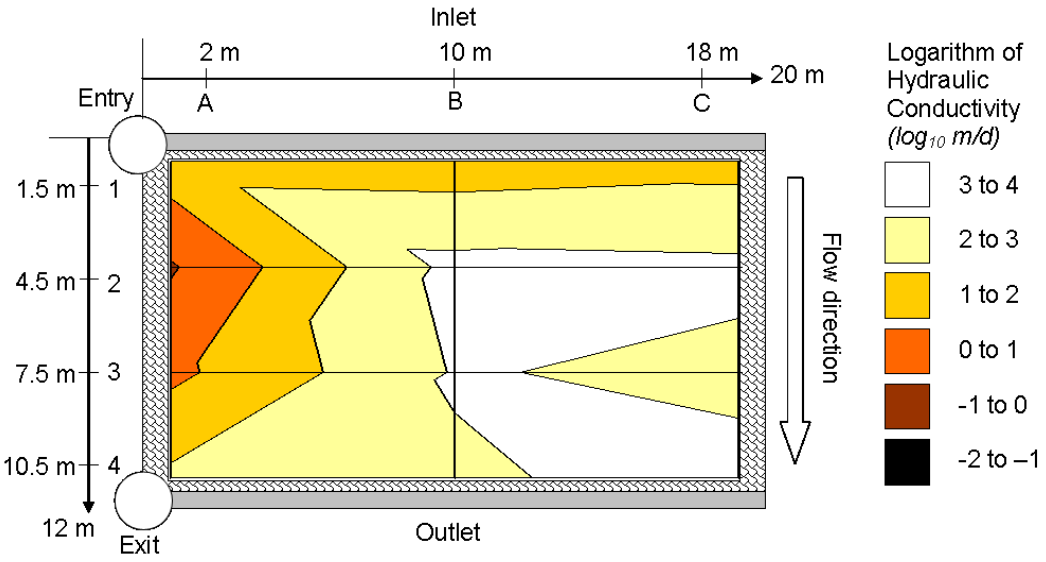

Figure 5-7 The 2D vertical hydraulic conductivity profile at Knightcote

Figure 5-8 The largely mineralised surface sludge layer at Knighcote just four weeks after the site was surveyed. The picture is taken behind Point C4 looking towards Point A1.

5.4. Fenny Compton (February 2007)

Fenny Compton is a 12 m long by 4 m wide system that provides tertiary support for an RBC. The major system features and layout of sampling locations are given in **Figure 5-9**. At the time of the test Fenny Compton had just undergone a partial refurbishment, whereby the top 200 mm of clogged gravel media had been removed and replaced with clean gravel. It was considered that the bottom 400 mm of gravel was not clogged enough to require replacement, and had been left intact. The spec of the original gravel was 3-6 mm and the new upper gravel layer was 6-12 mm. Despite the partial refurbishment it was assumed that Fenny Compton represented a good benchmark upon which to base the hydraulic conductivity of a new system. The influent distribution system at Fenny Compton comprises 6 horizontal ports connected to the inlet pipe. As evident in **Figure 5-9** the effluent discharge is located on the opposite corner of the bed to where the influent enters the inlet pipe. A 4X3 sampling matrix was used as indicated in **Figure 5-9**. The results of the 2D hydraulic conductivity survey are shown in **Figure 5-10**.

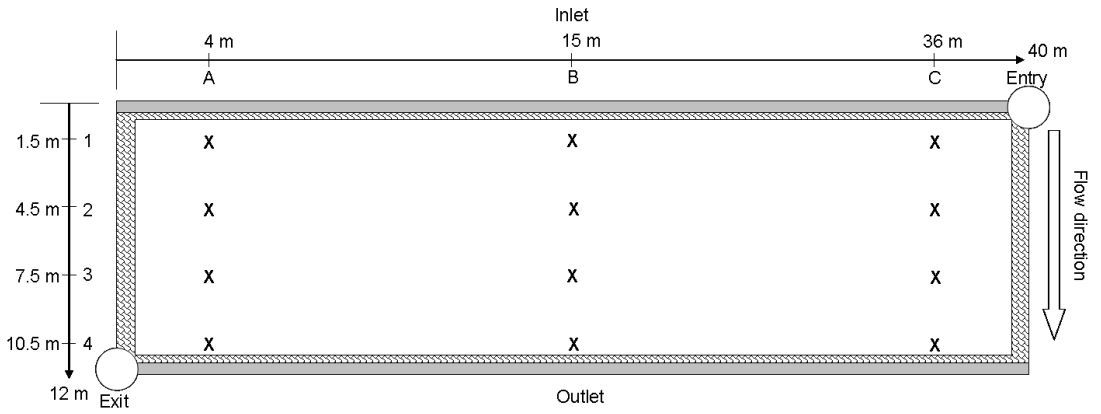

Figure 5-9 Plan view of Fenny Compton HSSF TW showing major architectural features and locations of sampling points for the February 2007 test. The influent distributor comprises 6 horizontal ports equally distributed along the length of the inlet pipe between Transects A and C.

Generally speaking, the gravel hydraulic conductivity at Fenny Compton was high, with values varying between 57 m/d at point C1 and 6,035 m/d at point C3. However, sampling point C2 had as uncharacteristically low hydraulic conductivity of approximately 0.01 m/d. Excavations at this point showed that the gravel material contained a large quantity of inorganic fines typical of unwashed gravel. This may have been introduced during construction. There was also a general increase in conductivity from inlet to outlet demonstrated by values along sampling plane 4 being between 1,907 m/d and 4,572 m/d.

Over the test period it was observed that the majority of the influent was distributed through the two ports closest to Transect A, and the ports nearer Transects B and C received less flow. Early signs of uneven clog matter formation in front of the different ports are demonstrated in **Figure 5-11**, after only a few weeks of operation.

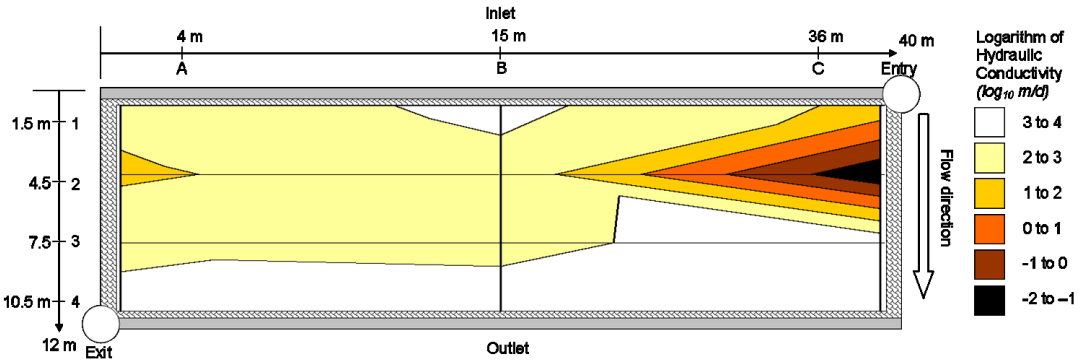

Figure 5-10 The 2D vertical hydraulic conductivity profile at Fenny Compton

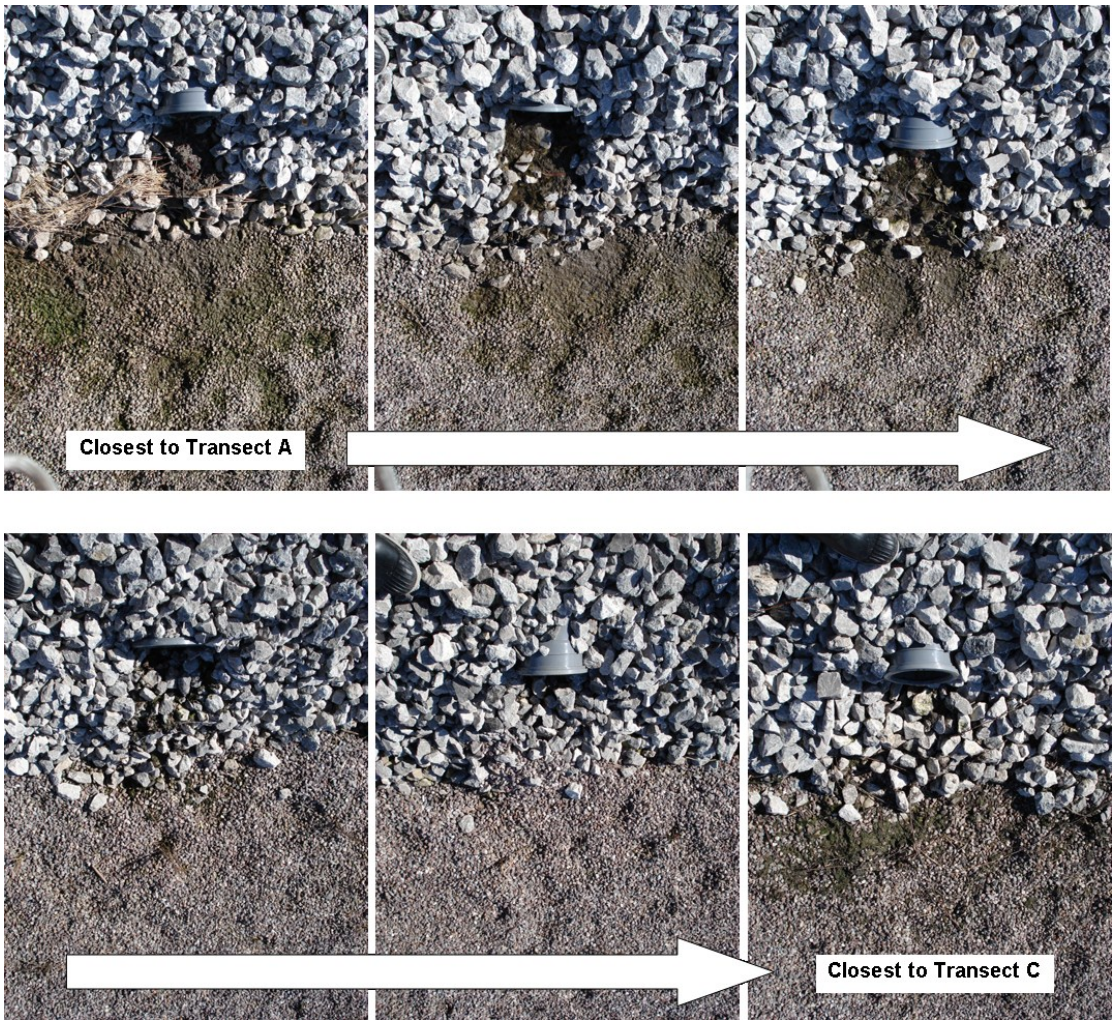

Figure 5-11 Uneven clog matter development, due to uneven influent distribution, in front of the horizontal ports at Fenny Compton, a few weeks after refurbishment.

5.5. Fenny Compton (February 2008)

The same system at Fenny Compton was revisited a year after the February 2007 test to observe the development of clogging over the first year of operation. Hydraulic conductivity measurements were performed on a 4X5 sampling matrix (**Figure 5-12**) using the then newly developed 3D surveying method. The 2D vertical hydraulic conductivity profile is shown in **Figure 5-13**, and the 3D hydraulic conductivity results comprising the longitudinal-vertical hydraulic conductivity profiles of Transects A to D, are shown in **Figure 5-14**.

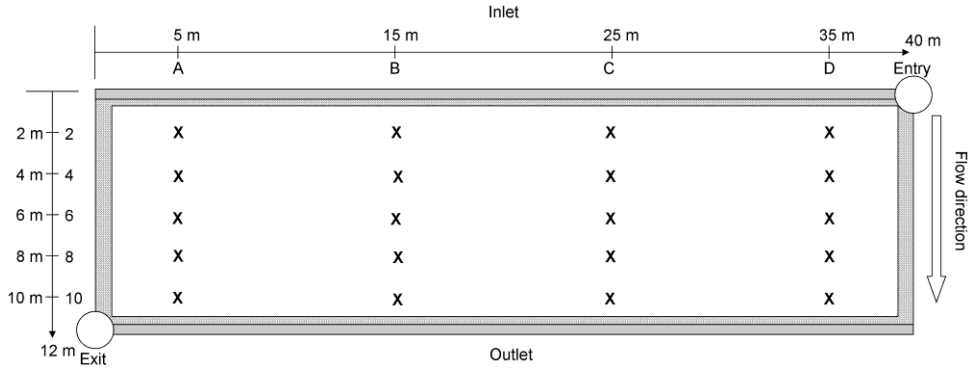

Figure 5-12 The locations of sampling points for the February 2008 test at Fenny Compton.

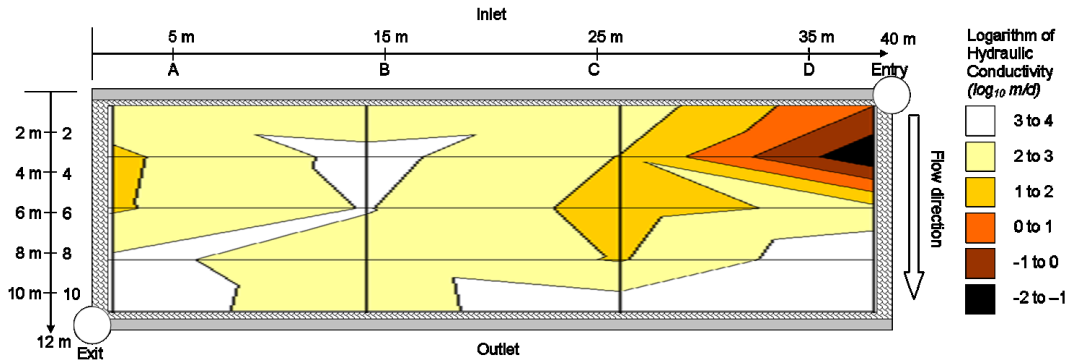

Figure 5-13 The 2D vertical hydraulic conductivity profile for Fenny Compton at February 2008.

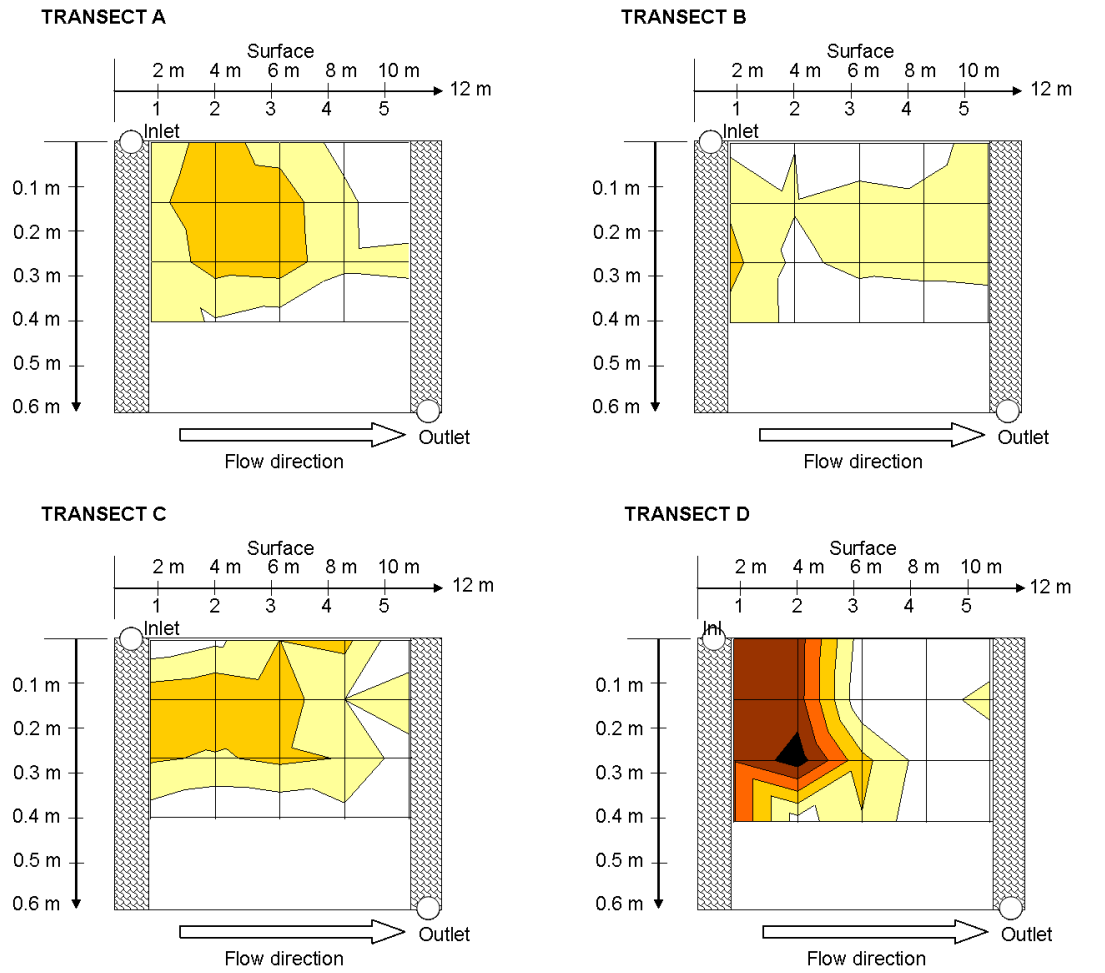

Figure 5-14 The 3D hydraulic conductivity profile of Fenny Compton at February 2008. The longitudinal versus vertical hydraulic profiles are shown for the four transverse cross-sections that correspond to sampling Transects A to D. Sampling was performed to a 0.4 m depth below the surface of the bed and results are linearly interpolated between sampling points. Colour contours indicate orders of magnitude of media hydraulic conductivity.

No results were obtained for Points B4 and D1 and data used for these points are inearly interpolated from the results obtained for surrounding points. The 2D profile illustrated in **Figure 5-13** is similar to that obtained in 2007 (**Figure 5-10**), and show a general increase from 100-1,000 m/d at the inlet to 1,000-10,000 m/d at the outlet. The 3D results shown in **Figure 5-14** support the observation of localised clogging at sampling point D2, finding hydraulic conductivity values as low as 0.03 m/d at a depth 0.3 m below the gravel surface.

This agrees with the findings of the 2007 test at Fenny Compton, which indicated localised clogging at point D2 as a result of construction fines occupying the pore spaces in between the gravel particles. Apart from Transect D, the other Transect profiles suggest that hydraulic conductivity increases by one to two orders of magnitude from inlet to outlet. Furthermore clogging generally appears to be most apparent at depths of 0.1 to 0.3 m below the gravel surface, which corresponds to the transition between the 6 - 12 mm gravel in the upper layer and the 3 - 6 mm gravel in the lower layer. The conductivity values between these depths were often being 1 to 2 orders of magnitude lower than those measured in the rest of the vertical cores. Apart from point D2, the lowest hydraulic conductivity value found on the bed was 1.05 m/d which corresponded to the top 0.1 m of gravel at point D1. The highest hydraulic conductivity of 83,000 m/d was recorded through the top 0.1 m of gravel at point C5.

It was noted that reed growth during the first year had been poor and establishment across the bed was isolated to sporadic patches. For example, the region downstream of the low hydraulic conductivity region at point D2 was practically bare of reeds, whereas the zone upstream of point D2 exhibited far better establishment (**Figure 5-15**). Visual survey revealed the establishment of surface clogging near the influent distributor ports, which is illustrated in **Figure 5-15** for the port closest to Transect D.

Figure 5-15 (Left) Sporadic reed establishment at Fenny Compton after one year of growth. The picture is taken looking along Transect D from outlet to inlet. The region in the forefront with sparse reed population corresponds to sampling points D3 and D4, whereas the comparatively lush growth at points D1 and D2 can be seen in the background. (Right) Surface clogging development in front of the influent distributor port closest to Transect D.

5.6. Fenny Compton (February 2009)

A 4X4 sampling matrix was utilised for the 2009 sampling test, as described in **Figure 5-16**. Prior to the test, the weather had been snowy and the treatment plant was receiving a large volume of snow-melt. The vertical 2D and 3D interpolated hydraulic conductivity profiles are given in **Figure 5-17** and **Figure 5-18** respectively. Compared with the 2D profiles for the previous two years, the 2009 results show a general decline in hydraulic conductivity over the entire bed, with no results exceeding 1000 m/d. Hydraulic conductivity in the inlet regions of Transects A and D had decreased to 0.64 m/d and 0.18 m/d respectively. Furthermore, the low hydraulic conductivity values associated with point D2 were now also apparent at point C2, where the core conductivity was 0.06 m/d. A general increase of 2-3 orders of magnitude hydraulic conductivity is evident from inlet to outlet.

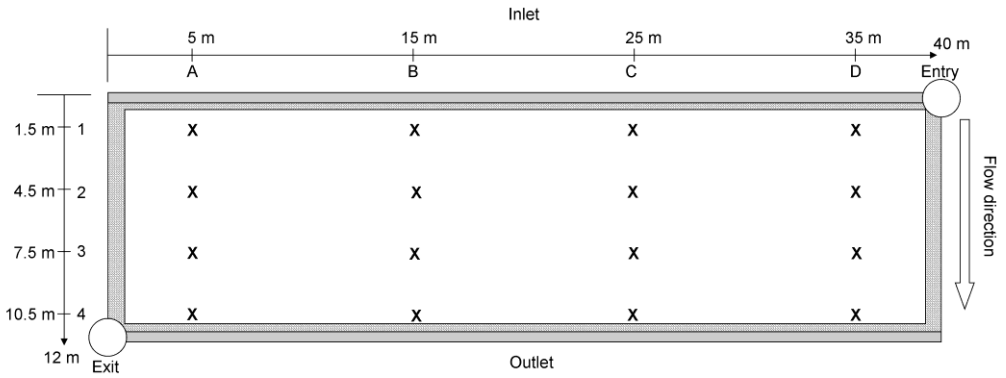

Figure 5-16 The locations of sampling points for the February 2009 test at Fenny Compton

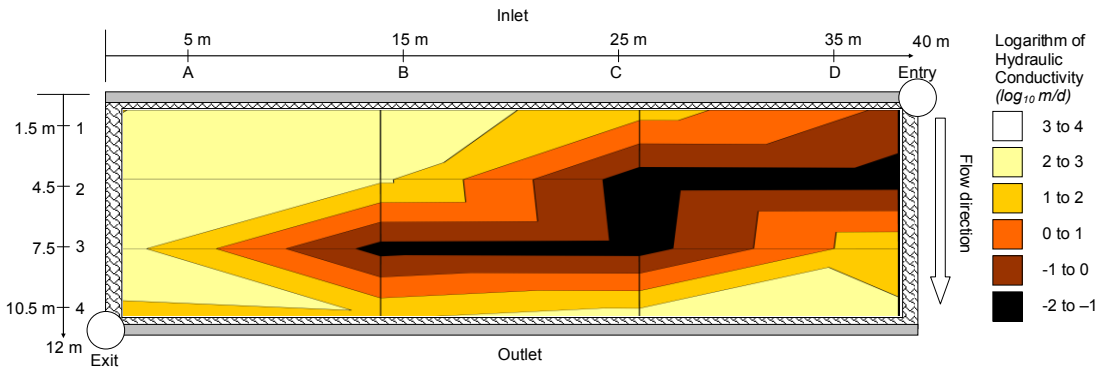

Figure 5-17 The 2D vertical hydraulic conductivity profile for Fenny Compton at February 2009

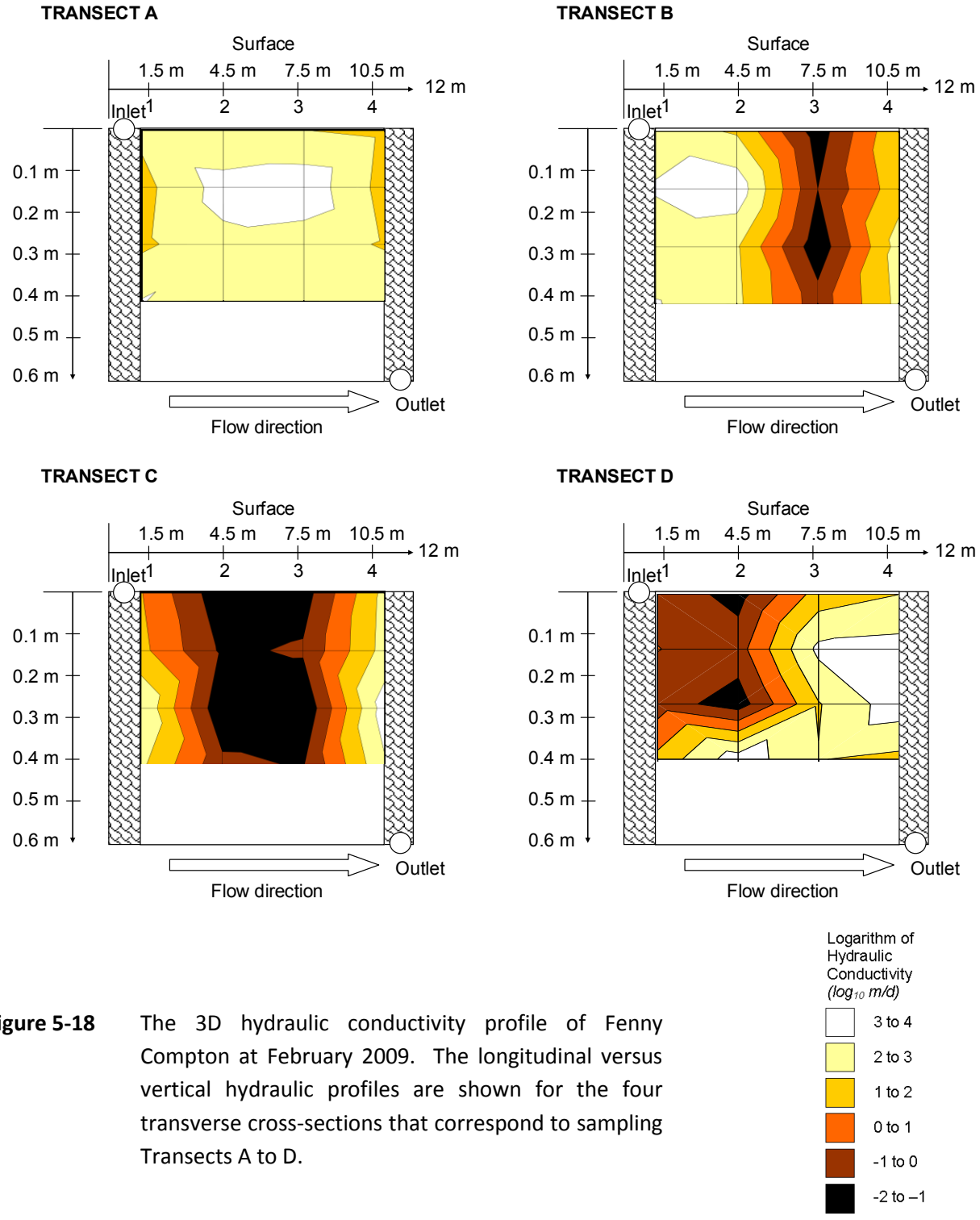

Figure 5-18 The 3D hydraulic conductivity profile of Fenny Compton at February 2009. The longitudinal versus vertical hydraulic profiles are shown for the four transverse cross-sections that correspond to sampling Transects A to D.

The 3D results show a significant change from the year before. The vertical distribution of hydraulic conductivity at the inlets of Transect A and B is relatively uniform. The vertical profile at C2 confirms that a zone of very low hydraulic conductivity has developed across the entire reactor depth, which is most significant in the top 0.1 m of gravel where the

hydraulic conductivity had dropped to 0.03 m/d. The profile for the downstream half of Transect D indicates that a small increase in clogging has occurred above 0.1 m and below 0.4 m depth, with negligible deviation from clean media values between these bounds. Clogging may have developed in this way because the inlet region adjacent to point D1 receives a disproportionately large fraction of the influent flow. Once in the subsurface, this flow takes the path of least resistance around the clogged media at the 0.3 m depth of point D2, and preferential flow-paths occur through point C2. This has caused the hydraulic conductivity at point C2 to decrease by two orders of magnitude between 2008 and 2009.

The general decrease in media hydraulic conductivity in the top 0.1 m of the bed can be attributed to plant detritus that has accumulated on the surface of the bed after winter plant die-off. This is confirmed by **Figure 5-19** (right), which also shows that reed growth in the downstream areas of Transect C and D is still poor (left). Second year reed growth generally exceeded first year growth, with reed crop height exceeding 1.5 m in places.

Figure 5-19 (Left) Continued evidence of poor reed establishment in the downstream half of Transects C and D, at Fenny Compton two years after planting. The photo is taken from sampling point D4 looking towards sampling point A1, such that the poorly vegetated foreground roughly encompasses points D4 and C3. (Right) Surface clog matter accumulations after two years operation, mainly comprising plant detritus and bio-solids washout from upstream processes. A small amount of surface ponding is evident.

5.7. Fenny Compton (March 2010)

A 5X4 sampling matrix was utilised for the 2010 test at Fenny Compton, as described in **Figure 5-20**. The vertical 2D and 3D interpolated hydraulic conductivity profiles are given in **Figure 5-21** and **Figure 5-22** respectively. Prior to the test the weather had been relatively dry and sunny. Compared with the 2D profiles for the February 2009 test, the 2010 results show a general increase in hydraulic conductivity over the entire bed, with no results below 1 m/d. A general increase of 3 orders of magnitude hydraulic conductivity is evident from inlet to outlet and the majority of the bed has vertical hydraulic conductivity between 10 m/d and 1000 m/d. The hydraulic conductivity at the inlet adjacent to Transect A, C and E was between 1 m/d and 10 m/d. The hydraulic conductivity in the vicinity of point E2 has increased by three orders of magnitude to 75 m/d.

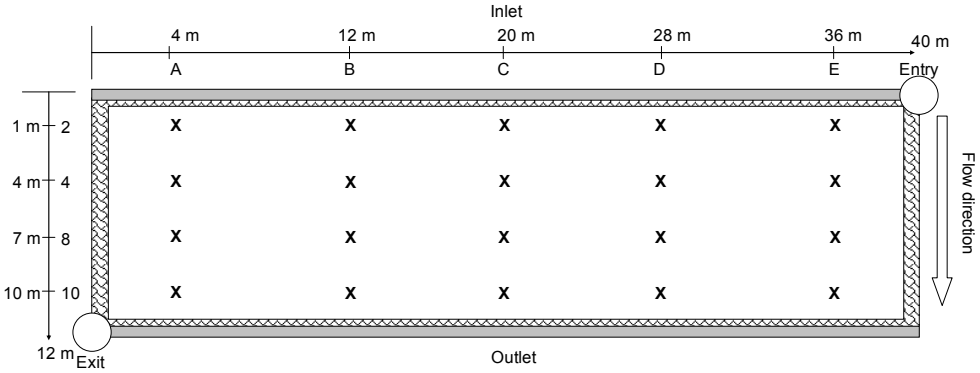

Figure 5-20 The locations of sampling points for the March 2010 test at Fenny Compton

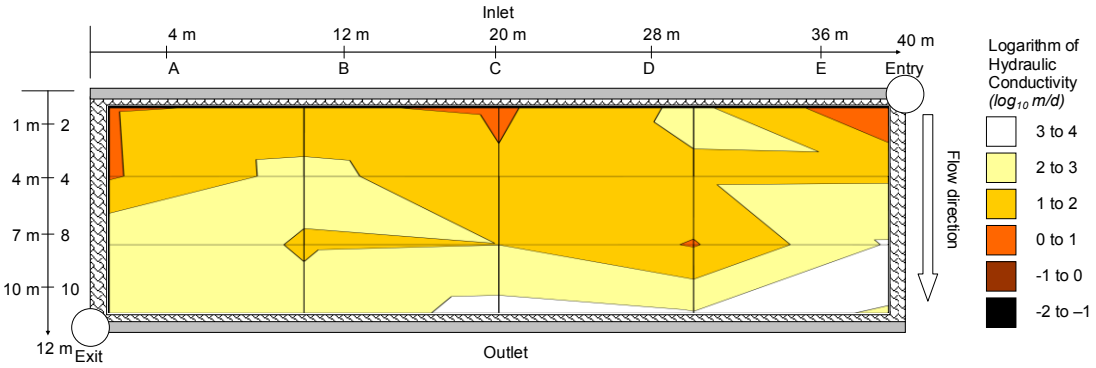

Figure 5-21 The 2D vertical hydraulic conductivity profile for Fenny Compton at March 2010

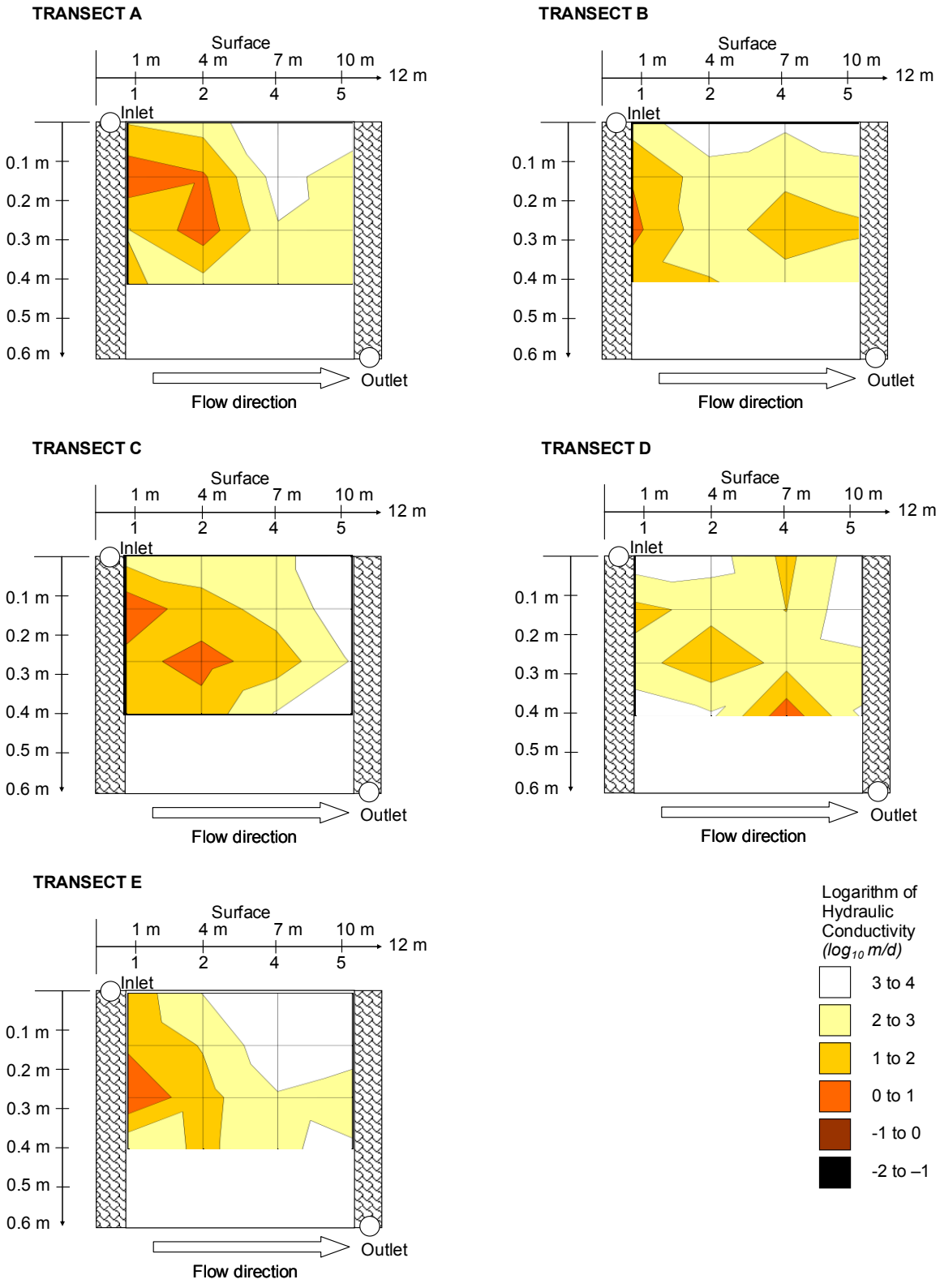

Figure 5-22 The 3D hydraulic conductivity profile of Fenny Compton at March 2010. The longitudinal versus vertical hydraulic profiles are shown for the five transverse cross-sections that correspond to sampling Transects A to E.

No measurements were made of hydraulic conductivity below 1 m/d during the 2010 3D profiling of Fenny Compton. The 3D hydraulic conductivity profiles illustrated in **Figure 5-22** confirm that even the low hydraulic conductivity that was previously measured at a 0.3 m depth at point E2 had increased to 44 m/d. Reeds were well established at point E2 by 2010 and investigation confirmed that roots had penetrated to a depth of 0.3 m below the surface, which would serve to disrupt the fines accumulated in the gravel pore spaces and increase hydraulic conductivity through the media.

Also notable by comparing **Figure 5-18** with **Figure 5-22** is that hydraulic conductivity in the top 0.1 m of gravel has returned to between 100 and 10,000 m/d across the majority of the bed. In 2010 there was less evidence of plant detritus on the surface of the system and the surface layer appeared well mineralised, which can be attributed to the period of relatively dry sunny weather that preceded the test. The hydraulic conductivity at a 0.4 m depth in the vicinity of the effluent collector had decreased to below 1,000 m/d for the first time. This suggests that clogging is increasing in the vicinity of the effluent collector, perhaps because the effluent collector is the focal point for all flow leaving the bed.

5.8. Moreton Morrell (June 2008)

Tertiary treatment support is provided to two RBC units at Moreton Morrell, using four identical, square HSSF TWs with sides of 15 m. The influent distributors consist of four vertical risers evenly spaced along the width of the inlet pipe. A flow splitter is used to distribute the influent between the four beds. One bed in particular showed symptoms of advanced stage clogging, including thick surface sludge accumulation, extensive overland flow and blocked influent distributors, and was therefore selected for investigation. **Figure 5-23** details the major architectural features of the Moreton Morrell system, and the arrangement of the 4X4 sampling matrix used for the survey. As evident in **Figure 5-23** the effluent discharge is transversely located on the same side of the bed to where the influent enters the inlet pipe. The 2D and 3D hydraulic conductivity profiles are given in **Figure 5-24** and **Figure 5-25** respectively.

The 2D vertical hydraulic profile presented indicates that clogging generally increases by three to four orders of magnitude from inlet to outlet. Values at the inlet are between 0.1 m/d and 10 m/d. The 3D hydraulic conductivity results support that hydraulic conductivity is two to three orders of magnitude lower at the inlet than elsewhere in the bed, with values between 0.01 m/d and 10 m/d, and is distributed relatively uniformly across the vertical depth. Downstream hydraulic conductivity values vary between 100 m/d and 10,000 m/d, and on average the upper gravel layers appear more clogged than lower depths. Below 0.3 m, the hydraulic conductivity along Transect A is an order of magnitude lower than elsewhere in the bed. The hydraulic conductivity across the length of Transect D is generally an order of magnitude greater than the hydraulic conductivity across the other three transects.

The reed establishment at Moreton Morrell was relatively uniform with reed height exceeding 2.5 m near the inlet. The locations of the four vertical risers closely corresponded to the locations of the four Transects. It was noted that those risers at Transects C and D were completely blocked with bio-solids. The majority of the flow was emanating from the riser at Transect A, with a small fraction emanating from the riser at Transect B.

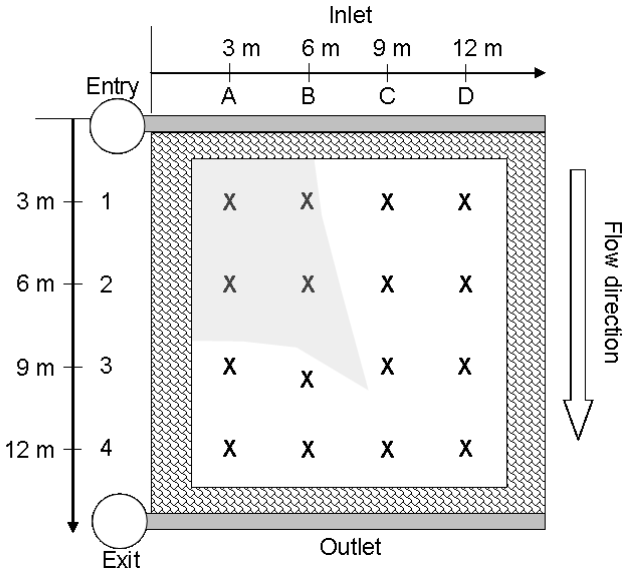

Figure 5-23 Plan view of Moreton Morrell HSSF TW showing major architectural features and locations of sampling points for the June 2008 test. The influent distributor comprises 4 vertical risers equally distributed along the length of the inlet pipe between Transects A and D.

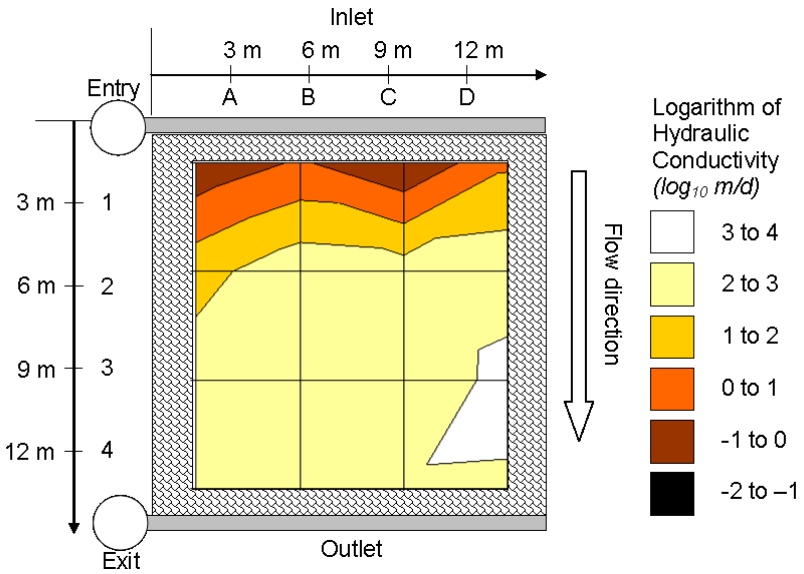

Figure 5-24 The 2D vertical hydraulic conductivity profile of Moreton Morrell at July 2008.

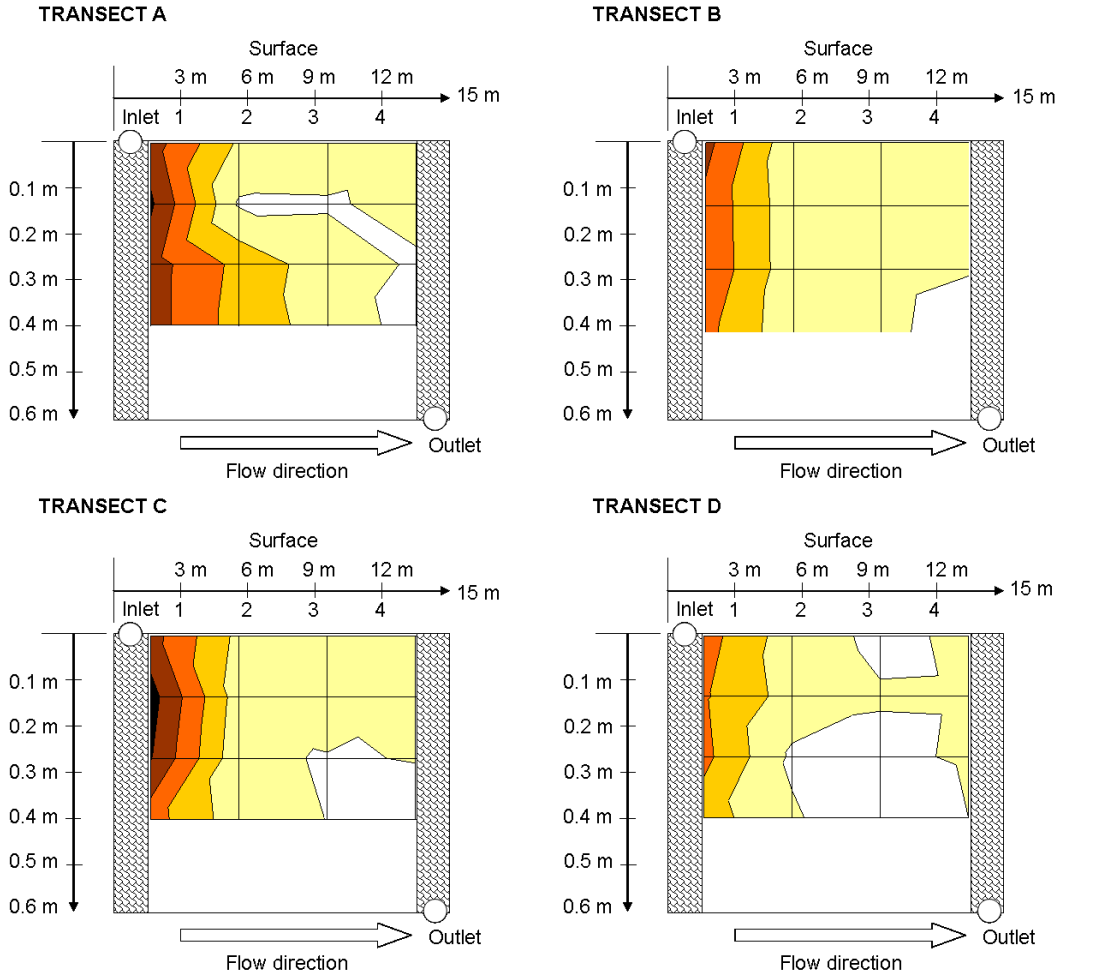

Figure 5-25 The 3D hydraulic conductivity profile of Moreton Morrell at June 2008. The longitudinal versus vertical hydraulic profiles are shown for the four transverse cross-sections that correspond to sampling Transects A to D. Sampling was performed to a 0.4 m depth below the surface of the bed and results are interpolated between sampling points. Colour contours indicate order of magnitude divisions in hydraulic conductivity.

5.9. Moreton Morrell (February 2009)

The same system at Moreton Morrell was revisited in February 2009 and resurveyed. High winter flow-rates had increased the extent of overland flow on the bed, as indicated in **Figure 5-26**, which also illustrates the sampling matrix used (identical to the sampling matrix used in June 2008). The results of the 2D and 3D hydraulic conductivity surveys are given in **Figure 5-27** and **Figure 5-28**, respectively.

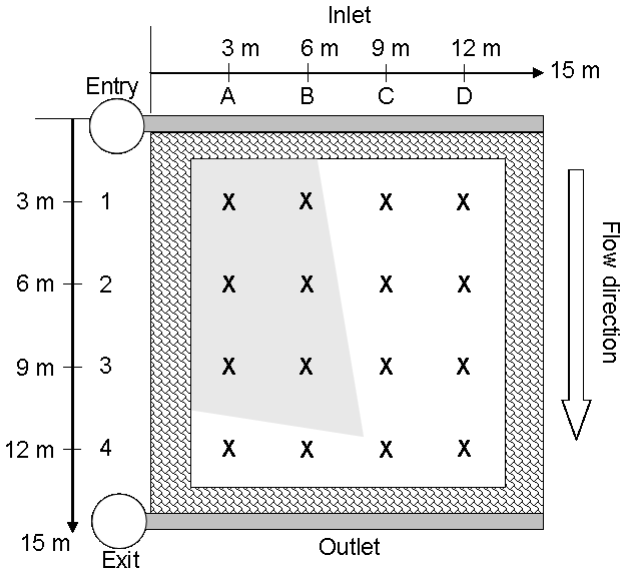

Figure 5-26 Plan view of Moreton Morrell HSSF TW showing major architectural features and locations of sampling points for the February 2009 test. The region of overland flow has extended compared to the situation in July 2008.

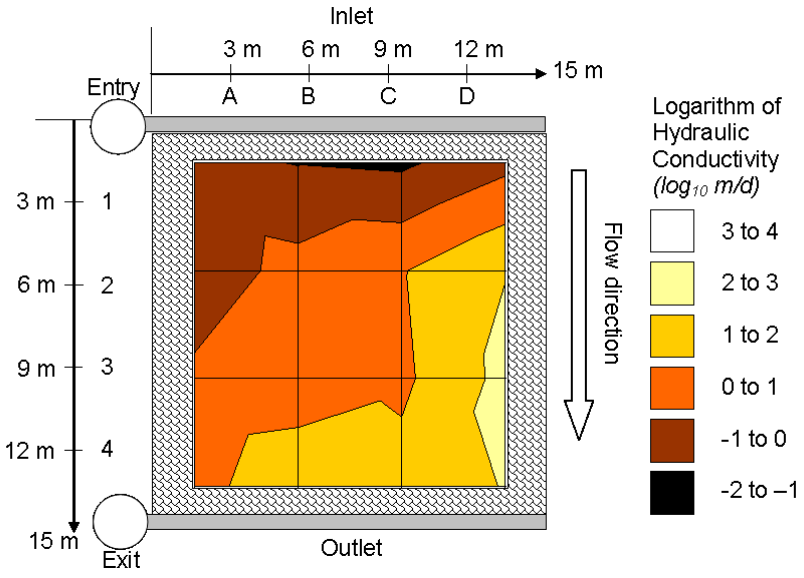

Figure 5-27 The 2D vertical hydraulic conductivity profile of Moreton Morrell at February 2009.

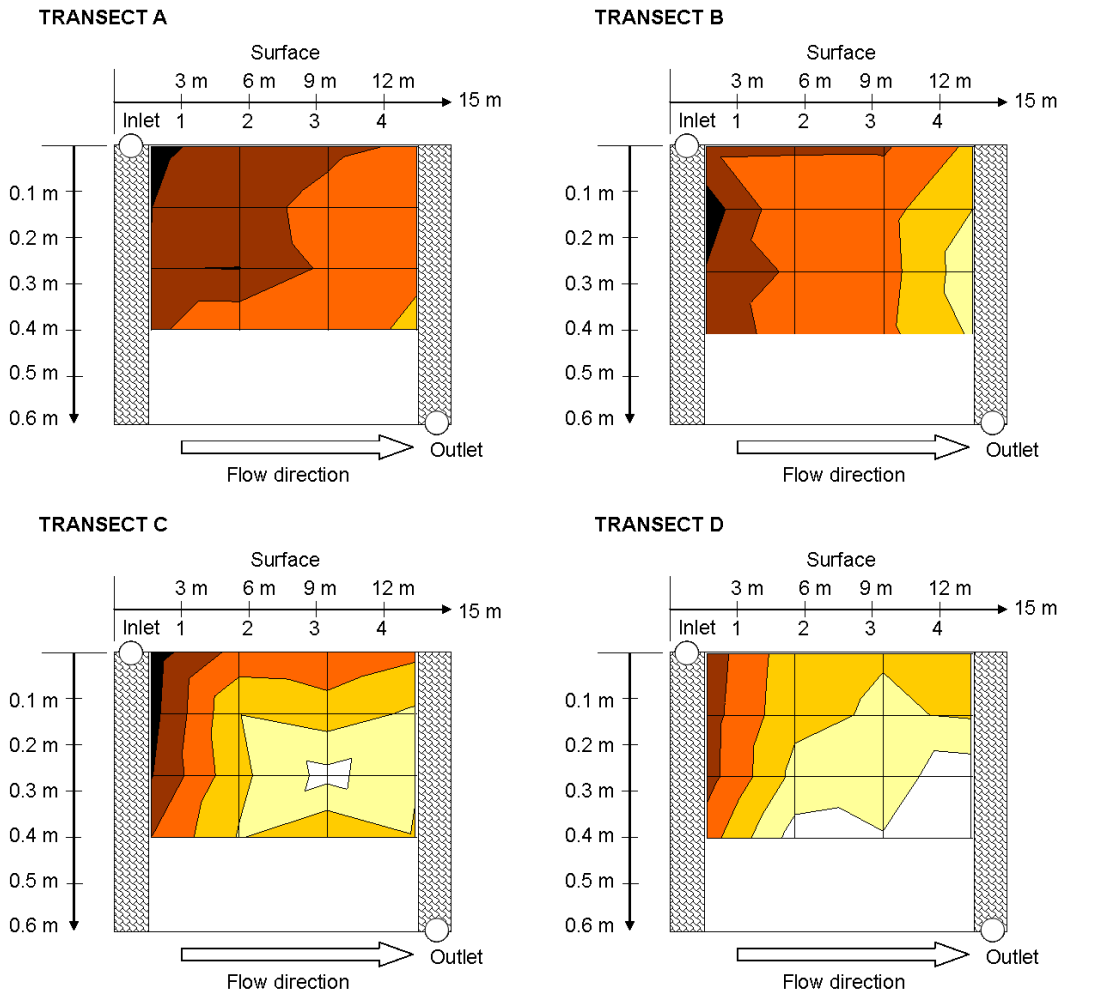

Figure 5-28 The 3D hydraulic conductivity profile of Moreton Morrell at February 2009. The longitudinal versus vertical profiles are shown for the four transverse cross-sections that correspond to sampling Transects A to D.

According to the 2D hydraulic conductivity profile (**Figure 5-27**) clogging in the system has worsened between the period June 2008 and February 2009. Previously, hydraulic conductivity below 10 m/d was only detected in the vicinity of the inlet; however, 9 out of the 16 sampling locations tested in 2009 exhibited hydraulic conductivity below 10 m/d. The majority of Transect A was covered by overland flow and hydraulic conductivity only

increased by two orders of magnitude from 0.1 m/d to 100 m/d. Comparisons between transects shows that hydraulic conductivity increases by two orders of magnitude in the transverse direction between Transect A and Transect D. This effect was not apparent for the June 2008 experiment.

Comparison between the June 2008 (**Figure 5-25**) and February 2009 (**Figure 5-28**) transect profiles indicates that along Transects C and D the increase in clogging has mainly been in the upper surface, where hydraulic conductivity values have dropped from between 100 and 1,000 m/d to between 1 and 100 m/d. Clogging has spread both vertically and horizontally along Transects A and B, which is particularly apparent along the 6-9 m mid-section, where values have decreased by 2 to 3 orders of magnitude between sampling periods. The upper gravel media tends to be more clogged than the lower gravel media in Transects A and B. Visual survey confirmed that influent distribution risers still suffer variable degrees of clogging, with the two risers at Transects A and B receiving all of the flow (**Figure 5-29**).

Figure 5-29 (Left) Flowing inlet riser at Transect A. The extent of surface ponding and washout of sanitary storm solids is identifiable. (Right) An inlet riser at Transect D which is clogged by bio-solids.

5.10. Moreton Morrell (September 2009)

Moreton Morrell was revisited at the end of September 2009 and resurveyed using the same sampling matrix as the previous two tests. The profile of overland flow was very similar to that reported in June 2008 in **Figure 5-23**. The 2D vertical and 3D hydraulic conductivity profiles are presented in **Figure 5-30** and **Figure 5-31**, respectively.

Comparison between **Figure 5-30** and **Figure 5-27** indicates that clogging at Moreton Morrell has again worsened over the period February to September 2009. No vertical core hydraulic conductivity values above 100 m/d were found and over three quarters of the samples now exhibit values below 10 m/d. Similar to February, highest values were found at point D4, and hydraulic conductivity generally deceased by two orders of magnitude in the longitudinal and transverse direction.

The 3D hydraulic conductivity results presented in **Figure 5-31** confirm that clogging across all transects is more severe in October than in February. For Transects A and B, the upper 0.3 m of media in the first half of the bed generally has hydraulic conductivity below 1 m/d. Hydraulic conductivity above 10 m/d was only detected at 0.4 m depths at points downstream of the inlet. Conductivity of the upper media has continued to decrease for all points along Transects C and D. Along Transect C the vast majority of the bed now has hydraulic conductivity below 100 m/d.

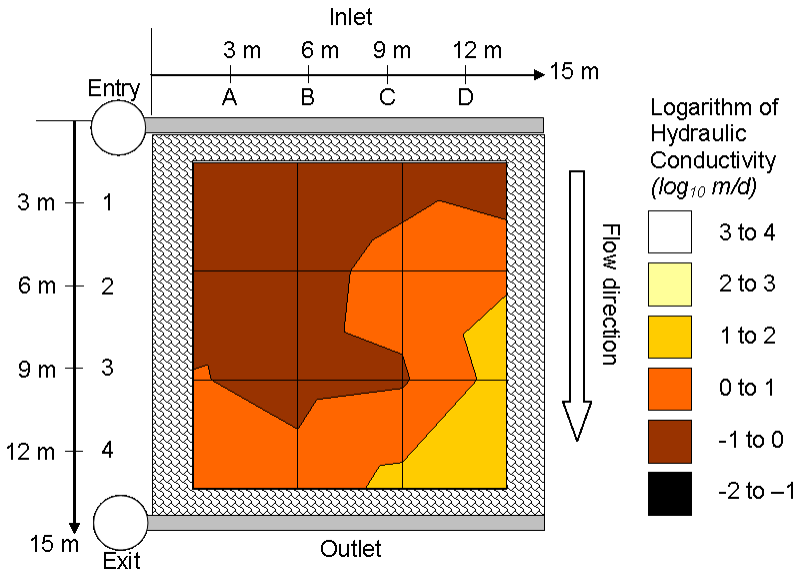

Figure 5-30 The 2D vertical hydraulic conductivity profile for Moreton Morrell at September 2009.

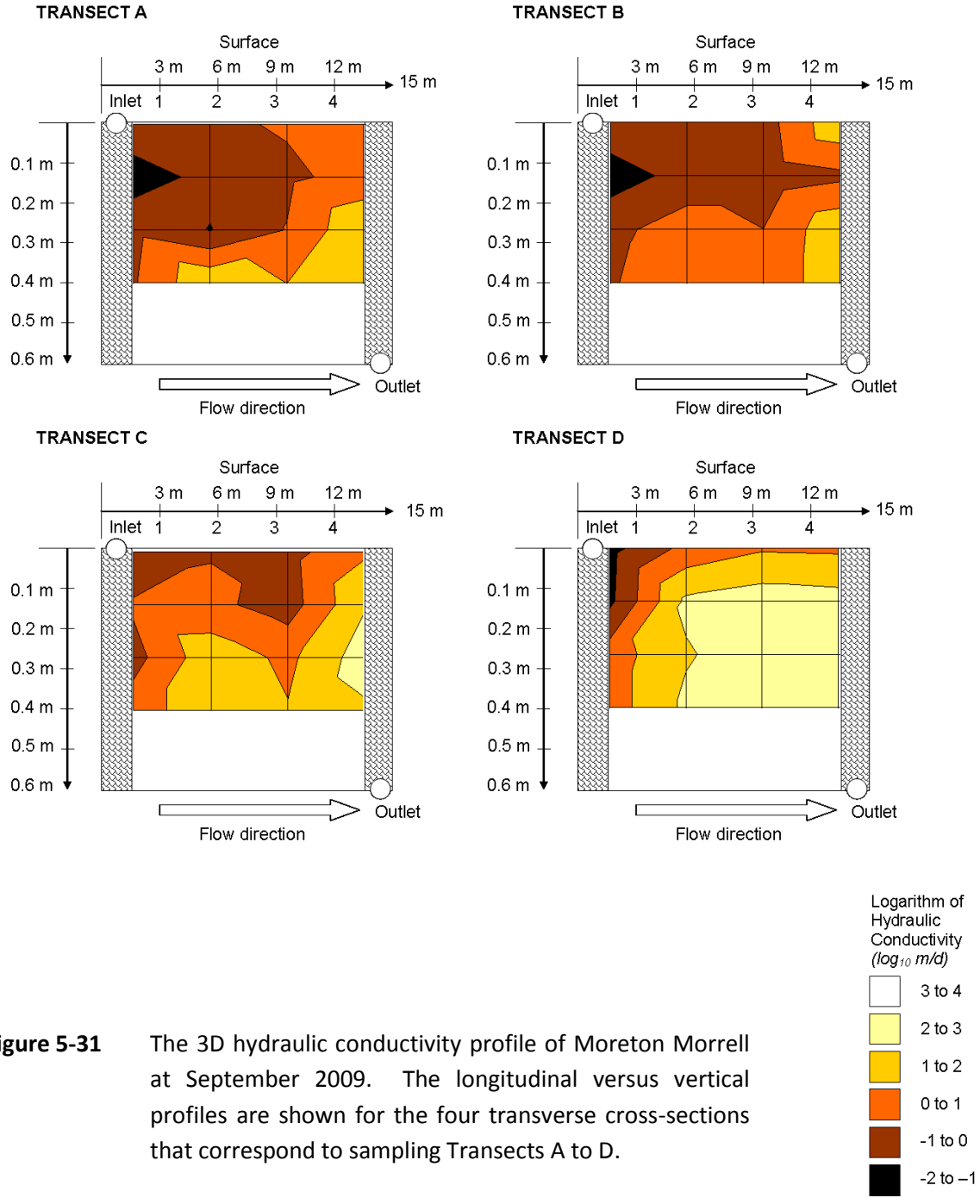

Figure 5-31 The 3D hydraulic conductivity profile of Moreton Morrell at September 2009. The longitudinal versus vertical profiles are shown for the four transverse cross-sections that correspond to sampling Transects A to D.

5.11. Moreton Morrell Control Case (October 2009)

When Moreton Morrell wastewater treatment plant was first visited in June 2008, all four HSSF TW cells were receiving flow and exhibiting symptoms of clogging. Between June 2008 and October 2009, flow was stopped to the cell adjacent to that profiled in the three studies previously described. The control cell was surveyed in October 2009 after 15 months of resting. The hypothesis is that at October 2009 clogging in the control cell would be less than clogging in the operational cell because the control case had not been treating wastewater, and perhaps clogging in the control case at October 2009 would be less than clogging in the operational cell at June 2008 because resting the bed would enable clog matter to mineralise and reverse clogging in the system. Despite the lack of flow, the system had maintained a relatively good reed cover that was approximately 1 m tall. The dimensions of the cell are akin to those of the other Moreton Morrell cell, and a 4X3 sampling matrix was used, as illustrated in **Figure 5-32**. The only difference between the systems is the side of the bed along which flow is loaded and discharged. The 2D vertical and 3D hydraulic conductivity profiles are shown in **Figure 5-33** and **Figure 5-34**, respectively.

As evident in **Figure 5-33**, 11 out of the 12 sampling points had hydraulic conductivity values between 100 and 1,000 m/d. The 3D results indicate that hydraulic conductivity only varies across two orders of magnitude, between the minimum of 24 m/d measured at a 0.2 m depth at point A1, and a maximum of 9,150 m/d measured at a 0.4 m depth at points A4. Generally speaking, the lowest hydraulic conductivity values occur between the 0.1 m and 0.3 m depth at points close to the inlet. The highest hydraulic conductivity values occur between 0.3 m and 0.4 m depth at points close to the outlet. The clogging in the control case is far less severe than that measured in the other Moreton Morrell cell, despite the fact that the cells were commissioned at the same time.

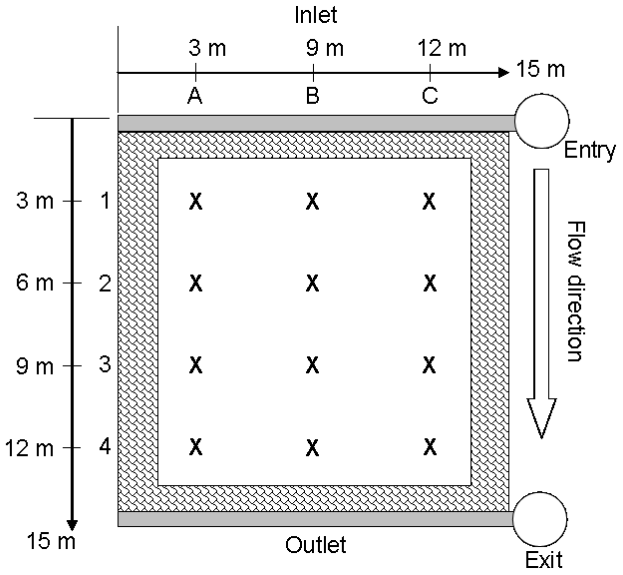

Figure 5-32 Plan view of the HSSF TW at Moreton Morrell which was a 'zero-flow' control case, showing major architectural features and locations of sampling points.

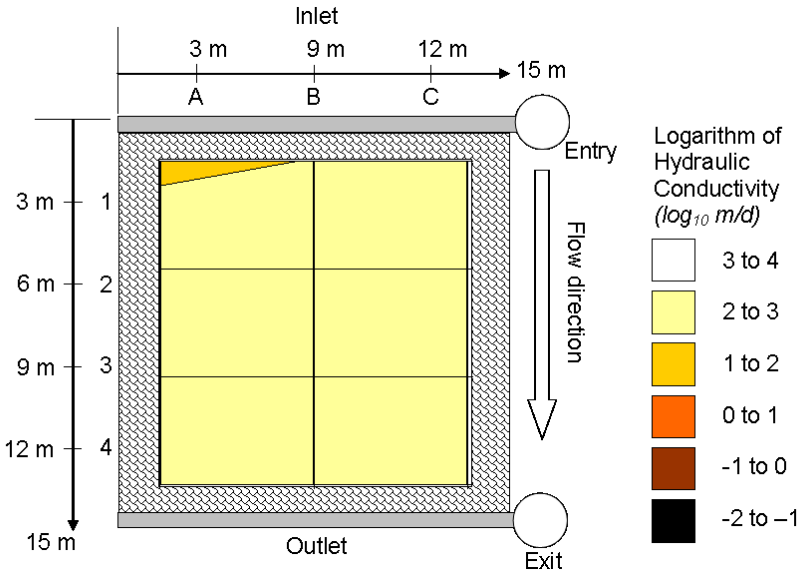

Figure 5-33 The 2D vertical hydraulic conductivity profile for the control case at Moreton Morrell.

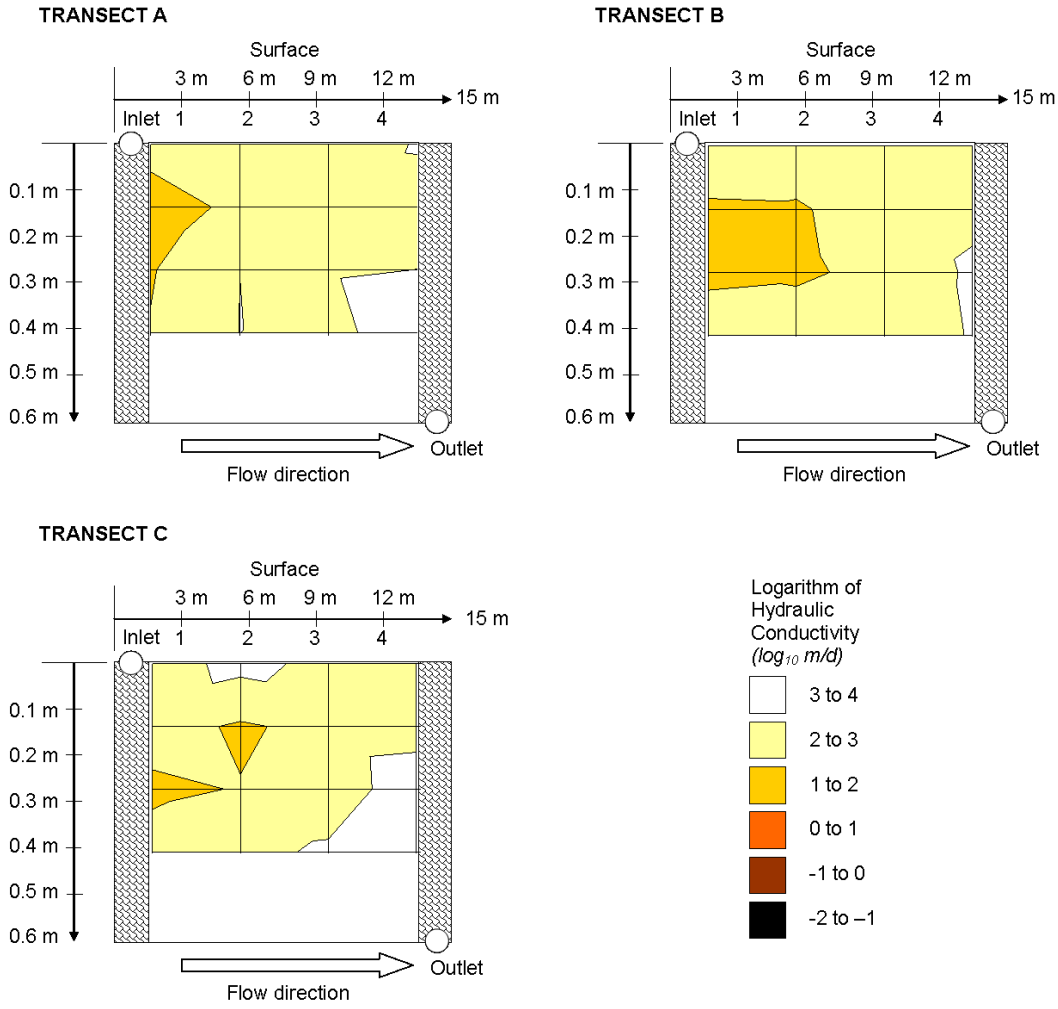

Figure 5-34 The 3D hydraulic conductivity profile of the Moreton Morrell control case. The longitudinal versus vertical hydraulic profiles are shown for the four transverse cross-sections that correspond to sampling Transects A to C.

5.12. Weston Under Wetherley (May 2009)

The HSSF TW at Weston Under Wetherley provides tertiary treatment after two trickling filters. The system is 16 m long by 46 m wide, and is fed by an influent distribution trough with numerous v-notch weirs cut along its length. At the time of the test, the system was approximately 5 years old and had been operating with a flooded water level. The water level was dropped to below the gravel surface to allow the system to be surveyed using a 4X5 sampling matrix, as indicated in **Figure 5-35**. The 2D vertical and 3D hydraulic conductivity profiles are shown in **Figure 5-36** and **Figure 5-37**, respectively.

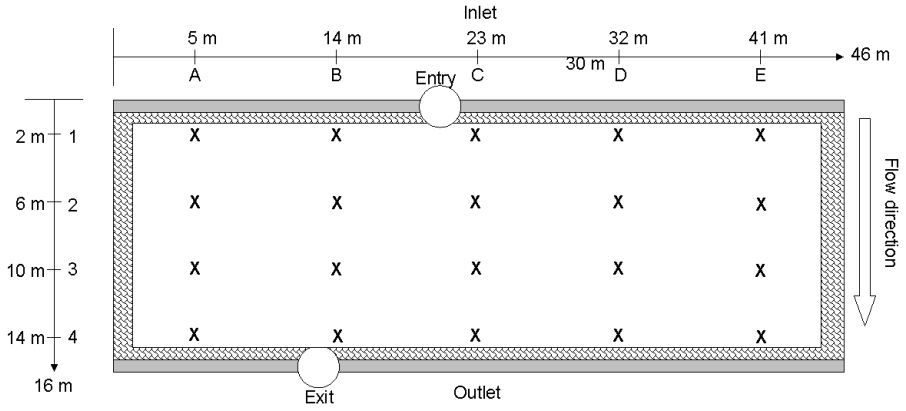

Figure 5-35 Plan view of the HSSF TW at Weston Under Wetherley, showing the major architectural features and the locations of sampling points for the hydraulic conductivity survey. The influent distributor is of the 'v-notch trough' variety.

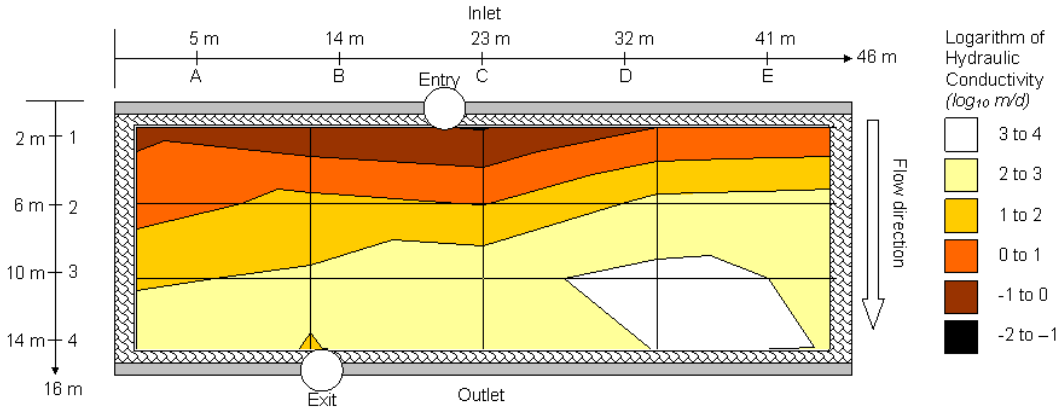

Figure 5-36 The 2D vertical hydraulic conductivity profile at Weston Under Wetherley.

As evident in **Figure 5-36**, the points that flow enters the influent distributor exist the effluent collector are located on a similar transverse plane; roughly between Transects B and C. According to **Figure 5-36**, the vertical hydraulic conductivity measured at different sampling locations varies by five orders of magnitude overall. At the inlet region across Transects A, B and C the measured hydraulic conductivity was below 1 m/d. Generally speaking values increase by four orders of magnitude from inlet to outlet, although the media at points D3 and D4 had hydraulic conductivities above 1000 m/d.

It can be seen in **Figure 5-37** that Transects B and C are those worst affected by clogging, with hydraulic conductivity below 0.1 m/d at the surface close to the inlet region. Clogging across Transects D and E is comparatively less severe than elsewhere in the bed, with hydraulic conductivity being consistently above 1000 m/d at lower depths downstream of 6 m. The contours illustrate that the most severe clogging detected across each measuring point was often near the gravel surface, with hydraulic conductivity values at lower depths often being one to two orders of magnitude greater. The minimum hydraulic conductivity of 0.04 m/d corresponded to a 0.2 m depth at point C1.

Notable features from the visual survey of Weston Under Wetherley are given in **Figure 5-38**. It was found that reed establishment was sporadic, with little vegetation in the region bounded by points C2 to E3. Furthermore, invasive trees had colonised certain parts of the bed. The long term flooded operation had led to the deposition of a fine surface sludge layer over most of the bed. **Figure 5-38** provides evidence of holes created in the sludge layer by macro-invertebrates and wind-rocking of reed stems, which would improve surface infiltration rates. In downstream regions where the surface deposit was relatively thin the gravel underneath appeared relatively clean. The thinnest parts of the surface layer mineralise rapidly after the bed was drained.

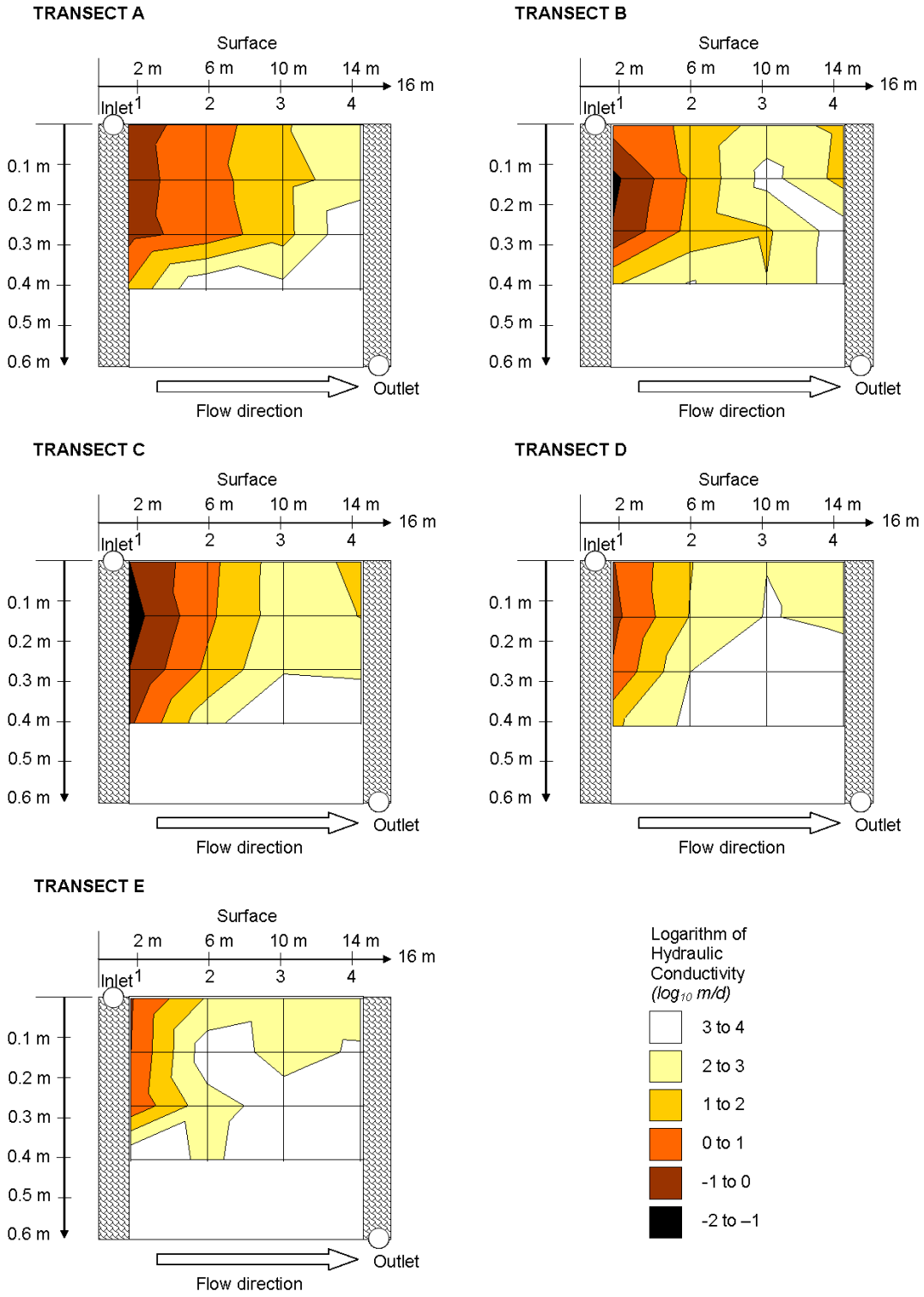

Figure 5-37 The 3D hydraulic conductivity profile of Weston Under Wetherley. The longitudinal versus vertical hydraulic profiles are shown for the four transverse cross sections that correspond to sampling Transects A to E. Sampling was performed to a 0.4 m depth below the surface of the bed and results are interpolated between sampling points. Colour contours indicate order of magnitude divisions in hydraulic conductivity.

Figure 5-38 (Left) The constant head permeameter equipment in-situ at Weston Under Wetherley. This photograph was taken at point D3 looking towards point E2. As evident the reed growth in this region is non-existent. Evidence of the mineralised surface layer can be seen in the mid-ground between the exposed gravel and reeds. (Middle) Relatively clean gravel below the surface deposit at point A4. (Right) Holes through the surface deposit created by macro-invertebrates and wind induced reed rocking.

5.13. Ashorne (June 2009)

By June 2009 the HSSF TW as Ashorne was 16 years old and provided tertiary treatment after one upstream RBC. The system is 15 m long by 18 m wide and is equipped with a reverse facing 'v-notch trough' style influent distributor. Details of the system layout and 4X4 sampling matrix used for the test are given in **Figure 5-39**. Results from the 2D and 3D hydraulic conductivity survey are given in **Figure 5-40** and **Figure 5-41**, respectively.

As evident in **Figure 5-39**, Ashorne was exhibiting a small degree of overland flow in the corner closest to the wastewater entry point. The discharge point is situated on the opposite side of the system to the entry point. Reed growth at Ashorne was generally poor with low stem density and few reeds exceeding 1 m in height. The lack of plant shade had dried out the surface of the bed wherever overland flow was absent.

The 2D vertical hydraulic conductivity profile presented in **Figure 5-40** illustrates a four order of magnitude variation in values, moving in the direction from wastewater entry point to exit point. Media adjacent to the inlet and the region corresponding to overland flow have hydraulic conductivity below 1 m/d. Adjacent to the outlet and in the corner by the exit point, hydraulic conductivity is between 100 and 1,000 m/d. At points B1 and D2, vertical core hydraulic conductivities lower that 0.1 m/d were detected.

An interesting effect can be observed In the 3D hydraulic conductivity results illustrated in **Figure 5-41**. All transects demonstrate that the lowest hydraulic conductivity (below 0.1 m/d) in the vicinity of the inlet occurs in the top 0.2 m gravel. However, downstream of the inlet Transects A and B indicate that the lowest conductivities are to be found at mid-depth between 0.1 and 0.3 m, whereas the surface layer and the region at 0.4 m depth had generally higher conductivities. This effect is not as apparent in Transect C and D where, for the first 9 m length of bed, the lowest hydraulic conductivities occur near the surface. At points near the outlet of Transect C and Transect D the upper layers of gravel are more conductive than the lower layers of gravel.

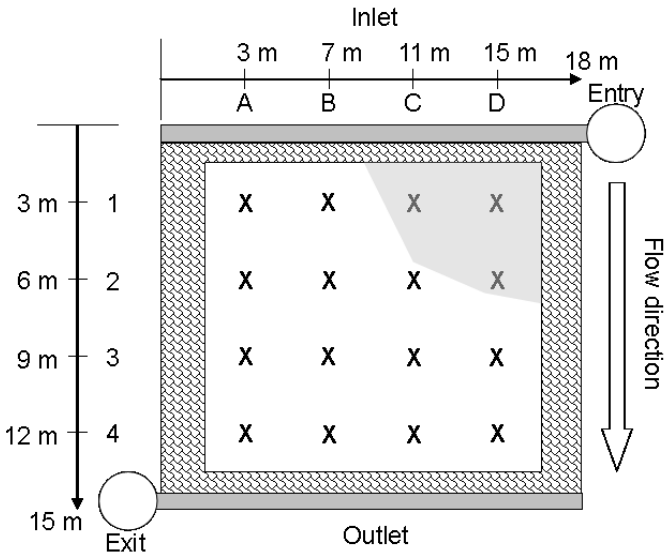

Figure 5-39 Plan view of Ashorne HSSF TW showing major architectural features and the layout of experimental sampling points. The influent distributor is of the reverse facing 'v-notch trough' variety.

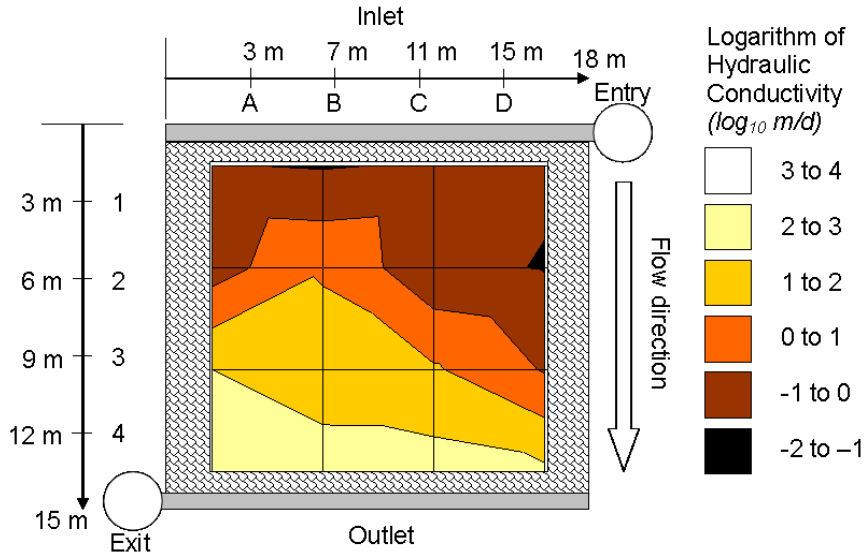

Figure 5-40 The 2D vertical hydraulic conductivity profile for Ashorne.

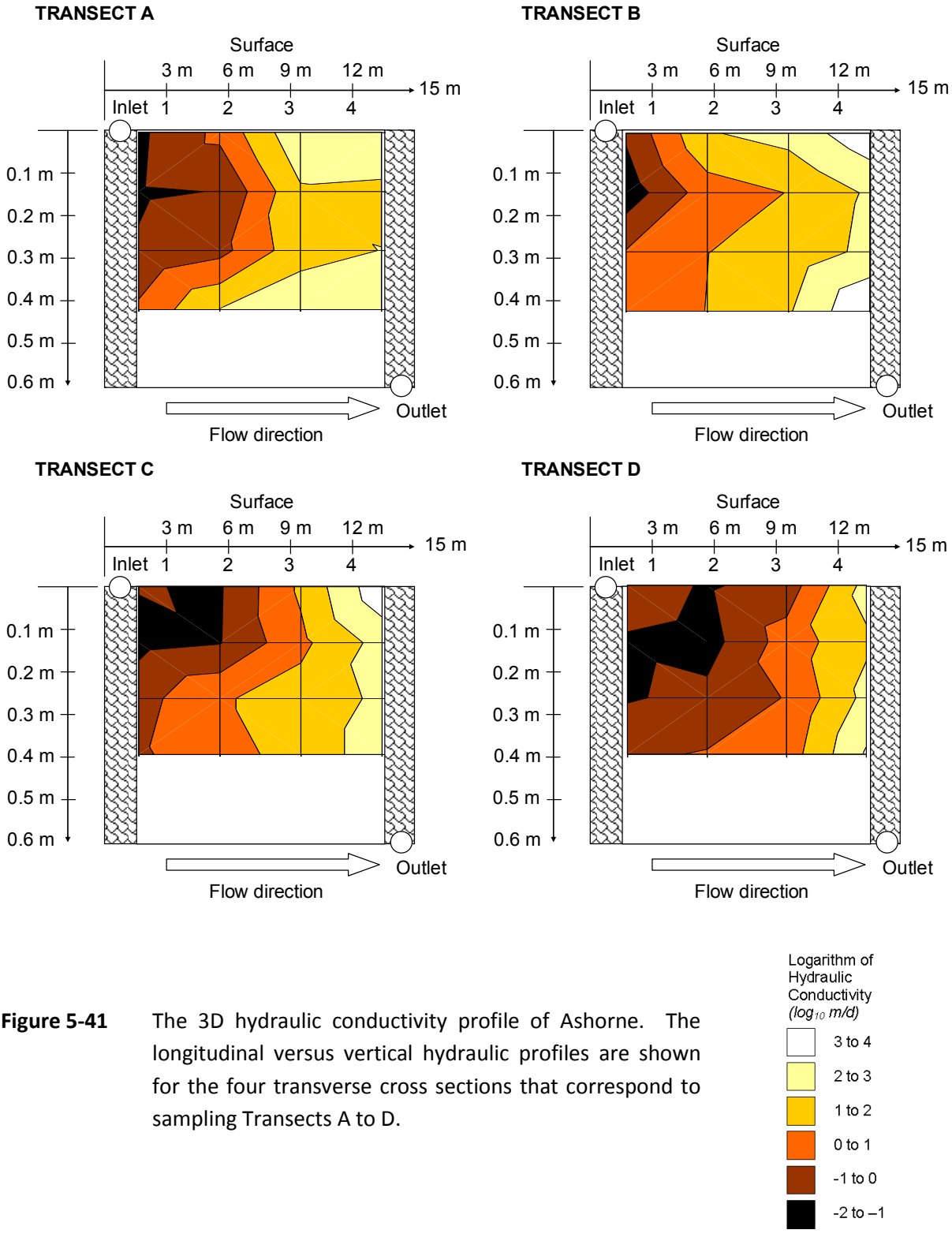

Figure 5-41 The 3D hydraulic conductivity profile of Ashorne. The longitudinal versus vertical hydraulic profiles are shown for the four transverse cross sections that correspond to sampling Transects A to D.

5.14. Leek Wooton (June 2009)

Leek Wooton HSSF TW was fully refurbished in 2006 and therefore the filter media was 3 years old when tested. The TW cell is 16 m long by 28 m wide and provides tertiary treatment after a trickling filter. The influent distribution system consists of five horizontal ports, and the wastewater enters the influent distributor and exits the effluent collector at opposite corners. In June 2009 the reed establishment was excellent, with high stem density throughout the filter and much of the growth exceeding 2.5 m in height. There was little evidence of overland flow or surface sludge accumulation. The system layout and experimental sampling matrix is detailed in **Figure 5-42**. The 2D and 3D hydraulic conductivity survey results are given in **Figure 5-43** and **Figure 5-44**, respectively.

Consideration of **Figure 5-44** reveals that clogging along all transects is mainly confined to the surface region. On Transects A, B and C, the top 0.1 m of most sampling locations returned hydraulic conductivities between 10 and 100 m/d. Particularly in Transects C and D, depths below 0.3 m had hydraulic conductivities above 1000 m/d. For Transects A and B the most clogged region appears to be adjacent to the inlet. Interestingly, all Transects suggest that conductivities sampled close to the outlet, at a 14 m length, where lower than those found at a 10 m length. For Transects C and E in particular, the lowest hydraulic conductivities found within the Transect corresponded to the region close to the outlet.

According to **Figure 5-43**, the vertical hydraulic conductivity of the media at Leek Wooton is relatively homogeneous with hydraulic conductivity predominantly between 100 and 1000 m/d. The corner that is closest to the influent entry point and one extra isolated measurement at point B4 returned hydraulic conductivities between 10 and 100 m/d.

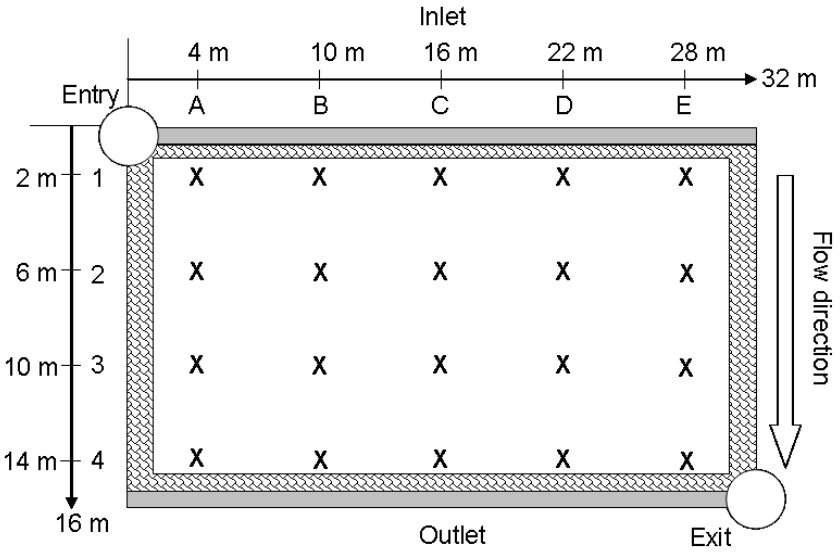

Figure 5-42 Plan view of Leek Wooton HSSF TW showing major architectural features and the distribution of sampling locations. The influent distribution system comprises five horizontal ports equally distributed along the inlet pipe between Transects A and E.

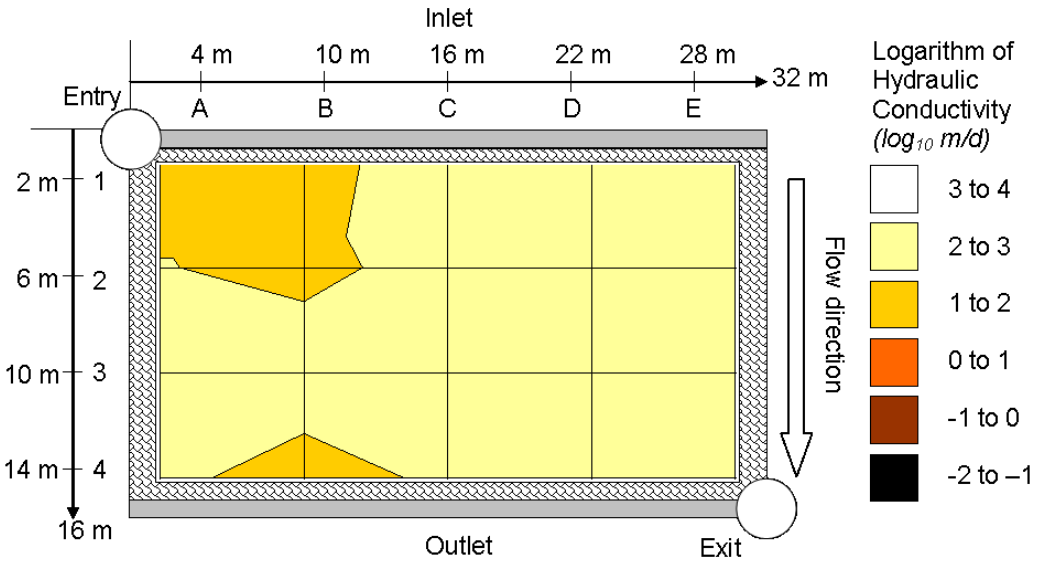

Figure 5-43 The 2D vertical hydraulic conductivity profile for Leek Wooton.

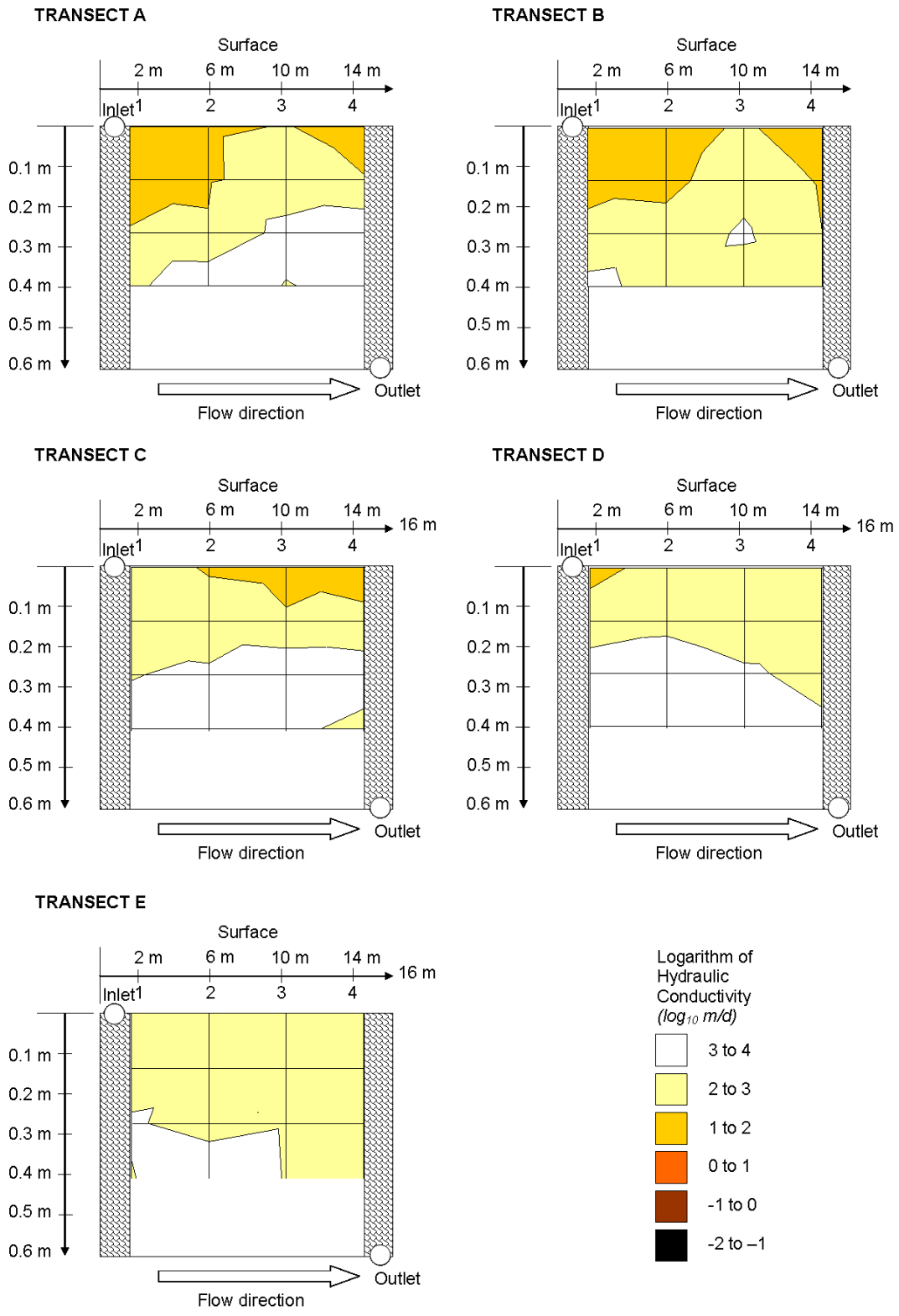

Figure 5-44 The 3D hydraulic conductivity profile of Leek Wooton. The longitudinal versus vertical hydraulic profiles are shown for the four transverse cross sections that correspond to sampling Transects A to E. Sampling was performed to a 0.4 m depth below the surface of the bed and results are interpolated between sampling points. Colour contours indicate order of magnitude divisions in hydraulic conductivity.

5.15. Northend (June 2009)

Northend was revisited more than two years after a 2D survey had been completed in April 2007, in order to perform a 3D survey. To reiterate on some details provided in Section 5.1, the influent distributor consists of 6 vertical risers that are width distributed either side of a centrally located influent entry point. The risers are buried by surface accumulation and can no longer be seen from the surface. There is no distribution of wastewater directly in front of the entry point. The effluent exit point is located at a corner point on the outlet side of the bed. Since the previous test the reed stock had partially re-established itself, although the quality of growth varied substantially across the bed. According to the sampling matrix outlined in **Figure 5-45**, the region roughly encompassed by Transects B and C showed dense growth with reed height above 2 m. The region parallel to Transect A and the corner closest to the effluent exit point showed patchy growth with reeds generally below 1.5 m height. Overland flow was evident over the length of the bed at Transects B and C but was not apparent elsewhere. It is assumed that the preferential flow at Transects B and C occurs as a result of plugging in the risers that feed the other transects. The 2D vertical and 3D results of the hydraulic conductivity survey are illustrated in **Figure 5-46** and **Figure 5-47**, respectively.

According to **Figure 5-46**, two low hydraulic conductivity areas have developed within the media at Northend, roughly corresponding to Transects B and D, which predominantly returned hydraulic conductivity values below 1 m/d. In particular, Points B2 and B3 which correspond to the overland flow region with high vegetation density were found to have vertical core hydraulic conductivities below 0.1 m/d. Transects A and E, and points along Transect C had hydraulic conductivities above 1 m/d, although nowhere on the bed did the core hydraulic conductivity exceed 100 m/d.

Considering the 3D version of the hydraulic conductivity results which are portrayed in **Figure 5-47**, it can be seen that most of upper 0.2 m of media along Transect B has hydraulic conductivity below 0.1 m/d, which closely corresponds to the overland flow. Elsewhere, hydraulic conductivity below 0.1m/d is confined to the surface at the inlet region of Transect D. Generally speaking, it can be observed that the hydraulic conductivity of the upper media is lower than the hydraulic conductivity of the lower media. All sampling points demonstrate a one or two order of magnitude increase of hydraulic conductivity from surface to a 0.4 m depth, which is attributed to dense vegetation establishment in the upper layers of gravel. Only Transect A had media with hydraulic conductivity predominantly

greater than 1 m/d. The highest conductivities recorded for each transect where at a 0.4 m depth towards the outlet pipe. Certain 0.3 and 0.4 m depths at the outlet of Transects A, C, D and E had media conductivities above 100 m/d.

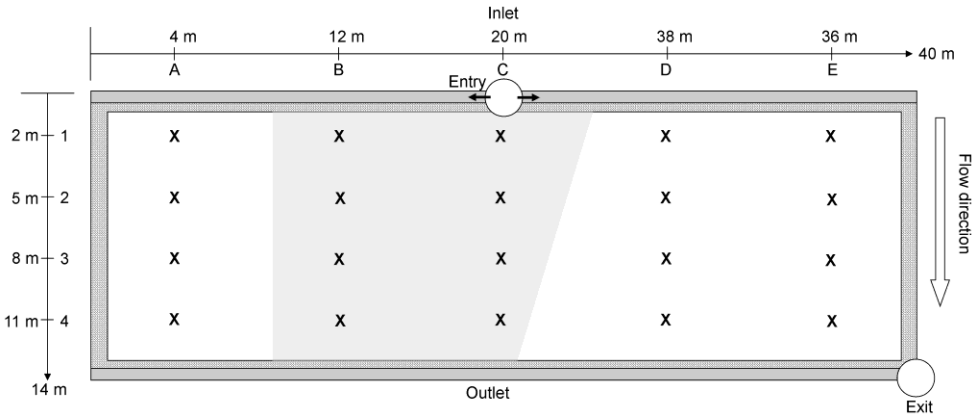

Figure 5-45 Plan view of Northend HSSF TW showing the major architectural features and locations of sampling points for the June 2009 test. The influent distributor comprises 6 vertical risers distributed either side of a central influent entry point. The shaded region represents overland flow.

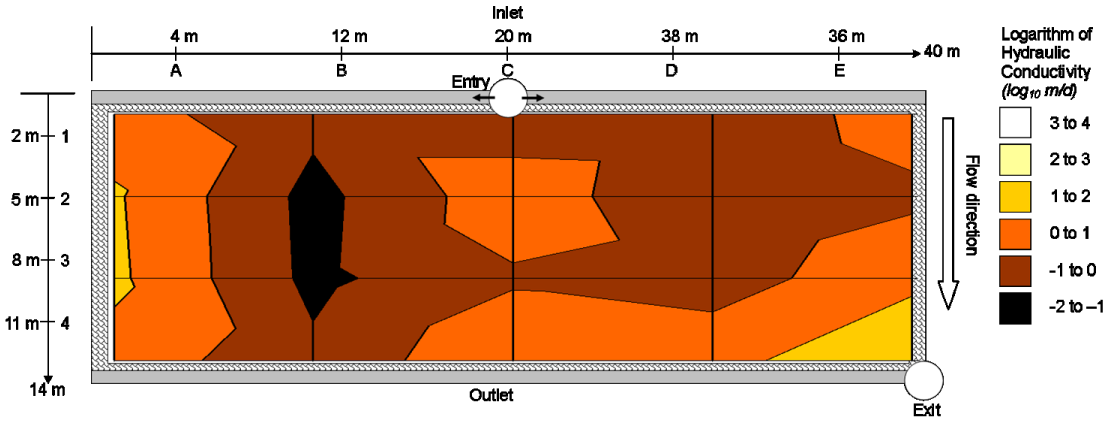

Figure 5-46 The 2D vertical hydraulic conductivity profile obtained at Northend during the June 2009 test.

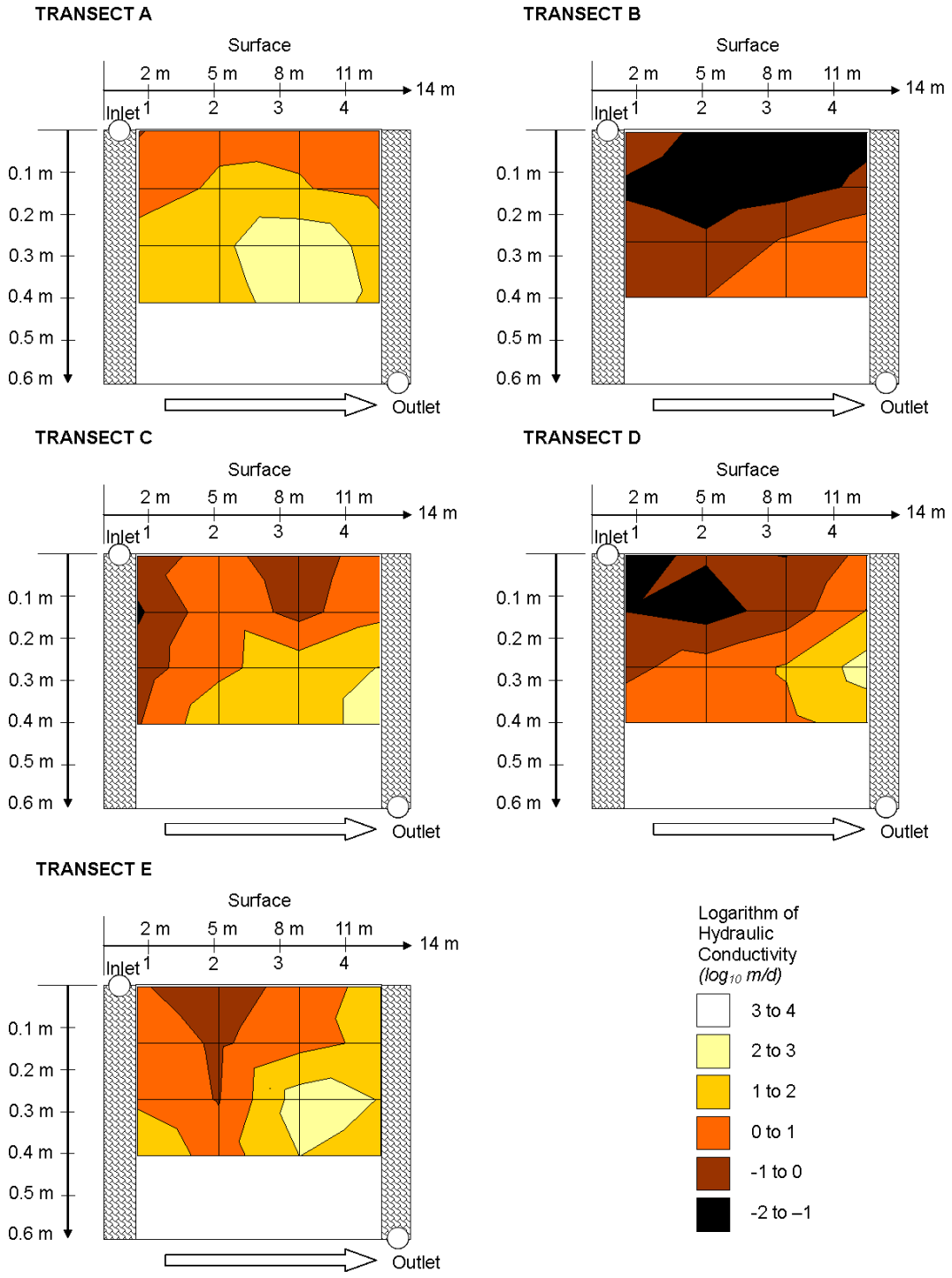

Figure 5-47 The 3D hydraulic conductivity profile of Northend as measured in June 2009. The longitudinal versus vertical hydraulic profiles are shown for the four transverse cross sections that correspond to sampling Transects A to E. Sampling was performed to a 0.4 m depth below the surface of the bed and results are interpolated between sampling points. Colour contours indicate order of magnitude divisions of hydraulic conductivity.

5.16. Rowington (July 2009)

The HSSF TW at Rowington comprises one bed of 25 m length and 54 m width that is divided down the mid-length by a berm that houses an effluent collector pipe, and thus creates two cells. A flow splitter spreads the influent along both sides of the bed. These cells provide tertiary treatment after a trickling filter and were 8 years old at the time of testing. Figure 5.45 represents the cell that was chosen for surveying and the utilised sampling matrix. The influent is distributed via six horizontal ports that are equally spaced along the width of the inlet pipe, either side of the influent entry point that is located at mid-width. The effluent exit point is located at one end of the outlet pipe. When the test was conducted reed growth was good with moderate to high stem density over the entire surface and reed height generally exceeding 2 m. A large region of the bed surface was covered by overland flow, as indicated by the shaded region on **Figure 5-48**. The 2D vertical and 3D versions of the hydraulic conductivity results are depicted in **Figure 5-49** and **Figure 5-50**, respectively.

The prevalence of clogging at Rowington is emphasised in **Figure 5-49**, which depicts vertical hydraulic conductivities below 0.1 m/d over much of the bed. Point D1 was the only inlet location where hydraulic conductivity fell in the 0.1 to 1 m/d range. Generally speaking values from inlet to outlet increase by four orders of magnitude, to between 10 and 100 m/d at Points C4, D4 and E4. The media in the outlet region located on the opposite side of the bed from the effluent exit point had the highest conductivity, with Points A3, A4 and B4 returning values in the 100 to 1000 m/d range.

As illustrated in **Figure 5-50**, the media has hydraulic conductivity below 0.1 m/d at all depths from the inlet to the mid-length of Transect C. Elsewhere along the inlet region the gravel layer between 0.1 and 0.2 m depth has lower hydraulic conductivity than the media at the surface. Across the depths of Transects C and D, hydraulic conductivity increases by three orders of magnitude between the region affected by overland flow and the outlet. Along Transect A and B, the increase from minimum values measured at the inlet to maximum values measured at the outlet is four orders of magnitude. In Transect A, the downstream half of the bed, especially, has hydraulic conductivities between 100 and 1000 m/d.

In the downstream half of Transects B, C and D the hydraulic conductivity generally increases by one order of magnitude between the surface and a depth of 0.4 m. Along Transect E the lowest hydraulic conductivities are found at mid-depth in the inlet region, with values of the surface layer consistently being between 1 and 10 m/d. For each transect the highest

hydraulic conductivities were consistently found at a 0.3 to 0.4 m depth in the vicinity of the outlet pipe, with values generally lying between 100 and 1000 m/d. The highest value of hydraulic conductivity found in the system was 1900 m/d at a 0.3 m depth at Point E4.

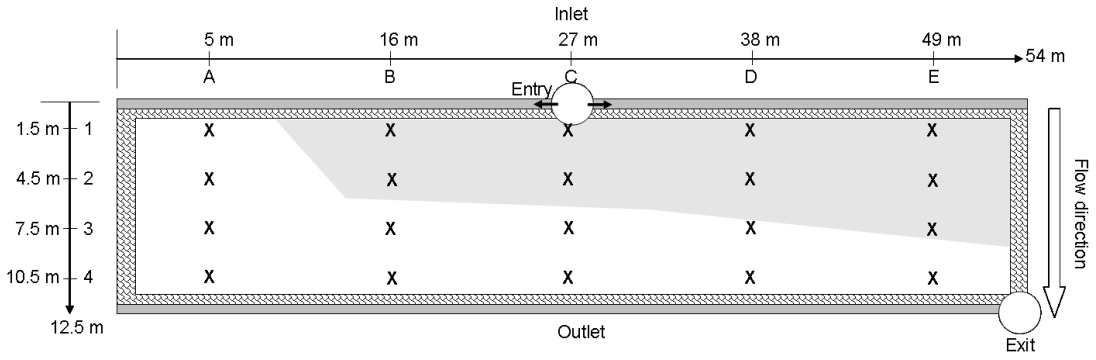

Figure 5-48 Plan view of Rowington HSSF TW showing the major architectural features and locations of sampling points. The influent distribution is via 6 horizontal ports distributed either side of the central influent entry point. The shaded region represents overland flow.

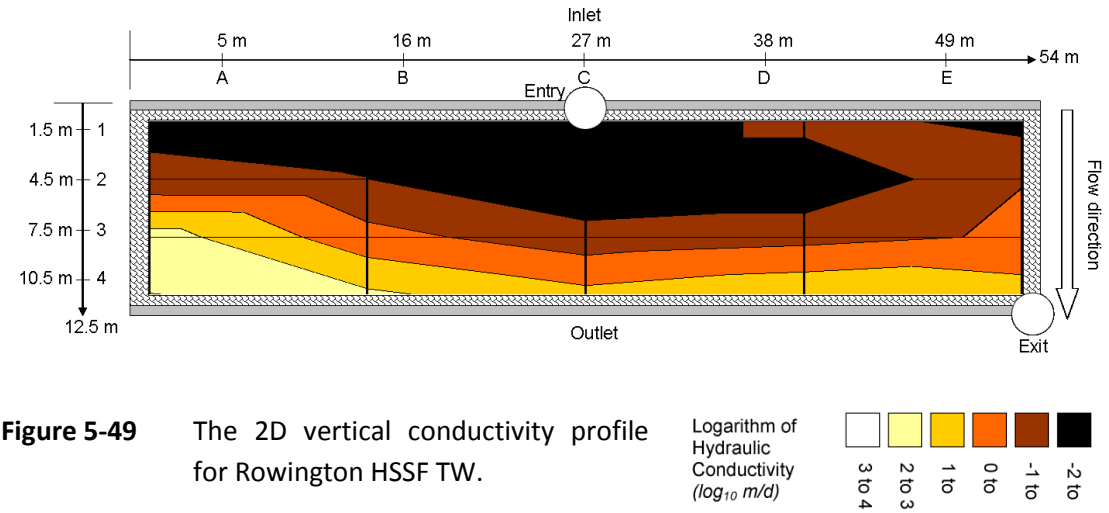

Figure 5-49 The 2D vertical conductivity profile for Rowington HSSF TW.

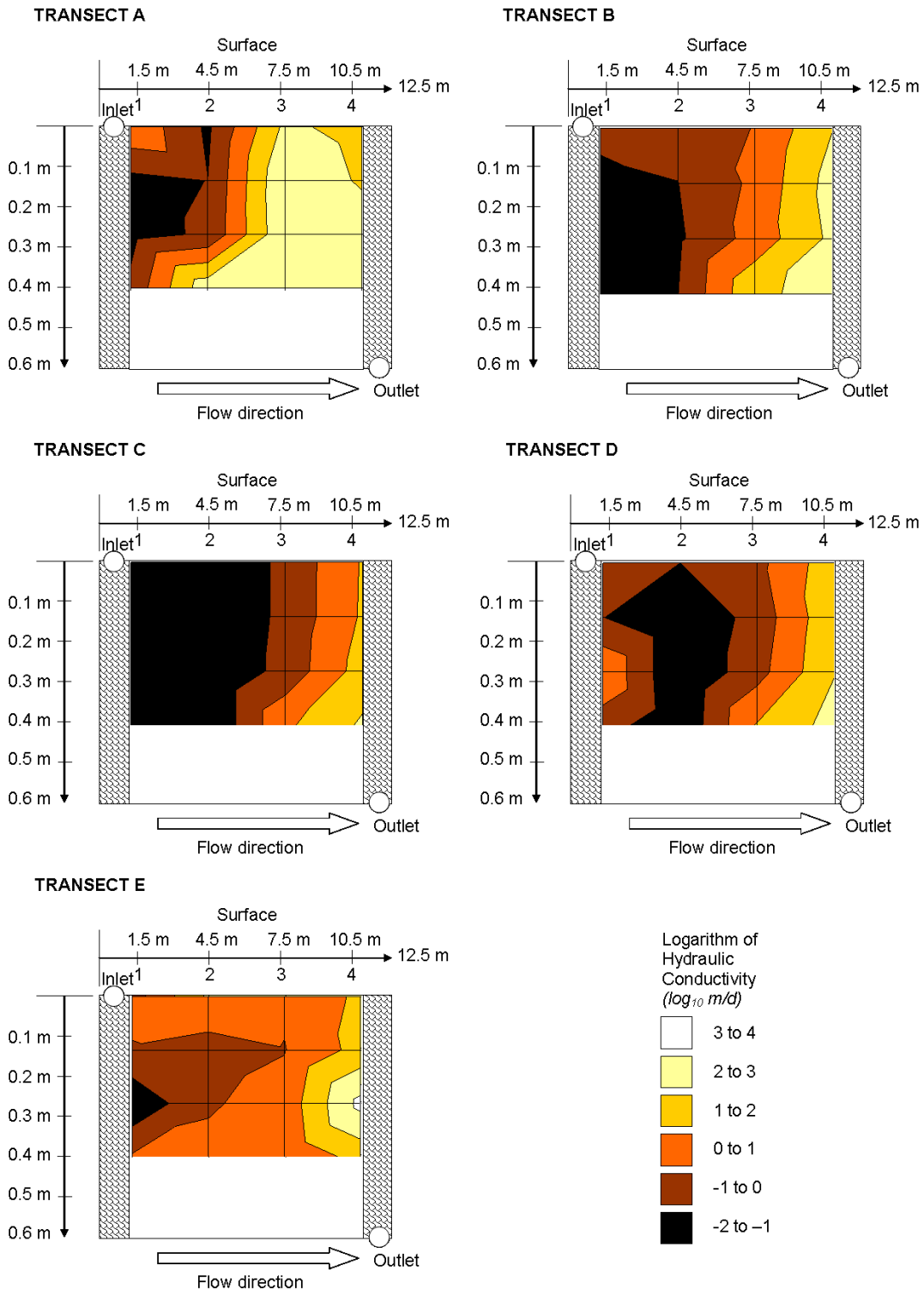

Figure 5-50 The 3D hydraulic conductivity profile of Rowington. The longitudinal versus vertical hydraulic profiles are shown for the four transverse cross sections that correspond to sampling Transects A to E. Sampling was performed to a 0.4 m depth below the surface of the bed and results are interpolated between sampling points. Colour contours indicate order of magnitude divisions in hydraulic conductivity.

5.17. Snitterfield (August 2009)

As of August 2009 Snitterfield HSSF TW had been providing tertiary treatment after RBCs for a period of 15 years. The bed is 16 m long by 30 m wide and is depicted in **Figure 5-51**, along with the location of sampling points. Influent distribution is achieved by 6 vertical risers equally spaced along the inlet pipe. The entry point to the inlet pipe and exit point from the effluent pipe are similarly located at the bed mid-width. At the time of the test the reed growth at Snitterfield was healthy, with good stem density and plant height above 2.5 m. Overland flow was severe and occupied approximately 80 % of the bed surface, reaching from inlet to outlet between Transects B and D. The 2D vertical and 3D interpretations of the system hydraulic conductivity profile are given in **Figure 5-52** and **Figure 5-53**, respectively.

As presented in **Figure 5-52**, the most severe clogging at Snittefrield occurs along Transect C where vertical core conductivities were consistently below 1 m/d. Across the inlet region hydraulic conductivity was generally on the order of 0.01 to 0.1 m/d, although for Transects A, C, D and E this increased by two orders of magnitude in the downstream half of the bed.

The 3D hydraulic conductivity profiles presented in **Figure 5-53** suggest that inlet clogging at Transects C and D is fairly uniform over the tested depth of media, with values consistently below 0.1 m/d. Transects A, B and D show a three order of magnitude increase in hydraulic conductivity between the upper gravel layers at the inlet and the lower gravel layers at the outlet. Transect C is the most clogged and only shows a two order of magnitude increase in hydraulic conductivity between the inlet and the 0.3 to 0.4 m depth at the outlet.

In the downstream region of all five transects there is a one to two order of magnitude increase in hydraulic conductivity from the surface to a depth of 0.4 m. Transect E is the least clogged with surface values downstream of the inlet consistently remaining between 1 and 10 m/d, and the maximum hydraulic conductivity of 170 m/d being recorded at the 0.3 m depth at Point E3.

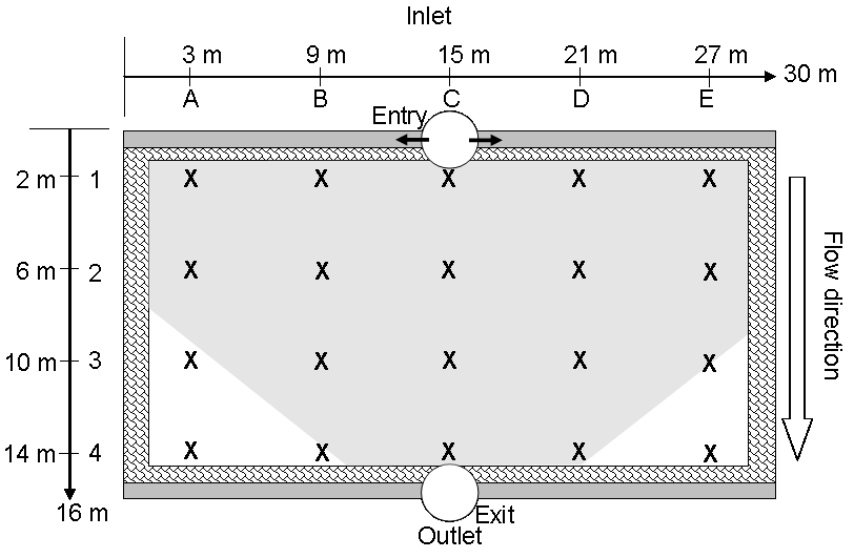

Figure 5-51 Plan view of Snitterfield HSSF TW showing the major architectural features and locations of sampling points. The influent distribution is via 6 vertical risers distributed either side of the central influent entry point. The shaded region represents overland flow.

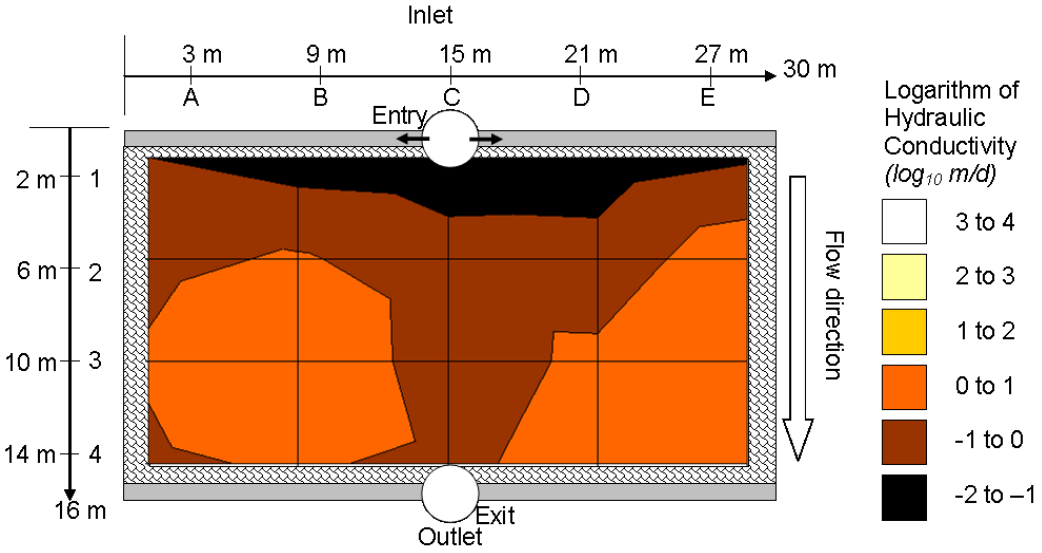

Figure 5-52 The 2D hydraulic conductivity profile obtained at Snitterfield HSSF TW.

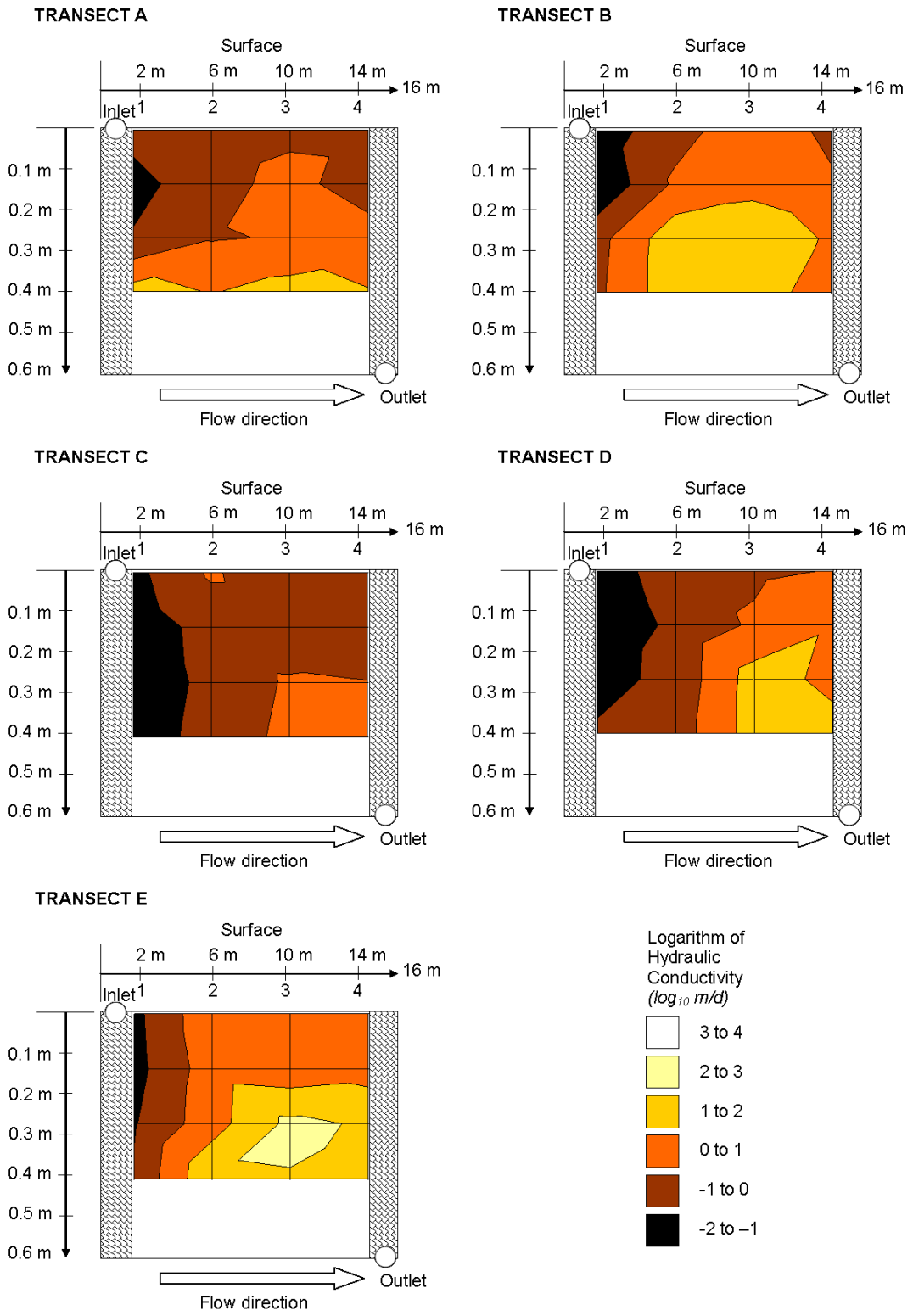

Figure 5-53 The 3D hydraulic conductivity profile of Snitterfield. The longitudinal versus vertical hydraulic profiles are shown for the five transverse cross sections that correspond to sampling Transects A to E. Sampling was performed to a 0.4 m depth below the surface of the bed and results are interpolated between sampling points. Colour contours indicate order of magnitude divisions of hydraulic conductivity.

5.18. Greens of Delwood, Minnesota, US (July 2009)

At the time of testing Greens of Delwood (Delwood) had been providing secondary domestic wastewater treatment to a small conurbation for 12 years. In the months before July 2009 Delwood had reportedly suffered flow surfacing that required corrective action to be taken. To reiterate, the Minnesotan systems have subsurface influent distribution and a 30 cm mulch layer atop the gravel layer, such that flow surfacing is indicative of severe gravel clogging. The site was therefore selected as representing a 'clogged' system by US standards. Delwood is a 20 m long by 15 m wide HSSF TW that is depicted in **Figure 5-54** along with the 4X4 sampling matrix that was used in the survey. The influent distribution system comprises a perforated inlet pipe buried just below the gravel surface that spans the width of the bed, and is fed from a header tank that introduces wastewater to the pipe at an entry point between Transect A and B. The effluent exit point is located at the end of the outlet pipe adjacent to Transect D. The survey was performed by removing the mulch layer at sampling points so that only the hydraulic conductivity of the gravel media was measured. The 2D vertical and 3D interpretations of the hydraulic conductivity data are provided in **Figure 5-55** and **Figure 5-56**.

As evident from **Figure 5-55** the lowest core conductivity measured for the system was at Point D4, closest to the effluent exit point, which corresponded to a value of 0.09 m/d. Hydraulic conductivity at the inlet of Transects A, B and D lay between 1 and 10 m/d, and apart from Transect D values across the outlet where between 10 and 100 m/d. In between the inlet and outlet the vast majority of the 2D results were on the order of 100 to 1000 m/d.

As discernible from **Figure 5-56**, the hydraulic conductivity of the top 0.1 m of gravel in the inlet region is between 1 and 10 m/d across all transects. Generally speaking the hydraulic conductivity across the depth at the inlet region does not exceed 100 m/d. The top 0.1 m of gravel at points A2 and B2 and certain depths at the outlet of Transects A, B and C also exhibit hydraulic conductivity between 10 and 100 m/d. The central portion of the bed has fairly high conductivity above 100 m/d and, below the top 0.1 m of gravel, all transects had hydraulic conductivities greater than 1,000 m/d for at least one depth. The highest hydraulic conductivity of 12,500 m/d was measured at Point B2 between depths of 0.1 and 0.2 m.

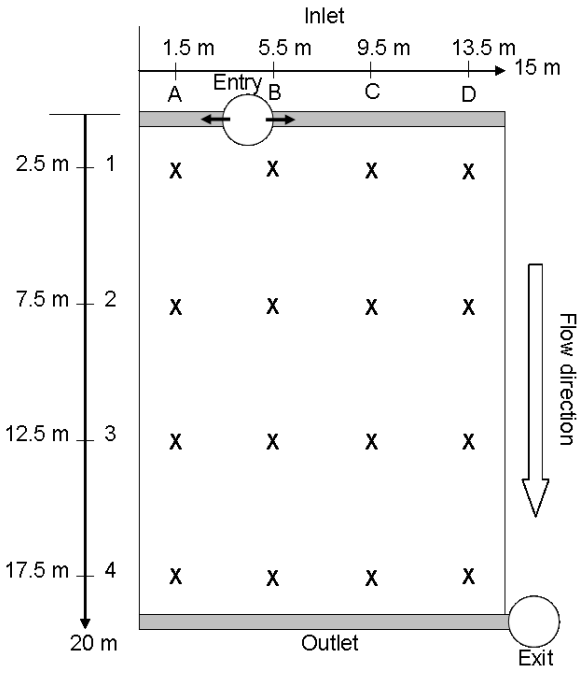

Figure 5-54 Plan view of the HSSF TW at Delwood, detailing major architectural features and the location of sampling points. The influent distribution comprises a subsurface perforated pipe.

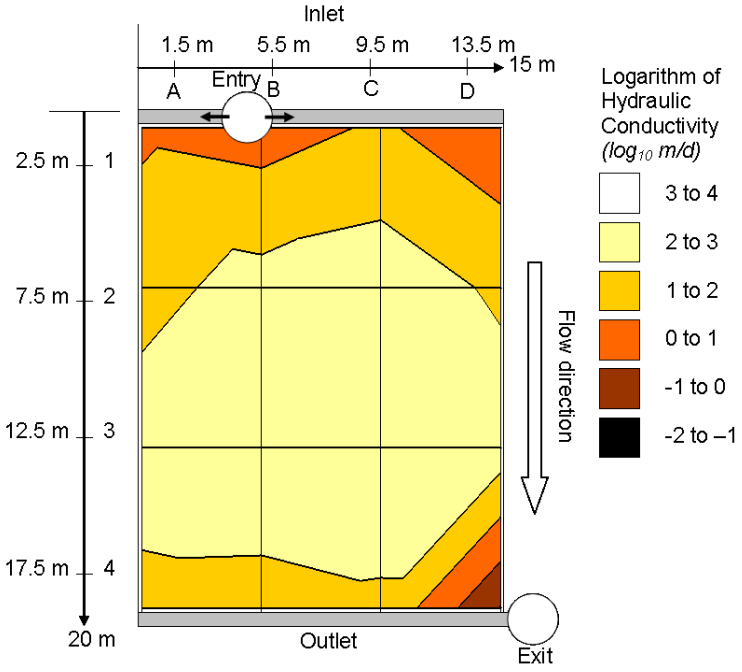

Figure 5-55 The 2D vertical hydraulic conductivity profile at Delwood.

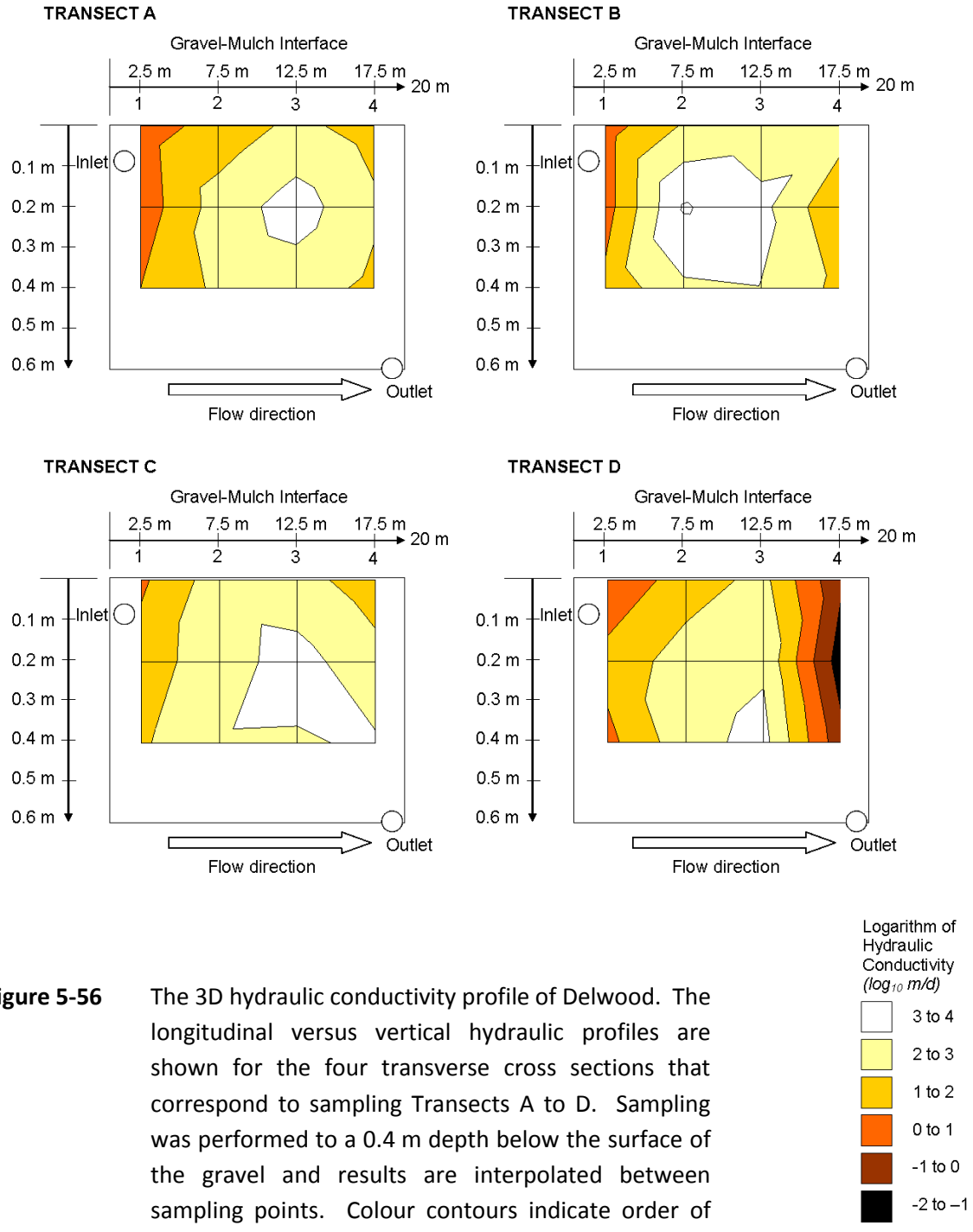

Figure 5-56 The 3D hydraulic conductivity profile of Delwood. The longitudinal versus vertical hydraulic profiles are shown for the four transverse cross sections that correspond to sampling Transects A to D. Sampling was performed to a 0.4 m depth below the surface of the gravel and results are interpolated between sampling points. Colour contours indicate order of magnitude divisions of hydraulic conductivity.

5.19. Tamarack Farms Estate, Minnesota, US (July 2009)

The HSSF TW at Tamarack Farms Estate (Tamarack) was selected for survey as it had previously been the subject of a novel clogging remediation strategy, whereby hydrogen peroxide was injected directly into the clogged porous media to mineralise the organic clog matter. By July 2009 Tamarack had been providing secondary domestic wastewater treatment for 8 years and the chemical oxidant application had occurred in 2007 (Nivala and Rousseau, 2009). The system is 33 m long by 18 m wide and the influent distributor is a subsurface perforated pipe that runs the width of the bed. This information is illustrated in **Figure 5-57** along with the distribution of the 3X5 sampling matrix. As evident from **Figure 5-57**, the influent entry point is located close to Transect C whereas the effluent exit point is closest to Transect A. **Figure 5-58** and **Figure 5-59** reveal the 2D vertical and 3D interpolations of the hydraulic conductivity results.

The results conveyed in **Figure 5-58** suggest that the vast majority of the bed has hydraulic conductivity between 10 and 100 m/d. Measurements at points A1, A2, A3, B2 and C1 produced slightly higher conductivities between 100 and 1000 m/d, which roughly coincided with the locations of hydrogen peroxide application. The lowest hydraulic conductivity value measured was 9/md and occurred at point B1, where the surface ponding had previously been most severe.

The 3D interpretation provided in **Figure 5-59** indicates that clogging at the inlet is mainly confined to Transect B, especially in the upper gravel layers that are close to the inlet pipe, where hydraulic conductivity was between 1 and 10 m/d. The upper layers at Point C1 also exhibit signs of mild clogging where hydraulic conductivity was found to be 71 m/d. However, elsewhere at the inlet the media generally displayed conductivity readings above 100 m/d, suggesting that subsurface influent distribution may be uneven between Transects B and the other two transects.

An interesting effect can be observed downstream of the inlet within Transects B and C. A region with lower hydraulic conductivity values (between 10 and 100 m/d) has developed across the gravel depth, between the 9 m and 21 m length. The low hydraulic conductivity region extends to the upper layers of gravel towards the outlet, but appears disjointed from any clogging associated with the inlet region in these transects. It is hypothesised that the vigorous oxidation caused by the hydrogen peroxide application disturbed clog matter accumulations in the inlet region and caused them to migrate further downstream; in this case settling out in the central region of the bed.

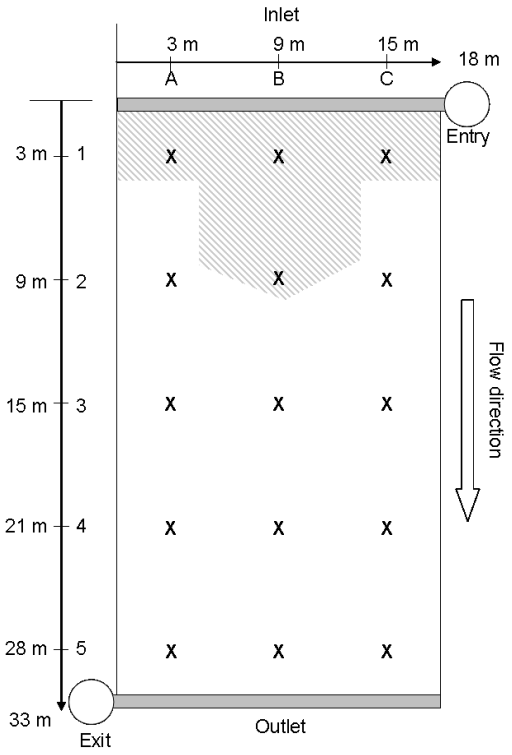

Figure 5-57 Plan view of the HSSF TW at Tamarack, detailing major architectural features and the location of sampling points. The influent distributor is a subsurface perforated pipe. In this figure the grey shaded region represents the area that received hydrogen peroxide treatment to reverse clogging.

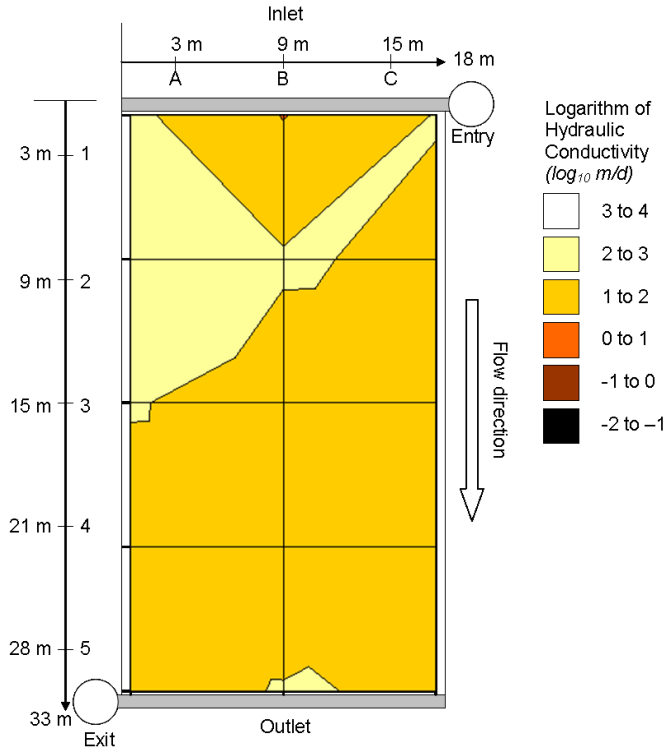

Figure 5-58 The 2D vertical hydraulic conductivity profile at Tamarack.

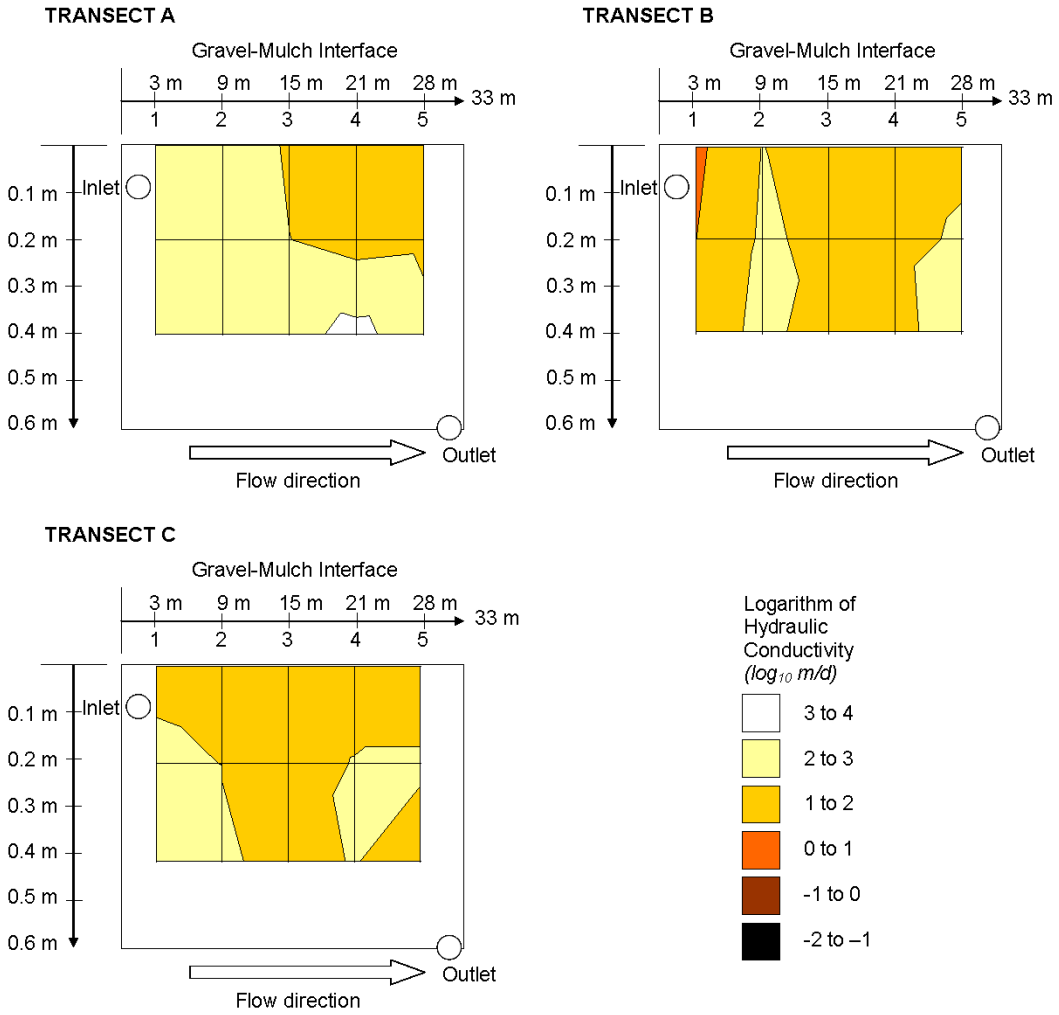

Figure 5-59 The 3D hydraulic conductivity profile of Tamarack. The longitudinal versus vertical hydraulic profiles are shown for the three transverse cross sections that correspond to sampling Transects A to C. Sampling was performed to a 0.4 m depth below the surface of the gravel and results are interpolated between sampling points. Colour contours indicate order of magnitude divisions in hydraulic conductivity.

For Transect A, the vast majority of the media was fairly permeable and only the upper gravel region downstream of 15 m had hydraulic conductivity values below 100 m/d. The highest hydraulic conductivity value of approximately 2000 m/d was measured at the 0.4 m depth at Point A3, in the vicinity of the effluent exit point.

5.20. Jackson Meadow South, Minnesota, US (August 2009)

The gravel media in the HSSF TW at Jackson Meadow has been receiving septic tank treated domestic wastewater for 12 years. In 2004 the system was retrofitted with forced aeration and the flow direction reoriented within the cell, so that in **Figure 5-60** where flow moves from top to bottom in the diagram, it previously moved from left to right. The position of the old influent header is illustrated by grey shading, approximately coinciding with Transect A. The media was not replaced as part of the system upgrade.

The resultant layout is 20 m long by 30 m wide and the influent distributor comprises an infiltration chamber which introduces wastewater over the entire depth at the inlet. The influent entry point is located close to Transect A whereas the effluent exit point is adjacent to Transect D. A 4X4 sampling matrix was used for the hydraulic conductivity experiment, and the 2D vertical and 3D results are illustrated in **Figure 5-61** and **Figure 5-62**, respectively.

As illustrated in **Figure 5-61**, clogging in the system was most significant in the vicinity of the influent entry point, where points A1 and B1 displayed core conductivities of 65 m/d and 5 m/d, respectively. The vertical conductivities across the new inlet region did not exceed 150 m/d and values representative of the old inlet region, along Transect A where always below 1000 m/d. This is in contrast to the other three transects which generally returned hydraulic conductivities between 1000 and 3000 m/d for regions downstream of the inlet. However, a second area of clogging appears to be developing adjacent to the effluent exit point because Points C3, C4 and D4 all registered hydraulic conductivity between 200 and 400 m/d.

Figure 5-62 elucidates that inlet clogging is generally detected across the gravel depth, and only the 0.2 m depth at Point D1 had a hydraulic conductivity above 1000 m/d. Downstream of the inlet, clogging in each transect tends to only occur in the top 0.1 m of gravel media, where the majority of values recorded are below 1000 m/d (usually 1 to 2 orders of magnitude below the rest of the core). This is particularly evident in Transects B, C and D where gravel at lower depths has many occurrences of media conductivity between 10,000 and 20,000 m/d. The highest recorded value of 62,500 m/d occurred at a 0.4 m depth within Point D2, and the lowest reported hydraulic conductivity was 1.5 m/d in the top 0.1 m of media at point B1.

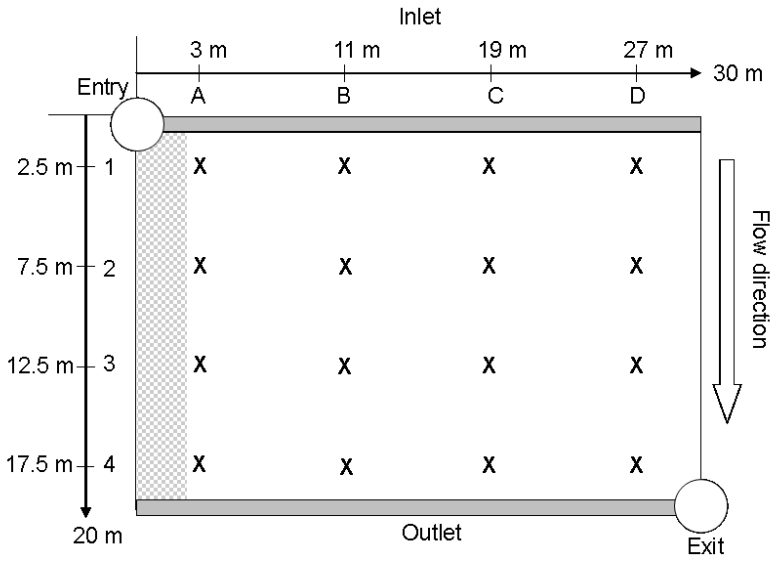

Figure 5-60 Plan view of the HSSF TW at Jackson Meadow, detailing major architectural features and the location of sampling points. The influent distributor is a subsurface infiltration chamber. The location of the old influent distributor is indicated by the grey shaded region, and was upgraded to the current configuration in 2004.

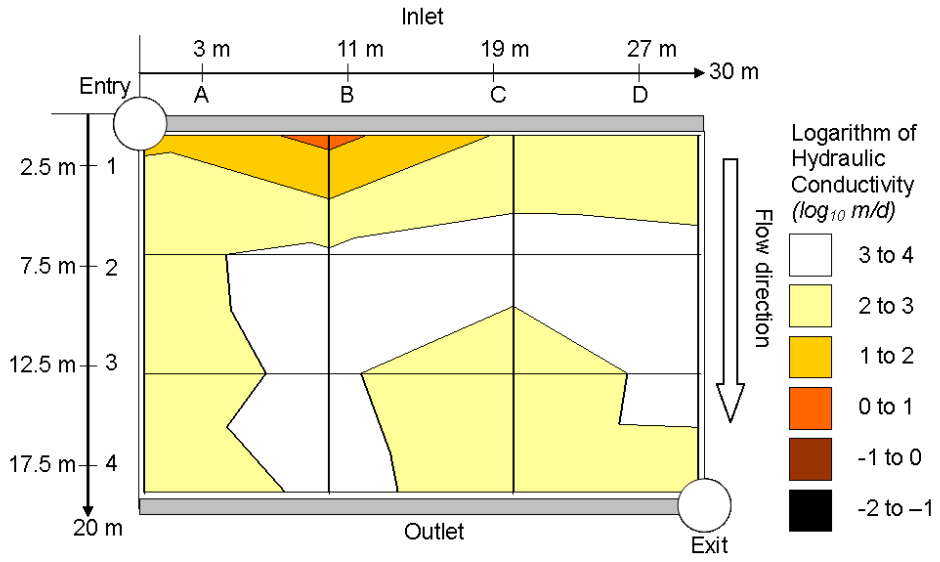

Figure 5-61 The 2D vertical hydraulic conductivity profile at Jackson Meadow.

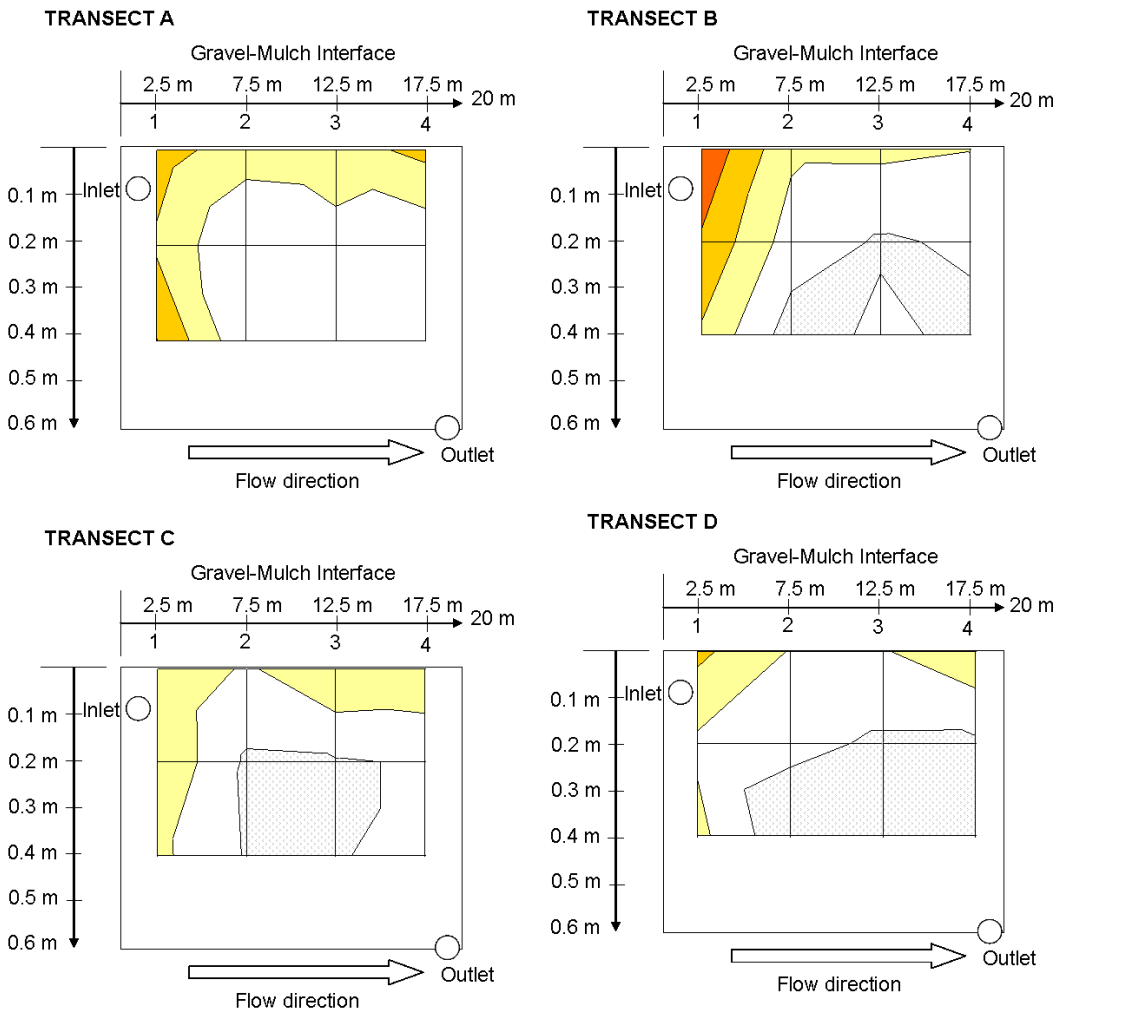

Figure 5-62 The 3D hydraulic conductivity profile of Jackson Meadow. The longitudinal versus vertical hydraulic profiles are shown for the four transverse cross sections that correspond to sampling Transects A to D. Sampling was performed to a 0.4 m depth below the surface of the gravel and results are interpolated between sampling points. Colour contours indicate order of magnitude divisions of hydraulic conductivity. For this system an extra contour has been introduced in comparison to the previously reported systems (grey shading) to reflect high conductivities between 10,000 and 100,000 m/d.

5.21. Conclusions

Spatial hydraulic conductivity profiles have been measured for 20 separate tests on 13 different HSSF TWs in the UK and the US. Systems varied in geometry and age and incorporated varying media, influent distributors and upstream processes. The development of reeds varied between filters, as did the degree of visible surface clog matter accumulation and overland flow. Systems that exhibited surface clogging and overland flow over a large fraction of the bed surface, such as Moreton Morrell A, Snitterfield and Rowington, generally exhibited good reed cover and growth. Systems that did not exhibit extensive surface clogging and overland flow, such as Fenny Compton, Weston-Under-Wetherley, Ashorne and Northend, had patchy reed cover. It is deduced that overland flow encourages healthy reed establishment by maintaining root-zone saturation and distributing influent nutrients across the surface of the bed.

Most systems displayed at least a 2 to 3 order of magnitude variation in hydraulic conductivity, across all planes. The minimum value measured during the study was 0.03 m/d at Fenny Compton in February 2008, which was attributed to a concentration of construction fines clogging the gravel void spaces. The maximum value measured was 62,500 m/d at Jackson Meadows South in 2009, although it was not possible to maintain laminar flow velocities through the permeameter cell for this measurement, which means that the accuracy of the calculated hydraulic conductivity is limited (see **Section 4.2.2**). It should be noted that the US systems had hydraulic loading rates that are approximately an order of magnitude lower than hydraulic loading rates for the UK systems. As discussed in **Section 2.5.4,** high hydraulic loading rates encourage bed clogging by providing less opportunity for aerobic mineralisation of accumulated organic clog matter.

It became apparent during this research that clogging in HSSF TWs is a complex process and the specific design and operational parameters of the system must be taken into account to explain the development of clogging. Factors such as season, vegetation quality and influent distributor and effluent collector architecture appear to greatly influence the profiles that develop. The obtained results will now be used to make general observations about clogging in HSSF TWs, and to derive Clog Factor relationships for Severn Trent systems.

6. Discussion and Analysis

Chapter 5 reported findings from investigations into the spatial variation of hydraulic conductivity within Horizontal Subsurface Flow Treatment Wetlands (HSSF TWs), as obtained using the Aston Permeameter method developed in **Chapter 4**. Altogether 1,053 results were obtained during 20 field tests, representing three-dimensionally resolved hydraulic conductivity values in 13 different systems that varied by age, design and location. Through discussion and analysis of the obtained data, this chapter aims to improve the following areas of understanding regarding hydrological behaviour in Severn Trent HSSF TWs:

1) An improved understanding of how design and operational factors, such as wastewater treatment, plant growth, influent distribution and effluent collection, influence clogging.
2) A general relationship to describe the manner in which clogging develops in Severn Trent HSSF TWs.
3) A generalised understanding of how the development of clogging influences hydraulic operation in Severn Trent HSSF TWs.
4) A generalised understanding of how the development of clogging influences hydrodynamic performance over time.

This Chapter will achieve the above objectives by using the novel theory introduced in **Chapter 3**. Only data from the 3D hydraulic conductivity investigations will be used because of the intention to identify vertical variations of hydraulic conductivity. Additionally, due to fundamental differences in design that may influence the ability to deduce trends, the data from the Minnesotan HSSF TWs will not form part of this analysis. In **Section 6.1,** hydraulic conductivity results will be converted to Clog Factor ***CF*** values using the theory presented in **Section 3.6.2**.

The ***CF*** values will be used in **Section 6.2** to make inferences regarding the influence of wastewater treatment and plant growth on clogging. A 3-way statistical Analysis of Variance (ANOVA) test will be performed using StatGraphics Centurion XVI (StatPoint Technologies, Warrington, Virginia). The analysis will be used to infer whether the influent and effluent arrangement exacerbate uneven clogging in the transverse direction.

In **Section 6.3**, a non-dimensionalised 3-Way ANOVA test will be used to identify trends in ***CF*** in the longitudinal and vertical direction, depending on the bulk system Clog Factor $\boldsymbol{CF_T}$.

The extracted trends will be used to create a general equation that will allow hydraulic conductivity profiles to be recreated for any Severn Trent HSSF TWs using only a single value; $\boldsymbol{CF_T}$.

Hydraulic conductivity profiles that correspond to the general equation are modelled in **Section 6.4** and imported into the FEA model derived in **Chapter 3**. This makes it possible to gauge the influence that Clog Factor has on hydraulics. The water table profiles produced by the model are calibrated against parameters in the novel 1D analytical equation derived in **Chapter 3**. The accuracy of the FEA model is evaluated by comparing to experimental measurements of the water table profile in a HSSF TW where the hydraulic conductivity profile is known.

The FEA model is then used to explore the influence of $\boldsymbol{CF_T}$ on hydrodynamics in **Section 6.5**. The solute transport module of the FEA model is used to produce RTDs that correspond to the clogging and hydraulic profiles derived from $\boldsymbol{CF_T}$ values. The RTDs are fit using Tanks-in-Series models such that the number of tanks $\boldsymbol{n}$ for different stages of clogging can be deduced. This allows $\boldsymbol{CF_T}$ to be correlated against number of tanks. The solute transport module of the FEA model is validated against RTD measurements obtained from a field scale HSSF TW where the hydraulic conductivity profile and water table profile are known.

The outputs from these analyses will provide wetland designers with several simple tools that help elucidate how the hydrological performance of HSSF TWs varies over time.

6.1. Derivation of Clog Factor results

From the 1,053 hydraulic conductivity measurements taken, the results for 816 are summarised in **Table 6-1**, **Table 6-2**, **Table 6-3** and **Table 6-4**. These tables only give a matrix of 4X4X4 sampling points for the Severn Trent systems, such that the results can be conveniently visualised. The calculated Clog Factor values for each system are given in **Appendix C**. Each table shows values for four transects (A-D) and the first four longitudinal sampling points from the inlet (1-4). **Table 6-1** represents hydraulic conductivity between the bed surface and a 0.1 m depth, **Table 6-2** represents hydraulic conductivity between 0.1 m and 0.2 m depth, **Table 6-3** represents hydraulic conductivity between 0.2 m and 0.3 m depth, and **Table 6-4** represents hydraulic conductivity between 0.3 m and 0.4 m depth.

The corresponding Clog Factors for the measurements shown in **Table 6-1**, **Table 6-2**, **Table 6-3** and **Table 6-4** are respectively shown in **Table 6-5**, **Table 6-6**, **Table 6-7** and **Table 6-8**. The Clog Factors were calculated from hydraulic conductivity results using the d_{50} values for the gravel indicated in **Table 5-1**, and a value of 0.35 for clean media porosity ε throughout the entire bed in **Equation 3-57** and **Equation 3-59**.

Table 6-9 provides a summary of the data shown in **Table 6-1** to **Table 6-8**, and shows the range of hydraulic conductivities measured in different systems, the arithmetic mean of the hydraulic conductivity, the standard deviation of hydraulic conductivity results and the arithmetic mean of the Clog Factor results. As evident in **Table 6-9**, the standard deviation of hydraulic conductivity values is generally greater than the arithmetic mean, which confirms that averages of datasets should not be used to represent physical properties that vary by several orders of magnitude about the mean and are neither intensive nor extensive properties of a physical system. In contrast, the Clog Factor is an intensive property and can be representatively averaged. The arithmetic mean of Clog Factor results therefore represents the Clog Factor for the bulk system (CF_T) and can be used as a useful benchmarking tool to compare the state of clogging in different systems (**Equation 3-60**).

The values of CF_T shown in **Table 6-9** vary between 0.54 for the 2008 study on Fenny Compton and 0.92 for the Snitterfield survey. For an ideal medium the ***CF*** value will vary from 0 to 1 as the system clogs, based on the deviation from ideal theoretical hydraulic performance. As discussed in **Chapter 3,** the clean ***CF*** of a non-ideal medium will be greater than 0 because of deviation from ideal theoretical hydraulic performance caused by particle size distribution around d_{50} and non-spherical particle geometries. **Chapter 3** explains that minimum ***CF*** values of 0.35 are realistic for real samples of gravel, and this value can be used to quantify the reduction on design hydraulic performance associated with the quality of the procured media before any clogging occurs. Fenny Compton had been partially refurbished in 2008 and the top 0.2 m of 3-6 mm media had been replaced with 6-12 mm media. The large particle size distribution around the effective d_{50} of the combined media, and the age of the bottom 0.4 m of media, may explain why the CF_T is not lower despite the refurbishment. Regarding the high CF_T value at Snitterfield, this corresponds well to the large degree of ponding observed in this system.

Table 6-1 Hydraulic conductivity results obtained from thirteen surveys of Severn Trent HSSF TWs. The results represent the hydraulic conductivity of the media in m/d between the bed surface and a depth of 0.1 m depth below the surface.

	Transect A				Transect B				Transect C				Transect D			
	Longitudinal Sampling Point				Longitudinal Sampling Point				Longitudinal Sampling Point				Longitudinal Sampling Point			
	1	2	3	4	1	2	3	4	1	2	3	4	1	2	3	4
Ashorne - Jun 09	6.42 E-02	1.80 E+00	6.42 E+02	9.56 E+02	1.44 E-01	8.19 E+01	2.37 E+02	4.80 E+03	1.12 E-01	8.11 E-02	1.52 E+01	5.34 E+03	4.45 E-01	7.36 E-02	2.84 E-01	2.21 E+02
Fenny Compton - Feb 08	1.05 E+00	3.46 E-01	3.28 E+03	7.57 E+03	6.32 E+03	1.67 E+03	9.77 E+01	4.98 E+01	1.82 E+03	1.03 E+03	9.18 E+03	2.88 E+03	2.74 E+02	4.99 E+01	2.27 E+02	2.01 E+03
Fenny Compton - Feb 09	5.09 E-01	2.82 E-02	2.72 E+01	8.96 E+01	1.10 E+01	1.98 E-02	3.30 E-02	1.94 E+02	3.34 E+02	7.77 E+01	3.08 E-02	8.70 E+01	1.73 E+02	1.21 E+02	1.06 E+02	6.04 E+01
Fenny Compton - Feb 10	1.09 E+02	2.62 E+02	1.06 E+04	5.25 E+03	2.57 E+02	6.76 E+03	1.40 E+03	6.91 E+03	2.52 E+02	4.65 E+02	6.10 E+02	4.17 E+03	4.53 E+03	2.96 E+03	5.54 E+01	4.22 E+03
Leek Wooton - Jun 09	1.92 E+01	8.75 E+01	1.04 E+02	6.87 E+01	1.52 E+01	2.51 E+01	1.56 E+02	1.42 E+01	1.93 E+02	8.80 E+01	7.64 E+01	5.49 E+01	5.48 E+01	2.01 E+02	1.22 E+02	1.45 E+02
Moreton Morrell - Feb 09	6.59 E-02	2.09 E-01	6.41 E-01	1.31 E+00	6.57 E-01	7.19 E-01	7.61 E-01	1.62 E+01	3.25 E-02	2.24 E+00	1.71 E+00	5.86 E+00	2.87 E-01	4.55 E+01	8.86 E+01	4.71 E+01
Moreton Morrell - Jun 08	3.80 E+00	3.58 E+02	1.57 E+03	7.01 E+02	4.16 E-01	1.86 E+02	5.12 E+02	6.09 E+02	4.90 E-01	5.54 E+02	7.34 E+02	3.73 E+02	3.35 E-01	1.46 E+02	2.94 E+02	5.05 E+02
Moreton Morrell - Sep 09	4.70 E-01	6.65 E-01	1.26 E+00	1.40 E+00	4.70 E-01	2.30 E-01	3.58 E-01	6.21 E+01	1.06 E-01	8.53 E-01	4.31 E-01	7.10 E+00	4.66 E-02	1.92 E+00	7.55 E+00	6.58 E+00
Moreton Morrell - Oct 09	3.03 E+02	4.99 E+02	2.06 E+02	1.19 E+03	5.41 E+02	3.73 E+02	5.04 E+02	7.75 E+02	3.28 E+02	2.01 E+03	5.33 E+02	3.06 E+02				
Northend Jun 09	8.82 E-01	5.42 E+00	6.45 E+00	1.40 E+00	4.31 E-01	5.65 E-02	2.19 E-02	6.11 E-02	4.31 E-01	1.96 E+00	2.93 E-01	3.23 E+00	6.77 E-02	1.26 E-01	9.62 E-02	2.02 E+00
Rowington - Jul 09	7.29 E+00	6.69 E-02	1.65 E+02	3.99 E+01	1.50 E-01	2.54 E-01	1.08 E+00	9.12 E+01	3.12 E-03	9.12 E-03	1.75 E-01	1.21 E+01	3.25 E-01	9.98 E-02	5.31 E-01	4.36 E+01
Snitterfield - Aug 09	5.51 E-02	5.88 E+00	1.76 E+00	1.41 E+00	3.07 E-02	3.21 E-01	6.69 E-01	1.10 E+00	5.13 E-02	1.39 E+00	1.43 E-01	4.55 E-01	2.76 E-02	4.48 E-01	3.93 E+00	6.25 E-01
Weston u. W. - May 09	4.62 E-01	2.23 E+00	9.00 E+01	2.25 E+02	2.52 E+00	1.48 E+01	2.65 E+02	5.67 E+01	1.04 E-01	4.80 E+00	3.65 E+02	5.43 E+01	8.92 E-01	9.00 E+01	9.58 E+02	5.79 E+02

Table 6-2 Hydraulic conductivity results obtained from thirteen surveys of Severn Trent HSSF TWs. The results represent the hydraulic conductivity of the media in m/d between the depths of 0.1 m and 0.2 m below the bed surface.

	Transect A				Transect B				Transect C				Transect D			
	Longitudinal Sampling Point				Longitudinal Sampling Point				Longitudinal Sampling Point				Longitudinal Sampling Point			
	1	2	3	4	1	2	3	4	1	2	3	4	1	2	3	4
Ashorne - Jun 09	7.78 E-02	1.06 E-01	7.27 E+01	5.50 E+01	2.60 E-02	3.24 E+00	1.06 E+01	1.39 E+02	5.14 E-02	8.83 E-02	5.86 E+00	2.37 E+02	7.26 E-02	4.06 E-02	2.66 E+00	6.96 E+01
Fenny Compton - Feb 08	8.64 E-01	2.66 E-01	6.56 E+03	3.59 E+03	1.84 E+01	1.01 E+01	2.44 E+01	9.77 E+02	1.43 E+02	8.63 E+02	2.73 E+02	5.00 E+02	1.73 E+02	2.61 E+01	3.39 E+01	5.98 E+02
Fenny Compton - Feb 09	1.05 E+00	2.66 E-01	3.18 E+02	6.68 E+03	1.89 E+01	6.65 E-02	1.34 E-01	2.39 E+02	1.25 E+03	4.55 E+03	1.00 E-01	3.99 E+01	4.92 E+01	2.58 E+03	4.67 E+03	4.28 E+01
Fenny Compton - Feb 10	2.17 E+00	7.27 E+00	2.65 E+03	2.06 E+02	1.20 E+01	3.07 E+02	1.75 E+02	3.00 E+02	2.12 E+00	3.58 E+01	2.44 E+02	4.17 E+03	5.33 E+01	1.97 E+02	9.70 E+01	7.39 E+03
Leek Wooton - Jun 09	3.02 E+01	8.61 E+01	1.78 E+02	1.04 E+02	6.00 E+01	4.80 E+01	4.93 E+02	8.09 E+01	2.80 E+02	1.88 E+02	1.10 E+02	1.39 E+02	2.50 E+02	5.42 E+02	2.04 E+02	1.80 E+02
Moreton Morrell - Feb 09	9.89 E-02	4.98 E-01	1.86 E+00	8.49 E+00	2.93 E-02	8.27 E+00	4.69 E+00	1.01 E+02	4.51 E-02	9.42 E+01	2.87 E+01	1.49 E+02	3.80 E-01	5.74 E+01	1.32 E+02	7.83 E+01
Moreton Morrell - Jun 08	7.73 E+00	2.59 E+02	8.38 E+02	7.94 E+02	4.18 E-02	3.20 E+02	1.35 E+02	6.74 E+02	1.83 E+00	4.41 E+02	5.86 E+02	5.94 E+02	6.95 E-02	1.29 E+03	1.22 E+03	5.70 E+02
Moreton Morrell - Sep 09	3.31 E-02	1.95 E-01	6.38 E-01	2.27 E+00	3.31 E-02	2.22 E-01	2.28 E-01	5.97 E-01	1.43 E+00	1.77 E+00	3.33 E-01	8.52 E+01	5.97 E-02	1.59 E+02	3.62 E+02	2.60 E+02
Moreton Morrell - Oct 09	2.48 E+01	1.91 E+02	3.40 E+02	4.04 E+02	7.05 E+01	7.82 E+01	3.02 E+02	6.43 E+02	2.21 E+02	7.72 E+01	1.80 E+02	2.68 E+02				
Northend Jun 09	3.04 E+00	1.48 E+01	1.16 E+01	4.97 E+00	6.92 E-02	1.73 E-02	4.04 E-02	1.54 E-01	6.92 E-02	5.06 E+00	4.67 E-01	5.88 E+00	9.42 E-02	3.55 E-02	2.74 E-01	1.07 E+01
Rowington - Jul 09	4.89 E-02	1.03 E-01	8.58 E+02	7.19 E+01	6.59 E-02	9.64 E-02	1.61 E+00	2.53 E+02	9.85 E-03	1.32 E-03	1.78 E-01	1.32 E+01	1.06 E-01	3.44 E-03	2.52 E-01	6.48 E+01
Snitterfield - Aug 09	4.56 E-02	3.45 E+00	2.19 E+00	3.69 E+00	1.24 E-02	1.88 E-01	1.42 E+00	7.96 E+00	2.60 E-02	2.29 E-01	2.04 E-01	2.78 E-01	1.38 E-02	1.51 E+00	4.45 E+00	1.35 E+00
Weston u. W. - May 09	3.78 E-01	4.15 E+00	5.01 E+01	2.63 E+02	5.73 E-02	1.21 E+01	2.25 E+03	4.18 E+01	3.87 E-02	5.99 E+00	3.56 E+02	9.31 E+01	5.29 E-01	1.09 E+02	1.14 E+03	5.48 E+02

Table 6-3 Hydraulic conductivity results obtained from thirteen surveys of Severn Trent HSSF TWs. The results represent the hydraulic conductivity of the media in m/d between the depths of 0.2 m and 0.3 m below the bed surface.

	Transect A				Transect B				Transect C				Transect D			
	Longitudinal Sampling Point				Longitudinal Sampling Point				Longitudinal Sampling Point				Longitudinal Sampling Point			
	1	2	3	4	1	2	3	4	1	2	3	4	1	2	3	4
Ashorne - Jun 09	1.22 E-01	4.86 E-01	4.28 E+01	1.04 E+02	3.46 E+00	9.63 E+00	2.25 E+01	1.78 E+02	4.15 E-01	7.94 E+00	2.54 E+01	1.55 E+02	8.25 E-02	1.77 E-01	1.14 E+00	1.95 E+02
Fenny Compton - Feb 08	8.64 E-01	2.06 E-02	4.97 E+01	2.99 E+03	7.45 E+01	1.33 E+02	6.04 E+01	1.13 E+02	4.69 E+01	1.70 E+03	5.12 E+02	3.62 E+02	4.85 E+02	3.77 E+01	2.73 E+01	5.74 E+02
Fenny Compton - Feb 09	3.32 E-01	2.06 E-02	1.09 E+02	1.80 E+03	8.93 E+02	1.36 E-02	1.22 E-02	3.06 E+03	2.25 E+02	1.26 E+02	2.16 E-02	2.60 E+02	6.52 E+01	5.12 E+02	3.28 E+02	7.87 E+01
Fenny Compton - Feb 10	1.09 E+02	2.78 E+00	8.15 E+02	2.50 E+02	5.59 E+00	4.23 E+02	2.34 E+01	7.35 E+01	2.10 E+01	4.43 E+00	2.93 E+01	1.15 E+03	2.27 E+02	2.10 E+01	1.94 E+02	4.48 E+02
Leek Wooton - Jun 09	1.20 E+02	1.14 E+02	2.31 E+03	6.25 E+03	1.57 E+02	2.74 E+02	1.34 E+03	1.02 E+02	9.15 E+02	1.58 E+03	8.70 E+03	5.00 E+03	3.78 E+03	4.57 E+03	1.50 E+03	4.43 E+02
Moreton Morrell - Feb 09	1.03 E-01	9.61 E-02	1.62 E+00	7.25 E+00	1.15 E-01	1.59 E+00	3.92 E+00	4.07 E+02	8.61 E-02	5.81 E+01	2.07 E+03	1.16 E+02	4.01 E-01	1.94 E+02	3.60 E+02	4.36 E+03
Moreton Morrell - Jun 08	5.46 E+00	1.49 E+03	1.72 E+03	7.33 E+02	9.07 E-02	5.11 E+02	1.24 E+03	9.03 E+02	1.63 E+00	4.36 E+02	2.17 E+02	7.70 E+02	3.74 E-01	1.95 E+01	3.61 E+02	1.27 E+03
Moreton Morrell - Sep 09	5.22 E-01	9.07 E-02	1.08 E+00	7.26 E+01	5.22 E-01	3.28 E+00	1.02 E+00	6.21 E+01	4.45 E-01	4.43 E+01	5.82 E+00	3.41 E+02	3.17 E+00	7.97 E+01	3.62 E+02	2.60 E+02
Moreton Morrell - Oct 09	8.53 E+01	9.98 E+02	7.11 E+02	1.02 E+03	4.84 E+01	6.67 E+01	1.95 E+02	1.37 E+03	7.03 E+01	1.08 E+02	1.51 E+02	6.53 E+03				
Northend Jun 09	3.19 E+01	6.43 E+01	6.76 E+02	3.60 E+01	3.43 E-01	1.74 E-01	1.36 E+00	7.39 E+00	3.43 E-01	5.54 E+00	4.05 E+01	1.06 E+02	5.54 E-01	2.77 E+00	1.21 E+01	2.59 E+02
Rowington - Jul 09	4.68 E-02	1.37 E-01	7.11 E+02	5.04 E+02	2.35 E-02	6.90 E-02	2.52 E+00	1.66 E+02	1.99 E-03	2.41 E-03	2.21 E-01	2.76 E+01	7.47 E+00	1.93 E-03	4.21 E-01	9.05 E+01
Snitterfield - Aug 09	8.40 E-02	4.01 E+00	1.74 E+02	7.56 E+01	4.39 E-02	2.02 E-01	2.74 E+01	5.79 E+00	1.73 E-02	2.04 E-01	1.32 E+00	1.05 E+00	4.62 E-01	4.52 E+01	6.68 E+01	6.98 E+00
Weston u. W. - May 09	4.60 E-01	2.53 E+00	4.50 E+01	2.03 E+04	1.19 E-01	1.94 E+01	7.38 E+01	3.34 E+03	1.10 E-01	1.52 E+01	8.21 E+02	6.45 E+02	1.29 E+00	9.85 E+02	9.39 E+03	3.84 E+03

Table 6-4 Hydraulic conductivity results obtained from thirteen surveys of Severn Trent HSSF TWs. The results represent the hydraulic conductivity of the media in m/d between the depths of 0.3 m and 0.4 m below the bed surface.

	Transect A				Transect B				Transect C				Transect D			
	Longitudinal Sampling Point				Longitudinal Sampling Point				Longitudinal Sampling Point				Longitudinal Sampling Point			
	1	2	3	4	1	2	3	4	1	2	3	4	1	2	3	4
Ashorne - Jun 09	1.56 E+00	1.04 E+02	4.82 E+02	6.83 E+02	1.15 E+00	1.06 E+01	7.88 E+01	9.59 E+03	7.26 E-01	3.97 E+00	2.54 E+01	3.24 E+02	6.68 E-01	1.18 E+00	2.96 E+00	1.27 E+03
Fenny Compton - Feb 08	8.64 E-01	2.99 E+03	1.15 E+02	6.38 E+03	2.98 E+03	2.44 E+04	8.26 E+03	2.05 E+03	2.22 E+02	1.67 E+03	6.46 E+03	2.29 E+04	3.44 E+02	1.24 E+03	3.12 E+03	1.08 E+04
Fenny Compton - Feb 09	1.93 E+01	1.80 E+03	1.33 E+02	5.26 E+01	1.52 E+02	1.90 E-01	8.36 E-02	7.00 E+02	1.17 E+03	1.63 E+02	2.89 E-01	1.90 E+02	1.14 E+03	1.15 E+02	1.97 E+02	8.17 E+02
Fenny Compton - Feb 10	7.24 E+01	2.50 E+02	3.93 E+02	6.56 E+02	3.96 E+01	8.35 E+01	3.12 E+02	4.93 E+02	1.94 E+01	2.58 E+01	1.22 E+03	4.17 E+03	4.53 E+03	1.48 E+03	2.19 E+00	1.23 E+03
Leek Wooton - Jun 09	5.56 E+02	6.25 E+03	8.88 E+02	2.08 E+03	2.05 E+03	3.91 E+02	3.28 E+02	2.04 E+02	2.17 E+03	1.85 E+03	2.18 E+03	3.85 E+02	7.56 E+03	2.08 E+03	1.50 E+03	1.62 E+03
Moreton Morrell - Feb 09	5.93 E-01	7.25 E+00	4.05 E+00	1.48 E+01	6.31 E-01	1.41 E+00	5.50 E+00	1.34 E+02	9.61 E-01	1.19 E+02	1.01 E+01	8.44 E+01	3.42 E+00	2.75 E+03	1.14 E+03	1.31 E+04
Moreton Morrell - Jun 08	3.60 E+01	7.33 E+02	7.26 E+03	1.00 E+03	3.90 E+00	3.74 E+02	1.02 E+03	3.38 E+03	5.08 E+00	5.43 E+02	3.09 E+02	3.94 E+04	3.79 E-01	2.76 E+01	2.55 E+02	2.41 E+03
Moreton Morrell - Sep 09	7.83 E-01	7.26 E+01	9.73 E+00	7.26 E+01	7.83 E-01	6.56 E+00	1.32 E+00	6.21 E+01	3.22 E+00	4.43 E+01	1.16 E+01	6.81 E+01	3.17 E+00	1.59 E+02	3.62 E+02	2.60 E+02
Moreton Morrell - Oct 09	1.14 E+02	1.02 E+03	3.40 E+02	9.15 E+03	6.49 E+02	4.22 E+02	2.37 E+02	1.16 E+03	2.12 E+02	4.22 E+02	1.60 E+03	3.27 E+03				
Northend Jun 09	1.06 E+01	3.60 E+01	3.38 E+02	6.00 E+01	8.35 E-01	9.98 E-01	2.71 E+00	7.39 E+00	8.35 E-01	5.98 E+01	4.05 E+01	2.12 E+02	4.16 E+00	2.77 E+00	6.05 E+00	2.35 E+01
Rowington - Jul 09	1.82 E-01	5.04 E+02	3.99 E+02	5.04 E+02	6.59 E-02	9.73 E-02	6.94 E+01	1.98 E+02	5.86 E-03	2.56 E-03	6.48 E+00	1.41 E+02	2.67 E-01	1.31 E-02	1.29 E+01	2.27 E+02
Snitterfield - Aug 09	1.37 E-01	7.56 E+01	8.68 E+01	5.04 E+01	1.38 E-01	3.12 E-01	2.74 E+01	2.12 E+01	2.23 E-02	2.75 E-01	1.73 E+00	3.90 E+00	6.16 E-01	4.52 E+01	3.82 E+01	2.46 E+00
Weston u. W. - May 09	1.42 E+01	2.03 E+04	1.98 E+03	2.03 E+04	7.75 E+01	1.22 E+03	1.07 E+02	3.34 E+03	7.26 E-01	5.03 E+02	2.96 E+04	7.10 E+03	6.60 E+01	1.77 E+03	7.82 E+03	1.02 E+04

Table 6-5 Clog Factor (***CF***) results that correspond to the hydraulic conductivity results shown in **Table 6.1**. A ***CF*** value of 0 represents no clogging and a ***CF*** value of 1 represents complete clogging. The results represent the ***CF*** of the media between the bed surface and a depth of 0.1 m depth below the surface.

	Transect A				**Transect B**				**Transect C**				**Transect D**			
	Longitudinal Sampling Point				Longitudinal Sampling Point				Longitudinal Sampling Point				Longitudinal Sampling Point			
	1	2	3	4	1	2	3	4	1	2	3	4	1	2	3	4
Ashorne - Jun 09	1.00	0.93	0.53	0.47	0.98	0.75	0.65	0.18	0.98	1.00	0.85	0.15	0.96	1.00	0.96	0.66
Fenny Compton - Feb 08	0.94	0.96	0.26	0.07	0.12	0.38	0.74	0.79	0.37	0.46	0.03	0.28	0.64	0.79	0.66	0.35
Fenny Compton - Feb 09	0.95	1.00	0.82	0.74	0.87	1.00	1.00	0.67	0.61	0.75	1.00	0.75	1.00	0.72	0.73	0.77
Fenny Compton - Feb 10	0.79	0.73	0.19	0.33	0.73	0.28	0.54	0.28	0.73	0.67	0.64	0.37	0.36	0.43	0.83	0.37
Leek Wooton - Jun 09	0.88	0.81	0.79	0.82	0.89	0.87	0.77	0.89	0.75	0.81	0.81	0.83	0.83	0.75	0.78	0.77
Moreton Morrell - Feb 09	1.00	0.97	0.95	0.94	0.95	0.95	0.94	0.85	0.98	0.92	0.93	0.89	0.96	0.79	0.74	0.79
Moreton Morrell - Jun 08	0.91	0.62	0.42	0.54	0.96	0.69	0.58	0.56	0.96	0.57	0.53	0.62	0.96	0.71	0.65	0.58
Moreton Morrell - Sep 09	0.96	0.95	0.93	0.93	0.95	0.97	0.96	0.77	0.98	0.94	0.95	0.89	1.00	0.93	0.88	0.89
Moreton Morrell - Oct 09	0.63	0.57	0.67	0.44	0.55	0.60	0.56	0.50	0.62	0.35	0.56	0.62				
Northend Jun 09	0.94	0.89	0.89	0.93	0.95	1.00	1.00	1.00	0.95	0.92	0.96	0.91	1.00	0.98	0.97	0.92
Rowington - Jul 09	0.88	1.00	0.69	0.80	0.97	0.96	0.94	0.74	1.00	1.00	0.96	0.86	0.96	0.99	0.95	0.80
Snitterfield - Aug 09	1.00	0.89	0.93	0.93	1.00	0.96	0.95	0.94	1.00	0.93	0.96	0.95	1.00	0.95	0.91	0.95
Weston u. W. - May 09	0.95	0.92	0.74	0.66	0.92	0.85	0.64	0.78	0.98	0.90	0.60	0.78	0.94	0.74	0.47	0.55

Table 6-6 Clog Factor (***CF***) results that correspond to the hydraulic conductivity results shown in **Table 6.2**. A ***CF*** value of 0 represents no clogging and a ***CF*** value of 1 represents complete clogging. The results represent the ***CF*** of the media between the depths of 0.1 m and 0.2 m below the bed surface.

	Transect A				**Transect B**				**Transect C**				**Transect D**			
	Longitudinal Sampling Point				Longitudinal Sampling Point				Longitudinal Sampling Point				Longitudinal Sampling Point			
	1	2	3	4	1	2	3	4	1	2	3	4	1	2	3	4
Ashorne - Jun 09	1.00	0.97	0.76	0.78	1.00	0.91	0.87	0.71	1.00	0.99	0.89	0.65	1.00	0.98	0.92	0.76
Fenny Compton - Feb 08	0.94	0.96	0.11	0.24	0.84	0.87	0.83	0.47	0.70	0.49	0.64	0.56	0.68	0.83	0.81	0.54
Fenny Compton - Feb 09	0.94	0.96	0.62	0.10	1.00	1.00	0.97	0.65	0.43	0.19	0.98	0.80	1.00	1.00	0.18	0.80
Fenny Compton - Feb 10	0.94	0.91	0.45	0.75	0.90	0.71	0.76	0.71	0.94	0.85	0.73	0.37	0.83	0.75	0.80	0.27
Leek Wooton - Jun 09	0.86	0.81	0.76	0.79	0.83	0.84	0.67	0.81	0.72	0.75	0.79	0.77	0.73	0.66	0.75	0.76
Moreton Morrell - Feb 09	0.98	0.95	0.93	0.88	1.00	0.88	0.90	0.73	1.00	0.74	0.82	0.70	0.95	0.78	0.71	0.75
Moreton Morrell - Jun 08	0.89	0.66	0.51	0.52	1.00	0.64	0.72	0.55	0.93	0.60	0.56	0.56	1.00	0.45	0.46	0.57
Moreton Morrell - Sep 09	1.00	0.97	0.95	0.92	1.00	0.96	0.97	0.95	0.93	0.93	0.96	0.75	1.00	0.69	0.60	0.64
Moreton Morrell - Oct 09	0.83	0.68	0.61	0.59	0.76	0.75	0.63	0.53	0.66	0.75	0.68	0.64				
Northend Jun 09	0.91	0.85	0.87	0.90	1.00	1.00	1.00	0.96	1.00	0.90	0.95	0.89	0.98	1.00	0.96	0.87
Rowington - Jul 09	1.00	0.98	0.49	0.76	1.00	0.98	0.93	0.65	1.00	1.00	0.96	0.86	0.98	1.00	0.96	0.77
Snitterfield - Aug 09	1.00	0.91	0.92	0.91	1.00	0.96	0.93	0.88	1.00	0.96	0.96	0.96	1.00	0.93	0.90	0.93
Weston u. W. - May 09	0.95	0.90	0.79	0.64	1.00	0.86	0.33	0.80	1.00	0.89	0.61	0.74	0.95	0.73	0.45	0.55

Table 6-7 Clog Factor (***CF***) results that correspond to the hydraulic conductivity results shown in **Table 6.3**. A ***CF*** value of 0 represents no clogging and a ***CF*** value of 1 represents complete clogging. The results represent the ***CF*** of the media between the depths of 0.2 m and 0.3 m below the bed surface.

	Transect A				**Transect B**				**Transect C**				**Transect D**			
	Longitudinal Sampling Point				Longitudinal Sampling Point				Longitudinal Sampling Point				Longitudinal Sampling Point			
	1	2	3	4	1	2	3	4	1	2	3	4	1	2	3	4
Ashorne - Jun 09	0.98	0.95	0.80	0.73	0.91	0.87	0.83	0.68	0.95	0.88	0.83	0.70	1.00	0.97	0.94	0.67
Fenny Compton - Feb 08	0.94	1.00	0.79	0.27	0.76	0.71	0.77	0.72	0.79	0.38	0.56	0.61	0.57	0.80	0.82	0.55
Fenny Compton - Feb 09	0.96	0.99	0.73	0.37	0.48	1.00	1.00	0.27	0.66	0.71	1.00	0.64	0.77	0.59	0.62	0.75
Fenny Compton - Feb 10	0.73	0.92	0.50	0.65	0.89	0.59	0.83	0.76	0.84	0.90	0.82	0.44	0.66	0.84	0.67	0.58
Leek Wooton - Jun 09	0.79	0.79	0.47	0.30	0.77	0.72	0.55	0.80	0.60	0.53	0.23	0.34	0.39	0.36	0.53	0.68
Moreton Morrell - Feb 09	0.98	0.99	0.93	0.89	0.98	0.93	0.91	0.59	1.00	0.78	0.34	0.72	0.96	0.67	0.61	0.20
Moreton Morrell - Jun 08	0.90	0.43	0.40	0.53	0.97	0.58	0.46	0.50	0.93	0.60	0.68	0.53	0.96	0.85	0.62	0.45
Moreton Morrell - Sep 09	0.95	0.99	0.94	0.76	0.95	0.91	0.94	0.77	0.95	0.79	0.89	0.61	0.91	0.75	0.60	0.64
Moreton Morrell - Oct 09	0.75	0.47	0.52	0.46	0.79	0.77	0.67	0.42	0.76	0.73	0.70	0.11				
Northend Jun 09	0.81	0.77	0.52	0.81	0.96	0.97	0.93	0.88	0.96	0.89	0.80	0.73	0.95	0.92	0.86	0.64
Rowington - Jul 09	1.00	0.97	0.52	0.56	1.00	1.00	0.92	0.69	0.98	1.00	0.96	0.82	0.88	0.98	0.96	0.74
Snitterfield - Aug 09	1.00	0.91	0.68	0.76	1.00	0.97	0.82	0.89	0.98	0.97	0.94	0.94	0.95	0.79	0.77	0.89
Weston u. W. - May 09	0.95	0.92	0.79	0.00	0.98	0.84	0.76	0.25	0.98	0.85	0.50	0.53	0.94	0.47	0.02	0.22

Table 6-8 Clog Factor (***CF***) results that correspond to the hydraulic conductivity results shown in **Table 6.4**. A ***CF*** value of 0 represents no clogging and a ***CF*** value of 1 represents complete clogging. The results represent the ***CF*** of the media between the depths of 0.3 m and 0.4 m below the bed surface.

	Transect A				**Transect B**				**Transect C**				**Transect D**			
	Longitudinal Sampling Point				Longitudinal Sampling Point				Longitudinal Sampling Point				Longitudinal Sampling Point			
	1	2	3	4	1	2	3	4	1	2	3	4	1	2	3	4
Ashorne - Jun 09	0.93	0.73	0.57	0.52	0.94	0.87	0.75	0.02	0.95	0.91	0.83	0.62	0.95	0.94	0.91	0.43
Fenny Compton - Feb 08	0.94	0.27	0.72	0.11	0.28	0.00	0.05	0.35	0.66	0.38	0.11	0.00	0.61	0.43	0.27	0.00
Fenny Compton - Feb 09	0.84	0.37	0.71	0.78	0.70	0.97	1.00	0.52	0.44	0.69	0.96	0.68	0.45	0.72	0.67	0.50
Fenny Compton - Feb 10	0.76	0.65	0.60	0.53	0.80	0.75	0.62	0.57	0.84	0.83	0.44	0.21	0.19	0.40	0.92	0.43
Leek Wooton - Jun 09	0.65	0.30	0.60	0.49	0.49	0.69	0.71	0.75	0.48	0.50	0.48	0.69	0.26	0.49	0.53	0.52
Moreton Morrell - Feb 09	0.95	0.89	0.91	0.86	0.95	0.93	0.90	0.71	0.94	0.72	0.87	0.75	0.91	0.29	0.45	0.00
Moreton Morrell - Jun 08	0.82	0.53	0.12	0.49	0.91	0.62	0.49	0.28	0.90	0.57	0.64	0.00	0.96	0.83	0.66	0.34
Moreton Morrell - Sep 09	0.94	0.76	0.87	0.76	0.94	0.89	0.93	0.77	0.91	0.79	0.87	0.76	0.91	0.69	0.60	0.64
Moreton Morrell - Oct 09	0.72	0.46	0.61	0.03	0.53	0.59	0.65	0.44	0.66	0.59	0.39	0.26				
Northend Jun 09	0.87	0.81	0.61	0.77	0.94	0.94	0.92	0.88	0.94	0.77	0.80	0.66	0.90	0.92	0.89	0.83
Rowington - Jul 09	0.97	0.56	0.59	0.56	1.00	0.97	0.76	0.67	0.98	1.00	0.89	0.70	0.96	0.98	0.86	0.66
Snitterfield - Aug 09	0.98	0.76	0.75	0.79	0.97	0.96	0.82	0.84	0.98	0.96	0.93	0.91	0.95	0.79	0.80	0.92
Weston u. W. - May 09	0.86	0.00	0.35	0.00	0.75	0.43	0.73	0.25	0.95	0.56	0.00	0.09	0.77	0.37	0.07	0.00

Table 6-9 A summary of results from hydraulic surveys on 13 field scale Severn Trent HSSF TWs. Moreton Morrell B was a bed that had been rested for 13 months. All other systems were operational. Areal Overland Flow and Plant Cover indices are approximate and qualitative. Data includes: the media size range; the measured range of range hydraulic conductivity; arithmetic mean and standard deviation of hydraulic conductivity datasets; and the system Clog Factor (CF_T) value.

Test Date	System Name	Age	Media Size Range	Hyd. Cond. Range	Hyd. Cond. mean	Hyd. Cond. Std. Dev.	CF_T	Areal Over Land Flow	Areal Plant Cover
		(yrs)	(mm)	(m/d)	(m/d)	(m/d)	(-)	(%)	(%)
Feb '08	Fenny Compton	1	3-12	0.02 - 83,000	4,000	10,265	0.54	<5	5
Feb '09	Fenny Compton	2	3-12	0.01 – 6,700	560	1,240	0.74	<5	50
Mar '10	Fenny Compton	3	3-12	1.2 – 10,600	1,396	2,355	0.63	<5	85
Jun '09	Leek Wooton	3	6-9	14 - 8,700	1,077	1,817	0.67	<5	100
May '09	Weston Under Wetherley	5	3-6	0.04 - 30,000	2,560	5,568	0.60	10	50
Jul '09	Rowington	8	3-6	0.001 - 1,900	90	262	0.88	40	100
Aug '09	Snitterfield	15	3-6	0.01 - 170	11	26	0.92	80	100
Jun '08	Moreton Morrell A	16	3-6	0.04 - 40,000	1,260	4,950	0.64	15	100
Feb '09	Moreton Morrell A	16.5	3-6	0.03 - 13,000	403	1,752	0.82	20	100
Sep '09	Moreton Morrell A	17	3-6	0.03 - 360	52	100	0.87	25	100
Oct '09	Moreton Morrell B	17	3-6	24 - 9,100	840	1,613	0.58	<5	80
Jun '09	Ashorne	16	3-6	0.03 - 9,500	409	1,473	0.81	15	70
Jun '09	Northend	17	3-6	0.02 - 680	35	96	0.89	20	70

6.2. The influence of design and operation parameters on clogging

The ***CF*** results can be used to deduce information regarding the impacts of wastewater treatment and vegetation on clogging, and the influence of inlet and outlet architecture. Some of these discussions only require consideration of $\boldsymbol{CF_T}$ values, whereas others require statistical analysis of spatial trends in discrete ***CF*** values.

6.2.1. The influence of wastewater treatment

Two identical HSSF TWs operated in parallel at Moreton Morrell A (operational) Moreton Morrell B (rested) were used to test the influence of normal operation on hydraulic conductivity. Both beds appeared to be in similar states of clogging in July 2008 (although only Moreton Morrell A was surveyed). Moreton Morrell B was taken off-line for 14 months and in September 2009 surveys were conducted on both Moreton Morrell A and B. Visually, Moreton Morrell A appeared more clogged than Moreton Morrell B, with Moreton Morrell B showing a smaller degree of surface accumulation and stunted plant growth in comparison to Moreton Morrell A. This is supported by the $\boldsymbol{CF_T}$ results that show a value of 0.58 for Moreton Morrell B, a value of 0.87 for Moreton Morrell A at October 2009, and a value of 0.64 for Moreton Morrell A at June 2008. This result supports the idea that bed resting allows organic clog matter accumulations to mineralise and restores hydraulic conductivity.

6.2.2. The influence of vegetation

The ***CF*** results for each system were analysed using a 3-Way ANOVA test; the three factorials being the vertical, longitudinal and transverse location of the sampling point. This enabled the relative component of ***CF*** variability in each direction to be factorialised, such that it was possible to study the influence of vegetation on vertical trends in ***CF*** results. Only tests performed during the relatively warm and dry 6 month period May-September 2009 were considered. Although vegetation health was not quantified through biomass assay or stem density counts, a qualitative relationship was noticed between the vegetation cover over the surface of the bed, and the vertical ***CF*** relationships in each system. Those systems that were sparsely vegetated exhibited lower vertical ***CF*** values in the top 0.1 m of media than in media between depths of 0.1 to 0.2 m. Those systems that had dense vegetation cover exhibited the highest vertical ***CF*** values in the top 0.1 m of measured media. This effect occurs because plants contributes an additional solids load through leaf-litter fall, and shade

the bed surface from being dried-out by the elements, such that aerobic mineralization is decelerated. This information is summarised in **Table 6-10**.

Further evidence of the importance of vegetation is indicated by the repeat tests performed on Fenny Compton and Moreton Morrel A. The tests of February 2009 were performed in very cold weather and measured CF_T values were 0.74 and 0.82 respectively. Fenny Compton partially recovered over the following year (March 2010 CF_T value of 0.63), whereas the situation at Moreton Morrell became compounded (September 2009 CF_T value of 0.87). This evidence suggests that sparse vegetation cover at Fenny Compton enabled adequate mineralization during summer, and dense cover at Moreton Morrell prevented mineralization and CF_T for the system continued to increase.

Table 6-10 Least Square Means for the vertical component of Clog Factor variability at the 95% Confidence Level, for those systems surveyed between May 2009 and September 2009. The summer of 2009 was relatively warm and dry. The percentage Areal Plant Cover (APC) is given to compare the influence of incomplete vegetation cover on vertical CF relationships.

	Depth below surface (m)				
	0.0 : 0.1	0.1 : 0.2	0.2 : 0.3	0.3 : 0.4	**APC* (%)**
Ashorne	0.75	0.89	0.86	0.74	**60**
Leek Wooton	0.81	0.76	0.57	0.54	**100**
Moreton Morrell A	0.93	0.89	0.84	0.82	**100**
Moreton Morrell B	0.56	0.68	0.59	0.5	**75**
Rowington	0.91	0.9	0.86	0.84	**100**
Northend	0.93	0.94	0.83	0.83	**75**
Snitterfield	0.95	0.95	0.9	0.88	**100**
Weston Under W*	0.77	0.72	0.59	0.34	**60**

* The system at Weston Under Wetherley had been operating with a flooded surface prior to the test

6.2.3. The influence of inlet and outlet architecture

The ANOVA analysis was also used to explore the influence of inlet and outlet architecture on transverse variations in Clog Factor. An ideal HSSF TW that behaves as a plug-flow reactor would not experience any preferential flow induced by transverse variations in ***CF.*** To avoid transverse variations of preferential flow, the system would have to employ an influent distributor that achieves uniform width distribution and have an effluent collector

that does not induce preferential flow. It is assumed that if these conditions are met, vegetation density across the width of the bed would be uniform, and therefore transverse variations of hydraulic conductivity due to varying vegetation establishment would be negligible. If the HSSF TW is operating as designed, the ***CF*** results between different transects should not exhibit statistically significant differences, and the results from all transects should be in one homogeneous group. Homogeneity in the transverse direction does not require homogeneity in the vertical or longitudinal direction. The hypothesis was tested on each system by comparing the Least Significant Difference between transects at the 95% confidence level. **Table 6-11** summarises the number of homogeneous groups found for each study.

As evident in **Table 6-11**, for most systems the statistical differences between ***CF*** results along each transect can be grouped into 2 or more homogeneous groups. The only systems that do not exhibit variance between transects are Fenny Compton, which had recently undergone partial refurbishment, and Moreton Morrell B, which was not in operation. As discussed during **Chapter 5**, clogging towards the inlet was generally highest within those transects that are closest to the point at which flow enters the influent distribution system. Clogging towards the outlet is generally highest within those transects that are closest to the point at which flow exits the effluent collection system. These findings support the notion that pressure losses in inlet and outlet plumbing arrangements cause flow to short-circuit along the shortest path between the point at which flow enters and exits the system (Speer et al., 2004, Suliman et al., 2006b, García et al., 2003).

Table 6-11 The number of statistically different homogeneous groupings (HG) of the results from each system, based on the Least Significant Difference between Clog Factor results for each transect, at the 95% confidence level.

Date	System	HG	Date	System	HG
Feb '08	Fenny Compton	1	**Jul '08**	Moreton Morrell A	2
Feb '09	Fenny Compton	1	**Feb '09**	Moreton Morrell A	3
Mar '10	Fenny Compton	1	**Sep '09**	Moreton Morrell A	3
Jun '09	Leek Wooton	2	**Oct '09**	Moreton Morrell B	1
May '09	Weston Under W.	2	**Jun '09**	Ashorne	3
Jul '09	Rowington	2	**Jun '09**	Northend	4
Aug '09	Snitterfield	4			

6.3. The development of clogging

The obtained ***CF*** data can also be used to explore the typical development of clogging in HSSF TWs in the longitudinal-vertical plane. To achieve this, the entire ***CF*** data-set is statistically analysed to ascertain whether a relationship exists between the bulk system clog factor CF_T and the variations in the vertical and horizontal values of ***CF***. Vertical and longitudinal coordinates associated with each value of ***CF*** were non-dimensionalised relative to the overall dimensions of the system (longitudinal position was non-dimensionalised relative to system length ***L*** and vertical position was non-dimensionalised relative to the total testing depth of 0.4 m). It is recognised that there is some limitation to this approach because the surveyed systems had values of ***L*** that varied between 12 m and 20 m, and it is therefore assumed that the influence of ***L*** on ***CF*** is constant between this range. However, it is deemed necessary to non-dimensionalise the dataset to allow a general equation to be developed that can reproduce longitudinal clogging profiles irrespective of system length.

The ***CF*** data-sets for each system were subjected to 3-Way ANOVA tests with the three factorials set as CF_T, dimensionless longitudinal sampling location $(\bar{x})$ and dimensionless vertical sampling location $(\bar{z})$ (sampling locations were non-dimensionalised against the relative system dimensions). Dimensionless transverse sampling location was not included as a factor because formulations are desired which describe clogging in the longitudinal-vertical plane. As discussed in the previous section, well-functioning HSSF TWs should not develop transverse variations in clogging as part of a normal clogging mechanism. Including all 13 sets of ***CF*** data in the analysis damped the influence of intra-system variability and allowed the general relationships between ***CF*** and CF_T, $\bar{x}$ and $\bar{z}$ to be derived.

A Type III Sums of Squares Analysis was used to perform a multifactor analysis of variance test for ***CF***. The test calculates the Least Square Means for ***CF*** to determine which factors have a statistically significant effect on ***CF*** at the 95% confidence interval. Given the 2D nature of the dataset, the interaction between $\bar{x}$ and $\bar{z}$ can be separated into vertical and horizontal components. This allows the interaction between $\bar{x}$ and the components of ***CF*** in the longitudinal direction (CF_X), and the interaction between $\bar{z}$ and the components of ***CF*** in the vertical direction (CF_Z), to be derived for different values of CF_T (**Figure 6-1** and **Figure 6-2**). Statistical analyses were performed using StatGraphics Centurion XVI (StatPoint Technologies, Warrington, Virginia). The outputs produced by StatGraphics Centurion XVI for each data-set are included in **Appendix C**.

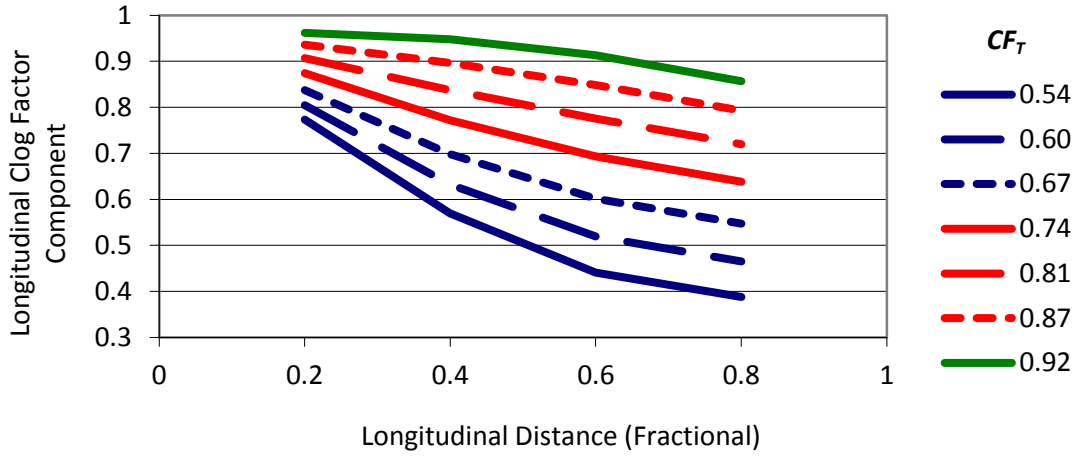

Figure 6-1 The relationship between longitudinal distance and longitudinal component of Clog Factor ***(CF_X)*** for various values of bulk system Clog Factor ***(CF_T)***

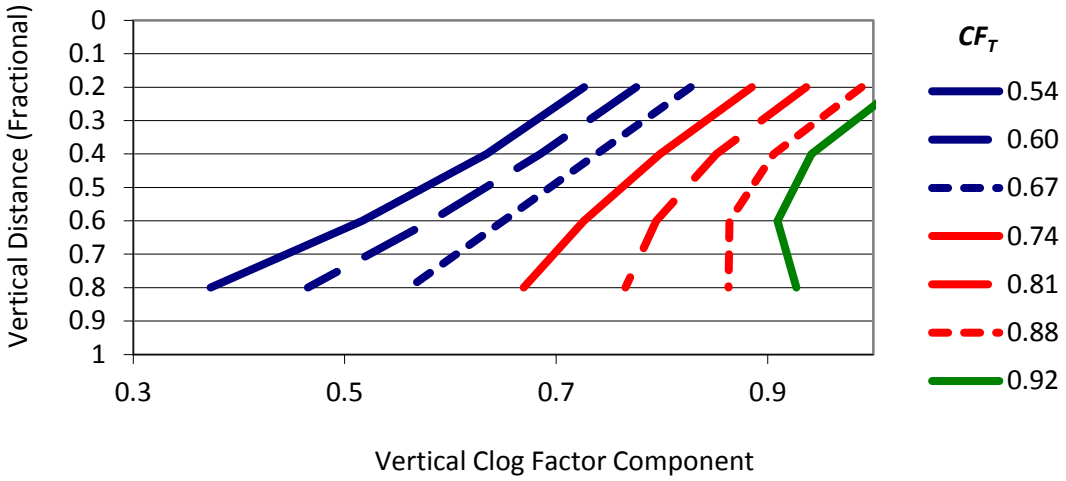

Figure 6-2 The relationship between vertical depth and vertical component of Clog Factor ***(CF_Z)*** for various values of bulk system Clog Factor ***(CF_T)***

A surface fit equation to **Figure 6-1** was derived that describes how the value of CF_X changes for different values of $\bar{x}$ and CF_T (**Equation 6-1**) and a surface fit equation to **Figure 6-2** was derived that describes how the value of CF_Z changes for different values of $\bar{z}$ and CF_T (**Equation 6-2**). The analysis used to derive the coefficients that govern **Equation 6-1** and **Equation 6-2** is given in **Appendix B**. The coefficients given in **Equation 6-1** and **Equation 6-2** are quoted to five significant figures, which improves the accuracy of calculated values for CF_X and CF_Z by approximately 3 %.

$$CF_X = CF_T(-3.1881\bar{x}^2 + 4.4203\bar{x} - 0.2613) + (2.6644\bar{x}^2 - 3.9731\bar{x} + 1.1942)$$ **Equation 6-1**

$$CF_Z = CF_T(1.5842\bar{z}^2 - 1.0787\bar{z} + 0.9520) + (-1.0580\bar{z}^2 + 0.3648\bar{z} + 0.2795)$$ **Equation 6-2**

According to the theory underlying the ANOVA test, the relationship between ***CF, CF_X, CF_Z*** and ***CF_T*** for a dataset is given by **Equation 6-3**:

$$CF = \frac{CF_X\, CF_Z}{CF_T}$$ **Equation 6-3**

By substituting **Equation 6-1** and **Equation 6-2** into **Equation 6-3** it is possible to derive a surface equation for ***CF*** purely in terms of ***CF_T***, $\bar{x}$ and $\bar{z}$; i.e. it would be possible to calculate a value of ***CF*** at any point in the system and at any stage of clogging, which represents the relationships illustrated in **Figure 6-1** and **Figure 6-2**. It should be emphasised that this relationship is specific to Severn Trent HSSF TWs and is considered valid for values of ***CF_T*** between 0.5 and 0.95.

The goodness of fit produced when **Equation 6-1**, **Equation 6-2** and **Equation 6-3** are combined to describe ***CF*** profiles of Severn Trent HSSF TWs can be tested by trying to reproduce the experimental measurements from which the expressions where derived. Values for 208 width normalised combinations of ***CF_T*** , $\bar{x}$ and $\bar{z}$, which correspond to measurements made during the 13 field surveys, were substituted into the above expressions. The closeness of fit between the 208 modelled ***CF*** values and the corresponding experimental results are shown on a scatterplot in **Figure 6-3**. As evident from **Figure 6-3**, the derived surface plot closely represents the experimental dataset, as the average linear trend is almost 1:1. The clogging in these systems will develop differently subject to natural variations. The ANOVA test has enabled the statistically significant general trend to be separated from the naturally occurring scatter in the data-set. The obtained general trend has a goodness of fit corresponding to an R^2 value of 0.64.

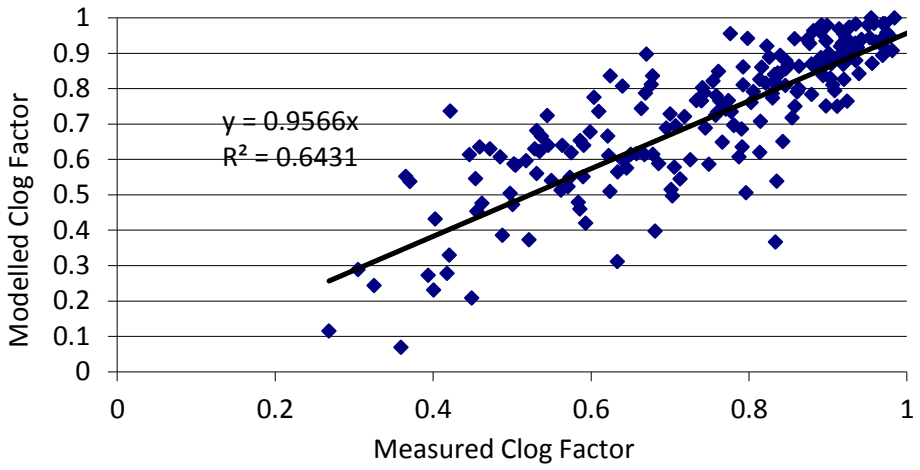

Figure 6-3 The agreement between measured and modelled Clog Factor values for 208 data sets obtained over the sampling period. The empirical model is based on statistical analysis of the data, whereby transverse variance is removed, and shows good agreement with data.

Figure 6-4 illustrates the ability of **Equation 6-1**, **Equation 6-2** and **Equation 6-3** to reproduce representative 2D ***CF*** profiles by comparing against ***CF*** data that was derived from one of the Severn Trent HSSF TW surveys. At February 2009 the HSSF TW at Fenny Compton had an experimentally derived CF_T of 0.74, with a corresponding 2D ***CF*** profile (with transverse variance statistically removed) as illustrated in **Figure 6-4a**. **Figure 6-4b** provides the corresponding 2D ***CF*** profile derived for this system using a CF_T value of 0.74 in **Equation 6-1**, **Equation 6-2** and **Equation 6-3**. **Figure 6-4**b represents a good fit to **Figure 6-4**a, but with system specific anomalies removed, as per the influence of the ANOVA test.

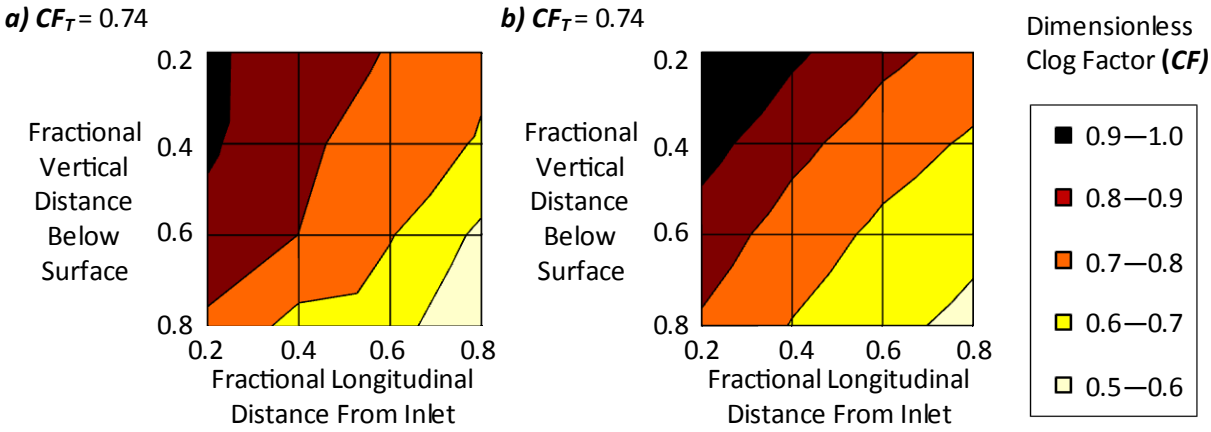

Figure 6-4 Comparisons between the measured (a) and modelled (b) Clog Factor profiles for the February 2009 survey of Fenny Compton.

The ***CF*** profiles produced by **Equation 6-1**, **Equation 6-2** and **Equation 6-3** can be used to recreate hydraulic conductivity profiles for HSSF TWs at different stages of clogging. This procedure involves using **Equation 3-59** to reproduce porosity profiles for the system, and then using the Kozeny-Carman equation (**Equation 3-57**) with a value for d_{50} to reproduce hydraulic conductivity profiles for different values of CF_T that are similar to those measured during the field surveys. The profile must be dimensionalised according to the geometry of the system. In this way engineers can recreate hydraulic conductivity profiles from a simple set of variables. The same simple variables will now be used to help calibrate the novel 1D analytical solution that describes the hydraulic response of the system at different stages of clogging (**Equation 3-52** and **Equation 3-55**).

6.4. A Clog Factor Based Expression for water table profile

Chapter 3 introduced three parameter based expressions to describe how the water table profile varies in the longitudinal direction, due to spatial and temporal variations in hydraulic conductivity, overland flow and flow-rate. **Equation 3-49**, **Equation 3-52** and **Equation 3-55** are restated here for convenience.

$$f = \frac{1}{b} ln\left(\frac{q_{in}\, b}{k\, a} + 1\right) \qquad \textbf{Equation 3-49}$$

$$\lim_{f \to L} h^2(x) = \frac{2}{b^2}\left[e^{-bL} + e^{b(f-x)} - e^{-bx} - e^{b(f-L)}\right] + h_{out}^2 \qquad \textbf{Equation 3-52}$$

$$\lim_{0 \to f} h^2(x) = \frac{2}{b^2}\left[e^{-bf} - e^{-bx} + b(f-x)\right] + h_f^2 \qquad \textbf{Equation 3-55}$$

h	*Water depth at a point* ***x*** *(m)*
h_{out}	*Water depth at the outlet (m)*
h_f	*Water depth at* ***f*** *(m)*
q_{in}	*Hydraulic loading rate (m^3/d)*
k	*Clean gravel hydraulic conductivity (m/d)*
L	*System length (m)*
f	*Length of overland flow from inlet (m)*

where ***a*** and ***b*** are parameters to be found. Parameters ***a*** and ***b*** can be calibrated to functions of system Clog Factor ***(CF_T)*** so that the above expressions can be simply used to describe how the hydraulic response of the system varies as ***CF_T*** varies between 0.55 and 0.9. The FEA model derived in **Chapter 3** will be used to achieve this calibration. Firstly, a test case will be presented for the FEA model and the 1D analytical equation, to assess their ability to simulate hydraulic performance of field-scale HSSF TWs. Secondly, theoretical hydraulic conductivity profiles will be modelled for different values of ***CF_T*** by using the surface fit equations derived in the last section. The FEA model will produce water table profiles that correspond to the hydraulic conductivity profile. Values of ***a*** and ***b*** that produce best fit solutions to the water table profile produced by FEA will be derived for **Equation 3-49**, **Equation 3-52** and **Equation 3-55**. Lastly, a relationship will be derived to describe how values of ***a*** and ***b*** change with ***CF_T***.

6.4.1. Hydraulic model validation using a real-life test case

The proposed 1D analytical solution for water table profile, and FEA model were benchmarked against existing hydraulic tools for HSSF TWs, namely Darcy's Law (EC/EWPCA, 1990), Dual-Zone Darcy's Law (USEPA, 2000), and the Dupuit-Forchheimer Assumption (Kadlec and Watson, 1993). The models were compared on their ability to fit water table measurements along Transect A at Moreton Morrell A, which were obtained during the February 2009 test. Six spot measurements of water table depth were made at regular intervals between the inlet and outlet. During the survey overland flow was visible along the measuring transect to a distance of approximately 5 m from the inlet.

To implement the FEA model a mesh consisting of 4,416 triangular elements, with a 10 times scaling factor in the longitudinal direction was used to represent the system. A linear interpolation between hydraulic conductivity values measured along Transect A of Moreton Morrell A during the February 2009 test was used to create a spatially varying hydraulic conductivity profile on the model subdomain. The boundary conditions that correspond to values measured during the Moreton Morrell A February 2009 test are stipulated in **Table 6-12**. The boundary conditions given in **Table 6-12** were used as variables in **Equation 3-49**, **Equation 3-52** and **Equation 3-55** to create a water table-profile. The SOLVER function embedded in Microsoft Excel™ was used as a data-fitting tool to find values of ***a*** and ***b*** that best fit the analytical model to the measured water table profile.

Table 6-12 Experimental data and modelling parameters as measured during the Moreton Morrell A, February 2009 sampling test.

Parameter	Symbol	Value	Unit
Experimentally measured inlet water depth	h_{in}	0.68	m
Experimentally measured outlet water depth	h_{out}	0.542	m
System Length	L	15	m
System Width	W	15	m
Gravel Depth	H	0.6	m
Estimated wetted cross-section	A_W	8.86	m^2
Gravel Cross Sectional Area along flow axis	$L*H$	9	m^2
Hydraulic Loading Rate	q_{in}	175	m^3/d
Clean media hydraulic conductivity	k	5,000	m/d

Using each method, a water table profile was fitted that reproduced the inlet and outlet depths as closely as possible, as this is how equivalent values of hydraulic conductivity are often experimentally derived.

The proposed analytical formulation was able to closely reproduce the downstream portion of the water table, although no solution could be found that mimicked the broad upstream water profile whilst achieving the observed inlet water height. Parameter values for ***a*** and ***b*** were found to be 0.025 and 0.198, respectively. It was found that assuming different values of ***a*** and ***b*** upstream and downstream of ***f*** enabled the water table profile to be closely fitted. The requirement to use two sets of values for ***a*** and ***b*** physically represents the distinct difference between the hydraulic properties of the region upstream of ***f,*** where flow must vertically infiltrate through a surface layer of clog matter, and the region downstream of ***f,*** where flow moves horizontally though the gravel subsurface. For the remainder of this study it is assumed that ***a*** and ***b*** can assume different values upstream and downstream of ***f.*** The parameter names a_{up} and b_{up} will be used upstream of ***f*** and a_{down} and b_{down} will be used downstream of ***f***. The following parameter values were found to closely replicate the water table profile: a_{up} = 0.00025, b_{up} = 200, a_{down} = 0.015, b_{down} = 0.45. In this case, a_{up} and b_{down} are used to calculate ***f***.

The water table profiles obtained by each method are illustrated in **Figure 6-5** and the corresponding wetted volume and closeness of fit to the measured water table profile are

given in **Table 6-13**. The Dupuit-Forchheimer and Darcy's Law approaches overestimate the water table profile, whereas the Dual-Zone Darcy approach underestimates the water table profile. The FEA model closely describes all portions of the water table profile with a Root Mean Square Error (RMSE) of 0.008 m. Using two sets of fitting parameters (Anaytical 2 in **Figure 6-5**) instead of one set of fitting parameters (Anaytical 1 in **Figure 6-5**) improved the RMSE of the Analytical solution from 0.010 m to 0.006 m.

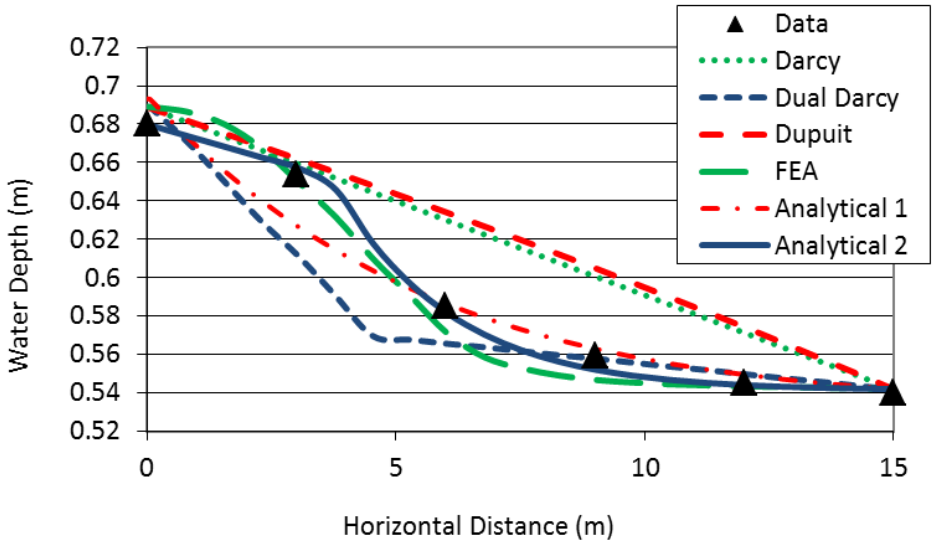

Figure 6-5 The water table profiles that were fitted to the experimental water table survey, according to the different methods discussed in this report: Darcy's Law, Dual Zone Darcy's Law, Dupuit-Forchheimer Assumption, Finite Element Analysis and the proposed analytical solution.

Table 6-13 Simulation results for reproduction of the water table measured at Moreton Morrell A, according to three existing hydraulic design tools, the FEA model, and the proposed analytical formulation.

Method	Darcy	Dual Darcy	Dupuit	FEA	Analytical 1	Analytical 2
Root Mean Square Error (m)	0.027	0.020	0.030	0.009	0.013	0.006
Wetted cross-section (m^2)	9.28	8.67	9.23	8.79	8.81	8.83

Figure 6-6 illustrates the interpolated hydraulic conductivity profile of the FEA model, with values varying across 6 orders of magnitude in concordance with field observations. The most clogged region corresponds to the surface layer at the inlet with values on the order of

0.01 m/d, whilst lower depths towards the outlet of the bed have a hydraulic conductivity on the order of clean gravel (1000 m/d).

The computed flow regime that corresponds to this hydraulic conductivity profile at a flow-rate of 2 L/s is shown in **Figure 6-7**. The length of the ponding region ***f*** required to achieve a flow-rate of 175 m^3/day was found to be 7.72 m, and two different resulting zones of flow are clear: a vertical infiltration region below the ponding length indicated by the presence of vertical head-loss contours (upper sub-domain); and a horizontally flowing water-table with a profile governed by recharge from the upper sub-domain, as indicated by the greyscale shading from left to right (lower sub-domain). The area of the upper sub-domain with no contours confirms zero flow through this part of the system. These characteristics concur with the hydraulic theory of HSSF TWs described in **Chapter 3**.

The model indicates that surface infiltration increases with distance downstream according to increasing hydraulic conductivity. Infiltration rates at the termination of the ponding region are 72 m/d whilst rates at the inlet are approximately an order of magnitude lower (**Figure 6-8**). The high flux towards the middle of the bed results in the 'S-shaped' water table profile illustrated in **Figure 6-5**, which corresponds closely to that measured by the field survey.

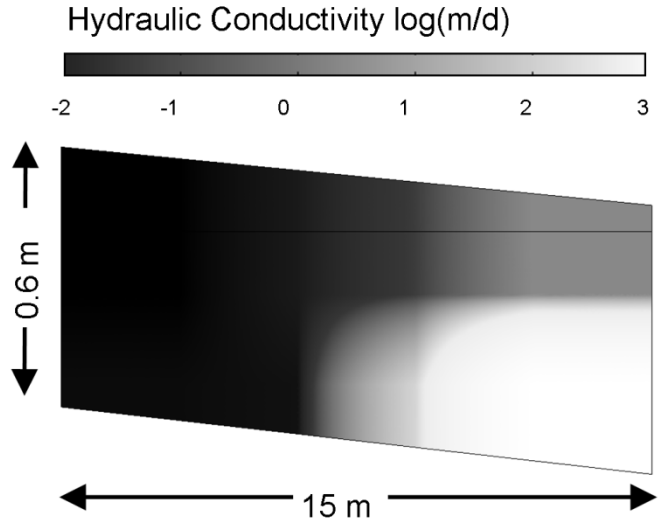

Figure 6-6 Model of the hydraulic conductivity profile of Transect A at Moreton Morrell A, based on the hydraulic conductivity survey of February 2009. The logarithmic shading bar represents order of magnitude variations where dark areas are more clogged. Reproduced from Knowles and Davies (2011).

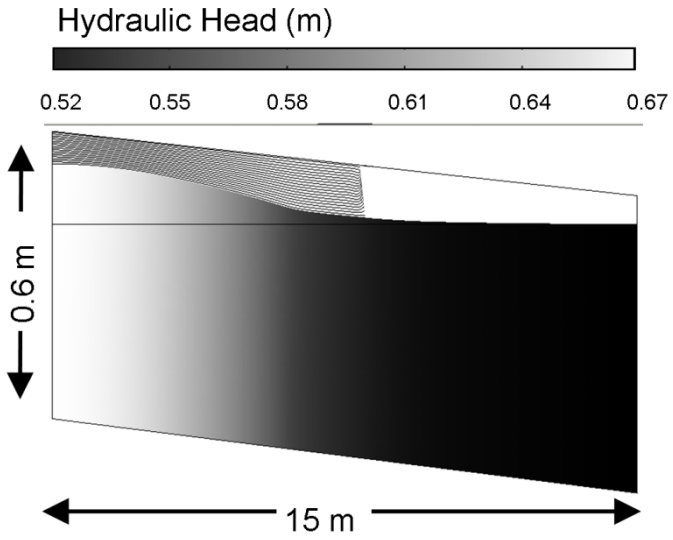

Figure 6-7 The flow field that corresponds to the modelling parameters specified in **Table 6-12** and the hydraulic conductivity profile illustrated in **Figure 6-6**. The vertical contours in the upper sub-domain represent vertical infiltration through the surface layer and the shaded profile represents the variation of hydraulic head in the horizontal water table. Reproduced from Knowles and Davies (2011).

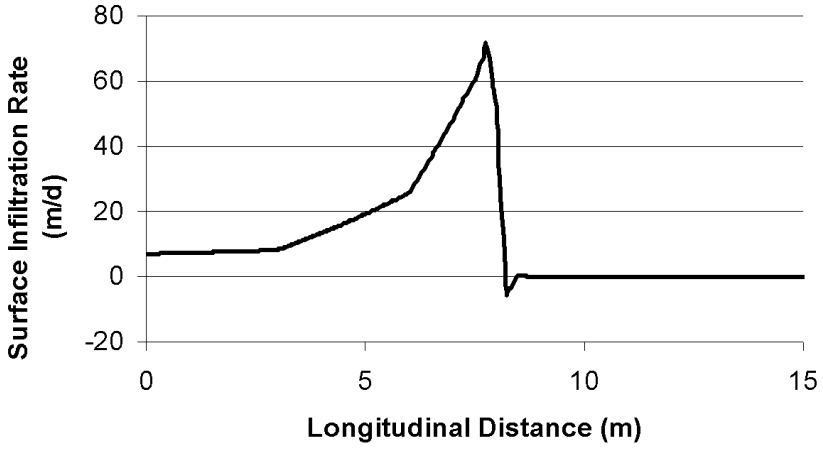

Figure 6-8 The variable surface infiltration rate across the overland flow region at Moreton Morrell, as modelled using FEA. This recharge profile creates an 'S-shaped' water table profile, similar to that illustrated in **Figure 6-7**. Reproduced from Knowles and Davies (2011).

6.4.2. Calibration of analytical equation using FEA model

According to **Table 6-9**, the values of CF_T measured in field scale HSSF TWs by this study varied between 0.54 and 0.92. Based on this, eight (8) ***CF*** profiles were generated using **Equation 6-1**, **Equation 6-2** and **Equation 6-3**, corresponding to CF_T values ranging from 0.55 to 0.90, in increments of 0.05. The resulting ***CF*** profiles are illustrated in **Figure 6-9** on dimensionless transects.

Each ***CF*** profile was converted into a non-dimensional hydraulic conductivity profile via the Kozeny Carmen Equation using a value of 5 mm for d_{50} and a value of 0.35 for ε. Each hydraulic conductivity profile was dimensionalised to create a spatially interpolated hydraulic conductivity profile for the FEA model. The FEA model is based on a hypothetical 2D HSSF TW that has a gravel filled cell with length L of 15 m, height H of 0.6 m and a maximum height of 0.1 m for surface sludge accumulation. The outlet water depth h_{out} was set to 0.4 m. For each ***CF*** profile, the length of the ponding region f (inlet boundary condition) required to achieve Q_{in} of 2 L/s across the outlet boundary was found using an iterative solver included in COMSOL. The water-table profile that corresponds to each ***CF*** Profile is shown in **Figure 6-10**.

The same boundary conditions were used for parameter values Q_{in}, L, h_{out} and f in **Equation 3-49**, **Equation 3-52** and **Equation 3-55**. The SOLVER function embedded in Microsoft Excel™ was used as a data-fitting tool to find values of a_{up}, b_{up}, a_{down} and b_{down} that best fit the analytical model to the modelled water table profile. The corresponding parameter values for each fit, and the salient results for values of h_{in}, f, A_W are tabulated in **Table 6-14**. Post-processing visualisations from COMSOL that correspond to the FEA model created for each value of CF_T are provided in **Appendix D**, and illustrate: the FEA modelling mesh; the hydraulic conductivity profile produced from **Equation 6-1**, **Equation 6-2**, **Equation 6-3** and **Equation 3-7**; and the water table profile produced by the FEA model.

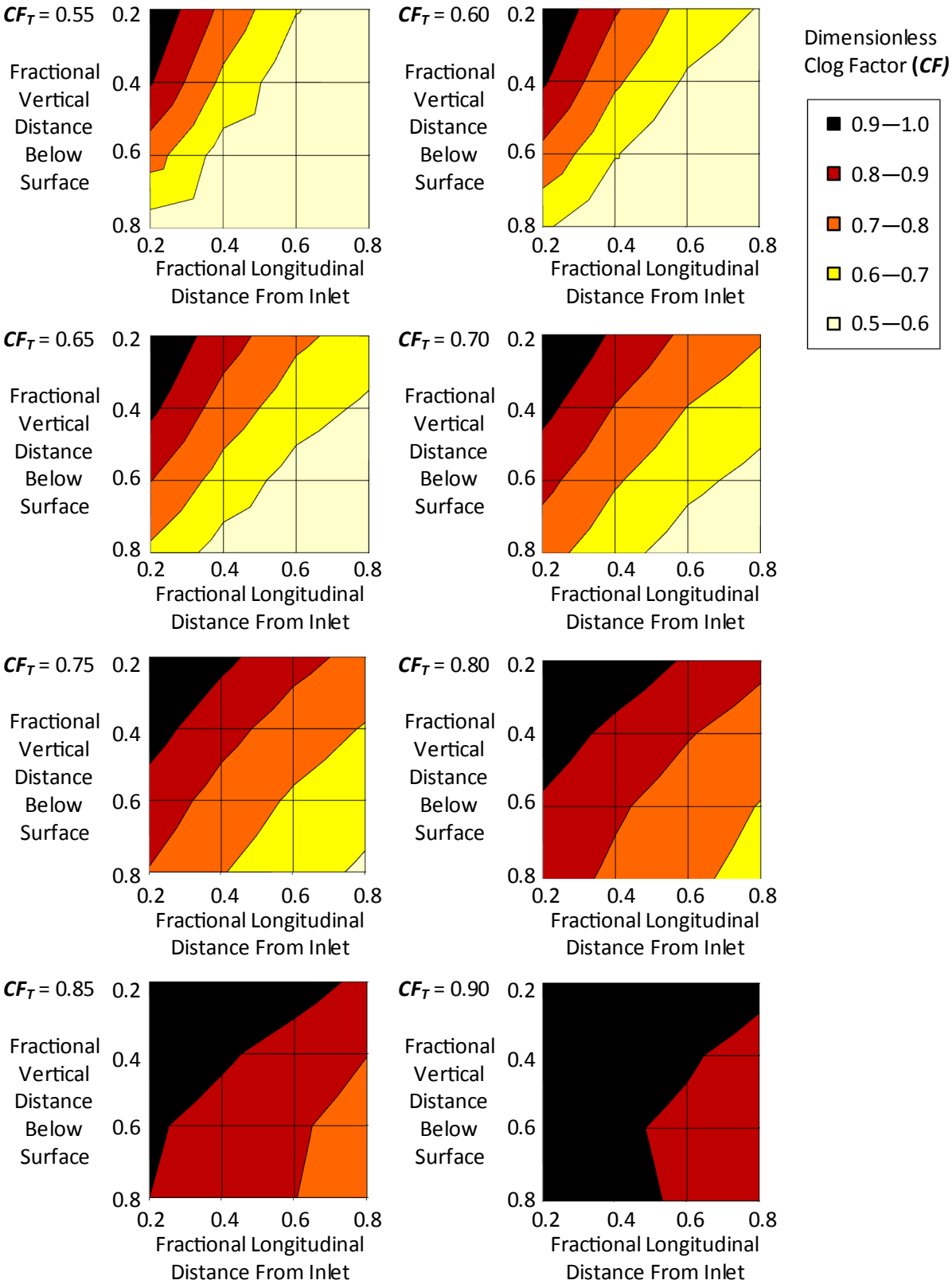

Figure 6-9 Dimensionless Clog Factor profiles corresponding to **Equation 6-1**, **Equation 6-2** and **Equation 6-3** using values of CF_T between 0.55 and 0.90, in increments of 0.05. The progression of profiles from 0.55 to 0.90 corresponds to the perceived progression of clogging in Severn Trent HSSF TWs, as derived from hydraulic conductivity surveys on field scale systems.

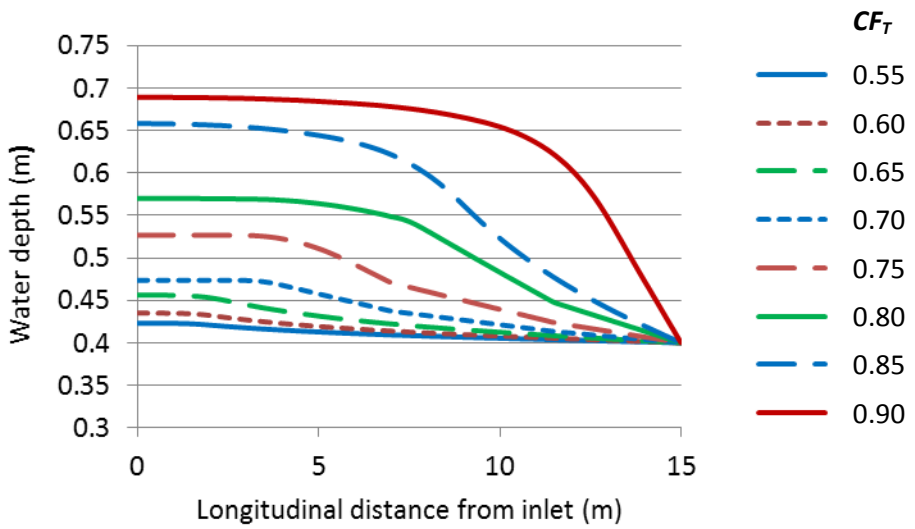

Figure 6-10 Longitudinal water-table profile for different values of bulk system Clog Factor CF_T as obtained using the COMSOL FEA model of HSSF TW hydrology.

Table 6-14 Values of f that satisfiy the boundary conditions of the FEA model and corresponding values for A_w and h_f and h_{in}. Parameter values are given for a and b in **Equation 3-49**, **Equation 3-32** and **Equation 3-55** that produce a close fit to the water-table profiles produced by each FEA model.

CF_T	f (m)	h_{in} (m)	h_f (m)	A_w (m^2)	a_{up} -	b_{up} -	a_{down} -	b_{down} -
0.55	1.83	0.42	0.42	4.13	1.08E-03	3,387	1.00	1.70E-01
0.60	2.05	0.43	0.43	4.20	1.01E-03	1,632	1.00	1.04E-01
0.65	2.41	0.46	0.45	4.29	9.20E-04	954	1.00	3.59E-02
0.70	3.90	0.47	0.47	4.56	5.94E-04	600	0.85	1.00E-03
0.75	6.90	0.53	0.51	5.01	4.50E-04	350	0.60	1.00E-04
0.80	7.76	0.57	0.54	5.62	2.98E-04	400	0.30	1.00E-05
0.85	9.00	0.66	0.59	5.93	2.57E-04	200	0.18	1.00E-03
0.90	13.10	0.69	0.64	6.54	1.99E-04	321	0.07	1.00E-02

6.4.3. The relationship between analytical equation and system Clog Factor

The relationships between system clog factor CF_T and parameter values for a_{up}, b_{up}, a_{down} and b_{down} are respectively shown in **Figure 6-11**, **Figure 6-12**, **Figure 6-13** and **Figure 6-14**. The perceived relationships of best-fit for each parameter are illustrated on each figure, and are provided in **Equation 6-4**, **Equation 6-5**, **Equation 6-6** and **Equation 6-7**. Substituting these relationships into **Equation 3-49**, **Equation 3-52** and **Equation 3-55** allows an expression for water table profile to be derived that is based on the input variables for CF_T, k, h_{out} and Q_{in}.

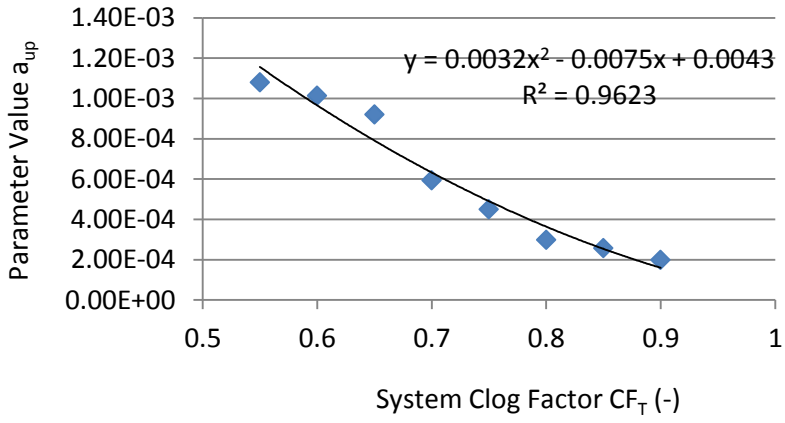

Figure 6-11 The relationship between parameter value a_{up} and system Clog Factor CF_T based on the data-fit to the results of the FEA modelling.

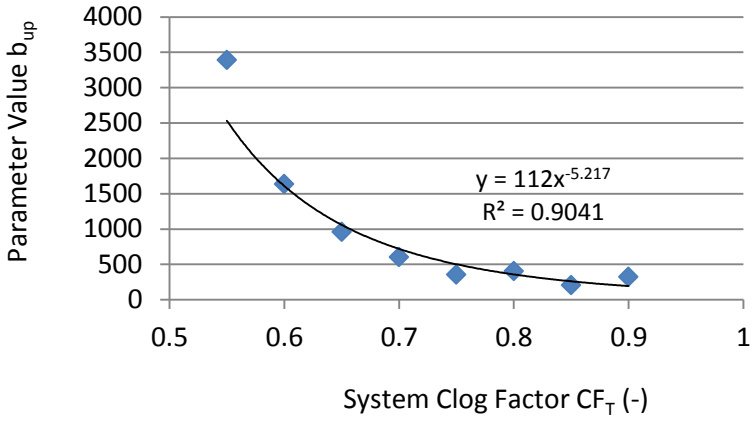

Figure 6-12 The relationship between parameter value b_{up} and system Clog Factor CF_T based on the data-fit to the results of the FEA modelling.

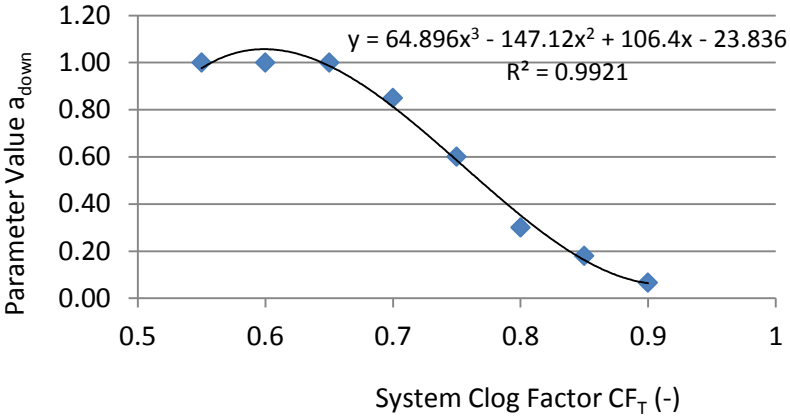

Figure 6-13 The relationship between parameter value a_{down} and system Clog Factor CF_T based on the data-fit to the results of the FEA modelling.

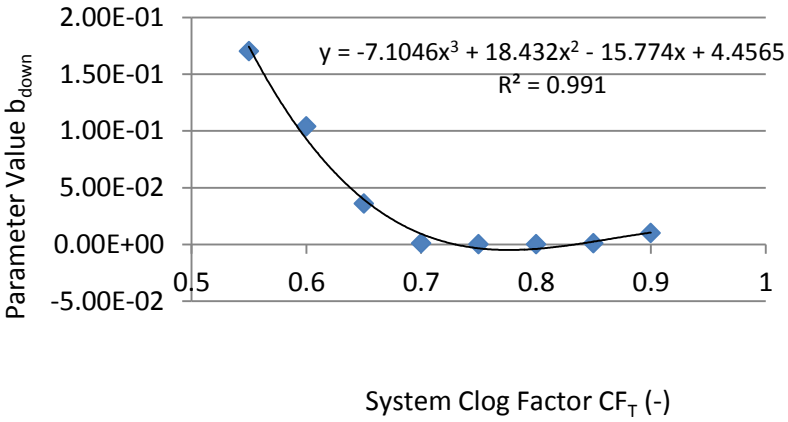

Figure 6-14 The relationship between parameter value b_{down} and system Clog Factor CF_T based on the data-fit to the results of the FEA modelling.

$$a_{up} = 0.0032\ {CF_T}^2 - 0.0075\ CF_T + 0.0043 \qquad \textbf{Equation 6-4}$$

$$b_{up} = 112\ {CF_T}^{-5.217} \qquad \textbf{Equation 6-5}$$

$$a_{down} = 65\ {CF_T}^3 - 147\ {CF_T}^2 + 106\ CF_T - 24 \qquad \textbf{Equation 6-6}$$

$$b_{down} = -7.1\ {CF_T}^3 + 18.4\ {CF_T}^2 - 15.8\ CF_T + 4.5 \qquad \textbf{Equation 6-7}$$

The results of the parameter-fitting exercise, and the resulting water table profiles produced by substituting **Equation 6-4**, **Equation 6-5**, **Equation 6-6** and **Equation 6-7** into **Equation 3-49**, **Equation 3-52** and **Equation 3-55**, are shown in **Figure 6-15**. As evident from **Figure 6-15**, the resulting expression is able to well describe the geometry of the water-table for values of CF_T between 0.55 and 0.9, and therefore can simulate the changing hydrology of a Severn Trent HSSF TWs as they undergo clogging. The water table profile results produced by the FEA model and the analytical equation are provided in **Appendix F**.

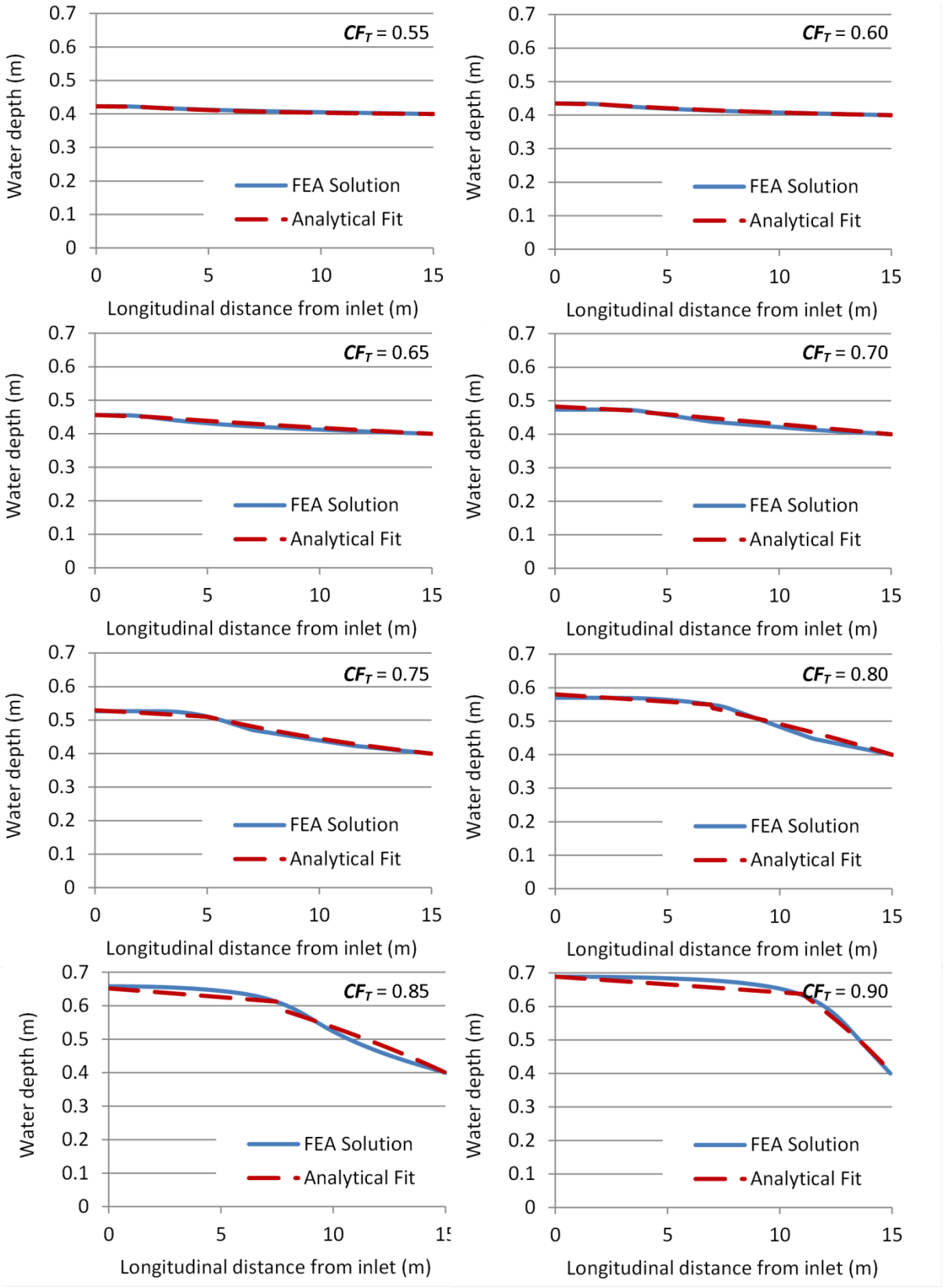

Figure 6-15 Results of the data-fitting exercise, to fit the analytical equation to the water table profile produced for each ***CF*** profile by the COMSOL FEA model.

6.5. The relationship between Clog Factor and hydrodynamics

The relationship between hydrodynamics and CF_T will be explored in a similar manner to how the relationship between hydraulics and CF_T has been explored. Firstly the hydrodynamic module of the FEA model will be validated against tracer tests performed on a field scale HSSF TW. Pending validation, the FEA model will be used to produce RTDs for different ***CF*** profiles, such that relationships can be deduced between the values of CF_T and: a) Number of Tanks-In-Series ***n*** that fit the RTD; and b) overall hydraulic efficiency λ.

6.5.1. Hydrodynamic model validation using a real-life test case

The validity of the FEA hydrodynamic module will be verified against tracer tests performed at Moreton Morrell during the February 2009 test. Internal tracer monitoring was performed at multiple points corresponding to the sampling locations for hydraulic conductivity measurements (as illustrated in **Figure 5-26**). All sampling was made at a 0.5 m depth below the bed surface to investigate the occurrence of vertical short-circuiting in these systems. Additionally, the breakthrough curve from the outlet was monitored to elucidate the influence that system hydrology has on bulk hydrodynamics. A 5 ml single-shot impulse of concentrated Rhodamine WT solution was added to the inlet manifold, upstream of the wetland cell. In response to there being no affordable proprietary fluorimeter for synchronous measurement from a matrix of sampling points, a novel multi-in-line-channel, data-logging fluorimeter was created. Details of the design, calibration, sensitivity and manufacture of this device are included in **Appendix E**. **Figure 6-13** is a photograph of the interior of the multichannel fluorimeter at a TW in South Warwickshire. The Rhodamine breakthrough curve was measured at the outlet using a Cyclops 7 submersible fluorimeter (Turner Designs, USA). Tracer recovery was 71 % with the loss mainly attributed to adsorption by clog matter. An instrument error meant no information was collected for point D2.

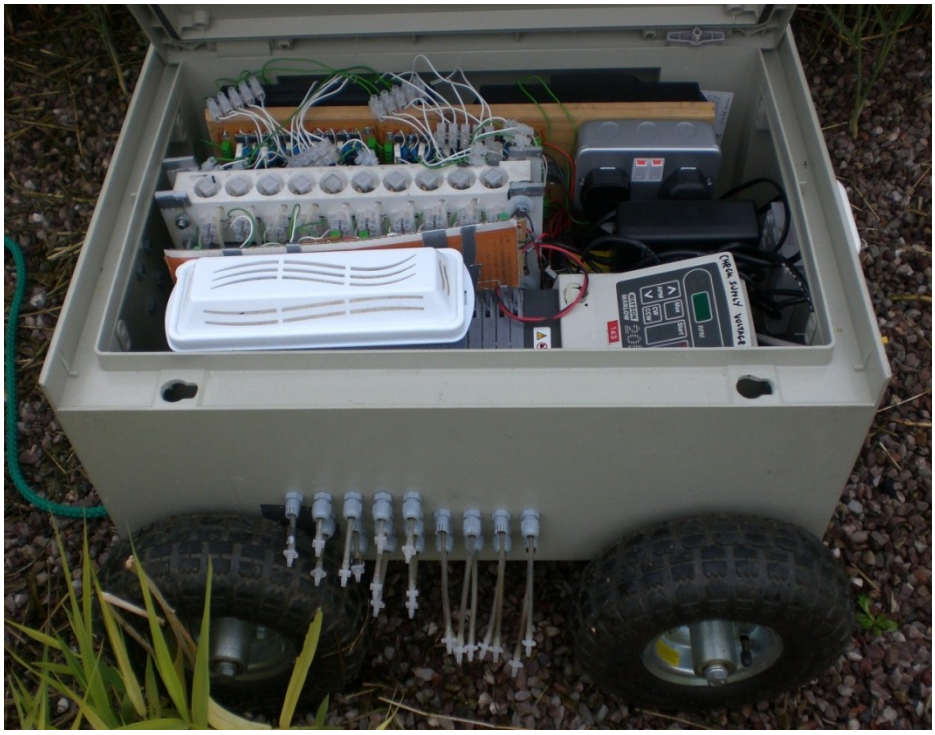

Figure 6-16 Photographs of the developed multichannel, flow-through, data-logging fluorimeter for multipoint dye tracing experiments, installed at Fenny Compton. Reproduced from Knowles et al. (2010).

Figure 6-17 compares the total dye detected at each point with the average detected over the 500 mm vertical plane. This indicates the relative location of preferential flow-paths and dead-zones as values greater and less than one respectively. The biggest preferential flow-path is detected at point A3 (5.4 times the average flow) which roughly coincides with the point at which overland flow ceases in this system. Contrastingly, upstream points A1 and A2 have very little involvement in the flow field, confirming observations that the majority of the flow short-circuits over the surface sludge until it can infiltrate into the subsurface and follow the path of least resistance below the root zone. In accordance with the hydraulic conductivity results obtained for this system (**Section 5.8**), flow follows the path of least resistance downstream from point A3, by steering towards points A3, B4, C4 and D4; perhaps avoiding a clogged outlet collector at point A4 (Cooper et al., 2008). Calculation of the hydraulic efficiency factor $\boldsymbol{\lambda}$ (Muñoz et al., 2006, Persson et al., 1999) emphasises the inefficiency created by this flow regime. Point A2, B2, A3 and B3 have $\boldsymbol{\lambda}$ values of 0.16 to 0.39 (**Table 6-15**) reflecting the premature passage of the RTD peak associated with where the overland flow secedes, in comparison to the centroid of the flow. Some upstream points have $\boldsymbol{\lambda}$ values greater than 1 due to low subsurface flow-rates at the inlet.

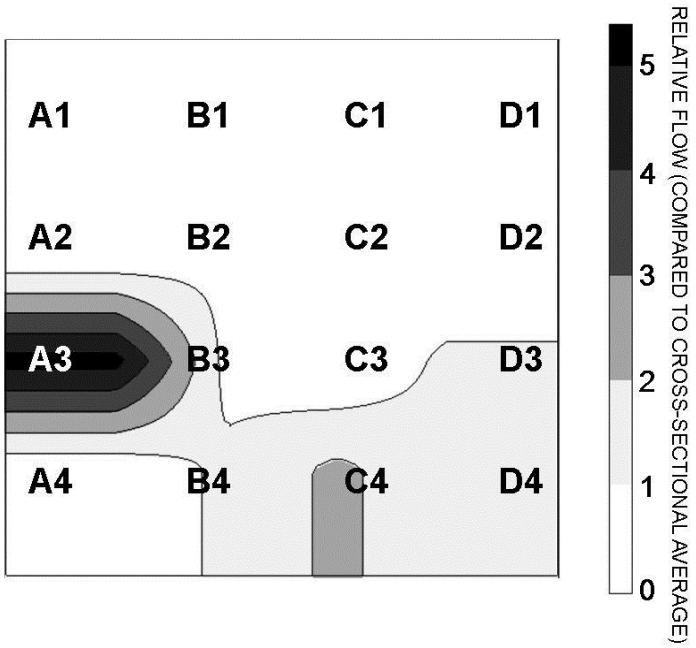

Figure 6-17 The variation of Relative Flow Fraction measured at the 500 mm depth plane within the TW subsurface. The darker regions represent those that receive more flow. Reproduced from Knowles et al. (2010).

Table 6-15 Parameters derived from the breakthrough (BT) curves of each sampling point, studied using the multi-point fluorimeter.

	Peak Time (d)	Centroid Time (d)	16% BT (d)	50% BT (d)	84% BT (d)	Short-Circuiting Factor	Hydraulic Efficiency Factor	Relative Flow Fraction
A1	0.22	0.07	0.06	0.14	0.2	0.45	3.09	0.57
A2	0.06	0.14	0.08	0.33	0.58	0.23	0.39	0.01
A3	0.07	0.22	0.14	0.31	0.51	0.44	0.32	5.4
A4	0.19	0.29	0.15	0.22	0.39	0.71	0.65	0.3
B1	0.02	0.07	0.03	0.26	0.49	0.13	0.29	0.24
B2	0.06	0.14	0.13	0.33	0.5	0.38	0.39	0.71
B3	0.03	0.22	0.03	0.07	0.17	0.4	0.16	0.67
B4	0.06	0.29	0.17	0.37	0.55	0.47	0.19	1.2
C1	0.21	0.07	0.11	0.17	0.21	0.64	2.89	0.46
C2	0.13	0.14	0.13	0.31	0.49	0.43	0.92	0.74
C3	0.09	0.22	0.08	0.19	0.26	0.43	0.42	0
C4	0.39	0.29	0.19	0.33	0.44	0.57	1.35	2.22
D1	0.04	0.07	0.03	0.07	0.15	0.5	0.58	0
D2	NR	NR	NR	NR	NR	NR	NR	NR
D3	0.66	0.22	0.61	0.65	0.69	0.94	3.06	1.23
D4	0.25	0.29	0.18	0.32	0.49	0.57	0.87	1.25

The outlet RTD very clearly indicates the existence of two major flow-paths through the HSSF TW (**Figure 6-18**) which have been partitioned according to the parameters reported in **Table 6-16**. The first path to arrive at the outlet corresponds to the overland flow that short-circuits to point A3, carrying 79% of the flow and arriving after only 5.3 hrs. The second represents the highly retarded flow-path from upstream infiltration into the subsurface, which arrives 41 hrs later than the overland flow path.

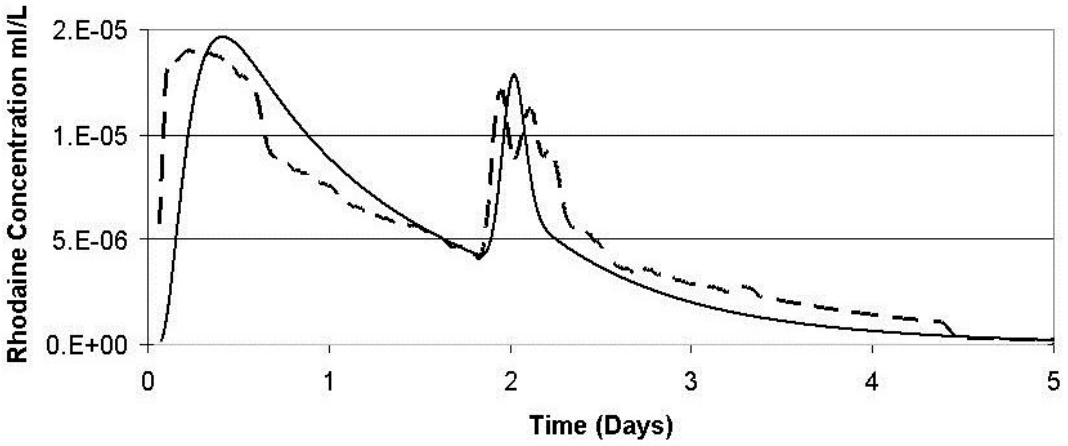

Figure 6-18 The obtained Rhodamine WT Residence Time Distribution Curve (dashed line) and a dual-path Tanks-In-Series model fitted to the obtained results.

Table 6-16 Hydraulic parameters for the various flow paths derived from the outlet residence time distribution. The Hydraulic Loading Rate is 175,000 m^3, the theoretical hydraulic residence time is 0.27 days and the total volume of tracer injected is 3 ml.

		SINGLE PATH	OVERLAND PATH	SUBSURFACE PATH
Peak Time	**d**	0.22	0.22	1.93
16% Tracer Recovery Time	**d**	0.33	0.27	1.96
50% Tracer Recovery Time	**d**	1.23	0.9	2.26
84% Tracer Recovery Time	**d**	3.23	3.22	4.46
Total Tracer Recovered	**ml**	2.13	1.74	0.45
Flow-Split		1	0.82	0.21
Volumetric Efficiency		5.22	4.47	9.82
Number of TIS (N)		5.44	5.44	-0.16
Hydraulic Efficiency (λ)		0.18	0.24	0.85
Short Circuiting (S)		0.26	0.3	0.87

Three snap-shots from the tracer impulse simulation modelled using COMSOL are shown in **Figure 6-19**, **Figure 6-20** and **Figure 6-21** for times 20, 40 and 140 minutes respectively. The shading shows the spatial concentration profile of the tracer plume normalised against the inlet tracer concentration, where darker shades indicate greater concentration. Note that the shading bar is rescaled for each different time frame so that the concentration gradient is still discernible as the plume becomes more dispersed with time.

In **Figure 6-19** the variable infiltration below the ponding region can be seen. Plume advancement near the inlet is fairly stagnant whereas faster infiltration rates downstream have led to rapid vertical spreading of the plume. This effect is emphasised in **Figure 6-20** where the vast majority of the injected tracer is engaging the water-table at about 8 m downstream and has quickly spread towards the bottom of the bed.

Figure 6-21 shows that the plume migrates horizontally once it is within the water-table, although low hydraulic conductivity through the root-zone causes the majority of the plume to vertically short-circuit through the relatively clean media along the bottom of the bed. The fraction of the tracer that infiltrates through the surface layer near the inlet moves at contrastingly lower horizontal speeds, such that an interesting effect happens that may help to explain the results obtained in the tracer tests at Moreton Morrell. The plume breaks into two visible phases: the first to reach the outlet represents the majority of the flow which rapidly propagates along the overland flow-path and then short-circuits below the root-zone; whilst the second phase represents flow through the clogged upstream media and consequently reaches the outlet much later.

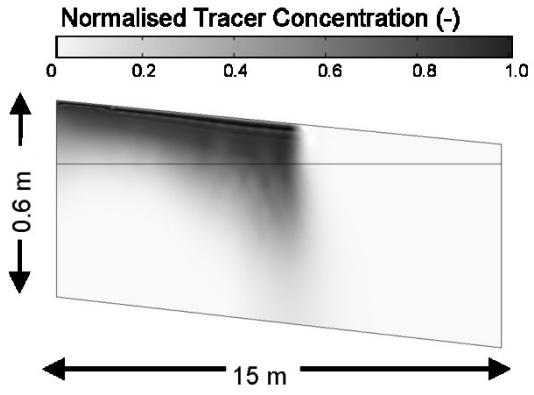

Figure 6-19 The passage of tracer through Moreton Morrell as simulated through the FEA model developed in COMSOL. The shading represents the spatial concentration of the tracer plume relative to the influent concentration at 20 minutes. Reproduced from Knowles and Davies (2011).

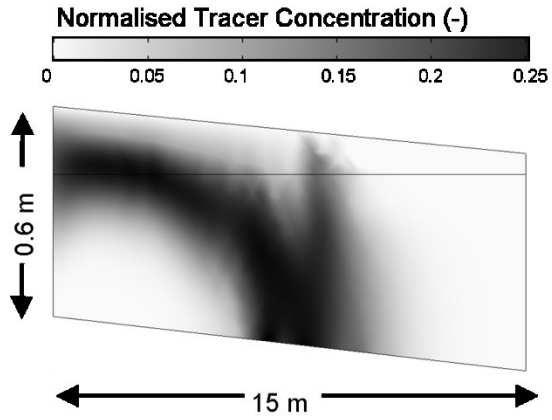

Figure 6-20 The passage of tracer through Moreton Morrell as simulated through the FEA model developed in COMSOL. The shading represents the spatial concentration of the tracer plume relative to the influent concentration at 40 minutes. Reproduced from Knowles and Davies (2011).

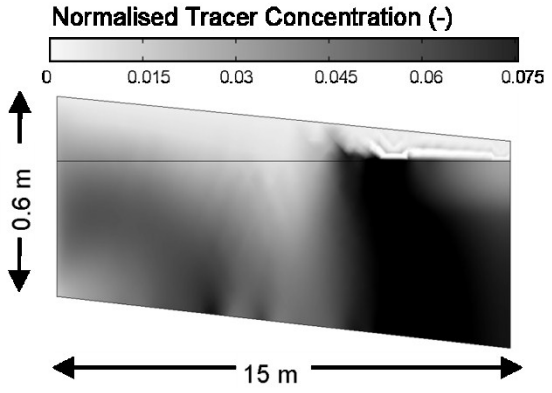

Figure 6-21 The passage of tracer through Moreton Morrell as simulated through the FEA model developed in COMSOL. The shading represents the spatial concentration of the tracer plume relative to the influent concentration at 60 minutes. Reproduced from Knowles and Davies (2011).

6.5.2. Calibration of RTDs using the TIS model

The COMSOL FEA static hydraulic models produced in **Section 6.4** are used to perform dynamic solute transport modelling, and generate RTDs that correspond to the hydraulic scenario for each value of CF_T in the model HSSF TW. The influent pulse used in the model was based on an influent concentration c_{in} of 1 mg/L applied across the boundary covered by length f for a period of 60 seconds. The RTDs produced for each CF_T are shown in **Figure 6-22**.

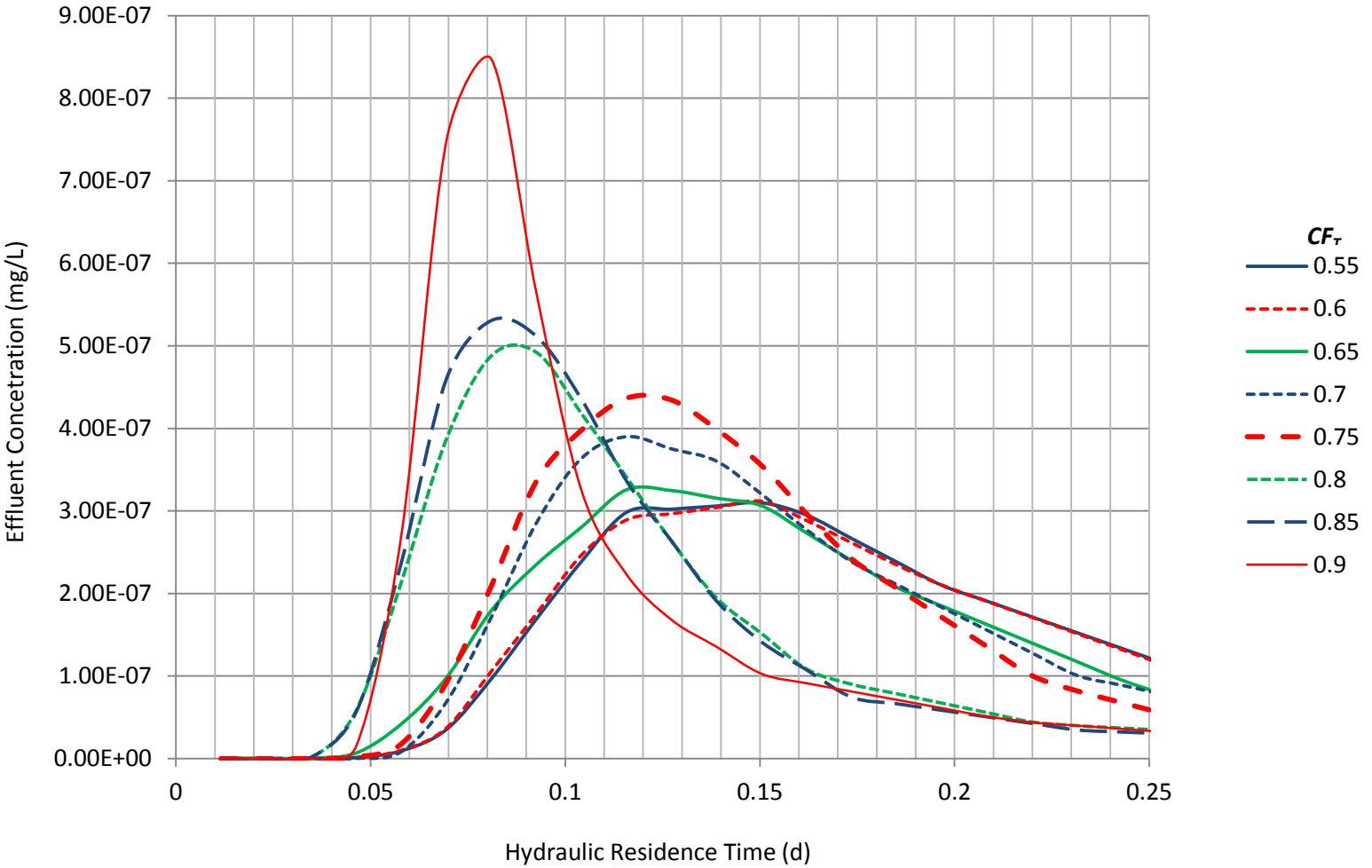

Figure 6-22 Residence Time Distributions (RTDs) produced by the COMSOL FEA models of a Severn Trent HSSF TW for multiple values of system Clog Factor ***(CF_T).***

Equation 3-43 was used to fit a Tanks-In-Series (TIS) model to each RTD, according to parameter values for number of TIS n and mean hydraulic residence time τ. The TIS fit for each RTD is shown in **Figure 6-23**. The RTD results produced by the FEA and TIS models are provided in **Appendix G**. Each TIS fit is used to calculate the volumetric efficiency e_V, mixing efficiency e_M and hydraulic efficiency λ for each RTD. To take into account the reactor volume lost to clogging, the CF_T value is used to adjust the results for A_w, e_V and λ. The results for each modelled value of CF_T are summarised in **Table 6-17**.

Table 6-17 Salient results from the COMSOL FEA hydrodynamic modelling and TIS model fitting exercise, that describe how system hydrodynamics change according to CF_T (as the system clogs).

CF_T		**0.55**	**0.60**	**0.65**	**0.70**	**0.75**	**0.80**	**0.85**	**0.90**
q_{in}	(m^2/d)	11.52	11.52	11.52	11.52	11.52	11.52	11.52	11.52
A_w	(m^2)	4.13	4.20	4.29	4.56	5.01	5.62	5.93	6.54
$A_w(CF_T)$	(m^2)	1.86	1.68	1.50	1.37	1.25	1.12	0.89	0.65
τ_T	(d)	0.36	0.36	0.37	0.40	0.44	0.49	0.51	0.57
$\tau_T(CF_T)$	(d)	0.16	0.15	0.13	0.12	0.11	0.10	0.08	0.06
n	(-)	4.3	4.7	5.0	5.5	5.9	6.6	6.9	8.4
τ	(d)	0.16	0.17	0.17	0.14	0.13	0.09	0.09	0.08
e_M	(-)	77%	79%	80%	82%	83%	85%	86%	88%
e_V	(-)	44%	46%	47%	37%	31%	19%	17%	13%
$e_V(CF_T)$	(-)	97%	115%	133%	122%	122%	95%	112%	133%
λ	(-)	33%	36%	37%	30%	25%	16%	14%	12%
$\lambda(CF_T)$	(-)	74%	91%	106%	100%	101%	80%	96%	117%

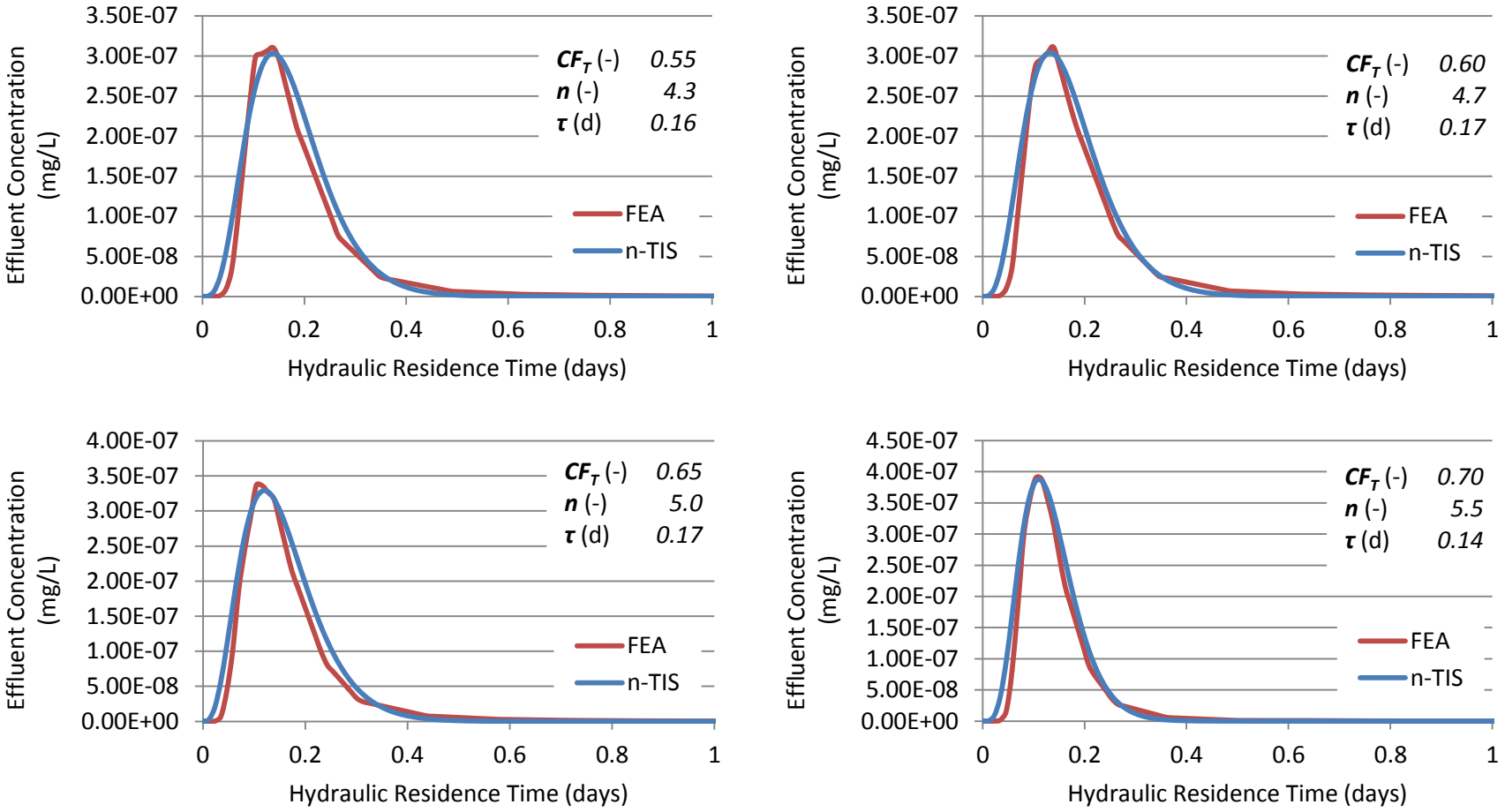

Figure 6-23 Tanks-In-Series fits to the RTD produced for each CF_T scenario (continued overleaf)

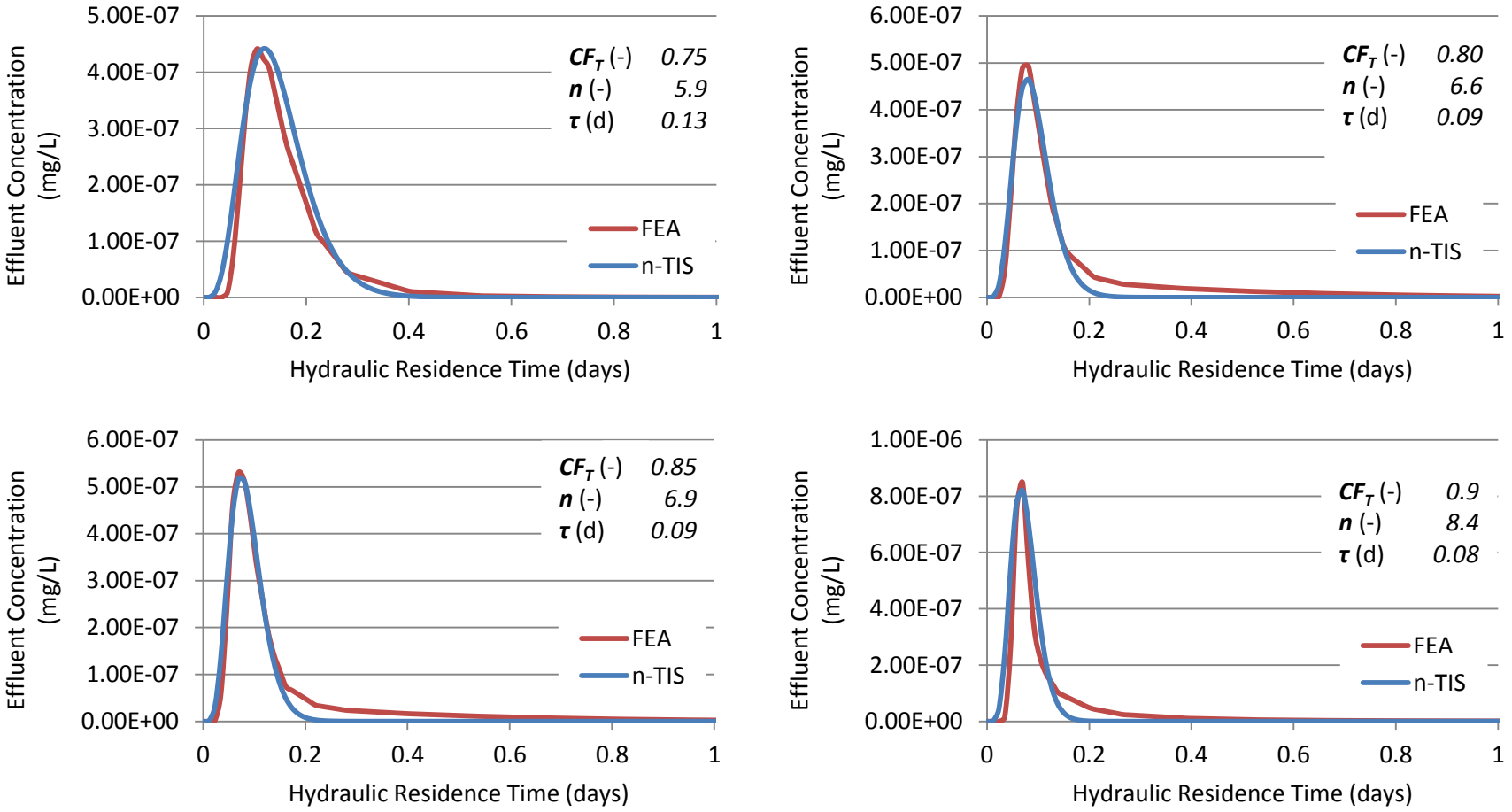

Figure 6-23 Tanks-In-Series fits to the RTD produced for each CF_T scenario

6.6. The relationship between HSSF TW hydrology and Clog Factor

It should be emphasised that the exact relationship and variable values discussed in this section are specific to the constant values of k, h_{out}, Q_{in} and **L** used in the modelled scenario. The general relationships between CF_T and the modelled system are discussed but numerical relationships are not derived.

Figure 6-24 illustrates the relationship between system Clog Factor CF_T and overland flow front f in the modelled system. As CF_T increases from 0.55 to 0.9 the value of f increases from 1.8 m to 13.1 m. The general relationship illustrated by **Figure 6-24** indicates that the rate of increase of f with respect to CF_T increases as CF_T increases. The extent of overland flow in Severn Trent HSSF TWs becomes a compounding problem as reactor porosity is lost.

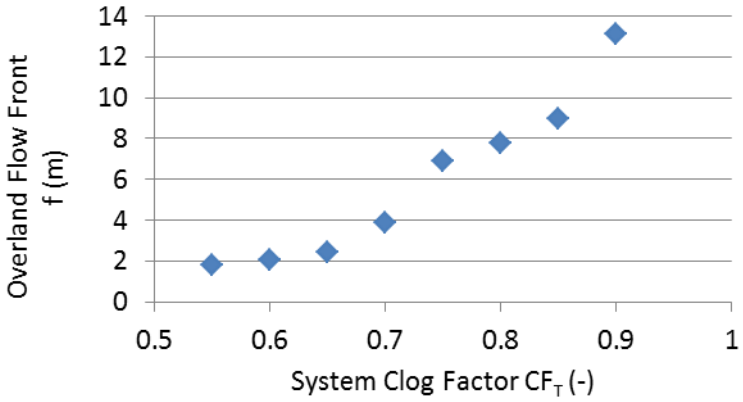

Figure 6-24 The relationship between CF_T and f for the modelled system.

Figure 6-25 illustrates the relationship between system Clog Factor CF_T and the depth of the subsurface water table at the inlet h_{in} in the modelled system. As CF_T increases from 0.55 to 0.9 the value of h_{in} increases from 0.42 m to 0.69 m. The general relationship illustrated by **Figure 6-25** indicates that the rate of increase of h_{in} with respect to CF_T increases as CF_T increases. In the modelled system the maximum water depth at which point ponding occurs is 0.7 m. The possibility that ponding will occur in Severn Trent HSSF TWs becomes increasingly likely as reactor porosity is lost.

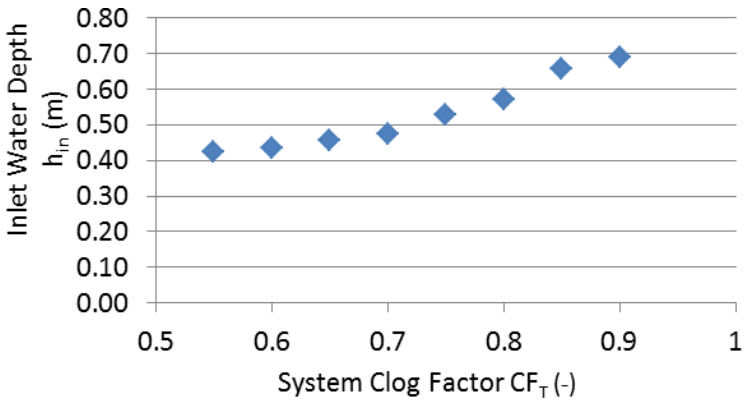

Figure 6-25 The relationship between CF_T and h_{in} for the modelled system.

Figure 6-26 illustrates the relationship between system Clog Factor CF_T and the wetted reactor area A_W in the modelled system. A_W is expressed both in terms of theoretical clean media porosity and adjusted using CF_T to account for the loss of porosity due to clogging. The general relationship illustrated by **Figure 6-26** indicates that the rate of change of A_W with respect to CF_T increases as CF_T increases. As CF_T increases from 0.55 to 0.9 the value of A_W increases from 4.1 m^2 to 6.4 m^2. However, once adjusted for loss in porosity, it can be seen from **Figure 6-26** that the wetted cross-sectional area available for flow actually decreases from 1.9 m^2 to 0.7 m^2. This important results confirms that the increase in wetted volume in response to clogging does not compensate for the loss of porosity due to clogging, and the reactor volume available for flow does decrease as the system clogs. The general relationship illustrated by **Figure 6-26** indicates that when adjusted for clogging the rate of decrease of A_W with respect to CF_T gradually increases as CF_T increases.

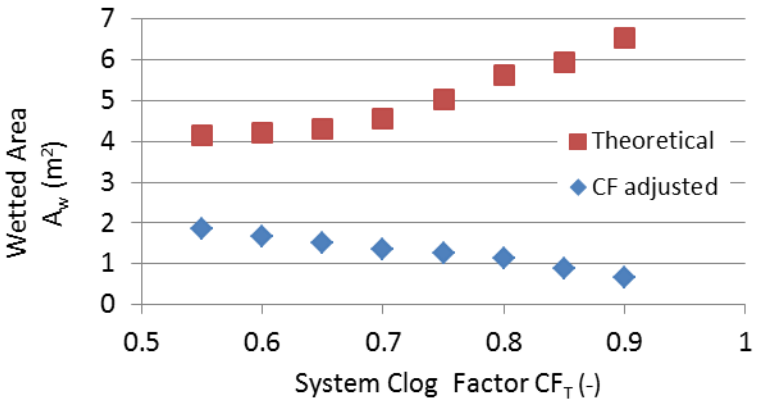

Figure 6-26 The relationship between CF_T and A_W for the modelled system, based on the theoretical clean media porosity and CF adjusted to account for the loss of porosity due to clogging.

Figure 6-27 illustrates the relationship between system Clog Factor CF_T and theoretical mean residence time τ_T in the modelled system. τ_T is expressed both in terms of theoretical clean media porosity and adjusted using CF_T to account for the loss of porosity due to clogging. The change of τ_T is directly proportional to the change of A_W. As CF_T increases from 0.55 to 0.9 the value of τ_T increases from 0.36 days to 0.57 days. Similar to A_W, once adjusted for loss in porosity, it can be seen from **Figure 6-27** that the value of τ_T should be anticipated to decrease from 0.16 days to 0.06 days. The increase in wetted volume in response to clogging does not compensate for the loss of porosity due to clogging and the theoretical residence time will decrease in proportion to the reactor volume available for flow.

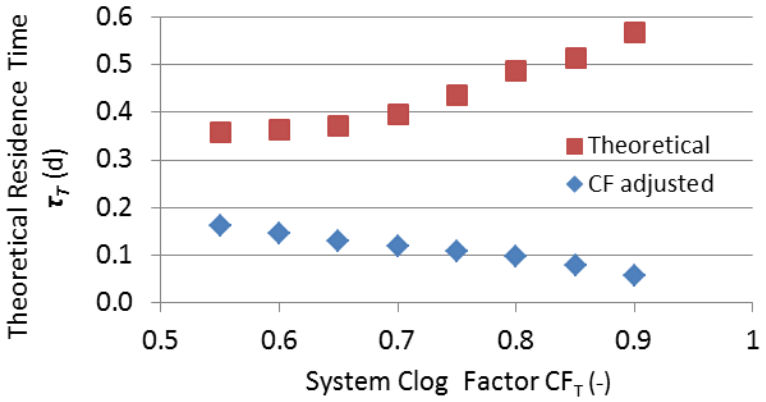

Figure 6-27 The relationship between CF_T and τ_T for the modelled system, based on the theoretical clean media porosity and CF adjusted to account for the loss of porosity due to clogging.

Figure 6-28 illustrates the relationship between system Clog Factor CF_T and number of Tanks-In-Series ***n***. As CF_T increases from 0.55 to 0.9 the value of ***n*** increases from 4.3 to 8.4. The general relationship illustrated by **Figure 6-25** indicates that the rate of increase of ***n*** with respect to CF_T increases as CF_T increases. The relationship suggests an increasing shift towards plug-flow hydrodynamics as the system clogs. The more flow that short-circuits overland, the less time the flow spends in the subsurface where tortuosity and hydraulic resistance would increase dispersion. As such, the mixing efficiency e_M of the HSSF TW increases from 77 % to 88 % as the system clogs.

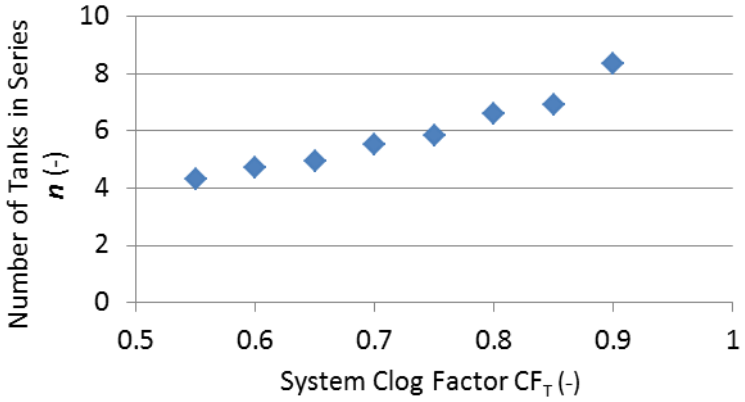

Figure 6-28 The relationship between CF_T and n produced by the FEA hydrodynamic model.

Figure 6-29 illustrates the relationship between system Clog Factor CF_T and the mean residence time τ produced by the FEA hydrodynamic model. The value of τ increases from 0.16 days when CF_T is 0.55 and peaks at 0.18 days when CF_T is 0.65, after which τ decreases to a value of 0.08 days when CF_T is 0.90. The general trend illustrated in **Figure 6-29** suggests that a small degree of clogging causes mean hydraulic residence time to increase, probably because of the increase in subsurface wetted volume that is involved in dispersion. However, as clogging increases and the extent of overland flow increases the fraction of subsurface volume bypassed by the flow also increases. As the system clogs, the decrease in dispersion, indicated by the increasing value of n, combined with the reduction in A_W results in a decrease in mean hydraulic residence time.

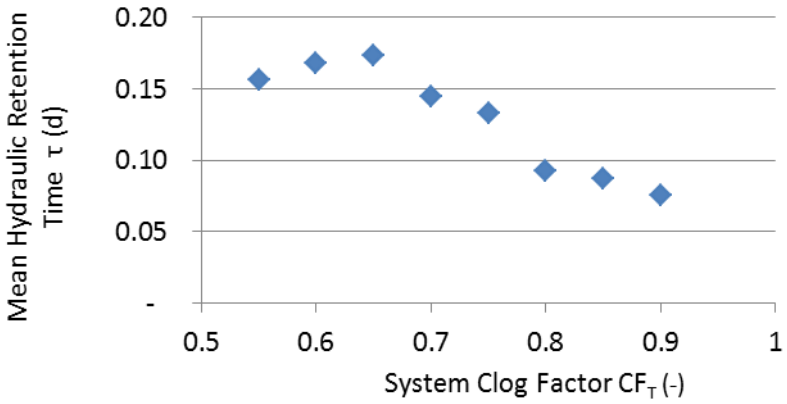

Figure 6-29 The relationship between CF_T and τ produced by the FEA hydrodynamic model.

According to **Figure 6-30**, the volumetric efficiency ***(e_V)*** of the HSSF TW increases from 44 % to 47 % as ***CF_T*** increases from 0.55 to 0.65, and then ***e_V*** decreases from 47 % to 13 % as the ***CF_T*** increases from 0.65 to 0.90. However, the ***CF_T*** adjusted values of ***e_v*** are between 95 % and 133 %. This phenomenon suggests that adjusting the value of volumetric efficiency using ***CF_T*** well accounts for the impact of clogging on volumetric efficiency (i.e. no results that are significantly lower than 100 %). Evapotranspiration may be responsible for counteracting the effects of clogging by up to 33 % in some systems, although a flow balance between the inlet and outlet would need to be performed to confirm this suggestion.

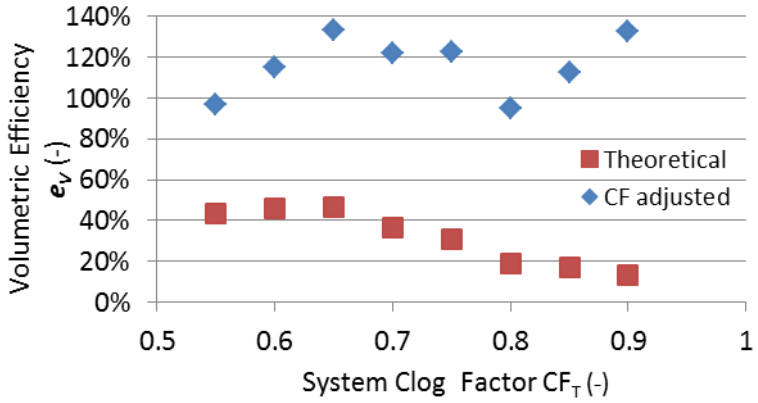

Figure 6-30 The relationship between ***CF_T*** and ***e_V*** produced by the FEA hydrodynamic model.

The relationship between ***CF_T*** and hydraulic efficiency ***λ*** is similar to the relationship between ***CF_T*** and ***e_V***. The value of ***λ*** decreases from a maximum of 37 % to a minimum of 12 % as the system clogs. The ***CF_T*** adjusted values of ***λ*** vary between 74 % and 117 %.

6.7. Conclusions

This Chapter has demonstrated the usefulness and flexibility of the Clog Factor to describe the hydraulics of HSSF TWs. Clog Factor values were derived for Severn Trent HSSF TWs using the hydraulic conductivity results obtained in **Chapter 5**. The arithmetic mean of these results produced a bulk system Clog Factor ***CF_T*** that was used to benchmark the state of clogging in each system. The value of ***CF_T*** is referenced against the theoretical hydraulic conductivity for a homogeneous media with particle diameter equivalent to the mean

particle diameter of the clean media, and porosity equivalent to the porosity of the clean media. The system is clean and ideal when $\boldsymbol{CF_T}$ is 0, non-ideal with a particle size distribution when the system is clean and $\boldsymbol{CF_T}$ is greater than 0, and completely clogged when $\boldsymbol{CF_T}$ is 1.

It was found that $\boldsymbol{CF_T}$ varied between 0.54 for a system that had recently been refurbished (clean and non-ideal), and 0.90 for a 15 year old system that exhibited overland flow across the majority of the bed surface (heavily clogged). The value of 0.54 for the clean system suggests that the actual hydraulic performance of the system is less than half of the design hydraulic performance because of the tendency for small media particles to occupy the pore spaces between large media particles in media with a particle size distribution.

Based on additional statistical analysis of ***CF*** data-sets, the following observations were made regarding the influence of system design and operation on clogging:

- Statistically significant transverse variations in hydraulic conductivity were found in 70% of the systems surveyed. Clogging towards the inlet was generally highest within those transects that are closest to the point at which flow enters the influent distribution system. Clogging towards the outlet was generally highest within those transects that are closest to the point at which flow exits the effluent collection system. Pressure losses in inlet and outlet plumbing encourage preferential flow along a path of least resistance between the point at which flow enters and exits the system.
- Those systems that were sparsely vegetated exhibited reduced vertical ***CF*** values in the top 0.1 m of measured media, in comparison to the 0.1 to 0.2 m depth of media. Those systems that had dense vegetation cover exhibited the highest vertical ***CF*** values in the top 0.1 m of measured media. Sparse cover enables accelerated clog matter mineralisation via surface evaporation, whereas dense cover prevents this occurrence and exacerbates the onset of clogging.
- Resting strategies can be used to restore hydraulic conductivity and reduce $\boldsymbol{CF_T}$. A side-by-side test indicated that a system that had been rested for 14 months had a $\boldsymbol{CF_T}$ value that was 29% lower than a system that had been operating continuously.

Transverse variations in clogging were removed from the dataset to allow a dimensionless 2D surface expression to be derived that describes the variation of ***CF*** within the subsurface for various values of $\boldsymbol{CF_T}$. This equation relates the spatial development of clogging within the system to temporal changes of overall clogging within the system. The agreement

between measured and modelled values of ***CF*** was found to be good and allowed the statistically significant trend in clogging to be separated from scatter in the data that arises from natural randomistic variations in the way that systems clog.

An experimentally validated hydrological FEA model was used to investigate how a Severn Trent HSSF TW hydraulically and hydrodynamically responds to various values of CF_T. The 2D surface expression was used to generate hydraulic conductivity profiles for values of CF_T between 0.55 and 0.90. For each hydraulic conductivity profile and specific values of flow-rate, outlet water depth, clean media hydraulic conductivity and system length, the FEA model was used to find: the length of overland flow; the water table profile; and the residence time distribution within the reactor. It was possible to closely replicate the water table profile corresponding to each value of CF_T by using different values of ***a*** and ***b*** in **Equation 3-49**, **Equation 3-52** and **Equation 3-55**, for the regions upstream and downstream of ***f***. The RTDs were closely replicated using a Tanks-in-Series model with a gamma distribution.

The results of the modelling exercise were used to further analyse the relationship between CF_T and system hydrology. It was found that the length of overland flow, the inlet water depth, the wetted reactor area, and the number of Tanks-in-Series all increased as CF_T increased from 0.55 to 0.90. This combination of results confirms that as the system clogs an increasing fraction of the reactor subsurface is bypassed by flow that short-circuits as overland flow. The elevation of water table profile that results from increased hydraulic resistance in the subsurface cannot compensate for the loss of subsurface porosity and the reactor volumetric efficiency and mean hydraulic residence time in the reactor both decrease. Hydrodynamics shifts towards plug-flow because the flow spends less time in the subsurface where dispersive effects are greater. However, the increase in mixing efficiency cannot compensate for the loss of volumetric efficiency and the overall hydraulic efficiency of the reactor decreases from 37 % to 12 % as the system clogs. Adjusting the wetted reactor area to account for the reduction of porosity confirms that even though the wetted reactor area increases the area available for flow decreases as the system clogs.

It should be emphasised that these general findings are only valid for Severn Trent HSSF TWs for tertiary treatment of municipal wastewater and due to the deviations from ideal media mentioned above only provide representative answers for values of CF_T greater than 0.5.

7. Conclusions

The research described within this thesis entails four years of study, the majority of which was undertaken on operational, field-scale Horizontal Subsurface Flow Treatment Wetlands (HSSF TWs). Together, the preceding chapters describe a systematic approach to understanding the way that clogging develops in HSSF TWs operated by Severn Trent, and the impact that this has on system hydrodynamics and hydraulics.

This final chapter draws overall conclusions based on the detailed findings of the study. Discussion is given to the ability of the outcomes to satisfy the report objectives and the overall aim. Finally, recommendations for using the study output are made along with suggestions for further work.

7.1. General Conclusions

The major findings from each Chapter will be considered in an overall discussion of the general conclusions that can be made from the research.

The review of **Chapter 2** found that the development of clogging in Subsurface Flow Treatment Wetlands depends on the design and operation of the system. There are several factors that cause the systems of Severn Trent to clog in the manner that they do.

- The systems are sized on the principle of 0.7 m^2/PE, in contrast to secondary treatment HSSF TWs that are sized for 5 m^2/PE. Therefore, the hydraulic loading rate of tertiary HSSF TWs is over five times greater than secondary HSSF TWs.
- One of the major roles of the beds is to intercept biomass solids that are sloughed from upstream secondary stages. The solids are often filamentous flocs with diameter that are greater than the media pore diameters, such that they are quickly strained from the flow. Furthermore, these microbial strains are often slime producing.
- It was found that tertiary HSSF TWs have a combination of relatively high hydraulic loading rate and solids loading rates when compared to variants of Subsurface Flow Treatment Wetlands employed elsewhere in the world (e.g.: Severn Trent HSSF TWs for tertiary treatment - median HLR = 0.12 m/d and median TSS = 7 g/m^2.day; US

HSSF TWs for secondary treatment - median HLR = 0.02 m/d and median TSS = 2 g/m^2.day).

- The systems ordinarily incorporate influent distrubtors that are located above the gravel surface and load the wastewater across the width of the bed, onto a rock berm that is intended to improve uniform distribution. Common distributors incorporate a horizontal pipe with several outward facing tees located at regular intervals along the pipe length, or a trough with v-notch weir incisions at regular intervals.

The above combination of high hydraulic loading rate and surface loading rate of filamentous biomass solids results in the formation of a low permeability surface sludge layer on the surface of the bed, accompanied by overland flow. This is particularly so once the upper layers of gravel have become extensively clogged, such that infiltration rates into the subsurface are limited. The overland flow covers the sludge layer and prevents aerobic mineralisation such that sludge layer development becomes progressive. Sludge layer accumulation is exacerbated by patchy masses of leaf litter in various stages of decomposition. Analysis of data presented by (Wilson, 2007) showed that surface sludge layer depth at the inlet increases by approximately 16 mm for every kilogram of solids loaded per square meter of system footprint. A median Severn Trent system will therefore accumulate approximately 40 mm/year of surface sludge at the inlet region.

Chapter 3 presented a novel mathematical derivation that describes the hydraulic response of HSSF TWs as they clog. The model was derived in response to the need for an intermediate approach between over-simplified unrepresentative methods that have been applied historically in wetland design and sophisticated methods that are either time consuming or require computational expertise that extends beyond a good working knowledge of HSSF TWs. The derived formulation is considered to be an intermediate approach that is relatively simple to apply without neglecting features that significantly influence clogging in HSSF TWs, i.e. variable hydraulic conductivity and overland flow.

The expression is based on the assumption that media hydraulic conductivity varies from inlet to outlet according to an exponential relationship, the parameters of which vary as the system clogged. A condition is included to describe the interaction between overland flow and the hydraulic conductivity profile. In **Chapter 6** the formulation was benchmarked against existing hydraulic tools for HSSF TWs, namely Darcy's Law (EC/EWPCA, 1990), Dual-Zone Darcy's Law (USEPA, 2000), the Dupuit-Forchheimer Assumption (Kadlec and Watson,

1993) and the FEA model of (Knowles and Davies, 2011). The models were compared on their ability to fit the data obtained in a water table survey of a HSSF TW at Moreton Morrell. The equivalent hydraulic conductivity parameter values, corresponding wetted volume and closeness of fit to the measured water table profile were deduced for each method and the the proposed method presented an error reduction in the calculation of $\boldsymbol{V_W}$ compared to all other methods, including the FEA model. The novel derivation succeeded in achieving an intermediate accuracy between simple rules and complex computation models. It therefore provides a useful design guideline for wetland practitioners.

Chapter 3 also introduced the Clog Factor ***CF***: a novel metric that converts hydraulic conductivity, a physical property that is neither intensive nor extensive, into an intensive bulk property that can be representatively averaged for subsequent analysis. ***CF*** is based on the Kozeny-Carman equation and can be applied over any scale, thus allowing internal variations of ***CF*** and aggregate values for system Clog Factor $\boldsymbol{CF_T}$ to be derived from experimental hydraulic conductivity measurements. The Clog Factor has the following advantages:

- Intensive bulk property that can be applied to any scale porous media flow system
- Non-dimensionalises data so that comparisons can be performed between systems with different dimensions and media sizes
- Highlights deviations from theoretical clean conductivity due to both clogging and media non-ideality
- Allows reasonable statistical comparisons where orders of magnitude changes in hydraulic conductivity would skew a data set
- Allows single-parameter values to be published to indicate health of bed at a point in time

In **Chapter 4**, a novel method was devised to allow the three dimensional hydraulic conductivity of HSSF TWs to be determined *in situ*. The method recreates the laboratory constant head permeameter test *in situ* by using a submersible permeameter cell that encapsulates a test specimen of media, and a Mariotte Siphon actuated recharge reservoir to maintain constant head conditions in the cell. The apparatus is designed for use by one person in remote locations, weighing approximately 10 kg and utilizing 10 L of water for one test, and is sized to be appropriate for the range of media hydraulic conductivities typically encountered in mature HSSF TWs (from 0 to 10,000 m/d). Manometer take off tubes are immersed to different depths within the permeameter cell so that the vertical variation of

hydraulic conductivity can be elucidated. By repeating the test at different locations over the surface of the bed and interpolating between results it is possible to generate a three-dimensional hydraulic conductivity profile for the HSSF TW.

Chapter 5 reported results for spatial variations in hydraulic conductivity for 20 separate tests on 13 different HSSF TWs, in the UK and the US. Systems varied by geometry and age and incorporated varying media, influent distributors and upstream processes. The Aston Permeamter measured 1,053 sample hydraulic conductivities that ranged across 6 orders of magnitude. Hydraulic conductivity was typically lowest on the surface of the bed at the inlet, where hydraulic conductivity values below 1 m/d often corresponded to a surface sludge layers covered by overland flow. Hydraulic conductivity was typically highest at the base of the bed near the outlet and was generally always above 100 m/d, even in extensively clogged systems. Most systems displayed at least a 2 to 3 order of magnitude variation in hydraulic conductivity, across all planes. The minimum value measured during the test was 0.03 m/d at Fenny Compton in February 2008, which was attributed to a concentration of construction fines clogging the gravel void space. The maximum value measured was 62,500 m/d at Jackson Meadows South in 2009, although hydraulic conductivity of this magnitude is close to the practical measuring limit of The Aston Permeameter.

In **Chapter 6**, the hydraulic conductivity results were converted to Clog Factors and subjected to an ANOVA test to explore the development of clogging and how this is influenced by various design parameters. It was found that $\boldsymbol{CF_T}$ values are typically between 0.5 and 0.9, even for relatively clean beds (representing hydraulic performance that is equivalent to 50-90% of porosity reduction in the Kozeny Carman equation). This is due to the influence of media non-ideality, such as particle size distribution, that reduces the hydraulic performance of the media below theoretical ideal design values.

A 2D surface fit equation (transverse variance removed) was calibrated based on the relationship between $\boldsymbol{CF_T}$ and internal variations of ***CF***. Effectively, this equation relates the spatial development of clogging within the system to temporal changes of overall clogging within the system. It should be emphasised that the empirical surface fit is only valid for Severn Trent HSSF TWs for tertiary treatment of municipal wastewater and, due to the deviations from ideal media mentioned above, only provides representative answers for values of $\boldsymbol{CF_T}$ greater than 0.5. The agreement between measured and modelled values of ***CF*** was found to be good and allowed the statistically significant trend in clogging to be

separated from scatter in the data that arises from natural randomistic variations in the way that systems clog. The equations will allow wetland modellers to conveniently reproduce 2D hydraulic conductivity profiles for Severn Trent HSSF TWs at any stage of clogging development.

Based on additional statistical analyses of ***CF*** data-sets, the following conclusions were drawn:

- Statistically significant transverse variations in hydraulic conductivity were found in 70% of the systems surveyed. Clogging towards the inlet was generally highest within those transects that are closest to the point at which flow enters the influent distribution system. Clogging towards the outlet was generally highest within those transects that are closest to the point at which flow exits the effluent collection system. Pressure losses in inlet and outlet plumbing encourage preferential flow along a path of least resistance between the point at which flow enters and exits the system.
- Those systems that were sparsely vegetated exhibited reduced vertical ***CF*** values in the top 0.1 m of measured media, in comparison to the 0.1 to 0.2 m depth of media. Those systems that had dense vegetation cover exhibited the highest vertical ***CF*** values in the top 0.1 m of measured media. Sparse cover enables accelerated clog matter mineralisation via surface evaporation, whereas dense cover prevents this occurrence and exacerbates the onset of clogging.
- Resting strategies can be used to restore hydraulic conductivity and reduce $\boldsymbol{CF_T}$. A side-by-side test indicated that a system that had been rested for 14 months had a $\boldsymbol{CF_T}$ value that was 29% lower than a system that had been operating continuously.

The effect that clogging has on hydraulics was explored using a custom FEA model of a 2D HSSF TW that was validated via experimentation. The results of the model confirmed that low hydraulic conductivity in the subsurface does not govern the occurrence of overland flow in Severn Trent HSSF TWs. Rather, overland flow is controlled by slow vertical infiltration rates through the surface sludge layer into the subsurface. This effect creates a dual hydrological regime in Severn Trent HSSF TWs, whereby the overland flow provides variable recharge to the subsurface water table and extends over the surface of the bed until the infiltration rate matches the influent flow-rate. The FEA model proved that infiltration rates are slower near the inlet, where surface clogging and hydraulic resistance are greatest, and increase with distance downstream. The higher infiltration rates towards

the end of the overland flow region create an 'S-shaped' water table profile within Severn Trent HSSF TWs. In advanced stages of clogging, the subsurface water table and surface layer infiltration region connect as a singular hydrology.

Tracer tests were used to illustrate the effect that clogging has on hydrodynamics. Results showed that negligible tracer was detected at lower depths neat the inlet because most flow bypassed this region as overland flow. Downstream of the overland flow region, large concentrations of tracer were detected at lower depths, suggesting that flow short-circuits below the root-zone once within the subsurface. This behaviour was supported by an FEA model. A dye-tracing test on a field-scale HSSF TW confirmed that transverse short-circuiting occurs due to non-uniform width distribution and a resultant variation of clogging along the bed width.

7.2. Ability to meet research objectives

The salient findings of the report are discussed with regard to the major objectives outlined in **Chapter 1**:

Problem	**The factors that cause clogging are not well understood.**
Obstacle	Numerous sources exist proffering various observations, hypotheses and conclusions regarding clogging; however, a comparative review of the literature which identifies trends and salient factors does not exist.
Objective	**Summarise the relevant literature on HSSF TW clogging.**
Output	Determination of current best practice design guidelines for mitigation of clogging, and identification of where more research is required.

For the first time, an objective literature review was performed into the underlying causes and effects of clogging in Subsurface Flow TWs. Through comparison with other variants of Subsurface Flow TW, and analysis of the Severn Trent Water Wetland database provided by ARM Ltd., it was possible to conclude the following about the longevity of Severn Trent HSSF TWs:

1. Strong enough evidence did not exist to suggest that systems with lower hydraulic loading rates per unit area of system footprint are less likely to have been refurbished.

2. Strong enough evidence did not exist to suggest that systems with larger width-to-length ratios are less likely to have been refurbished.
3. Systems that incorporate troughs have greater longevity than those with ports.
4. Severn Trent tertiary HSSF TWs receive high solids loading rates and hydraulic loading rates in comparison to international variants of secondary and primary Subsurface Flow TWs.
5. A solids loading rate of 1 kg/m^2.yr results in a surface sludge accumulation rate of 16 mm/year at the inlet.
6. Systems that support rotating biological contactors are less likely to clog than systems that support trickling filters. Compared with rotating biological contactors, it is proposed that trickling filters are more susceptible to solids washout during wet weather flows and are less able to remove small solids.
7. The ability of clog matter to fill pore space is not proportional to the dry mass of solids. Associations between highly hydrated biological matter and inorganic constituents create low-density viscous sols that fill pores spaces and provide high resistance to flow.

It was concluded that measurements of the magnitude and distribution of clogging in HSSF TWs are lacking in the literature, and are required to understand better the relationship between clogging and hydraulics and how clogging limits system longevity.

Problem	**Little is known about the relationship between clogging, hydraulics and treatment and how this develops over time.**
Obstacle	Current design tools for HSSF TW hydrology are too simple to be representative, and computational models are too complicated to be useful. Not enough information exists to allow better tools to be derived.
Objective	**Derive design tools that are representative and practical to apply, and validate them through experimentation and dynamic modelling.**
Output	Design tools that relate the changing hydrology of HSSF TWs to changes in clogging, calibrated using experimentally derived data.

This objective has been achieved in several stages:

1. The Clog Factor ***CF*** was derived as a way of ranking the deviation of hydraulic performance from ideal conditions and relating this to effective loss of porosity.
2. The Clog Factor is an intensive parameter that can be applied over any scale. As such, it was possible to calibrate a surface fit equation that relates the bulk system Clog Factor $\boldsymbol{CF_T}$ to the spatial distribution of ***CF*** values throughout the system. The surface fit equation well reproduced the experimental values of ***CF*** obtained from Severn Trent HSSF TWs.
3. A 1D analytical solution was derived that relates hydraulics to clogging by describing how the water table profile varies along the length of the system, and how this changes as the system clogs. To be representative, the analytical solution includes features that significantly influence hydrology, such as overland flow and spatially varying hydraulic conductivity profile.
4. The analytical solution is parameter based and was calibrated to Severn Trent HSSF TWs by using different values of $\boldsymbol{CF_T}$ in the ***CF*** surface fit expression and superimposing the obtained ***CF*** profiles onto the subdomain of an FEA model of a HSSF TW. The FEA model computed the water table profile that corresponded to different $\boldsymbol{CF_T}$ profiles. The model was validated using an experimental test case. To complete the calibration, the relationship between $\boldsymbol{CF_T}$ and the parameter values in the analytical equation were deduced, so that the analytical equation could be expressed solely as a function of $\boldsymbol{CF_T}$.
5. To provide the relationship between clogging and hydrodynamics, the FEA model was used to determine the hydrodynamic response of the system to different $\boldsymbol{CF_T}$ profiles. The hydraulic efficiency and number of TIS were calculated for the RTD produced by each hydrodynamic simulation, and these parameters were correlated against $\boldsymbol{CF_T}$.

The derived expressions are specific to Severn Trent Water HSSF TWs, but the approach can be applied to model the interrelationship between clogging, hydrodynamics and hydraulics for any system.

Problem	**Not enough information is available on the magnitude and distribution of hydraulic conductivity to make conclusions about design or allow models to be developed.**
Obstacle	Many conventional methods for *in situ* measurement of hydraulic conductivity are not suitable for HSSF TWs, and as such no simple method exists to obtain data.
Objective	**Design an *in situ* method to obtain this information.**
Output	Hydraulic conductivity profiles for several tertiary HSSF TWs of various ages that can then be used to calibrate hydraulic models. This will also allow the influence of design and operational parameters on clogging to be studied.

The ***CF*** analyses described above were made possible due to the data obtained via the novel method and apparatus used in this thesis: the Aston Permeameter. By this method, for the first time, it was possible to measure the three-dimensional variation of media hydraulic conductivity throughout systems in different stages of clogging. The apparatus could be operated by an individual, was applicable over a wide range of hydraulic conductivity, and was relatively low cost. The Aston Permeameter has now been transferred to Severn Trent Water and treatment plant operators are being trained in its use.

7.3. Ability to meet overall research aim

The first page of this thesis stated the overall aim of this doctoral study:

"To help designers and operators make informed decisions that result in improved asset longevity, by improving the knowledge and understanding of clogging in Severn Trent HSSF TWs"

This thesis has achieved this aim through three main, original contributions to wetland science:

1. The development of the Aston Permeameter to measure three-dimensional hydraulic conductivity profiles.

2. The Clog Factor analysis to interpret hydraulic conductivity profiles, and infer the overall state of clogging in a system, for the purpose of comparison and ranking.
3. Several design tools that describe the relationships between clogging, hydraulics and hydrodynamics in Severn Trent HSSF TWs. These design tools can be applied without the need for computational modelling and consider significant influences on mature hydrology, such as variable hydraulic conductivity and overland flow.

It is hoped that these contributions have provided a framework for wetland scientists to study clogging within other subsurface flow wetland treatment systems. With this improved understanding of clogging and access to better design tools, wetland practitioners should be able to design more robust wetlands that achieve greater longevity and assured financial feasibility.

7.4. Recommendations and future work

There are several major outcomes from this study that can be used to make recommendations to Severn Trent and provide grounds for further work.

1. *Outcome: Clogging is greatest at the inlet at the surface. Clogging is compounded when overland flow covers the surface layer.*

   Recommendation: It is suggested that future Severn Trent HSSF TWs are designed with inlet headers and effluent collectors at both ends. This will allow the flow direction to be changed between years. Clog matter which has accumulated at the inlet over the year will then have a whole year to mineralise before flow is reintroduced to this area. It is thought that this action would be very affordable if implemented at the time of system construction and would greatly extend the useful life of the system. This is similar to the equivalent of zonal bed resting. The base of the wetland could still have a slope in one direction to facilitate complete draining when desired.

2. *Outcome: Lush foliage shades the surface and prevents the surface layer from mineralising during summer months. Surface clogging is exacerbated by accumulation of patchy masses of leaf litter in various stages of decomposition.*

   Recommendation: The leaf litter layer only provides insulation benefit in cold climates. In the UK it would be possible to harvest the reed stock during late summer without

threatening winter operation. This would provide the surface with some time to mineralise and would prevent accumulation of leaf litter on the surface. Several Severn Trent Water systems in the East Region jurisdiction currently operate with reed harvesting. An internal review should be performed into the cost benefit analysis of annual harvesting, versus potential improvement in asset longevity.

3. *Outcome: The Aston Permeameter and Clog Factor analysis have been provided as a way of studying the development of clogging in wetland systems. A bed with aeration was the least clogged system of all the systems studied.*

   Further work: The method performed in this study should be repeated for other wetland variants to identify differences in the development and magnitude of clogging. One such study would be into engineered wetland systems that employ subsurface aeration to enhance treatment, and additionally purport to control clogging. Clog Factor results from Jackson Meadow indicated that this system, fitted with aeration, was the least clogged of all systems, which may validate this claim. Further system studies would need to be performed to confirm this hypothesis.

4. *Outcome: A simple design equation has been provided that has been validated using experimental data from one system and a representative computational model.*

   Further work: The accuracy and usefulness of this equation should be further validated through water level surveys of additional systems. This would be an easy research exercise for an MSc or MEng student.

5. *Outcome: A relationship has been found which describes how hydrodynamic performance of a system changes in response to clogging. This has been validated using experimental data from one system and a representative computational model.*

   Further work: The accuracy and usefulness of this relationship should be further validated through tracer tests on additional systems. This would be an easy research exercise for an MSc or MEng student. The relationship that describes the temporal change in system hydrodynamic performance as the system clogs should be incorporated into a Treatment Wetland treatment performance model, such as Constructed Wetlands Model 1 (Langergraber et al., 2009), to infer how treatment performance changes as the system clogs.

6. *Outcome: If it can be easily measured, the bulk Clog Factor is a useful metric to assess the overall hydraulic health of a system. It can be used by operators to help decision making.*

   Further work: During this research, a spin-off research project evolved in collaboration with the Physical Science department at Nottingham Trent University. This project involved the development of a new tool to measure clogging in porous media flow systems and utilised *in situ* Nuclear spin Magnetic Resonance Imaging Technology (Morris et al., 2011). A prototype device dubbed 'The Clogging Probe' was developed by a Nottingham Trent University incubator spin-out company called 'Mr Eye' and is ready for field testing. It is recommended that a trial study be performed whereby this instrument is left *in situ* to monitor clogging in a new wetland over 3 years. If the probe can be calibrated to return Clog Factor values this would provide useful information to operators. For example, if a model is developed to link Clog Factor and treatment performance then this information and the probe would provide wetland operators with a useful indicator of when a system should be refurbished/rested in order to avoid substandard treatment performance. Furthermore, in engineered wetlands, the Clogging Probe could inform operators when to add nutrients to the system to increase biomass establishment, or when to increase aeration to maintain system hydraulic health.

References

ÁLVAREZ, J. A., RUÍZ, I. & SOTO, M. 2008. Anaerobic digesters as a pretreatment for constructed wetlands. *Ecological Engineering,* 33 (1)**,** 54-67.

AMOOZEGAR, A. 1989. A compact constant-head permeameter for measuring saturated hydraulic conductivity of the vadose zone. *Soil Science Society of America journal,* 53 (5)**,** 1356-1361.

ASAEDA, T., NAM, L. H., HIETZ, P., TANAKA, N. & KARUNARATNE, S. 2002. Seasonal fluctuations in live and dead biomass of Phragmites australis as described by a growth and decomposition model: implications of duration of aerobic conditions for litter mineralization and sedimentation. *Aquatic Botany,* 73 (3)**,** 223-239.

ASTM-D3385 2003. Standard Test Method for Infiltration Rate of Soils in Field Using Double-Ring Infiltrometer. American Society for the Testing of Materials.

ASTM-D5126 2004. Standard Guide for Comparison of Field Methods for Determining Hydraulic Conductivity in the Vadose Zone. West Conshohocken, PA, USA: American Society for the Testing of Materials.

ATV 1998. Grundsätze für Bemessung, Bau und von Pflanzenbeeten für kommunales Abwasser bei Ausbaugrößen bis 1000 Einwohnern. 1141 St. Augustin, Germany.

AUSTIN, D. C. 2005. Patent: Tidal vertical flow wastewater treatment system and method. United States US 6,896,805 B2. October 20, 2003.

BAIRD, A. J., SURRIDGE, B. W. J. & MONEY, R. P. 2004. An assessment of the piezometer method for measuring the hydraulic conductivity of a Cladium mariscus—Phragmites australis root mat in a Norfolk (UK) fen. *Hydrological Processes,* 18**,** 275-291.

BARNES, G. E. 2000. *Soil mechanics : principles and practice: 2nd ed.,* Basingstoke, Macmillan.xviii, 493 p.

BARROS, P., RUIZ, I. & SOTO, M. 2008. Performance of an anaerobic digester-constructed wetland system for a small community. *Ecological Engineering,* 33 (2)**,** 142-149.

BATCHELOR, A. & LOOTS, P. 1997. A critical evaluation of a pilot scale subsurface flow wetland: 10 years after commissioning. *Water Science and Technology,* 35 (5)**,** 337-343.

BAVEYE, P., VANDEVIVERE, P., HOYLE, B. L., DELEO, P. C. & DE LOZADA, D. S. 1998. Environmental Impact and Mechanisms of the Biological Clogging of Saturated Soils and Aquifer Materials. *Critical Reviews in Environmental Science and Technology,* 28**,** 123-191.

BAVOR, H. J. & SCHULZ, T. J. 1993. Sustainable Suspended Solids and Nutrient Removal in Large-Scale, Solid Matrix, Constructed Wetlands Systems. *In:* MOSHIRI, G. A. E. (ed.) *Constructed wetlands for water quality improvement : Conference : Selected papers.* Boca Raton: Lewis Pub, pp 219-225.

BEAR, J. 1979. *Hydraulics of groundwater:* New York ; London, McGraw-Hill.xiii,567p.

BECKWITH, C. W., BAIRD, A. J. & HEATHWAITE, A. L. 2003. Anisotropy and depth-related heterogeneity of hydraulic conductivity in a bog peat. I: laboratory measurements. *Hydrological processes,* 17 (1)**,** 89-101.

BEHRENDS, L. L., HOUKE, L., BAILEY, E., JANSEN, P. & BROWN, D. 2001. Reciprocating constructed wetlands for treating industrial, municipal, and agricultural wastewater. *Water Science and Technology,* 44 (11-12)**,** 399-405.

BENSON, C. & GRIBB, M. Measuring Unsaturated Hydraulic Conductivity in the Laboratory and the Field. Unsaturated Soil Engineering Practice: Geotechnical Special Publication, 1997 Logan, Utah 113-168.

BEZBARUAH, A. N. & ZHANG, T. C. 2004. pH, redox, and oxygen microprofiles in rhizosphere of bulrush(Scirpus validus) in a constructed wetland treating municipal wastewater. *Biotechnology and bioengineering,* 88 (1)**,** 60-70.

BHATTARAI, R. R. & GRIFFIN JR, D. M. 1999. Results of tracer tests in rock-plant filters. *Journal of Environmental Engineering,* 125 (2)**,** 117-125.

BINLEY, A., BEVEN, K. & ELGY, J. 1989. Physically Based Model of Heterogeneous Hillslopes: 2. Effective Hydraulic Conductivities. *Water Resources Research,* 25 (6)**,** 1227-1233.

BLAKE, W. C. 1922. The resistance of packing to fluid flow. *Transactions of the American Institute of Chemical Engineers,* 14**,** 415-421.

BLAZEJEWSKI, R. & MURAT-BLAZEJEWSKA, S. 1997. Soil clogging phenomena in constructed wetlands with subsurface flow. *Water Science and Technology,* 35 (5)**,** 183-188.

BOON, A. G. 1985. Report of a visit by members and staff of WRc to Germany to investigate the Root Zone Methods for treatment of wastewaters. Stevenage UK: WRc Report 376-S/1.

BÖRNER, T., VON FELDE, K., GSCHLÖSSL, E., GSCHLÖSSL, T., KUNST, S. & WISSING, F. W. 1998. Germany. *In:* VYMAZAL, J., BRIX, H., COOPER, P. F., GREEN, M. B. & HABERL, R. (eds.) *Constructed Wetlands for Wastewater Treatment in Europe.* Lieden, The Netherlands: Backhuys Publishers, 169-190.

BOUTIN, C., LIENARD, A. & ESSER, D. 1997. Development of a new generation of reed-bed filters in France: first results. *Water Science and Technology,* 35**,** 315-322.

BOUWER, H. 2002. Artificial recharge of groundwater: hydrogeology and engineering. *Hydrogeology Journal,* 10 (1)**,** 121-142.

BOUWER, H. & RICE, R. C. 1976. A slug test for determining hydraulic conductivity of unconfined aquifers with completely or partially penetrating wells. *Water Resources Research,* 12 (3)**,** 423-428.

BOWMER, K. H. 1987. Nutrient removal from effluents by an artificial wetland: Influence of rhizosphere aeration and referential flow studied using bromide and dye tracers. *Water Research,* 21 (5)**,** 591-599.

BREEN, P. F. & CHICK, A. J. 1995. Rootzone dynamics in constructed wetlands receiving wastewater: A comparison of vertical and horizontal flow systems. *Water Science and Technology,* 32 (3)**,** 281-290.

BRIX, H. 1987. Treatment of wastewater in the rhizosphere of wetland plants-the root-zone method. *Wat. Sci. Tech,* 19 (1/2)**,** 107-118.

BRIX, H. 1993. Wastewater treatment in constructed wetlands: system design, removal processes and treatment performance. *In:* MOSHIRI, G. A. E. (ed.) *Constructed wetlands for water quality improvement : Conference : Selected papers.* Boca Raton: Lewis Pub, 9-22.

BRIX, H. 1994a. Functions of macrophytes in constructed wetlands. *Water Science and Technology,* 29 (4)**,** 71-78.

BRIX, H. 1994b. Use of constructed wetlands in water pollution control: Historical development, present status, and future perspectives. *Water Science and Technology,* 30 (8)**,** 209-223.

BRIX, H. 1997. Do macrophytes play a role in constructed treatment wetlands? *Water Science and Technology,* 35 (5)**,** 11-17.

BRIX, H. & ARIAS, C. A. 2005. The use of vertical flow constructed wetlands for on-site treatment of domestic wastewater: New Danish guidelines. *Ecological Engineering,* 25 (5)**,** 491-500.

BRIX, H. & JOHANSEN, N. H. 1999. Treatment of Domestic Sewage in a Two-Stage Constructed Wetland - Design Principles. *In:* VYMAZAL, J. (ed.) *Nutrient cycling and retention in natural and constructed wetlands.* Netherlands: Backhuys, 155-163.

BRIX, H. & SCHIERUP, H. 1989. Sewage treatment in constructed reed beds. Danish experiences. *Water Science & Technology,* 21 (12)**,** 1665-1668.
BRIX, H. & SCHIERUP, H. 1990. Soil oxygenation in constructed reed beds: the role of macrophyte and soil-atmosphere interface oxygen transport. *In:* COOPER, P. F. & FINDLATER, B. C. (eds.) *Constructed Wetlands in Water Pollution Control.* Cambridge, UK: Pergamon Press, Oxford, UK, 53-66.
BROOKS, R. H. & COREY, A. T. 1964. Hydraulic Properties of Porous Media. *Hydrology Papers, Colorado State University,* (March).
BS-EN-872 2005. Water quality. Determination of suspended solids. Method by filtration through glass fibre filters British Standards Institute.
BS-ISO-17313 2004. Soil quality. Determination of hydraulic conductivity of saturated porous materials using a flexible wall permeameter. British Standards Institute.
BURKA, U. & LAWRENCE, P. C. 1990. A New Community Approach to Waste Treatment with Higher Water Plants. *In:* COOPER, P. F. & FINDLATER, B. C. (eds.) *Constructed Wetlands in Water Pollution Control.* Cambridge, UK: Pergamon Press, Oxford, UK, 359-371.
BURKE, S. P. & PLUMMER, W. B. 1928. Gas Flow through Packed Columns. *Industrial & Engineering Chemistry,* 20 (11)**,** 1196-1200.
CAMPBELL, C. S. & OGDEN, M. H. 1999. *Constructed Wetlands in the Sustainable Landscape*, John Wiley & Sons: New York, New York
CARMAN, P. C. 1937. Fluid flow through granular beds. *Chemical Engineering Research and Design,* 15 (a)**,** 150-166.
CASELLES-OSORIO, A. & GARCÍA, J. 2006. Performance of experimental horizontal subsurface flow constructed wetlands fed with dissolved or particulate organic matter. *Water Research,* 40 (19)**,** 3603-3611.
CASELLES-OSORIO, A. & GARCÍA, J. 2007. Effect of physico-chemical pretreatment on the removal efficiency of horizontal subsurface-flow constructed wetlands. *Environmental Pollution,* 146 (1)**,** 55-63.
CASELLES-OSORIO, A., PUIGAGUT, J., SEGU, E., VAELLO, N., GRANÉS, F., GARCÍA, D. & GARCÍA, J. 2007. Solids accumulation in six full-scale subsurface flow constructed wetlands. *Water Research,* 41 (6)**,** 1388-1398.
CHAZARENC, F., MALTAIS-LANDRY, G., TROESCH, S., COMEAU, Y. & BRISSON, J. 2007. Effect of loading rate on performance of constructed wetlands treating an anaerobic supernatant. *Water Science and Technology,* 56**,** 23-29.
CHAZARENC, F. & MERLIN, G. 2005. Influence of surface layer on hydrology and biology of gravel bed vertical flow constructed wetlands. *Water Science and Technology,* 51 (9)**,** 91-97.
CHAZARENC, F., MERLIN, G. & GONTHIER, Y. 2003. Hydrodynamics of horizontal subsurface flow constructed wetlands. *Ecological Engineering,* 21 (2-3)**,** 165-173.
CHEN, S., TE WANG, G. & XUE, S. K. 1999. Modeling BOD removal in constructed wetlands with mixing cell method. *Journal of environmental engineering,* 125 (1)**,** 64-71.
CHILDS, E. C. 1952. The measurement of the hydraulic permeability of saturated soil in situ. I. Principles of a proposed method. *Proceedings of the Royal Society of London. Series A, Mathematical and Physical Sciences,* 215 (1123)**,** 525-535.
CHIMNEY, M. J. & PIETRO, K. C. 2006. Decomposition of macrophyte litter in a subtropical constructed wetland in south Florida (USA). *Ecological engineering,* 27 (4)**,** 301-321.
CHRISTENSEN, J. B., JENSEN, D. L., GRØN, C., FILIP, Z. & CHRISTENSEN, T. H. 1998. CHARACTERIZATION OF THE DISSOLVED ORGANIC CARBON IN LANDFILL LEACHATE-POLLUTED GROUNDWATER. *Water Research,* 32 (1)**,** 125-135.
CHRISTIAN, J. N. W. 1990. Reed bed treatment systems: Experimental gravel beds at Gravesend - The Southern Water Experience. *In:* COOPER, P. F. & FINDLATER, B. C.

(eds.) *Constructed Wetlands in Water Pollution Control.* Cambridge, UK: Pergamon Press, Oxford, UK, 309-319.
CIRIA, M. P., SOLANO, M. L. & SORIANO, P. 2005. Role of Macrophyte Typha latifolia in a Constructed Wetland for Wastewater Treatment and Assessment of Its Potential as a Biomass Fuel. *Biosystems Engineering,* 92 (4)**,** 535-544.
COMMISSION, E. 1999. Implementation of Council Directive 91/271/EEC of 21 May 1991 concerning urban waste water treatment, as amended by Commission Directive 98/15/EC of 27 February 1998 : summary of the measures implemented by the member states and assessment of the information received pursuant to Articles 17 and 13 of the directive. Luxembourg; Lanham, Md.: Office for Official Publications of the European Communities ; Bernan Associates [distributor].
CONLEY, L. M., DICK, R. I. & LION, L. W. 1991. An assessment of the root zone method of wastewater treatment. *Research Journal of the Water Pollution Control Federation,* 63 (3)**,** 239-247.
COOKE, A. J. & ROWE, R. K. 1999. Extension of Porosity and Surface Area Models for Uniform Porous Media. *Journal of Environmental Engineering,* 125 (2)**,** 126-136.
COOKE, A. J. & ROWE, R. K. 2008. 2D modelling of clogging in landfill leachate collection systems. *Canadian Geotechnical Journal,* 45 (10)**,** 1393-1409.
COOMBES, C. 1990. Reed bed treatment systems in Anglian Water. *In:* COOPER, P. F. & FINDLATER, B. C. (eds.) *Constructed Wetlands in Water Pollution Control.* Cambridge, UK: Pergamon Press, Oxford, UK, 223-234.
COOPER, D., GRIFFIN, P. & COOPER, P. 2005. Factors affecting the longevity of sub-surface horizontal flow systems operating as tertiary treatment for sewage effluent. *Water Science and Technology,* 51 (9)**,** 127-135.
COOPER, D., GRIFFIN, P. & COOPER, P. 2008. Factors affecting the longevity of sub-surface horizontal flow systems operating as tertiary treatment for sewage effluent. *In:* VYMAZAL, J. (ed.) *Wastewater Treatment, Plant Dynamics and Management in Constructed and Natural Wetlands.* Dordrecht, The Netherlands: Springer, 191-198.
COOPER, P. 2007. The Constructed Wetland Association UK database of constructed wetland systems. *Water Science and Technology,* 56 (3)**,** 1-6.
COOPER, P. & GREEN, B. 1995. Reed bed treatment systems for sewage treatment in the United Kingdom- the first 10 years' experience. *Water Science & Technology,* 32 (3)**,** 317-327.
COOPER, P. F. (ed.) 1990. *European Design and Operations Guidelines for Reed Bed Treatment Systems,* Swindon, UK: WRc.
COOPER, P. F. Performance of Vertical Flow Constructed Wetland systems with special reference to the significance of Oxygen Transfer and Hydraulic Loading Rates. Proceedings of the 9th International Conference on Wetland Systems for Water Pollution Control, 2004 Avignon, France.
COOPER, P. F. & COOPER, D. 2005. Evaluation of a Tidal Flow Reed Bed System for the Treatment of domestic sewage - Nitrification trials. *In:* VYMAZAL, J. (ed.) *Natural and Constructed Wetlands : Nutrients, Metals and Management.* Leiden: Backhuys, 222-232.
COOPER, P. F. & GREEN, B. 1998. United Kingdom. *In:* VYMAZAL, J., BRIX, H., COOPER, P. F., GREEN, M. B. & HABERL, R. (eds.) *Constructed Wetlands for Wastewater Treatment in Europe.* Leiden, The Netherlands: Backhuys Publishers,, 315-335.
COOPER, P. F., JOB, G. D. & GREEN, M. B. 1996. *Reed beds and constructed wetlands for wastewater treatment:* Swindon, United Kingdom, Water Research Centre
CORZO, A., PEDESCOLL, A., ÁLVAREZ, E. & GARCÍA, J. Solids accumulation and drainable porosity in experimental subsurface flow constructed wetlands with different primary treatments and operating strategies. *In:* BILLORE, S. K., DASS, P. &

VYMAZAL, J., eds. Proceedings of the 11th International Conference on Wetland Systems for Water Pollution Control, 1–7 November, 2008 Indore, India. Vikram University and IWA, 290-295.
CRAIG, R. F. 2004. *Craig's soil mechanics: 7th ed.,* Abingdon, Taylor & Francis.vii, 447 p.
CRITES, R. W. & TCHOBANOGLOUS, G. 1998. *Small and decentralized wastewater management systems:* Boston, WCB/McGraw-Hill.xix, 1084 p.
CUI, Y., WOOSTER, J. K., BAKER, P. F., DUSTERHOFF, S. R., SKLAR, L. S. & DIETRICH, W. E. 2008. Theory of Fine Sediment Infiltration into Immobile Gravel Bed. *Journal of Hydraulic Engineering,* 134 (10)**,** 1421-1429.
CWA 2006. Constructed Wetlands Interactive Database *In:* COOPER, P. F. & JOB, G. D. (eds.) 9.02 ed. Gloucestershire, United Kingdom: United Kingdom Constructed Wetland Association.
DANIEL, D. E. 1994. State-of-the-art: Laboratory hydraulic conductivity tests for saturated soils. *In:* DANIEL, D. E. & TRAUTWEIN, S. J. (eds.) *Hydraulic conductivity and waste contaminant transport in soil.* Philadelphia, PA: American Society for the Testing of Materials (ASTM), 30-78.
DARCY, H. 1856. Les fontaines publiques de la ville de Dijon. *Dalmont, Paris,* 647.
DEBEER, D. & STOODLEY, P. 1995. Relation between the structure of an aerobic biofilm and transport phenomena. *Water Sci. Technol.,* 32 (8)**,** 11-18.
DISERENS, E. 1934. Beitrag zur Bestimmung der Durchlässigkeit des Bodens in natürlicher Bodenlagerung. *Schweiz. Landw. Monatshefte,* 12**,** 1-19.
DITTRICH, E. 2006. Experiences on Hydraulic Performance of Sub-Surface Flow Constructed Wetlands. *Pollack Periodica,* 1 (1)**,** 53-66.
DORNELAS, F. L., MACHADO, M. B. & VON SPERLING, M. 2009. Performance evaluation of planted and unplanted subsurface-flow constructed wetlands for the post-treatment of UASB reactor effluents. *Water Science & Technology,* 60 (12)**,** 3025–3033.
DRURY, W. J. & MAINZHAUSEN, K. Hydraulic Characteristics of Subsurface Flow Wetlands. 2000 Billings Land Reclamation Symposium, March 20-24, 2000 2000 Billings, MT, USA
DUPIN, H. J., KITANIDIS, P. K. & MCCARTY, P. L. 2001. Simulations of two-dimensional modeling of biomass aggregate growth in network models. *Water Resources Research,* 37 (12)**,** 2981-2994.
DUPIN, H. J. & MCCARTY, P. L. 1999. Mesoscale and microscale observations of biological growth in a silicon pore imaging element. *ENVIRONMENTAL SCIENCE AND TECHNOLOGY-WASHINGTON DC-,* 33**,** 1230-1236.
EC/EWPCA 1990. *European Design and Operations Guidelines for Reed Bed Treatment Systems:* Swindon, UK, WRc
EINSTEIN, H. A. 1968. Deposition of suspended particles in a gravel bed. *Journal of the Hydraulics Division, American Society of Civil Engineers,* 95 (5)**,** 1197-1205.
ERGUN, S. 1952. Fluid flow through packed columns. *Chem. Eng. Prog.,* 48 (2)**,** 89-94.
FAN, L., RETI, H., WANG, W., LU, Z. & YANG, Z. 2008. Application of computational fluid dynamic to model the hydraulic performance of subsurface flow wetlands. *Journal of Environmental Sciences,* 20 (12)**,** 1415-1422.
FETTER, C. W., JR., SLOEY, W. E. & SPANGLER, F. L. 1976. Potential Replacement of Septic Tank Drain Fields by Artificial Marsh Wastewater Treatment Systems^a. *Ground Water,* 14 (6)**,** 396-402.
FISHER, P. J. 1990. Hydraulic characteristics of constructed wetlands at Richmond, NSW, Australia. *In:* COOPER, P. F. & FINDLATER, B. C. (eds.) *Constructed Wetlands in Water Pollution Control.* Cambridge, UK: Pergamon Press, Oxford, UK, 21-31.
FLEMING, I. R., ROWE, R. K. & CULLIMORE, D. R. 1999. Field observations of clogging in a landfill leachate collection system. *Canadian Geotechnical Journal,* 36 (4)**,** 685-707.

FLURY, M. & WAI, N. N. 2003. Dyes as tracers for vadose zone hydrology. *Reviews of Geophysics,* 41 (1)**,** 2-1.

FOGG, P. 2007. A novel approach to assess organic material accumulation in constructed reed beds: Phase 2. Nottingham, UK: ADAS UK Ltd.

FONDER, N. & HEADLEY, T. 2011. Systematic nomenclature and reporting for treatment wetlands. *In:* VYMAZAL, J. (ed.) *Water and Nutrient Management in Natural and Constructed Wetlands.* Dordrecht: Springer

FONDER, N. & XANTHOULIS, D. Influence of the media granular size of small pilot subsurface flow wetlands on axial dispersion and the hydraulic behaviour. 11th International Conference on Wetland Systems for Water Pollution Control, 1-7 November 2008 2008 Indore, India. Vikram University and IWA., 798-806.

FREIRE, F. G., DAVIES, L. C., VACAS, A. M., NOVAIS, J. M. & MARTINS-DIAS, S. 2009. Influence of operating conditions on the degradation kinetics of an azo-dye in a vertical flow constructed wetland using a simple mechanistic model. *Ecological Engineering,* 35 (10)**,** 1379-1386.

GARCÍA, J., CHIVA, J., AGUIRRE, P., ALVAREZ, E., SIERRA, J. P. & MUJERIEGO, R. 2004. Hydraulic behaviour of horizontal subsurface flow constructed wetlands with different aspect ratio and granular medium size. *Ecological Engineering,* 23 (3)**,** 177-187.

GARCÍA, J. & CORZO, A. 2008. Depuración con Humedales Construidos. Guía Práctica de Diseño, Construcción y Explotación de Sistemas de Humedales de Flujo Subsuperficial. Universitat Politècnica de Catalunya. Departament d'Enginyeria Hidràulica, Marítima i Ambiental.

GARCÍA, J., OJEDA, E., SALES, E., CHICO, F., PÍRIZ, T., AGUIRRE, P. & MUJERIEGO, R. 2003. Spatial variations of temperature, redox potential, and contaminants in horizontal flow reed beds. *Ecological Engineering,* 21 (2-3)**,** 129-142.

GARCÍA, J., ROUSSEAU, D., CASELLES-OSORIO, A., STORY, A., DE PAUW, N. & VANROLLEGHEM, P. 2007. Impact of prior physico-chemical treatment on the clogging process of subsurface flow constructed wetlands: Model-based evaluation. *Water, Air, and Soil Pollution,* 185 (1-4)**,** 101-109.

GERSBERG, R. M., ELKINS, B. V. & GOLDMAN, C. R. 1983. Nitrogen removal in artificial wetlands. *Water Research,* 17 (9)**,** 1009-1014.

GERSBERG, R. M., ELKINS, B. V. & GOLDMAN, C. R. 1984. Use of artificial wetlands to remove nitrogen from wastewater. *Journal (Water Pollution Control Federation),* 56 (2)**,** 152-156.

GIRALDI, D., DE MICHIELI VITTURI, M. & IANNELLI, R. 2010. FITOVERT: A dynamic numerical model of subsurface vertical flow constructed wetlands. *Environmental Modelling & Software,* 25 (5)**,** 633-640.

GOPAL, B. 1999. Natural and Constructed Wetlands for Wastewater Treatment: Potentials and Problems. *Water Science and Technology,* 40**,** 27-35.

GRAY, I. S. 2008. *An Evaluation of Floating Reed Beds, and Comparison with Gravel Reed Beds for Combined Domestic Tertiary / Storm Sewage Treatment.* Doctor of Philiosophy, University of Birmingham.

GREEN, M., SHAUL, N., BELIAVSKI, M., SABBAH, I., GHATTAS, B. & TARRE, S. 2006. Minimizing land requirement and evaporation in small wastewater treatment systems. *Ecological Engineering,* 26 (3)**,** 266-271.

GREEN, M. B. & MARTIN, J. R. 1996. Constructed reed beds clean up storm overflows on small wastewater treatment works. *Water environment research***,** 1054-1060.

GREEN, M. B., O'CONNELL, P. J. & GRIFFIN, P. 1998. Uprating and rescuing small wastewater treatment facilities by adding tertiary treatment reed beds. *Water environment research***,** 1307-1313.

GREEN, M. B. & UPTON, J. 1993. Reed bed treatment for small communities: UK experience. *In:* MOSHIRI, G. A. (ed.) *Constructed wetlands for water quality improvement.* Chelsea, MI: Lewis Publishers, 517-524.

GREEN, M. B. & UPTON, J. 1994. Constructed reed beds: a cost-effective way to polish wastewater effluents for small communities. *Water Environment Research,* 66 (3)**,** 188-192.

GREEN, M. B. & UPTON, J. 1995. Constructed reed beds: Appropriate technology for small communities. *Water Science and Technology,* 32 (3)**,** 339-348.

GRIFFIN, P. 2003. Ten years experience of treating all flows from combined sewerage systems using package plant and constructed wetland combinations. *Water Science & Technology,* 48 (11)**,** 93-99.

GRIFFIN, P. & PAMPLIN, C. 1998. The advantages of a constructed reed bed based strategy for small sewage treatment works. *Water Science and Technology,* 38**,** 143-150.

GRIFFIN, P., WILSON, L. & COOPER, D. Changes in the use, operation and design of sub-surface flow constructed wetlands in a major UK water utility. 11th International Conference on Wetland Systems for Water Pollution Control, 2008 Indore, India. Vikram University and IWA, 419-426.

GRISMER, M. E., TAUSENDSCHOEN, M. & SHEPHERD, H. L. 2001. Hydraulic characteristics of a subsurface flow constructed wetland for winery effluent treatment. *Water Environment Research,* 73 (4)**,** 466-477.

HABERL, R. & PERFLER, R. 1990. Seven years of research work and experience with wastewater treatment by a reed bed system. *In:* COOPER, P. F. & FINDLATER, B. C. (eds.) *Constructed Wetlands in Water Pollution Control.* Cambridge, UK: Pergamon Press, Oxford, UK, 205-214.

HE, Q. & MANKIN, K. R. 2001. Seasonal variations in hydraulic performance of rock-plant filters. *Environmental Technology,* 22 (9)**,** 991-999.

HEADLEY, T. R. & KADLEC, R. H. 2007. Conducting hydraulic tracer studies of constructed wetlands: a practical guide. *International Journal of Ecohydrology & Hydrobiology,* 7 (3-4)**,** 269-282.

HEDGES, P. D., FERMOR, P. M. & DUŠEK, J. 2008. The Hydrological Sustainability of Constructed Wetlands for Wastewater Treatment. *In:* VYMAZAL, J. (ed.) *Wastewater Treatment, Plant Dynamics and Management in Constructed and Natural Wetlands.* 111-120.

HERMANSSON, M. 1999. The DLVO theory in microbial adhesion. *Colloids and Surfaces B: Biointerfaces,* 14 (1-4)**,** 105-119.

HOLLAND, J. F., MARTIN, J. F., GRANATA, T., BOUCHARD, V., QUIGLEY, M. & BROWN, L. 2004. Effects of wetland depth and flow rate on residence time distribution characteristics. *Ecological Engineering,* 23 (3)**,** 189-203.

HORTON, D. 2003. *Review of tertiary and storm reed bed operation in Severn Trent Water.* MSc thesis, , Anglia Polytechnic University.

HUBBE, M. A., CHEN, H. & HEITMANN, J. A. 2009. PERMEABILITY REDUCTION PHENOMENA IN PACKED BEDS, FIBER MATS, AND WET WEBS OF PAPER EXPOSED TO FLOW OF LIQUIDS AND SUSPENSIONS: A REVIEW. *BioResources,* 4 (1)**,** 405-451.

HVORSLEV, M. J. 1951. Time lag and soil permeability in ground-water observations. US Army, Corps of engineers, Waterways experiment station.

HYÁNKOVÁ, E., KRIŠKA-DUNAJSKÝ, M., ROZKOŠNÝ, M. & SÁLEK, J. The Knowledge Based on the Research of the Filtration Properties of the Filter Media and on the Determination of Clogging Causes. 10th International Conference on Wetland Systems for Water Pollution Control, September 23-29 2006 Lisbon, Portugal. Ministério de Ambiente, do Ordenamento do Territórie do Desenvolvimento Regional (MAOTDR) and IWA, 1331-1338.

IDELCHIK, I. E. & FRIED, E. 1986. *Handbook of hydraulic resistance: Second Edition,* New York, NY, Hemisphere Publishing.Pages: 650.
INGEBRITSEN, S. E., NEUZIL, C. E. & SANFORD, W. E. 2006. *Groundwater in geologic processes: 2nd ed.,* Cambridge, Cambridge University Press.xxv, 536 p.
IVES, K. J. & PIENVICHITR, V. 1965. Kinetics of the filtration of dilute suspensions. *Chemical Engineering Science,* 20 (11)**,** 965-973.
IWA 2000. Constructed wetlands for pollution control : processes, performance, design and operation. *In:* KADLEC, R. H., KNIGHT, R. L., VYMAZAL, J., BRIX, H., COOPER, P. F. & HABERL, R. (eds.). IWA Publishing
IWASAKI, T. 1937. Some notes on sand filtration. *J. Am. Water Works Assoc,* 29 (10)**,** 1591-1602.
IWEMA, A., RABY, D., LESAVRE, J., BOUTIN, C., DODANE, P. H., LIENARD, A., MOLLE, P., BECK, C., SADOWSKI, A., MERLIN, G., DAP, S., OHRESSER, C., POULET, J. B., REEB, G., WERCKMANN, M. & ESSER, D. 2005. Épuration des eaux usées domestiques par filtres plantés de macrophytes. Recommandations techniques pour la conception et la réalisation.
KADLEC, R. H. 1989. Hydrologic factors in wetland water treatment. *In:* HAMMER, D. A. (ed.) *Constructed Wetlands for Wastewater Treatment: Municipal, Industrial and Agricultural.* Chelsea, Mich.: Lewis, 21-40.
KADLEC, R. H. 2000. The inadequacy of first-order treatment wetland models. *Ecological Engineering,* 15 (1-2)**,** 105-119.
KADLEC, R. H. 2009. Comparison of free water and horizontal subsurface treatment wetlands. *Ecological Engineering,* 35 (2)**,** 159-174.
KADLEC, R. H. & KNIGHT, R. L. 1996. *Treatment wetlands:* Boca Raton ; London, CRC.893p.
KADLEC, R. H. & WALLACE, S. 2010. *Treatment wetlands, Second Edition: 2nd,* Boca Raton, Fla., CRC ; London : Taylor & Francis [distributor].1 v.
KADLEC, R. H. & WATSON, J. T. 1993. Hydraulics and Solids Accumulation in a Gravel Bed Treatment Wetland. *In:* MOSHIRI, G. A. E. (ed.) *Constructed wetlands for water quality improvement : Conference : Selected papers.* Boca Raton: Lewis Pub, pp 227-235.
KAYSER, K. & KUNST, S. 2005. Processes in vertical-flow reed beds: Nitrification, oxygen transfer and soil clogging. *Water Science and Technology,* 51 (9)**,** 177-184.
KHATIWADA, N. R. & POLPRASERT, C. 1999. Assessment of Effective Specific Surface Area for Free Water Surface Constructed Wetlands. *Water Science and Technology,* 40**,** 83-89.
KICKUTH, R. W. Degradation and incoporation of of nutrients from rural wastewaters by plant rhizosphere under limnic conditions. Utilisation of manure by land spreading, 1977 London. Commision of the European Communities, 235-243.
KICKUTH, R. W. & KONEMANN, N. 1988. *Method for the purification of sewage waters* United States of America patent application.
KING, A. C., MITCHELL, C. A. & HOWES, T. 1997. Hydraulic tracer studies in a pilot scale subsurface flow constructed wetland. *Water Science and Technology,* 35 (5)**,** 189-196.
KIRSCHNER, ALEXANDER, K. T., RIEGL, BERNHARD, VELIMIROV & BRANKO 2001. Degradation of emergent and submerged macrophytes in an oxbow lake of an embanked backwater system : Implications for the terrestrialization process. *International Review of Hydrobiology,* 86 (4-5)**,** 555-571.
KJELLIN, J., WÖRMAN, A., JOHANSSON, H. & LINDAHL, A. 2007. Controlling factors for water residence time and flow patterns in Ekeby treatment wetland, Sweden. *Advances in Water Resources,* 30 (4)**,** 838-850.

KNIGHT, R. L., CLARKE, R. A. & BASTIAN, R. K. Treatment wetlands as habitat for wildlife and humans. Proceedings of the 7th IWA International Conference on Wetland Systems for Water Pollution Control, 2000 Orlando, FL, USA. 37-52.

KNOWLES, P. R. & DAVIES, P. A. 2009. A method for the in-situ determination of the hydraulic conductivity of gravels as used in constructed wetlands for wastewater treatment. *Desalination and Water Treatment,* 1 (5)**,** 257–266.

KNOWLES, P. R. & DAVIES, P. A. 2011. A Finite Element Approach to Modelling the Hydrological Regime in Horizontal Subsurface Flow Constructed Wetlands for Wastewater Treatment *In:* VYMAZAL, J. (ed.) *Water and Nutrient Management in Natural and Constructed Wetlands.* Dordrecht: Springer Science+Business Media B.V

KNOWLES, P. R., DOTRO, G. C., NIVALA, J. & GARCÍA, J. 2011. Clogging in subsurface-flow treatment wetlands: Occurrence, contributing factors, and management strategies. *Ecological Engineering,* 37 (2)**,** 99-112.

KNOWLES, P. R., GRIFFIN, P. & DAVIES, P. A. 2010. Complementary methods to investigate the development of clogging within a horizontal sub-surface flow tertiary treatment wetland. *Water Research,* 44 (1)**,** 320-330.

KOZENY, J. 1927. Ueber kapillare leitung des wassers im boden. *Sitzungsber. Akad. Wiss. Wien,* 136**,** 271-306.

KRUSE, J., LENNARTZ, B. & LEINWEBER, P. 2008. A modified method for measuring saturated hydraulic conductivity and anisotropy of fen peat samples. *Wetlands,* 28 (2)**,** 527-531.

LAHAV, O., ARTZI, E., TARRE, S. & GREEN, M. 2001. Ammonium removal using a novel unsaturated flow biological filter with passive aeration. *Water Research,* 35 (2)**,** 397-404.

LAKSHMAN, G. 1979. An ecosystem approach to the treatment of waste waters. *Journal of Environmental Quality,* 8 (3)**,** 353-361.

LANGERGRABER, G. 2003. Simulation of subsurface flow constructed wetlands-results and further research needs. *Water Science and Technology,* 48 (5)**,** 157-166.

LANGERGRABER, G. 2008. Modeling of processes in subsurface flow constructed wetlands: A review. *Vadose Zone Journal,* 7 (2)**,** 830-842.

LANGERGRABER, G., HABERL, R., LABER, J. & PRESSL, A. 2003. Evaluation of substrate clogging processes in vertical flow constructed wetlands. *Water Science and Technology,* 48 (5)**,** 25-34.

LANGERGRABER, G., ROUSSEAU, D. P. L., GARCÍA, J. & MENA, J. 2009. CWM1: a general model to describe biokinetic processes in subsurface flow constructed wetlands. *Water Science & Technology,* 59 (9)**,** 1687-1687.

LANGERGRABER, G. & ŠIMŮNEK, J. 2005. Modeling Variably Saturated Water Flow and Multicomponent Reactive Transport in Constructed Wetlands. *Vadose Zone Journal,* 4**,** 924-938.

LAPEN, D. R., MOORMAN, B. J. & PRICE, J. S. 1996. Using Ground-Penetrating Radar to Delineate Subsurface Features along a Wetland Catena. *Soil Sci Soc Am J,* 60 (3)**,** 923-931.

LEVENSPIEL, O. 1999. *Chemical reaction engineering: 3rd ed.,* New York ; Chichester, Wiley.xvi,668p.

LEVINE, A. D., TSCHOBANOGLOUS, G. & ASANO, T. 1991. Size distributions of particulate contaminants in wastewater and their impact on treatability. *Water Research,* 25 (8)**,** 911-922.

LIENARD, A., BOUTIN, C. & ESSER, D. 1990. Domestic wastewater treatment with emergent hydrophyte beds in France. *In:* COOPER, P. F. & FINDLATER, B. C. (eds.) *Constructed Wetlands in Water Pollution Control.* Cambridge, UK: Pergamon Press, Oxford, UK, 183-192.

LIENARD, A., BOUTIN, C. & ESSER, D. 1998. France. *In:* VYMAZAL, J., BRIX, H., COOPER, P. F., GREEN, M. B. & HABERL, R. (eds.) *Constructed Wetlands for Wastewater Treatment in Europe.* Leiden, The Netherlands: Backhuys Publishers, 153-167.

LIN, A. Y. C., DEBROUX, J. F., CUNNINGHAM, J. A. & REINHARD, M. 2003. Comparison of rhodamine WT and bromide in the determination of hydraulic characteristics of constructed wetlands. *Ecological Engineering,* 20 (1)**,** 75-88.

LLORENS, E., PUIGAGUT, J. & GARCÍA, J. 2009. Distribution and biodegradability of sludge accumulated in a full-scale horizontal subsurface-flow constructed wetland. *Desalination and Water Treatment,* 1 (4)**,** 54-58.

LLORENS, E., SAALTINK, M. W. & GARCÍA, J. 2011a. CWM1 implementation in RetrasoCodeBright: First results using horizontal subsurface flow constructed wetland data. *Chemical Engineering Journal,* 166 (1)**,** 224-232.

LLORENS, E., SAALTINK, M. W., POCH, M. & GARCÍA, J. 2011b. Bacterial transformation and biodegradation processes simulation in horizontal subsurface flow constructed wetlands using CWM1-RETRASO. *Bioresource technology,* 102 (2)**,** 928-936.

LÖFFLER, H. 1990. Human uses. *In:* PATTEN, B. C. (ed.) *Wetlands and Shallow Continental Water Bodies.* The Hague, The Netherlands: SPB Academic Publishing, 17-27.

LOGAN, B. E., JEWETT, D. G., ARNOLD, R. G., BOUWER, E. J. & O'MELIA, C. R. 1995. Clarification of Clean-Bed Filtration Models. *Journal of Environmental Engineering,* 121 (12)**,** 869-873.

LUTHIN, J. N. & KIRKHAM, D. O. N. 1949. A Piezometer Method for Measuring Permeability of Soil in Situ Below A Water Table. *Soil Science,* 68 (5)**,** 349-358.

MADIGAN, M. T., MARTINKO, J. M. & BROCK, T. D. B. O. M. 2006. *Brock biology of microorganisms: 11th ed.,* Upper Saddle River, NJ, Pearson Prentice Hall.p.

MALOSZEWSKI, P., WACHNIEW, P. & CZUPRYNSKI, P. 2006. Study of hydraulic parameters in heterogeneous gravel beds: Constructed wetland in Nowa Słupia (Poland). *Journal of Hydrology,* 331 (3-4)**,** 630-642.

MANDER, U. & JENSSEN, P. D. (eds.) 2003. *Constructed wetlands for waste water treatment in cold climates,* Southampton: WIT.

MARSILI-LIBELLI, S. & CHECCHI, N. 2005. Identification of dynamic models for horizontal subsurface constructed wetlands. *Ecological Modelling,* 187 (2-3)**,** 201-218.

MARTINEZ, C. J. & WISE, W. R. 2003. Analysis of constructed treatment wetland hydraulics with the transient storage model OTIS. *Ecological Engineering,* 20 (3)**,** 211-222.

MASCH, F. D. & DENNY, K. J. 1966. Grain Size Distribution and Its Effect on The Permeability of Unconsolidated Sands. *Water Resources Research,* 4 (2)**,** 665-677.

MASHAURI, D. A. & KAYOMBO, S. 2002. Application of the two coupled models for water quality management: facultative pond cum constructed wetland models. *Physics and Chemistry of the Earth, Parts A/B/C,* 27 (11-22)**,** 773-781.

MAYO, A. W. & BIGAMBO, T. 2005. Nitrogen transformation in horizontal subsurface flow constructed wetlands I: Model development. *Physics and Chemistry of the Earth, Parts A/B/C,* 30 (11-16)**,** 658-667.

MAYS, D. C. & HUNT, R. J. 2005. Hydrodynamic aspects of particle clogging in porous media. *Environ. Sci. Technol.,* 39 (2)**,** 577-584.

MCGECHAN, M. B., MOIR, S. E., SYM, G. & CASTLE, K. 2005. Estimating inorganic and organic nitrogen transformation rates in a model of a constructed wetland purification system for dilute farm effluents. *Biosystems engineering,* 91 (1)**,** 61-75.

MITSCH, W. J. & GOSSELINK, J. G. 2007. *Wetlands: 4th ed.,* Hoboken, N.J., Wiley ; Chichester : John Wiley [distributor].xi, 582 p.

MOLLE, P., LIENARD, A., BOUTIN, C., MERLIN, G. & IWEMA, A. 2005. How to treat raw sewage with constructed wetlands: an overview of the French systems. *Water Science & Technology* 51 (9)**,** 11-21.

MOLLE, P., LIÉNARD, A., GRASMICK, A. & IWEMA, A. 2006. Effect of reeds and feeding operations on hydraulic behaviour of vertical flow constructed wetlands under hydraulic overloads. *Water Research,* 40 (3)**,** 606-612.

MORRIS, R. H., NEWTON, M. I., KNOWLES, P. R., BENCSIK, M., DAVIES, P. A., GRIFFIN, P. & MCHALE, G. 2011. Analysis of clogging in constructed wetlands using magnetic resonance. *Analyst,* 136 (11)**,** 2283-2286.

MUÑOZ-CARPENA, R., REGALADO, C. M., ÁLVAREZ-BENEDI, J. & BARTOLI, F. 2002. Field evaluation of the new Philip-Dunne permeameter for measuring saturated hydraulic conductivity. *Soil Science,* 167 (1)**,** 9-24.

MUÑOZ, P., DRIZO, A. & CULLY HESSION, W. 2006. Flow patterns of dairy wastewater constructed wetlands in a cold climate. *Water Research,* 40 (17)**,** 3209-3218.

MURPHY, C. & COOPER, D. 2010. The Evolution of Horizontal Sub-Surface Flow Reed Bed Design for Tertiary Treatment of Sewage Effluents in the UK. *In:* VYMAZAL, J. (ed.) *Water and Nutrient Management in Natural and Constructed Wetlands.* Dordrecht: Springer

NAVFAC 1986. *Soil Mechanics. Design Manual 7.01:* Alexandria, Virginia, USA, Naval Facilities Engineering Command.389pp.

NETTER, R. & BISCHOFSBERGER, W. 1990. Hydraulic investigations on planted soil filters. *In:* COOPER, P. F. & FINDLATER, B. C. (eds.) *Constructed Wetlands in Water Pollution Control.* Cambridge, UK: Pergamon Press, Oxford, UK, 11-20.

NGUYEN, L. 2000. Organic matter composition, microbial biomass and microbial activity in gravel-bed constructed wetlands treating farm dairy wastewaters. *Ecological Engineering,* 16 (2)**,** 199-221.

NGUYEN, L. 2001. Accumulation of organic matter fractions in a gravel-bed constructed wetland. *Water Science and Technology,* 44 (11-12)**,** 281-287.

NIVALA, J., HOOS, M. B., CROSS, C., WALLACE, S. & PARKIN, G. 2007. Treatment of landfill leachate using an aerated, horizontal subsurface-flow constructed wetland. *Science of the Total Environment, The,* 380 (1-3)**,** 19-27.

NIVALA, J., KNOWLES, P. R., DOTRO, G. C., GARCÍA, J. & WALLACE, S. 2012. Clogging in subsurface-flow treatment wetlands: Measurement, modeling and management. *Water Research,* 46 (6)**,** 1625-1640.

NIVALA, J. A. 2005. *Treatment of landfill leachate using as enhanced subsurface-flow sontructed wetland.* MS, University of Iowa.

NUTTALL, P. M., BOON, A. G. & ROWELL, M. R. 1997. *Review of the design and management of constructed wetlands:* London, CIRIA.267p.

O'MELIA, C. R. & ALI, W. 1978. The role of retained particles in deep bed filtration. *Progress in Water Research,* 10 (5-6)**,** 167-182.

OJEDA, E., CALDENTEY, J., SAALTINK, M. W. & GARCÍA, J. 2008. Evaluation of relative importance of different microbial reactions on organic matter removal in horizontal subsurface-flow constructed wetlands using a 2D simulation model. *Ecological Engineering,* 34 (1)**,** 65-75.

ÖNORM-B-2505 1997. Bepflanzte Bodenfilter (Pflanzenkläranlagen) - Anwendung, Bemessung, Bau und Betrieb. Österreichisches Normungsinstitut, Vertrieb.

OOSTERBAAN, R. J., BOONSTRA, J. & RAO, K. 1996. The energy balance of groundwater flow. *In:* SINGH, V. P. & KUMAR, B. (eds.) *Subsurface-Water Hydrology.* The Netherlands: Kluwer Academic publishers, 153-160.

PARR, T. W. 1990. Factors affecting the reed (Phragmites Australis) growth in UK reed bed treatment systems. *In:* COOPER, P. F. & FINDLATER, B. C. (eds.) *Constructed Wetlands in Water Pollution Control.* Cambridge, UK: Pergamon Press, Oxford, UK, 67-76.

PAULY, U. 1990. Performance data of a wastewater sludge treatment plant derived from the rootzone method set against the background of detention times. *In:* COOPER, P. F. & FINDLATER, B. C. (eds.) *Constructed Wetlands in Water Pollution Control.* Cambridge, UK: Pergamon Press, Oxford, UK, 289-300.

PEDESCOLL, A. 24th February 2009 2009. *RE: Personal Communication.* Type to KNOWLES, P. R.

PEDESCOLL, A., UGGETTI, E., LLORENS, E., GRANÉS, F., GARCÍA, D. & GARCÍA, J. 2009. Practical method based on saturated hydraulic conductivity used to assess clogging in subsurface flow constructed wetlands. *Ecological Engineering,* 35 (8)**,** 1216-1224.

PERSSON, J., SOMES, N. L. G. & WONG, T. H. F. 1999. Hydraulic efficiency of constructed wetlands and ponds. *Water Science and Technology,* 40 (3)**,** 291-300.

PILGRIM, D. H., SCHULZ, T. J. & PILGRIM, I. D. 1992. Tracer investigation of the flow patterns in two field-scale constructed wetland units with subsurface flow. *3rd International Specialist Conference on Wetland Systems in Water Pollution Control***,** 191-199.

PLATZER, C. & MAUCH, K. 1997. Soil clogging in vertical flow reed beds - Mechanisms, parameters, consequences and.....solutions? *Water Science and Technology,* 35 (5)**,** 175-181.

PUIGAGUT, J., CASELLES-OSORIO, A., VAELLO, N. & GARCÍA, J. 2008. Fractionation, Biodegradability and Particle-Size Distribution of Organic Matter in Horizontal Subsurface-Flow Constructed Wetlands. *In:* VYMAZAL, J. (ed.) *Wastewater Treatment, Plant Dynamics and Management in Constructed and Natural Wetlands.* 289-297.

RAGUSA, S. R., MCNEVIN, D., QASEM, S. & MITCHELL, C. 2004. Indicators of biofilm development and activity in constructed wetlands microcosms. *Water Research,* 38 (12)**,** 2865-2873.

RANIERI, E. 2003. Hydraulics of sub-superficial flow constructed wetlands in semi arid climate conditions. *Water Science and Technology,* 47 (7-8)**,** 49-55.

RASH, J. K. & LIEHR, S. K. 1999. Flow pattern analysis of constructed wetlands treating landfill leachate. *Water Science and Technology,* 40 (3)**,** 309-315.

REED, S. C., CRITES, R. W. & MIDDLEBROOKS, E. J. 1995. *Natural systems for waste management and treatment: 2nd ed.,* New York ; London, McGraw-Hill.xi,433p.

REED, S. C., LEE, R. E. & BASTIAN, R. 1993. *Subsurface Flow Constructed Wetlands for Watewater Treatment: A Technology Assessment*, United States Environmental Protection Agency

RENARD, P., GENTY, A. & STAUFFER, F. 2001. Laboratory determination of the full permeability tensor. *J. Geophys. Res,* 160 (B11)**,** 26,443-426,452.

REYNOLDS, W. D. & ELRICK, D. E. 1986. A method for simultaneous in situ measurement in the vadose zone of field-saturated hydraulic conductivity, sorptivity and the conductivity-pressure head relationship. *Ground Water Monitoring Review,* 6 (1)**,** 84-95.

RITTMANN, B. E. & MCCARTY, P. L. 1980. Evaluation of steady-state-biofilm kinetics. *Biotechnology and Bioengineering,* 22 (11)**,** 2359-2373.

ROSA, E. & LAROCQUE, M. 2008. Investigating peat hydrological properties using field and laboratory methods: application to the Lanoraie peatland complex (southern Quebec, Canada). *Hydrological Processes,* 22 (12)**,** 1866-1875.

ROUSSEAU, D. P. L. 2005. *Performance of constructed treatment wetlands: modelbased evaluation and impact of operation and maintenance* PhD PhD, Ghent University, Belgium.

ROUSSEAU, D. P. L., GRIFFIN, P., VANROLLEGHEM, P. A. & DE PAUW, N. 2005a. Model study of short-term dynamics of secondary treatment reed beds at Saxby (Leicestershire,

UK). *Journal of Environmental Science and Health - Part A Toxic/Hazardous Substances and Environmental Engineering,* 40 (6-7)**,** 1479-1492.
ROUSSEAU, D. P. L., HORTON, D., GRIFFIN, P., VANROLLEGHEM, P. A. & DE PAUW, N. 2005b. Impact of operational maintenance on the asset life of storm reed beds. *Water Science and Technology,* 51 (9)**,** 243-250.
ROUSSEAU, D. P. L., LESAGE, E., STORY, A., VANROLLEGHEM, P. A. & DE PAUW, N. 2008. Constructed wetlands for water reclamation. *Desalination,* 218 (1-3)**,** 181-189.
ROUSSEAU, D. P. L., VANROLLEGHEM, P. A. & DE PAUW, N. 2004. Model-based design of horizontal subsurface flow constructed treatment wetlands: A review. *Water Research,* 38 (6)**,** 1484-1493.
RYBCZYK, J. M., DAY JR, J. W. & CONNER, W. H. 2002. The impact of wastewater effluent on accretion and decomposition in a subsiding forested wetland. *Wetlands,* 22 (1)**,** 18-32.
SANFORD, W. E., STEENHUIS, T. S., PARLANGE, J. Y., SURFACE, J. M. & PEVERLY, J. H. 1995a. Hydraulic conductivity of gravel and sand as substrates in rock-reed filters. *Ecological Engineering,* 4 (4)**,** 321-326.
SANFORD, W. E., STEENHUIS, T. S., SURFACE, J. M. & PEVERLY, J. H. 1995b. Flow characteristics of rock-reed filters for treatment of landfill leachate. *Ecological Engineering,* 5 (1)**,** 37-50.
SCHIFF, L. & JOHNSON, C. E. 1958. Some methods of alleviating surface clogging in water spreading with emphasis on filters. *Trans. Amer. Geophys. Un,* 39 (2)**,** 292-297.
SEIDEL, K. 1966. Reinigung von Gewässern durch höhere Pflanzen. *Naturwissenschaften,* 53 (12)**,** 289-297.
SEIDEL, K. 1976. Macrophytes and water purification. *In:* TOURBIER, J. & PIERSON JR., R. W. (eds.) *Biological Control of Water Pollution.* Philadelphia: University of Pennsylvania Press, 109-123.
SHAMY, U. E. & ZEGHAL, M. 2007. A micro-mechanical investigation of the dynamic response and liquefaction of saturated granular soils. *Soil Dynamics and Earthquake Engineering,* 27 (8)**,** 712-729.
SHEORAN, A. S. & SHEORAN, V. 2006. Heavy metal removal mechanism of acid mine drainage in wetlands: A critical review. *Minerals engineering,* 19 (2)**,** 105-116.
SHILTON, A. N. & PRASAD, J. N. 1996. Tracer studies of a gravel bed wetland. *Water Science and Technology,* 34 (4)**,** 421-425.
SIMI, A. L. & MITCHELL, C. A. 1999. Design and hydraulic performance of a constructed wetland treating oil refinery wastewater. *Water Science and Technology,* 40 (3)**,** 301-307.
SMITH, G. N. & SMITH, G. N. 1990. *Elements of soil mechanics: 6th ed.*, BSP Professional.[xii,506]p.
SPANGLER, F. L., SLOEY, W. E. & FETTER, C. W., JR. Artificial and Natural Marshes as Wastewater Treatment Systems in Winsconsin. *In:* TILTON, D. L., KADLEC, R. H. & RICHARDSON, C. J., eds. Proceedings of Freshwater Wetlands and Swwage Effluent Disposal, 1976 Ann Arbor, Michigan. University of Michigan, 215-240.
SPEER, S., CHAMPAGNE, P., CROLLA, A. & KINSLEY, C. Hydrodynamic Pathways in a Maturing Constructed Wetland. 8th International Conference on Wetland Systems for Water Pollution Control, September 26-30 2006 2004 Avignon, France.
STEINER, G. R. & FREEMAN JR., R. J. 1989. Configuration and Substrate Design Considerations for Constructed Wetlands for Wastewater Treatment. *In:* HAMMER, D. A. (ed.) *Constructed wetlands for wastewater treatment : municipal, industrial and agricultural.* Chelsea, Mich.: Lewis, 363-377.

SULIMAN, F., FRENCH, H. K., HAUGEN, L. E. & SØVIK, A. K. 2006a. Change in flow and transport patterns in horizontal subsurface flow constructed wetlands as a result of biological growth. *Ecological Engineering,* 27 (2)**,** 124-133.

SULIMAN, F., FUTSAETHER, C., OXAAL, U., HAUGEN, L. E. & JENSSEN, P. 2006b. Effect of the inlet-outlet positions on the hydraulic performance of horizontal subsurface-flow wetlands constructed with heterogeneous porous media. *Journal of Contaminant Hydrology,* 87 (1-2)**,** 22-36.

SUN, G., ZHAO, Y. & ALLEN, S. 2007. An Alternative Arrangement of Gravel Media in Tidal Flow Reed Beds Treating Pig Farm Wastewater. *Water, Air, & Soil Pollution,* 182 (1)**,** 13-19.

SURRIDGE, B. W. J., BAIRD, A. J. & HEATHWAITE, A. L. 2005. Evaluating the quality of hydraulic conductivity estimates from piezometer slug tests in peat. *Hydrological Processes,* 19 (6)**,** 1227-1244.

SWIFT, D. L. & FRIEDLANDER, S. K. 1964. The coagulation of hydrosols by brownian motion and laminar shear flow* 1. *Journal of Colloid Science,* 19 (7)**,** 621-647.

TANNER, C. C. 1994. Growth and nutrition of Schoenoplectus validus in agricultural wastewaters. *Aquatic botany,* 47 (2)**,** 131-153.

TANNER, C. C. & SUKIAS, J. P. 1995. Accumulation of organic solids in gravel-bed constructed wetlands. *Water Science and Technology,* 32 (3)**,** 229-239.

TANNER, C. C., SUKIAS, J. P. S. & UPSDELL, M. P. 1998. Organic matter accumulation during maturation of gravel-bed constructed wetlands treating farm dairy wastewaters. *Water Research,* 32 (10)**,** 3046-3054.

TAYLOR, S. W., MILLY, P. C. D. & JAFFE, P. R. 1990. Biofilm growth and the related changes in the physical properties of a porous medium. 2. Permeability. *Water Resources Research,* 26 (9)**,** 2161-2169.

TCHOBANOGLOUS, G. 1993. Constructed Wetlands and Aquatic Plant Systems: Research, Design, Operational and Monitoring Issues. *In:* MOSHIRI, G. A. E. (ed.) *Constructed wetlands for water quality improvement : Conference : Selected papers.* Boca Raton: Lewis Pub, pp 23-34.

TCHOBANOGLOUS, G. Preliminary treatment in Constructed Wetlands. *In:* DIAS, V. N. & VYMAZAL, J., eds. 1st International Seminar on the Use of Aquatic Macrophytes for Wastewater Treatment in Constructed Wetlands, 2003 Lisbon, Portugal. Instituto da Conservação de Natureza, Instituo Nacional de Água., 13-33.

THEIS, C. V. 1935. The relation between the lowering of the piezometric surface and the rate and duration of discharge of a well using groundwater storage. *Trans. Amer. Geophys. Union,* 16 (1)**,** 519–524.

THULLNER, M. 2010. Comparison of bioclogging effects in saturated porous media within one- and two-dimensional flow systems. *Ecological Engineering,* 36 (2)**,** 176-196.

TIETZ, A., KIRSCHNER, A., LANGERGRABER, G., SLEYTR, K. & HABERL, R. 2007. Characterisation of microbial biocoenosis in vertical subsurface flow constructed wetlands. *Science of The Total Environment,* 380 (1-3)**,** 163-172.

TOSCANO, A., LANGERGRABER, G., CONSOLI, S. & CIRELLI, G. L. 2009. Modelling pollutant removal in a pilot-scale two-stage subsurface flow constructed wetlands. *Ecological Engineering,* 35 (2)**,** 281-289.

TUFENKJI, N. 2007. Modeling microbial transport in porous media: Traditional approaches and recent developments. *Advances in Water Resources,* 30 (6-7)**,** 1455-1469.

TVA 1993. *General design, construction and operation guidelines: Constructed wetlands wastewater treatment systems for small users including individual residences, 2nd Edition*, Tennessee Valley Authority (TVA) Resource Group Water Management: Chattanooga, Tennessee

USEPA 1988. Design Manual: Constructed wetlands and aquatic plant systems for municipal wastewater treatment. Cincinnati, OH: U.S. EPA Office of Water.
USEPA 1993. Subsurface flow constructed wetlands for wastewater treatment: A technology assessment. U.S. EPA Office of Water: Washington, D.C., United Staes.
USEPA 2000. Constructed wetlands treatment of municipal wastewaters. U.S. EPA Office of Research and Development: Washington, D.C., United Staes.
USEPA 2002. Onsite Wastewater Treatment Systems Manual. U.S. EPA Office of Research and Development: Washington, D.C., United Staes.
VAN GENUCHTEN, M. T. 1980. A closed-form equation for predicting the hydraulic conductivity of unsaturated soils. *Soil Sci. Soc. Am. J,* 44 (5)**,** 892-898.
VANDEVIVERE, P. & BAVEYE, P. 1992a. Effect of bacterial extracellular polymers on the saturated hydraulic conductivity of sand columns. *Applied and Environmental Microbiology,* 58 (5)**,** 1690.
VANDEVIVERE, P. & BAVEYE, P. 1992b. Relationship between transport of bacteria and their clogging efficiency in sand columns. *Applied and Environmental Microbiology,* 58 (8)**,** 2523.
VANDEVIVERE, P. & BAVEYE, P. 1992c. Saturated hydraulic conductivity reduction caused by aerobic bacteria in sand columns. *Soil Science Society of America Journal,* 56 (1)**,** 1.
VYMAZAL, J. 1996. The use of subsurface-flow constructed wetlands for wastewater treatment in the Czech Republic. *Ecological Engineering,* 7 (1)**,** 1-14.
VYMAZAL, J. 2001. Types of constructed wetlands for wastewater treatment: their potential for nutrient removal. *In:* VYMAZAL, J. (ed.) *Transformations of nutrients in natural and constructed wetlands.* Netherlands: Backhuys, 1-93.
VYMAZAL, J. Types of Constructed Wetlands. *In:* DIAS, V. N. & VYMAZAL, J., eds. 1st International Seminar on the Use of Aquatic Macrophytes for Wastewater Treatment in Constructed Wetlands, 2003 Lisbon, Portugal. Instituto da Conservação de Natureza, Instituo Nacional de Água., 35-79.
VYMAZAL, J., BRIX, H., COOPER, P. F., GREEN, M. B. & HABERL, R. (eds.) 1998. *Constructed wetlands for wastewater treatment in Europe,* Leiden: Backhuys.
VYMAZAL, J. & KROPFELOVA, L. 2008. *Wastewater treatment in constructed wetlands with horizontal sub-surface flow:* Dordrecht, The Netherlands, Springer.xiv, 566 p.
WALLACE, S. D. 2001. *System for Removing Pollutants from Water*. United States of America patent application.
WALLACE, S. D. & KNIGHT, R. L. 2006. *Small-scale constructed wetland treatment systems : feasibility, design criteria and O & M requirements*, Water Environment Research Foundation (WERF), Virginia, Alexandria.1 v. (various pagings).
WANG, H. & JAWITZ, J. W. 2006. Hydraulic analysis of cell-network treatment wetlands. *Journal of Hydrology,* 330 (3-4)**,** 721-734.
WANKO, A., TAPIA, G., MOSE, R. & GREGOIRE, C. 2009. Adsorption distribution impact on preferential transport within horizontal flow constructed wetland(HFCW). *Ecological Modelling,* 220 (23)**,** 3342-3352.
WATERS, M. T., PILGRIM, D. H., SCHULZ, T. J. & PILGRIM, I. D. Variability of hydraulic response of constructed wetlands. Proceedings - National Conference on Hydraulic Engineering, 1993. 406-411.
WATSON, J. T. & CHOATE, K. D. Hydraulic conductivity of onsite constructed wetlands. On-Site Wastewater Treatment, Proceedings of the Ninth National Symposium on Individual and Small Community Sewage Systems, 2001 St. Joseph, Michigan. 631-648.
WATSON, J. T., CHOATE, K. D. & STEINER, G. R. 1990. Performance of Constructed Wetland Treatment Systems at Benton, Hardin and Pembroke, Kentucky, during the early vegetation establishment. *In:* COOPER, P. F. & FINDLATER, B. C. (eds.) *Constructed*

Wetlands in Water Pollution Control. Cambridge, UK: Pergamon Press, Oxford, UK, 171-182.

WATSON, J. T. & HOBSON, J. A. 1989. Hydraulic Design Considerations and Control Structure for Constructed Wetlands for Wastewater Treatment. *In:* HAMMER, D. A. (ed.) *Constructed wetlands for wastewater treatment : municipal, industrial and agricultural.* Chelsea, Mich.: Lewis, 379-391.

WERF 2006. Small-Scale Constructed Wetland Treatment Systems Database. *In:* WALLACE, S. D. & KNIGHT, R. L. (eds.). Project 01-CTS-5. Compiled by J.A.Nivala and R.A.Clarke.

WERNER, T. M. & KADLEC, R. H. 2000. Wetland residence time distribution modeling. *Ecological Engineering,* 15 (1-2)**,** 77-90.

WILSON, L. 2007. Reed Beds: Factors Affecting Asset Life and Current Operation. Severn Trent Water.

WINTER, K. J. & GOETZ, D. 2003. The impact of sewage composition on the soil clogging phenomena of vertical flow constructued wetlands. *Water Science and Technology,* 48 (5)**,** 9-14.

WOLVERTON, B. 1982. Hybrid wastewater treatment system using anaerobic microorganisms and reed (Phragmites communis). *Economic Botany,* 36 (4)**,** 373-380.

WORRALL, P., PEBERDY, K. J. & MILLETT, M. C. 1997. Constructed wetlands and nature conservation. *Water Science and Technology,* 35 (5)**,** 205-213.

WYNN, T. M. & LIEHR, S. K. 2001. Development of a constructed subsurface-flow wetland simulation model. *Ecological Engineering,* 16 (4)**,** 519-536.

YAO, K.-M., HABIBIAN, M. T. & O'MELIA, C. R. 1971. Water and waste water filtration. Concepts and applications. *Environmental Science & Technology,* 5 (11)**,** 1105-1112.

ZACHRITZ, W. H. & FULLER, J. W. 1993. Performance of an Artificial Wetlands Filter Treating Facultative Lagoon Effluent at Carville, Louisiana. *Water Environment Research,* 65 (1)**,** 46-52.

ZAMANI, A. & MAINI, B. 2009. Flow of dispersed particles through porous media -- Deep bed filtration. *Journal of Petroleum Science and Engineering,* 69 (1-2)**,** 71-88.

ZHAO, Y. Q., SUN, G. & ALLEN, S. J. 2004. Anti-sized reed bed system for animal wastewater treatment: a comparative study. *Water Research,* 38 (12)**,** 2907-2917.

ZHU, T., JENSSEN, P. D., MAEHLUM, T. & KROGSTAD, T. 1997. Phosphorus sorption and chemical characteristics of lightweight aggregates (LWA)-potential filter media in treatment wetlands. *Water Science and Technology,* 35 (5)**,** 103-108.

ZOELLER, K. E. & BYERS, M. E. 1999. *Patent: Wastewater treatment system. United States US 5,897,777. October 3, 1997.* United States patent application.

ZURITA, F., LÓPEZ, Z., DE ANDA, J. & BELMONT, M. A. The use of commercial-valuable ornamental plants in subsurface flow constructed wetlands. 11th International Conference on Wetland Systems for Water Pollution Control, 1-7 November 2008 2008 Indore, India. Vikram University and IWA, 328-335.

Appendices

Appendix A.1 Field Results – Northend (February 2007). See Section 5.1

Position	h_T	Δt	$\Delta D_{(rsvr)}$	Q	k_T
	cm	s	cm	cm^3/s	m/d
A1	14.1	1,459	2.6	0.62	7.52
A2	10	1,383	2.2	0.55	9.47
A3	12.6	569	2.8	1.70	23.25
A4	10.4	200	9.5	16.45	271.91
B1	10.2	1,110	15.8	4.93	83.08
B2	11.9	1,515	14.8	3.38	48.87
B3	10	844	9.2	3.78	64.90
B4	7.5	159	12	26.14	599.09
C1	10	3,473	7.5	0.75	12.86
C2	9	2,977	6	0.70	13.33
C3	9.2	297	2.8	3.27	61.01
C4	9.8	261	10.8	14.33	251.38

Appendix A.2 Field Results – Gaydon (March 2007). See Section 5.2

Position	h_T	Δt	$\Delta D_{(rsvr)}$	Q	k_T
	cm	s	cm	cm^3/s	m/d
A1	6	4080	3	0.28	8.026
A2	7.6	3,600	0.3	0.03	0.653
A3	24.8	2,980	2.1	0.24	1.692
A4	25.3	263	7.5	9.88	67.1
B1	7.8	2,712	0.5	0.06	1.4
B2	24.2	2,239	0.5	0.08	0.5
B3	25.3	2,323	1.1	0.16	1.1
B4	26.3	257	12.4	16.71	109.2
C1	10	1757	0.1	0.02	0.34
C2	25.7	2,534	1.5	0.21	1.4
C3	26.2	266	15.5	20.18	132.4
C4	25.8	365	13.4	12.72	84.7

Appendix A.3 Field Results – Knightcote (March 2007). See Section 5.3

Position	h_T	Δt	$\Delta D_{(rsvr)}$	Q	k_T
	cm	s	cm	cm^3/s	m/d
A1	6.8	3,180	10.7	1.17	18.5
A2	12.2	1,220	0.1	0.03	0.5
A3	13.2	2,955	3.8	0.45	7.1
A4	13.8	445	16	12.45	198.2
B1	11.8	2,185	12.3	1.95	31.0
B2	12.5	100	54.6	140.23	2231.9
B3	14	149	54.6	93.96	1495.5
B4	14.1	215	54.6	65.23	1038.2
C1	10.8	1,260	10.4	2.86	45.5
C2	12.8	120	54.6	116.38	1852.2
C3	13.1	88	11	43.30	689.1
C4	13.4	97	54.6	143.37	2281.8

Appendix A.4 Field Results – Fenny Compton (February 2007). See Section 5.4

Position	h_T	Δt	$\Delta D_{(rsvr)}$	Q	k_T
	cm	s	cm	cm^3/s	m/d
A1	70	1,860	21.8	4.1	58.56
A2	138	3,600	0.1	0.010	0.09
A3	75	36	54.6	393.0	6,035.93
A4	57	73	54.6	192.4	4,572.58
B1	101	96	54.6	146.5	1,845.48
B2	88	473	54.6	29.6	442.27
B3	129	268	54.6	52.2	466.36
B4	91	50	54.6	280.5	4,249.32
C1	46	1,080	23.6	7.6	195.85
C2	91	1,440	18.8	4.5	67.26
C3	112	230	54.6	63.5	621.52
C4	73	105	54.6	133.4	1,907.83

Appendix A.5 Field Results – Fenny Compton (February 2008). See Section 5.5

FENNY COMPTON - FEB 08			Point	A1	Measuring Depth (mm)			
Measurements (see Chapter 4)			(See Fig 4-6)		400	300	200	100
$D_{1(rsvr)}$	cm	0.0	1	mm	200	200	200	200
$D_{2(rsvr)}$	cm	5.0	2	mm	62	58	57	53
Δt	s	63	3	mm	82	92	132	153
$\Delta D_{(rsvr)}$	cm	5.0	4	mm	50	50	50	50
Q	m^3/d	140	$h_{T(probe)}$	mm	88	92	94	97
$h_{T(ave)}$	mm	93	h_n	mm	20	35	75	101
k_T	m/d	73.91	Δh_n	mm	14	40	26	101
			k_n	m/d	343.8	484.7	172.8	273.7

FENNY COMPTON - FEB 08			Point	A2	Measuring Depth (mm)			
Measurements (see Chapter 4)			(See Fig 4-6)		400	300	200	100
$D_{1(rsvr)}$	cm	0.0	1	mm	200	200	200	200
$D_{2(rsvr)}$	cm	4.0	2	mm	22	18	22	18
Δt	s	234	3	mm	23	58	119	146
$\Delta D_{(rsvr)}$	cm	4.0	4	mm	50	50	50	50
Q	m^3/d	112	$h_{T(probe)}$	mm	129	132	129	132
$h_{T(ave)}$	mm	130	h_n	mm	1	41	98	128
k_T	m/d	11.38	Δh_n	mm	40	57	30	128
			k_n	m/d	1,242.76	37.73	26.13	49.86

FENNY COMPTON - FEB 08			Point	A3	Measuring Depth (mm)			
Measurements (see Chapter 4)			(See Fig 4-6)		400	300	200	100
$D_{1(rsvr)}$	cm	0.0	1	mm	300	300	300	200
$D_{2(rsvr)}$	cm	3.0	2	mm	100	115	110	5
Δt	s	131	3	mm	100	188	242	146
$\Delta D_{(rsvr)}$	cm	3.0	4	mm	58	58	58	58
Q	m^3/d	84	$h_{T(probe)}$	mm	158	143	148	153
$h_{T(ave)}$	mm	151	h_n	mm	1	73	132	141
k_T	m/d	13.48	Δh_n	mm	72	59	9	141
			k_n	m/d	3,110	27	34	227

FENNY COMPTON - FEB 08			Point	A4	Measuring Depth (mm)			
Measurements (see Chapter 4)			(See Fig 4-6)		400	300	200	100
$D_{1(rsvr)}$	cm	0.0	1	mm	200	200	200	200
$D_{2(rsvr)}$	cm	12.0	2	mm	27	32	22	25
Δt	s	42	3	mm	25	74	106	121
$\Delta D_{(rsvr)}$	cm	12.0	4	mm	20	20	20	20
Q	m^3/d	337	$h_{T(probe)}$	mm	93	88	98	95
$h_{T(ave)}$	mm	93	h_n	mm	2	41	83	96
k_T	m/d	266.69	Δh_n	mm	39	42	12	96
			k_n	m/d	10,823	574	598	2,010

FENNY COMPTON - FEB 08			Point	A5	Measuring Depth (mm)			
Measurements (see Chapter 4)			(See Fig 4-6)		400	300	200	100
$D_{1(rsvr)}$	cm	0.0	1	mm	200	200	200	200
$D_{2(rsvr)}$	cm	11.0	2	mm	58	40	44	45
Δt	s	32	3	mm	57	113	121	125
$\Delta D_{(rsvr)}$	cm	11.0	4	mm	20	20	20	20
Q	m^3/d	309	$h_{T(probe)}$	mm	63	80	76	76
$h_{T(ave)}$	mm	73	h_n	mm	1	73	77	81
k_T	m/d	395.31	Δh_n	mm	72	5	3	81
			k_n	m/d	14,599	418	6,623	9,232

FENNY COMPTON - FEB 08			Point	B1	Measuring Depth (mm)			
Measurements (see Chapter 4)			(See Fig 4-6)		400	300	200	100
$D_{1(rsvr)}$	cm	0.0	1	mm	200	200	200	200
$D_{2(rsvr)}$	cm	2.0	2	mm	50	45	41	45
Δt	s	60	3	mm	63	120	137	142
$\Delta D_{(rsvr)}$	cm	2.0	4	mm	31	31	31	31
Q	m^3/d	56	$h_{T(probe)}$	mm	81	86	90	86
$h_{T(ave)}$	mm	86	h_n	mm	13	75	95	97
k_T	m/d	33.29	Δh_n	mm	62	20	2	97
			k_n	m/d	221.99	46.90	143.25	1,817.54

FENNY COMPTON - FEB 08			Point	B2	Measuring Depth (mm)			
Measurements (see Chapter 4)			(See Fig 4-6)		400	300	200	100
$D_{1(rsvr)}$	cm	0.0	1	mm	200	200	200	200
$D_{2(rsvr)}$	cm	7.0	2	mm	40	43	43	38
Δt	s	20	3	mm	59	79	115	140
$\Delta D_{(rsvr)}$	cm	7.0	4	mm	27	27	27	27
Q	m^3/d	197	$h_{T(probe)}$	mm	87	84	84	89
$h_{T(ave)}$	mm	86	h_n	mm	18	36	72	101
k_T	m/d	356.58	Δh_n	mm	18	35	30	101
			k_n	m/d	1,668.56	1,696.37	862.56	1,028.11

FENNY COMPTON - FEB 08			Point	B3	Measuring Depth (mm)			
Measurements (see Chapter 4)			(See Fig 4-6)		400	300	200	100
$D_{1(rsvr)}$	cm	0.0	1	mm	200	200	200	200
$D_{2(rsvr)}$	cm	7.0	2	mm	43	42	33	36
Δt	s	35	3	mm	46	79	134	139
$\Delta D_{(rsvr)}$	cm	7.0	4	mm	24	24	24	24
Q	m^3/d	197	$h_{T(probe)}$	mm	81	82	91	88
$h_{T(ave)}$	mm	86	h_n	mm	3	37	101	103
k_T	m/d	200.25	Δh_n	mm	34	64	2	103
			k_n	m/d	6,462	512	273	9,183

FENNY COMPTON - FEB 08			Point	B4	Measuring Depth (mm)			
Measurements (see Chapter 4)			(See Fig 4-6)		400	300	200	100
$D_{1(rsvr)}$	cm	0.0	1	mm	-	-	-	-
$D_{2(rsvr)}$	cm	0.0	2	mm	-	-	-	-
Δt	s	0	3	mm	-	-	-	-
$\Delta D_{(rsvr)}$	cm	0.0	4	mm	-	-	-	-
Q	m^3/d	0	$h_{T(probe)}$	mm	-	-	-	-
$h_{T(ave)}$	mm	0	h_n	mm	-	-	-	-
k_T	m/d	0.00	Δh_n	mm	-	-	-	-
			k_n	m/d	-	-	-	-

FENNY COMPTON - FEB 08			Point	B5	Measuring Depth (mm)			
Measurements (see Chapter 4)			(See Fig 4-6)		400	300	200	100
$D_{1(rsvr)}$	cm	0.0	1	mm	250	250	250	200
$D_{2(rsvr)}$	cm	8.0	2	mm	47	48	49	6
Δt	s	61	3	mm	48	94	170	166
$\Delta D_{(rsvr)}$	cm	8.0	4	mm	56	56	56	56
Q	m^3/d	225	$h_{T(probe)}$	mm	159	158	157	150
$h_{T(ave)}$	mm	156	h_n	mm	1	47	121	160
k_T	m/d	73.80	Δh_n	mm	46	74	39	160
			k_n	m/d	22,883	249	154	294

FENNY COMPTON - FEB 08			Point	C1	Measuring Depth (mm)			
Measurements (see Chapter 4)			(See Fig 4-6)		400	300	200	100
$D_{1(rsvr)}$	cm	0.0	1	mm	200	200	200	200
$D_{2(rsvr)}$	cm	6.0	2	mm	13	17	15	16
Δt	s	60	3	mm	16	83	85	84
$\Delta D_{(rsvr)}$	cm	6.0	4	mm	35	35	35	35
Q	m^3/d	169	$h_{T(probe)}$	mm	122	118	120	119
$h_{T(ave)}$	mm	120	h_n	mm	3	120	127	129
k_T	m/d	73.38	Δh_n	mm	117	7	1	129
			k_n	m/d	2,978	74	1,193	6,322

FENNY COMPTON - FEB 08			Point	C2	Measuring Depth (mm)			
Measurements (see Chapter 4)			(See Fig 4-6)		400	300	200	100
$D_{1(rsvr)}$	cm	0.0	1	mm	200	200	200	200
$D_{2(rsvr)}$	cm	2.8	2	mm	19	21	17	18
Δt	s	125	3	mm	19	35	138	140
$\Delta D_{(rsvr)}$	cm	2.8	4	mm	35	35	35	35
Q	m^3/d	79	$h_{T(probe)}$	mm	116	115	118	117
$h_{T(ave)}$	mm	117	h_n	mm	0	15	121	122
k_T	m/d	16.76	Δh_n	mm	15	106	1	122
			k_n	m/d	1,243	38	26	50

FENNY COMPTON - FEB 08			Point	C3	Measuring Depth (mm)			
Measurements (see Chapter 4)			(See Fig 4-6)		400	300	200	100
$D_{1(rsvr)}$	cm	0.0	1	mm	250	250	250	200
$D_{2(rsvr)}$	cm	4.0	2	mm	39	38	34	-
Δt	s	279	3	mm	38	58	178	157
$\Delta D_{(rsvr)}$	cm	4.0	4	mm	53	53	53	53
Q	m^3/d	112	$h_{T(probe)}$	mm	164	165	169	153
$h_{T(ave)}$	mm	163	h_n	mm	1	20	144	157
k_T	m/d	7.71	Δh_n	mm	19	124	13	157
			k_n	m/d	8,259.84	27.26	33.86	226.52

FENNY COMPTON - FEB 08			Point	C4	Measuring Depth (mm)			
Measurements (see Chapter 4)			(See Fig 4-6)		400	300	200	100
$D_{1(rsvr)}$	cm	0.0	1	mm	200	200	200	200
$D_{2(rsvr)}$	cm	12.0	2	mm	5	5	5	5
Δt	s	42	3	mm	6	26	118	164
$\Delta D_{(rsvr)}$	cm	12.0	4	mm	50	50	50	50
Q	m^3/d	337	$h_{T(probe)}$	mm	145	145	145	145
$h_{T(ave)}$	mm	145	h_n	mm	1	21	113	159
k_T	m/d	266.69	Δh_n	mm	20	92	45	159
			k_n	m/d	2,051	574	598	2,010

FENNY COMPTON - FEB 08			Point	C5	Measuring Depth (mm)			
Measurements (see Chapter 4)			(See Fig 4-6)		400	300	200	100
$D_{1(rsvr)}$	cm	0.0	1	mm	200	200	200	200
$D_{2(rsvr)}$	cm	11.0	2	mm	15	9	14	17
Δt	s	32	3	mm	31	44	126	130
$\Delta D_{(rsvr)}$	cm	11.0	4	mm	15	15	15	15
Q	m^3/d	309	$h_{T(probe)}$	mm	100	106	102	99
$h_{T(ave)}$	mm	102	h_n	mm	16	36	113	114
k_T	m/d	395.31	Δh_n	mm	19	77	1	114
			k_n	m/d	4,609	418	6,623	9,232

FENNY COMPTON - FEB 08			Point	D1	Measuring Depth (mm)			
Measurements (see Chapter 4)			(See Fig 4-6)		400	300	200	100
$D_{1(rsvr)}$	cm	0.0	1	mm	-	-	-	-
$D_{2(rsvr)}$	cm	0.0	2	mm	-	-	-	-
Δt	s	0	3	mm	-	-	-	-
$\Delta D_{(rsvr)}$	cm	0.0	4	mm	-	-	-	-
Q	m^3/d	0	$h_{T(probe)}$	mm	-	-	-	-
$h_{T(ave)}$	mm	0	h_n	mm	-	-	-	-
k_T	m/d	0.00	Δh_n	mm	-	-	-	-
			k_n	m/d	-	-	-	-

FENNY COMPTON - FEB 08			Point	D2	Measuring Depth (mm)			
Measurements (see Chapter 4)			(See Fig 4-6)		400	300	200	100
$D_{1(rsvr)}$	cm	0.0	1	mm	200	200	200	200
$D_{2(rsvr)}$	cm	0.0	2	mm	50	50	50	50
Δt	s	600	3	mm	177	185	186	182
$\Delta D_{(rsvr)}$	cm	0.0	4	mm	50	50	50	50
Q	m^3/d	9	$h_{T(probe)}$	mm	180	180	180	180
$h_{T(ave)}$	mm	180	h_n	mm	127	135	136	132
k_T	m/d	0.25	Δh_n	mm	177	8	1	-
			k_n	m/d	0	6	45	0

FENNY COMPTON - FEB 08			Point	D3	Measuring Depth (mm)			
Measurements (see Chapter 4)			(See Fig 4-6)		400	300	200	100
$D_{1(rsvr)}$	cm	0.0	1	mm	200	200	200	200
$D_{2(rsvr)}$	cm	8.5	2	mm	50	50	50	50
Δt	s	113	3	mm	57	189	190	192
$\Delta D_{(rsvr)}$	cm	8.5	4	mm	50	50	50	50
Q	m^3/d	239	$h_{T(probe)}$	mm	180	180	180	180
$h_{T(ave)}$	mm	180	h_n	mm	7	139	140	142
k_T	m/d	36.46	Δh_n	mm	57	132	1	2
			k_n	m/d	115	50	6,562	3,281

FENNY COMPTON - FEB 08			Point	D4	Measuring Depth (mm)			
Measurements (see Chapter 4)			(See Fig 4-6)		400	300	200	100
$D_{1(rsvr)}$	cm	0.0	1	mm	200	200	200	200
$D_{2(rsvr)}$	cm	0.0	2	mm	60	48	48	49
Δt	s	29	3	mm	51	82	119	138
$\Delta D_{(rsvr)}$	cm	0.0	4	mm	50	50	50	50
Q	m^3/d	1210	$h_{T(probe)}$	mm	90	102	102	101
$h_{T(ave)}$	mm	99	h_n	mm	1	35	71	89
k_T	m/d	1293.87	Δh_n	mm	34	37	17	89
			k_n	m/d	6,382	2,989	3,591	7,575

FENNY COMPTON - FEB 08			Point	D5	Measuring Depth (mm)			
Measurements (see Chapter 4)			(See Fig 4-6)		400	300	200	100
$D_{1(rsvr)}$	cm	0.0	1	mm	200	200	200	200
$D_{2(rsvr)}$	cm	6.5	2	mm	75	57	28	30
Δt	s	16	3	mm	77	64	132	138
$\Delta D_{(rsvr)}$	cm	6.5	4	mm	35	35	35	35
Q	m^3/d	183	$h_{T(probe)}$	mm	61	78	107	105
$h_{T(ave)}$	mm	88	h_n	mm	2	7	105	108
k_T	m/d	368.44	Δh_n	mm	5	97	3	108
			k_n	m/d	16,983	7,133	366	10,490

Appendix A.6 Field Results – Fenny Compton (February 2009). See Section 5.6

FENNY COMPTON - FEB 2009			Point	A1	Measuring Depth (mm)			
Measurements (see Chapter 4)			(See Fig 4-6)		400	300	200	100
$D_{1(rsvr)}$	cm	5.5	1	mm	200	200	200	100
$D_{2(rsvr)}$	cm	9.0	2	mm	52	49	48	
Δt	s	136	3	mm	52	49	102	71
$\Delta D_{(rsvr)}$	cm	3.5	4	mm	9	9	9	9
Q	m^3/d	98	$h_{T(probe)}$	mm	139	143	143	
$h_{T(ave)}$	mm	141	h_n	mm	139	142	89	20
k_T	m/d	96.82	Δh_n	mm	3	53	70	20
			k_n	m/d	1,141	65	49	173

FENNY COMPTON - FEB 2009			Point	A2	Measuring Depth (mm)			
Measurements (see Chapter 4)			(See Fig 4-6)		400	300	200	100
$D_{1(rsvr)}$	cm	15.0	1	mm	200	200	200	150
$D_{2(rsvr)}$	cm	20.0	2	mm	36	29	42	
Δt	s	89	3	mm	42	107	124	74
$\Delta D_{(rsvr)}$	cm	5.0	4	mm	14	14	11	14
Q	m^3/d	140	$h_{T(probe)}$	mm	150	157	147	
$h_{T(ave)}$	mm	151	h_n	mm	145	79	65	62
k_T	m/d	197.66	Δh_n	mm	65	15	3	62
			k_n	m/d	115	512	2,576	121

FENNY COMPTON - FEB 2009			Point	A3	Measuring Depth (mm)			
Measurements (see Chapter 4)			(See Fig 4-6)		400	300	200	100
$D_{1(rsvr)}$	cm	7.0	1	mm	200	200	200	150
$D_{2(rsvr)}$	cm	12.0	2	mm	59	67	59	
Δt	s	89	3	mm	61	99	124	74
$\Delta D_{(rsvr)}$	cm	5.0	4	mm	6	6	4	6
Q	m^3/d	140	$h_{T(probe)}$	mm	135	127	137	
$h_{T(ave)}$	mm	133	h_n	mm	133	95	72	71
k_T	m/d	224.93	Δh_n	mm	38	23	2	71
			k_n	m/d	197	328	4,670	106

FENNY COMPTON - FEB 2009			Point	A4	Measuring Depth (mm)			
Measurements (see Chapter 4)			(See Fig 4-6)		400	300	200	100
$D_{1(rsvr)}$	cm	4.0	1	mm	200	200	200	150
$D_{2(rsvr)}$	cm	10.0	2	mm	3	4	14	
Δt	s	222	3	mm	3	7	53	87
$\Delta D_{(rsvr)}$	cm	6.0	4	mm	4	4	4	4
Q	m^3/d	169	$h_{T(probe)}$	mm	193	192	182	
$h_{T(ave)}$	mm	189	h_n	mm	194	189	143	60
k_T	m/d	76.04	Δh_n	mm	4	46	84	60
			k_n	m/d	817	79	43	60

FENNY COMPTON - FEB 2009			Point	B1	Measuring Depth (mm)			
Measurements (see Chapter 4)			(See Fig 4-6)		400	300	200	100
$D_{1(rsvr)}$	cm	7.5	1	mm	200	200	200	150
$D_{2(rsvr)}$	cm	18.0	2	mm	67	77	65	
Δt	s	126	3	mm	71	87	127	86
$\Delta D_{(rsvr)}$	cm	10.5	4	mm	28	22	31	31
Q	m^3/d	295	$h_{T(probe)}$	mm	105	101	104	
$h_{T(ave)}$	mm	103	h_n	mm	101	91	42	33
k_T	m/d	428.73	Δh_n	mm	10	49	9	33
			k_n	m/d	1,167	225	1,245	334

FENNY COMPTON - FEB 2009			Point	B2	Measuring Depth (mm)			
Measurements (see Chapter 4)			(See Fig 4-6)		400	300	200	100
$D_{1(rsvr)}$	cm	6.6	1	mm	200	200	200	150
$D_{2(rsvr)}$	cm	16.0	2	mm	62	71	51	
Δt	s	275	3	mm	57	85	123	73
$\Delta D_{(rsvr)}$	cm	9.4	4	mm	15	25	19	13
Q	m^3/d	264	$h_{T(probe)}$	mm	118	109	131	
$h_{T(ave)}$	mm	119	h_n	mm	124	96	60	59
k_T	m/d	152.45	Δh_n	mm	28	36	1	59
			k_n	m/d	163	126	4,546	78

FENNY COMPTON - FEB 2009			Point	B3	Measuring Depth (mm)			
Measurements (see Chapter 4)			(See Fig 4-6)		400	300	200	100
$D_{1(rsvr)}$	cm	0.0	1	mm	200	200	200	150
$D_{2(rsvr)}$	cm	0.1	2	mm	50	55	69	
Δt	s	10000	3	mm	57	62	126	87
$\Delta D_{(rsvr)}$	cm	0.1	4	mm	20	20	18	20
Q	m^3/d	3	$h_{T(probe)}$	mm	130	125	113	
$h_{T(ave)}$	mm	122	h_n	mm	123	118	57	43
k_T	m/d	0.04	Δh_n	mm	5	62	13	43
			k_n	m/d	0.29	0.02	0.10	0.03

FENNY COMPTON - FEB 2009			Point	B4	Measuring Depth (mm)			
Measurements (see Chapter 4)			(See Fig 4-6)		400	300	200	100
$D_{1(rsvr)}$	cm	4.4	1	mm	200	200	200	150
$D_{2(rsvr)}$	cm	9.0	2	mm	53	56	60	
Δt	s	240	3	mm	55	57	84	98
$\Delta D_{(rsvr)}$	cm	4.6	4	mm	29	40	23	23
Q	m^3/d	129	$h_{T(probe)}$	mm	118	104	117	
$h_{T(ave)}$	mm	113	h_n	mm	116	103	93	29
k_T	m/d	90.31	Δh_n	mm	13	10	64	29
			k_n	m/d	190	260	40	87

FENNY COMPTON - FEB 2009			Point	C1	Measuring Depth (mm)			
Measurements (see Chapter 4)			(See Fig 4-6)		400	300	200	100
$D_{1(rsvr)}$	cm	6.4	1	mm	200	200	200	150
$D_{2(rsvr)}$	cm	7.7	2	mm	73	89	82	
Δt	s	242	3	mm	74	82	86	74
$\Delta D_{(rsvr)}$	cm	1.3	4	mm	18	15	11	11
Q	m^3/d	37	$h_{T(probe)}$	mm	109	96	108	
$h_{T(ave)}$	mm	104	h_n	mm	108	103	103	65
k_T	m/d	27.42	Δh_n	mm	5	1	38	65
			k_n	m/d	152	893	19	11

FENNY COMPTON - FEB 2009			Point	C2	Measuring Depth (mm)			
Measurements (see Chapter 4)			(See Fig 4-6)		400	300	200	100
$D_{1(rsvr)}$	cm	10.7	1	mm	250	250	250	150
$D_{2(rsvr)}$	cm	10.8	2	mm	56	62	59	
Δt	s	10000	3	mm	61	57	144	74
$\Delta D_{(rsvr)}$	cm	0.1	4	mm	11	8	19	9
Q	m^3/d	3	$h_{T(probe)}$	mm	183	180	173	
$h_{T(ave)}$	mm	179	h_n	mm	178	185	87	67
k_T	m/d	0.03	Δh_n	mm	7	98	20	67
			k_n	m/d	0.19	0.01	0.07	0.02

FENNY COMPTON - FEB 2009			Point	C3	Measuring Depth (mm)			
Measurements (see Chapter 4)			(See Fig 4-6)		400	300	200	100
$D_{1(rsvr)}$	cm	0.0	1	mm	200	200	200	150
$D_{2(rsvr)}$	cm	0.1	2	mm	30	30	41	
Δt	s	10000	3	mm	51	32	143	84
$\Delta D_{(rsvr)}$	cm	0.1	4	mm	26	29	27	26
Q	m^3/d	3	$h_{T(probe)}$	mm	145	141	132	
$h_{T(ave)}$	mm	139	h_n	mm	123	139	30	40
k_T	m/d	0.04	Δh_n	mm	16	109	10	40
			k_n	m/d	0.08	0.01	0.13	0.03

FENNY COMPTON - FEB 2009			Point	C4	Measuring Depth (mm)			
Measurements (see Chapter 4)			(See Fig 4-6)		400	300	200	100
$D_{1(rsvr)}$	cm	17.2	1	mm	200	200	200	150
$D_{2(rsvr)}$	cm	20.5	2	mm	58	65	58	
Δt	s	41	3	mm	59	78	81	74
$\Delta D_{(rsvr)}$	cm	3.3	4	mm	22	19	19	21
Q	m^3/d	93	$h_{T(probe)}$	mm	120	117	123	
$h_{T(ave)}$	mm	120	h_n	mm	119	103	100	55
k_T	m/d	357.00	Δh_n	mm	15	4	45	55
			k_n	m/d	700	3,058	239	194

FENNY COMPTON - FEB 2009			Point	D1	Measuring Depth (mm)			
Measurements (see Chapter 4)			(See Fig 4-6)		400	300	200	100
$D_{1(rsvr)}$	cm	4.8	1	mm	200	200	250	150
$D_{2(rsvr)}$	cm	4.9	2	mm	9	13	35	
Δt	s	460	3	mm	11	13	141	62
$\Delta D_{(rsvr)}$	cm	0.1	4	mm	16	16	25	31
Q	m^3/d	3	$h_{T(probe)}$	mm	175	171	190	
$h_{T(ave)}$	mm	178	h_n	mm	173	172	84	57
k_T	m/d	0.65	Δh_n	mm	2	87	28	57
			k_n	m/d	19.3	0.3	1.0	0.5

FENNY COMPTON - FEB 2009			Point	D2	Measuring Depth (mm)			
Measurements (see Chapter 4)			(See Fig 4-6)		400	300	200	100
$D_{1(rsvr)}$	cm	8.9	1	mm	200	200	200	150
$D_{2(rsvr)}$	cm	9.0	2	mm	13	11	11	
Δt	s	10000	3	mm	16	54	122	81
$\Delta D_{(rsvr)}$	cm	0.1	4	mm	18	29	26	22
Q	m^3/d	3	$h_{T(probe)}$	mm	169	160	163	
$h_{T(ave)}$	mm	164	h_n	mm	166	117	52	47
k_T	m/d	0.03	Δh_n	mm	49	65	5	47
			k_n	m/d	0.03	0.02	0.27	0.03

FENNY COMPTON - FEB 2009			Point	D3	Measuring Depth (mm)			
Measurements (see Chapter 4)			(See Fig 4-6)		400	300	200	100
$D_{1(rsvr)}$	cm	15.0	1	mm	200	200	200	150
$D_{2(rsvr)}$	cm	17.5	2	mm	36	37	27	
Δt	s	143	3	mm	43	71	92	51
$\Delta D_{(rsvr)}$	cm	2.5	4	mm	25	15	15	14
Q	m^3/d	70	$h_{T(probe)}$	mm	139	148	158	
$h_{T(ave)}$	mm	149	h_n	mm	132	114	93	86
k_T	m/d	62.58	Δh_n	mm	18	21	7	86
			k_n	m/d	133	109	318	27

FENNY COMPTON - FEB 2009			Point	D4	Measuring Depth (mm)			
Measurements (see Chapter 4)			(See Fig 4-6)		400	300	200	100
$D_{1(rsvr)}$	cm	10.0	1	mm	200	200	200	150
$D_{2(rsvr)}$	cm	17.0	2	mm	43	16	13	
Δt	s	199	3	mm	38	125	124	78
$\Delta D_{(rsvr)}$	cm	7.0	4	mm	23	25	23	20
Q	m^3/d	197	$h_{T(probe)}$	mm	134	159	164	
$h_{T(ave)}$	mm	152	h_n	mm	139	50	53	52
k_T	m/d	122.76	Δh_n	mm	89	3	1	52
			k_n	m/d	53	1,799	6,683	90

Appendix A.7 Field Results – Fenny Compton (March 2010). See Section 5.7

FENNY COMPTON - MAR 2010			**Point**	**A1**	***Measuring Depth (mm)***			
Measurements (see Chapter 4)			***(See Fig 4-6)***		**400**	**300**	**200**	**100**
$D_{1(rsvr)}$	cm	12.3	***1***	mm	190	190	190	70
$D_{2(rsvr)}$	cm	13.9	***2***	mm	18	24	23	
Δt	s	979	***3***	mm	15	23	23	3
$\Delta D_{(rsvr)}$	cm	1.6	***4***	mm	68	63	65	65
Q	m^3/d	45	$h_{T(probe)}$	mm	104	103		
$h_{T(ave)}$	mm	104	h_n	mm	107	104	102	2
k_T	m/d	8.40	Δh_n	mm	3	2	100	2
			k_n	m/d	72	109	2	109

FENNY COMPTON - MAR 2010			**Point**	**A2**	***Measuring Depth (mm)***			
Measurements (see Chapter 4)			***(See Fig 4-6)***		**400**	**300**	**200**	**100**
$D_{1(rsvr)}$	cm	6.2	***1***	mm	200	200	200	50
$D_{2(rsvr)}$	cm	7.3	***2***	mm	17	21	17	
Δt	s	559	***3***	mm	19	22	117	4
$\Delta D_{(rsvr)}$	cm	1.1	***4***	mm	48	47	46	45
Q	m^3/d	31	$h_{T(probe)}$	mm	135	132	137	
$h_{T(ave)}$	mm	135	h_n	mm	133	131	37	1
k_T	m/d	7.77	Δh_n	mm	2	94	36	1
			k_n	m/d	131	3	7	262

FENNY COMPTON - MAR 2010			**Point**	**A3**	***Measuring Depth (mm)***			
Measurements (see Chapter 4)			***(See Fig 4-6)***		**400**	**300**	**200**	**100**
$D_{1(rsvr)}$	cm	8.0	***1***	mm	180	180	180	90
$D_{2(rsvr)}$	cm	23.3	***2***	mm	20	16	14	
Δt	s	96	***3***	mm	28	78	102	16
$\Delta D_{(rsvr)}$	cm	15.3	***4***	mm	62	66	68	72
Q	m^3/d	430	$h_{T(probe)}$	mm	98	98	98	
$h_{T(ave)}$	mm	98	h_n	mm	90	36	10	2
k_T	m/d	865.12	Δh_n	mm	54	26	8	2
			k_n	m/d	393	815	2,649	10,598

FENNY COMPTON - MAR 2010			**Point**	**A4**	***Measuring Depth (mm)***			
Measurements (see Chapter 4)			***(See Fig 4-6)***		**400**	**300**	**200**	**100**
$D_{1(rsvr)}$	cm	10.0	***1***	mm	170	170	170	50
$D_{2(rsvr)}$	cm	22.0	***2***	mm	20	23	18	
Δt	s	152	***3***	mm	19	29	76	5
$\Delta D_{(rsvr)}$	cm	12.0	***4***	mm	40	46	41	43
Q	m^3/d	337	$h_{T(probe)}$	mm	110	101	111	
$h_{T(ave)}$	mm	107	h_n	mm	111	95	53	2
k_T	m/d	391.28	Δh_n	mm	16	3	51	2
			k_n	m/d	656	250	206	5,250

FENNY COMPTON - MAR 2010			Point	B1	Measuring Depth (mm)			
Measurements (see Chapter 4)			(See Fig 4-6)		400	300	200	100
$D_{1(rsvr)}$	cm	21.1	1	mm	210	210	210	50
$D_{2(rsvr)}$	cm	26.2	2	mm	13	20	15	
Δt	s	1318	3	mm	16	25	122	5
$\Delta D_{(rsvr)}$	cm	5.1	4	mm	44	48	43	43
Q	m^3/d	143	$h_{T(probe)}$	mm	153	142	152	
$h_{T(ave)}$	mm	149	h_n	mm	150	137	45	2
k_T	m/d	13.81	Δh_n	mm	13	92	43	2
			k_n	m/d	40	6	12	257

FENNY COMPTON - MAR 2010			Point	B2	Measuring Depth (mm)			
Measurements (see Chapter 4)			(See Fig 4-6)		400	300	200	100
$D_{1(rsvr)}$	cm	8.0	1	mm	200	200	200	65
$D_{2(rsvr)}$	cm	14.0	2	mm	20	23	23	
Δt	s	118	3	mm	23	104	120	4
$\Delta D_{(rsvr)}$	cm	6.0	4	mm	57	57	57	60
Q	m^3/d	169	$h_{T(probe)}$	mm	123	120	120	
$h_{T(ave)}$	mm	121	h_n	mm	120	39	23	1
k_T	m/d	223.55	Δh_n	mm	7	16	22	1
			k_n	m/d	83	423	307	6,762

FENNY COMPTON - MAR 2010			Point	B3	Measuring Depth (mm)			
Measurements (see Chapter 4)			(See Fig 4-6)		400	300	200	100
$D_{1(rsvr)}$	cm	19.5	1	mm	210	210	210	50
$D_{2(rsvr)}$	cm	23.0	2	mm	24	26	22	
Δt	s	166	3	mm	21	32	148	4
$\Delta D_{(rsvr)}$	cm	3.5	4	mm	42	40	44	44
Q	m^3/d	98	$h_{T(probe)}$	mm	144	144	144	
$h_{T(ave)}$	mm	144	h_n	mm	147	138	18	2
k_T	m/d	77.89	Δh_n	mm	16	120	10	2
			k_n	m/d	312	23	175	1,402

FENNY COMPTON - MAR 2010			Point	B4	Measuring Depth (mm)			
Measurements (see Chapter 4)			(See Fig 4-6)		400	300	200	100
$D_{1(rsvr)}$	cm	8.0	1	mm	200	200	200	70
$D_{2(rsvr)}$	cm	16.0	2	mm	12	14	15	
Δt	s	154	3	mm	9	27	121	16
$\Delta D_{(rsvr)}$	cm	8.0	4	mm	59	55	55	53
Q	m^3/d	225	$h_{T(probe)}$	mm	129	131	130	
$h_{T(ave)}$	mm	130	h_n	mm	132	118	24	1
k_T	m/d	212.57	Δh_n	mm	14	94	23	1
			k_n	m/d	493	73	300	6,909

FENNY COMPTON - MAR 2010			Point	C1	Measuring Depth (mm)			
Measurements (see Chapter 4)			(See Fig 4-6)		400	300	200	100
$D_{1(rsvr)}$	cm	4.0	1	mm	200	200	200	60
$D_{2(rsvr)}$	cm	6.2	2	mm	20	12	3	
Δt	s	1159	3	mm	10	20	28	3
$\Delta D_{(rsvr)}$	cm	2.2	4	mm	45	48	52	56
Q	m^3/d	62	$h_{T(probe)}$	mm	135	140	145	
$h_{T(ave)}$	mm	140	h_n	mm	145	132	120	1
k_T	m/d	7.21	Δh_n	mm	13	12	119	1
			k_n	m/d	19	21	2	252

FENNY COMPTON - MAR 2010			Point	C2	Measuring Depth (mm)			
Measurements (see Chapter 4)			(See Fig 4-6)		400	300	200	100
$D_{1(rsvr)}$	cm	10.0	1	mm	210	200	200	50
$D_{2(rsvr)}$	cm	14.4	2	mm	25	17	14	
Δt	s	1259	3	mm	24	37	142	6
$\Delta D_{(rsvr)}$	cm	4.4	4	mm	49	44	44	43
Q	m^3/d	124	$h_{T(probe)}$	mm	136	139		
$h_{T(ave)}$	mm	138	h_n	mm	137	119	14	1
k_T	m/d	13.52	Δh_n	mm	18	105	13	1
			k_n	m/d	26	4	36	465

FENNY COMPTON - MAR 2010			Point	C3	Measuring Depth (mm)			
Measurements (see Chapter 4)			(See Fig 4-6)		400	300	200	100
$D_{1(rsvr)}$	cm	7.9	1	mm	200	200	200	50
$D_{2(rsvr)}$	cm	15.5	2	mm	14	13	13	
Δt	s	276	3	mm	12	18	142	6
$\Delta D_{(rsvr)}$	cm	7.6	4	mm	39	36	37	38
Q	m^3/d	214	$h_{T(probe)}$	mm	147	151		
$h_{T(ave)}$	mm	149	h_n	mm	149	146	21	6
k_T	m/d	98.31	Δh_n	mm	3	125	15	6
			k_n	m/d	1,221	29	244	610

FENNY COMPTON - MAR 2010			Point	C4	Measuring Depth (mm)			
Measurements (see Chapter 4)			(See Fig 4-6)		400	300	200	100
$D_{1(rsvr)}$	cm	14.0	1	mm	150	150	150	60
$D_{2(rsvr)}$	cm	25.0	2	mm	19	11	7	
Δt	s	27	3	mm	22	35	82	5
$\Delta D_{(rsvr)}$	cm	11.0	4	mm	42	42	42	42
Q	m^3/d	309	$h_{T(probe)}$	mm	89	97	101	
$h_{T(ave)}$	mm	96	h_n	mm	86	73	26	13
k_T	m/d	2265.43	Δh_n	mm	13	47	13	13
			k_n	m/d	4,168	1,153	4,168	4,168

FENNY COMPTON - MAR 2010			Point	D1	Measuring Depth (mm)			
Measurements (see Chapter 4)			(See Fig 4-6)		400	300	200	100
$D_{1(rsvr)}$	cm	20.0	1	mm	200	200	200	60
$D_{2(rsvr)}$	cm	24.5	2	mm	40	38	37	
Δt	s	132	3	mm	42	39	61	5
$\Delta D_{(rsvr)}$	cm	4.5	4	mm	51	55	53	54
Q	m^3/d	126	$h_{T(probe)}$	mm	109	107	110	
$h_{T(ave)}$	mm	109	h_n	mm	107	106	86	1
k_T	m/d	166.89	Δh_n	mm	3	20	85	1
			k_n	m/d	4,534	227	53	4,534

FENNY COMPTON - MAR 2010			Point	D2	Measuring Depth (mm)			
Measurements (see Chapter 4)			(See Fig 4-6)		400	300	200	100
$D_{1(rsvr)}$	cm	6.5	1	mm	230	230	230	50
$D_{2(rsvr)}$	cm	12.5	2	mm	25	20	17	
Δt	s	270	3	mm	30	32	168	8
$\Delta D_{(rsvr)}$	cm	6.0	4	mm	41	41	46	41
Q	m^3/d	169	$h_{T(probe)}$	mm	164	169	167	
$h_{T(ave)}$	mm	167	h_n	mm	159	157	16	1
k_T	m/d	70.93	Δh_n	mm	2	141	15	1
			k_n	m/d	1,478	21	197	2,955

FENNY COMPTON - MAR 2010			Point	D3	Measuring Depth (mm)			
Measurements (see Chapter 4)			(See Fig 4-6)		400	300	200	100
$D_{1(rsvr)}$	cm	5.8	1	mm	250	250	250	175
$D_{2(rsvr)}$	cm	11.1	2	mm	27	21	24	
Δt	s	1422	3	mm	22	199	195	136
$\Delta D_{(rsvr)}$	cm	5.3	4	mm	38	38	44	32
Q	m^3/d	117	$h_{T(probe)}$	mm	185	191	182	
$h_{T(ave)}$	mm	186	h_n	mm	190	13	11	7
k_T	m/d	8.35	Δh_n	mm	177	2	4	7
			k_n	m/d	2	194	97	55

FENNY COMPTON - MAR 2010			Point	D4	Measuring Depth (mm)			
Measurements (see Chapter 4)			(See Fig 4-6)		400	300	200	100
$D_{1(rsvr)}$	cm	14.0	1	mm	200	200	200	175
$D_{2(rsvr)}$	cm	20.0	2	mm	28	28	28	
Δt	s	27	3	mm	30	57	119	98
$\Delta D_{(rsvr)}$	cm	6.0	4	mm	69	66	70	70
Q	m^3/d	169	$h_{T(probe)}$	mm	103	106		
$h_{T(ave)}$	mm	105	h_n	mm	101	77	11	7
k_T	m/d	1131.24	Δh_n	mm	24	66	4	7
			k_n	m/d	1,231	448	7,388	4,222

FENNY COMPTON - MAR 2010			Point	E1	Measuring Depth (mm)			
Measurements (see Chapter 4)			(See Fig 4-6)		400	300	200	100
$D_{1(rsvr)}$	cm	19.9	1	mm	210	210	210	70
$D_{2(rsvr)}$	cm	20.2	2	mm	13	14	15	
Δt	s	894	3	mm	12	115	154	9
$\Delta D_{(rsvr)}$	cm	0.3	4	mm	54	55	51	59
Q	m^3/d	8	$h_{T(probe)}$	mm	143	141	144	
$h_{T(ave)}$	mm	143	h_n	mm	144	40	5	2
k_T	m/d	1.25	Δh_n	mm	3	35	3	2
			k_n	m/d	0.43	1.28	14.88	22.31

FENNY COMPTON - MAR 2010			Point	E2	Measuring Depth (mm)			
Measurements (see Chapter 4)			(See Fig 4-6)		400	300	200	100
$D_{1(rsvr)}$	cm	5.0	1	mm	230	230	230	55
$D_{2(rsvr)}$	cm	11.5	2	mm	33	25	15	
Δt	s	273	3	mm	36	94	158	13
$\Delta D_{(rsvr)}$	cm	6.5	4	mm	34	35	42	39
Q	m^3/d	183	$h_{T(probe)}$	mm	163	170	173	
$h_{T(ave)}$	mm	169	h_n	mm	160	101	30	3
k_T	m/d	75.09	Δh_n	mm	59	71	27	3
			k_n	m/d	54	45	117	1,055

FENNY COMPTON - MAR 2010			Point	E3	Measuring Depth (mm)			
Measurements (see Chapter 4)			(See Fig 4-6)		400	300	200	100
$D_{1(rsvr)}$	cm	9.1	1	mm	210	210	210	175
$D_{2(rsvr)}$	cm	16.0	2	mm	18	19	16	
Δt	s	23	3	mm	35	82	132	104
$\Delta D_{(rsvr)}$	cm	6.9	4	mm	63	62	62	62
Q	m^3/d	194	$h_{T(probe)}$	mm	129	129	132	
$h_{T(ave)}$	mm	130	h_n	mm	112	66	16	9
k_T	m/d	1227.61	Δh_n	mm	46	50	7	9
			k_n	m/d	867	798	5,700	4,433

FENNY COMPTON - MAR 2010			Point	E4	Measuring Depth (mm)			
Measurements (see Chapter 4)			(See Fig 4-6)		400	300	200	100
$D_{1(rsvr)}$	cm	9.0	1	mm	220	220	220	175
$D_{2(rsvr)}$	cm	18.0	2	mm	34	35	27	
Δt	s	39	3	mm	35	61	142	117
$\Delta D_{(rsvr)}$	cm	9.0	4	mm	61	58	62	55
Q	m^3/d	253	$h_{T(probe)}$	mm	125	127		
$h_{T(ave)}$	mm	126	h_n	mm	124	101	16	3
k_T	m/d	974.29	Δh_n	mm	23	85	13	3
			k_n	m/d	1,334	361	2,361	10,230

Appendix A.8 Field Results – Moreton Morrell (July 2008). See Section 5.8

MORETON MORRELL - July 2008			**Point**	**A1**	***Measuring Depth (mm)***			
Measurements (see Chapter 4)			***(See Fig 4-6)***		**400**	**300**	**200**	**100**
$D_{1(rsvr)}$	cm	19.8	***1***	mm	250	250	250	100
$D_{2(rsvr)}$	cm	19.9	***2***	mm	35	74	61	-
Δt	s	1586	***3***	mm	40	77	94	60
$\Delta D_{(rsvr)}$	cm	0.1	***4***	mm	20	5	10	15
Q	m^3/d	3	$h_{T(probe)}$	mm	195	172	179	
$h_{T(ave)}$	mm	182	h_n	mm	190	168	146	25
k_T	m/d	0.18	Δh_n	mm	22	22	121	25
			k_n	m/d	0.38	0.37	0.07	0.34

MORETON MORRELL - July 2008			**Point**	**A2**	***Measuring Depth (mm)***			
Measurements (see Chapter 4)			***(See Fig 4-6)***		**400**	**300**	**200**	**100**
$D_{1(rsvr)}$	cm	9.2	***1***	mm	350	350	250	150
$D_{2(rsvr)}$	cm	13.7	***2***	mm	9	16		
Δt	s	193	***3***	mm	10	122	186	89
$\Delta D_{(rsvr)}$	cm	4.5	***4***	mm	45	45	40	40
Q	m^3/d	126	$h_{T(probe)}$	mm	296	289		
$h_{T(ave)}$	mm	293	h_n	mm	295	183	24	21
k_T	m/d	42.39	Δh_n	mm	112	159	2	21
			k_n	m/d	28	19	1,292	146

MORETON MORRELL - July 2008			**Point**	**A3**	***Measuring Depth (mm)***			
Measurements (see Chapter 4)			***(See Fig 4-6)***		**400**	**300**	**200**	**100**
$D_{1(rsvr)}$	cm	7.0	***1***	mm	350	350	250	150
$D_{2(rsvr)}$	cm	15.0	***2***	mm	85	31		
Δt	s	52	***3***	mm	82	162	124	40
$\Delta D_{(rsvr)}$	cm	8.0	***4***	mm	45	45	40	40
Q	m^3/d	225	$h_{T(probe)}$	mm	220	274		
$h_{T(ave)}$	mm	247	h_n	mm	224	143	87	70
k_T	m/d	331.78	Δh_n	mm	80	57	17	70
			k_n	m/d	255	361	1,220	294

MORETON MORRELL - July 2008			**Point**	**A4**	***Measuring Depth (mm)***			
Measurements (see Chapter 4)			***(See Fig 4-6)***		**400**	**300**	**200**	**100**
$D_{1(rsvr)}$	cm	9.0	***1***	mm	250	250	250	150
$D_{2(rsvr)}$	cm	17.0	***2***	mm	10	7	3	
Δt	s	28	***3***	mm	15	31	66	34
$\Delta D_{(rsvr)}$	cm	8.0	***4***	mm	45	45	40	40
Q	m^3/d	225	$h_{T(probe)}$	mm	195	198		
$h_{T(ave)}$	mm	196	h_n	mm	190	174	144	76
k_T	m/d	785.45	Δh_n	mm	16	30	68	76
			k_n	m/d	2,409	1,272	570	505

MORETON MORRELL - July 2008			Point	B1	Measuring Depth (mm)			
Measurements (see Chapter 4)			(See Fig 4-6)		400	300	200	100
$D_{1(rsvr)}$	cm	8.2	1	mm	200	200	200	150
$D_{2(rsvr)}$	cm	8.3	2	mm	45	44	46	
Δt	s	340	3	mm	32	45	64	35
$\Delta D_{(rsvr)}$	cm	0.1	4	mm	35	30	35	35
Q	m^3/d	3	$h_{T(probe)}$	mm	120	126	119	
$h_{T(ave)}$	mm	122	h_n	mm	133	125	101	80
k_T	m/d	1.29	Δh_n	mm	8	24	21	80
			k_n	m/d	5.1	1.6	1.8	0.5

MORETON MORRELL - July 2008			Point	B2	Measuring Depth (mm)			
Measurements (see Chapter 4)			(See Fig 4-6)		400	300	200	100
$D_{1(rsvr)}$	cm	15.0	1	mm	300	300	250	150
$D_{2(rsvr)}$	cm	20.0	2	mm	20	9		
Δt	s	21	3	mm	18	71	93	64
$\Delta D_{(rsvr)}$	cm	5.0	4	mm	25	30	30	30
Q	m^3/d	140	$h_{T(probe)}$	mm	255	261		
$h_{T(ave)}$	mm	258	h_n	mm	257	199	127	56
k_T	m/d	485.35	Δh_n	mm	58	72	71	56
			k_n	m/d	543	436	441	554

MORETON MORRELL - July 2008			Point	B3	Measuring Depth (mm)			
Measurements (see Chapter 4)			(See Fig 4-6)		400	300	200	100
$D_{1(rsvr)}$	cm	5.5	1	mm	300	300	250	150
$D_{2(rsvr)}$	cm	17.0	2	mm	34	26		
Δt	s	76	3	mm	30	95	138	78
$\Delta D_{(rsvr)}$	cm	11.5	4	mm	50	50	50	45
Q	m^3/d	323	$h_{T(probe)}$	mm	216	224		
$h_{T(ave)}$	mm	220	h_n	mm	220	155	62	27
k_T	m/d	365.59	Δh_n	mm	65	93	34	27
			k_n	m/d	309	217	586	734

MORETON MORRELL - July 2008			Point	B4	Measuring Depth (mm)			
Measurements (see Chapter 4)			(See Fig 4-6)		400	300	200	100
$D_{1(rsvr)}$	cm	10.0	1	mm	250	300	250	150
$D_{2(rsvr)}$	cm	21.0	2	mm	19	47	11	
Δt	s	37	3	mm	21	62	68	35
$\Delta D_{(rsvr)}$	cm	11.0	4	mm	5	15	10	10
Q	m^3/d	309	$h_{T(probe)}$	mm	226	238	229	
$h_{T(ave)}$	mm	231	h_n	mm	224	223	172	105
k_T	m/d	681.11	Δh_n	mm	1	51	66	105
			k_n	m/d	39,357	770	594	373

MORETON MORRELL - July 2008			Point	C1	Measuring Depth (mm)			
Measurements (see Chapter 4)			(See Fig 4-6)		400	300	200	100
$D_{1(rsvr)}$	cm	9.6	1	mm	350	350	250	150
$D_{2(rsvr)}$	cm	9.7	2	mm	44	-	-	-
Δt	s	1600	3	mm	17	15	1	100
$\Delta D_{(rsvr)}$	cm	0.1	4	mm	20	25	30	30
Q	m^3/d	3	$h_{T(probe)}$	mm	286			
$h_{T(ave)}$	mm	286	h_n	mm	313	310	219	20
k_T	m/d	0.12	Δh_n	mm	2	92	199	20
			k_n	m/d	3.90	0.09	0.04	0.42

MORETON MORRELL - July 2008			Point	C2	Measuring Depth (mm)			
Measurements (see Chapter 4)			(See Fig 4-6)		400	300	200	100
$D_{1(rsvr)}$	cm	6.0	1	mm	300	300	250	150
$D_{2(rsvr)}$	cm	12.0	2	mm	5	34		
Δt	s	41	3	mm	5	57	25	0
$\Delta D_{(rsvr)}$	cm	6.0	4	mm	40	40	60	45
Q	m^3/d	169	$h_{T(probe)}$	mm	255	226		
$h_{T(ave)}$	mm	240	h_n	mm	255	203	165	105
k_T	m/d	323.88	Δh_n	mm	52	38	61	105
			k_n	m/d	374	511	320	186

MORETON MORRELL - July 2008			Point	C3	Measuring Depth (mm)			
Measurements (see Chapter 4)			(See Fig 4-6)		400	300	200	100
$D_{1(rsvr)}$	cm	5.0	1	mm	300	300	270	150
$D_{2(rsvr)}$	cm	16.0	2	mm	2	9		
Δt	s	69	3	mm	4	30	7	44
$\Delta D_{(rsvr)}$	cm	11.0	4	mm	60	55	65	65
Q	m^3/d	309	$h_{T(probe)}$	mm	238	236		
$h_{T(ave)}$	mm	237	h_n	mm	236	215	198	41
k_T	m/d	356.74	Δh_n	mm	21	17	157	41
			k_n	m/d	1,022	1,236	135	512

MORETON MORRELL - July 2008			Point	C4	Measuring Depth (mm)			
Measurements (see Chapter 4)			(See Fig 4-6)		400	300	200	100
$D_{1(rsvr)}$	cm	7.5	1	mm	300	300	250	150
$D_{2(rsvr)}$	cm	16.0	2	mm	33	34		
Δt	s	25	3	mm	34	47	41	12
$\Delta D_{(rsvr)}$	cm	8.5	4	mm	65	65	70	65
Q	m^3/d	239	$h_{T(probe)}$	mm	202	201		
$h_{T(ave)}$	mm	201	h_n	mm	202	188	139	73
k_T	m/d	884.33	Δh_n	mm	13	49	66	73
			k_n	m/d	3,377	903	674	609

MORETON MORRELL - July 2008			Point	D1	Measuring Depth (mm)			
Measurements (see Chapter 4)			(See Fig 4-6)		400	300	200	100
$D_{1(rsvr)}$	cm	3.7	1	mm	300	300	250	150
$D_{2(rsvr)}$	cm	5.3	2	mm	9	14		
Δt	s	468	3	mm	6	18	52	0
$\Delta D_{(rsvr)}$	cm	1.6	4	mm	20	20	20	30
Q	m^3/d	45	$h_{T(probe)}$	mm	271	266		
$h_{T(ave)}$	mm	268	h_n	mm	274	262	178	120
k_T	m/d	6.77	Δh_n	mm	13	83	59	120
			k_n	m/d	36	5	8	4

MORETON MORRELL - July 2008			Point	D2	Measuring Depth (mm)			
Measurements (see Chapter 4)			(See Fig 4-6)		400	300	200	100
$D_{1(rsvr)}$	cm	7.5	1	mm	250	300	275	150
$D_{2(rsvr)}$	cm	18.0	2	mm	1	37	12	
Δt	s	56	3	mm	0	47	39	10
$\Delta D_{(rsvr)}$	cm	10.5	4	mm	60	70	70	70
Q	m^3/d	295	$h_{T(probe)}$	mm	189	193	193	
$h_{T(ave)}$	mm	191	h_n	mm	190	183	166	70
k_T	m/d	520.86	Δh_n	mm	7	17	96	70
			k_n	m/d	3,454	1,486	259	358

MORETON MORRELL - July 2008			Point	D3	Measuring Depth (mm)			
Measurements (see Chapter 4)			(See Fig 4-6)		400	300	200	100
$D_{1(rsvr)}$	cm	9.0	1	mm	250	250	250	150
$D_{2(rsvr)}$	cm	23.0	2	mm	2	2	9	
Δt	s	33	3	mm	6	14	47	14
$\Delta D_{(rsvr)}$	cm	14.0	4	mm	100	100	100	100
Q	m^3/d	393	$h_{T(probe)}$	mm	148	148	141	
$h_{T(ave)}$	mm	146	h_n	mm	144	136	103	36
k_T	m/d	1549.76	Δh_n	mm	8	33	67	36
			k_n	m/d	7,261	1,715	838	1,567

MORETON MORRELL - July 2008			Point	D4	Measuring Depth (mm)			
Measurements (see Chapter 4)			(See Fig 4-6)		400	300	200	100
$D_{1(rsvr)}$	cm	7.0	1	mm	300	300	250	150
$D_{2(rsvr)}$	cm	22.0	2	mm	6	4		
Δt	s	41	3	mm	5	23	39	11
$\Delta D_{(rsvr)}$	cm	15.0	4	mm	50	80	80	70
Q	m^3/d	421	$h_{T(probe)}$	mm	244	216		
$h_{T(ave)}$	mm	230	h_n	mm	246	197	131	69
k_T	m/d	847.08	Δh_n	mm	48	66	61	69
			k_n	m/d	1,005	733	794	701

Appendix A.9 Field Results – Moreton Morrell (February 2009). See Section 5.9

MORETON MORRELL - FEB 2009			Point	A1	Measuring Depth (mm)			
Measurements (see Chapter 4)			(See Fig 4-6)		400	300	200	100
$D_{1(rsvr)}$	cm	9.7	1	mm	250	250	250	150
$D_{2(rsvr)}$	cm	9.8	2	mm	48	49		
Δt	s	1345	3	mm				
$\Delta D_{(rsvr)}$	cm	0.1	4	mm				
Q	m^3/d	3	$h_{T(probe)}$	mm	202	201	250	
$h_{T(ave)}$	mm	218	h_n	mm	250	250	250	150
k_T	m/d	0.18	Δh_n	mm	-	-	100	150
			k_n	m/d	0.59	0.10	0.10	0.07

MORETON MORRELL - FEB 2009			Point	A2	Measuring Depth (mm)			
Measurements (see Chapter 4)			(See Fig 4-6)		400	300	200	100
$D_{1(rsvr)}$	cm	13.8	1	mm	250	250	200	150
$D_{2(rsvr)}$	cm	13.9	2	mm	17	15		
Δt	s	958	3	mm	2	15	110	88
$\Delta D_{(rsvr)}$	cm	0.1	4	mm	-	-	-	-
Q	m^3/d	3	$h_{T(probe)}$	mm	233	235	200	
$h_{T(ave)}$	mm	222	h_n	mm	248	235	90	63
k_T	m/d	0.25	Δh_n	mm	13	144	28	63
			k_n	m/d	1.04	0.10	0.50	0.22

MORETON MORRELL - FEB 2009			Point	A3	Measuring Depth (mm)			
Measurements (see Chapter 4)			(See Fig 4-6)		400	300	200	100
$D_{1(rsvr)}$	cm	6.6	1	mm	200	200	200	150
$D_{2(rsvr)}$	cm	7.6	2	mm	38	24	26	
Δt	s	2105	3	mm	5	21	60	44
$\Delta D_{(rsvr)}$	cm	1.0	4	mm	8	8	8	8
Q	m^3/d	28	$h_{T(probe)}$	mm	154	168	166	
$h_{T(ave)}$	mm	163	h_n	mm	187	171	132	99
k_T	m/d	1.55	Δh_n	mm	16	39	34	99
			k_n	m/d	4.05	1.62	1.86	0.64

MORETON MORRELL - FEB 2009			Point	A4	Measuring Depth (mm)			
Measurements (see Chapter 4)			(See Fig 4-6)		400	300	200	100
$D_{1(rsvr)}$	cm	4.5	1	mm	200	250	200	150
$D_{2(rsvr)}$	cm	5.0	2	mm	54	94	63	
Δt	s	445	3	mm	33	93	64	31
$\Delta D_{(rsvr)}$	cm	0.5	4	mm	5	5	5	5
Q	m^3/d	14	$h_{T(probe)}$	mm	142	151	133	
$h_{T(ave)}$	mm	142	h_n	mm	162	152	132	114
k_T	m/d	4.22	Δh_n	mm	10	21	18	114
			k_n	m/d	14.8	7.3	8.5	1.3

MORETON MORRELL - FEB 2009			Point	B1	Measuring Depth (mm)			
Measurements (see Chapter 4)			(See Fig 4-6)		400	300	200	100
$D_{1(rsvr)}$	cm	4.5	1	mm	250	250	250	150
$D_{2(rsvr)}$	cm	4.6	2	mm	25	22	23	
Δt	s	2850	3	mm	14	21	62	121
$\Delta D_{(rsvr)}$	cm	0.1	4	mm	22	22	22	22
Q	m^3/d	3	$h_{T(probe)}$	mm	203	206	206	
$h_{T(ave)}$	mm	205	h_n	mm	214	207	166	7
k_T	m/d	0.09	Δh_n	mm	7	41	159	7
			k_n	m/d	0.63	0.11	0.03	0.66

MORETON MORRELL - FEB 2009			Point	B2	Measuring Depth (mm)			
Measurements (see Chapter 4)			(See Fig 4-6)		400	300	200	100
$D_{1(rsvr)}$	cm	15.0	1	mm	300	200	200	150
$D_{2(rsvr)}$	cm	16.6	2	mm	3	2	31	
Δt	s	2140	3	mm	31	1	40	2
$\Delta D_{(rsvr)}$	cm	1.6	4	mm	10	10	10	10
Q	m^3/d	45	$h_{T(probe)}$	mm	287	188	159	
$h_{T(ave)}$	mm	211	h_n	mm	259	189	150	138
k_T	m/d	1.88	Δh_n	mm	70	38	12	138
			k_n	m/d	1.41	2.59	8.27	0.72

MORETON MORRELL - FEB 2009			Point	B3	Measuring Depth (mm)			
Measurements (see Chapter 4)			(See Fig 4-6)		400	300	200	100
$D_{1(rsvr)}$	cm	12.1	1	mm	250	200	200	150
$D_{2(rsvr)}$	cm	12.5	2	mm	33	20	16	
Δt	s	534	3	mm	44	13	38	9
$\Delta D_{(rsvr)}$	cm	0.4	4	mm	10	10	10	10
Q	m^3/d	11	$h_{T(probe)}$	mm	207	171	174	
$h_{T(ave)}$	mm	184	h_n	mm	196	178	152	131
k_T	m/d	2.17	Δh_n	mm	18	25	21	131
			k_n	m/d	5.50	3.92	4.69	0.76

MORETON MORRELL - FEB 2009			Point	B4	Measuring Depth (mm)			
Measurements (see Chapter 4)			(See Fig 4-6)		400	300	200	100
$D_{1(rsvr)}$	cm	3.5	1	mm	150	150	150	150
$D_{2(rsvr)}$	cm	8.5	2	mm	26	15	15	
Δt	s	400	3	mm	2	14	18	35
$\Delta D_{(rsvr)}$	cm	5.0	4	mm	13	13	13	13
Q	m^3/d	140	$h_{T(probe)}$	mm	111	123	122	
$h_{T(ave)}$	mm	118	h_n	mm	135	123	119	102
k_T	m/d	56.13	Δh_n	mm	12	4	17	102
			k_n	m/d	134	407	101	16

MORETON MORRELL - FEB 2009			Point	C1	Measuring Depth (mm)			
Measurements (see Chapter 4)			(See Fig 4-6)		400	300	200	100
$D_{1(rsvr)}$	cm	16.3	1	mm	350	350	250	150
$D_{2(rsvr)}$	cm	16.4	2	mm	56	47		
Δt	s	2975	3	mm	47	52	4	3
$\Delta D_{(rsvr)}$	cm	0.1	4	mm	10	10	10	10
Q	m^3/d	3	$h_{T(probe)}$	mm	285	294	241	
$h_{T(ave)}$	mm	273	h_n	mm	293	288	237	137
k_T	m/d	0.07	Δh_n	mm	5	52	99	137
			k_n	m/d	0.96	0.09	0.05	0.03

MORETON MORRELL - FEB 2009			Point	C2	Measuring Depth (mm)			
Measurements (see Chapter 4)			(See Fig 4-6)		400	300	200	100
$D_{1(rsvr)}$	cm	10.4	1	mm	150	150	150	150
$D_{2(rsvr)}$	cm	11.6	2	mm	15	14	16	
Δt	s	584	3	mm	9	12	16	19
$\Delta D_{(rsvr)}$	cm	1.2	4	mm	9	9	9	9
Q	m^3/d	34	$h_{T(probe)}$	mm	127	127	126	
$h_{T(ave)}$	mm	127	h_n	mm	132	130	125	122
k_T	m/d	8.63	Δh_n	mm	2	5	3	122
			k_n	m/d	118.8	58.1	94.2	2.2

MORETON MORRELL - FEB 2009			Point	C3	Measuring Depth (mm)			
Measurements (see Chapter 4)			(See Fig 4-6)		400	300	200	100
$D_{1(rsvr)}$	cm	2.6	1	mm	250	200	150	150
$D_{2(rsvr)}$	cm	4.2	2	mm	9	67	12	
Δt	s	1028	3	mm	41	12	15	22
$\Delta D_{(rsvr)}$	cm	1.6	4	mm	8	8	8	8
Q	m^3/d	45	$h_{T(probe)}$	mm	234	126	130	
$h_{T(ave)}$	mm	163	h_n	mm	201	181	128	121
k_T	m/d	5.07	Δh_n	mm	21	0.10	7	121
			k_n	m/d	10	2,070	29	2

MORETON MORRELL - FEB 2009			Point	C4	Measuring Depth (mm)			
Measurements (see Chapter 4)			(See Fig 4-6)		400	300	200	100
$D_{1(rsvr)}$	cm	3.3	1	mm	200	200	200	150
$D_{2(rsvr)}$	cm	12.0	2	mm	73	66	71	
Δt	s	1693	3	mm	56	64	70	25
$\Delta D_{(rsvr)}$	cm	8.7	4	mm	9	9	9	9
Q	m^3/d	244	$h_{T(probe)}$	mm	118	126	121	
$h_{T(ave)}$	mm	121	h_n	mm	135	127	121	117
k_T	m/d	22.51	Δh_n	mm	8	6	5	117
			k_n	m/d	84.4	115.8	148.6	5.9

MORETON MORRELL - FEB 2009			Point	D1	Measuring Depth (mm)			
Measurements (see Chapter 4)			(See Fig 4-6)		400	300	200	100
$D_{1(rsvr)}$	cm	4.9	1	mm	350	350	250	150
$D_{2(rsvr)}$	cm	5.5	2	mm	15	5	0	
Δt	s	2099	3	mm	6	15		
$\Delta D_{(rsvr)}$	cm	0.6	4	mm	18	18	18	18
Q	m^3/d	17	$h_{T(probe)}$	mm	317	328	232	
$h_{T(ave)}$	mm	292	h_n	mm	328	317	233	133
k_T	m/d	0.52	Δh_n	mm	11	85	100	133
			k_n	m/d	3.42	0.45	0.38	0.29

MORETON MORRELL - FEB 2009			Point	D2	Measuring Depth (mm)			
Measurements (see Chapter 4)			(See Fig 4-6)		400	300	200	100
$D_{1(rsvr)}$	cm	4.0	1	mm	350	350	250	150
$D_{2(rsvr)}$	cm	10.0	2	mm	66	57	1	
Δt	s	132	3	mm	67	70	1	6
$\Delta D_{(rsvr)}$	cm	6.0	4	mm	11	11	11	11
Q	m^3/d	169	$h_{T(probe)}$	mm	273	282	238	
$h_{T(ave)}$	mm	264	h_n	mm	272	270	238	133
k_T	m/d	91.43	Δh_n	mm	2	31	105	133
			k_n	m/d	2,748	194	57	45

MORETON MORRELL - FEB 2009			Point	D3	Measuring Depth (mm)			
Measurements (see Chapter 4)			(See Fig 4-6)		400	300	200	100
$D_{1(rsvr)}$	cm	16.5	1	mm	300	300	250	150
$D_{2(rsvr)}$	cm	21.0	2	mm	21	14		
Δt	s	47	3	mm	7	18	4	0
$\Delta D_{(rsvr)}$	cm	4.5	4	mm	6	6	6	6
Q	m^3/d	126	$h_{T(probe)}$	mm	273	280	244	
$h_{T(ave)}$	mm	266	h_n	mm	287	276	240	144
k_T	m/d	191.71	Δh_n	mm	11	35	97	144
			k_n	m/d	1,137	360	132	89

MORETON MORRELL - FEB 2009			Point	D4	Measuring Depth (mm)			
Measurements (see Chapter 4)			(See Fig 4-6)		400	300	200	100
$D_{1(rsvr)}$	cm	14.3	1	mm	200	200	200	150
$D_{2(rsvr)}$	cm	21.0	2	mm	48	51	44	
Δt	s	227	3	mm	53	53	54	54
$\Delta D_{(rsvr)}$	cm	6.7	4	mm	13	13	13	13
Q	m^3/d	188	$h_{T(probe)}$	mm	140	136	144	
$h_{T(ave)}$	mm	140	h_n	mm	135	134	133	83
k_T	m/d	112.12	Δh_n	mm	0	1	50	83
			k_n	m/d	13,084	4,361	78	47

Appendix A.10: Field Results – Moreton Morrell (September 2009). See Section 5.10

MORETON MORRELL - SEPT 2009			**Point**	**A1**	***Measuring Depth (mm)***			
Measurements (see Chapter 4)			***(See Fig 4-6)***		**400**	**300**	**200**	**100**
$D_{1(rsvr)}$	cm	11.3	***1***	mm	220	220	220	175
$D_{2(rsvr)}$	cm	11.4	***2***	mm	12	18	11	
Δt	s	1415	***3***	mm	13	25	26	123
$\Delta D_{(rsvr)}$	cm	0.0	***4***	mm	40	34	42	42
Q	m^3/d	1	$h_{T(probe)}$	mm	168	168	167	
$h_{T(ave)}$	mm	168	h_n	mm	167	161	152	10
k_T	m/d	0.11	Δh_n	mm	6	9	142	10
			k_n	m/d	0.78	0.52	0.03	0.47

MORETON MORRELL – SEPT 2009			**Point**	**A2**	***Measuring Depth (mm)***			
Measurements (see Chapter 4)			***(See Fig 4-6)***		**400**	**300**	**200**	**100**
$D_{1(rsvr)}$	cm	16.9	***1***	mm	210	210	210	150
$D_{2(rsvr)}$	cm	17.0	***2***	mm	12	9	23	30
Δt	s	1666	***3***	mm	14	13	102	86
$\Delta D_{(rsvr)}$	cm	0.1	***4***	mm	54	56	55	52
Q	m^3/d	3	$h_{T(probe)}$	mm	144	145	132	68
$h_{T(ave)}$	mm	122	h_n	mm	142	141	53	12
k_T	m/d	0.26	Δh_n	mm	1	88	41	12
			k_n	m/d	7.98	0.09	0.19	0.67

MORETON MORRELL - SEPT 2009			**Point**	**A3**	***Measuring Depth (mm)***			
Measurements (see Chapter 4)			***(See Fig 4-6)***		**400**	**300**	**200**	**100**
$D_{1(rsvr)}$	cm	7.8	***1***	mm	200	200	200	175
$D_{2(rsvr)}$	cm	8.4	***2***	mm	13	8	9	
Δt	s	2050	***3***	mm	14	17	52	82
$\Delta D_{(rsvr)}$	cm	0.6	***4***	mm	54	55	56	62
Q	m^3/d	17	$h_{T(probe)}$	mm	133	137	135	
$h_{T(ave)}$	mm	135	h_n	mm	132	128	92	31
k_T	m/d	1.15	Δh_n	mm	4	36	61	31
			k_n	m/d	9.7	1.1	0.6	1.3

MORETON MORRELL - SEPT 2009			**Point**	**A4**	***Measuring Depth (mm)***			
Measurements (see Chapter 4)			***(See Fig 4-6)***		**400**	**300**	**200**	**100**
$D_{1(rsvr)}$	cm	12.1	***1***	mm	200	190	190	175
$D_{2(rsvr)}$	cm	13.3	***2***	mm	29	20	24	21
Δt	s	2106	***3***	mm	29	21	25	44
$\Delta D_{(rsvr)}$	cm	1.2	***4***	mm	85	84	81	79
Q	m^3/d	32	$h_{T(probe)}$	mm	86	86	85	75
$h_{T(ave)}$	mm	83	h_n	mm	86	85	84	52
k_T	m/d	3.50	Δh_n	mm	1	1	32	52
			k_n	m/d	72.6	72.6	2.3	1.4

MORETON MORRELL - SEPT 2009			Point	B1	Measuring Depth (mm)			
Measurements (see Chapter 4)			(See Fig 4-6)		400	300	200	100
$D_{1(rsvr)}$	cm	11.3	1	mm	220	220	220	175
$D_{2(rsvr)}$	cm	11.4	2	mm	12	18	11	
Δt	s	1415	3	mm	13	25	26	123
$\Delta D_{(rsvr)}$	cm	0.0	4	mm	40	34	42	42
Q	m^3/d	1	$h_{T(probe)}$	mm	168	168	167	
$h_{T(ave)}$	mm	168	h_n	mm	167	161	152	10
k_T	m/d	0.11	Δh_n	mm	6	9	142	10
			k_n	m/d	0.78	0.52	0.03	0.47

MORETON MORRELL - SEPT 2009			Point	B2	Measuring Depth (mm)			
Measurements (see Chapter 4)			(See Fig 4-6)		400	300	200	100
$D_{1(rsvr)}$	cm	5.3	1	mm	220	220	220	175
$D_{2(rsvr)}$	cm	5.6	2	mm	13	14	15	
Δt	s	2533	3	mm	18	19	26	44
$\Delta D_{(rsvr)}$	cm	0.3	4	mm	80	81	78	74
Q	m^3/d	7	$h_{T(probe)}$	mm	127	125	127	
$h_{T(ave)}$	mm	126	h_n	mm	122	120	116	57
k_T	m/d	0.42	Δh_n	mm	2	4	59	57
			k_n	m/d	6.56	3.28	0.22	0.23

MORETON MORRELL - SEPT 2009			Point	B3	Measuring Depth (mm)			
Measurements (see Chapter 4)			(See Fig 4-6)		400	300	200	100
$D_{1(rsvr)}$	cm	20.9	1	mm	200	190	190	175
$D_{2(rsvr)}$	cm	21.0	2	mm	27	26	15	
Δt	s	1506	3	mm	21	16	26	63
$\Delta D_{(rsvr)}$	cm	0.1	4	mm	61	66	69	75
Q	m^3/d	4	$h_{T(probe)}$	mm	112	98	106	
$h_{T(ave)}$	mm	105	h_n	mm	118	108	95	37
k_T	m/d	0.50	Δh_n	mm	10	13	58	37
			k_n	m/d	1.32	1.02	0.23	0.36

MORETON MORRELL - SEPT 2009			Point	B4	Measuring Depth (mm)			
Measurements (see Chapter 4)			(See Fig 4-6)		400	300	200	100
$D_{1(rsvr)}$	cm	17.4	1	mm	200	200	200	175
$D_{2(rsvr)}$	cm	18.4	2	mm	16	14	7	
Δt	s	2249	3	mm	19	14	13	89
$\Delta D_{(rsvr)}$	cm	1.1	4	mm	74	80	82	85
Q	m^3/d	29	$h_{T(probe)}$	mm	110	106	111	
$h_{T(ave)}$	mm	109	h_n	mm	107	106	105	1
k_T	m/d	2.28	Δh_n	mm	1	1	104	1
			k_n	m/d	62	62	1	62

MORETON MORRELL - SEPT 2009			Point	C1	Measuring Depth (mm)			
Measurements (see Chapter 4)			(See Fig 4-6)		400	300	200	100
$D_{1(rsvr)}$	cm	17.4	1	mm	210	210	210	175
$D_{2(rsvr)}$	cm	17.6	2	mm	13	16		
Δt	s	2062	3	mm	1	8	38	27
$\Delta D_{(rsvr)}$	cm	0.2	4	mm	45	42	41	26
Q	m^3/d	6	$h_{T(probe)}$	mm	152	152		
$h_{T(ave)}$	mm	152	h_n	mm	164	160	131	122
k_T	m/d	0.34	Δh_n	mm	4	29	9	122
			k_n	m/d	3.22	0.44	1.43	0.11

MORETON MORRELL - SEPT 2009			Point	C2	Measuring Depth (mm)			
Measurements (see Chapter 4)			(See Fig 4-6)		400	300	200	100
$D_{1(rsvr)}$	cm	11.1	1	mm	165	160	160	160
$D_{2(rsvr)}$	cm	11.7	2	mm	10	6	7	14
Δt	s	1800	3	mm	5	3	4	35
$\Delta D_{(rsvr)}$	cm	0.6	4	mm	81	79	79	73
Q	m^3/d	17	$h_{T(probe)}$	mm	74	75	74	73
$h_{T(ave)}$	mm	74	h_n	mm	79	78	77	52
k_T	m/d	2.40	Δh_n	mm	1	1	25	52
			k_n	m/d	44	44	2	1

MORETON MORRELL - SEPT 2009			Point	C3	Measuring Depth (mm)			
Measurements (see Chapter 4)			(See Fig 4-6)		400	300	200	100
$D_{1(rsvr)}$	cm	6.1	1	mm	145	145	145	160
$D_{2(rsvr)}$	cm	6.3	2	mm	20	15	24	21
Δt	s	1713	3	mm	14	11	17	63
$\Delta D_{(rsvr)}$	cm	0.2	4	mm	66	70	66	70
Q	m^3/d	4	$h_{T(probe)}$	mm	59	60	55	69
$h_{T(ave)}$	mm	61	h_n	mm	65	64	62	27
k_T	m/d	0.77	Δh_n	mm	1	2	35	27
			k_n	m/d	11.6	5.8	0.3	0.4

MORETON MORRELL - SEPT 2009			Point	C4	Measuring Depth (mm)			
Measurements (see Chapter 4)			(See Fig 4-6)		400	300	200	100
$D_{1(rsvr)}$	cm	9.2	1	mm	140	140	140	140
$D_{2(rsvr)}$	cm	10.8	2	mm	25	22	21	21
Δt	s	605	3	mm	27	26	31	36
$\Delta D_{(rsvr)}$	cm	1.6	4	mm	55	61	57	56
Q	m^3/d	44	$h_{T(probe)}$	mm	60	57	62	63
$h_{T(ave)}$	mm	61	h_n	mm	58	53	52	48
k_T	m/d	22.53	Δh_n	mm	5	1	4	48
			k_n	m/d	68.1	340.7	85.2	7.1

MORETON MORRELL - SEPT 2009			Point	D1	Measuring Depth (mm)			
Measurements (see Chapter 4)			(See Fig 4-6)		400	300	200	100
$D_{1(rsvr)}$	cm	12.0	1	mm	180	180	190	175
$D_{2(rsvr)}$	cm	12.1	2	mm	6	6	10	
Δt	s	2100	3	mm	7	8	14	52
$\Delta D_{(rsvr)}$	cm	0.1	4	mm	50	50	55	55
Q	m^3/d	1	$h_{T(probe)}$	mm	124	124	125	
$h_{T(ave)}$	mm	124	h_n	mm	123	122	121	68
k_T	m/d	0.10	Δh_n	mm	1	1	53	68
			k_n	m/d	3.17	3.17	0.06	0.05

MORETON MORRELL - SEPT 2009			Point	D2	Measuring Depth (mm)			
Measurements (see Chapter 4)			(See Fig 4-6)		400	300	200	100
$D_{1(rsvr)}$	cm	6.5	1	mm	160	160	160	160
$D_{2(rsvr)}$	cm	9.3	2	mm	15	13	11	14
Δt	s	2377	3	mm	14	13	11	13
$\Delta D_{(rsvr)}$	cm	2.9	4	mm	59	61	65	64
Q	m^3/d	80	$h_{T(probe)}$	mm	86	86	84	82
$h_{T(ave)}$	mm	85	h_n	mm	87	86	84	83
k_T	m/d	7.55	Δh_n	mm	1	2	1	83
			k_n	m/d	159	80	159	2

MORETON MORRELL - SEPT 2009			Point	D3	Measuring Depth (mm)			
Measurements (see Chapter 4)			(See Fig 4-6)		400	300	200	100
$D_{1(rsvr)}$	cm	18.8	1	mm	115	120	120	120
$D_{2(rsvr)}$	cm	20.4	2	mm	13	7	5	6
Δt	s	587	3	mm	14	10	6	6
$\Delta D_{(rsvr)}$	cm	1.6	4	mm	50	60	65	66
Q	m^3/d	45	$h_{T(probe)}$	mm	52			
$h_{T(ave)}$	mm	52	h_n	mm	51	50	49	48
k_T	m/d	27.88	Δh_n	mm	1	1	1	48
			k_n	m/d	362	362	362	8

MORETON MORRELL - SEPT 2009			Point	D4	Measuring Depth (mm)			
Measurements (see Chapter 4)			(See Fig 4-6)		400	300	200	100
$D_{1(rsvr)}$	cm	15.2	1	mm	160	160	160	160
$D_{2(rsvr)}$	cm	17.6	2	mm	16	16	15	18
Δt	s	614	3	mm	20	20	18	21
$\Delta D_{(rsvr)}$	cm	2.4	4	mm	55	57	61	60
Q	m^3/d	67	$h_{T(probe)}$	mm	89	87	84	82
$h_{T(ave)}$	mm	86	h_n	mm	85	83	81	79
k_T	m/d	24.32	Δh_n	mm	2	2	2	79
			k_n	m/d	260	260	260	7

Appendix A.11: Field Results – Moreton Morrell (October 2009). See Section 5.11

MORETON MORRELL - OCT 2009			Point	A1	Measuring Depth (mm)			
Measurements (see Chapter 4)			(See Fig 4-6)		400	300	200	100
$D_{1(rsvr)}$	cm	5.0	1	mm	220	220	220	175
$D_{2(rsvr)}$	cm	9.0	2	mm	2	11	22	
Δt	s	195	3	mm	3	33	71	136
$\Delta D_{(rsvr)}$	cm	4.0	4	mm	42	36	30	30
Q	m^3/d	112	$h_{T(probe)}$	mm	176	173	168	
$h_{T(ave)}$	mm	172	h_n	mm	175	151	119	9
k_T	m/d	63.32	Δh_n	mm	24	32	110	9
			k_n	m/d	114	85	25	303

MORETON MORRELL - OCT 2009			Point	A2	Measuring Depth (mm)			
Measurements (see Chapter 4)			(See Fig 4-6)		400	300	200	100
$D_{1(rsvr)}$	cm	4.0	1	mm	200	200	200	175
$D_{2(rsvr)}$	cm	16.0	2	mm	25	30	25	3
Δt	s	123	3	mm	25	38	44	85
$\Delta D_{(rsvr)}$	cm	12.0	4	mm	57	55	62	64
Q	m^3/d	337	$h_{T(probe)}$	mm	118	115	113	
$h_{T(ave)}$	mm	115	h_n	mm	118	107	94	26
k_T	m/d	449.99	Δh_n	mm	11	13	68	26
			k_n	m/d	1,180	998	191	499

MORETON MORRELL - OCT 2009			Point	A3	Measuring Depth (mm)			
Measurements (see Chapter 4)			(See Fig 4-6)		400	300	200	100
$D_{1(rsvr)}$	cm	5.0	1	mm	150	150	150	150
$D_{2(rsvr)}$	cm	13.0	2	mm	9	17	16	16
Δt	s	136	3	mm	9	42	49	70
$\Delta D_{(rsvr)}$	cm	8.0	4	mm	46	36	40	42
Q	m^3/d	225	$h_{T(probe)}$	mm	95	97	94	
$h_{T(ave)}$	mm	95	h_n	mm	95	72	61	38
k_T	m/d	328.24	Δh_n	mm	23	11	23	38
			k_n	m/d	340	711	340	206

MORETON MORRELL - OCT 2009			Point	A4	Measuring Depth (mm)			
Measurements (see Chapter 4)			(See Fig 4-6)		400	300	200	100
$D_{1(rsvr)}$	cm	5.0	1	mm	220	220	220	175
$D_{2(rsvr)}$	cm	18.0	2	mm	23	17	30	
Δt	s	63	3	mm	72	70	74	74
$\Delta D_{(rsvr)}$	cm	13.0	4	mm	27	32	55	78
Q	m^3/d	365	$h_{T(probe)}$	mm	170	171	135	
$h_{T(ave)}$	mm	159	h_n	mm	121	118	91	23
k_T	m/d	691.83	Δh_n	mm	3	27	68	23
			k_n	m/d	9,148	1,016	404	1,193

MORETON MORRELL - OCT 2009			Point	B1	Measuring Depth (mm)			
Measurements (see Chapter 4)			(See Fig 4-6)		400	300	200	100
$D_{1(rsvr)}$	cm	6.0	1	mm	300	300	270	175
$D_{2(rsvr)}$	cm	12.0	2	mm	3	5		
Δt	s	123	3	mm	1	17	123	127
$\Delta D_{(rsvr)}$	cm	6.0	4	mm	51	45	43	36
Q	m^3/d	169	$h_{T(probe)}$	mm	246	250		
$h_{T(ave)}$	mm	248	h_n	mm	248	238	104	12
k_T	m/d	104.63	Δh_n	mm	10	134	92	12
			k_n	m/d	649	48	71	541

MORETON MORRELL - OCT 2009			Point	B2	Measuring Depth (mm)			
Measurements (see Chapter 4)			(See Fig 4-6)		400	300	200	100
$D_{1(rsvr)}$	cm	4.0	1	mm	260	250	260	175
$D_{2(rsvr)}$	cm	11.0	2	mm	8	5	11	
Δt	s	147	3	mm	10	18	119	121
$\Delta D_{(rsvr)}$	cm	7.0	4	mm	42	39	43	37
Q	m^3/d	197	$h_{T(probe)}$	mm	210	206	206	
$h_{T(ave)}$	mm	207	h_n	mm	208	193	98	17
k_T	m/d	122.18	Δh_n	mm	15	95	81	17
			k_n	m/d	422	67	78	373

MORETON MORRELL - OCT 2009			Point	B3	Measuring Depth (mm)			
Measurements (see Chapter 4)			(See Fig 4-6)		400	300	200	100
$D_{1(rsvr)}$	cm	5.0	1	mm	240	240	240	175
$D_{2(rsvr)}$	cm	16.0	2	mm	15	21	25	
Δt	s	121	3	mm	19	72	135	112
$\Delta D_{(rsvr)}$	cm	11.0	4	mm	44	42	41	39
Q	m^3/d	309	$h_{T(probe)}$	mm	181	177	174	
$h_{T(ave)}$	mm	177	h_n	mm	177	126	64	24
k_T	m/d	272.71	Δh_n	mm	51	62	40	24
			k_n	m/d	237	195	302	504

MORETON MORRELL - OCT 2009			Point	B4	Measuring Depth (mm)			
Measurements (see Chapter 4)			(See Fig 4-6)		400	300	200	100
$D_{1(rsvr)}$	cm	7.5	1	mm	220	220	220	175
$D_{2(rsvr)}$	cm	20.0	2	mm	14	24	29	
Δt	s	55	3	mm	22	55	80	85
$\Delta D_{(rsvr)}$	cm	12.5	4	mm	64	57	54	51
Q	m^3/d	351	$h_{T(probe)}$	mm	142	139	137	
$h_{T(ave)}$	mm	139	h_n	mm	134	108	86	39
k_T	m/d	867.71	Δh_n	mm	26	22	47	39
			k_n	m/d	1,163	1,374	643	775

MORETON MORRELL - OCT 2009			Point	C1	Measuring Depth (mm)			
Measurements (see Chapter 4)			(See Fig 4-6)		400	300	200	100
$D_{1(rsvr)}$	cm	8.5	1	mm	350	350	270	175
$D_{2(rsvr)}$	cm	19.0	2	mm	4	15		
Δt	s	129	3	mm	6	62	135	88
$\Delta D_{(rsvr)}$	cm	10.5	4	mm	57	52	53	54
Q	m^3/d	295	$h_{T(probe)}$	mm	289	283		
$h_{T(ave)}$	mm	286	h_n	mm	287	236	82	33
k_T	m/d	151.40	Δh_n	mm	51	154	49	33
			k_n	m/d	212	70	221	328

MORETON MORRELL - OCT 2009			Point	C2	Measuring Depth (mm)			
Measurements (see Chapter 4)			(See Fig 4-6)		400	300	200	100
$D_{1(rsvr)}$	cm	3.5	1	mm	260	260	260	175
$D_{2(rsvr)}$	cm	10.5	2	mm	5	6	9	
Δt	s	116	3	mm	6	28	100	119
$\Delta D_{(rsvr)}$	cm	7.0	4	mm	53	50	52	52
Q	m^3/d	197	$h_{T(probe)}$	mm	202	204	199	
$h_{T(ave)}$	mm	202	h_n	mm	201	182	108	4
k_T	m/d	159.18	Δh_n	mm	19	74	104	4
			k_n	m/d	422	108	77	2,006

MORETON MORRELL - OCT 2009			Point	C3	Measuring Depth (mm)			
Measurements (see Chapter 4)			(See Fig 4-6)		400	300	200	100
$D_{1(rsvr)}$	cm	6.0	1	mm	240	240	240	175
$D_{2(rsvr)}$	cm	15.0	2	mm	11	16	20	
Δt	s	107	3	mm	14	26	103	109
$\Delta D_{(rsvr)}$	cm	9.0	4	mm	62	57	54	45
Q	m^3/d	253	$h_{T(probe)}$	mm	167	167	166	
$h_{T(ave)}$	mm	167	h_n	mm	164	157	83	21
k_T	m/d	268.47	Δh_n	mm	7	74	62	21
			k_n	m/d	1,598	151	180	533

MORETON MORRELL - OCT 2009			Point	C4	Measuring Depth (mm)			
Measurements (see Chapter 4)			(See Fig 4-6)		400	300	200	100
$D_{1(rsvr)}$	cm	5.0	1	mm	230	230	230	175
$D_{2(rsvr)}$	cm	19.0	2	mm	16	18	19	
Δt	s	95	3	mm	20	28	37	52
$\Delta D_{(rsvr)}$	cm	14.0	4	mm	64	62	56	59
Q	m^3/d	393	$h_{T(probe)}$	mm	150	150	155	
$h_{T(ave)}$	mm	152	h_n	mm	146	140	137	64
k_T	m/d	516.89	Δh_n	mm	6	3	73	64
			k_n	m/d	3,266	6,533	268	306

Appendix A.12: Field Results – Weston-U-Wetherley (May 2009). See Section 5.12

WESTON-U-WETHERLEY - MAY 2009			**Point**	**A1**	***Measuring Depth (mm)***			
Measurements (see Chapter 4)			***(See Fig 4-6)***		**400**	**300**	**200**	**100**
$D_{1(rsvr)}$	cm	7.6	***1***	mm	400	380	270	180
$D_{2(rsvr)}$	cm	8.2	***2***	mm	26	7		
Δt	s	1876	***3***	mm	35	18	0	83
$\Delta D_{(rsvr)}$	cm	0.6	***4***	mm	65	65	65	5
Q	m^3/d	17	$h_{T(probe)}$	mm	309	308		
$h_{T(ave)}$	mm	309	h_n	mm	300	297	205	92
k_T	m/d	0.55	Δh_n	mm	3	92	113	92
			k_n	m/d	14.2	0.5	0.4	0.5

WESTON-U-WETHERLEY - MAY 2009			**Point**	**A2**	***Measuring Depth (mm)***			
Measurements (see Chapter 4)			***(See Fig 4-6)***		**400**	**300**	**200**	**100**
$D_{1(rsvr)}$	cm	5.4	***1***	mm	350	350	250	180
$D_{2(rsvr)}$	cm	7.2	***2***	mm	6	7		
Δt	s	902	***3***	mm	7	11	17	17
$\Delta D_{(rsvr)}$	cm	1.8	***4***	mm	47	51	50	44
Q	m^3/d	51	$h_{T(probe)}$	mm	297	292		
$h_{T(ave)}$	mm	295	h_n	mm	296	288	183	119
k_T	m/d	3.60	Δh_n	mm	8	105	64	119
			k_n	m/d	33	3	4	2

WESTON-U-WETHERLEY - MAY 2009			**Point**	**A3**	***Measuring Depth (mm)***			
Measurements (see Chapter 4)			***(See Fig 4-6)***		**400**	**300**	**200**	**100**
$D_{1(rsvr)}$	cm	6.0	***1***	mm	300	300	250	150
$D_{2(rsvr)}$	cm	13.8	***2***	mm	25	16		
Δt	s	262	***3***	mm	24	18	57	50
$\Delta D_{(rsvr)}$	cm	7.8	***4***	mm	63	71	70	56
Q	m^3/d	219	$h_{T(probe)}$	mm	212	213		
$h_{T(ave)}$	mm	213	h_n	mm	213	211	123	44
k_T	m/d	74.53	Δh_n	mm	2	88	79	44
			k_n	m/d	1,980	45	50	90

WESTON-U-WETHERLEY - MAY 2009			**Point**	**A4**	***Measuring Depth (mm)***			
Measurements (see Chapter 4)			***(See Fig 4-6)***		**400**	**300**	**200**	**100**
$D_{1(rsvr)}$	cm	6.5	***1***	mm	250	250	250	150
$D_{2(rsvr)}$	cm	19.5	***2***	mm	35	32	15	
Δt	s	85	***3***	mm	35	36	22	4
$\Delta D_{(rsvr)}$	cm	13.0	***4***	mm	45	45	60	55
Q	m^3/d	365	$h_{T(probe)}$	mm	170	173	175	
$h_{T(ave)}$	mm	173	h_n	mm	170	169	168	91
k_T	m/d	471.19	Δh_n	mm	1	1	77	91
			k_n	m/d	20,340	20,340	263	225

WESTON-U-WETHERLEY - MAY 2009			Point	B1	Measuring Depth (mm)			
Measurements (see Chapter 4)			(See Fig 4-6)		400	300	200	100
$D_{1(rsvr)}$	cm	5.9	1	mm	350	350	250	175
$D_{2(rsvr)}$	cm	6.0	2	mm	44	-	-	-
Δt	s	1320	3	mm	17	15	1	75
$\Delta D_{(rsvr)}$	cm	0.1	4	mm	68	71	69	96
Q	m^3/d	3	$h_{T(probe)}$	mm	238			
$h_{T(ave)}$	mm	238	h_n	mm	265	264	180	4
k_T	m/d	0.17	Δh_n	mm	0	85	176	4
			k_n	m/d	77.5	0.1	0.1	2.5

WESTON-U-WETHERLEY - MAY 2009			Point	B2	Measuring Depth (mm)			
Measurements (see Chapter 4)			(See Fig 4-6)		400	300	200	100
$D_{1(rsvr)}$	cm	5.0	1	mm	350	350	250	150
$D_{2(rsvr)}$	cm	12.0	2	mm	47	38		
Δt	s	760	3	mm	54	42	1	-
$\Delta D_{(rsvr)}$	cm	7.0	4	mm	48	61	65	67
Q	m^3/d	197	$h_{T(probe)}$	mm	255	251		
$h_{T(ave)}$	mm	253	h_n	mm	248	247	184	83
k_T	m/d	19.37	Δh_n	mm	1	63	101	83
			k_n	m/d	1,225	19	12	15

WESTON-U-WETHERLEY - MAY 2009			Point	B3	Measuring Depth (mm)			
Measurements (see Chapter 4)			(See Fig 4-6)		400	300	200	100
$D_{1(rsvr)}$	cm	7.6	1	mm	350	350	150	150
$D_{2(rsvr)}$	cm	21.0	2	mm	35	41		
Δt	s	198	3	mm	48	130	48	45
$\Delta D_{(rsvr)}$	cm	13.4	4	mm	58	60	64	71
Q	m^3/d	376	$h_{T(probe)}$	mm	257	249		
$h_{T(ave)}$	mm	253	h_n	mm	244	160	38	34
k_T	m/d	142.30	Δh_n	mm	84	122	4	34
			k_n	m/d	107	74	2,250	265

WESTON-U-WETHERLEY - MAY 2009			Point	B4	Measuring Depth (mm)			
Measurements (see Chapter 4)			(See Fig 4-6)		400	300	200	100
$D_{1(rsvr)}$	cm	5.2	1	mm	250	250	250	150
$D_{2(rsvr)}$	cm	9.7	2	mm	31	31	29	
Δt	s	179	3	mm	43	45	30	17
$\Delta D_{(rsvr)}$	cm	4.5	4	mm	66	65	81	74
Q	m^3/d	126	$h_{T(probe)}$	mm	153	154		
$h_{T(ave)}$	mm	154	h_n	mm	141	140	139	59
k_T	m/d	87.12	Δh_n	mm	1	1	80	59
			k_n	m/d	3,343	3,343	42	57

WESTON-U-WETHERLEY - MAY 2009			Point	C1	Measuring Depth (mm)			
Measurements (see Chapter 4)			(See Fig 4-6)		400	300	200	100
$D_{1(rsvr)}$	cm	10.1	1	mm	350	350	270	180
$D_{2(rsvr)}$	cm	10.2	2	mm	15	6		
Δt	s	2289	3	mm	8	6	3	58
$\Delta D_{(rsvr)}$	cm	0.1	4	mm	75	85	61	66
Q	m^3/d	3	$h_{T(probe)}$	mm	260	259		
$h_{T(ave)}$	mm	260	h_n	mm	267	259	206	56
k_T	m/d	0.09	Δh_n	mm	8	53	150	56
			k_n	m/d	0.73	0.11	0.04	0.10

WESTON-U-WETHERLEY - MAY 2009			Point	C2	Measuring Depth (mm)			
Measurements (see Chapter 4)			(See Fig 4-6)		400	300	200	100
$D_{1(rsvr)}$	cm	5.4	1	mm	350	350	270	180
$D_{2(rsvr)}$	cm	9.2	2	mm	47	44		
Δt	s	1004	3	mm	48	47	0	0
$\Delta D_{(rsvr)}$	cm	3.8	4	mm	79	81	81	75
Q	m^3/d	107	$h_{T(probe)}$	mm	224	225		
$h_{T(ave)}$	mm	225	h_n	mm	223	222	189	105
k_T	m/d	8.97	Δh_n	mm	1	33	84	105
			k_n	m/d	503	15	6	5

WESTON-U-WETHERLEY - MAY 2009			Point	C3	Measuring Depth (mm)			
Measurements (see Chapter 4)			(See Fig 4-6)		400	300	200	100
$D_{1(rsvr)}$	cm	7.0	1	mm	300	300	270	180
$D_{2(rsvr)}$	cm	19.0	2	mm	33	11	0	
Δt	s	54	3	mm	34	19	22	13
$\Delta D_{(rsvr)}$	cm	12.0	4	mm	65	81	84	86
Q	m^3/d	337	$h_{T(probe)}$	mm	202	208	186	
$h_{T(ave)}$	mm	199	h_n	mm	201	200	164	81
k_T	m/d	595.24	Δh_n	mm	1	36	83	81
			k_n	m/d	29,554	821	356	365

WESTON-U-WETHERLEY - MAY 2009			Point	C4	Measuring Depth (mm)			
Measurements (see Chapter 4)			(See Fig 4-6)		400	300	200	100
$D_{1(rsvr)}$	cm	3.5	1	mm	300	300	270	180
$D_{2(rsvr)}$	cm	13.0	2	mm	33	26	2	
Δt	s	178	3	mm	31	24	11	0
$\Delta D_{(rsvr)}$	cm	9.5	4	mm	50	58	52	49
Q	m^3/d	267	$h_{T(probe)}$	mm	217	216	216	
$h_{T(ave)}$	mm	216	h_n	mm	219	218	207	131
k_T	m/d	131.24	Δh_n	mm	1	11	76	131
			k_n	m/d	7,098	645	93	54

WESTON-U-WETHERLEY - MAY 2009			Point	D1	Measuring Depth (mm)			
Measurements (see Chapter 4)			(See Fig 4-6)		400	300	200	100
$D_{1(rsvr)}$	cm	3.6	1	mm	350	350	270	180
$D_{2(rsvr)}$	cm	4.3	2	mm	11	17		
Δt	s	1410	3	mm	29	24	0	35
$\Delta D_{(rsvr)}$	cm	0.7	4	mm	70	76	71	71
Q	m^3/d	20	$h_{T(probe)}$	mm	269	257		
$h_{T(ave)}$	mm	263	h_n	mm	251	250	199	74
k_T	m/d	1.00	Δh_n	mm	1	51	125	74
			k_n	m/d	66.0	1.3	0.5	0.9

WESTON-U-WETHERLEY - MAY 2009			Point	D2	Measuring Depth (mm)			
Measurements (see Chapter 4)			(See Fig 4-6)		400	300	200	100
$D_{1(rsvr)}$	cm	9.5	1	mm	300	300	270	180
$D_{2(rsvr)}$	cm	18.5	2	mm	38	25		
Δt	s	135	3	mm	41	31	4	1
$\Delta D_{(rsvr)}$	cm	9.0	4	mm	65	80	86	81
Q	m^3/d	253	$h_{T(probe)}$	mm	197	195		
$h_{T(ave)}$	mm	196	h_n	mm	194	189	180	99
k_T	m/d	180.94	Δh_n	mm	5	9	82	99
			k_n	m/d	1,773	985	109	90

WESTON-U-WETHERLEY - MAY 2009			Point	D3	Measuring Depth (mm)			
Measurements (see Chapter 4)			(See Fig 4-6)		400	300	200	100
$D_{1(rsvr)}$	cm	5.0	1	mm	250	250	250	150
$D_{2(rsvr)}$	cm	17.0	2	mm	65	57	57	
Δt	s	34	3	mm	69	65	70	11
$\Delta D_{(rsvr)}$	cm	12.0	4	mm	80	90	90	90
Q	m^3/d	337	$h_{T(probe)}$	mm	105	103		
$h_{T(ave)}$	mm	104	h_n	mm	101	95	90	49
k_T	m/d	1805.31	Δh_n	mm	6	5	41	49
			k_n	m/d	7,823	9,388	1,145	958

WESTON-U-WETHERLEY - MAY 2009			Point	D4	Measuring Depth (mm)			
Measurements (see Chapter 4)			(See Fig 4-6)		400	300	200	100
$D_{1(rsvr)}$	cm	7.0	1	mm	250	250	250	150
$D_{2(rsvr)}$	cm	22.0	2	mm	68	68	68	
Δt	s	65	3	mm	70	74	81	27
$\Delta D_{(rsvr)}$	cm	15.0	4	mm	60	59	60	70
Q	m^3/d	421	$h_{T(probe)}$	mm	122	123		
$h_{T(ave)}$	mm	123	h_n	mm	120	117	109	53
k_T	m/d	1002.13	Δh_n	mm	3	8	56	53
			k_n	m/d	10,230	3,836	548	579

WESTON-U-WETHERLEY - MAY 2009			Point	E1	Measuring Depth (mm)			
Measurements (see Chapter 4)			(See Fig 4-6)		400	300	200	100
$D_{1(rsvr)}$	cm	5.6	1	mm	350	350	270	180
$D_{2(rsvr)}$	cm	6.7	2	mm	9	9		
Δt	s	1642	3	mm	13	14	0	7
$\Delta D_{(rsvr)}$	cm	1.1	4	mm	68	68	57	55
Q	m^3/d	31	$h_{T(probe)}$	mm	273	273	213	
$h_{T(ave)}$	mm	253	h_n	mm	269	268	213	118
k_T	m/d	1.41	Δh_n	mm	1	55	95	118
			k_n	m/d	89.1	1.6	0.9	0.8

WESTON-U-WETHERLEY - MAY 2009			Point	E2	Measuring Depth (mm)			
Measurements (see Chapter 4)			(See Fig 4-6)		400	300	200	100
$D_{1(rsvr)}$	cm	12.5	1	mm	300	300	270	180
$D_{2(rsvr)}$	cm	19.0	2	mm	30	23		
Δt	s	71	3	mm	60	75	90	0
$\Delta D_{(rsvr)}$	cm	6.5	4	mm	87	95	81	84
Q	m^3/d	183	$h_{T(probe)}$	mm	183	182		
$h_{T(ave)}$	mm	183	h_n	mm	153	130	99	96
k_T	m/d	266.85	Δh_n	mm	23	31	3	96
			k_n	m/d	529	393	3,927	127

WESTON-U-WETHERLEY - MAY 2009			Point	E3	Measuring Depth (mm)			
Measurements (see Chapter 4)			(See Fig 4-6)		400	300	200	100
$D_{1(rsvr)}$	cm	7.0	1	mm	250	250	250	180
$D_{2(rsvr)}$	cm	20.0	2	mm	12	12	19	
Δt	s	57	3	mm	13	14	25	1
$\Delta D_{(rsvr)}$	cm	13.0	4	mm	68	70	70	95
Q	m^3/d	365	$h_{T(probe)}$	mm	170	168		
$h_{T(ave)}$	mm	169	h_n	mm	169	166	155	84
k_T	m/d	717.90	Δh_n	mm	3	11	71	84
			k_n	m/d	10,110	2,757	427	361

WESTON-U-WETHERLEY - MAY 2009			Point	E4	Measuring Depth (mm)			
Measurements (see Chapter 4)			(See Fig 4-6)		400	300	200	100
$D_{1(rsvr)}$	cm	5.0	1	mm	250	250	250	180
$D_{2(rsvr)}$	cm	18.5	2	mm	55	57	59	
Δt	s	66	3	mm	58	59	60	6
$\Delta D_{(rsvr)}$	cm	13.5	4	mm	78	79	81	85
Q	m^3/d	379	$h_{T(probe)}$	mm	117	114		
$h_{T(ave)}$	mm	116	h_n	mm	114	112	109	89
k_T	m/d	942.08	Δh_n	mm	2	3	20	89
			k_n	m/d	13,601	9,068	1,360	306

Appendix A.13: Field Results – Ashorne (June 2009). See Section 5.13

ASHORNE - JUNE 2009			Point	A1	Measuring Depth (mm)			
Measurements (see Chapter 4)			(See Fig 4-6)		400	300	200	100
$D_{1(rsvr)}$	cm	7.5	1	mm	300	300	270	180
$D_{2(rsvr)}$	cm	7.6	2	mm	14	13	20	
Δt	s	2136	3	mm	10	11	42	22
$\Delta D_{(rsvr)}$	cm	0.1	4	mm	58	61	51	61
Q	m^3/d	3	$h_{T(probe)}$	mm	228	226	199	
$h_{T(ave)}$	mm	218	h_n	mm	232	228	177	97
k_T	m/d	0.11	Δh_n	mm	4	51	80	97
			k_n	m/d	1.56	0.12	0.08	0.06

ASHORNE - JUNE 2009			Point	A2	Measuring Depth (mm)			
Measurements (see Chapter 4)			(See Fig 4-6)		400	300	200	100
$D_{1(rsvr)}$	cm	2.3	1	mm	230	230	230	100
$D_{2(rsvr)}$	cm	2.5	2	mm	14	14	38	
Δt	s	2106	3	mm	17	10	55	26
$\Delta D_{(rsvr)}$	cm	0.2	4	mm	58	68	49	67
Q	m^3/d	6	$h_{T(probe)}$	mm	158	148	143	
$h_{T(ave)}$	mm	150	h_n	mm	155	152	126	7
k_T	m/d	0.34	Δh_n	mm	3	26	119	7
			k_n	m/d	4.21	0.49	0.11	1.80

ASHORNE - JUNE 2009			Point	A3	Measuring Depth (mm)			
Measurements (see Chapter 4)			(See Fig 4-6)		400	300	200	100
$D_{1(rsvr)}$	cm	5.5	1	mm	240	240	240	150
$D_{2(rsvr)}$	cm	9.5	2	mm	8	22	28	
Δt	s	138	3	mm	13	23	117	81
$\Delta D_{(rsvr)}$	cm	4.0	4	mm	70	68	64	63
Q	m^3/d	112	$h_{T(probe)}$	mm	162	150	148	
$h_{T(ave)}$	mm	153	h_n	mm	157	149	59	6
k_T	m/d	100.56	Δh_n	mm	8	90	53	6
			k_n	m/d	482	43	73	642

ASHORNE - JUNE 2009			Point	A4	Measuring Depth (mm)			
Measurements (see Chapter 4)			(See Fig 4-6)		400	300	200	100
$D_{1(rsvr)}$	cm	4.0	1	mm	240	240	240	100
$D_{2(rsvr)}$	cm	9.5	2	mm	10	17	11	
Δt	s	153	3	mm	11	25	63	14
$\Delta D_{(rsvr)}$	cm	5.5	4	mm	84	77	85	81
Q	m^3/d	155	$h_{T(probe)}$	mm	146	146	144	
$h_{T(ave)}$	mm	145	h_n	mm	145	138	92	5
k_T	m/d	131.58	Δh_n	mm	7	46	87	5
			k_n	m/d	683	104	55	956

ASHORNE - JUNE 2009			Point	B1	Measuring Depth (mm)			
Measurements (see Chapter 4)			(See Fig 4-6)		400	300	200	100
$D_{1(rsvr)}$	cm	3.9	1	mm	240	240	240	100
$D_{2(rsvr)}$	cm	4.0	2	mm	7	15	18	
Δt	s	1920	3	mm	9	23	19	15
$\Delta D_{(rsvr)}$	cm	0.1	4	mm	70	59	64	61
Q	m^3/d	1	$h_{T(probe)}$	mm	163	166	158	
$h_{T(ave)}$	mm	162	h_n	mm	161	158	157	24
k_T	m/d	0.09	Δh_n	mm	3	1	133	24
			k_n	m/d	1.15	3.46	0.03	0.14

ASHORNE - JUNE 2009			Point	B2	Measuring Depth (mm)			
Measurements (see Chapter 4)			(See Fig 4-6)		400	300	200	100
$D_{1(rsvr)}$	cm	7.5	1	mm	250	250	250	80
$D_{2(rsvr)}$	cm	9.0	2	mm	6	22	13	
Δt	s	609	3	mm	8	36	73	6
$\Delta D_{(rsvr)}$	cm	1.5	4	mm	72	75	72	70
Q	m^3/d	42	$h_{T(probe)}$	mm	172	153	165	
$h_{T(ave)}$	mm	163	h_n	mm	170	139	105	4
k_T	m/d	8.02	Δh_n	mm	31	34	101	4
			k_n	m/d	11	10	3	82

ASHORNE - JUNE 2009			Point	B3	Measuring Depth (mm)			
Measurements (see Chapter 4)			(See Fig 4-6)		400	300	200	100
$D_{1(rsvr)}$	cm	3.4	1	mm	230	230	230	100
$D_{2(rsvr)}$	cm	5.2	2	mm	15	21	25	
Δt	s	253	3	mm	9	20	73	25
$\Delta D_{(rsvr)}$	cm	1.8	4	mm	74	75	64	71
Q	m^3/d	51	$h_{T(probe)}$	mm	141	134	141	
$h_{T(ave)}$	mm	139	h_n	mm	147	135	93	4
k_T	m/d	27.29	Δh_n	mm	12	42	89	4
			k_n	m/d	79	23	11	237

ASHORNE - JUNE 2009			Point	B4	Measuring Depth (mm)			
Measurements (see Chapter 4)			(See Fig 4-6)		400	300	200	100
$D_{1(rsvr)}$	cm	8.0	1	mm	230	230	230	100
$D_{2(rsvr)}$	cm	15.5	2	mm	38	33	30	
Δt	s	104	3	mm	39	40	89	33
$\Delta D_{(rsvr)}$	cm	7.5	4	mm	65	65	70	65
Q	m^3/d	211	$h_{T(probe)}$	mm	127	132	130	
$h_{T(ave)}$	mm	130	h_n	mm	126	125	71	2
k_T	m/d	295.86	Δh_n	mm	1	54	69	2
			k_n	m/d	9,591	178	139	4,795

ASHORNE - JUNE 2009			Point	C1	Measuring Depth (mm)			
Measurements (see Chapter 4)			(See Fig 4-6)		400	300	200	100
$D_{1(rsvr)}$	cm	10.1	1	mm	270	270	270	150
$D_{2(rsvr)}$	cm	10.2	2	mm	20	26	36	
Δt	s	2289	3	mm	23	28	43	44
$\Delta D_{(rsvr)}$	cm	0.1	4	mm	60	63	62	54
Q	m^3/d	3	$h_{T(probe)}$	mm	190	181	172	
$h_{T(ave)}$	mm	181	h_n	mm	187	179	165	52
k_T	m/d	0.13	Δh_n	mm	8	14	113	52
			k_n	m/d	0.73	0.42	0.05	0.11

ASHORNE - JUNE 2009			Point	C2	Measuring Depth (mm)			
Measurements (see Chapter 4)			(See Fig 4-6)		400	300	200	100
$D_{1(rsvr)}$	cm	4.9	1	mm	250	250	250	180
$D_{2(rsvr)}$	cm	5.0	2	mm	32	29	25	
Δt	s	1674	3	mm	22	21	20	42
$\Delta D_{(rsvr)}$	cm	0.1	4	mm	37	40	42	40
Q	m^3/d	3	$h_{T(probe)}$	mm	181	181		
$h_{T(ave)}$	mm	181	h_n	mm	191	189	188	98
k_T	m/d	0.18	Δh_n	mm	2	1	90	98
			k_n	m/d	3.97	7.94	0.09	0.08

ASHORNE - JUNE 2009			Point	C3	Measuring Depth (mm)			
Measurements (see Chapter 4)			(See Fig 4-6)		400	300	200	100
$D_{1(rsvr)}$	cm	6.4	1	mm	210	200	200	100
$D_{2(rsvr)}$	cm	11.2	2	mm	13	17	8	
Δt	s	1675	3	mm	15	22	39	9
$\Delta D_{(rsvr)}$	cm	4.8	4	mm	75	73	71	66
Q	m^3/d	135	$h_{T(probe)}$	mm	122	110		
$h_{T(ave)}$	mm	116	h_n	mm	120	105	90	25
k_T	m/d	13.14	Δh_n	mm	15	15	65	25
			k_n	m/d	25	25	6	15

ASHORNE - JUNE 2009			Point	C4	Measuring Depth (mm)			
Measurements (see Chapter 4)			(See Fig 4-6)		400	300	200	100
$D_{1(rsvr)}$	cm	6.0	1	mm	220	220	220	100
$D_{2(rsvr)}$	cm	17.0	2	mm	19	21	15	
Δt	s	137	3	mm	23	52	120	52
$\Delta D_{(rsvr)}$	cm	11.0	4	mm	48	52	53	46
Q	m^3/d	309	$h_{T(probe)}$	mm	153	147	152	
$h_{T(ave)}$	mm	151	h_n	mm	149	116	47	2
k_T	m/d	283.49	Δh_n	mm	33	69	45	2
			k_n	m/d	324	155	237	5,339

ASHORNE - JUNE 2009			Point	D1	Measuring Depth (mm)			
Measurements (see Chapter 4)			(See Fig 4-6)		400	300	200	100
$D_{1(rsvr)}$	cm	10.3	1	mm	270	270	270	100
$D_{2(rsvr)}$	cm	10.4	2	mm	10	12		
Δt	s	1991	3	mm	13	23	96	31
$\Delta D_{(rsvr)}$	cm	0.1	4	mm	59	59	67	54
Q	m^3/d	3	$h_{T(probe)}$	mm	201	199	203	
$h_{T(ave)}$	mm	201	h_n	mm	198	188	107	15
k_T	m/d	0.13	Δh_n	mm	10	81	92	15
			k_n	m/d	0.67	0.08	0.07	0.45

ASHORNE - JUNE 2009			Point	D2	Measuring Depth (mm)			
Measurements (see Chapter 4)			(See Fig 4-6)		400	300	200	100
$D_{1(rsvr)}$	cm	8.0	1	mm	250	250	260	150
$D_{2(rsvr)}$	cm	8.0	2	mm	2	13	25	
Δt	s	1882	3	mm	5	14	43	19
$\Delta D_{(rsvr)}$	cm	0.0	4	mm	87	81	82	83
Q	m^3/d	1	$h_{T(probe)}$	mm	161	156	153	
$h_{T(ave)}$	mm	157	h_n	mm	158	155	135	48
k_T	m/d	0.09	Δh_n	mm	3	20	87	48
			k_n	m/d	1.18	0.18	0.04	0.07

ASHORNE - JUNE 2009			Point	D3	Measuring Depth (mm)			
Measurements (see Chapter 4)			(See Fig 4-6)		400	300	200	100
$D_{1(rsvr)}$	cm	5.9	1	mm	240	240	240	180
$D_{2(rsvr)}$	cm	6.3	2	mm	22	24	15	
Δt	s	1800	3	mm	13	19	44	0
$\Delta D_{(rsvr)}$	cm	0.4	4	mm	76	80	81	76
Q	m^3/d	11	$h_{T(probe)}$	mm	142	136	144	
$h_{T(ave)}$	mm	141	h_n	mm	151	141	115	104
k_T	m/d	0.84	Δh_n	mm	10	26	11	104
			k_n	m/d	2.96	1.14	2.66	0.28

ASHORNE - JUNE 2009			Point	D4	Measuring Depth (mm)			
Measurements (see Chapter 4)			(See Fig 4-6)		400	300	200	100
$D_{1(rsvr)}$	cm	7.0	1	mm	220	220	220	180
$D_{2(rsvr)}$	cm	13.0	2	mm	21	27	21	
Δt	s	157	3	mm	24	32	60	92
$\Delta D_{(rsvr)}$	cm	6.0	4	mm	70	66	64	65
Q	m^3/d	169	$h_{T(probe)}$	mm	129	127		
$h_{T(ave)}$	mm	128	h_n	mm	126	122	96	23
k_T	m/d	158.83	Δh_n	mm	4	26	73	23
			k_n	m/d	1,271	195	70	221

Appendix A.14: Field Results – Leek Wooton (June 2009). See Section 5.14

LEEK WOOTON - JUNE 2009			Point	A1	Measuring Depth (mm)			
Measurements (see Chapter 4)			(See Fig 4-6)		400	300	200	100
$D_{1(rsvr)}$	cm	15.5	1	mm	300	300	270	180
$D_{2(rsvr)}$	cm	21.0	2	mm	2	6		
Δt	s	263	3	mm	4	9	0	0
$\Delta D_{(rsvr)}$	cm	5.5	4	mm	31	31	33	35
Q	m^3/d	155	$h_{T(probe)}$	mm	267	263		
$h_{T(ave)}$	mm	265	h_n	mm	265	260	237	145
k_T	m/d	41.98	Δh_n	mm	5	23	92	145
			k_n	m/d	556	120	30	19

LEEK WOOTON - JUNE 2009			Point	A2	Measuring Depth (mm)			
Measurements (see Chapter 4)			(See Fig 4-6)		400	300	200	100
$D_{1(rsvr)}$	cm	4.0	1	mm	270	270	270	150
$D_{2(rsvr)}$	cm	9.9	2	mm	14	2	5	
Δt	s	138	3	mm	14	29	82	26
$\Delta D_{(rsvr)}$	cm	5.9	4	mm	46	60	57	59
Q	m^3/d	166	$h_{T(probe)}$	mm	210	208	208	
$h_{T(ave)}$	mm	209	h_n	mm	210	181	131	65
k_T	m/d	108.99	Δh_n	mm	29	50	66	65
			k_n	m/d	196	114	86	87

LEEK WOOTON - JUNE 2009			Point	A3	Measuring Depth (mm)			
Measurements (see Chapter 4)			(See Fig 4-6)		400	300	200	100
$D_{1(rsvr)}$	cm	3.5	1	mm	250	250	250	180
$D_{2(rsvr)}$	cm	16.0	2	mm	10	15	6	
Δt	s	144	3	mm	10	25	28	18
$\Delta D_{(rsvr)}$	cm	12.5	4	mm	46	44	46	51
Q	m^3/d	351	$h_{T(probe)}$	mm	194	191	198	
$h_{T(ave)}$	mm	194	h_n	mm	194	181	176	111
k_T	m/d	237.62	Δh_n	mm	13	5	65	111
			k_n	m/d	888	2,309	178	104

LEEK WOOTON - JUNE 2009			Point	A4	Measuring Depth (mm)			
Measurements (see Chapter 4)			(See Fig 4-6)		400	300	200	100
$D_{1(rsvr)}$	cm	9.0	1	mm	230	220	220	150
$D_{2(rsvr)}$	cm	18.5	2	mm	22	12	5	
Δt	s	202	3	mm	23	13	14	9
$\Delta D_{(rsvr)}$	cm	9.5	4	mm	52	55	55	50
Q	m^3/d	267	$h_{T(probe)}$	mm	156	153	160	
$h_{T(ave)}$	mm	156	h_n	mm	155	152	151	91
k_T	m/d	160.03	Δh_n	mm	3	1	60	91
			k_n	m/d	2,085	6,255	104	69

LEEK WOOTON - JUNE 2009			Point	B1	Measuring Depth (mm)			
Measurements (see Chapter 4)			(See Fig 4-6)		400	300	200	100
$D_{1(rsvr)}$	cm	12.0	1	mm	250	250	250	180
$D_{2(rsvr)}$	cm	16.0	2	mm	15	16	4	100
Δt	s	260	3	mm	23	24	35	0
$\Delta D_{(rsvr)}$	cm	4.0	4	mm	44	44	46	45
Q	m^3/d	112	$h_{T(probe)}$	mm	191	190	200	
$h_{T(ave)}$	mm	194	h_n	mm	183	182	169	135
k_T	m/d	42.26	Δh_n	mm	1	13	34	135
			k_n	m/d	2,046	157	60	15

LEEK WOOTON - JUNE 2009			Point	B2	Measuring Depth (mm)			
Measurements (see Chapter 4)			(See Fig 4-6)		400	300	200	100
$D_{1(rsvr)}$	cm	5.0	1	mm	270	280	270	180
$D_{2(rsvr)}$	cm	8.5	2	mm	16	7	7	
Δt	s	170	3	mm	15	29	32	1
$\Delta D_{(rsvr)}$	cm	3.5	4	mm	72	75	72	70
Q	m^3/d	98	$h_{T(probe)}$	mm	182	198	191	
$h_{T(ave)}$	mm	190	h_n	mm	183	176	166	109
k_T	m/d	57.54	Δh_n	mm	7	10	57	109
			k_n	m/d	391	274	48	25

LEEK WOOTON - JUNE 2009			Point	B3	Measuring Depth (mm)			
Measurements (see Chapter 4)			(See Fig 4-6)		400	300	200	100
$D_{1(rsvr)}$	cm	6.0	1	mm	270	270	270	180
$D_{2(rsvr)}$	cm	17.0	2	mm	15	16	19	
Δt	s	99	3	mm	16	68	79	14
$\Delta D_{(rsvr)}$	cm	11.0	4	mm	73	66	66	71
Q	m^3/d	309	$h_{T(probe)}$	mm	182	188	185	
$h_{T(ave)}$	mm	185	h_n	mm	181	136	125	95
k_T	m/d	319.50	Δh_n	mm	45	11	30	95
			k_n	m/d	328	1,343	493	156

LEEK WOOTON - JUNE 2009			Point	B4	Measuring Depth (mm)			
Measurements (see Chapter 4)			(See Fig 4-6)		400	300	200	100
$D_{1(rsvr)}$	cm	9.0	1	mm	230	230	230	180
$D_{2(rsvr)}$	cm	12.5	2	mm	5	6	21	
Δt	s	285	3	mm	6	14	25	0
$\Delta D_{(rsvr)}$	cm	3.5	4	mm	65	65	70	65
Q	m^3/d	98	$h_{T(probe)}$	mm	160	159	139	
$h_{T(ave)}$	mm	153	h_n	mm	159	151	135	115
k_T	m/d	42.79	Δh_n	mm	8	16	20	115
			k_n	m/d	204	102	81	14

LEEK WOOTON - JUNE 2009			Point	C1	Measuring Depth (mm)			
Measurements (see Chapter 4)			(See Fig 4-6)		400	300	200	100
$D_{1(rsvr)}$	cm	6.0	1	mm	250	250	250	180
$D_{2(rsvr)}$	cm	17.5	2	mm	2	6	8	
Δt	s	88	3	mm	6	18	39	18
$\Delta D_{(rsvr)}$	cm	11.5	4	mm	65	61	59	72
Q	m^3/d	323	$h_{T(probe)}$	mm	183	183	183	
$h_{T(ave)}$	mm	183	h_n	mm	179	171	152	90
k_T	m/d	379.88	Δh_n	mm	8	19	62	90
			k_n	m/d	2,172	915	280	193

LEEK WOOTON - JUNE 2009			Point	C2	Measuring Depth (mm)			
Measurements (see Chapter 4)			(See Fig 4-6)		400	300	200	100
$D_{1(rsvr)}$	cm	7.0	1	mm	270	270	270	180
$D_{2(rsvr)}$	cm	15.0	2	mm	13	17	16	
Δt	s	96	3	mm	15	22	27	2
$\Delta D_{(rsvr)}$	cm	8.0	4	mm	57	56	58	52
Q	m^3/d	225	$h_{T(probe)}$	mm	200	197		
$h_{T(ave)}$	mm	199	h_n	mm	198	192	185	126
k_T	m/d	223.33	Δh_n	mm	6	7	59	126
			k_n	m/d	1,847	1,583	188	88

LEEK WOOTON - JUNE 2009			Point	C3	Measuring Depth (mm)			
Measurements (see Chapter 4)			(See Fig 4-6)		400	300	200	100
$D_{1(rsvr)}$	cm	7.0	1	mm	270	270	270	170
$D_{2(rsvr)}$	cm	14.0	2	mm	6	14	11	
Δt	s	107	3	mm	10	19	20	0
$\Delta D_{(rsvr)}$	cm	7.0	4	mm	62	57	57	56
Q	m^3/d	197	$h_{T(probe)}$	mm	202	199		
$h_{T(ave)}$	mm	201	h_n	mm	198	194	193	114
k_T	m/d	173.57	Δh_n	mm	4	1	79	114
			k_n	m/d	2,175	8,700	110	76

LEEK WOOTON - JUNE 2009			Point	C4	Measuring Depth (mm)			
Measurements (see Chapter 4)			(See Fig 4-6)		400	300	200	100
$D_{1(rsvr)}$	cm	6.0	1	mm	220	220	220	175
$D_{2(rsvr)}$	cm	16.0	2	mm	16	12	17	
Δt	s	266	3	mm	16	23	26	14
$\Delta D_{(rsvr)}$	cm	10.0	4	mm	63	69	67	70
Q	m^3/d	281	$h_{T(probe)}$	mm	141	139	136	
$h_{T(ave)}$	mm	139	h_n	mm	141	128	127	91
k_T	m/d	144.22	Δh_n	mm	13	1	36	91
			k_n	m/d	385	5,000	139	55

LEEK WOOTON - JUNE 2009			Point	D1	Measuring Depth (mm)			
Measurements (see Chapter 4)			(See Fig 4-6)		400	300	200	100
$D_{1(rsvr)}$	cm	6.0	1	mm	250	220	220	180
$D_{2(rsvr)}$	cm	16.0	2	mm	14	12	13	
Δt	s	176	3	mm	17	16	23	0
$\Delta D_{(rsvr)}$	cm	10.0	4	mm	62	34	29	42
Q	m^3/d	281	$h_{T(probe)}$	mm	174	174	178	
$h_{T(ave)}$	mm	175	h_n	mm	171	170	168	138
k_T	m/d	172.39	Δh_n	mm	1	2	30	138
			k_n	m/d	7,556	3,778	250	55

LEEK WOOTON - JUNE 2009			Point	D2	Measuring Depth (mm)			
Measurements (see Chapter 4)			(See Fig 4-6)		400	300	200	100
$D_{1(rsvr)}$	cm	9.0	1	mm	250	250	250	180
$D_{2(rsvr)}$	cm	20.0	2	mm	9	17	7	
Δt	s	64	3	mm	15	28	27	0
$\Delta D_{(rsvr)}$	cm	11.0	4	mm	63	61	67	66
Q	m^3/d	309	$h_{T(probe)}$	mm	178	172	176	
$h_{T(ave)}$	mm	175	h_n	mm	172	161	156	114
k_T	m/d	521.47	Δh_n	mm	11	5	42	114
			k_n	m/d	2,078	4,572	542	201

LEEK WOOTON - JUNE 2009			Point	D3	Measuring Depth (mm)			
Measurements (see Chapter 4)			(See Fig 4-6)		400	300	200	100
$D_{1(rsvr)}$	cm	10.0	1	mm	260	260	260	180
$D_{2(rsvr)}$	cm	18.0	2	mm	3	8	4	
Δt	s	79	3	mm	9	16	19	9
$\Delta D_{(rsvr)}$	cm	8.0	4	mm	57	59	65	61
Q	m^3/d	225	$h_{T(probe)}$	mm	200	193	191	
$h_{T(ave)}$	mm	195	h_n	mm	194	185	176	110
k_T	m/d	276.73	Δh_n	mm	9	9	66	110
			k_n	m/d	1,496	1,496	204	122

LEEK WOOTON - JUNE 2009			Point	D4	Measuring Depth (mm)			
Measurements (see Chapter 4)			(See Fig 4-6)		400	300	200	100
$D_{1(rsvr)}$	cm	6.5	1	mm	230	230	230	150
$D_{2(rsvr)}$	cm	18.0	2	mm	34	32	38	
Δt	s	157	3	mm	36	40	68	39
$\Delta D_{(rsvr)}$	cm	11.5	4	mm	45	47	41	44
Q	m^3/d	323	$h_{T(probe)}$	mm	151	151		
$h_{T(ave)}$	mm	151	h_n	mm	149	143	121	67
k_T	m/d	258.05	Δh_n	mm	6	22	54	67
			k_n	m/d	1,624	443	180	145

LEEK WOOTON - JUNE 2009			Point	E1	Measuring Depth (mm)			
Measurements (see Chapter 4)			(See Fig 4-6)		400	300	200	100
$D_{1(rsvr)}$	cm	8.0	1	mm	250	250	250	180
$D_{2(rsvr)}$	cm	18.0	2	mm	14	13	27	
Δt	s	106	3	mm	15	19	37	0
$\Delta D_{(rsvr)}$	cm	10.0	4	mm	75	75	67	64
Q	m^3/d	281	$h_{T(probe)}$	mm	161	162	156	
$h_{T(ave)}$	mm	160	h_n	mm	160	156	146	116
k_T	m/d	314.31	Δh_n	mm	4	10	30	116
			k_n	m/d	3,137	1,255	414	108

LEEK WOOTON - JUNE 2009			Point	E2	Measuring Depth (mm)			
Measurements (see Chapter 4)			(See Fig 4-6)		400	300	200	100
$D_{1(rsvr)}$	cm	10.0	1	mm	270	270	260	180
$D_{2(rsvr)}$	cm	20.0	2	mm	8	5	12	
Δt	s	79	3	mm	10	13	46	0
$\Delta D_{(rsvr)}$	cm	10.0	4	mm	71	71	67	63
Q	m^3/d	281	$h_{T(probe)}$	mm	191	194	181	
$h_{T(ave)}$	mm	189	h_n	mm	189	186	147	117
k_T	m/d	356.91	Δh_n	mm	3	39	30	117
			k_n	m/d	5,611	432	559	144

LEEK WOOTON - JUNE 2009			Point	E3	Measuring Depth (mm)			
Measurements (see Chapter 4)			(See Fig 4-6)		400	300	200	100
$D_{1(rsvr)}$	cm	6.0	1	mm	240	240	240	180
$D_{2(rsvr)}$	cm	18.0	2	mm	12	18	16	
Δt	s	148	3	mm	13	25	33	30
$\Delta D_{(rsvr)}$	cm	12.0	4	mm	56	56	61	64
Q	m^3/d	337	$h_{T(probe)}$	mm	172	166	163	
$h_{T(ave)}$	mm	167	h_n	mm	171	159	146	86
k_T	m/d	258.28	Δh_n	mm	12	13	60	86
			k_n	m/d	899	829	180	125

LEEK WOOTON - JUNE 2009			Point	E4	Measuring Depth (mm)			
Measurements (see Chapter 4)			(See Fig 4-6)		400	300	200	100
$D_{1(rsvr)}$	cm	6.0	1	mm	200	200	200	150
$D_{2(rsvr)}$	cm	20.0	2	mm	10	5	22	
Δt	s	233	3	mm	15	46	69	55
$\Delta D_{(rsvr)}$	cm	14.0	4	mm	57	59	56	57
Q	m^3/d	393	$h_{T(probe)}$	mm	133	136		
$h_{T(ave)}$	mm	135	h_n	mm	128	95	75	38
k_T	m/d	237.65	Δh_n	mm	33	20	37	38
			k_n	m/d	242	400	216	210

Appendix A.15: Field Results – Northend (June 2009). See Section 5.15

NORTHEND - JUNE 2009			Point	A1	Measuring Depth (mm)			
Measurements (see Chapter 4)			(See Fig 4-6)		400	300	200	100
$D_{1(rsvr)}$	cm	3.7	1	mm	250	250	250	180
$D_{2(rsvr)}$	cm	5.2	2	mm	15	30	21	
Δt	s	1561	3	mm	16	28	30	0
$\Delta D_{(rsvr)}$	cm	1.5	4	mm	31	31	33	35
Q	m^3/d	42	$h_{T(probe)}$	mm	204	189	196	
$h_{T(ave)}$	mm	196	h_n	mm	203	191	187	145
k_T	m/d	2.60	Δh_n	mm	12	4	42	145
			k_n	m/d	10.6	31.9	3.0	0.9

NORTHEND - JUNE 2009			Point	A2	Measuring Depth (mm)			
Measurements (see Chapter 4)			(See Fig 4-6)		400	300	200	100
$D_{1(rsvr)}$	cm	7.6	1	mm	270	270	270	180
$D_{2(rsvr)}$	cm	11.8	2	mm	15	21	15	
Δt	s	869	3	mm	22	31	45	1
$\Delta D_{(rsvr)}$	cm	4.2	4	mm	65	67	63	61
Q	m^3/d	118	$h_{T(probe)}$	mm	190	182	192	
$h_{T(ave)}$	mm	188	h_n	mm	183	172	162	119
k_T	m/d	13.68	Δh_n	mm	11	10	44	119
			k_n	m/d	58	64	15	5

NORTHEND - JUNE 2009			Point	A3	Measuring Depth (mm)			
Measurements (see Chapter 4)			(See Fig 4-6)		400	300	200	100
$D_{1(rsvr)}$	cm	20.5	1	mm	250	250	250	180
$D_{2(rsvr)}$	cm	22.0	2	mm	10	15	8	
Δt	s	295	3	mm	13	16	12	0
$\Delta D_{(rsvr)}$	cm	1.5	4	mm	71	70	75	75
Q	m^3/d	42	$h_{T(probe)}$	mm	169	165	167	
$h_{T(ave)}$	mm	167	h_n	mm	166	164	163	105
k_T	m/d	16.20	Δh_n	mm	2	1	58	105
			k_n	m/d	338	676	12	6

NORTHEND - JUNE 2009			Point	A4	Measuring Depth (mm)			
Measurements (see Chapter 4)			(See Fig 4-6)		400	300	200	100
$D_{1(rsvr)}$	cm	2.2	1	mm	240	240	240	180
$D_{2(rsvr)}$	cm	4.3	2	mm	17	12	9	
Δt	s	1551	3	mm	13	14	23	0
$\Delta D_{(rsvr)}$	cm	2.1	4	mm	54	56	52	51
Q	m^3/d	59	$h_{T(probe)}$	mm	169	172	179	
$h_{T(ave)}$	mm	173	h_n	mm	173	170	165	129
k_T	m/d	4.16	Δh_n	mm	3	5	36	129
			k_n	m/d	60	36	5	1

NORTHEND - JUNE 2009			Point	B1	Measuring Depth (mm)			
Measurements (see Chapter 4)			(See Fig 4-6)		400	300	200	100
$D_{1(rsvr)}$	cm	10.8	1	mm	320	320	270	100
$D_{2(rsvr)}$	cm	11.0	2	mm	7	18		
Δt	s	1991	3	mm	8	27	17	41
$\Delta D_{(rsvr)}$	cm	0.2	4	mm	33	30	29	28
Q	m^3/d	6	$h_{T(probe)}$	mm	280	272		
$h_{T(ave)}$	mm	276	h_n	mm	279	263	224	31
k_T	m/d	0.19	Δh_n	mm	16	39	193	31
			k_n	m/d	0.83	0.34	0.07	0.43

NORTHEND - JUNE 2009			Point	B2	Measuring Depth (mm)			
Measurements (see Chapter 4)			(See Fig 4-6)		400	300	200	100
$D_{1(rsvr)}$	cm	3.2	1	mm	300	300	270	120
$D_{2(rsvr)}$	cm	3.2	2	mm	14	8		
Δt	s	2220	3	mm	15	9	0	21
$\Delta D_{(rsvr)}$	cm	0.1	4	mm	39	48	44	46
Q	m^3/d	1	$h_{T(probe)}$	mm	247	244	226	
$h_{T(ave)}$	mm	239	h_n	mm	246	243	226	53
k_T	m/d	0.05	Δh_n	mm	3	17	173	53
			k_n	m/d	1.00	0.17	0.02	0.06

NORTHEND - JUNE 2009			Point	B3	Measuring Depth (mm)			
Measurements (see Chapter 4)			(See Fig 4-6)		400	300	200	100
$D_{1(rsvr)}$	cm	4.0	1	mm	270	270	270	180
$D_{2(rsvr)}$	cm	4.1	2	mm	21	18	17	
Δt	s	2450	3	mm	20	16	19	0
$\Delta D_{(rsvr)}$	cm	0.0	4	mm	56	61	60	56
Q	m^3/d	1	$h_{T(probe)}$	mm	193	191	193	
$h_{T(ave)}$	mm	192	h_n	mm	194	193	191	124
k_T	m/d	0.06	Δh_n	mm	1	2	67	124
			k_n	m/d	2.71	1.36	0.04	0.02

NORTHEND - JUNE 2009			Point	B4	Measuring Depth (mm)			
Measurements (see Chapter 4)			(See Fig 4-6)		400	300	200	100
$D_{1(rsvr)}$	cm	7.7	1	mm	240	240	240	180
$D_{2(rsvr)}$	cm	7.8	2	mm	17	18		
Δt	s	1800	3	mm	18	19	9	2
$\Delta D_{(rsvr)}$	cm	0.1	4	mm	51	51	62	57
Q	m^3/d	3	$h_{T(probe)}$	mm	172	171	178	
$h_{T(ave)}$	mm	174	h_n	mm	171	170	169	121
k_T	m/d	0.17	Δh_n	mm	1	1	48	121
			k_n	m/d	7.39	7.39	0.15	0.06

NORTHEND - JUNE 2009			Point	C1	Measuring Depth (mm)			
Measurements (see Chapter 4)			(See Fig 4-6)		400	300	200	100
$D_{1(rsvr)}$	cm	10.8	1	mm	320	320	270	100
$D_{2(rsvr)}$	cm	11.0	2	mm	7	18		
Δt	s	1991	3	mm	8	27	17	41
$\Delta D_{(rsvr)}$	cm	0.2	4	mm	33	30	29	28
Q	m^3/d	6	$h_{T(probe)}$	mm	280	272		
$h_{T(ave)}$	mm	276	h_n	mm	279	263	224	31
k_T	m/d	0.19	Δh_n	mm	16	39	193	31
			k_n	m/d	0.83	0.34	0.07	0.43

NORTHEND - JUNE 2009			Point	C2	Measuring Depth (mm)			
Measurements (see Chapter 4)			(See Fig 4-6)		400	300	200	100
$D_{1(rsvr)}$	cm	8.5	1	mm	300	300	270	180
$D_{2(rsvr)}$	cm	9.9	2	mm	10	1	16	
Δt	s	600	3	mm	9	5	26	0
$\Delta D_{(rsvr)}$	cm	1.4	4	mm	20	29	32	27
Q	m^3/d	38	$h_{T(probe)}$	mm	270	270		
$h_{T(ave)}$	mm	270	h_n	mm	271	266	212	153
k_T	m/d	4.43	Δh_n	mm	5	54	59	153
			k_n	m/d	60	6	5	2

NORTHEND - JUNE 2009			Point	C3	Measuring Depth (mm)			
Measurements (see Chapter 4)			(See Fig 4-6)		400	300	200	100
$D_{1(rsvr)}$	cm	18.7	1	mm	280	280	270	180
$D_{2(rsvr)}$	cm	19.2	2	mm	21	12	4	
Δt	s	1641	3	mm	22	15	7	1
$\Delta D_{(rsvr)}$	cm	0.5	4	mm	31	39	38	41
Q	m^3/d	14	$h_{T(probe)}$	mm	228	229		
$h_{T(ave)}$	mm	229	h_n	mm	227	226	225	138
k_T	m/d	0.71	Δh_n	mm	1	1	87	138
			k_n	m/d	40.5	40.5	0.5	0.3

NORTHEND - JUNE 2009			Point	C4	Measuring Depth (mm)			
Measurements (see Chapter 4)			(See Fig 4-6)		400	300	200	100
$D_{1(rsvr)}$	cm	12.4	1	mm	250	250	250	180
$D_{2(rsvr)}$	cm	15.6	2	mm	10	11	15	
Δt	s	1006	3	mm	15	14	14	15
$\Delta D_{(rsvr)}$	cm	3.2	4	mm	26	29	33	34
Q	m^3/d	90	$h_{T(probe)}$	mm	214	210	202	
$h_{T(ave)}$	mm	209	h_n	mm	209	207	203	131
k_T	m/d	8.11	Δh_n	mm	2	4	72	131
			k_n	m/d	212	106	6	3

NORTHEND - JUNE 2009			Point	D1	Measuring Depth (mm)			
Measurements (see Chapter 4)			(See Fig 4-6)		400	300	200	100
$D_{1(rsvr)}$	cm	4.1	1	mm	250	250	250	150
$D_{2(rsvr)}$	cm	4.3	2	mm	(3)	(2)	15	
Δt	s	2400	3	mm	4	8	18	0
$\Delta D_{(rsvr)}$	cm	0.2	4	mm	18	16	21	27
Q	m^3/d	4	$h_{T(probe)}$	mm	235	236	214	
$h_{T(ave)}$	mm	228	h_n	mm	228	226	211	123
k_T	m/d	0.15	Δh_n	mm	2	15	88	123
			k_n	m/d	4.16	0.55	0.09	0.07

NORTHEND - JUNE 2009			Point	D2	Measuring Depth (mm)			
Measurements (see Chapter 4)			(See Fig 4-6)		400	300	200	100
$D_{1(rsvr)}$	cm	6.8	1	mm	280	280	260	100
$D_{2(rsvr)}$	cm	6.9	2	mm	18	9	8	
Δt	s	3600	3	mm	28	27	7	3
$\Delta D_{(rsvr)}$	cm	0.2	4	mm	48	51	53	53
Q	m^3/d	4	$h_{T(probe)}$	mm	214	220	199	
$h_{T(ave)}$	mm	211	h_n	mm	204	202	200	44
k_T	m/d	0.11	Δh_n	mm	2	2	156	44
			k_n	m/d	2.77	2.77	0.04	0.13

NORTHEND - JUNE 2009			Point	D3	Measuring Depth (mm)			
Measurements (see Chapter 4)			(See Fig 4-6)		400	300	200	100
$D_{1(rsvr)}$	cm	9.4	1	mm	250	250	250	180
$D_{2(rsvr)}$	cm	9.6	2	mm	21	19	22	
Δt	s	2197	3	mm	26	27	28	0
$\Delta D_{(rsvr)}$	cm	0.2	4	mm	51	52	52	54
Q	m^3/d	6	$h_{T(probe)}$	mm	178	179	176	
$h_{T(ave)}$	mm	178	h_n	mm	173	171	170	126
k_T	m/d	0.27	Δh_n	mm	2	1	44	126
			k_n	m/d	6.05	12.11	0.27	0.10

NORTHEND - JUNE 2009			Point	D4	Measuring Depth (mm)			
Measurements (see Chapter 4)			(See Fig 4-6)		400	300	200	100
$D_{1(rsvr)}$	cm	11.9	1	mm	220	220	230	180
$D_{2(rsvr)}$	cm	13.3	2	mm	1	6	10	
Δt	s	720	3	mm	2	8	19	0
$\Delta D_{(rsvr)}$	cm	1.4	4	mm	54	59	59	52
Q	m^3/d	39	$h_{T(probe)}$	mm	165	155		
$h_{T(ave)}$	mm	160	h_n	mm	164	153	152	128
k_T	m/d	6.46	Δh_n	mm	11	1	24	128
			k_n	m/d	24	259	11	2

NORTHEND - JUNE 2009			Point	E1	Measuring Depth (mm)			
Measurements (see Chapter 4)			(See Fig 4-6)		400	300	200	100
$D_{1(rsvr)}$	cm	6.9	1	mm	270	270	270	180
$D_{2(rsvr)}$	cm	9.3	2	mm	22	13	8	
Δt	s	1881	3	mm	24	17	44	0
$\Delta D_{(rsvr)}$	cm	2.4	4	mm	53	62	62	52
Q	m^3/d	67	$h_{T(probe)}$	mm	195	195	200	
$h_{T(ave)}$	mm	197	h_n	mm	193	191	164	128
k_T	m/d	3.45	Δh_n	mm	2	27	36	128
			k_n	m/d	85	6	5	1

NORTHEND - JUNE 2009			Point	E2	Measuring Depth (mm)			
Measurements (see Chapter 4)			(See Fig 4-6)		400	300	200	100
$D_{1(rsvr)}$	cm	3.3	1	mm	260	240	240	180
$D_{2(rsvr)}$	cm	3.7	2	mm	20	4	6	
Δt	s	2100	3	mm	21	6	30	0
$\Delta D_{(rsvr)}$	cm	0.4	4	mm	57	60	65	71
Q	m^3/d	11	$h_{T(probe)}$	mm	183	176	169	
$h_{T(ave)}$	mm	176	h_n	mm	182	174	145	109
k_T	m/d	0.58	Δh_n	mm	8	29	36	109
			k_n	m/d	3.2	0.9	0.7	0.2

NORTHEND - JUNE 2009			Point	E3	Measuring Depth (mm)			
Measurements (see Chapter 4)			(See Fig 4-6)		400	300	200	100
$D_{1(rsvr)}$	cm	11.8	1	mm	240	240	240	180
$D_{2(rsvr)}$	cm	14.5	2	mm	14	11	11	
Δt	s	1187	3	mm	9	7	13	0
$\Delta D_{(rsvr)}$	cm	2.7	4	mm	58	63	58	72
Q	m^3/d	76	$h_{T(probe)}$	mm	168	166	171	
$h_{T(ave)}$	mm	168	h_n	mm	173	170	169	108
k_T	m/d	7.19	Δh_n	mm	3	1	61	108
			k_n	m/d	101	303	5	3

NORTHEND - JUNE 2009			Point	E4	Measuring Depth (mm)			
Measurements (see Chapter 4)			(See Fig 4-6)		400	300	200	100
$D_{1(rsvr)}$	cm	4.6	1	mm	220	200	200	150
$D_{2(rsvr)}$	cm	9.6	2	mm	25	13	16	
Δt	s	652	3	mm	16	24	41	36
$\Delta D_{(rsvr)}$	cm	5.0	4	mm	66	64	58	72
Q	m^3/d	140	$h_{T(probe)}$	mm	129	123		
$h_{T(ave)}$	mm	126	h_n	mm	138	112	101	42
k_T	m/d	32.38	Δh_n	mm	26	11	59	42
			k_n	m/d	39	93	17	24

Appendix A.16: Field Results – Rowington (July 2009). See Section 5.16

ROWINGTON - JULY 2009			Point	A1	Measuring Depth (mm)			
Measurements (see Chapter 4)			(See Fig 4-6)		400	300	200	100
$D_{1(rsvr)}$	cm	4.9	1	mm	410	370	270	100
$D_{2(rsvr)}$	cm	5.0	2	mm	3			
Δt	s	2736	3	mm	0	0	61	40
$\Delta D_{(rsvr)}$	cm	0.2	4	mm	64	64	59	59
Q	m^3/d	4	$h_{T(probe)}$	mm	343			
$h_{T(ave)}$	mm	343	h_n	mm	346	306	150	1
k_T	m/d	0.09	Δh_n	mm	40	156	149	1
			k_n	m/d	0.18	0.05	0.05	7.29

ROWINGTON - JULY 2009			Point	A2	Measuring Depth (mm)			
Measurements (see Chapter 4)			(See Fig 4-6)		400	300	200	100
$D_{1(rsvr)}$	cm	8.8	1	mm	370	370	270	180
$D_{2(rsvr)}$	cm	8.9	2	mm	6	7		
Δt	s	2100	3	mm	28	34	0	0
$\Delta D_{(rsvr)}$	cm	0.2	4	mm	36	33	36	38
Q	m^3/d	4	$h_{T(probe)}$	mm	328	330		
$h_{T(ave)}$	mm	329	h_n	mm	306	303	234	142
k_T	m/d	0.12	Δh_n	mm	3	69	92	142
			k_n	m/d	3.17	0.14	0.10	0.07

ROWINGTON - JULY 2009			Point	A3	Measuring Depth (mm)			
Measurements (see Chapter 4)			(See Fig 4-6)		400	300	200	100
$D_{1(rsvr)}$	cm	11.0	1	mm	340	340	270	180
$D_{2(rsvr)}$	cm	17.5	2	mm	20	15		
Δt	s	38	3	mm	47	92	63	1
$\Delta D_{(rsvr)}$	cm	6.5	4	mm	40	52	43	42
Q	m^3/d	183	$h_{T(probe)}$	mm	280	273		
$h_{T(ave)}$	mm	277	h_n	mm	253	196	164	138
k_T	m/d	329.09	Δh_n	mm	57	32	27	138
			k_n	m/d	399	711	858	165

ROWINGTON - JULY 2009			Point	A4	Measuring Depth (mm)			
Measurements (see Chapter 4)			(See Fig 4-6)		400	300	200	100
$D_{1(rsvr)}$	cm	10.0	1	mm	300	280	270	180
$D_{2(rsvr)}$	cm	18.0	2	mm	9	5	9	
Δt	s	192	3	mm	10	11	14	0
$\Delta D_{(rsvr)}$	cm	8.0	4	mm	52	42	40	41
Q	m^3/d	225	$h_{T(probe)}$	mm	239	233	221	
$h_{T(ave)}$	mm	231	h_n	mm	238	227	216	139
k_T	m/d	95.95	Δh_n	mm	11	11	77	139
			k_n	m/d	504	504	72	40

ROWINGTON - JULY 2009			Point	B1	Measuring Depth (mm)			
Measurements (see Chapter 4)			(See Fig 4-6)		400	300	200	100
$D_{1(rsvr)}$	cm	3.6	1	mm	290	270	270	100
$D_{2(rsvr)}$	cm	3.6	2	mm	16			
Δt	s	2460	3	mm	8	33	155	20
$\Delta D_{(rsvr)}$	cm	0.1	4	mm	67	63	56	62
Q	m^3/d	1	$h_{T(probe)}$	mm	207			
$h_{T(ave)}$	mm	207	h_n	mm	215	174	59	18
k_T	m/d	0.05	Δh_n	mm	41	115	41	18
			k_n	m/d	0.07	0.02	0.07	0.15

ROWINGTON - JULY 2009			Point	B2	Measuring Depth (mm)			
Measurements (see Chapter 4)			(See Fig 4-6)		400	300	200	100
$D_{1(rsvr)}$	cm	7.2	1	mm	490	370	270	130
$D_{2(rsvr)}$	cm	7.4	2	mm	17			
Δt	s	2554	3	mm	17	7	65	27
$\Delta D_{(rsvr)}$	cm	0.2	4	mm	66	63	56	62
Q	m^3/d	6	$h_{T(probe)}$	mm	407			
$h_{T(ave)}$	mm	407	h_n	mm	407	300	149	41
k_T	m/d	0.10	Δh_n	mm	107	151	108	41
			k_n	m/d	0.10	0.07	0.10	0.25

ROWINGTON - JULY 2009			Point	B3	Measuring Depth (mm)			
Measurements (see Chapter 4)			(See Fig 4-6)		400	300	200	100
$D_{1(rsvr)}$	cm	12.7	1	mm	350	350	270	180
$D_{2(rsvr)}$	cm	14.7	2	mm	31	31		
Δt	s	1965	3	mm	24	26	0	0
$\Delta D_{(rsvr)}$	cm	2.1	4	mm	55	55	56	52
Q	m^3/d	58	$h_{T(probe)}$	mm	264	264	214	
$h_{T(ave)}$	mm	247	h_n	mm	271	269	214	128
k_T	m/d	2.24	Δh_n	mm	2	55	86	128
			k_n	m/d	69	3	2	1

ROWINGTON - JULY 2009			Point	B4	Measuring Depth (mm)			
Measurements (see Chapter 4)			(See Fig 4-6)		400	300	200	100
$D_{1(rsvr)}$	cm	4.0	1	mm	330	330	270	180
$D_{2(rsvr)}$	cm	16.0	2	mm	31	32		
Δt	s	175	3	mm	32	79	78	25
$\Delta D_{(rsvr)}$	cm	12.0	4	mm	61	60	56	55
Q	m^3/d	337	$h_{T(probe)}$	mm	238	238	214	
$h_{T(ave)}$	mm	230	h_n	mm	237	191	136	100
k_T	m/d	158.60	Δh_n	mm	46	55	36	100
			k_n	m/d	198	166	253	91

ROWINGTON - JULY 2009			Point	C1	Measuring Depth (mm)			
Measurements (see Chapter 4)			(See Fig 4-6)		400	300	200	100
$D_{1(rsvr)}$	cm	9.2	1	mm	320	320	270	120
$D_{2(rsvr)}$	cm	9.2	2	mm	15			
Δt	s	2700	3	mm	15	56	127	17
$\Delta D_{(rsvr)}$	cm	0.0	4	mm	35	36	39	24
Q	m^3/d	0	$h_{T(probe)}$	mm	270			
$h_{T(ave)}$	mm	270	h_n	mm	270	228	104	79
k_T	m/d	0.004	Δh_n	mm	42	124	25	79
			k_n	m/d	0.006	0.002	0.010	0.003

ROWINGTON - JULY 2009			Point	C2	Measuring Depth (mm)			
Measurements (see Chapter 4)			(See Fig 4-6)		400	300	200	100
$D_{1(rsvr)}$	cm	14.1	1	mm	480	370	270	150
$D_{2(rsvr)}$	cm	14.1	2	mm	11			
Δt	s	2700	3	mm	13	0	0	70
$\Delta D_{(rsvr)}$	cm	0.0	4	mm	56	55	57	53
Q	m^3/d	0	$h_{T(probe)}$	mm	413	315		
$h_{T(ave)}$	mm	364	h_n	mm	411	315	213	27
k_T	m/d	0.003	Δh_n	mm	96	102	186	27
			k_n	m/d	0.003	0.002	0.001	0.009

ROWINGTON - JULY 2009			Point	C3	Measuring Depth (mm)			
Measurements (see Chapter 4)			(See Fig 4-6)		400	300	200	100
$D_{1(rsvr)}$	cm	20.2	1	mm	390	370	270	180
$D_{2(rsvr)}$	cm	20.4	2	mm	12			
Δt	s	1325	3	mm	13	0	0	19
$\Delta D_{(rsvr)}$	cm	0.2	4	mm	55	51	42	46
Q	m^3/d	6	$h_{T(probe)}$	mm	323	319		
$h_{T(ave)}$	mm	321	h_n	mm	322	319	228	115
k_T	m/d	0.25	Δh_n	mm	3	91	113	115
			k_n	m/d	6.48	0.22	0.18	0.17

ROWINGTON - JULY 2009			Point	C4	Measuring Depth (mm)			
Measurements (see Chapter 4)			(See Fig 4-6)		400	300	200	100
$D_{1(rsvr)}$	cm	3.8	1	mm	340	340	270	180
$D_{2(rsvr)}$	cm	10.0	2	mm	35	30		
Δt	s	654	3	mm	23	31	0	0
$\Delta D_{(rsvr)}$	cm	6.3	4	mm	61	62	69	75
Q	m^3/d	176	$h_{T(probe)}$	mm	244	248		
$h_{T(ave)}$	mm	246	h_n	mm	256	247	201	105
k_T	m/d	20.67	Δh_n	mm	9	46	96	105
			k_n	m/d	141	28	13	12

ROWINGTON - JULY 2009			Point	D1	Measuring Depth (mm)			
Measurements (see Chapter 4)			(See Fig 4-6)		400	300	200	100
$D_{1(rsvr)}$	cm	12.1	1	mm	310	260	260	130
$D_{2(rsvr)}$	cm	12.3	2	mm	14			
Δt	s	1781	3	mm	11	18	20	28
$\Delta D_{(rsvr)}$	cm	0.2	4	mm	54	53	53	56
Q	m^3/d	6	$h_{T(probe)}$	mm	242			
$h_{T(ave)}$	mm	242	h_n	mm	245	189	187	46
k_T	m/d	0.25	Δh_n	mm	56	2	141	46
			k_n	m/d	0.27	7.47	0.11	0.32

ROWINGTON - JULY 2009			Point	D2	Measuring Depth (mm)			
Measurements (see Chapter 4)			(See Fig 4-6)		400	300	200	100
$D_{1(rsvr)}$	cm	7.3	1	mm	350	330	180	100
$D_{2(rsvr)}$	cm	7.3	2	mm	3			
Δt	s	2220	3	mm	0	5	17	22
$\Delta D_{(rsvr)}$	cm	0.0	4	mm	82	80	73	75
Q	m^3/d	0	$h_{T(probe)}$	mm	265			
$h_{T(ave)}$	mm	265	h_n	mm	268	245	90	3
k_T	m/d	0.005	Δh_n	mm	23	155	87	3
			k_n	m/d	0.013	0.002	0.003	0.100

ROWINGTON - JULY 2009			Point	D3	Measuring Depth (mm)			
Measurements (see Chapter 4)			(See Fig 4-6)		400	300	200	100
$D_{1(rsvr)}$	cm	3.4	1	mm	370	370	270	150
$D_{2(rsvr)}$	cm	4.1	2	mm	6			
Δt	s	2400	3	mm	6	0	0	35
$\Delta D_{(rsvr)}$	cm	0.7	4	mm	42	51	43	42
Q	m^3/d	20	$h_{T(probe)}$	mm	322			
$h_{T(ave)}$	mm	322	h_n	mm	322	319	227	73
k_T	m/d	0.48	Δh_n	mm	3	92	154	73
			k_n	m/d	13	0	0	1

ROWINGTON - JULY 2009			Point	D4	Measuring Depth (mm)			
Measurements (see Chapter 4)			(See Fig 4-6)		400	300	200	100
$D_{1(rsvr)}$	cm	14.5	1	mm	370	370	270	180
$D_{2(rsvr)}$	cm	19.0	2	mm	13	8		
Δt	s	110	3	mm	14	38	0	0
$\Delta D_{(rsvr)}$	cm	4.5	4	mm	63	63	61	55
Q	m^3/d	126	$h_{T(probe)}$	mm	294	299		
$h_{T(ave)}$	mm	297	h_n	mm	293	269	209	125
k_T	m/d	73.40	Δh_n	mm	24	60	84	125
			k_n	m/d	227	91	65	44

ROWINGTON - JULY 2009			Point	E1	Measuring Depth (mm)			
Measurements (see Chapter 4)			(See Fig 4-6)		400	300	200	100
$D_{1(rsvr)}$	cm	18.2	1	mm	270	220	60	40
$D_{2(rsvr)}$	cm	18.3	2	mm	14			
Δt	s	2700	3	mm	13	9	19	8
$\Delta D_{(rsvr)}$	cm	0.1	4	mm	35	35	37	31
Q	m^3/d	1	$h_{T(probe)}$	mm	221			
$h_{T(ave)}$	mm	221	h_n	mm	222	176	4	1
k_T	m/d	0.04	Δh_n	mm	46	172	3	1
			k_n	m/d	0.05	0.01	0.82	2.46

ROWINGTON - JULY 2009			Point	E2	Measuring Depth (mm)			
Measurements (see Chapter 4)			(See Fig 4-6)		400	300	200	100
$D_{1(rsvr)}$	cm	5.8	1	mm	250	240	170	80
$D_{2(rsvr)}$	cm	6.4	2	mm	6			
Δt	s	1680	3	mm	8	19	7	17
$\Delta D_{(rsvr)}$	cm	0.6	4	mm	45	51	52	52
Q	m^3/d	17	$h_{T(probe)}$	mm	199			
$h_{T(ave)}$	mm	199	h_n	mm	197	170	111	11
k_T	m/d	0.95	Δh_n	mm	27	59	100	11
			k_n	m/d	1.8	0.8	0.5	4.3

ROWINGTON - JULY 2009			Point	E3	Measuring Depth (mm)			
Measurements (see Chapter 4)			(See Fig 4-6)		400	300	200	100
$D_{1(rsvr)}$	cm	8.3	1	mm	390	300	250	150
$D_{2(rsvr)}$	cm	9.1	2	mm	14			
Δt	s	1094	3	mm	22	6	6	10
$\Delta D_{(rsvr)}$	cm	0.9	4	mm	61	64	60	69
Q	m^3/d	24	$h_{T(probe)}$	mm	315			
$h_{T(ave)}$	mm	315	h_n	mm	307	230	184	71
k_T	m/d	1.31	Δh_n	mm	77	46	113	71
			k_n	m/d	1.3	2.2	0.9	1.5

ROWINGTON - JULY 2009			Point	E4	Measuring Depth (mm)			
Measurements (see Chapter 4)			(See Fig 4-6)		400	300	200	100
$D_{1(rsvr)}$	cm	11.7	1	mm	360	270	270	180
$D_{2(rsvr)}$	cm	19.0	2	mm	15			
Δt	s	508	3	mm	19	7	10	0
$\Delta D_{(rsvr)}$	cm	7.3	4	mm	47	53	51	55
Q	m^3/d	205	$h_{T(probe)}$	mm	298	217		
$h_{T(ave)}$	mm	258	h_n	mm	294	210	209	125
k_T	m/d	29.69	Δh_n	mm	84	1	84	125
			k_n	m/d	23	1,911	23	15

Appendix A.17: Field Results – Snitterfield (August 2009). See Section 5.17

SNITTERFIELD - AUGUST 2009			Point	A1	Measuring Depth (mm)			
Measurements (see Chapter 4)			(See Fig 4-6)		400	300	200	100
$D_{1(rsvr)}$	cm	9.6	1	mm	240	240	260	175
$D_{2(rsvr)}$	cm	9.7	2	mm	25	26	14	
Δt	s	3300	3	mm	30	37	93	102
$\Delta D_{(rsvr)}$	cm	0.1	4	mm	66	61	58	55
Q	m^3/d	3	$h_{T(probe)}$	mm	149	153	188	
$h_{T(ave)}$	mm	163	h_n	mm	144	142	109	18
k_T	m/d	0.10	Δh_n	mm	2	33	91	18
			k_n	m/d	2.02	0.12	0.04	0.22

SNITTERFIELD - AUGUST 2009			Point	A2	Measuring Depth (mm)			
Measurements (see Chapter 4)			(See Fig 4-6)		400	300	200	100
$D_{1(rsvr)}$	cm	10.4	1	mm	220	220	220	175
$D_{2(rsvr)}$	cm	10.7	2	mm	25	28	24	
Δt	s	2265	3	mm	30	32	51	54
$\Delta D_{(rsvr)}$	cm	0.3	4	mm	71	71	73	65
Q	m^3/d	8	$h_{T(probe)}$	mm	124	121	123	
$h_{T(ave)}$	mm	123	h_n	mm	119	117	96	56
k_T	m/d	0.57	Δh_n	mm	2	21	40	56
			k_n	m/d	8.81	0.84	0.44	0.31

SNITTERFIELD - AUGUST 2009			Point	A3	Measuring Depth (mm)			
Measurements (see Chapter 4)			(See Fig 4-6)		400	300	200	100
$D_{1(rsvr)}$	cm	15.4	1	mm	230	230	230	175
$D_{2(rsvr)}$	cm	15.8	2	mm	30	24		
Δt	s	1200	3	mm	29	31	70	47
$\Delta D_{(rsvr)}$	cm	0.5	4	mm	50	50	53	45
Q	m^3/d	13	$h_{T(probe)}$	mm	150	156		
$h_{T(ave)}$	mm	153	h_n	mm	151	149	107	83
k_T	m/d	1.30	Δh_n	mm	2	42	24	83
			k_n	m/d	24.9	1.2	2.1	0.6

SNITTERFIELD - AUGUST 2009			Point	A4	Measuring Depth (mm)			
Measurements (see Chapter 4)			(See Fig 4-6)		400	300	200	100
$D_{1(rsvr)}$	cm	21.1	1	mm	140	150	150	150
$D_{2(rsvr)}$	cm	21.2	2	mm	20	20	16	18
Δt	s	1200	3	mm	25	23	23	51
$\Delta D_{(rsvr)}$	cm	0.1	4	mm	50	63	67	76
Q	m^3/d	3	$h_{T(probe)}$	mm	70	67	67	56
$h_{T(ave)}$	mm	65	h_n	mm	65	64	60	23
k_T	m/d	0.68	Δh_n	mm	1	4	37	23
			k_n	m/d	11.08	2.77	0.30	0.48

SNITTERFIELD - AUGUST 2009			Point	B1	Measuring Depth (mm)			
Measurements (see Chapter 4)			(See Fig 4-6)		400	300	200	100
$D_{1(rsvr)}$	cm	2.5	1	mm	270	270	270	175
$D_{2(rsvr)}$	cm	2.5	2	mm	13	17		
Δt	s	3600	3	mm	19	25	32	72
$\Delta D_{(rsvr)}$	cm	0.0	4	mm	43	40	37	36
Q	m^3/d	1	$h_{T(probe)}$	mm	214			
$h_{T(ave)}$	mm	214	h_n	mm	208	205	201	67
k_T	m/d	0.03	Δh_n	mm	3	4	134	67
			k_n	m/d	0.62	0.46	0.01	0.03

SNITTERFIELD - AUGUST 2009			Point	B2	Measuring Depth (mm)			
Measurements (see Chapter 4)			(See Fig 4-6)		400	300	200	100
$D_{1(rsvr)}$	cm	7.9	1	mm	220	220	220	175
$D_{2(rsvr)}$	cm	8.4	2	mm	11	6	8	
Δt	s	1618	3	mm	14	14	17	2
$\Delta D_{(rsvr)}$	cm	0.6	4	mm	73	74	72	72
Q	m^3/d	15	$h_{T(probe)}$	mm	136	140	140	
$h_{T(ave)}$	mm	139	h_n	mm	133	132	131	101
k_T	m/d	1.30	Δh_n	mm	1	1	30	101
			k_n	m/d	45.2	45.2	1.5	0.4

SNITTERFIELD - AUGUST 2009			Point	B3	Measuring Depth (mm)			
Measurements (see Chapter 4)			(See Fig 4-6)		400	300	200	100
$D_{1(rsvr)}$	cm	11.7	1	mm	220	220	220	175
$D_{2(rsvr)}$	cm	14.2	2	mm	5	8	8	
Δt	s	1244	3	mm	6	17	18	34
$\Delta D_{(rsvr)}$	cm	2.5	4	mm	75	71	74	73
Q	m^3/d	70	$h_{T(probe)}$	mm	140	141	138	
$h_{T(ave)}$	mm	140	h_n	mm	139	132	128	68
k_T	m/d	7.65	Δh_n	mm	7	4	60	68
			k_n	m/d	38.2	66.8	4.5	3.9

SNITTERFIELD - AUGUST 2009			Point	B4	Measuring Depth (mm)			
Measurements (see Chapter 4)			(See Fig 4-6)		400	300	200	100
$D_{1(rsvr)}$	cm	21.1	1	mm	190	200	200	175
$D_{2(rsvr)}$	cm	21.5	2	mm	24	24	20	9
Δt	s	1270	3	mm	25	47	49	59
$\Delta D_{(rsvr)}$	cm	0.4	4	mm	44	49	53	49
Q	m^3/d	11	$h_{T(probe)}$	mm	122	127		
$h_{T(ave)}$	mm	125	h_n	mm	121	104	98	67
k_T	m/d	1.35	Δh_n	mm	17	6	31	67
			k_n	m/d	2.5	7.0	1.4	0.6

SNITTERFIELD - AUGUST 2009			Point	C1	Measuring Depth (mm)			
Measurements (see Chapter 4)			(See Fig 4-6)		400	300	200	100
$D_{1(rsvr)}$	cm	14.2	1	mm	360	350	270	175
$D_{2(rsvr)}$	cm	14.2	2	mm	8			
Δt	s	3600	3	mm	14	85	104	84
$\Delta D_{(rsvr)}$	cm	0.0	4	mm	49	51	59	55
Q	m^3/d	1	$h_{T(probe)}$	mm	303			
$h_{T(ave)}$	mm	303	h_n	mm	297	214	107	36
k_T	m/d	0.02	Δh_n	mm	83	107	71	36
			k_n	m/d	0.02	0.02	0.03	0.05

SNITTERFIELD - AUGUST 2009			Point	C2	Measuring Depth (mm)			
Measurements (see Chapter 4)			(See Fig 4-6)		400	300	200	100
$D_{1(rsvr)}$	cm	19.1	1	mm	310	320	270	175
$D_{2(rsvr)}$	cm	19.5	2	mm	8			
Δt	s	2936	3	mm	15	88	124	100
$\Delta D_{(rsvr)}$	cm	0.4	4	mm	48	51	54	62
Q	m^3/d	11	$h_{T(probe)}$	mm	254	269		
$h_{T(ave)}$	mm	262	h_n	mm	247	181	92	13
k_T	m/d	0.28	Δh_n	mm	66	89	79	13
			k_n	m/d	0.27	0.20	0.23	1.39

SNITTERFIELD - AUGUST 2009			Point	C3	Measuring Depth (mm)			
Measurements (see Chapter 4)			(See Fig 4-6)		400	300	200	100
$D_{1(rsvr)}$	cm	8.6	1	mm	310	300	270	175
$D_{2(rsvr)}$	cm	8.8	2	mm	12	11		
Δt	s	1537	3	mm	14	15	0	0
$\Delta D_{(rsvr)}$	cm	0.2	4	mm	67	66	64	54
Q	m^3/d	6	$h_{T(probe)}$	mm	231	223		
$h_{T(ave)}$	mm	227	h_n	mm	229	219	206	121
k_T	m/d	0.30	Δh_n	mm	10	13	85	121
			k_n	m/d	1.73	1.32	0.20	0.14

SNITTERFIELD - AUGUST 2009			Point	C4	Measuring Depth (mm)			
Measurements (see Chapter 4)			(See Fig 4-6)		400	300	200	100
$D_{1(rsvr)}$	cm	2.1	1	mm	260	260	260	175
$D_{2(rsvr)}$	cm	2.4	2	mm	9	8	5	
Δt	s	1463	3	mm	11	16	40	53
$\Delta D_{(rsvr)}$	cm	0.3	4	mm	58	60	62	62
Q	m^3/d	8	$h_{T(probe)}$	mm	193	192		
$h_{T(ave)}$	mm	193	h_n	mm	191	184	158	60
k_T	m/d	0.57	Δh_n	mm	7	26	98	60
			k_n	m/d	3.90	1.05	0.28	0.45

SNITTERFIELD - AUGUST 2009			Point	D1	Measuring Depth (mm)			
Measurements (see Chapter 4)			(See Fig 4-6)		400	300	200	100
$D_{1(rsvr)}$	cm	24.0	1	mm	330	340	270	175
$D_{2(rsvr)}$	cm	24.1	2	mm	3	16		
Δt	s	3438	3	mm	6	27	0	61
$\Delta D_{(rsvr)}$	cm	0.1	4	mm	47	50	51	51
Q	m^3/d	1	$h_{T(probe)}$	mm	280			
$h_{T(ave)}$	mm	280	h_n	mm	277	263	219	63
k_T	m/d	0.03	Δh_n	mm	14	44	156	63
			k_n	m/d	0.14	0.04	0.01	0.03

SNITTERFIELD - AUGUST 2009			Point	D2	Measuring Depth (mm)			
Measurements (see Chapter 4)			(See Fig 4-6)		400	300	200	100
$D_{1(rsvr)}$	cm	6.2	1	mm	260	260	260	175
$D_{2(rsvr)}$	cm	6.3	2	mm	13	20		
Δt	s	1219	3	mm	13	51	112	79
$\Delta D_{(rsvr)}$	cm	0.1	4	mm	66	63	56	62
Q	m^3/d	3	$h_{T(probe)}$	mm	181			
$h_{T(ave)}$	mm	181	h_n	mm	181	146	92	34
k_T	m/d	0.24	Δh_n	mm	35	54	58	34
			k_n	m/d	0.31	0.20	0.19	0.32

SNITTERFIELD - AUGUST 2009			Point	D3	Measuring Depth (mm)			
Measurements (see Chapter 4)			(See Fig 4-6)		400	300	200	100
$D_{1(rsvr)}$	cm	16.7	1	mm	250	240	250	175
$D_{2(rsvr)}$	cm	17.7	2	mm	8	4	9	
Δt	s	1617	3	mm	14	13	21	0
$\Delta D_{(rsvr)}$	cm	1.0	4	mm	49	43	48	52
Q	m^3/d	28	$h_{T(probe)}$	mm	193	193	193	
$h_{T(ave)}$	mm	193	h_n	mm	187	184	181	123
k_T	m/d	1.70	Δh_n	mm	3	3	58	123
			k_n	m/d	27.4	27.4	1.4	0.7

SNITTERFIELD - AUGUST 2009			Point	D4	Measuring Depth (mm)			
Measurements (see Chapter 4)			(See Fig 4-6)		400	300	200	100
$D_{1(rsvr)}$	cm	12.4	1	mm	230	230	230	175
$D_{2(rsvr)}$	cm	13.8	2	mm	11	10	7	
Δt	s	1461	3	mm	13	20	43	5
$\Delta D_{(rsvr)}$	cm	1.4	4	mm	57	56	55	54
Q	m^3/d	39	$h_{T(probe)}$	mm	162	164	168	
$h_{T(ave)}$	mm	165	h_n	mm	160	154	132	116
k_T	m/d	3.10	Δh_n	mm	6	22	16	116
			k_n	m/d	21.2	5.8	8.0	1.1

SNITTERFIELD - AUGUST 2009			Point	E1	Measuring Depth (mm)			
Measurements (see Chapter 4)			(See Fig 4-6)		400	300	200	100
$D_{1(rsvr)}$	cm	9.0	1	mm	280	270	250	175
$D_{2(rsvr)}$	cm	9.0	2	mm	16	25	27	
Δt	s	1800	3	mm	17	32	54	57
$\Delta D_{(rsvr)}$	cm	0.1	4	mm	44	46	48	51
Q	m^3/d	1	$h_{T(probe)}$	mm	220	199	175	
$h_{T(ave)}$	mm	198	h_n	mm	219	192	148	67
k_T	m/d	0.07	Δh_n	mm	27	44	81	67
			k_n	m/d	0.14	0.08	0.05	0.06

SNITTERFIELD - AUGUST 2009			Point	E2	Measuring Depth (mm)			
Measurements (see Chapter 4)			(See Fig 4-6)		400	300	200	100
$D_{1(rsvr)}$	cm	19.2	1	mm	270	260	270	175
$D_{2(rsvr)}$	cm	21.7	2	mm	9	3	18	
Δt	s	1203	3	mm	17	14	90	75
$\Delta D_{(rsvr)}$	cm	2.5	4	mm	51	50	53	53
Q	m^3/d	70	$h_{T(probe)}$	mm	210	207	199	
$h_{T(ave)}$	mm	205	h_n	mm	202	196	127	47
k_T	m/d	5.38	Δh_n	mm	6	69	80	47
			k_n	m/d	46	4	3	6

SNITTERFIELD - AUGUST 2009			Point	E3	Measuring Depth (mm)			
Measurements (see Chapter 4)			(See Fig 4-6)		400	300	200	100
$D_{1(rsvr)}$	cm	16.6	1	mm	260	250	260	175
$D_{2(rsvr)}$	cm	18.1	2	mm	12	6	7	
Δt	s	1149	3	mm	17	11	12	0
$\Delta D_{(rsvr)}$	cm	1.5	4	mm	62	60	70	76
Q	m^3/d	42	$h_{T(probe)}$	mm	186	184	183	
$h_{T(ave)}$	mm	184	h_n	mm	181	179	178	99
k_T	m/d	3.77	Δh_n	mm	2	1	79	99
			k_n	m/d	87	174	2	2

SNITTERFIELD - AUGUST 2009			Point	E4	Measuring Depth (mm)			
Measurements (see Chapter 4)			(See Fig 4-6)		400	300	200	100
$D_{1(rsvr)}$	cm	4.2	1	mm	220	210	210	175
$D_{2(rsvr)}$	cm	6.2	2	mm	14	7	5	
Δt	s	1716	3	mm	17	12	9	26
$\Delta D_{(rsvr)}$	cm	2.0	4	mm	50	48	53	42
Q	m^3/d	55	$h_{T(probe)}$	mm	156	155	152	
$h_{T(ave)}$	mm	154	h_n	mm	153	150	148	107
k_T	m/d	3.92	Δh_n	mm	3	2	41	107
			k_n	m/d	50	76	4	1

Appendix A.18: Field Results – Greens of Delwood (July 2009). See Section 5.18

Greens of Delwood - July 2009			Point	A1	*Measuring Depth (mm)*		
Measurements (see Chapter 4)			*(See Fig 4-6)*		400	300	200
$D_{1(rsvr)}$	cm	2.7	*1*	mm	110	110	110
$D_{2(rsvr)}$	cm	3.6	*2*	mm	18	14	20
Δt	s	3965	*3*	mm	9	7	20
$\Delta D_{(rsvr)}$	cm	0.9	*4*	mm	73	78	77
Q	m^3/d	25	$h_{T(probe)}$	mm	19	18	13
$h_{T(ave)}$	mm	17	h_n	mm	28	25	13
k_T	m/d	6.29	Δh_n	mm	3	12	13
			k_n	m/d	10.1	2.5	3.4

Greens of Delwood - July 2009			Point	A2	*Measuring Depth (mm)*		
Measurements (see Chapter 4)			*(See Fig 4-6)*		400	300	200
$D_{1(rsvr)}$	cm	9.4	*1*	mm	220	220	220
$D_{2(rsvr)}$	cm	24.7	*2*	mm	9	13	8
Δt	s	1425	*3*	mm	14	12	27
$\Delta D_{(rsvr)}$	cm	15.3	*4*	mm	105	110	100
Q	m^3/d	430	$h_{T(probe)}$	mm	106	97	112
$h_{T(ave)}$	mm	105	h_n	mm	101	98	93
k_T	m/d	47.26	Δh_n	mm	3	5	93
			k_n	m/d	476	286	23

Greens of Delwood - July 2009			Point	A3	*Measuring Depth (mm)*		
Measurements (see Chapter 4)			*(See Fig 4-6)*		400	300	200
$D_{1(rsvr)}$	cm	7.5	*1*	mm	260	260	260
$D_{2(rsvr)}$	cm	20.0	*2*	mm	3	7	14
Δt	s	120	*3*	mm	9	42	49
$\Delta D_{(rsvr)}$	cm	12.5	*4*	mm	88	99	97
Q	m^3/d	351	$h_{T(probe)}$	mm	169	154	149
$h_{T(ave)}$	mm	157	h_n	mm	163	119	114
k_T	m/d	306.01	Δh_n	mm	44	5	114
			k_n	m/d	315	2,771	179

Greens of Delwood - July 2009			Point	A4	*Measuring Depth (mm)*		
Measurements (see Chapter 4)			*(See Fig 4-6)*		400	300	200
$D_{1(rsvr)}$	cm	11.4	*1*	mm	200	200	200
$D_{2(rsvr)}$	cm	14.2	*2*	mm	26	20	20
Δt	s	292	*3*	mm	32	43	53
$\Delta D_{(rsvr)}$	cm	2.8	*4*	mm	88	99	97
Q	m^3/d	79	$h_{T(probe)}$	mm	86	81	83
$h_{T(ave)}$	mm	83	h_n	mm	80	58	50
k_T	m/d	53.18	Δh_n	mm	22	8	50
			k_n	m/d	58	159	38

Greens of Delwood - July 2009			Point	B1	*Measuring Depth (mm)*		
Measurements (see Chapter 4)			*(See Fig 4-6)*		400	300	200
$D_{1(rsvr)}$	cm	5.6	*1*	mm	110	110	120
$D_{2(rsvr)}$	cm	5.9	*2*	mm	10	16	15
Δt	s	2100	*3*	mm	10	19	35
$\Delta D_{(rsvr)}$	cm	0.3	*4*	mm	86	78	77
Q	m^3/d	8	$h_{T(probe)}$	mm	14	16	28
$h_{T(ave)}$	mm	19	h_n	mm	14	13	8
k_T	m/d	3.42	Δh_n	mm	1	5	8
			k_n	m/d	19.0	3.8	3.5

Greens of Delwood - July 2009			Point	B2	*Measuring Depth (mm)*		
Measurements (see Chapter 4)			*(See Fig 4-6)*		400	300	200
$D_{1(rsvr)}$	cm	13.5	*1*	mm	260	260	260
$D_{2(rsvr)}$	cm	20.0	*2*	mm	6	16	28
Δt	s	69	*3*	mm	18	47	54
$\Delta D_{(rsvr)}$	cm	6.5	*4*	mm	64	54	48
Q	m^3/d	183	$h_{T(probe)}$	mm	190	190	184
$h_{T(ave)}$	mm	188	h_n	mm	178	159	158
k_T	m/d	240.06	Δh_n	mm	19	1	158
			k_n	m/d	659	12,528	127

Greens of Delwood - July 2009			Point	B3	*Measuring Depth (mm)*		
Measurements (see Chapter 4)			*(See Fig 4-6)*		400	300	200
$D_{1(rsvr)}$	cm	9.0	*1*	mm	200	200	200
$D_{2(rsvr)}$	cm	17.0	*2*	mm	17	16	18
Δt	s	68	*3*	mm	32	36	55
$\Delta D_{(rsvr)}$	cm	8.0	*4*	mm	43	56	45
Q	m^3/d	225	$h_{T(probe)}$	mm	140	128	137
$h_{T(ave)}$	mm	135	h_n	mm	125	108	100
k_T	m/d	402.79	Δh_n	mm	17	8	100
			k_n	m/d	920	1,956	231

Greens of Delwood - July 2009			Point	B4	*Measuring Depth (mm)*		
Measurements (see Chapter 4)			*(See Fig 4-6)*		400	300	200
$D_{1(rsvr)}$	cm	11.6	*1*	mm	70	70	70
$D_{2(rsvr)}$	cm	14.5	*2*	mm	18	25	22
Δt	s	1722	*3*	mm	12	22	38
$\Delta D_{(rsvr)}$	cm	2.9	*4*	mm	36	30	31
Q	m^3/d	81	$h_{T(probe)}$	mm	16	15	17
$h_{T(ave)}$	mm	16	h_n	mm	22	18	1
k_T	m/d	50.43	Δh_n	mm	4	17	1
			k_n	m/d	56	13	359

Greens of Delwood - July 2009			Point	C1	*Measuring Depth (mm)*		
Measurements (see Chapter 4)			*(See Fig 4-6)*		400	300	200
$D_{1(rsvr)}$	cm	16.1	*1*	mm	100	100	100
$D_{2(rsvr)}$	cm	21.0	*2*	mm	1	1	1
Δt	s	3055	*3*	mm	0	2	5
$\Delta D_{(rsvr)}$	cm	4.9	*4*	mm	43	44	48
Q	m^3/d	138	$h_{T(probe)}$	mm	56	55	51
$h_{T(ave)}$	mm	54	h_n	mm	57	54	47
k_T	m/d	13.73	Δh_n	mm	3	7	47
			k_n	m/d	74	30	7

Greens of Delwood - July 2009			Point	C2	*Measuring Depth (mm)*		
Measurements (see Chapter 4)			*(See Fig 4-6)*		400	300	200
$D_{1(rsvr)}$	cm	13.5	*1*	mm	200	200	200
$D_{2(rsvr)}$	cm	21.5	*2*	mm	16	17	13
Δt	s	61	*3*	mm	26	42	85
$\Delta D_{(rsvr)}$	cm	8.0	*4*	mm	39	44	43
Q	m^3/d	225	$h_{T(probe)}$	mm	145	139	144
$h_{T(ave)}$	mm	143	h_n	mm	135	114	72
k_T	m/d	424.88	Δh_n	mm	21	42	72
			k_n	m/d	831	415	357

Greens of Delwood - July 2009			Point	C3	*Measuring Depth (mm)*		
Measurements (see Chapter 4)			*(See Fig 4-6)*		400	300	200
$D_{1(rsvr)}$	cm	9.0	*1*	mm	180	180	180
$D_{2(rsvr)}$	cm	20.0	*2*	mm	17	24	14
Δt	s	123	*3*	mm	48	52	63
$\Delta D_{(rsvr)}$	cm	11.0	*4*	mm	32	43	37
Q	m^3/d	309	$h_{T(probe)}$	mm	131	113	129
$h_{T(ave)}$	mm	124	h_n	mm	100	85	80
k_T	m/d	338.53	Δh_n	mm	15	5	80
			k_n	m/d	793	2,379	229

Greens of Delwood - July 2009			Point	C4	*Measuring Depth (mm)*		
Measurements (see Chapter 4)			*(See Fig 4-6)*		400	300	200
$D_{1(rsvr)}$	cm	6.7	*1*	mm	130	130	130
$D_{2(rsvr)}$	cm	10.8	*2*	mm	15	16	7
Δt	s	406	*3*	mm	2	7	8
$\Delta D_{(rsvr)}$	cm	4.1	*4*	mm	55	51	56
Q	m^3/d	115	$h_{T(probe)}$	mm	60	63	67
$h_{T(ave)}$	mm	63	h_n	mm	73	72	66
k_T	m/d	75.04	Δh_n	mm	1	6	66
			k_n	m/d	1,343	224	31

Greens of Delwood - July 2009			Point	D1	*Measuring Depth (mm)*		
Measurements (see Chapter 4)			*(See Fig 4-6)*		400	300	200
$D_{1(rsvr)}$	cm	9.1	*1*	mm	95	90	80
$D_{2(rsvr)}$	cm	9.8	*2*	mm	2	1	1
Δt	s	3600	*3*	mm	24	20	19
$\Delta D_{(rsvr)}$	cm	0.7	*4*	mm	36	40	32
Q	m^3/d	20	$h_{T(probe)}$	mm	57	49	47
$h_{T(ave)}$	mm	51	h_n	mm	35	30	29
k_T	m/d	1.73	Δh_n	mm	5	1	29
			k_n	m/d	5.2	25.9	1.3

Greens of Delwood - July 2009			Point	D2	*Measuring Depth (mm)*		
Measurements (see Chapter 4)			*(See Fig 4-6)*		400	300	200
$D_{1(rsvr)}$	cm	10.0	*1*	mm	180	180	180
$D_{2(rsvr)}$	cm	14.0	*2*	mm	5	7	8
Δt	s	201	*3*	mm	12	14	18
$\Delta D_{(rsvr)}$	cm	4.0	*4*	mm	28	32	38
Q	m^3/d	112	$h_{T(probe)}$	mm	147	141	134
$h_{T(ave)}$	mm	141	h_n	mm	140	134	124
k_T	m/d	67.78	Δh_n	mm	6	10	124
			k_n	m/d	441	265	34

Greens of Delwood - July 2009			Point	D3	*Measuring Depth (mm)*		
Measurements (see Chapter 4)			*(See Fig 4-6)*		400	300	200
$D_{1(rsvr)}$	cm	9.0	*1*	mm	150	150	150
$D_{2(rsvr)}$	cm	19.0	*2*	mm	8	13	22
Δt	s	161	*3*	mm	15	14	27
$\Delta D_{(rsvr)}$	cm	10.0	*4*	mm	53	58	57
Q	m^3/d	281	$h_{T(probe)}$	mm	89	79	71
$h_{T(ave)}$	mm	80	h_n	mm	82	78	66
k_T	m/d	360.35	Δh_n	mm	4	12	66
			k_n	m/d	2,065	688	185

Greens of Delwood - July 2009			Point	D4	*Measuring Depth (mm)*		
Measurements (see Chapter 4)			*(See Fig 4-6)*		400	300	200
$D_{1(rsvr)}$	cm	2.9	*1*	mm	70	70	70
$D_{2(rsvr)}$	cm	2.9	*2*	mm	9	24	5
Δt	s	2147	*3*	mm	4	5	33
$\Delta D_{(rsvr)}$	cm	0.0	*4*	mm	33	35	30
Q	m^3/d	0	$h_{T(probe)}$	mm	28	11	35
$h_{T(ave)}$	mm	25	h_n	mm	33	30	7
k_T	m/d	0.09	Δh_n	mm	3	23	7
			k_n	m/d	0.21	0.03	0.14

Appendix A.19: Field Results – Tamarack Farms Estate (July 2009). See Section 5.19

Tamarack Farms - July 2009			Point	A1	*Measuring Depth (mm)*		
Measurements (see Chapter 4)			*(See Fig 4-6)*		400	300	200
$D_{1(rsvr)}$	cm	3.0	*1*	mm	420	365	265
$D_{2(rsvr)}$	cm	17.3	*2*	mm	14		
Δt	s	117	*3*	mm	45	12	10
$\Delta D_{(rsvr)}$	cm	14.3	*4*	mm	76	77	74
Q	m^3/d	402	$h_{T(probe)}$	mm	330		
$h_{T(ave)}$	mm	330	h_n	mm	299	276	181
k_T	m/d	162.23	Δh_n	mm	23	95	181
			k_n	m/d	707	171	116

Tamarack Farms - July 2009			Point	A2	*Measuring Depth (mm)*		
Measurements (see Chapter 4)			*(See Fig 4-6)*		400	300	200
$D_{1(rsvr)}$	cm	4.8	*1*	mm	445	330	250
$D_{2(rsvr)}$	cm	19.0	*2*	mm	14		
Δt	s	30	*3*	mm	43	57	48
$\Delta D_{(rsvr)}$	cm	14.2	*4*	mm	99	93	92
Q	m^3/d	399	$h_{T(probe)}$	mm	332		
$h_{T(ave)}$	mm	332	h_n	mm	303	180	110
k_T	m/d	624.49	Δh_n	mm	123	70	110
			k_n	m/d	512	899	740

Tamarack Farms - July 2009			Point	A3	*Measuring Depth (mm)*		
Measurements (see Chapter 4)			*(See Fig 4-6)*		400	300	200
$D_{1(rsvr)}$	cm	5.0	*1*	mm	400	360	260
$D_{2(rsvr)}$	cm	21.0	*2*	mm	13		
Δt	s	209	*3*	mm	13	2	
$\Delta D_{(rsvr)}$	cm	16.0	*4*	mm	81	74	75
Q	m^3/d	449	$h_{T(probe)}$	mm	306	286	
$h_{T(ave)}$	mm	296	h_n	mm	306	284	185
k_T	m/d	113.29	Δh_n	mm	22	99	185
			k_n	m/d	463	103	71

Tamarack Farms - July 2009			Point	A4	*Measuring Depth (mm)*		
Measurements (see Chapter 4)			*(See Fig 4-6)*		400	300	200
$D_{1(rsvr)}$	cm	4.0	*1*	mm	380	365	270
$D_{2(rsvr)}$	cm	17.0	*2*	mm	5		
Δt	s	437	*3*	mm	14	7	1
$\Delta D_{(rsvr)}$	cm	13.0	*4*	mm	69	63	63
Q	m^3/d	365	$h_{T(probe)}$	mm	306	302	
$h_{T(ave)}$	mm	304	h_n	mm	297	295	206
k_T	m/d	44.52	Δh_n	mm	2	89	206
			k_n	m/d	1,978	45	27

Tamarack Farms - July 2009			Point	A5	Measuring Depth (mm)		
Measurements (see Chapter 4)			(See Fig 4-6)		400	300	200
$D_{1(rsvr)}$	cm	6.0	1	mm	418	360	267
$D_{2(rsvr)}$	cm	19.0	2	mm	10		
Δt	s	306	3	mm	21		
$\Delta D_{(rsvr)}$	cm	13.0	4	mm	63	51	53
Q	m^3/d	365	$h_{T(probe)}$	mm	345	309	
$h_{T(ave)}$	mm	327	h_n	mm	334	309	214
k_T	m/d	56.91	Δh_n	mm	25	95	214
			k_n	m/d	226	59	34

Tamarack Farms - July 2009			Point	B1	Measuring Depth (mm)		
Measurements (see Chapter 4)			(See Fig 4-6)		400	300	200
$D_{1(rsvr)}$	cm	10.1	1	mm	420	365	265
$D_{2(rsvr)}$	cm	12.6	2	mm	12		
Δt	s	373	3	mm	14	1	1
$\Delta D_{(rsvr)}$	cm	2.6	4	mm	81	77	71
Q	m^3/d	72	$h_{T(probe)}$	mm	327		
$h_{T(ave)}$	mm	327	h_n	mm	325	287	194
k_T	m/d	9.16	Δh_n	mm	38	94	194
			k_n	m/d	24	10	6

Tamarack Farms - July 2009			Point	B2	Measuring Depth (mm)		
Measurements (see Chapter 4)			(See Fig 4-6)		400	300	200
$D_{1(rsvr)}$	cm	2.0	1	mm	455	365	260
$D_{2(rsvr)}$	cm	11.0	2	mm	3		
Δt	s	85	3	mm	13	1	1
$\Delta D_{(rsvr)}$	cm	9.0	4	mm	82	83	85
Q	m^3/d	253	$h_{T(probe)}$	mm	370		
$h_{T(ave)}$	mm	370	h_n	mm	360	281	175
k_T	m/d	125.35	Δh_n	mm	79	107	175
			k_n	m/d	178	132	104

Tamarack Farms - July 2009			Point	B3	Measuring Depth (mm)		
Measurements (see Chapter 4)			(See Fig 4-6)		400	300	200
$D_{1(rsvr)}$	cm	5.9	1	mm	530	360	260
$D_{2(rsvr)}$	cm	13.5	2	mm	8		
Δt	s	171	3	mm	13		
$\Delta D_{(rsvr)}$	cm	7.6	4	mm	72	71	65
Q	m^3/d	214	$h_{T(probe)}$	mm	450		
$h_{T(ave)}$	mm	450	h_n	mm	445	289	195
k_T	m/d	43.26	Δh_n	mm	156	94	195
			k_n	m/d	38	63	39

Tamarack Farms - July 2009			Point	B4	Measuring Depth (mm)		
Measurements (see Chapter 4)			(See Fig 4-6)		400	300	200
$D_{1(rsvr)}$	cm	5.0	1	mm	483	365	270
$D_{2(rsvr)}$	cm	14.9	2	mm	5		
Δt	s	288	3	mm	9	18	18
$\Delta D_{(rsvr)}$	cm	9.9	4	mm	68	67	68
Q	m^3/d	278	$h_{T(probe)}$	mm	410	298	
$h_{T(ave)}$	mm	354	h_n	mm	406	280	184
k_T	m/d	42.53	Δh_n	mm	126	96	184
			k_n	m/d	36	48	32

Tamarack Farms - July 2009			Point	B5	Measuring Depth (mm)		
Measurements (see Chapter 4)			(See Fig 4-6)		400	300	200
$D_{1(rsvr)}$	cm	2.0	1	mm	350	340	270
$D_{2(rsvr)}$	cm	11.0	2	mm	3	5	
Δt	s	140	3	mm	9	12	0
$\Delta D_{(rsvr)}$	cm	9.0	4	mm	78	79	82
Q	m^3/d	253	$h_{T(probe)}$	mm	269	256	
$h_{T(ave)}$	mm	263	h_n	mm	263	249	188
k_T	m/d	107.27	Δh_n	mm	14	61	188
			k_n	m/d	611	139	59

Tamarack Farms - July 2009			Point	C1	Measuring Depth (mm)		
Measurements (see Chapter 4)			(See Fig 4-6)		400	300	200
$D_{1(rsvr)}$	cm	5.5	1	mm	360	360	270
$D_{2(rsvr)}$	cm	17.0	2	mm	10	12	
Δt	s	171	3	mm	37	49	32
$\Delta D_{(rsvr)}$	cm	11.5	4	mm	79	83	76
Q	m^3/d	323	$h_{T(probe)}$	mm	271	265	
$h_{T(ave)}$	mm	268	h_n	mm	244	228	162
k_T	m/d	109.92	Δh_n	mm	16	66	162
			k_n	m/d	559	136	71

Tamarack Farms - July 2009			Point	C2	Measuring Depth (mm)		
Measurements (see Chapter 4)			(See Fig 4-6)		400	300	200
$D_{1(rsvr)}$	cm	5.0	1	mm	525	350	260
$D_{2(rsvr)}$	cm	15.0	2	mm	10		
Δt	s	157	3	mm	20	0	1
$\Delta D_{(rsvr)}$	cm	10.0	4	mm	100	100	96
Q	m^3/d	281	$h_{T(probe)}$	mm	415		
$h_{T(ave)}$	mm	415	h_n	mm	405	250	164
k_T	m/d	64.63	Δh_n	mm	155	86	164
			k_n	m/d	55	98	60

Tamarack Farms - July 2009			Point	C3	*Measuring Depth (mm)*		
Measurements (see Chapter 4)			*(See Fig 4-6)*		**400**	**300**	**200**
$D_{1(rsvr)}$	cm	5.7	***1***	mm	430	360	260
$D_{2(rsvr)}$	cm	15.2	***2***	mm	10		
Δt	s	286	***3***	mm	17		
$\Delta D_{(rsvr)}$	cm	9.5	***4***	mm	75	74	75
Q	m^3/d	267	$h_{T(probe)}$	mm	345		
$h_{T(ave)}$	mm	345	h_n	mm	338	286	185
k_T	m/d	42.17	Δh_n	mm	52	101	185
			k_n	m/d	85	44	31

Tamarack Farms - July 2009			Point	C4	*Measuring Depth (mm)*		
Measurements (see Chapter 4)			*(See Fig 4-6)*		**400**	**300**	**200**
$D_{1(rsvr)}$	cm	4.7	***1***	mm	393	325	265
$D_{2(rsvr)}$	cm	16.2	***2***	mm	11		
Δt	s	257	***3***	mm	12	3	
$\Delta D_{(rsvr)}$	cm	11.5	***4***	mm	76	75	73
Q	m^3/d	323	$h_{T(probe)}$	mm	306	250	
$h_{T(ave)}$	mm	278	h_n	mm	305	247	192
k_T	m/d	70.50	Δh_n	mm	58	55	192
			k_n	m/d	103	108	40

Tamarack Farms - July 2009			Point	C5	*Measuring Depth (mm)*		
Measurements (see Chapter 4)			*(See Fig 4-6)*		**400**	**300**	**200**
$D_{1(rsvr)}$	cm	4.0	***1***	mm	445	360	275
$D_{2(rsvr)}$	cm	16.0	***2***	mm	3		
Δt	s	174	***3***	mm	10	44	44
$\Delta D_{(rsvr)}$	cm	12.0	***4***	mm	60	59	59
Q	m^3/d	337	$h_{T(probe)}$	mm	382	301	
$h_{T(ave)}$	mm	342	h_n	mm	375	257	172
k_T	m/d	88.46	Δh_n	mm	118	85	172
			k_n	m/d	78	108	69

Appendix A.20: Field Results – Jackson Meadow S. (August 2009). See Section 5.20

Jackson Meadow S. - August 2009			Point	A1	*Measuring Depth (mm)*		
Measurements (see Chapter 4)			*(See Fig 4-6)*		400	300	200
$D_{1(rsvr)}$	cm	0.5	*1*	mm	450	220	220
$D_{2(rsvr)}$	cm	7.5	*2*	mm		31	36
Δt	s	367	*3*	mm		54	73
$\Delta D_{(rsvr)}$	cm	7.0	*4*	mm	79	64	63
Q	m^3/d	197	$h_{T(probe)}$	mm		125	121
$h_{T(ave)}$	mm	123	h_n	mm	371	102	84
k_T	m/d	65.30	Δh_n	mm	269	18	84
			k_n	m/d	9	141	35

Jackson Meadow S. - August 2009			Point	A2	*Measuring Depth (mm)*		
Measurements (see Chapter 4)			*(See Fig 4-6)*		400	300	200
$D_{1(rsvr)}$	cm	5.0	*1*	mm	240	230	220
$D_{2(rsvr)}$	cm	16.0	*2*	mm	8	18	8
Δt	s	42	*3*	mm	27	31	27
$\Delta D_{(rsvr)}$	cm	11.0	*4*	mm	82	70	67
Q	m^3/d	309	$h_{T(probe)}$	mm	150	142	145
$h_{T(ave)}$	mm	146	h_n	mm	131	129	126
k_T	m/d	787.55	Δh_n	mm	2	3	126
			k_n	m/d	17,415	11,610	358

Jackson Meadow S. - August 2009			Point	A3	*Measuring Depth (mm)*		
Measurements (see Chapter 4)			*(See Fig 4-6)*		400	300	200
$D_{1(rsvr)}$	cm	5.5	*1*	mm	260	250	250
$D_{2(rsvr)}$	cm	16.0	*2*	mm	21	13	12
Δt	s	52	*3*	mm	25	24	35
$\Delta D_{(rsvr)}$	cm	10.5	*4*	mm	91	88	88
Q	m^3/d	295	$h_{T(probe)}$	mm	148	149	150
$h_{T(ave)}$	mm	149	h_n	mm	144	138	127
k_T	m/d	593.60	Δh_n	mm	6	11	127
			k_n	m/d	4,476	2,441	274

Jackson Meadow S. - August 2009			Point	A4	*Measuring Depth (mm)*		
Measurements (see Chapter 4)			*(See Fig 4-6)*		400	300	200
$D_{1(rsvr)}$	cm	4.0	*1*	mm	260	260	260
$D_{2(rsvr)}$	cm	11.0	*2*	mm	15	15	12
Δt	s	145	*3*	mm	17	17	15
$\Delta D_{(rsvr)}$	cm	7.0	*4*	mm	69	70	73
Q	m^3/d	197	$h_{T(probe)}$	mm	176	175	175
$h_{T(ave)}$	mm	175	h_n	mm	174	173	172
k_T	m/d	125.26	Δh_n	mm	1	1	172
			k_n	m/d	6,420	6,420	53

Jackson Meadow S. - August 2009			Point	B1	*Measuring Depth (mm)*		
Measurements (see Chapter 4)			*(See Fig 4-6)*		**400**	**300**	**200**
$D_{1(rsvr)}$	cm	10.1	***1***	mm	110	100	90
$D_{2(rsvr)}$	cm	11.0	***2***	mm	10	9	7
Δt	s	2975	***3***	mm	6	1	0
$\Delta D_{(rsvr)}$	cm	0.9	***4***	mm	71	66	60
Q	m^3/d	27	$h_{T(probe)}$	mm	29	25	23
$h_{T(ave)}$	mm	26	h_n	mm	33	33	30
k_T	m/d	5.03	Δh_n	mm	0	3	30
			k_n	m/d	142	14	1

Jackson Meadow S. - August 2009			Point	B2	*Measuring Depth (mm)*		
Measurements (see Chapter 4)			*(See Fig 4-6)*		**400**	**300**	**200**
$D_{1(rsvr)}$	cm	4.0	***1***	mm	170	170	170
$D_{2(rsvr)}$	cm	16.0	***2***	mm	15	18	21
Δt	s	55	***3***	mm	18	22	28
$\Delta D_{(rsvr)}$	cm	12.0	***4***	mm	82	79	83
Q	m^3/d	337	$h_{T(probe)}$	mm	73	73	66
$h_{T(ave)}$	mm	71	h_n	mm	70	69	59
k_T	m/d	1352.37	Δh_n	mm	1	10	59
			k_n	m/d	29,016	2,902	636

Jackson Meadow S. - August 2009			Point	B3	*Measuring Depth (mm)*		
Measurements (see Chapter 4)			*(See Fig 4-6)*		**400**	**300**	**200**
$D_{1(rsvr)}$	cm	11.0	***1***	mm	200	200	200
$D_{2(rsvr)}$	cm	19.0	***2***	mm	7	4	4
Δt	s	21	***3***	mm	12	18	27
$\Delta D_{(rsvr)}$	cm	8.0	***4***	mm	68	70	65
Q	m^3/d	225	$h_{T(probe)}$	mm	125	126	131
$h_{T(ave)}$	mm	127	h_n	mm	120	112	108
k_T	m/d	1310.45	Δh_n	mm	8	4	108
			k_n	m/d	6,333	12,666	607

Jackson Meadow S. - August 2009			Point	B4	*Measuring Depth (mm)*		
Measurements (see Chapter 4)			*(See Fig 4-6)*		**400**	**300**	**200**
$D_{1(rsvr)}$	cm	9.0	***1***	mm	260	260	260
$D_{2(rsvr)}$	cm	20.0	***2***	mm	13	10	6
Δt	s	15	***3***	mm	19	30	43
$\Delta D_{(rsvr)}$	cm	11.0	***4***	mm	85	80	80
Q	m^3/d	309	$h_{T(probe)}$	mm	162	170	174
$h_{T(ave)}$	mm	169	h_n	mm	156	150	137
k_T	m/d	1904.43	Δh_n	mm	6	13	137
			k_n	m/d	16,254	7,502	921

Jackson Meadow S. - August 2009			Point	C1	*Measuring Depth (mm)*		
Measurements (see Chapter 4)			*(See Fig 4-6)*		400	300	200
$D_{1(rsvr)}$	cm	6.5	*1*	mm	150	140	130
$D_{2(rsvr)}$	cm	11.0	*2*	mm	11	4	3
Δt	s	207	*3*	mm	28	13	19
$\Delta D_{(rsvr)}$	cm	4.5	*4*	mm	62	72	81
Q	m^3/d	126	$h_{T(probe)}$	mm	77	64	46
$h_{T(ave)}$	mm	62	h_n	mm	60	55	30
k_T	m/d	152.76	Δh_n	mm	5	25	30
			k_n	m/d	578	116	125

Jackson Meadow S. - August 2009			Point	C2	*Measuring Depth (mm)*		
Measurements (see Chapter 4)			*(See Fig 4-6)*		400	300	200
$D_{1(rsvr)}$	cm	7.0	*1*	mm	210	210	210
$D_{2(rsvr)}$	cm	17.0	*2*	mm	20	16	9
Δt	s	16	*3*	mm	25	28	34
$\Delta D_{(rsvr)}$	cm	10.0	*4*	mm	87	91	91
Q	m^3/d	281	$h_{T(probe)}$	mm	103	103	110
$h_{T(ave)}$	mm	105	h_n	mm	98	91	85
k_T	m/d	2699.26	Δh_n	mm	7	6	85
			k_n	m/d	11,874	13,853	1,389

Jackson Meadow S. - August 2009			Point	C3	*Measuring Depth (mm)*		
Measurements (see Chapter 4)			*(See Fig 4-6)*		400	300	200
$D_{1(rsvr)}$	cm	3.0	*1*	mm	250	250	250
$D_{2(rsvr)}$	cm	12.0	*2*	mm	17	14	14
Δt	s	98	*3*	mm	21	17	19
$\Delta D_{(rsvr)}$	cm	9.0	*4*	mm	85	90	89
Q	m^3/d	253	$h_{T(probe)}$	mm	148	146	147
$h_{T(ave)}$	mm	147	h_n	mm	144	143	142
k_T	m/d	273.65	Δh_n	mm	1	1	142
			k_n	m/d	12,213	12,213	111

Jackson Meadow S. - August 2009			Point	C4	*Measuring Depth (mm)*		
Measurements (see Chapter 4)			*(See Fig 4-6)*		400	300	200
$D_{1(rsvr)}$	cm	9.0	*1*	mm	250	250	250
$D_{2(rsvr)}$	cm	18.0	*2*	mm	7	14	19
Δt	s	73	*3*	mm	9	17	23
$\Delta D_{(rsvr)}$	cm	9.0	*4*	mm	76	72	68
Q	m^3/d	253	$h_{T(probe)}$	mm	167	164	163
$h_{T(ave)}$	mm	165	h_n	mm	165	161	159
k_T	m/d	340.60	Δh_n	mm	4	2	159
			k_n	m/d	4,099	8,198	146

Jackson Meadow S. - August 2009			Point	D1	*Measuring Depth (mm)*		
Measurements (see Chapter 4)			*(See Fig 4-6)*		400	300	200
$D_{1(rsvr)}$	cm	5.2	*1*	mm	70	60	50
$D_{2(rsvr)}$	cm	11.4	*2*	mm	7	4	1
Δt	s	526	*3*	mm	7	6	6
$\Delta D_{(rsvr)}$	cm	6.2	*4*	mm	29	23	14
Q	m^3/d	174	$h_{T(probe)}$	mm	34	33	35
$h_{T(ave)}$	mm	34	h_n	mm	34	31	30
k_T	m/d	142.48	Δh_n	mm	3	1	30
			k_n	m/d	523	1,568	57

Jackson Meadow S. - August 2009			Point	D2	*Measuring Depth (mm)*		
Measurements (see Chapter 4)			*(See Fig 4-6)*		400	300	200
$D_{1(rsvr)}$	cm	8.0	*1*	mm	210	200	200
$D_{2(rsvr)}$	cm	16.0	*2*	mm	15	20	13
Δt	s	17	*3*	mm	45	43	46
$\Delta D_{(rsvr)}$	cm	8.0	*4*	mm	77	70	79
Q	m^3/d	225	$h_{T(probe)}$	mm	118	110	108
$h_{T(ave)}$	mm	112	h_n	mm	88	87	75
k_T	m/d	1875.91	Δh_n	mm	1	12	75
			k_n	m/d	62,584	5,215	1,132

Jackson Meadow S. - August 2009			Point	D3	*Measuring Depth (mm)*		
Measurements (see Chapter 4)			*(See Fig 4-6)*		400	300	200
$D_{1(rsvr)}$	cm	8.0	*1*	mm	200	200	200
$D_{2(rsvr)}$	cm	18.0	*2*	mm	9	16	12
Δt	s	19	*3*	mm	19	31	39
$\Delta D_{(rsvr)}$	cm	10.0	*4*	mm	87	79	76
Q	m^3/d	281	$h_{T(probe)}$	mm	104	105	112
$h_{T(ave)}$	mm	107	h_n	mm	94	90	85
k_T	m/d	2237.66	Δh_n	mm	4	5	85
			k_n	m/d	17,499	13,999	1,170

Jackson Meadow S. - August 2009			Point	D4	*Measuring Depth (mm)*		
Measurements (see Chapter 4)			*(See Fig 4-6)*		400	300	200
$D_{1(rsvr)}$	cm	2.0	*1*	mm	220	220	220
$D_{2(rsvr)}$	cm	10.0	*2*	mm	7	14	6
Δt	s	74	*3*	mm	20	19	13
$\Delta D_{(rsvr)}$	cm	8.0	*4*	mm	80	82	89
Q	m^3/d	225	$h_{T(probe)}$	mm	133	124	125
$h_{T(ave)}$	mm	127	h_n	mm	120	119	118
k_T	m/d	379.06	Δh_n	mm	1	1	118
			k_n	m/d	14,377	14,377	165

Appendix B: Clog Factor Derivations

Table App.B.1 Average longitudinal factors CF_X and vertical factors CF_Z of Clog Factor CF, at different sampling locations for various values of CF_T as determined from the ANOVA test.

	Longitudinal Sampling Position				Vertical Sampling Position			
	1	2	3	4	1	2	3	4
CF_T	CFx Longitudinal Factor of CFT				CFz Vertical Factor of CF			
0.54	0.67	0.61	0.51	0.37	0.52	0.66	0.69	0.32
0.58	0.69	0.61	0.60	0.42	0.59	0.68	0.59	0.50
0.6	0.88	0.67	0.47	0.40	0.81	0.72	0.59	0.34
0.63	0.76	0.71	0.60	0.47	0.55	0.71	0.72	0.59
0.64	0.94	0.62	0.53	0.48	0.72	0.66	0.65	0.57
0.67	0.68	0.65	0.65	0.70	0.86	0.76	0.57	0.54
0.74	0.76	0.79	0.81	0.61	0.89	0.73	0.72	0.69
0.81	0.97	0.92	0.81	0.55	0.80	0.89	0.86	0.74
0.82	0.97	0.82	0.80	0.70	0.97	0.86	0.78	0.75
0.87	0.96	0.87	0.87	0.78	0.99	0.89	0.84	0.82
0.88	0.93	0.91	0.86	0.84	1.00	0.93	0.83	0.83
0.88	0.97	0.95	0.85	0.73	0.96	0.90	0.86	0.84
0.92	0.98	0.92	0.88	0.90	1.01	0.95	0.90	0.88

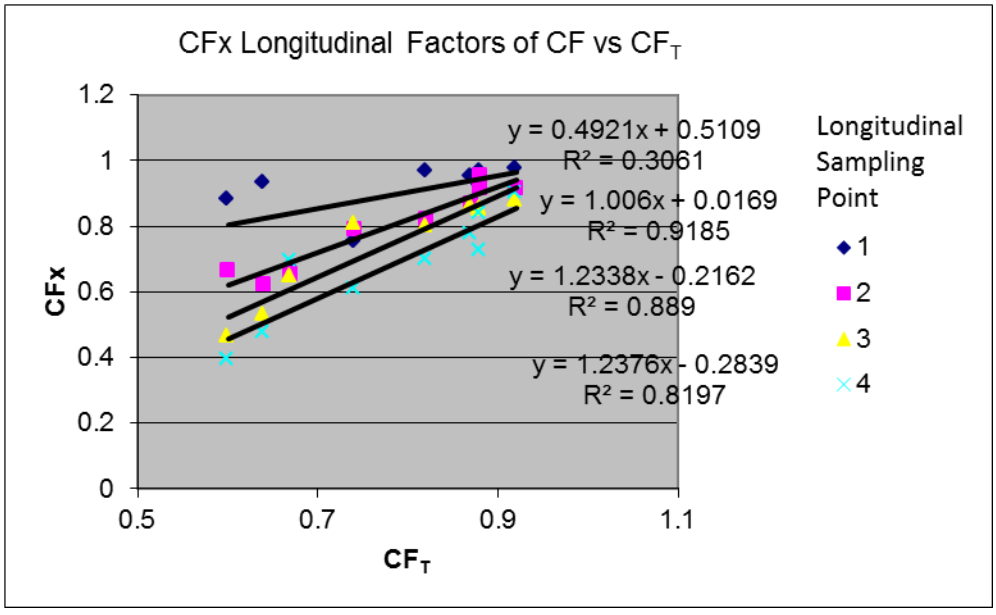

Figure App.B.1 Average linear trend of CF_X versus CF_T for different longitudinal sampling points, based on the data in **Table App.B.1.**

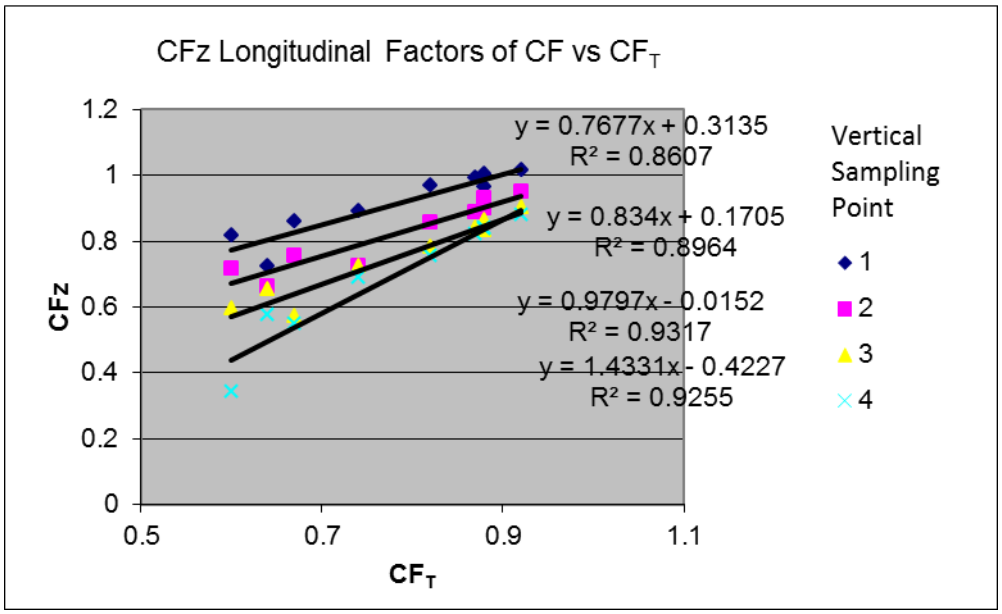

Figure App.B.2 Average linear trend of CF_z versus CF_T for different vertical sampling points, based on the data in **Table App.B.1.**

Table App.B.2 Gradient and intercept of the linear relationships illustrated in **Figure App.B.2,** for CF_X versus CF_T for different normalised longitudinal distance from inlet and CF_Z versus CF_T for different normalised vertical distance above base.

CFx vs CFT relationship			CFT vs CFz relationship		
$\bar{x}$	m	c	$\bar{z}$	m	c
0.2	0.4921	0.5109	0.25	0.7677	0.3135
0.4	1.006	0.0169	0.5	0.834	0.1705
0.6	1.2338	-0.2162	0.75	0.9797	-0.0152
0.8	1.2376	-0.2839	1	1.4331	-0.4227

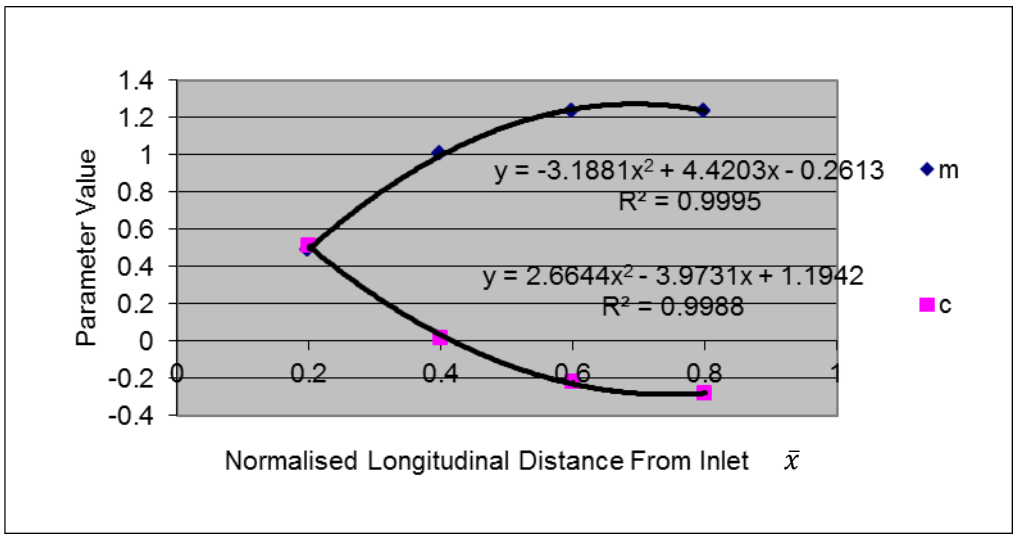

Figure App.B.3 Relationship between normalised longitudinal distance and the gradient and intercept of the linear trends illustrated in **Figure App.B.1.**

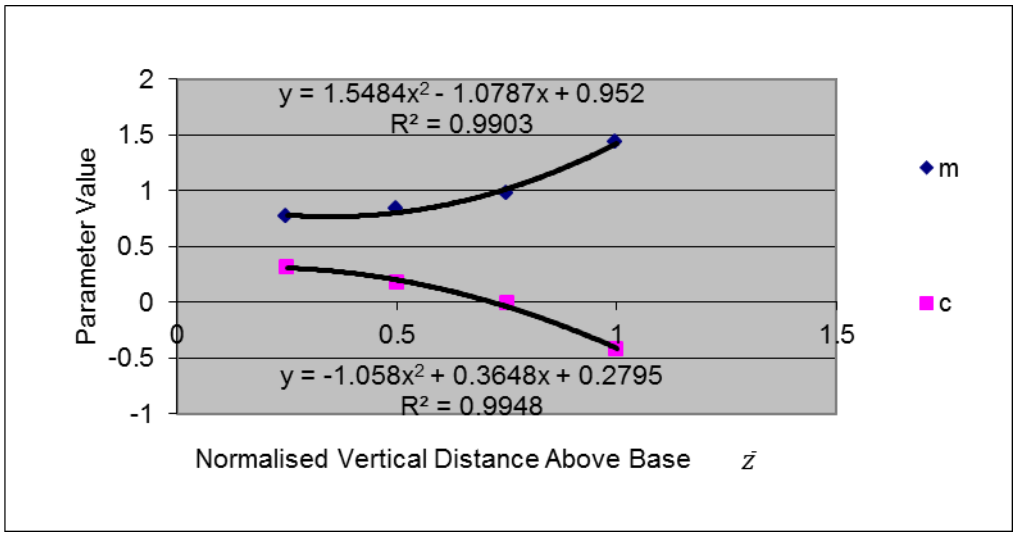

Figure App.B.4 Relationship between normalised vertical distance and the gradient and intercept of the linear trends illustrated in **Figure App.B.2.**

Appendix C: ANOVA Results

Summary ANOVA - CF

This ANOVA test performs a multifactor analysis of variance for CF. It constructs various tests and graphs to determine which factors have a statistically significant effect on CF. It also tests for significant interactions amongst the factors, given sufficient data. The F-tests in the ANOVA table will allow you to identify the significant factors. For each significant factor, the Multiple Range Tests will tell you which means are significantly different from which others. The Means Plot and Interaction Plot will help you interpret the significant effects. The Residual Plots will help you judge whether the assumptions underlying the analysis of variance are violated by the data.

Analysis of Variance Table

The ANOVA table decomposes the variability of CF into contributions due to various factors. Since Type III sums of squares (the default) have been chosen, the contribution of each factor is measured having removed the effects of all other factors. The P-values test the statistical significance of each of the factors. Since 4 P-values are less than 0.05, these factors have a statistically significant effect on CF at the 95.0% confidence level.

Table of Least Squares Means

This table shows the mean CF for each level of the factors. It also shows the standard error of each mean, which is a measure of its sampling variability. The rightmost two columns show 95.0% confidence intervals for each of the means. You can display these means and intervals by selecting Means Plot from the list of Graphical Options.

Multiple Range Tests

This table applies a multiple comparison procedure to determine which means are significantly different from which others. The bottom half of the output shows the estimated difference between each pair of means. An asterisk has been placed next to 5 pairs, indicating that these pairs show statistically significant differences at the 95.0% confidence level. At the top of the page, 3 homogenous groups are identified using columns of X's. Within each column, the levels containing X's form a group of means within which there are no statistically significant differences. The method currently being used to discriminate among the means is Fisher's least significant difference (LSD) procedure. With this method, there is a 5.0% risk of calling each pair of means significantly different when the actual difference equals 0.

Inter-system comparison, transverse variance removed - CF

Dependent variable: Clog Factor, Factors: Vert (Normalized vertical bed location), Bed Code (Referenced to bulk system Clog Factor CF_T), Long (Normalized longitudinal bed location). Transverse bed location is not included as a factor
Number of complete cases: 912

Bed Codes:

1	Ashorne
2	Fenny Compton (08)
3	Fenny Compton (09)
4	Fenny Compton (10)
5	Leek Wooton
6	Moreton Morrell (F9)
7	Moreton Morrell (J8)
8	Moreton Morrell (S9)
9	Moreton Morrell B
10	Northend
11	Rowington
12	Snitterfield
13	Weston

Analysis of Variance for Clog Factor - Type III Sums of Squares

Source	Sum of Squares	Df	Mean Square	F-Ratio	P-Value
MAIN EFFECTS					
A:Vert	2.82944	3	0.943147	42.45	0.0000
B:Bed Code	14.7369	12	1.22808	55.28	0.0000
C:Long	7.23109	3	2.41036	108.50	0.0000
INTERACTIONS					
AB	3.77201	36	0.104778	4.72	0.0000
AC	0.343483	9	0.0381648	1.72	0.0810
BC	4.01073	36	0.111409	5.01	0.0000
RESIDUAL	18.0391	812	0.0222157		
TOTAL (CORRECTED)	50.9734	911			

All F-ratios are based on the residual mean square error.

Table of Least Squares Means for Clog Factor with 95.0 Percent Confidence Intervals

Level	Count	Mean	Stnd. Error	Lower Limit	Upper Limit
GRAND MEAN	912	0.737833			
Vert					
1	228	0.772631	0.00998427	0.753062	0.792199
2	228	0.793616	0.00998427	0.774047	0.813185
3	228	0.738755	0.00998427	0.719187	0.758324
4	228	0.64633	0.00998427	0.626761	0.665899
Bed Code					
1	64	0.809459	0.0186312	0.772943	0.845976
2	64	0.540531	0.0186312	0.504015	0.577048
3	64	0.743004	0.0186312	0.706487	0.77952
4	80	0.632497	0.0166642	0.599836	0.665159
5	80	0.668897	0.0166642	0.636235	0.701558
6	64	0.823993	0.0186312	0.787476	0.860509
7	64	0.64152	0.0186312	0.605003	0.678036
8	64	0.867772	0.0186312	0.831255	0.904288
9	48	0.580474	0.0215134	0.538309	0.62264
10	80	0.884697	0.0166642	0.852035	0.917358
11	80	0.875823	0.0166642	0.843162	0.908485
12	80	0.919668	0.0166642	0.887007	0.952329
13	80	0.603495	0.0166642	0.570834	0.636156
Long					
1	228	0.85702	0.00998427	0.837451	0.876589
2	228	0.773342	0.00998427	0.753773	0.792911
3	228	0.710563	0.00998427	0.690994	0.730132
4	228	0.610408	0.00998427	0.590839	0.629977
Vert by Bed Code					
1	1	16	0.753593	0.0372623	0.68056	0.826626
1	2	16	0.489096	0.0372623	0.416063	0.562129
1	3	16	0.837085	0.0372623	0.764052	0.910118
1	4	20	0.515128	0.0333284	0.449805	0.58045
1	5	20	0.807274	0.0333284	0.741951	0.872597
1	6	16	0.909767	0.0372623	0.836735	0.9828
1	7	16	0.67936	0.0372623	0.606327	0.752393
1	8	16	0.930002	0.0372623	0.856969	1.00303
1	9	12	0.55598	0.0430268	0.471648	0.640311
1	10	20	0.943331	0.0333284	0.878009	1.00865
1	11	20	0.905139	0.0333284	0.839816	0.970461
1	12	20	0.952787	0.0333284	0.887465	1.01811
1	13	20	0.765654	0.0333284	0.700331	0.830976
2	1	16	0.886998	0.0372623	0.813965	0.960031
2	2	16	0.657709	0.0372623	0.584676	0.730742
2	3	16	0.726403	0.0372623	0.65337	0.799436
2	4	20	0.707017	0.0333284	0.641695	0.77234
2	5	20	0.756145	0.0333284	0.690823	0.821468
2	6	16	0.856645	0.0372623	0.783612	0.929678
2	7	16	0.663666	0.0372623	0.590633	0.736699

2	8	16	0.888933	0.0372623	0.8159	0.961966
2	9	12	0.676334	0.0430268	0.592003	0.760665
2	10	20	0.93124	0.0333284	0.865917	0.996562
2	11	20	0.898899	0.0333284	0.833577	0.964222
2	12	20	0.949483	0.0333284	0.884161	1.01481
2	13	20	0.717535	0.0333284	0.652212	0.782857
3	1	16	0.855985	0.0372623	0.782952	0.929018
3	2	16	0.690642	0.0372623	0.617609	0.763675
3	3	16	0.720957	0.0372623	0.647924	0.79399
3	4	20	0.722329	0.0333284	0.657006	0.787651
3	5	20	0.568223	0.0333284	0.5029	0.633545
3	6	16	0.77883	0.0372623	0.705797	0.851863
3	7	16	0.65021	0.0372623	0.577177	0.723243
3	8	16	0.835938	0.0372623	0.762906	0.908971
3	9	12	0.594504	0.0430268	0.510173	0.678835
3	10	20	0.831334	0.0333284	0.766012	0.896657
3	11	20	0.860996	0.0333284	0.795673	0.926319
3	12	20	0.900971	0.0333284	0.835648	0.966293
3	13	20	0.592902	0.0333284	0.52758	0.658225
4	1	16	0.741262	0.0372623	0.668229	0.814295
4	2	16	0.324678	0.0372623	0.251645	0.397711
4	3	16	0.687569	0.0372623	0.614536	0.760602
4	4	20	0.585516	0.0333284	0.520193	0.650838
4	5	20	0.543944	0.0333284	0.478622	0.609267
4	6	16	0.750728	0.0372623	0.677695	0.823761
4	7	16	0.572842	0.0372623	0.499809	0.645875
4	8	16	0.816214	0.0372623	0.743181	0.889246
4	9	12	0.495079	0.0430268	0.410748	0.57941
4	10	20	0.832881	0.0333284	0.767558	0.898204
4	11	20	0.83826	0.0333284	0.772937	0.903583
4	12	20	0.87543	0.0333284	0.810108	0.940753
4	13	20	0.33789	0.0333284	0.272567	0.403212
Vert by Long						
1	1	57	0.863767	0.0198415	0.824878	0.902655
1	2	57	0.805132	0.0198415	0.766244	0.844021
1	3	57	0.748524	0.0198415	0.709635	0.787412
1	4	57	0.673099	0.0198415	0.634211	0.711988
2	1	57	0.914788	0.0198415	0.8759	0.953677
2	2	57	0.822523	0.0198415	0.783635	0.861412
2	3	57	0.746605	0.0198415	0.707716	0.785494
2	4	57	0.690547	0.0198415	0.651658	0.729436
3	1	57	0.87198	0.0198415	0.833091	0.910868
3	2	57	0.800618	0.0198415	0.761729	0.839507
3	3	57	0.70392	0.0198415	0.665031	0.742808
3	4	57	0.578504	0.0198415	0.539616	0.617393
4	1	57	0.777544	0.0198415	0.738655	0.816433
4	2	57	0.665093	0.0198415	0.626205	0.703982
4	3	57	0.643203	0.0198415	0.604315	0.682092
4	4	57	0.49948	0.0198415	0.460592	0.538369
Bed Code by Long						
1	1	16	0.969789	0.0372623	0.896756	1.04282

1	2	16	0.91576	0.0372623	0.842727	0.988793
1	3	16	0.80639	0.0372623	0.733357	0.879423
1	4	16	0.545899	0.0372623	0.472866	0.618932
2	1	16	0.674301	0.0372623	0.601268	0.747334
2	2	16	0.607753	0.0372623	0.53472	0.680785
2	3	16	0.510177	0.0372623	0.437144	0.58321
2	4	16	0.369895	0.0372623	0.296862	0.442928
3	1	16	0.756393	0.0372623	0.68336	0.829426
3	2	16	0.791078	0.0372623	0.718045	0.864111
3	3	16	0.812153	0.0372623	0.73912	0.885186
3	4	16	0.61239	0.0372623	0.539358	0.685423
4	1	20	0.755989	0.0333284	0.690666	0.821312
4	2	20	0.707502	0.0333284	0.64218	0.772825
4	3	20	0.600778	0.0333284	0.535455	0.6661
4	4	20	0.465721	0.0333284	0.400398	0.531043
5	1	20	0.677355	0.0333284	0.612032	0.742677
5	2	20	0.653976	0.0333284	0.588654	0.719299
5	3	20	0.64858	0.0333284	0.583257	0.713903
5	4	20	0.695675	0.0333284	0.630353	0.760998
6	1	16	0.96862	0.0372623	0.895587	1.04165
6	2	16	0.823272	0.0372623	0.750239	0.896305
6	3	16	0.801573	0.0372623	0.72854	0.874606
6	4	16	0.702506	0.0372623	0.629473	0.775539
7	1	16	0.935362	0.0372623	0.862329	1.00839
7	2	16	0.622539	0.0372623	0.549507	0.695572
7	3	16	0.531456	0.0372623	0.458424	0.604489
7	4	16	0.476721	0.0372623	0.403688	0.549754
8	1	16	0.956848	0.0372623	0.883815	1.02988
8	2	16	0.869581	0.0372623	0.796548	0.942614
8	3	16	0.866	0.0372623	0.792967	0.939033
8	4	16	0.778658	0.0372623	0.705625	0.851691
9	1	12	0.688537	0.0430268	0.604206	0.772868
9	2	12	0.608198	0.0430268	0.523867	0.692529
9	3	12	0.604252	0.0430268	0.519921	0.688583
9	4	12	0.420909	0.0430268	0.336578	0.50524
10	1	20	0.927071	0.0333284	0.861748	0.992394
10	2	20	0.914875	0.0333284	0.849552	0.980197
10	3	20	0.85552	0.0333284	0.790198	0.920843
10	4	20	0.84132	0.0333284	0.775997	0.906643
11	1	20	0.968636	0.0333284	0.903313	1.03396
11	2	20	0.954828	0.0333284	0.889506	1.02015
11	3	20	0.853388	0.0333284	0.788065	0.918711
11	4	20	0.726442	0.0333284	0.661119	0.791764
12	1	20	0.978434	0.0333284	0.913111	1.04376
12	2	20	0.916857	0.0333284	0.851534	0.982179
12	3	20	0.880306	0.0333284	0.814983	0.945628
12	4	20	0.903075	0.0333284	0.837752	0.968398
13	1	20	0.883923	0.0333284	0.818601	0.949246
13	2	20	0.667224	0.0333284	0.601901	0.732547
13	3	20	0.466744	0.0333284	0.401422	0.532067
13	4	20	0.396089	0.0333284	0.330766	0.461411

Multiple Range Tests for Clog Factor by Long

Method: 95.0 percent LSD

Long	Count	LS Mean	LS Sigma	Homogeneous Groups
4	228	0.610408	0.00998427	X
3	228	0.710563	0.00998427	X
2	228	0.773342	0.00998427	X
1	228	0.85702	0.00998427	X

Contrast	Difference	+/- Limits
1 - 2	*0.083678	0.0276745
1 - 3	*0.146457	0.0276745
1 - 4	*0.246612	0.0276745
2 - 3	*0.0627788	0.0276745
2 - 4	*0.162934	0.0276745
3 - 4	*0.100155	0.0276745

* denotes a statistically significant difference.

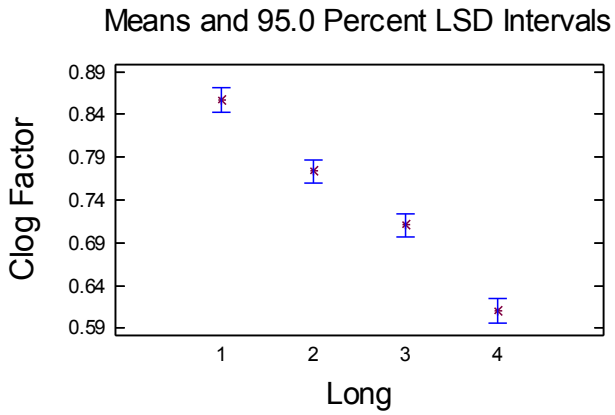

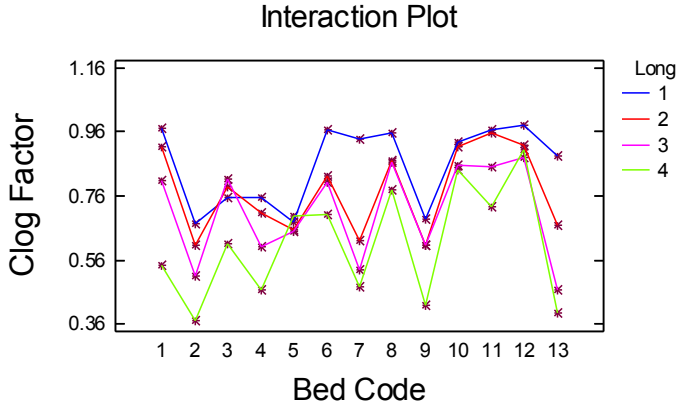

Multiple Range Tests for Clog Factor by Vert

Method: 95.0 percent LSD

Vert	Count	LS Mean	LS Sigma	Homogeneous Groups
4	228	0.64633	0.00998427	X
3	228	0.738755	0.00998427	X
1	228	0.772631	0.00998427	X
2	228	0.793616	0.00998427	X

Contrast	Difference	+/- Limits
1 - 2	-0.0209854	0.0276745
1 - 3	*0.0338751	0.0276745
1 - 4	*0.1263	0.0276745
2 - 3	*0.0548605	0.0276745
2 - 4	*0.147286	0.0276745
3 - 4	*0.0924252	0.0276745

---

* denotes a statistically significant difference.

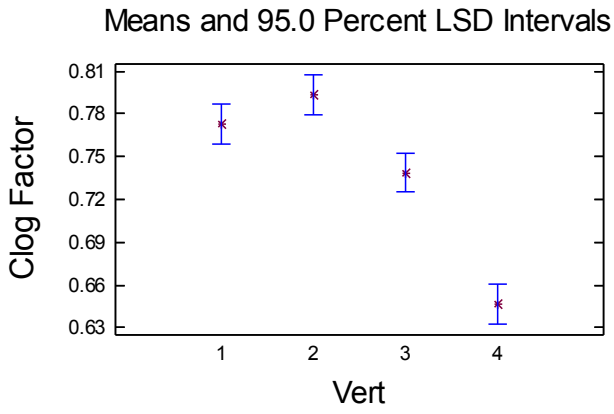

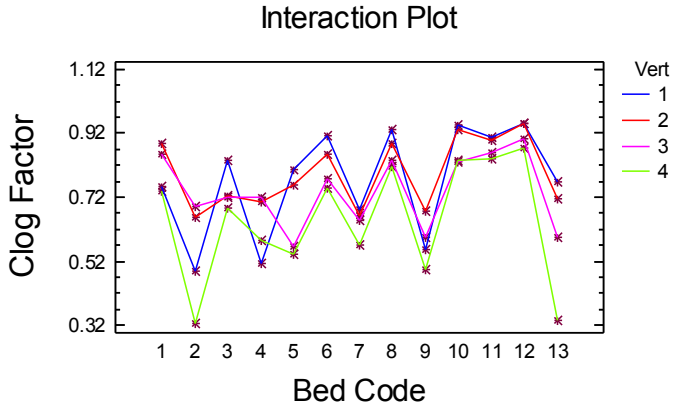

Multiple Range Tests for Clog Factor by Bed Code

Method: 95.0 percent LSD

Bed Code	Count	LS Mean	LS Sigma	Homogeneous Groups
2	64	0.540531	0.0186312	X
9	48	0.580474	0.0215134	XX
13	80	0.603495	0.0166642	XX
4	80	0.632497	0.0166642	XXX
7	64	0.64152	0.0186312	XX
5	80	0.668897	0.0166642	X
3	64	0.743004	0.0186312	X
1	64	0.809459	0.0186312	X
6	64	0.823993	0.0186312	XX
8	64	0.867772	0.0186312	XX
11	80	0.875823	0.0166642	XX
10	80	0.884697	0.0166642	XX
12	80	0.919668	0.0166642	X

Contrast	Difference	+/- Limits
1 - 2	*0.268928	0.0516421
1 - 3	*0.0664559	0.0516421
1 - 4	*0.176962	0.048992
1 - 5	*0.140563	0.048992
1 - 6	-0.0145332	0.0516421
1 - 7	*0.16794	0.0516421
1 - 8	*-0.0583124	0.0516421
1 - 9	*0.228985	0.0557798
1 - 10	*-0.0752372	0.048992
1 - 11	*-0.0663641	0.048992
1 - 12	*-0.110208	0.048992
1 - 13	*0.205964	0.048992
2 - 3	*-0.202472	0.0516421
2 - 4	*-0.091966	0.048992
2 - 5	*-0.128365	0.048992
2 - 6	*-0.283461	0.0516421
2 - 7	*-0.100988	0.0516421
2 - 8	*-0.32724	0.0516421
2 - 9	-0.0399427	0.0557798
2 - 10	*-0.344165	0.048992
2 - 11	*-0.335292	0.048992
2 - 12	*-0.379136	0.048992
2 - 13	*-0.0629636	0.048992
3 - 4	*0.110506	0.048992
3 - 5	*0.0741069	0.048992
3 - 6	*-0.080989	0.0516421
3 - 7	*0.101484	0.0516421
3 - 8	*-0.124768	0.0516421
3 - 9	*0.162529	0.0557798

3 - 10	*-0.141693	0.048992
3 - 11	*-0.13282	0.048992
3 - 12	*-0.176664	0.048992
3 - 13	*0.139508	0.048992
4 - 5	-0.0363992	0.0461901
4 - 6	*-0.191495	0.048992
4 - 7	-0.00902215	0.048992
4 - 8	*-0.235274	0.048992
4 - 9	0.0520233	0.0533357
4 - 10	*-0.252199	0.0461901
4 - 11	*-0.243326	0.0461901
4 - 12	*-0.28717	0.0461901
4 - 13	0.0290024	0.0461901
5 - 6	*-0.155096	0.048992
5 - 7	0.027377	0.048992
5 - 8	*-0.198875	0.048992
5 - 9	*0.0884225	0.0533357
5 - 10	*-0.2158	0.0461901
5 - 11	*-0.206927	0.0461901
5 - 12	*-0.250771	0.0461901
5 - 13	*0.0654016	0.0461901
6 - 7	*0.182473	0.0516421
6 - 8	-0.0437792	0.0516421
6 - 9	*0.243518	0.0557798
6 - 10	*-0.060704	0.048992
6 - 11	*-0.0518309	0.048992
6 - 12	*-0.0956753	0.048992
6 - 13	*0.220498	0.048992
7 - 8	*-0.226252	0.0516421
7 - 9	*0.0610455	0.0557798
7 - 10	*-0.243177	0.048992
7 - 11	*-0.234304	0.048992
7 - 12	*-0.278148	0.048992
7 - 13	0.0380245	0.048992
8 - 9	*0.287298	0.0557798
8 - 10	-0.0169249	0.048992
8 - 11	-0.00805175	0.048992
8 - 12	*-0.0518961	0.048992
8 - 13	*0.264277	0.048992
9 - 10	*-0.304222	0.0533357
9 - 11	*-0.295349	0.0533357
9 - 12	*-0.339194	0.0533357
9 - 13	-0.0230209	0.0533357
10 - 11	0.0088731	0.0461901
10 - 12	-0.0349712	0.0461901
10 - 13	*0.281202	0.0461901
11 - 12	-0.0438443	0.0461901
11 - 13	*0.272328	0.0461901
12 - 13	*0.316173	0.0461901

---

* denotes a statistically significant difference.

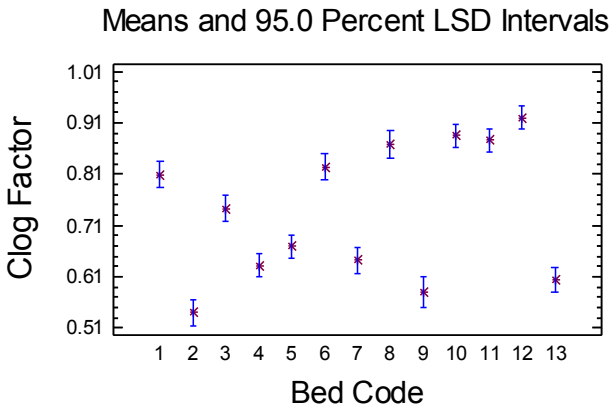
Means and 95.0 Percent LSD Intervals
Clog Factor
1.01
0.91
0.81
0.71
0.61
0.51
1 2 3 4 5 6 7 8 9 10 11 12 13
Bed Code

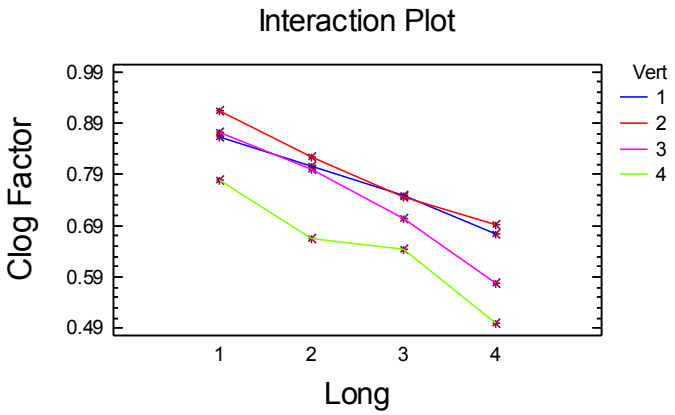
Interaction Plot
Clog Factor
0.99
0.89
0.79
0.69
0.59
0.49
1 2 3 4
Long
Vert
1
2
3
4

Appendix C.1: Ashorne Multifactor ANOVA - CF

Analysis Summary: Dependent variable: CF, Factors: trans, vert, long
Number of complete cases: 64

Analysis of Variance for CF - Type III Sums of Squares

Source	Sum of Squares	Df	Mean Square	F-Ratio	P-Value
MAIN EFFECTS					
A:trans	0.151333	3	0.0504444	5.32	0.0052
B:vert	0.25518	3	0.0850601	8.98	0.0003
C:long	1.70366	3	0.567888	59.94	0.0000
INTERACTIONS					
AB	0.0932374	9	0.0103597	1.09	0.3996
AC	0.187338	9	0.0208153	2.20	0.0551
BC	0.246288	9	0.0273653	2.89	0.0158
RESIDUAL	0.255784	27	0.00947349		
TOTAL (CORRECTED)	2.89282	63			

All F-ratios are based on the residual mean square error.

Table of Least Squares Means for CF with 95.0 Percent Confidence Intervals

Level	Count	Stnd. Mean	Error	Lower Limit	Upper Limit
GRAND MEAN	64	0.809459			
trans					
1	16	0.790749	0.024333	0.740822	0.840676
2	16	0.744899	0.024333	0.694972	0.794826
3	16	0.823954	0.024333	0.774027	0.873882
4	16	0.878235	0.024333	0.828308	0.928162
vert					
1	16	0.753593	0.024333	0.703666	0.80352
2	16	0.886998	0.024333	0.837071	0.936925
3	16	0.855985	0.024333	0.806057	0.905912
4	16	0.741262	0.024333	0.691335	0.791189
long					
1	16	0.969789	0.024333	0.919862	1.01972
2	16	0.91576	0.024333	0.865833	0.965687
3	16	0.80639	0.024333	0.756463	0.856317
4	16	0.545899	0.024333	0.495972	0.595826
trans by vert					
1 1	4	0.73301	0.0486659	0.633156	0.832865
1 2	4	0.877356	0.0486659	0.777501	0.97721

1	3	4	0.86397	0.0486659	0.764116	0.963825
1	4	4	0.688659	0.0486659	0.588804	0.788513
2	1	4	0.638946	0.0486659	0.539091	0.7388
2	2	4	0.871788	0.0486659	0.771933	0.971642
2	3	4	0.82459	0.0486659	0.724736	0.924444
2	4	4	0.644273	0.0486659	0.544418	0.744127
3	1	4	0.747335	0.0486659	0.64748	0.847189
3	2	4	0.88425	0.0486659	0.784395	0.984104
3	3	4	0.839518	0.0486659	0.739664	0.939373
3	4	4	0.824715	0.0486659	0.724861	0.92457
4	1	4	0.895081	0.0486659	0.795227	0.994935
4	2	4	0.914599	0.0486659	0.814744	1.01445
4	3	4	0.895861	0.0486659	0.796006	0.995715
4	4	4	0.807401	0.0486659	0.707546	0.907255
trans by long						
1	1	4	0.977118	0.0486659	0.877264	1.07697
1	2	4	0.89494	0.0486659	0.795086	0.994795
1	3	4	0.664184	0.0486659	0.564329	0.764038
1	4	4	0.626753	0.0486659	0.526898	0.726607
2	1	4	0.955107	0.0486659	0.855253	1.05496
2	2	4	0.851347	0.0486659	0.751493	0.951202
2	3	4	0.777381	0.0486659	0.677526	0.877235
2	4	4	0.395762	0.0486659	0.295907	0.495616
3	1	4	0.970648	0.0486659	0.870793	1.0705
3	2	4	0.944789	0.0486659	0.844934	1.04464
3	3	4	0.850352	0.0486659	0.750498	0.950207
3	4	4	0.530029	0.0486659	0.430175	0.629884
4	1	4	0.976282	0.0486659	0.876428	1.07614
4	2	4	0.971963	0.0486659	0.872109	1.07182
4	3	4	0.933644	0.0486659	0.833789	1.0335
4	4	4	0.631052	0.0486659	0.531197	0.730906
vert by long						
1	1	4	0.978344	0.0486659	0.87849	1.0782
1	2	4	0.919195	0.0486659	0.81934	1.01905
1	3	4	0.750542	0.0486659	0.650688	0.850397
1	4	4	0.366291	0.0486659	0.266436	0.466145
2	1	4	1.0	0.0486659	0.900146	1.09985
2	2	4	0.963159	0.0486659	0.863305	1.06301
2	3	4	0.859869	0.0486659	0.760014	0.959723
2	4	4	0.724964	0.0486659	0.625109	0.824818
3	1	4	0.95998	0.0486659	0.860126	1.05983
3	2	4	0.919797	0.0486659	0.819942	1.01965
3	3	4	0.848939	0.0486659	0.749084	0.948793
3	4	4	0.695223	0.0486659	0.595369	0.795078
4	1	4	0.940831	0.0486659	0.840977	1.04069
4	2	4	0.860889	0.0486659	0.761034	0.960743
4	3	4	0.766211	0.0486659	0.666356	0.866065
4	4	4	0.397117	0.0486659	0.297263	0.496972

Multiple Range Tests for CF by long

Method: 95.0 percent LSD

long	Count	LS Mean	LS Sigma	Homogeneous Groups
4	16	0.545899	0.024333	X
3	16	0.80639	0.024333	X
2	16	0.91576	0.024333	X
1	16	0.969789	0.024333	X

Contrast	Difference	+/- Limits
1 - 2	0.0540292	0.0706078
1 - 3	*0.163399	0.0706078
1 - 4	*0.42389	0.0706078
2 - 3	*0.10937	0.0706078
2 - 4	*0.369861	0.0706078
3 - 4	*0.260491	0.0706078

---

* denotes a statistically significant difference.

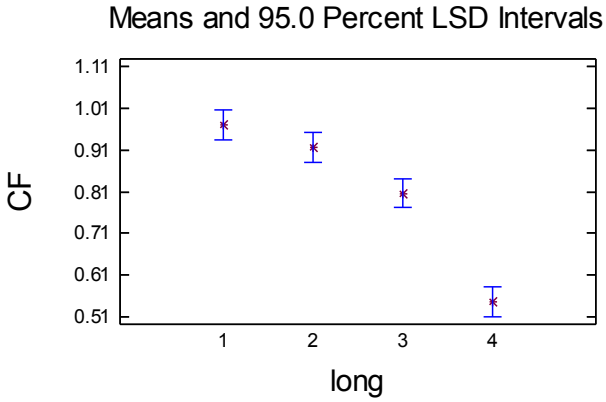

Multiple Range Tests for CF by vert

Method: 95.0 percent LSD

vert	Count	LS Mean	LS Sigma	Homogeneous Groups
4	16	0.741262	0.024333	X
1	16	0.753593	0.024333	X
3	16	0.855985	0.024333	X
2	16	0.886998	0.024333	X

Contrast	Difference	+/- Limits
1 - 2	*-0.133405	0.0706078
1 - 3	*-0.102392	0.0706078

1 - 4	0.0123311	0.0706078
2 - 3	0.0310132	0.0706078
2 - 4	*0.145736	0.0706078
3 - 4	*0.114723	0.0706078

---

* denotes a statistically significant difference.

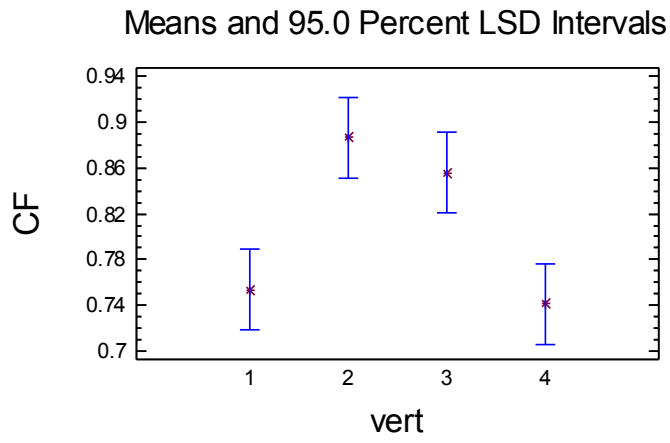

Multiple Range Tests for CF by trans

Method: 95.0 percent LSD

trans	Count	LS Mean	LS Sigma	Homogeneous Groups
2	16	0.744899	0.024333	X
1	16	0.790749	0.024333	XX
3	16	0.823954	0.024333	XX
4	16	0.878235	0.024333	X

Contrast	Difference	+/- Limits
1 - 2	0.0458496	0.0706078
1 - 3	-0.0332057	0.0706078
1 - 4	*-0.0874865	0.0706078
2 - 3	*-0.0790553	0.0706078
2 - 4	*-0.133336	0.0706078
3 - 4	-0.0542807	0.0706078

---

* denotes a statistically significant difference.

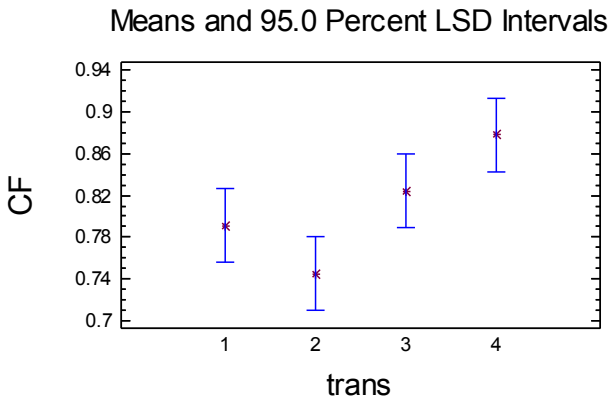
Means and 95.0 Percent LSD Intervals
CF
0.94
0.9
0.86
0.82
0.78
0.74
0.7
1
2
3
4
trans

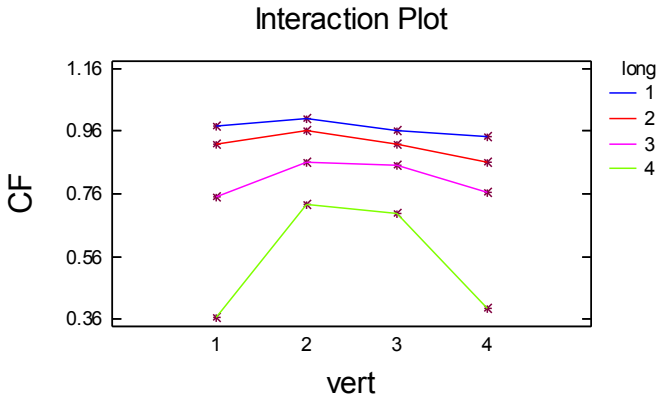
Interaction Plot
CF
1.16
0.96
0.76
0.56
0.36
1
2
3
4
vert
long
1
2
3
4

Appendix C.2: Fenny 08 Multifactor ANOVA - CF

Analysis Summary: Dependent variable: CF, Factors: long, trans, vert
Number of complete cases: 80

Analysis of Variance for CF - Type III Sums of Squares

Source	Sum of Squares	Df	Mean Square	F-Ratio	P-Value
MAIN EFFECTS					
A:long	1.69868	4	0.424671	8.57	0.0001
B:trans	0.0444461	3	0.0148154	0.30	0.8258
C:vert	1.85241	3	0.617469	12.47	0.0000
INTERACTIONS					
AB	1.58696	12	0.132246	2.67	0.0113
AC	0.409805	12	0.0341504	0.69	0.7503
BC	0.264548	9	0.0293942	0.59	0.7936
RESIDUAL	1.78289	36	0.0495248		
TOTAL (CORRECTED)	7.63974	79			

All F-ratios are based on the residual mean square error.

Table of Least Squares Means for CF
with 95.0 Percent Confidence Intervals

Level	Count	Mean	Stnd. Error	Lower Limit	Upper Limit
GRAND MEAN	80	0.488706			
long					
1	16	0.674301	0.0556354	0.561467	0.787135
2	16	0.607753	0.0556354	0.494918	0.720587
3	16	0.510177	0.0556354	0.397343	0.623011
4	16	0.369895	0.0556354	0.257061	0.482729
5	16	0.281406	0.0556354	0.168572	0.394241
trans					
1	20	0.511704	0.0497618	0.410782	0.612626
2	20	0.489407	0.0497618	0.388485	0.590329
3	20	0.450285	0.0497618	0.349364	0.551207
4	20	0.503429	0.0497618	0.402507	0.604351
vert					
1	20	0.42411	0.0497618	0.323188	0.525032
2	20	0.63156	0.0497618	0.530638	0.732481
3	20	0.629826	0.0497618	0.528904	0.730748
4	20	0.26933	0.0497618	0.168408	0.370252
long by trans					
1	1	4	0.943055	0.111271	0.717387	1.16872
1	2	4	0.498423	0.111271	0.272755	0.724091

1	3	4	0.630132	0.111271	0.404464	0.8558
1	4	4	0.625593	0.111271	0.399925	0.851262
2	1	4	0.798858	0.111271	0.57319	1.02453
2	2	4	0.491108	0.111271	0.26544	0.716776
2	3	4	0.42877	0.111271	0.203102	0.654438
2	4	4	0.712274	0.111271	0.486606	0.937942
3	1	4	0.468151	0.111271	0.242483	0.693819
3	2	4	0.598113	0.111271	0.372445	0.823782
3	3	4	0.334858	0.111271	0.109189	0.560526
3	4	4	0.639586	0.111271	0.413918	0.865255
4	1	4	0.175389	0.111271	-0.0502791	0.401057
4	2	4	0.581635	0.111271	0.355967	0.807303
4	3	4	0.363018	0.111271	0.13735	0.588686
4	4	4	0.359539	0.111271	0.133871	0.585207
5	1	4	0.173067	0.111271	-0.0526008	0.398735
5	2	4	0.277755	0.111271	0.0520871	0.503423
5	3	4	0.49465	0.111271	0.268982	0.720318
5	4	4	0.180153	0.111271	-0.0455148	0.405821
long by vert						
1	1	4	0.515329	0.111271	0.289661	0.740997
1	2	4	0.793967	0.111271	0.568299	1.01963
1	3	4	0.765231	0.111271	0.539563	0.990899
1	4	4	0.622676	0.111271	0.397008	0.848344
2	1	4	0.648203	0.111271	0.422535	0.873871
2	2	4	0.786689	0.111271	0.561021	1.01236
2	3	4	0.723484	0.111271	0.497815	0.949152
2	4	4	0.272634	0.111271	0.0469658	0.498302
3	1	4	0.41965	0.111271	0.193982	0.645318
3	2	4	0.596437	0.111271	0.370769	0.822105
3	3	4	0.736283	0.111271	0.510615	0.961951
3	4	4	0.288338	0.111271	0.0626702	0.514006
4	1	4	0.373202	0.111271	0.147534	0.59887
4	2	4	0.453744	0.111271	0.228076	0.679412
4	3	4	0.53757	0.111271	0.311902	0.763238
4	4	4	0.115064	0.111271	-0.110604	0.340733
5	1	4	0.164167	0.111271	-0.0615015	0.389835
5	2	4	0.526961	0.111271	0.301293	0.752629
5	3	4	0.386561	0.111271	0.160893	0.612229
5	4	4	0.0479373	0.111271	-0.177731	0.273605
trans by vert						
1	1	5	0.446382	0.0995236	0.244538	0.648225
1	2	5	0.570612	0.0995236	0.368768	0.772455
1	3	5	0.618811	0.0995236	0.416968	0.820655
1	4	5	0.411011	0.0995236	0.209167	0.612855
2	1	5	0.404253	0.0995236	0.20241	0.606097
2	2	5	0.743849	0.0995236	0.542005	0.945692
2	3	5	0.637148	0.0995236	0.435304	0.838991
2	4	5	0.172378	0.0995236	-0.0294653	0.374222
3	1	5	0.354109	0.0995236	0.152265	0.555953
3	2	5	0.618042	0.0995236	0.416198	0.819886
3	3	5	0.597057	0.0995236	0.395213	0.798901

3	4	5	0.231934	0.0995236	0.0300902	0.433778
4	1	5	0.491697	0.0995236	0.289854	0.693541
4	2	5	0.593736	0.0995236	0.391893	0.79558
4	3	5	0.666287	0.0995236	0.464443	0.868131
4	4	5	0.261997	0.0995236	0.0601529	0.46384

Multiple Range Tests for CF by long

Method: 95.0 percent LSD

long	Count	LS Mean	LS Sigma	Homogeneous Groups
5	16	0.281406	0.0556354	X
4	16	0.369895	0.0556354	XX
3	16	0.510177	0.0556354	XX
2	16	0.607753	0.0556354	XX
1	16	0.674301	0.0556354	X

Contrast	Difference	+/- Limits
1 - 2	0.0665483	0.159571
1 - 3	*0.164124	0.159571
1 - 4	*0.304406	0.159571
1 - 5	*0.392894	0.159571
2 - 3	0.0975754	0.159571
2 - 4	*0.237857	0.159571
2 - 5	*0.326346	0.159571
3 - 4	0.140282	0.159571
3 - 5	*0.228771	0.159571
4 - 5	0.0884887	0.159571

---

* denotes a statistically significant difference.

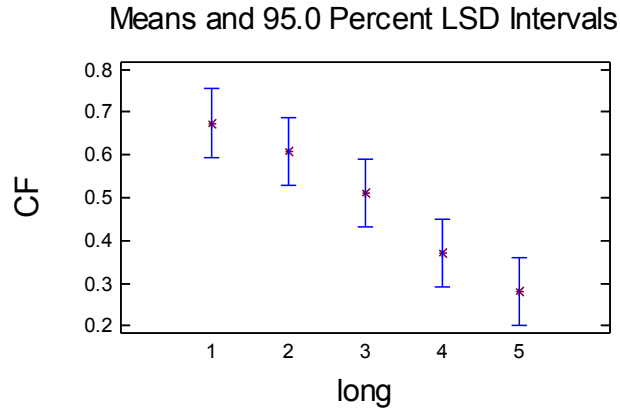

Multiple Range Tests for CF by trans

Method: 95.0 percent LSD

trans	Count	LS Mean	LS Sigma	Homogeneous Groups
3	20	0.450285	0.0497618	X
2	20	0.489407	0.0497618	X
4	20	0.503429	0.0497618	X
1	20	0.511704	0.0497618	X

Contrast	Difference	+/- Limits
1 - 2	0.022297	0.142725
1 - 3	0.0614184	0.142725
1 - 4	0.00827465	0.142725
2 - 3	0.0391215	0.142725
2 - 4	-0.0140223	0.142725
3 - 4	-0.0531438	0.142725

---

* denotes a statistically significant difference.

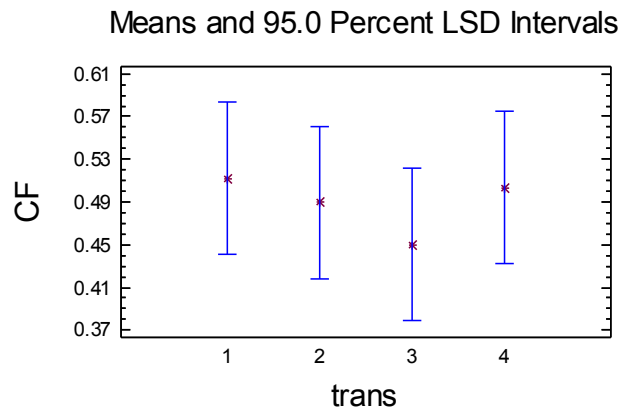

Multiple Range Tests for CF by vert

Method: 95.0 percent LSD

vert	Count	LS Mean	LS Sigma	Homogeneous Groups
4	20	0.26933	0.0497618	X
1	20	0.42411	0.0497618	X
3	20	0.629826	0.0497618	X
2	20	0.63156	0.0497618	X

Contrast	Difference	+/- Limits
1 - 2	*-0.207449	0.142725

1 - 3	*-0.205715	0.142725
1 - 4	*0.15478	0.142725
2 - 3	0.00173395	0.142725
2 - 4	*0.36223	0.142725
3 - 4	*0.360496	0.142725

---

* denotes a statistically significant difference.

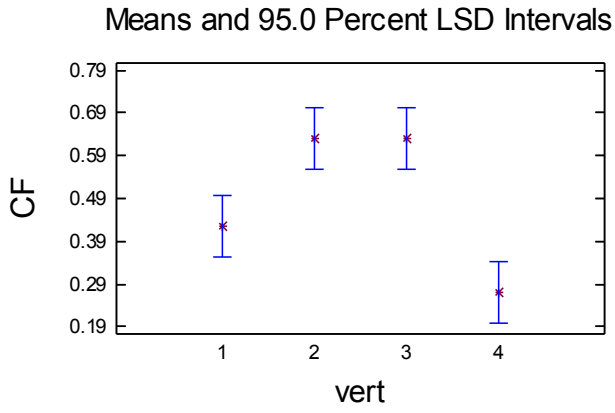

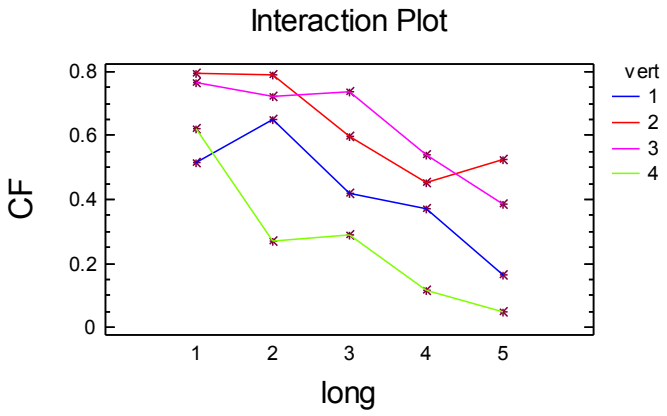

Appendix C.3: Fenny 09 Multifactor ANOVA - CF

Analysis Summary: Dependent variable: CF, Factors: long, trans, vert
Number of complete cases: 64

Analysis of Variance for CF - Type III Sums of Squares

Source	Sum of Squares	Df	Mean Square	F-Ratio	P-Value
MAIN EFFECTS					
A:long	0.389309	3	0.12977	3.37	0.0330
B:trans	0.138012	3	0.0460039	1.19	0.3305
C:vert	0.202976	3	0.0676586	1.76	0.1791
INTERACTIONS					
AB	1.22943	9	0.136603	3.55	0.0051
AC	0.226141	9	0.0251268	0.65	0.7429
BC	0.220491	9	0.024499	0.64	0.7563
RESIDUAL	1.0397	27	0.0385072		
TOTAL (CORRECTED)	3.44605	63			

All F-ratios are based on the residual mean square error.

Table of Least Squares Means for CF
with 95.0 Percent Confidence Intervals

Level	Count	Stnd. Mean	Lower Error	Upper Limit	Limit
GRAND MEAN	64	0.743004			
long					
1	16	0.756393	0.0490582	0.655734	0.857052
2	16	0.791078	0.0490582	0.690419	0.891737
3	16	0.812153	0.0490582	0.711494	0.912812
4	16	0.61239	0.0490582	0.511731	0.71305
trans					
1	16	0.742686	0.0490582	0.642027	0.843345
2	16	0.818923	0.0490582	0.718264	0.919582
3	16	0.706623	0.0490582	0.605964	0.807282
4	16	0.703782	0.0490582	0.603123	0.804441
vert					
1	16	0.837085	0.0490582	0.736426	0.937744
2	16	0.726403	0.0490582	0.625744	0.827062
3	16	0.720957	0.0490582	0.620298	0.821616
4	16	0.687569	0.0490582	0.58691	0.788228
long by trans					
1	1	4	0.922946	0.0981163	0.721627	1.12426
1	2	4	0.762245	0.0981163	0.560926	0.963563

1	3	4	0.536979	0.0981163	0.335661	0.738298
1	4	4	0.803401	0.0981163	0.602083	1.00472
2	1	4	0.828158	0.0981163	0.626839	1.02948
2	2	4	0.992745	0.0981163	0.791427	1.19406
2	3	4	0.5869	0.0981163	0.385581	0.788218
2	4	4	0.756509	0.0981163	0.555191	0.957828
3	1	4	0.719917	0.0981163	0.518598	0.921235
3	2	4	0.991896	0.0981163	0.790578	1.19321
3	3	4	0.98653	0.0981163	0.785212	1.18785
3	4	4	0.550269	0.0981163	0.34895	0.751587
4	1	4	0.499724	0.0981163	0.298406	0.701043
4	2	4	0.528806	0.0981163	0.327488	0.730125
4	3	4	0.716083	0.0981163	0.514764	0.917401
4	4	4	0.704949	0.0981163	0.503631	0.906267
long by vert						
1	1	4	0.858475	0.0981163	0.657157	1.05979
1	2	4	0.842479	0.0981163	0.64116	1.0438
1	3	4	0.717562	0.0981163	0.516243	0.91888
1	4	4	0.607055	0.0981163	0.405737	0.808374
2	1	4	0.868033	0.0981163	0.666715	1.06935
2	2	4	0.786564	0.0981163	0.585246	0.987883
2	3	4	0.821357	0.0981163	0.620039	1.02268
2	4	4	0.688357	0.0981163	0.487039	0.889676
3	1	4	0.888204	0.0981163	0.686886	1.08952
3	2	4	0.688439	0.0981163	0.487121	0.889757
3	3	4	0.835838	0.0981163	0.634519	1.03716
3	4	4	0.83613	0.0981163	0.634812	1.03745
4	1	4	0.733628	0.0981163	0.53231	0.934947
4	2	4	0.588129	0.0981163	0.386811	0.789448
4	3	4	0.509072	0.0981163	0.307753	0.71039
4	4	4	0.618733	0.0981163	0.417414	0.820051
trans by vert						
1	1	4	0.879491	0.0981163	0.678173	1.08081
1	2	4	0.654686	0.0981163	0.453368	0.856005
1	3	4	0.760557	0.0981163	0.559239	0.961876
1	4	4	0.676009	0.0981163	0.474691	0.877328
2	1	4	0.885286	0.0981163	0.683967	1.0866
2	2	4	0.90487	0.0981163	0.703551	1.10619
2	3	4	0.688635	0.0981163	0.487317	0.889954
2	4	4	0.796901	0.0981163	0.595583	0.99822
3	1	4	0.778561	0.0981163	0.577243	0.97988
3	2	4	0.601223	0.0981163	0.399904	0.802541
3	3	4	0.753835	0.0981163	0.552516	0.955153
3	4	4	0.692873	0.0981163	0.491555	0.894192
4	1	4	0.805003	0.0981163	0.603684	1.00632
4	2	4	0.744833	0.0981163	0.543514	0.946151
4	3	4	0.680801	0.0981163	0.479482	0.882119
4	4	4	0.584492	0.0981163	0.383173	0.78581

Multiple Range Tests for CF by long

Method: 95.0 percent LSD

long	Count	LS Mean	LS Sigma	Homogeneous Groups
4	16	0.61239	0.0490582	X
1	16	0.756393	0.0490582	X
2	16	0.791078	0.0490582	X
3	16	0.812153	0.0490582	X

Contrast	Difference	+/- Limits
1 - 2	-0.0346852	0.142354
1 - 3	-0.0557601	0.142354
1 - 4	*0.144002	0.142354
2 - 3	-0.0210749	0.142354
2 - 4	*0.178687	0.142354
3 - 4	*0.199762	0.142354

---

* denotes a statistically significant difference.

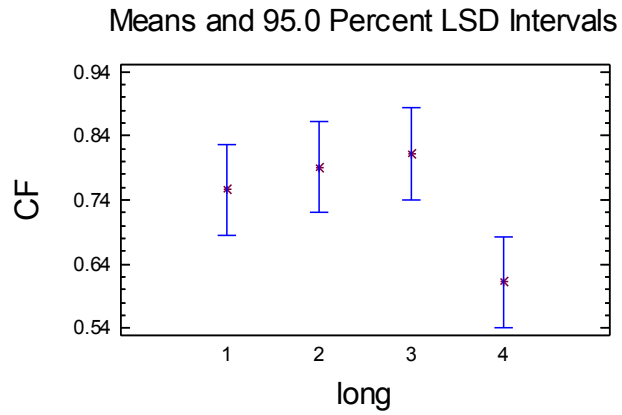

Multiple Range Tests for CF by trans

Method: 95.0 percent LSD

trans	Count	LS Mean	LS Sigma	Homogeneous Groups
4	16	0.703782	0.0490582	X
3	16	0.706623	0.0490582	X
1	16	0.742686	0.0490582	X
2	16	0.818923	0.0490582	X

Contrast	Difference	+/- Limits
1 - 2	-0.076237	0.142354
1 - 3	0.036063	0.142354
1 - 4	0.038904	0.142354

2 - 3	0.1123	0.142354
2 - 4	0.115141	0.142354
3 - 4	0.00284095	0.142354

* denotes a statistically significant difference.

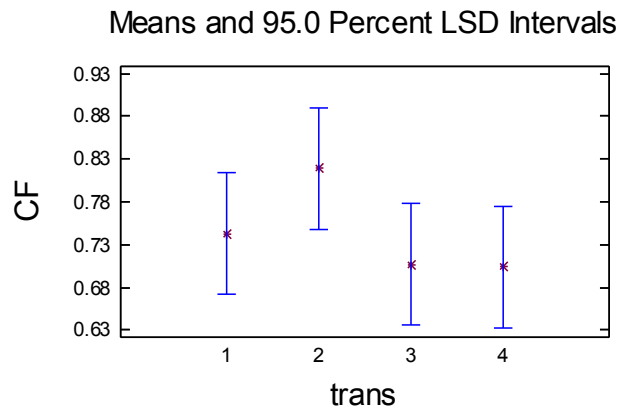

Multiple Range Tests for CF by vert

Method: 95.0 percent LSD

vert	Count	LS Mean	LS Sigma	Homogeneous Groups
4	16	0.687569	0.0490582	X
3	16	0.720957	0.0490582	XX
2	16	0.726403	0.0490582	XX
1	16	0.837085	0.0490582	X

Contrast	Difference	+/- Limits
1 - 2	0.110682	0.142354
1 - 3	0.116128	0.142354
1 - 4	*0.149516	0.142354
2 - 3	0.00544588	0.142354
2 - 4	0.038834	0.142354
3 - 4	0.0333881	0.142354

* denotes a statistically significant difference.

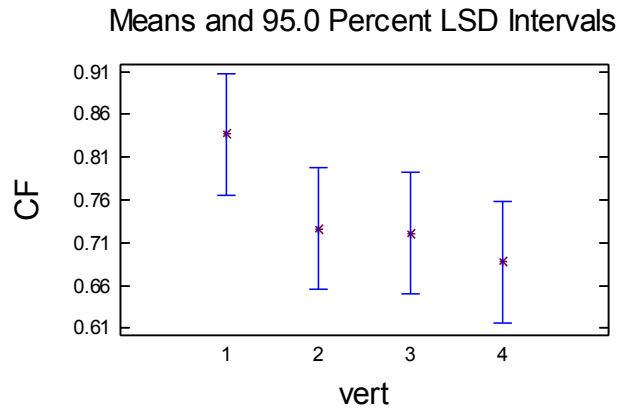
Means and 95.0 Percent LSD Intervals
CF
0.91
0.86
0.81
0.76
0.71
0.66
0.61
1
2
3
4
vert

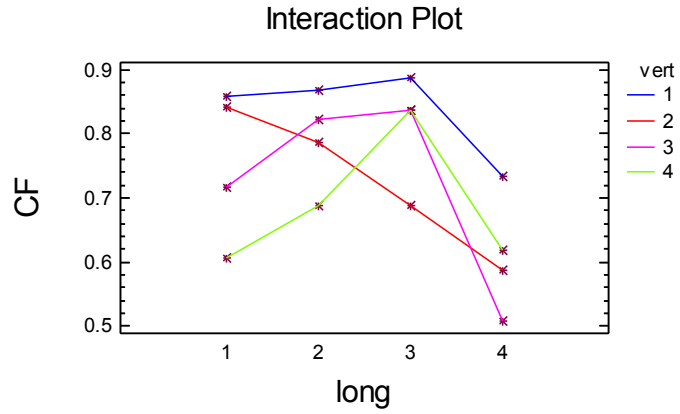
Interaction Plot
CF
0.9
0.8
0.7
0.6
0.5
1
2
3
4
long
vert
1
2
3
4

Appendix C.4: Fenny 10 Multifactor ANOVA - CF

Analysis Summary: Dependent variable: CF, Factors: long, trans, vert
Number of complete cases: 80

Analysis of Variance for CF - Type III Sums of Squares

Source	Sum of Squares	Df	Mean Square	F-Ratio	P-Value
MAIN EFFECTS					
A:long	0.99393	3	0.33131	18.89	0.0000
B:trans	0.10726	4	0.026815	1.53	0.2145
C:vert	0.592116	3	0.197372	11.25	0.0000
INTERACTIONS					
AB	1.00936	12	0.0841134	4.80	0.0001
AC	0.180089	9	0.0200098	1.14	0.3609
BC	0.124204	12	0.0103503	0.59	0.8355
RESIDUAL	0.631389	36	0.0175386		
TOTAL (CORRECTED)	3.63835	79			

All F-ratios are based on the residual mean square error.

Table of Least Squares Means for CF
with 95.0 Percent Confidence Intervals

Level	Count	Mean	Stnd. Error	Lower Limit	Upper Limit
GRAND MEAN	80	0.632497			
long					
1	20	0.755989	0.029613	0.695931	0.816047
2	20	0.707502	0.029613	0.647444	0.76756
3	20	0.600778	0.029613	0.54072	0.660836
4	20	0.465721	0.029613	0.405663	0.525779
trans					
1	16	0.650565	0.0331083	0.583418	0.717712
2	16	0.67028	0.0331083	0.603133	0.737427
3	16	0.66464	0.0331083	0.597493	0.731787
4	16	0.583746	0.0331083	0.516599	0.650893
5	16	0.593256	0.0331083	0.526109	0.660403
vert					
1	20	0.515128	0.029613	0.45507	0.575186
2	20	0.707017	0.029613	0.646959	0.767075
3	20	0.722329	0.029613	0.662271	0.782387
4	20	0.585516	0.029613	0.525458	0.645574
long by trans					

1	1	4	0.805029	0.0662167	0.670735	0.939323
1	2	4	0.830171	0.0662167	0.695877	0.964465
1	3	4	0.83759	0.0662167	0.703296	0.971884
1	4	4	0.509874	0.0662167	0.37558	0.644168
1	5	4	0.797281	0.0662167	0.662988	0.931575
2	1	4	0.800394	0.0662167	0.6661	0.934688
2	2	4	0.582551	0.0662167	0.448257	0.716845
2	3	4	0.813689	0.0662167	0.679395	0.947983
2	4	4	0.605566	0.0662167	0.471272	0.73986
2	5	4	0.735311	0.0662167	0.601017	0.869605
3	1	4	0.433603	0.0662167	0.299309	0.567897
3	2	4	0.688815	0.0662167	0.554522	0.823109
3	3	4	0.657515	0.0662167	0.523221	0.791809
3	4	4	0.806828	0.0662167	0.672534	0.941122
3	5	4	0.417127	0.0662167	0.282833	0.551421
4	1	4	0.563234	0.0662167	0.42894	0.697528
4	2	4	0.579584	0.0662167	0.44529	0.713878
4	3	4	0.349767	0.0662167	0.215473	0.484061
4	4	4	0.412714	0.0662167	0.27842	0.547008
4	5	4	0.423305	0.0662167	0.289011	0.557599
long by vert						
1	1	5	0.696114	0.059226	0.575998	0.81623
1	2	5	0.901209	0.059226	0.781092	1.02132
1	3	5	0.810521	0.059226	0.690405	0.930637
1	4	5	0.616113	0.059226	0.495997	0.736229
2	1	5	0.538583	0.059226	0.418467	0.658699
2	2	5	0.802794	0.059226	0.682678	0.92291
2	3	5	0.807161	0.059226	0.687045	0.927277
2	4	5	0.681471	0.059226	0.561354	0.801587
3	1	5	0.514597	0.059226	0.394481	0.634713
3	2	5	0.610846	0.059226	0.49073	0.730963
3	3	5	0.66469	0.059226	0.544574	0.784806
3	4	5	0.612978	0.059226	0.492862	0.733094
4	1	5	0.311217	0.059226	0.191101	0.431333
4	2	5	0.51322	0.059226	0.393104	0.633336
4	3	5	0.606943	0.059226	0.486827	0.727059
4	4	5	0.431502	0.059226	0.311386	0.551618
trans by vert						
1	1	4	0.510318	0.0662167	0.376024	0.644612
1	2	4	0.762375	0.0662167	0.628082	0.896669
1	3	4	0.696912	0.0662167	0.562618	0.831206
1	4	4	0.632654	0.0662167	0.49836	0.766948
2	1	4	0.458259	0.0662167	0.323965	0.592553
2	2	4	0.77013	0.0662167	0.635836	0.904424
2	3	4	0.767879	0.0662167	0.633585	0.902173
2	4	4	0.684854	0.0662167	0.55056	0.819148
3	1	4	0.604511	0.0662167	0.470217	0.738805
3	2	4	0.725343	0.0662167	0.591049	0.859637
3	3	4	0.750947	0.0662167	0.616653	0.885241
3	4	4	0.57776	0.0662167	0.443466	0.712054
4	1	4	0.498416	0.0662167	0.364122	0.63271

4	2	4	0.662068	0.0662167	0.527774	0.796362
4	3	4	0.686956	0.0662167	0.552662	0.82125
4	4	4	0.487543	0.0662167	0.353249	0.621837
5	1	4	0.504135	0.0662167	0.369841	0.638429
5	2	4	0.61517	0.0662167	0.480876	0.749464
5	3	4	0.708951	0.0662167	0.574657	0.843245
5	4	4	0.544768	0.0662167	0.410474	0.679062

Multiple Range Tests for CF by long

Method: 95.0 percent LSD

long	Count	LS Mean	LS Sigma	Homogeneous Groups
4	20	0.465721	0.029613	X
3	20	0.600778	0.029613	X
2	20	0.707502	0.029613	X
1	20	0.755989	0.029613	X

Contrast	Difference	+/- Limits
1 - 2	0.0484869	0.0849349
1 - 3	*0.155211	0.0849349
1 - 4	*0.290268	0.0849349
2 - 3	*0.106724	0.0849349
2 - 4	*0.241781	0.0849349
3 - 4	*0.135057	0.0849349

---

* denotes a statistically significant difference.

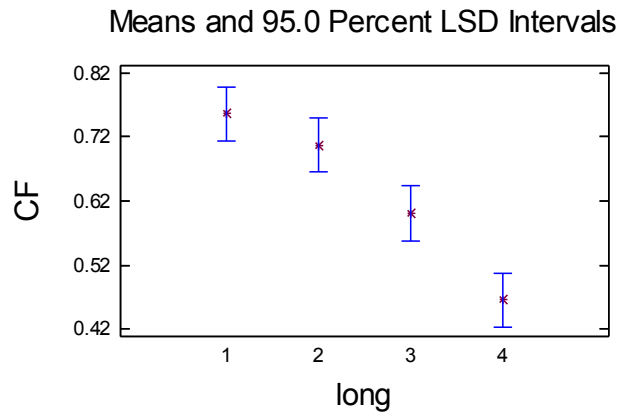

Multiple Range Tests for CF by trans

Method: 95.0 percent LSD

trans	Count	LS Mean	LS Sigma	Homogeneous Groups
4	16	0.583746	0.0331083	X
5	16	0.593256	0.0331083	X
1	16	0.650565	0.0331083	X
3	16	0.66464	0.0331083	X
2	16	0.67028	0.0331083	X

Contrast	Difference	+/- Limits
1 - 2	-0.0197155	0.0949601
1 - 3	-0.0140752	0.0949601
1 - 4	0.0668193	0.0949601
1 - 5	0.0573088	0.0949601
2 - 3	0.00564036	0.0949601
2 - 4	0.0865349	0.0949601
2 - 5	0.0770243	0.0949601
3 - 4	0.0808945	0.0949601
3 - 5	0.0713839	0.0949601
4 - 5	-0.00951056	0.0949601

---

* denotes a statistically significant difference.

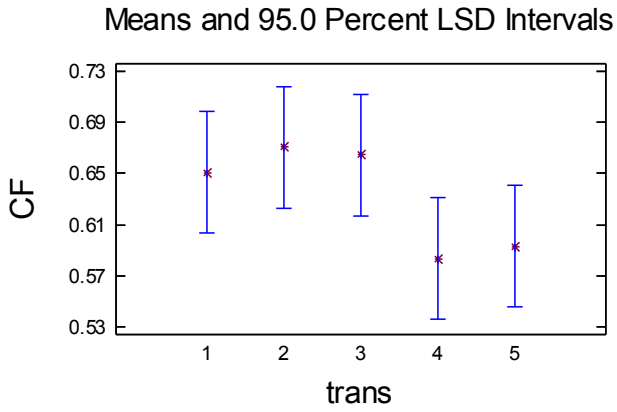

Multiple Range Tests for CF by vert

Method: 95.0 percent LSD

vert	Count	LS Mean	LS Sigma	Homogeneous Groups
1	20	0.515128	0.029613	X
4	20	0.585516	0.029613	X
2	20	0.707017	0.029613	X
3	20	0.722329	0.029613	X

Contrast	Difference	+/- Limits
1 - 2	*-0.19189	0.0849349
1 - 3	*-0.207201	0.0849349
1 - 4	-0.070388	0.0849349
2 - 3	-0.0153115	0.0849349
2 - 4	*0.121502	0.0849349
3 - 4	*0.136813	0.0849349

---

* denotes a statistically significant difference.

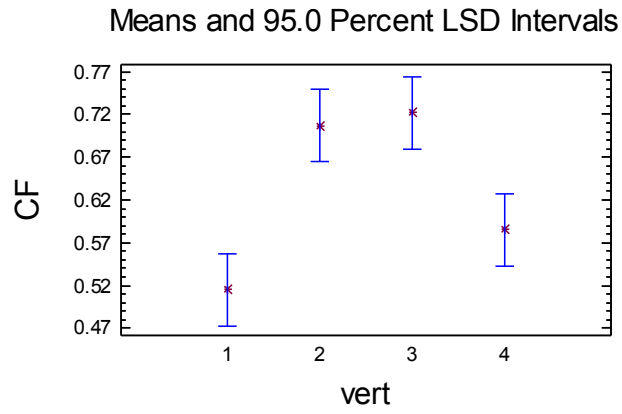

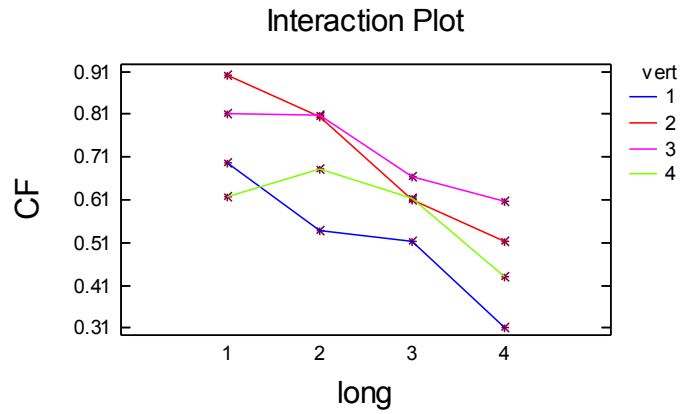

Appendix C.5: Leek Multifactor ANOVA - CF

Analysis Summary: Dependent variable: CF, Factors: long, trans, vert
Number of complete cases: 80

Analysis of Variance for CF - Type III Sums of Squares

Source	Sum of Squares	Df	Mean Square	F-Ratio	P-Value
MAIN EFFECTS					
A:long	0.0284804	3	0.00949347	0.94	0.4303
B:trans	0.187268	4	0.046817	4.65	0.0040
C:vert	1.05018	3	0.35006	34.75	0.0000
INTERACTIONS					
AB	0.190213	12	0.0158511	1.57	0.1438
AC	0.140549	9	0.0156166	1.55	0.1681
BC	0.152754	12	0.0127295	1.26	0.2813
RESIDUAL	0.362624	36	0.0100729		
TOTAL (CORRECTED)	2.11207	79			

All F-ratios are based on the residual mean square error.

Table of Least Squares Means for CF
with 95.0 Percent Confidence Intervals

Level	Count	Mean	Stnd. Error	Lower Limit	Upper Limit
GRAND MEAN	80	0.668897			
long					
1	20	0.677355	0.022442	0.63184	0.722869
2	20	0.653976	0.022442	0.608462	0.699491
3	20	0.64858	0.022442	0.603065	0.694095
4	20	0.695675	0.022442	0.650161	0.74119
trans					
1	16	0.681472	0.0250909	0.630585	0.732359
2	16	0.751419	0.0250909	0.700532	0.802306
3	16	0.630744	0.0250909	0.579857	0.681631
4	16	0.611622	0.0250909	0.560735	0.662508
5	16	0.669227	0.0250909	0.61834	0.720113
vert					
1	20	0.807274	0.022442	0.761759	0.852789
2	20	0.756145	0.022442	0.710631	0.80166
3	20	0.568223	0.022442	0.522708	0.613737
4	20	0.543944	0.022442	0.49843	0.589459
long by trans					

1	1	4	0.795279	0.0501819	0.693505	0.897053
1	2	4	0.742979	0.0501819	0.641205	0.844753
1	3	4	0.636812	0.0501819	0.535038	0.738586
1	4	4	0.553606	0.0501819	0.451832	0.655379
1	5	4	0.658097	0.0501819	0.556323	0.759871
2	1	4	0.674954	0.0501819	0.57318	0.776728
2	2	4	0.779988	0.0501819	0.678215	0.881762
2	3	4	0.646926	0.0501819	0.545152	0.7487
2	4	4	0.561887	0.0501819	0.460113	0.66366
2	5	4	0.606127	0.0501819	0.504353	0.7079
3	1	4	0.655766	0.0501819	0.553992	0.75754
3	2	4	0.671725	0.0501819	0.569951	0.773499
3	3	4	0.579479	0.0501819	0.477705	0.681252
3	4	4	0.649308	0.0501819	0.547535	0.751082
3	5	4	0.686623	0.0501819	0.584849	0.788396
4	1	4	0.599888	0.0501819	0.498115	0.701662
4	2	4	0.810984	0.0501819	0.70921	0.912758
4	3	4	0.659759	0.0501819	0.557986	0.761533
4	4	4	0.681686	0.0501819	0.579912	0.783459
4	5	4	0.72606	0.0501819	0.624286	0.827834
long by vert						
1	1	5	0.828958	0.044884	0.737929	0.919987
1	2	5	0.764369	0.044884	0.67334	0.855399
1	3	5	0.619299	0.044884	0.52827	0.710329
1	4	5	0.496791	0.044884	0.405762	0.587821
2	1	5	0.800051	0.044884	0.709021	0.89108
2	2	5	0.741613	0.044884	0.650584	0.832642
2	3	5	0.614595	0.044884	0.523566	0.705624
2	4	5	0.459647	0.044884	0.368618	0.550676
3	1	5	0.788209	0.044884	0.697179	0.879238
3	2	5	0.743207	0.044884	0.652178	0.834236
3	3	5	0.479036	0.044884	0.388007	0.570065
3	4	5	0.583868	0.044884	0.492839	0.674898
4	1	5	0.811879	0.044884	0.72085	0.902909
4	2	5	0.775393	0.044884	0.684363	0.866422
4	3	5	0.559959	0.044884	0.46893	0.650989
4	4	5	0.635471	0.044884	0.544441	0.7265
trans by vert						
1	1	4	0.8252	0.0501819	0.723426	0.926974
1	2	4	0.804892	0.0501819	0.703119	0.906666
1	3	4	0.58589	0.0501819	0.484116	0.687663
1	4	4	0.509906	0.0501819	0.408132	0.61168
2	1	4	0.854406	0.0501819	0.752633	0.95618
2	2	4	0.785952	0.0501819	0.684178	0.887726
2	3	4	0.707934	0.0501819	0.60616	0.809708
2	4	4	0.657384	0.0501819	0.55561	0.759158
3	1	4	0.800468	0.0501819	0.698694	0.902242
3	2	4	0.759502	0.0501819	0.657728	0.861275
3	3	4	0.424381	0.0501819	0.322607	0.526155
3	4	4	0.538625	0.0501819	0.436851	0.640399
4	1	4	0.783803	0.0501819	0.682029	0.885577

4	2	4	0.72186	0.0501819	0.620086	0.823634
4	3	4	0.489649	0.0501819	0.387875	0.591422
4	4	4	0.451175	0.0501819	0.349401	0.552949
5	1	4	0.772494	0.0501819	0.67072	0.874267
5	2	4	0.708522	0.0501819	0.606748	0.810296
5	3	4	0.633259	0.0501819	0.531485	0.735033
5	4	4	0.562632	0.0501819	0.460858	0.664406

Multiple Range Tests for CF by long

Method: 95.0 percent LSD

long	Count	LS Mean	LS Sigma	Homogeneous Groups
3	20	0.64858	0.022442	X
2	20	0.653976	0.022442	X
1	20	0.677355	0.022442	X
4	20	0.695675	0.022442	X

Contrast	Difference	+/- Limits
1 - 2	0.0233782	0.0643674
1 - 3	0.0287745	0.0643674
1 - 4	-0.0183209	0.0643674
2 - 3	0.00539626	0.0643674
2 - 4	-0.0416991	0.0643674
3 - 4	-0.0470954	0.0643674

---

* denotes a statistically significant difference.

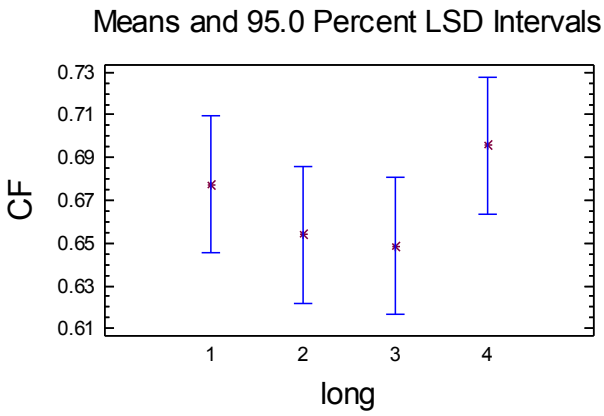

Multiple Range Tests for CF by trans

Method: 95.0 percent LSD

trans	Count	LS Mean	LS Sigma	Homogeneous Groups
4	16	0.611622	0.0250909	X
3	16	0.630744	0.0250909	X
5	16	0.669227	0.0250909	X
1	16	0.681472	0.0250909	XX
2	16	0.751419	0.0250909	X

Contrast	Difference	+/- Limits
1 - 2	-0.0699472	0.0719649
1 - 3	0.0507279	0.0719649
1 - 4	0.0698503	0.0719649
1 - 5	0.0122453	0.0719649
2 - 3	*0.120675	0.0719649
2 - 4	*0.139797	0.0719649
2 - 5	*0.0821924	0.0719649
3 - 4	0.0191224	0.0719649
3 - 5	-0.0384826	0.0719649
4 - 5	-0.057605	0.0719649

---

* denotes a statistically significant difference.

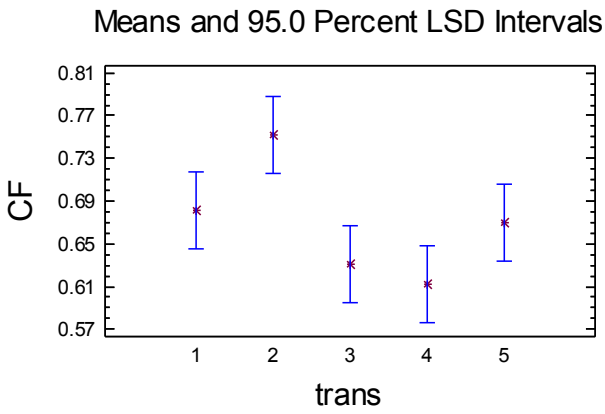

Multiple Range Tests for CF by vert

Method: 95.0 percent LSD

vert	Count	LS Mean	LS Sigma	Homogeneous Groups
4	20	0.543944	0.022442	X
3	20	0.568223	0.022442	X
2	20	0.756145	0.022442	X
1	20	0.807274	0.022442	X

Contrast	Difference	+/- Limits
1 - 2	0.0511286	0.0643674
1 - 3	*0.239052	0.0643674
1 - 4	*0.26333	0.0643674
2 - 3	*0.187923	0.0643674
2 - 4	*0.212201	0.0643674
3 - 4	0.0242782	0.0643674

* denotes a statistically significant difference.

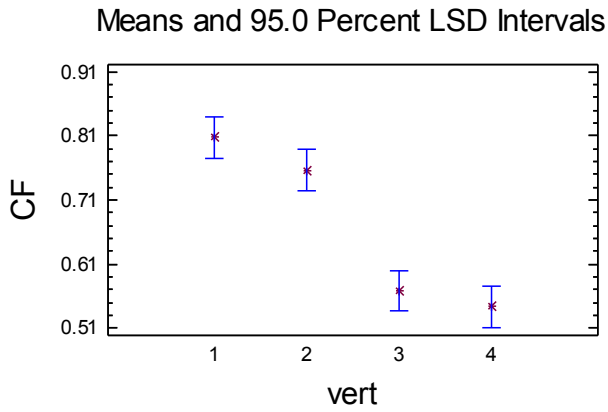

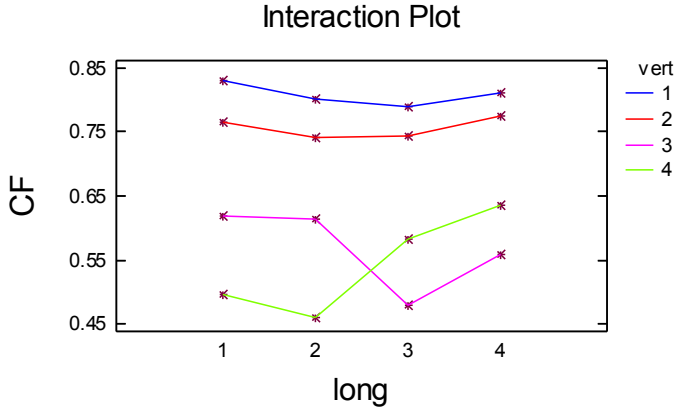

Appendix C.6: Moreton Feb 09 Multifactor ANOVA - CF

Analysis Summary: Dependent variable: CF, Factors: long, trans, vert
Number of complete cases: 64

Analysis of Variance for CF - Type III Sums of Squares

Source	Sum of Squares	Df	Mean Square	F-Ratio	P-Value
MAIN EFFECTS					
A:long	0.578866	3	0.192955	17.16	0.0000
B:trans	0.679894	3	0.226631	20.16	0.0000
C:vert	0.253293	3	0.084431	7.51	0.0008
INTERACTIONS					
AB	0.263299	9	0.0292554	2.60	0.0263
AC	0.149973	9	0.0166637	1.48	0.2046
BC	0.303066	9	0.033674	3.00	0.0131
RESIDUAL	0.303542	27	0.0112423		
TOTAL (CORRECTED)	2.53193	63			

All F-ratios are based on the residual mean square error.

Table of Least Squares Means for CF
with 95.0 Percent Confidence Intervals

Level	Count	Mean	Stnd. Error	Lower Limit	Upper Limit
GRAND MEAN	64	0.823993			
long					
1	16	0.96862	0.0265074	0.914231	1.02301
2	16	0.823272	0.0265074	0.768883	0.877661
3	16	0.801573	0.0265074	0.747184	0.855961
4	16	0.702506	0.0265074	0.648117	0.756895
trans					
1	16	0.935667	0.0265074	0.881279	0.990056
2	16	0.880815	0.0265074	0.826426	0.935204
3	16	0.819109	0.0265074	0.764721	0.873498
4	16	0.660379	0.0265074	0.60599	0.714768
vert					
1	16	0.909767	0.0265074	0.855379	0.964156
2	16	0.856645	0.0265074	0.802256	0.911034
3	16	0.77883	0.0265074	0.724441	0.833219
4	16	0.750728	0.0265074	0.69634	0.805117
long by trans					

1	1	4	0.978644	0.0530148	0.869866	1.08742
1	2	4	0.968595	0.0530148	0.859817	1.07737
1	3	4	0.981162	0.0530148	0.872384	1.08994
1	4	4	0.946078	0.0530148	0.837301	1.05486
2	1	4	0.948129	0.0530148	0.839351	1.05691
2	2	4	0.922705	0.0530148	0.813928	1.03148
2	3	4	0.78881	0.0530148	0.680033	0.897588
2	4	4	0.633443	0.0530148	0.524665	0.74222
3	1	4	0.927285	0.0530148	0.818508	1.03606
3	2	4	0.911089	0.0530148	0.802311	1.01987
3	3	4	0.741214	0.0530148	0.632436	0.849992
3	4	4	0.626702	0.0530148	0.517924	0.73548
4	1	4	0.888611	0.0530148	0.779834	0.997389
4	2	4	0.72087	0.0530148	0.612092	0.829648
4	3	4	0.765251	0.0530148	0.656474	0.874029
4	4	4	0.435292	0.0530148	0.326514	0.54407
long by vert						
1	1	4	0.973375	0.0530148	0.864598	1.08215
1	2	4	0.984139	0.0530148	0.875361	1.09292
1	3	4	0.979077	0.0530148	0.870299	1.08785
1	4	4	0.937888	0.0530148	0.82911	1.04667
2	1	4	0.907475	0.0530148	0.798698	1.01625
2	2	4	0.836959	0.0530148	0.728181	0.945737
2	3	4	0.841259	0.0530148	0.732481	0.950037
2	4	4	0.707394	0.0530148	0.598616	0.816172
3	1	4	0.891126	0.0530148	0.782348	0.999904
3	2	4	0.839184	0.0530148	0.730407	0.947962
3	3	4	0.696188	0.0530148	0.587411	0.804966
3	4	4	0.779792	0.0530148	0.671014	0.88857
4	1	4	0.867093	0.0530148	0.758316	0.975871
4	2	4	0.766297	0.0530148	0.657519	0.875075
4	3	4	0.598795	0.0530148	0.490017	0.707573
4	4	4	0.577839	0.0530148	0.469062	0.686617
trans by vert						
1	1	4	0.963434	0.0530148	0.854657	1.07221
1	2	4	0.935102	0.0530148	0.826324	1.04388
1	3	4	0.945059	0.0530148	0.836281	1.05384
1	4	4	0.899074	0.0530148	0.790297	1.00785
2	1	4	0.921815	0.0530148	0.813038	1.03059
2	2	4	0.878173	0.0530148	0.769395	0.98695
2	3	4	0.851579	0.0530148	0.742801	0.960356
2	4	4	0.871692	0.0530148	0.762915	0.98047
3	1	4	0.931223	0.0530148	0.822446	1.04
3	2	4	0.814622	0.0530148	0.705844	0.923399
3	3	4	0.710424	0.0530148	0.601647	0.819202
3	4	4	0.820168	0.0530148	0.71139	0.928946
4	1	4	0.822597	0.0530148	0.713819	0.931375
4	2	4	0.798682	0.0530148	0.689905	0.90746
4	3	4	0.608257	0.0530148	0.499479	0.717034
4	4	4	0.411979	0.0530148	0.303201	0.520756

Multiple Range Tests for CF by long

Method: 95.0 percent LSD

long	Count	LS Mean	LS Sigma	Homogeneous Groups
4	16	0.702506	0.0265074	X
3	16	0.801573	0.0265074	X
2	16	0.823272	0.0265074	X
1	16	0.96862	0.0265074	X

Contrast	Difference	+/- Limits
1 - 2	*0.145348	0.0769174
1 - 3	*0.167047	0.0769174
1 - 4	*0.266114	0.0769174
2 - 3	0.0216991	0.0769174
2 - 4	*0.120766	0.0769174
3 - 4	*0.0990665	0.0769174

---

* denotes a statistically significant difference.

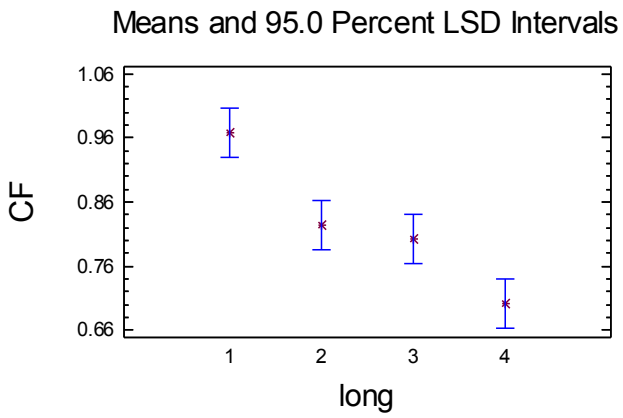

Multiple Range Tests for CF by trans

Method: 95.0 percent LSD

trans	Count	LS Mean	LS Sigma	Homogeneous Groups
4	16	0.660379	0.0265074	X
3	16	0.819109	0.0265074	X
2	16	0.880815	0.0265074	XX
1	16	0.935667	0.0265074	X

Contrast	Difference	+/- Limits
1 - 2	0.0548526	0.0769174
1 - 3	*0.116558	0.0769174
1 - 4	*0.275289	0.0769174
2 - 3	0.0617055	0.0769174
2 - 4	*0.220436	0.0769174
3 - 4	*0.158731	0.0769174

---

* denotes a statistically significant difference.

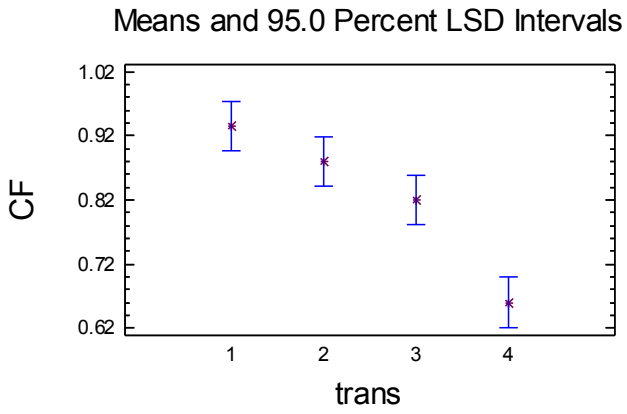

Multiple Range Tests for CF by vert

Method: 95.0 percent LSD

vert	Count	LS Mean	LS Sigma	Homogeneous Groups
4	16	0.750728	0.0265074	X
3	16	0.77883	0.0265074	X
2	16	0.856645	0.0265074	X
1	16	0.909767	0.0265074	X

Contrast	Difference	+/- Limits
1 - 2	0.0531227	0.0769174
1 - 3	*0.130938	0.0769174
1 - 4	*0.159039	0.0769174
2 - 3	*0.077815	0.0769174
2 - 4	*0.105916	0.0769174
3 - 4	0.0281014	0.0769174

---

* denotes a statistically significant difference.

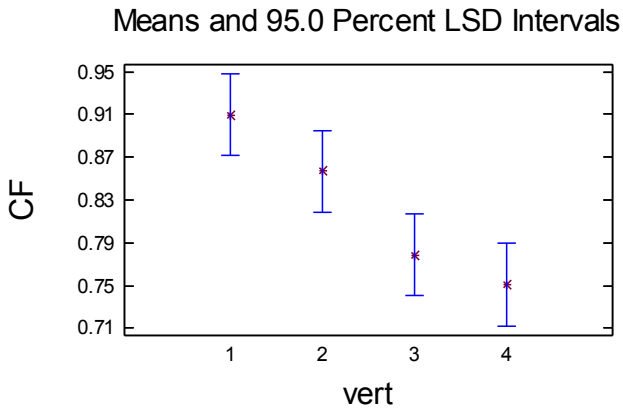

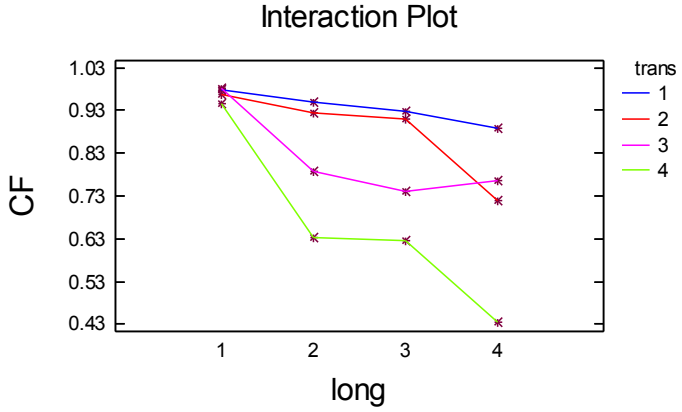

Appendix C.7: Moreton Morrell 08 Multifactor ANOVA - CF

Analysis Summary: Dependent variable: CF, Factors: long, trans, vert
Number of complete cases: 64

Analysis of Variance for CF - Type III Sums of Squares

Source	Sum of Squares	Df	Mean Square	F-Ratio	P-Value
MAIN EFFECTS					
A:trans	0.101853	3	0.0339512	3.02	0.0472
B:long	2.01562	3	0.671872	59.71	0.0000
C:vert	0.107431	3	0.0358105	3.18	0.0398
INTERACTIONS					
AB	0.142888	9	0.0158765	1.41	0.2324
AC	0.100105	9	0.0111227	0.99	0.4718
BC	0.148235	9	0.0164705	1.46	0.2115
RESIDUAL	0.303805	27	0.011252		
TOTAL (CORRECTED)	2.91993	63			

All F-ratios are based on the residual mean square error.

Table of Least Squares Means for CF
with 95.0 Percent Confidence Intervals

Level	Count	Stnd. Mean	Lower Error	Upper Limit	Limit
GRAND MEAN	64	0.64152			
trans					
1	16	0.581305	0.0265189	0.526892	0.635717
2	16	0.656473	0.0265189	0.602061	0.710886
3	16	0.636836	0.0265189	0.582424	0.691249
4	16	0.691464	0.0265189	0.637052	0.745876
long					
1	16	0.935362	0.0265189	0.880949	0.989774
2	16	0.622539	0.0265189	0.568127	0.676952
3	16	0.531456	0.0265189	0.477044	0.585869
4	16	0.476721	0.0265189	0.422308	0.531133
vert					
1	16	0.67936	0.0265189	0.624948	0.733773
2	16	0.663666	0.0265189	0.609253	0.718078
3	16	0.65021	0.0265189	0.595798	0.704622
4	16	0.572842	0.0265189	0.51843	0.627255
trans by long					
1	1	4	0.879011	0.0530378	0.770186	0.987836

1	2	4	0.561004	0.0530378	0.45218	0.669829
1	3	4	0.363949	0.0530378	0.255125	0.472774
1	4	4	0.521254	0.0530378	0.412429	0.630079
2	1	4	0.960528	0.0530378	0.851704	1.06935
2	2	4	0.632002	0.0530378	0.523177	0.740827
2	3	4	0.561306	0.0530378	0.452481	0.670131
2	4	4	0.472057	0.0530378	0.363232	0.580882
3	1	4	0.93069	0.0530378	0.821865	1.03952
3	2	4	0.58608	0.0530378	0.477255	0.694904
3	3	4	0.603617	0.0530378	0.494792	0.712442
3	4	4	0.426958	0.0530378	0.318133	0.535783
4	1	4	0.971217	0.0530378	0.862392	1.08004
4	2	4	0.711072	0.0530378	0.602247	0.819896
4	3	4	0.596954	0.0530378	0.488129	0.705779
4	4	4	0.486614	0.0530378	0.377789	0.595439
trans by vert						
1	1	4	0.623473	0.0530378	0.514648	0.732298
1	2	4	0.646214	0.0530378	0.537389	0.755039
1	3	4	0.566323	0.0530378	0.457498	0.675148
1	4	4	0.489208	0.0530378	0.380383	0.598033
2	1	4	0.697691	0.0530378	0.588867	0.806516
2	2	4	0.725661	0.0530378	0.616836	0.834486
2	3	4	0.628609	0.0530378	0.519784	0.737434
2	4	4	0.573932	0.0530378	0.465107	0.682757
3	1	4	0.669997	0.0530378	0.561172	0.778822
3	2	4	0.663697	0.0530378	0.554873	0.772522
3	3	4	0.684565	0.0530378	0.57574	0.79339
3	4	4	0.529085	0.0530378	0.420261	0.63791
4	1	4	0.72628	0.0530378	0.617455	0.835105
4	2	4	0.619091	0.0530378	0.510266	0.727915
4	3	4	0.721343	0.0530378	0.612518	0.830168
4	4	4	0.699143	0.0530378	0.590318	0.807968
long by vert						
1	1	4	0.947628	0.0530378	0.838803	1.05645
1	2	4	0.95448	0.0530378	0.845655	1.06331
1	3	4	0.941715	0.0530378	0.832891	1.05054
1	4	4	0.897623	0.0530378	0.788798	1.00645
2	1	4	0.650133	0.0530378	0.541308	0.758957
2	2	4	0.586151	0.0530378	0.477326	0.694975
2	3	4	0.614617	0.0530378	0.505792	0.723441
2	4	4	0.639258	0.0530378	0.530433	0.748083
3	1	4	0.544664	0.0530378	0.435839	0.653488
3	2	4	0.564751	0.0530378	0.455926	0.673575
3	3	4	0.540112	0.0530378	0.431287	0.648937
3	4	4	0.4763	0.0530378	0.367475	0.585125
4	1	4	0.575017	0.0530378	0.466192	0.683842
4	2	4	0.549281	0.0530378	0.440456	0.658106
4	3	4	0.504396	0.0530378	0.395571	0.613221
4	4	4	0.278189	0.0530378	0.169364	0.387013

Multiple Range Tests for CF by long

Method: 95.0 percent LSD

long	Count	LS Mean	LS Sigma	Homogeneous Groups
4	16	0.476721	0.0265189	X
3	16	0.531456	0.0265189	X
2	16	0.622539	0.0265189	X
1	16	0.935362	0.0265189	X

Contrast	Difference	+/- Limits
1 - 2	*0.312822	0.0769508
1 - 3	*0.403905	0.0769508
1 - 4	*0.458641	0.0769508
2 - 3	*0.091083	0.0769508
2 - 4	*0.145819	0.0769508
3 - 4	0.0547358	0.0769508

---

* denotes a statistically significant difference.

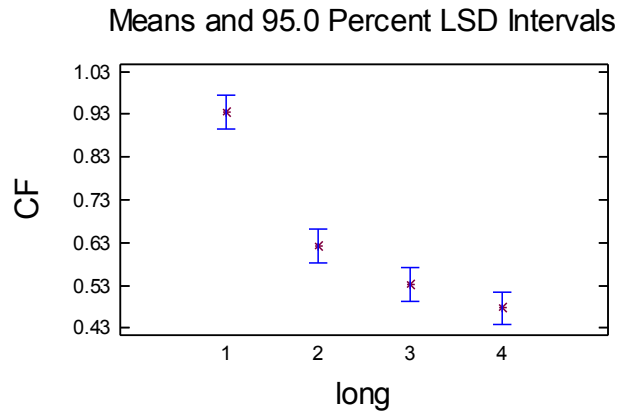

Multiple Range Tests for CF by trans

Method: 95.0 percent LSD

trans	Count	LS Mean	LS Sigma	Homogeneous Groups
1	16	0.581305	0.0265189	X
3	16	0.636836	0.0265189	XX
2	16	0.656473	0.0265189	XX
4	16	0.691464	0.0265189	X

Contrast	Difference	+/- Limits
1 - 2	-0.0751687	0.0769508
1 - 3	-0.0555315	0.0769508
1 - 4	*-0.110159	0.0769508
2 - 3	0.0196372	0.0769508
2 - 4	-0.0349907	0.0769508
3 - 4	-0.0546279	0.0769508

---

* denotes a statistically significant difference.

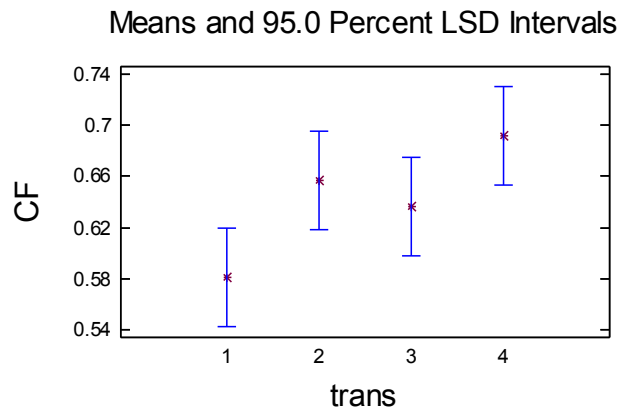

Multiple Range Tests for CF by vert

Method: 95.0 percent LSD

vert	Count	LS Mean	LS Sigma	Homogeneous Groups
4	16	0.572842	0.0265189	X
3	16	0.65021	0.0265189	X
2	16	0.663666	0.0265189	X
1	16	0.67936	0.0265189	X

Contrast	Difference	+/- Limits
1 - 2	0.0156946	0.0769508
1 - 3	0.0291502	0.0769508
1 - 4	*0.106518	0.0769508
2 - 3	0.0134556	0.0769508
2 - 4	*0.0908234	0.0769508
3 - 4	*0.0773678	0.0769508

---

* denotes a statistically significant difference.

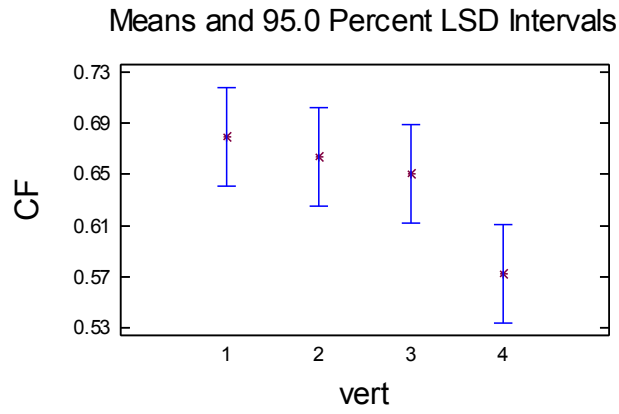

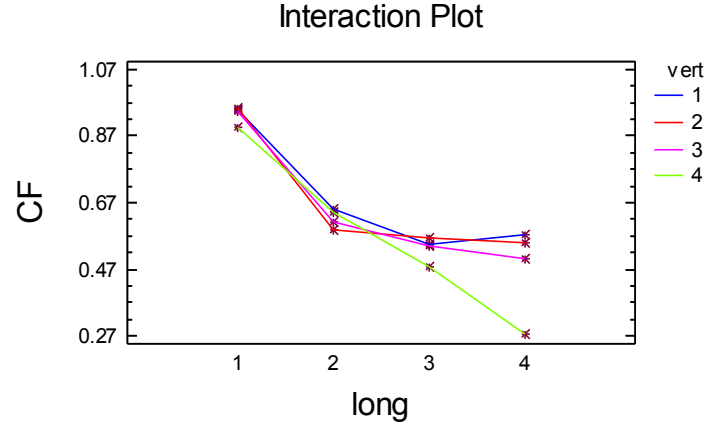

Appendix C.8: Moreton Sep 09 Multifactor ANOVA - CF

Analysis Summary: Dependent variable: CF, Factors: long, trans, vert
Number of complete cases: 64

Analysis of Variance for CF - Type III Sums of Squares

Source	Sum of Squares	Df	Mean Square	F-Ratio	P-Value
MAIN EFFECTS					
A:long	0.254115	3	0.084705	37.58	0.0000
B:trans	0.203867	3	0.0679557	30.15	0.0000
C:vert	0.127872	3	0.0426241	18.91	0.0000
INTERACTIONS					
AB	0.109771	9	0.0121968	5.41	0.0003
AC	0.0357109	9	0.00396788	1.76	0.1233
BC	0.0867717	9	0.0096413	4.28	0.0016
RESIDUAL	0.0608533	27	0.00225383		
TOTAL (CORRECTED)	0.878961	63			

All F-ratios are based on the residual mean square error.

Table of Least Squares Means for CF
with 95.0 Percent Confidence Intervals

Level	Count	Mean	Stnd. Error	Lower Limit	Upper Limit
GRAND MEAN	64	0.867772			
long					
1	16	0.956848	0.0118686	0.932495	0.9812
2	16	0.869581	0.0118686	0.845228	0.893933
3	16	0.866	0.0118686	0.841648	0.890352
4	16	0.778658	0.0118686	0.754306	0.803011
trans					
1	16	0.911307	0.0118686	0.886954	0.935659
2	16	0.91511	0.0118686	0.890758	0.939463
3	16	0.869645	0.0118686	0.845293	0.893997
4	16	0.775025	0.0118686	0.750673	0.799377
vert					
1	16	0.930002	0.0118686	0.90565	0.954354
2	16	0.888933	0.0118686	0.864581	0.913285
3	16	0.835938	0.0118686	0.811586	0.860291
4	16	0.816214	0.0118686	0.791861	0.840566
long by trans					
1	1	4	0.96342	0.0237372	0.914715	1.01213

1	2	4	0.963182	0.0237372	0.914477	1.01189
1	3	4	0.944864	0.0237372	0.896159	0.993569
1	4	4	0.955926	0.0237372	0.907221	1.00463
2	1	4	0.915589	0.0237372	0.866884	0.964293
2	2	4	0.932802	0.0237372	0.884097	0.981507
2	3	4	0.864374	0.0237372	0.815669	0.913078
2	4	4	0.765559	0.0237372	0.716854	0.814264
3	1	4	0.923237	0.0237372	0.874532	0.971942
3	2	4	0.94912	0.0237372	0.900415	0.997825
3	3	4	0.917164	0.0237372	0.868459	0.965869
3	4	4	0.674479	0.0237372	0.625774	0.723184
4	1	4	0.842981	0.0237372	0.794276	0.891686
4	2	4	0.815338	0.0237372	0.766633	0.864043
4	3	4	0.752178	0.0237372	0.703473	0.800883
4	4	4	0.704136	0.0237372	0.655431	0.752841
long by vert						
1	1	4	0.973366	0.0237372	0.924661	1.02207
1	2	4	0.982964	0.0237372	0.934259	1.03167
1	3	4	0.943264	0.0237372	0.894559	0.991969
1	4	4	0.927798	0.0237372	0.879093	0.976502
2	1	4	0.945556	0.0237372	0.896851	0.994261
2	2	4	0.888655	0.0237372	0.83995	0.93736
2	3	4	0.860591	0.0237372	0.811886	0.909296
2	4	4	0.783521	0.0237372	0.734816	0.832226
3	1	4	0.931907	0.0237372	0.883202	0.980612
3	2	4	0.869305	0.0237372	0.820601	0.91801
3	3	4	0.843555	0.0237372	0.79485	0.89226
3	4	4	0.819233	0.0237372	0.770528	0.867938
4	1	4	0.869179	0.0237372	0.820474	0.917884
4	2	4	0.814807	0.0237372	0.766102	0.863512
4	3	4	0.696345	0.0237372	0.64764	0.74505
4	4	4	0.734303	0.0237372	0.685598	0.783008
trans by vert						
1	1	4	0.942437	0.0237372	0.893732	0.991142
1	2	4	0.959757	0.0237372	0.911052	1.00846
1	3	4	0.909084	0.0237372	0.860379	0.957789
1	4	4	0.833949	0.0237372	0.785244	0.882654
2	1	4	0.912458	0.0237372	0.863753	0.961163
2	2	4	0.970155	0.0237372	0.92145	1.01886
2	3	4	0.893673	0.0237372	0.844968	0.942378
2	4	4	0.884156	0.0237372	0.835451	0.93286
3	1	4	0.941084	0.0237372	0.892379	0.989789
3	2	4	0.890746	0.0237372	0.842041	0.939451
3	3	4	0.813036	0.0237372	0.764331	0.861741
3	4	4	0.833714	0.0237372	0.785009	0.882419
4	1	4	0.924029	0.0237372	0.875325	0.972734
4	2	4	0.735074	0.0237372	0.686369	0.783778
4	3	4	0.727961	0.0237372	0.679256	0.776666
4	4	4	0.713036	0.0237372	0.664331	0.761741

Multiple Range Tests for CF by long

Method: 95.0 percent LSD

long	Count	LS Mean	LS Sigma	Homogeneous Groups
4	16	0.778658	0.0118686	X
3	16	0.866	0.0118686	X
2	16	0.869581	0.0118686	X
1	16	0.956848	0.0118686	X

Contrast	Difference	+/- Limits
1 - 2	*0.0872672	0.0344396
1 - 3	*0.0908479	0.0344396
1 - 4	*0.17819	0.0344396
2 - 3	0.00358075	0.0344396
2 - 4	*0.0909225	0.0344396
3 - 4	*0.0873418	0.0344396

---

* denotes a statistically significant difference.

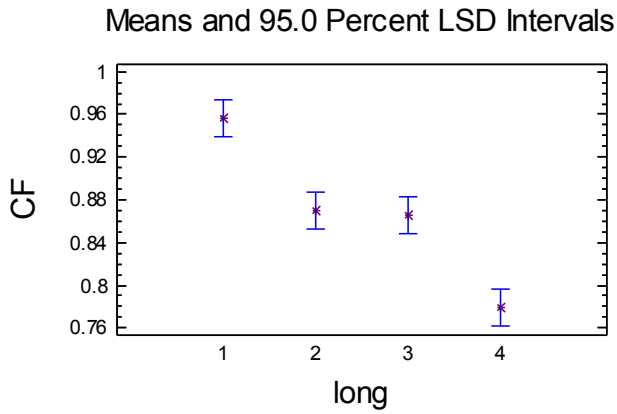

Multiple Range Tests for CF by trans

Method: 95.0 percent LSD

trans	Count	LS Mean	LS Sigma	Homogeneous Groups
4	16	0.775025	0.0118686	X
3	16	0.869645	0.0118686	X
1	16	0.911307	0.0118686	X
2	16	0.91511	0.0118686	X

Contrast	Difference	+/- Limits
1 - 2	-0.0038036	0.0344396
1 - 3	*0.0416618	0.0344396
1 - 4	*0.136282	0.0344396
2 - 3	*0.0454654	0.0344396
2 - 4	*0.140085	0.0344396
3 - 4	*0.0946199	0.0344396

* denotes a statistically significant difference.

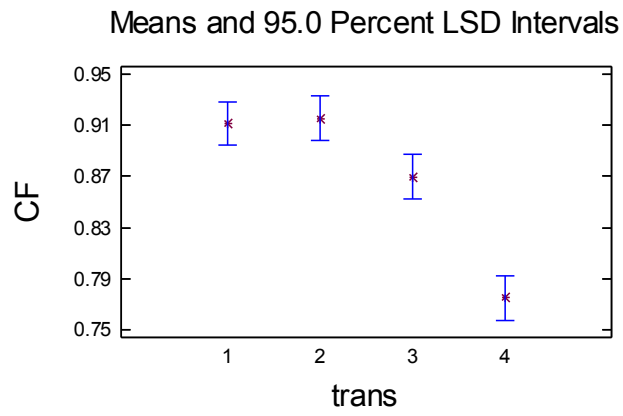

Multiple Range Tests for CF by vert

Method: 95.0 percent LSD

vert	Count	LS Mean	LS Sigma	Homogeneous Groups
4	16	0.816214	0.0118686	X
3	16	0.835938	0.0118686	X
2	16	0.888933	0.0118686	X
1	16	0.930002	0.0118686	X

Contrast	Difference	+/- Limits
1 - 2	*0.0410691	0.0344396
1 - 3	*0.0940636	0.0344396
1 - 4	*0.113789	0.0344396
2 - 3	*0.0529945	0.0344396
2 - 4	*0.0727194	0.0344396
3 - 4	0.0197249	0.0344396

---

* denotes a statistically significant difference.

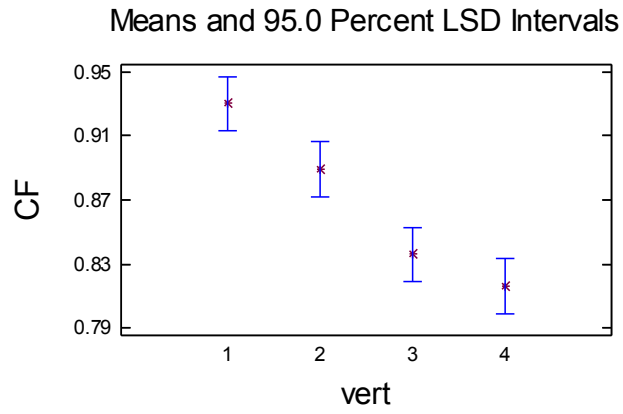

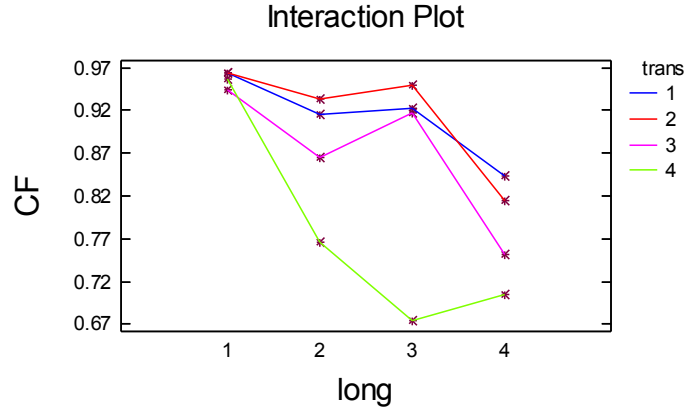

Appendix C.9: Moreton dry Multifactor ANOVA - CF

Analysis Summary: Dependent variable: CF, Factors: long, trans, vert
Number of complete cases: 48

Analysis of Variance for CF - Type III Sums of Squares

Source	Sum of Squares	Df	Mean Square	F-Ratio	P-Value
MAIN EFFECTS					
A:long	0.461671	3	0.15389	9.45	0.0006
B:trans	0.0204713	2	0.0102356	0.63	0.5448
C:vert	0.207339	3	0.0691131	4.24	0.0197
INTERACTIONS					
AB	0.0497492	6	0.00829153	0.51	0.7937
AC	0.193483	9	0.0214981	1.32	0.2937
BC	0.0311899	6	0.00519831	0.32	0.9185
RESIDUAL	0.293243	18	0.0162913		
TOTAL (CORRECTED)	1.25715	47			

All F-ratios are based on the residual mean square error.

Table of Least Squares Means for CF
with 95.0 Percent Confidence Intervals

Level	Count	Mean	Stnd. Error	Lower Limit	Upper Limit
GRAND MEAN	48	0.580474			
long					
1	12	0.688537	0.0368457	0.611127	0.765947
2	12	0.608198	0.0368457	0.530788	0.685608
3	12	0.604252	0.0368457	0.526842	0.681662
4	12	0.420909	0.0368457	0.343499	0.498319
trans					
1	16	0.564477	0.0319093	0.497438	0.631517
2	16	0.609634	0.0319093	0.542595	0.676673
3	16	0.567311	0.0319093	0.500272	0.63435
vert					
1	12	0.55598	0.0368457	0.478569	0.63339
2	12	0.676334	0.0368457	0.598924	0.753744
3	12	0.594504	0.0368457	0.517094	0.671914
4	12	0.495079	0.0368457	0.417669	0.572489
long by trans					
1	1	4	0.731163	0.0638187	0.597084	0.865241

1	2	4	0.65871	0.0638187	0.524631	0.792788
1	3	4	0.675739	0.0638187	0.541661	0.809817
2	1	4	0.543001	0.0638187	0.408923	0.67708
2	2	4	0.676937	0.0638187	0.542859	0.811016
2	3	4	0.604655	0.0638187	0.470577	0.738734
3	1	4	0.602429	0.0638187	0.46835	0.736507
3	2	4	0.628958	0.0638187	0.49488	0.763037
3	3	4	0.581369	0.0638187	0.447291	0.715448
4	1	4	0.381317	0.0638187	0.247239	0.515395
4	2	4	0.47393	0.0638187	0.339852	0.608009
4	3	4	0.40748	0.0638187	0.273402	0.541558

long by vert

1	1	3	0.599118	0.0736914	0.444297	0.753938
1	2	3	0.750175	0.0736914	0.595355	0.904995
1	3	3	0.765656	0.0736914	0.610836	0.920476
1	4	3	0.6392	0.0736914	0.48438	0.79402
2	1	3	0.505791	0.0736914	0.350971	0.660611
2	2	3	0.727843	0.0736914	0.573022	0.882663
2	3	3	0.653393	0.0736914	0.498572	0.808213
2	4	3	0.545766	0.0736914	0.390946	0.700586
3	1	3	0.596103	0.0736914	0.441283	0.750923
3	2	3	0.639733	0.0736914	0.484913	0.794554
3	3	3	0.629261	0.0736914	0.474441	0.784082
3	4	3	0.55191	0.0736914	0.39709	0.706731
4	1	3	0.522907	0.0736914	0.368087	0.677727
4	2	3	0.587585	0.0736914	0.432764	0.742405
4	3	3	0.329706	0.0736914	0.174886	0.484526
4	4	3	0.243439	0.0736914	0.0886188	0.398259

trans by vert

1	1	4	0.574402	0.0638187	0.440324	0.70848
1	2	4	0.67711	0.0638187	0.543032	0.811189
1	3	4	0.548961	0.0638187	0.414883	0.683039
1	4	4	0.457436	0.0638187	0.323358	0.591515
2	1	4	0.556421	0.0638187	0.422343	0.6905
2	2	4	0.668205	0.0638187	0.534127	0.802283
2	3	4	0.660738	0.0638187	0.52666	0.794816
2	4	4	0.553171	0.0638187	0.419093	0.68725
3	1	4	0.537115	0.0638187	0.403037	0.671194
3	2	4	0.683687	0.0638187	0.549608	0.817765
3	3	4	0.573813	0.0638187	0.439734	0.707891
3	4	4	0.474629	0.0638187	0.340551	0.608707

Multiple Range Tests for CF by long

Method: 95.0 percent LSD

long	Count	LS Mean	LS Sigma	Homogeneous Groups
4	12	0.420909	0.0368457	X
3	12	0.604252	0.0368457	X
2	12	0.608198	0.0368457	X
1	12	0.688537	0.0368457	X

Contrast	Difference	+/- Limits
1 - 2	0.0803391	0.109474
1 - 3	0.0842851	0.109474
1 - 4	*0.267628	0.109474
2 - 3	0.00394599	0.109474
2 - 4	*0.187289	0.109474
3 - 4	*0.183343	0.109474

---

* denotes a statistically significant difference.

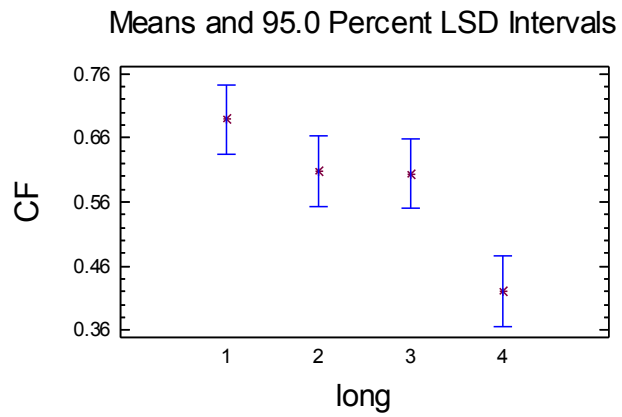

Multiple Range Tests for CF by trans

Method: 95.0 percent LSD

trans	Count	LS Mean	LS Sigma	Homogeneous Groups
1	16	0.564477	0.0319093	X
3	16	0.567311	0.0319093	X
2	16	0.609634	0.0319093	X

Contrast	Difference	+/- Limits
1 - 2	-0.0451564	0.0948077
1 - 3	-0.00283345	0.0948077
2 - 3	0.042323	0.0948077

---

* denotes a statistically significant difference.

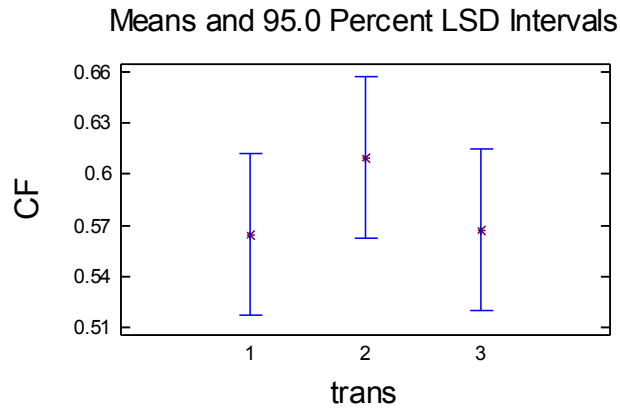

Multiple Range Tests for CF by vert

Method: 95.0 percent LSD

vert	Count	LS Mean	LS Sigma	Homogeneous Groups
4	12	0.495079	0.0368457	X
1	12	0.55598	0.0368457	X
3	12	0.594504	0.0368457	XX
2	12	0.676334	0.0368457	X

Contrast	Difference	+/- Limits
1 - 2	*-0.120354	0.109474
1 - 3	-0.0385243	0.109474
1 - 4	0.0609007	0.109474
2 - 3	0.0818301	0.109474
2 - 4	*0.181255	0.109474
3 - 4	0.099425	0.109474

---

* denotes a statistically significant difference.

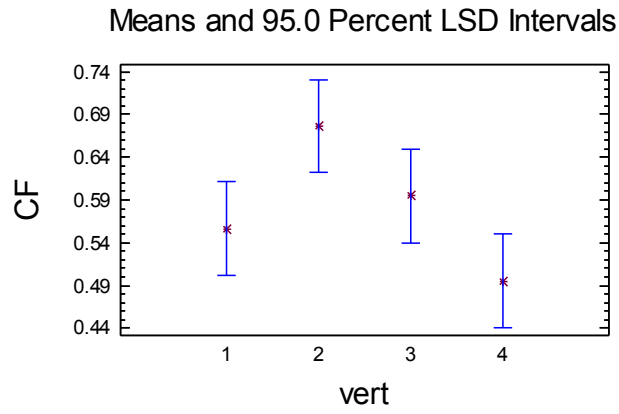

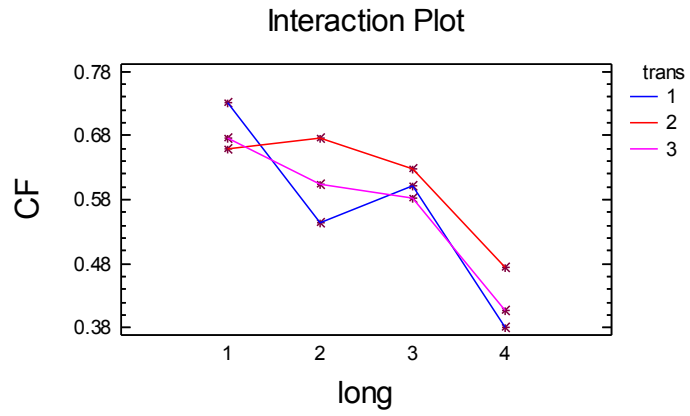

Appendix C.10: Northend Multifactor ANOVA - CF

Analysis Summary: Dependent variable: CF, Factors: long, trans, vert
Number of complete cases: 80

Analysis of Variance for CF - Type III Sums of Squares

Source	Sum of Squares	Df	Mean Square	F-Ratio	P-Value
MAIN EFFECTS					
A:long	0.108782	3	0.0362606	16.77	0.0000
B:trans	0.182244	4	0.0455609	21.07	0.0000
C:vert	0.222734	3	0.0742446	34.33	0.0000
INTERACTIONS					
AB	0.115332	12	0.00961103	4.44	0.0002
AC	0.0578568	9	0.00642853	2.97	0.0095
BC	0.0312222	12	0.00260185	1.20	0.3183
RESIDUAL	0.0778569	36	0.00216269		
TOTAL (CORRECTED)	0.796028	79			

All F-ratios are based on the residual mean square error.

Table of Least Squares Means for CF
with 95.0 Percent Confidence Intervals

Level	Count	Mean	Stnd. Error	Lower Limit	Upper Limit
GRAND MEAN	80	0.884697			
long					
1	20	0.927071	0.0103988	0.905981	0.948161
2	20	0.914875	0.0103988	0.893785	0.935964
3	20	0.85552	0.0103988	0.834431	0.87661
4	20	0.84132	0.0103988	0.82023	0.86241
trans					
1	16	0.822899	0.0116262	0.79932	0.846478
2	16	0.959442	0.0116262	0.935862	0.983021
3	16	0.878269	0.0116262	0.85469	0.901848
4	16	0.912436	0.0116262	0.888857	0.936015
5	16	0.850438	0.0116262	0.826859	0.874017
vert					
1	20	0.943331	0.0103988	0.922242	0.964421
2	20	0.93124	0.0103988	0.91015	0.95233
3	20	0.831334	0.0103988	0.810244	0.852424
4	20	0.832881	0.0103988	0.811791	0.853971

long by trans

1	1	4	0.884552	0.0232524	0.837394	0.93171
1	2	4	0.964386	0.0232524	0.917228	1.01154
1	3	4	0.964332	0.0232524	0.917174	1.01149
1	4	4	0.958183	0.0232524	0.911025	1.00534
1	5	4	0.863903	0.0232524	0.816745	0.911061
2	1	4	0.831328	0.0232524	0.784169	0.878486
2	2	4	0.977774	0.0232524	0.930616	1.02493
2	3	4	0.872329	0.0232524	0.825171	0.919487
2	4	4	0.952928	0.0232524	0.90577	1.00009
2	5	4	0.940015	0.0232524	0.892857	0.987173
3	1	4	0.722998	0.0232524	0.675839	0.770156
3	2	4	0.962821	0.0232524	0.915663	1.00998
3	3	4	0.876909	0.0232524	0.829751	0.924067
3	4	4	0.921862	0.0232524	0.874704	0.96902
3	5	4	0.793012	0.0232524	0.745854	0.84017
4	1	4	0.852717	0.0232524	0.805559	0.899875
4	2	4	0.932785	0.0232524	0.885626	0.979943
4	3	4	0.799507	0.0232524	0.752349	0.846665
4	4	4	0.816771	0.0232524	0.769613	0.863929
4	5	4	0.804821	0.0232524	0.757663	0.85198

long by vert

1	1	5	0.955398	0.0207976	0.913219	0.997578
1	2	5	0.958047	0.0207976	0.915867	1.00023
1	3	5	0.9156	0.0207976	0.873421	0.95778
1	4	5	0.87924	0.0207976	0.83706	0.921419
2	1	5	0.951437	0.0207976	0.909257	0.993616
2	2	5	0.938781	0.0207976	0.896601	0.98096
2	3	5	0.899003	0.0207976	0.856823	0.941182
2	4	5	0.870279	0.0207976	0.828099	0.912458
3	1	5	0.947094	0.0207976	0.904914	0.989273
3	2	5	0.934377	0.0207976	0.892197	0.976556
3	3	5	0.749808	0.0207976	0.707629	0.791988
3	4	5	0.790803	0.0207976	0.748623	0.832982
4	1	5	0.919396	0.0207976	0.877217	0.961576
4	2	5	0.893755	0.0207976	0.851576	0.935935
4	3	5	0.760925	0.0207976	0.718746	0.803105
4	4	5	0.791203	0.0207976	0.749024	0.833383

trans by vert

1	1	4	0.914158	0.0232524	0.867	0.961316
1	2	4	0.882943	0.0232524	0.835785	0.930101
1	3	4	0.728599	0.0232524	0.681441	0.775758
1	4	4	0.765894	0.0232524	0.718736	0.813052
2	1	4	0.988001	0.0232524	0.940843	1.03516
2	2	4	0.989875	0.0232524	0.942717	1.03703
2	3	4	0.938236	0.0232524	0.891078	0.985394
2	4	4	0.921654	0.0232524	0.874496	0.968812
3	1	4	0.936223	0.0232524	0.889065	0.983381
3	2	4	0.9351	0.0232524	0.887942	0.982258
3	3	4	0.846075	0.0232524	0.798916	0.893233
3	4	4	0.795679	0.0232524	0.748521	0.842838

4	1	4	0.969243	0.0232524	0.922085	1.0164
4	2	4	0.950817	0.0232524	0.903659	0.997975
4	3	4	0.843813	0.0232524	0.796655	0.890971
4	4	4	0.88587	0.0232524	0.838712	0.933028
5	1	4	0.909032	0.0232524	0.861873	0.95619
5	2	4	0.897464	0.0232524	0.850306	0.944622
5	3	4	0.799948	0.0232524	0.75279	0.847106
5	4	4	0.795308	0.0232524	0.74815	0.842466

Multiple Range Tests for CF by long

Method: 95.0 percent LSD

long	Count	LS Mean	LS Sigma	Homogeneous Groups
4	20	0.84132	0.0103988	X
3	20	0.85552	0.0103988	X
2	20	0.914875	0.0103988	X
1	20	0.927071	0.0103988	X

Contrast	Difference	+/- Limits
1 - 2	0.0121964	0.0298254
1 - 3	*0.0715507	0.0298254
1 - 4	*0.085751	0.0298254
2 - 3	*0.0593543	0.0298254
2 - 4	*0.0735546	0.0298254
3 - 4	0.0142003	0.0298254

* denotes a statistically significant difference.

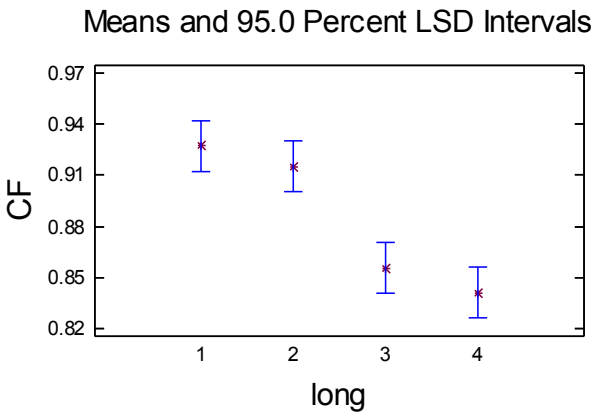

Multiple Range Tests for CF by trans

Method: 95.0 percent LSD

trans	Count	LS Mean	LS Sigma	Homogeneous Groups
1	16	0.822899	0.0116262	X
5	16	0.850438	0.0116262	XX
3	16	0.878269	0.0116262	X
4	16	0.912436	0.0116262	X
2	16	0.959442	0.0116262	X

Contrast	Difference	+/- Limits
1 - 2	*-0.136543	0.0333458
1 - 3	*-0.0553706	0.0333458
1 - 4	*-0.0895372	0.0333458
1 - 5	-0.0275393	0.0333458
2 - 3	*0.0811723	0.0333458
2 - 4	*0.0470057	0.0333458
2 - 5	*0.109004	0.0333458
3 - 4	*-0.0341666	0.0333458
3 - 5	0.0278313	0.0333458
4 - 5	*0.0619979	0.0333458

---

* denotes a statistically significant difference.

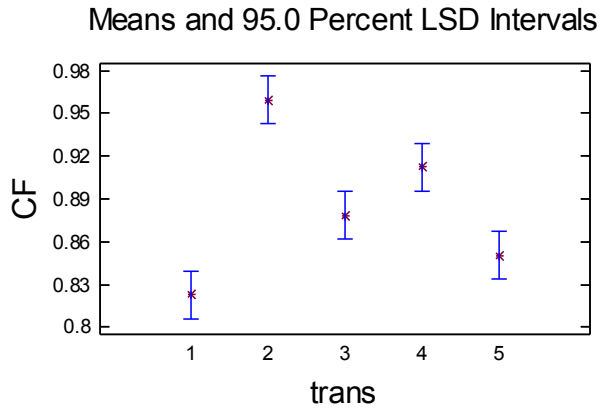

Multiple Range Tests for CF by vert

Method: 95.0 percent LSD

vert	Count	LS Mean	LS Sigma	Homogeneous Groups
3	20	0.831334	0.0103988	X
4	20	0.832881	0.0103988	X
2	20	0.93124	0.0103988	X
1	20	0.943331	0.0103988	X

Contrast	Difference	+/- Limits
1 - 2	0.0120915	0.0298254
1 - 3	*0.111997	0.0298254
1 - 4	*0.11045	0.0298254
2 - 3	*0.0999056	0.0298254
2 - 4	*0.0983587	0.0298254
3 - 4	-0.00154695	0.0298254

---

* denotes a statistically significant difference.

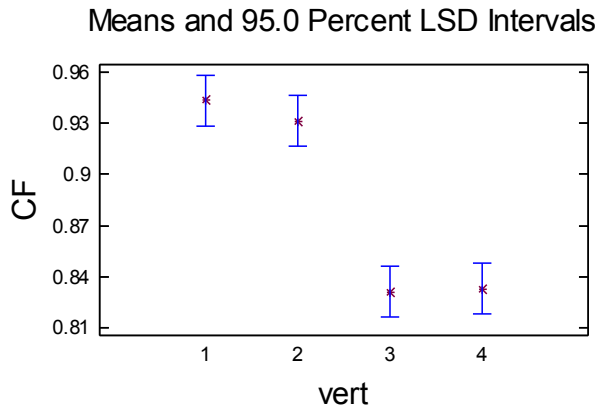

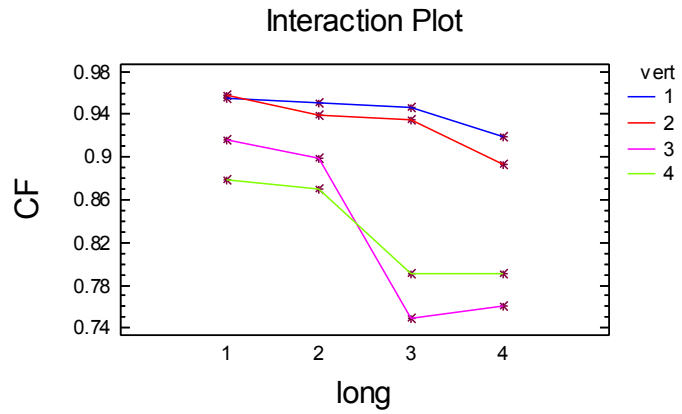

Appendix C.11: Rowington Multifactor ANOVA - CF

Analysis Summary: Dependent variable: CF, Factors: long, trans, vert
Number of complete cases:

Analysis of Variance for CF - Type III Sums of Squares

Source	Sum of Squares	Df	Mean Square	F-Ratio	P-Value
MAIN EFFECTS					
A:long	0.753483	3	0.251161	35.87	0.0000
B:trans	0.243887	4	0.0609717	8.71	0.0001
C:vert	0.060455	3	0.0201517	2.88	0.0493
INTERACTIONS					
AB	0.253845	12	0.0211537	3.02	0.0051
AC	0.0885744	9	0.0098416	1.41	0.2222
BC	0.0628715	12	0.0052393	0.75	0.6962
RESIDUAL	0.252037	36	0.00700102		
TOTAL (CORRECTED)	1.71515	79			

All F-ratios are based on the residual mean square error.

Table of Least Squares Means for CF
with 95.0 Percent Confidence Intervals

Level	Count	Mean	Stnd. Error	Lower Limit	Upper Limit
GRAND MEAN	80	0.875823			
long					
1	20	0.968636	0.0187097	0.930691	1.00658
2	20	0.954828	0.0187097	0.916883	0.992773
3	20	0.853388	0.0187097	0.815443	0.891333
4	20	0.726442	0.0187097	0.688497	0.764387
trans					
1	16	0.772169	0.020918	0.729745	0.814593
2	16	0.88636	0.020918	0.843936	0.928783
3	16	0.936781	0.020918	0.894357	0.979205
4	16	0.9007	0.020918	0.858276	0.943124
5	16	0.883108	0.020918	0.840684	0.925532
vert					
1	20	0.905139	0.0187097	0.867194	0.943084
2	20	0.898899	0.0187097	0.860954	0.936844
3	20	0.860996	0.0187097	0.823051	0.898941
4	20	0.83826	0.0187097	0.800315	0.876205
long by trans					

1	1	4	0.964063	0.0418361	0.879215	1.04891
1	2	4	0.993684	0.0418361	0.908836	1.07853
1	3	4	0.991284	0.0418361	0.906436	1.07613
1	4	4	0.945293	0.0418361	0.860445	1.03014
1	5	4	0.948856	0.0418361	0.864008	1.0337
2	1	4	0.879876	0.0418361	0.795029	0.964724
2	2	4	0.978019	0.0418361	0.893171	1.06287
2	3	4	0.999219	0.0418361	0.914372	1.08407
2	4	4	0.985371	0.0418361	0.900524	1.07022
2	5	4	0.931656	0.0418361	0.846808	1.0165
3	1	4	0.572432	0.0418361	0.487584	0.657279
3	2	4	0.886956	0.0418361	0.802109	0.971804
3	3	4	0.944006	0.0418361	0.859159	1.02885
3	4	4	0.931453	0.0418361	0.846605	1.0163
3	5	4	0.932094	0.0418361	0.847246	1.01694
4	1	4	0.672306	0.0418361	0.587458	0.757154
4	2	4	0.686779	0.0418361	0.601931	0.771627
4	3	4	0.812614	0.0418361	0.727766	0.897461
4	4	4	0.740684	0.0418361	0.655837	0.825532
4	5	4	0.719826	0.0418361	0.634979	0.804674
long by vert						
1	1	5	0.94672	0.0374193	0.870829	1.02261
1	2	5	0.983697	0.0374193	0.907807	1.05959
1	3	5	0.972929	0.0374193	0.897039	1.04882
1	4	5	0.971199	0.0374193	0.895309	1.04709
2	1	5	0.969246	0.0374193	0.893356	1.04514
2	2	5	0.982539	0.0374193	0.906649	1.05843
2	3	5	0.980081	0.0374193	0.904191	1.05597
2	4	5	0.887447	0.0374193	0.811557	0.963337
3	1	5	0.89368	0.0374193	0.81779	0.96957
3	2	5	0.855971	0.0374193	0.780081	0.931861
3	3	5	0.855558	0.0374193	0.779668	0.931448
3	4	5	0.808343	0.0374193	0.732453	0.884233
4	1	5	0.81091	0.0374193	0.73502	0.8868
4	2	5	0.773391	0.0374193	0.697501	0.849281
4	3	5	0.635416	0.0374193	0.559526	0.711306
4	4	5	0.68605	0.0374193	0.61016	0.76194
trans by vert						
1	1	4	0.843555	0.0418361	0.758708	0.928403
1	2	4	0.807865	0.0418361	0.723017	0.892712
1	3	4	0.76389	0.0418361	0.679042	0.848738
1	4	4	0.673367	0.0418361	0.588519	0.758214
2	1	4	0.902751	0.0418361	0.817903	0.987599
2	2	4	0.889798	0.0418361	0.80495	0.974645
2	3	4	0.901873	0.0418361	0.817026	0.986721
2	4	4	0.851016	0.0418361	0.766168	0.935864
3	1	4	0.956485	0.0418361	0.871637	1.04133
3	2	4	0.954712	0.0418361	0.869864	1.03956
3	3	4	0.941494	0.0418361	0.856646	1.02634
3	4	4	0.894432	0.0418361	0.809585	0.97928
4	1	4	0.921386	0.0418361	0.836538	1.00623

4	2	4	0.925741	0.0418361	0.840893	1.01059
4	3	4	0.89099	0.0418361	0.806143	0.975838
4	4	4	0.864684	0.0418361	0.779836	0.949532
5	1	4	0.901516	0.0418361	0.816669	0.986364
5	2	4	0.916381	0.0418361	0.831534	1.00123
5	3	4	0.806733	0.0418361	0.721885	0.89158
5	4	4	0.907801	0.0418361	0.822953	0.992648

Multiple Range Tests for CF by long

Method: 95.0 percent LSD

long	Count	LS Mean	LS Sigma	Homogeneous Groups
4	20	0.726442	0.0187097	X
3	20	0.853388	0.0187097	X
2	20	0.954828	0.0187097	X
1	20	0.968636	0.0187097	X

Contrast	Difference	+/- Limits
1 - 2	0.0138076	0.0536623
1 - 3	*0.115248	0.0536623
1 - 4	*0.242194	0.0536623
2 - 3	*0.10144	0.0536623
2 - 4	*0.228387	0.0536623
3 - 4	*0.126946	0.0536623

---

* denotes a statistically significant difference.

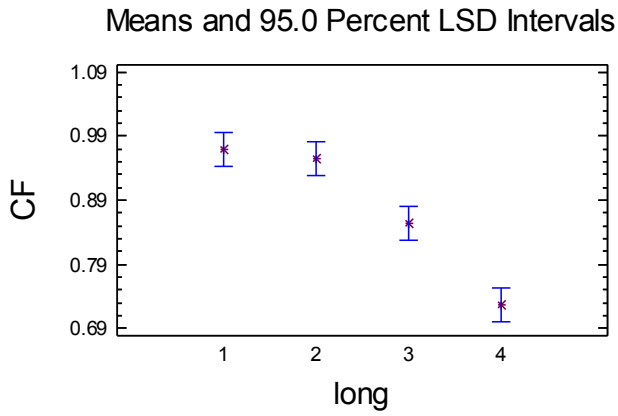

Multiple Range Tests for CF by trans

Method: 95.0 percent LSD

trans	Count	LS Mean	LS Sigma	Homogeneous Groups
1	16	0.772169	0.020918	X
5	16	0.883108	0.020918	X
2	16	0.88636	0.020918	X
4	16	0.9007	0.020918	X
3	16	0.936781	0.020918	X

Contrast	Difference	+/- Limits
1 - 2	*-0.11419	0.0599963
1 - 3	*-0.164612	0.0599963
1 - 4	*-0.128531	0.0599963
1 - 5	*-0.110939	0.0599963
2 - 3	-0.0504212	0.0599963
2 - 4	-0.0143408	0.0599963
2 - 5	0.00325175	0.0599963
3 - 4	0.0360805	0.0599963
3 - 5	0.053673	0.0599963
4 - 5	0.0175925	0.0599963

---

* denotes a statistically significant difference.

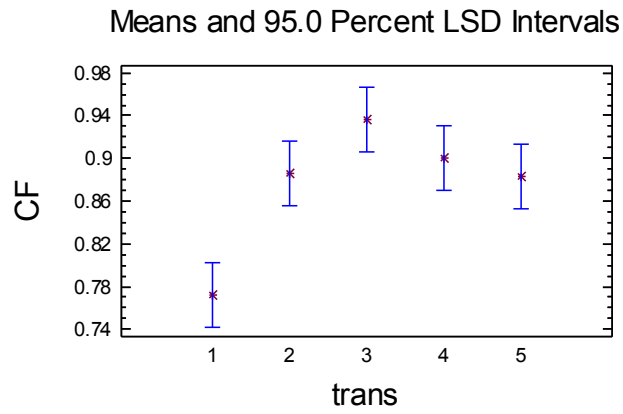

Multiple Range Tests for CF by vert

Method: 95.0 percent LSD

vert	Count	LS Mean	LS Sigma	Homogeneous Groups
4	20	0.83826	0.0187097	X
3	20	0.860996	0.0187097	XX
2	20	0.898899	0.0187097	X
1	20	0.905139	0.0187097	X

Contrast	Difference	+/- Limits
1 - 2	0.00623937	0.0536623
1 - 3	0.0441427	0.0536623
1 - 4	*0.0668788	0.0536623
2 - 3	0.0379033	0.0536623
2 - 4	*0.0606394	0.0536623
3 - 4	0.0227361	0.0536623

---

* denotes a statistically significant difference.

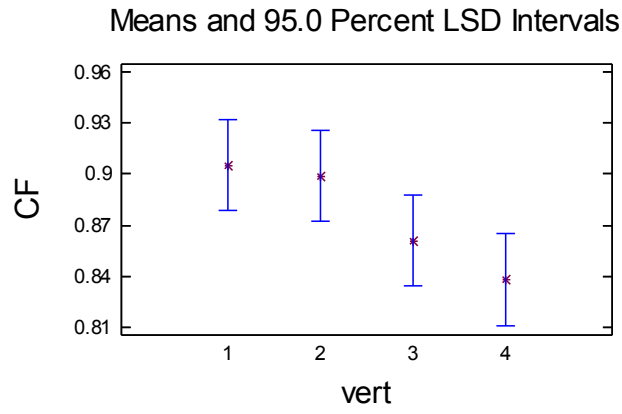

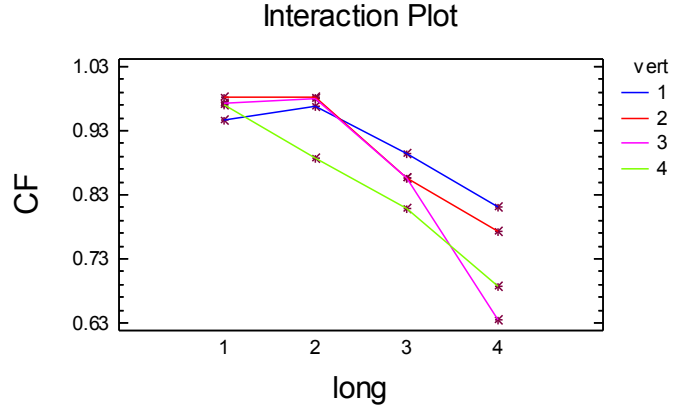

Appendix C.12: Snitterfield Multifactor ANOVA - CF

Analysis Summary: Dependent variable: CF, Factors: long, trans, vert
Number of complete cases: 80

Analysis of Variance for CF - Type III Sums of Squares

Source	Sum of Squares	Df	Mean Square	F-Ratio	P-Value
MAIN EFFECTS					
A:long	0.105721	3	0.0352404	28.28	0.0000
B:trans	0.0550869	4	0.0137717	11.05	0.0000
C:vert	0.0858482	3	0.0286161	22.97	0.0000
INTERACTIONS					
AB	0.0528952	12	0.00440793	3.54	0.0016
AC	0.0182414	9	0.00202682	1.63	0.1446
BC	0.0361293	12	0.00301078	2.42	0.0204
RESIDUAL	0.0448551	36	0.00124597		
TOTAL (CORRECTED)	0.398777	79			

All F-ratios are based on the residual mean square error.

Table of Least Squares Means for CF with 95.0 Percent Confidence Intervals

Level	Count	Mean	Stnd. Error	Lower Limit	Upper Limit
GRAND MEAN	80	0.919668			
long					
1	20	0.978434	0.00789295	0.962426	0.994442
2	20	0.916857	0.00789295	0.900849	0.932865
3	20	0.880306	0.00789295	0.864298	0.896313
4	20	0.903075	0.00789295	0.887067	0.919083
trans					
1	16	0.881328	0.00882459	0.863431	0.899225
2	16	0.930617	0.00882459	0.91272	0.948514
3	16	0.958327	0.00882459	0.94043	0.976224
4	16	0.901887	0.00882459	0.88399	0.919784
5	16	0.92618	0.00882459	0.908283	0.944077
vert					
1	20	0.952787	0.00789295	0.93678	0.968795
2	20	0.949483	0.00789295	0.933476	0.965491
3	20	0.900971	0.00789295	0.884963	0.916978
4	20	0.87543	0.00789295	0.859423	0.891438
long by trans					
1	1	4	0.994223	0.0176492	0.958428	1.03002

1	2	4	0.992402	0.0176492	0.956607	1.0282
1	3	4	0.991284	0.0176492	0.95549	1.02708
1	4	4	0.975223	0.0176492	0.939429	1.01102
1	5	4	0.939038	0.0176492	0.903243	0.974832
2	1	4	0.865999	0.0176492	0.830204	0.901793
2	2	4	0.962179	0.0176492	0.926384	0.997973
2	3	4	0.956533	0.0176492	0.920739	0.992328
2	4	4	0.867059	0.0176492	0.831265	0.902854
2	5	4	0.932514	0.0176492	0.89672	0.968309
3	1	4	0.819531	0.0176492	0.783737	0.855325
3	2	4	0.880958	0.0176492	0.845164	0.916753
3	3	4	0.94683	0.0176492	0.911036	0.982624
3	4	4	0.844071	0.0176492	0.808277	0.879865
3	5	4	0.910138	0.0176492	0.874344	0.945932
4	1	4	0.845561	0.0176492	0.809767	0.881355
4	2	4	0.886929	0.0176492	0.851134	0.922723
4	3	4	0.938662	0.0176492	0.902868	0.974456
4	4	4	0.921194	0.0176492	0.885399	0.956988
4	5	4	0.923029	0.0176492	0.887235	0.958823
long by vert						
1	1	5	0.991906	0.0157859	0.95989	1.02392
1	2	5	1.0	0.0157859	0.967985	1.03202
1	3	5	0.980009	0.0157859	0.947993	1.01202
1	4	5	0.941821	0.0157859	0.909806	0.973837
2	1	5	0.937604	0.0157859	0.905589	0.96962
2	2	5	0.942832	0.0157859	0.910817	0.974848
2	3	5	0.916261	0.0157859	0.884245	0.948276
2	4	5	0.87073	0.0157859	0.838715	0.902746
3	1	5	0.938351	0.0157859	0.906335	0.970366
3	2	5	0.9278	0.0157859	0.895785	0.959815
3	3	5	0.82916	0.0157859	0.797144	0.861175
3	4	5	0.825913	0.0157859	0.793897	0.857928
4	1	5	0.943288	0.0157859	0.911273	0.975304
4	2	5	0.927301	0.0157859	0.895285	0.959316
4	3	5	0.878454	0.0157859	0.846438	0.910469
4	4	5	0.863257	0.0157859	0.831242	0.895272
trans by vert						
1	1	4	0.937675	0.0176492	0.901881	0.97347
1	2	4	0.935015	0.0176492	0.899221	0.97081
1	3	4	0.836534	0.0176492	0.80074	0.872329
1	4	4	0.816088	0.0176492	0.780294	0.851882
2	1	4	0.959289	0.0176492	0.923494	0.995083
2	2	4	0.943507	0.0176492	0.907712	0.979301
2	3	4	0.921424	0.0176492	0.88563	0.957218
2	4	4	0.898248	0.0176492	0.862454	0.934043
3	1	4	0.961751	0.0176492	0.925956	0.997545
3	2	4	0.969498	0.0176492	0.933704	1.00529
3	3	4	0.956232	0.0176492	0.920438	0.992026
3	4	4	0.945829	0.0176492	0.910034	0.981623
4	1	4	0.950853	0.0176492	0.915058	0.986647
4	2	4	0.941384	0.0176492	0.905589	0.977178

4	3	4	0.849056	0.0176492	0.813262	0.884851
4	4	4	0.866255	0.0176492	0.830461	0.902049
5	1	4	0.954369	0.0176492	0.918575	0.990164
5	2	4	0.958012	0.0176492	0.922218	0.993806
5	3	4	0.941606	0.0176492	0.905812	0.977401
5	4	4	0.850731	0.0176492	0.814937	0.886526

Multiple Range Tests for CF by long

Method: 95.0 percent LSD

long	Count	LS Mean	LS Sigma	Homogeneous Groups
3	20	0.880306	0.00789295	X
4	20	0.903075	0.00789295	X
2	20	0.916857	0.00789295	X
1	20	0.978434	0.00789295	X

Contrast	Difference	+/- Limits
1 - 2	*0.0615771	0.0226383
1 - 3	*0.0981282	0.0226383
1 - 4	*0.075359	0.0226383
2 - 3	*0.0365512	0.0226383
2 - 4	0.0137819	0.0226383
3 - 4	*-0.0227692	0.0226383

---

* denotes a statistically significant difference.

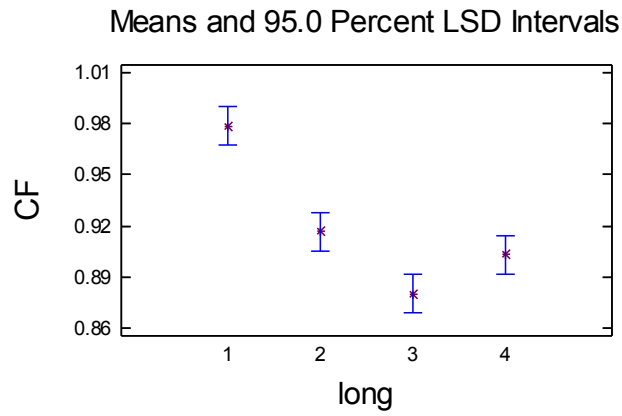

Multiple Range Tests for CF by trans

Method: 95.0 percent LSD

trans	Count	LS Mean	LS Sigma	Homogeneous Groups
1	16	0.881328	0.00882459	X
4	16	0.901887	0.00882459	XX
5	16	0.92618	0.00882459	XX
2	16	0.930617	0.00882459	X
3	16	0.958327	0.00882459	X

Contrast	Difference	+/- Limits
1 - 2	*-0.0492886	0.0253104
1 - 3	*-0.0769991	0.0253104
1 - 4	-0.0205586	0.0253104
1 - 5	*-0.0448516	0.0253104
2 - 3	*-0.0277105	0.0253104
2 - 4	*0.02873	0.0253104
2 - 5	0.00443709	0.0253104
3 - 4	*0.0564405	0.0253104
3 - 5	*0.0321475	0.0253104
4 - 5	-0.0242929	0.0253104

---

* denotes a statistically significant difference.

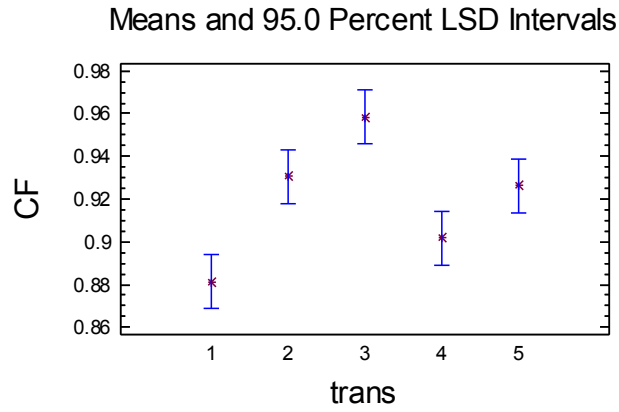

Multiple Range Tests for CF by vert

Method: 95.0 percent LSD

vert	Count	LS Mean	LS Sigma	Homogeneous Groups
4	20	0.87543	0.00789295	X
3	20	0.900971	0.00789295	X
2	20	0.949483	0.00789295	X
1	20	0.952787	0.00789295	X

Contrast	Difference	+/- Limits
1 - 2	0.00330413	0.0226383
1 - 3	*0.0518167	0.0226383
1 - 4	*0.0773571	0.0226383
2 - 3	*0.0485126	0.0226383
2 - 4	*0.074053	0.0226383
3 - 4	*0.0255404	0.0226383

---

* denotes a statistically significant difference.

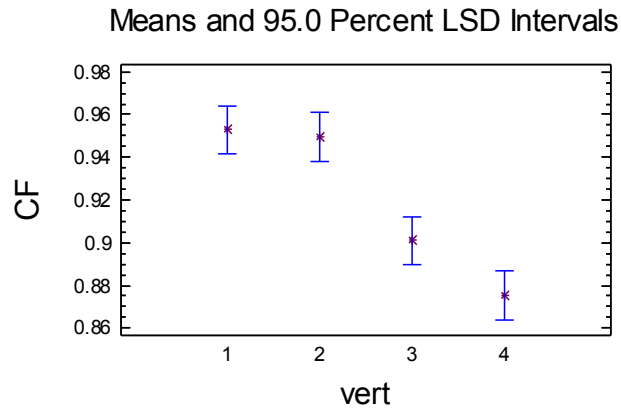

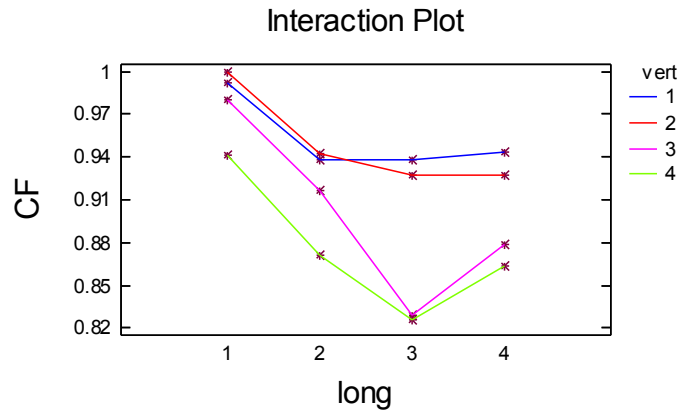

Appendix C.13: Weston Multifactor ANOVA - CF

Analysis Summary: Dependent variable: CF, Factors: long, trans, vert
Number of complete cases: 80

Analysis of Variance for CF - Type III Sums of Squares

Source	Sum of Squares	Df	Mean Square	F-Ratio	P-Value
MAIN EFFECTS					
A:long	2.88839	3	0.962798	26.95	0.0000
B:trans	0.716472	4	0.179118	5.01	0.0026
C:vert	2.19918	3	0.733059	20.52	0.0000
INTERACTIONS					
AB	0.393703	12	0.0328086	0.92	0.5391
AC	0.481397	9	0.0534885	1.50	0.1864
BC	0.243576	12	0.020298	0.57	0.8527
RESIDUAL	1.28608	36	0.0357244		
TOTAL (CORRECTED)	8.2088	79			

All F-ratios are based on the residual mean square error.

Table of Least Squares Means for CF
with 95.0 Percent Confidence Intervals

Level	Count	Mean	Stnd. Error	Lower Limit	Upper Limit
GRAND MEAN	80	0.603495			
long					
1	20	0.883923	0.0422637	0.798208	0.969638
2	20	0.667224	0.0422637	0.581509	0.752939
3	20	0.466744	0.0422637	0.381029	0.552459
4	20	0.396089	0.0422637	0.310374	0.481804
trans					
1	16	0.652038	0.0472523	0.556206	0.74787
2	16	0.699072	0.0472523	0.603239	0.794904
3	16	0.685056	0.0472523	0.589224	0.780889
4	16	0.51484	0.0472523	0.419008	0.610672
5	16	0.466469	0.0472523	0.370636	0.562301
vert					
1	20	0.765654	0.0422637	0.679939	0.851369
2	20	0.717535	0.0422637	0.63182	0.80325
3	20	0.592902	0.0422637	0.507187	0.678617
4	20	0.33789	0.0422637	0.252175	0.423605
long by trans					

1	1	4	0.92864	0.0945045	0.736976	1.1203
1	2	4	0.913201	0.0945045	0.721537	1.10487
1	3	4	0.975888	0.0945045	0.784224	1.16755
1	4	4	0.897753	0.0945045	0.706088	1.08942
1	5	4	0.704135	0.0945045	0.51247	0.895799
2	1	4	0.685893	0.0945045	0.494229	0.877558
2	2	4	0.748795	0.0945045	0.557131	0.94046
2	3	4	0.802165	0.0945045	0.610501	0.99383
2	4	4	0.577757	0.0945045	0.386092	0.769421
2	5	4	0.521509	0.0945045	0.329845	0.713174
3	1	4	0.668594	0.0945045	0.47693	0.860259
3	2	4	0.614113	0.0945045	0.422448	0.805777
3	3	4	0.426972	0.0945045	0.235307	0.618636
3	4	4	0.252399	0.0945045	0.0607344	0.444063
3	5	4	0.371644	0.0945045	0.179979	0.563308
4	1	4	0.325025	0.0945045	0.13336	0.516689
4	2	4	0.520178	0.0945045	0.328513	0.711842
4	3	4	0.5352	0.0945045	0.343535	0.726864
4	4	4	0.331453	0.0945045	0.139788	0.523117
4	5	4	0.268588	0.0945045	0.0769231	0.460252
long by vert						
1	1	5	0.945664	0.0845274	0.774234	1.11709
1	2	5	0.968386	0.0845274	0.796956	1.13982
1	3	5	0.955517	0.0845274	0.784087	1.12695
1	4	5	0.666126	0.0845274	0.494696	0.837556
2	1	5	0.826257	0.0845274	0.654827	0.997687
2	2	5	0.721124	0.0845274	0.549694	0.892554
2	3	5	0.735704	0.0845274	0.564274	0.907134
2	4	5	0.38581	0.0845274	0.21438	0.55724
3	1	5	0.613303	0.0845274	0.441873	0.784733
3	2	5	0.550612	0.0845274	0.379182	0.722042
3	3	5	0.4724	0.0845274	0.30097	0.64383
3	4	5	0.230662	0.0845274	0.059232	0.402092
4	1	5	0.67739	0.0845274	0.50596	0.84882
4	2	5	0.630016	0.0845274	0.458586	0.801446
4	3	5	0.207988	0.0845274	0.036558	0.379418
4	4	5	0.06896	0.0845274	-0.10247	0.24039
trans by vert						
1	1	4	0.818357	0.0945045	0.626692	1.01002
1	2	4	0.82132	0.0945045	0.629656	1.01298
1	3	4	0.66603	0.0945045	0.474365	0.857694
1	4	4	0.302446	0.0945045	0.110782	0.494111
2	1	4	0.797924	0.0945045	0.60626	0.989589
2	2	4	0.747727	0.0945045	0.556062	0.939391
2	3	4	0.708133	0.0945045	0.516468	0.899797
2	4	4	0.542503	0.0945045	0.350838	0.734167
3	1	4	0.814846	0.0945045	0.623181	1.00651
3	2	4	0.809587	0.0945045	0.617923	1.00125
3	3	4	0.715473	0.0945045	0.523809	0.907138
3	4	4	0.400319	0.0945045	0.208655	0.591984
4	1	4	0.675475	0.0945045	0.483811	0.86714

4	2	4	0.6686	0.0945045	0.476936	0.860264
4	3	4	0.413221	0.0945045	0.221556	0.604885
4	4	4	0.302065	0.0945045	0.1104	0.493729
5	1	4	0.721666	0.0945045	0.530001	0.91333
5	2	4	0.540439	0.0945045	0.348774	0.732103
5	3	4	0.461655	0.0945045	0.269991	0.65332
5	4	4	0.142115	0.0945045	-0.0495494	0.33378

Multiple Range Tests for CF by long

Method: 95.0 percent LSD

long	Count	LS Mean	LS Sigma	Homogeneous Groups
4	20	0.396089	0.0422637	X
3	20	0.466744	0.0422637	X
2	20	0.667224	0.0422637	X
1	20	0.883923	0.0422637	X

Contrast	Difference	+/- Limits
1 - 2	*0.216699	0.121219
1 - 3	*0.417179	0.121219
1 - 4	*0.487835	0.121219
2 - 3	*0.20048	0.121219
2 - 4	*0.271135	0.121219
3 - 4	0.0706556	0.121219

---

* denotes a statistically significant difference.

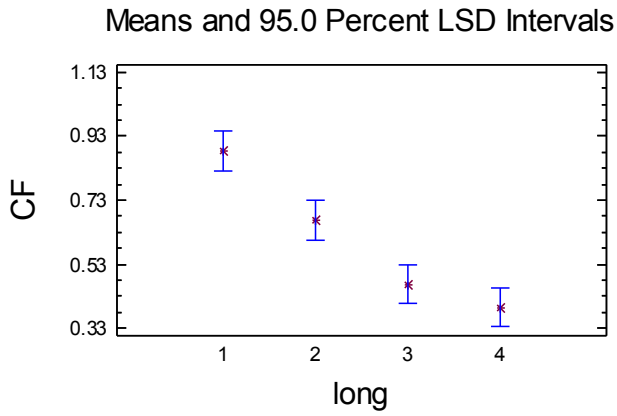

Multiple Range Tests for CF by trans

Method: 95.0 percent LSD

trans	Count	LS Mean	LS Sigma	Homogeneous Groups
5	16	0.466469	0.0472523	X
4	16	0.51484	0.0472523	X
1	16	0.652038	0.0472523	X
3	16	0.685056	0.0472523	X
2	16	0.699072	0.0472523	X

Contrast	Difference	+/- Limits
1 - 2	-0.0470335	0.135527
1 - 3	-0.0330181	0.135527
1 - 4	*0.137198	0.135527
1 - 5	*0.18557	0.135527
2 - 3	0.0140154	0.135527
2 - 4	*0.184232	0.135527
2 - 5	*0.232603	0.135527
3 - 4	*0.170216	0.135527
3 - 5	*0.218588	0.135527
4 - 5	0.0483715	0.135527

---

* denotes a statistically significant difference.

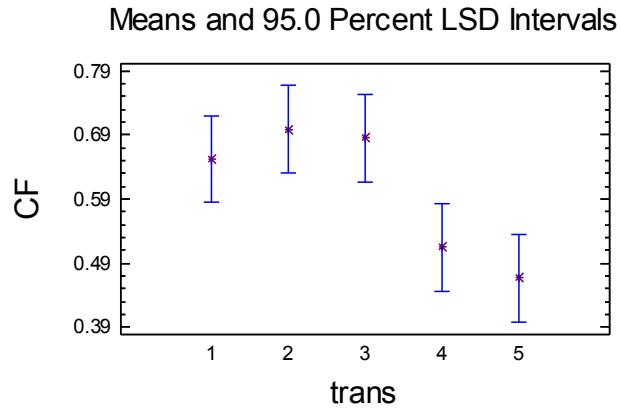

Multiple Range Tests for CF by vert

Method: 95.0 percent LSD

vert	Count	LS Mean	LS Sigma	Homogeneous Groups
4	20	0.33789	0.0422637	X
3	20	0.592902	0.0422637	X
2	20	0.717535	0.0422637	X
1	20	0.765654	0.0422637	X

Contrast	Difference	+/- Limits
1 - 2	0.048119	0.121219
1 - 3	*0.172751	0.121219
1 - 4	*0.427764	0.121219
2 - 3	*0.124632	0.121219
2 - 4	*0.379645	0.121219
3 - 4	*0.255013	0.121219

---

* denotes a statistically significant difference.

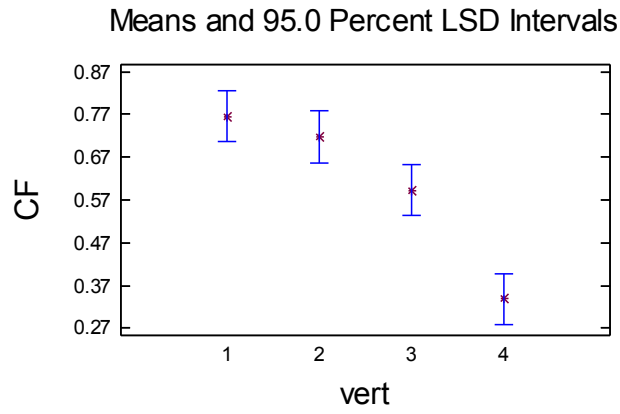

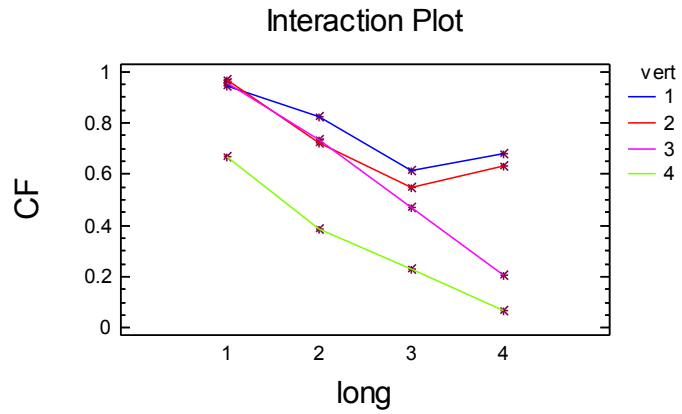

Appendix D.1: FEA Modelling Results – CF_T = 0.55, Hydraulic Conductivity Profile

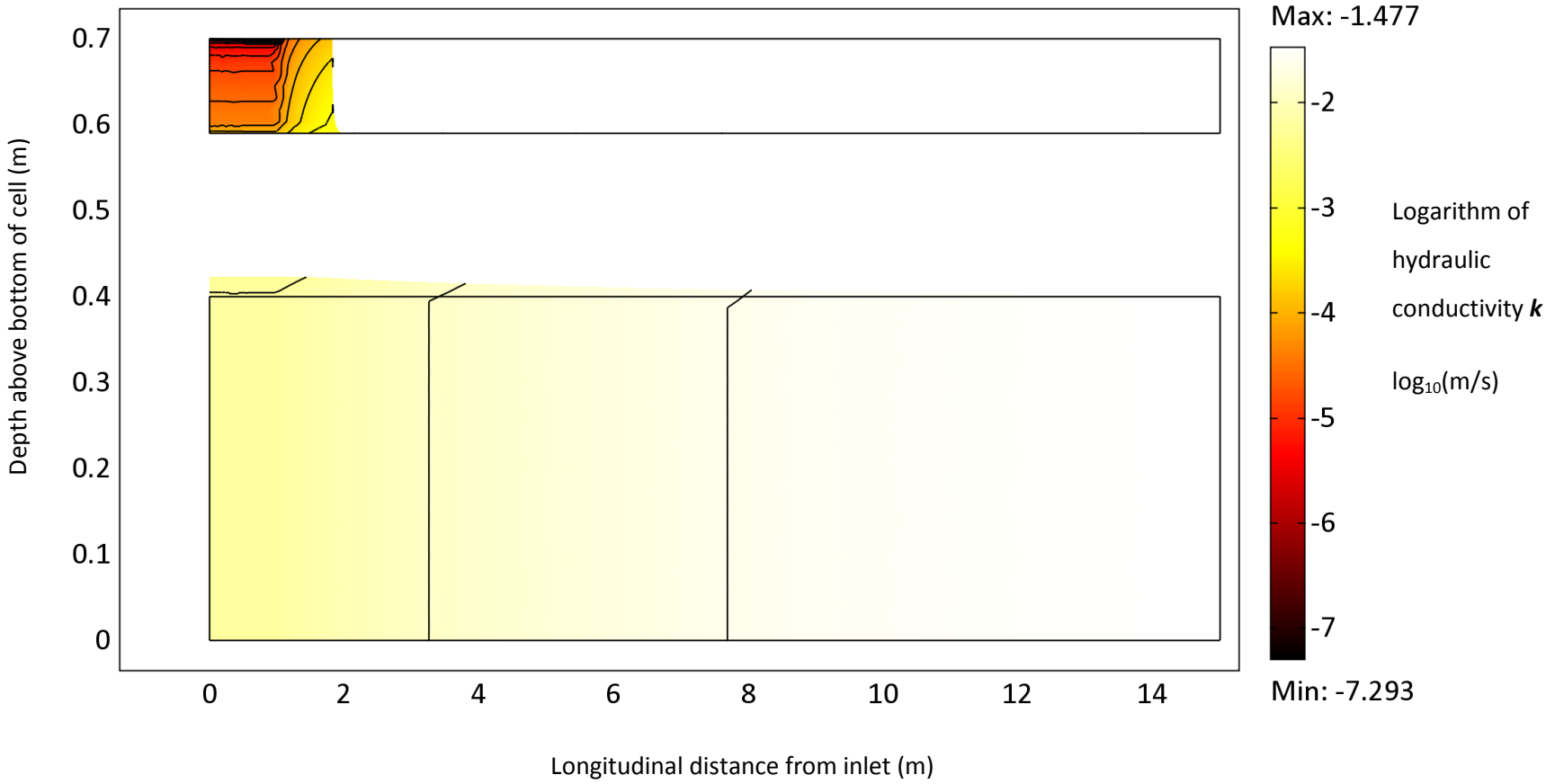

Appendix D.1: FEA Modelling Results – CF_T = 0.55, Adaptive Mesh

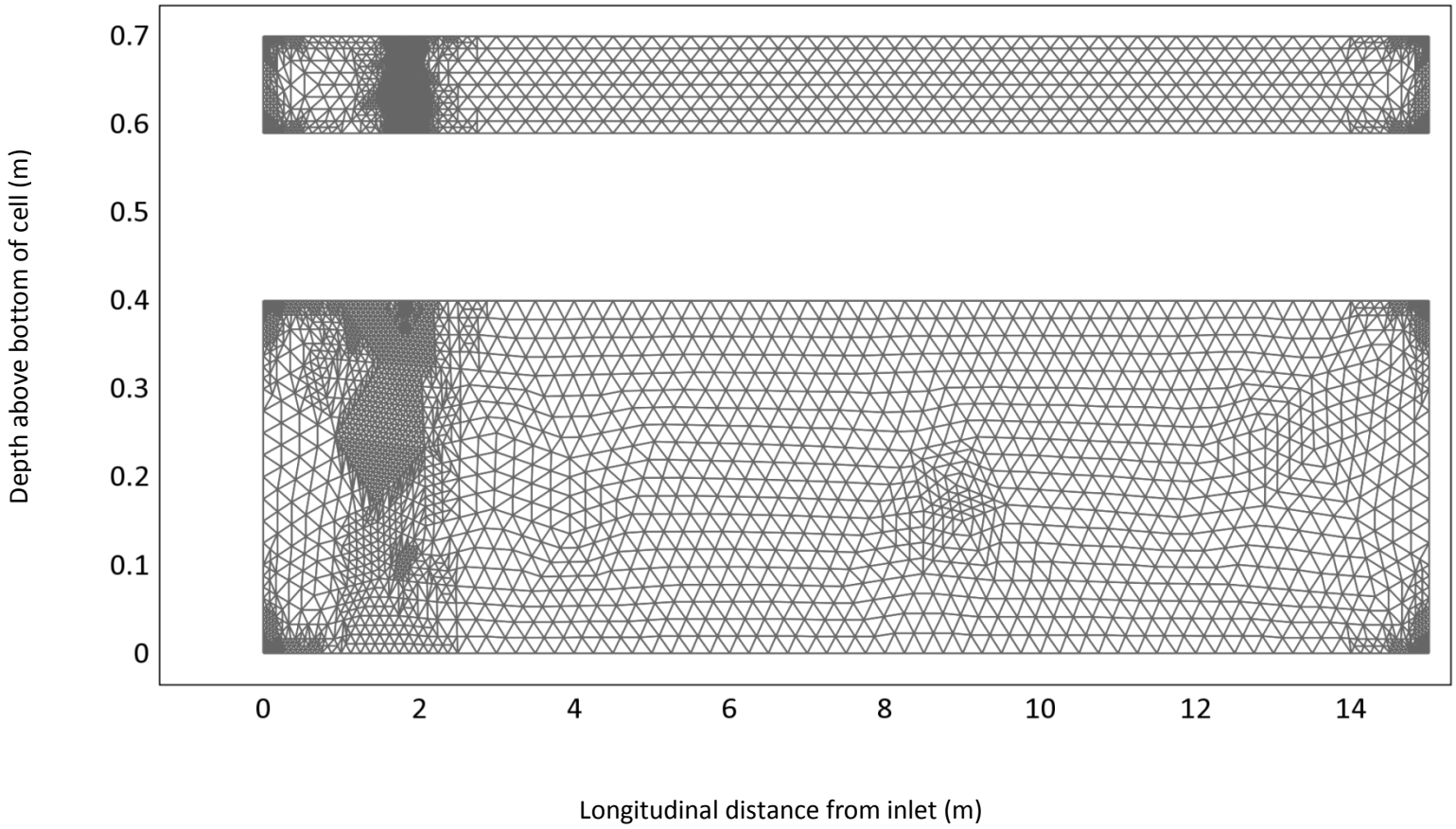

Appendix D.1: FEA Modelling Results – CF_T = 0.55, Hydraulic Head

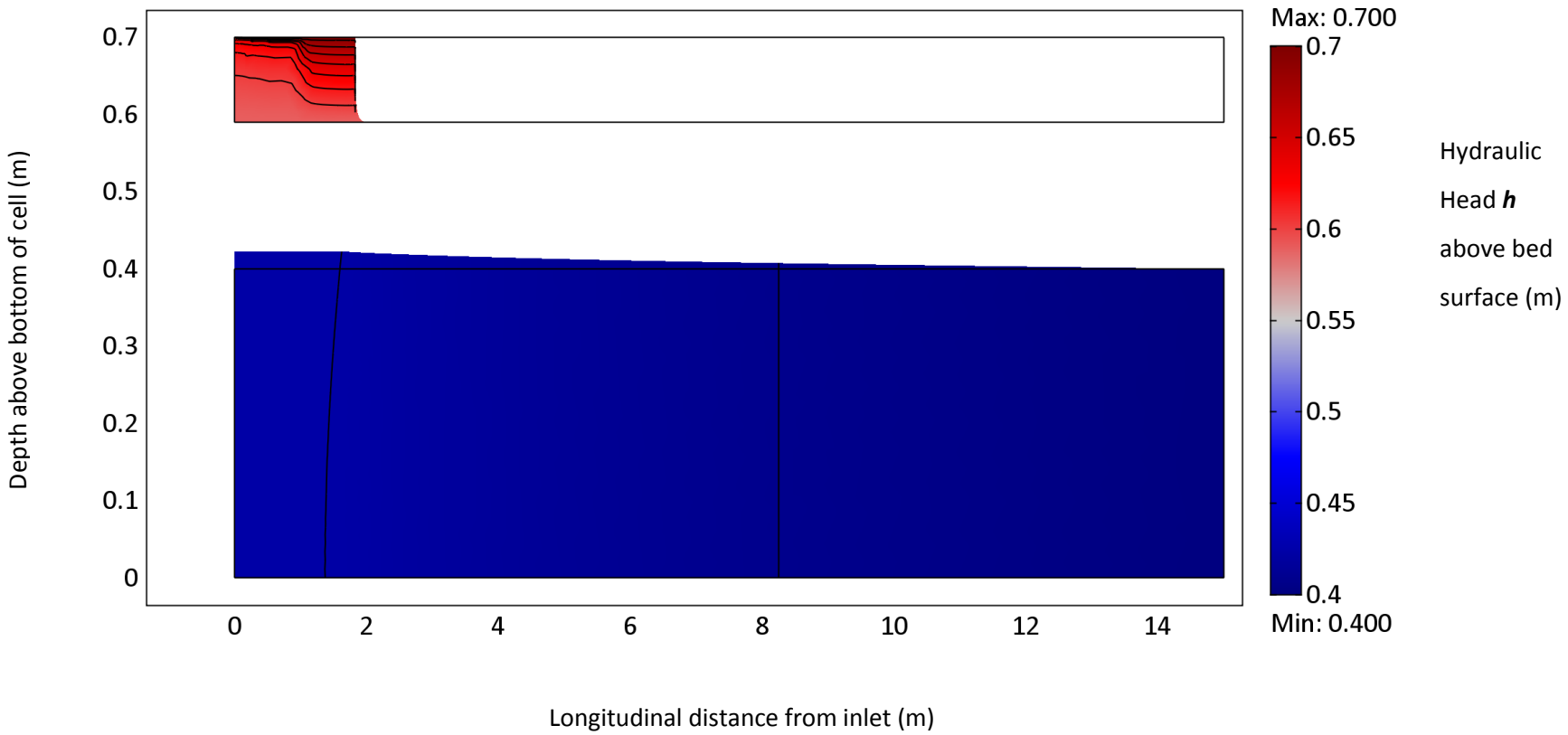

Appendix D.2: FEA Modelling Results – CF_T = 0.60, Hydraulic Conductivity Profile

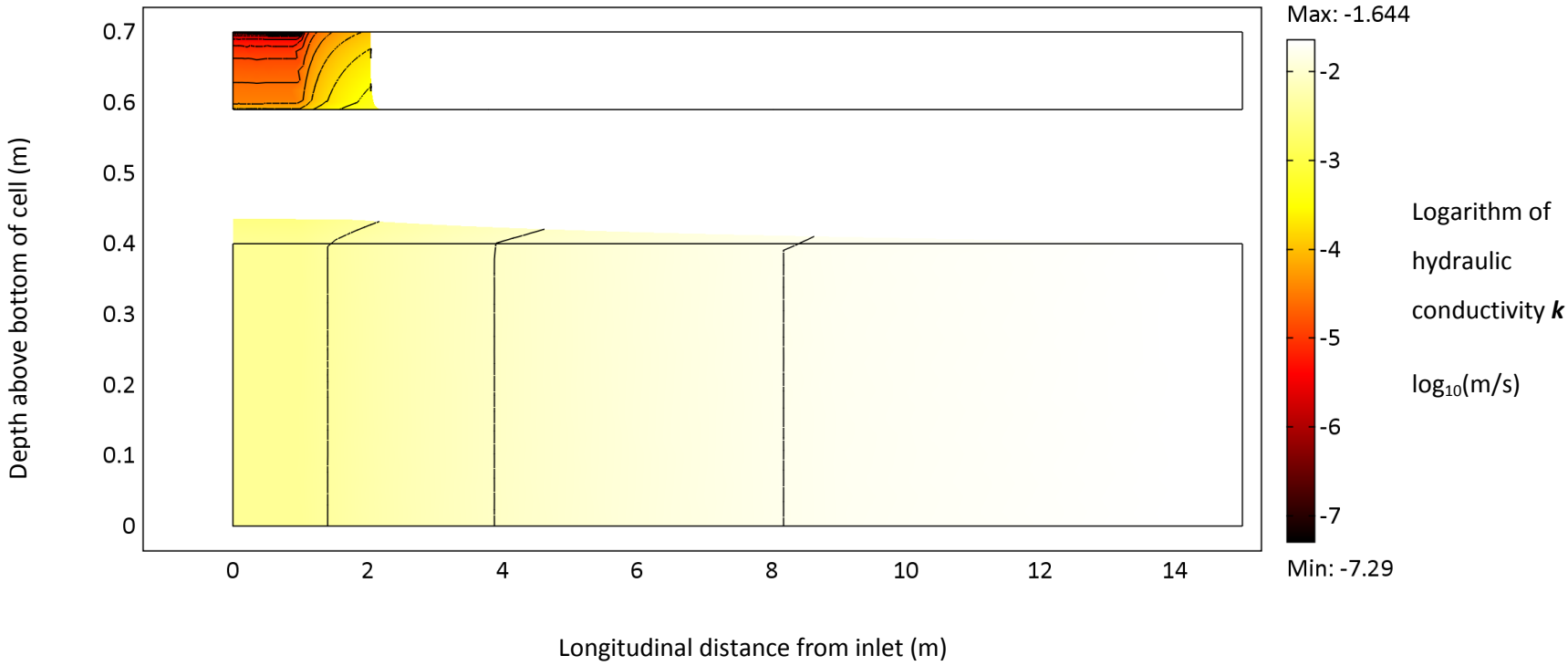

Appendix D.2: FEA Modelling Results – CF_T = 0.60, Adaptive Mesh

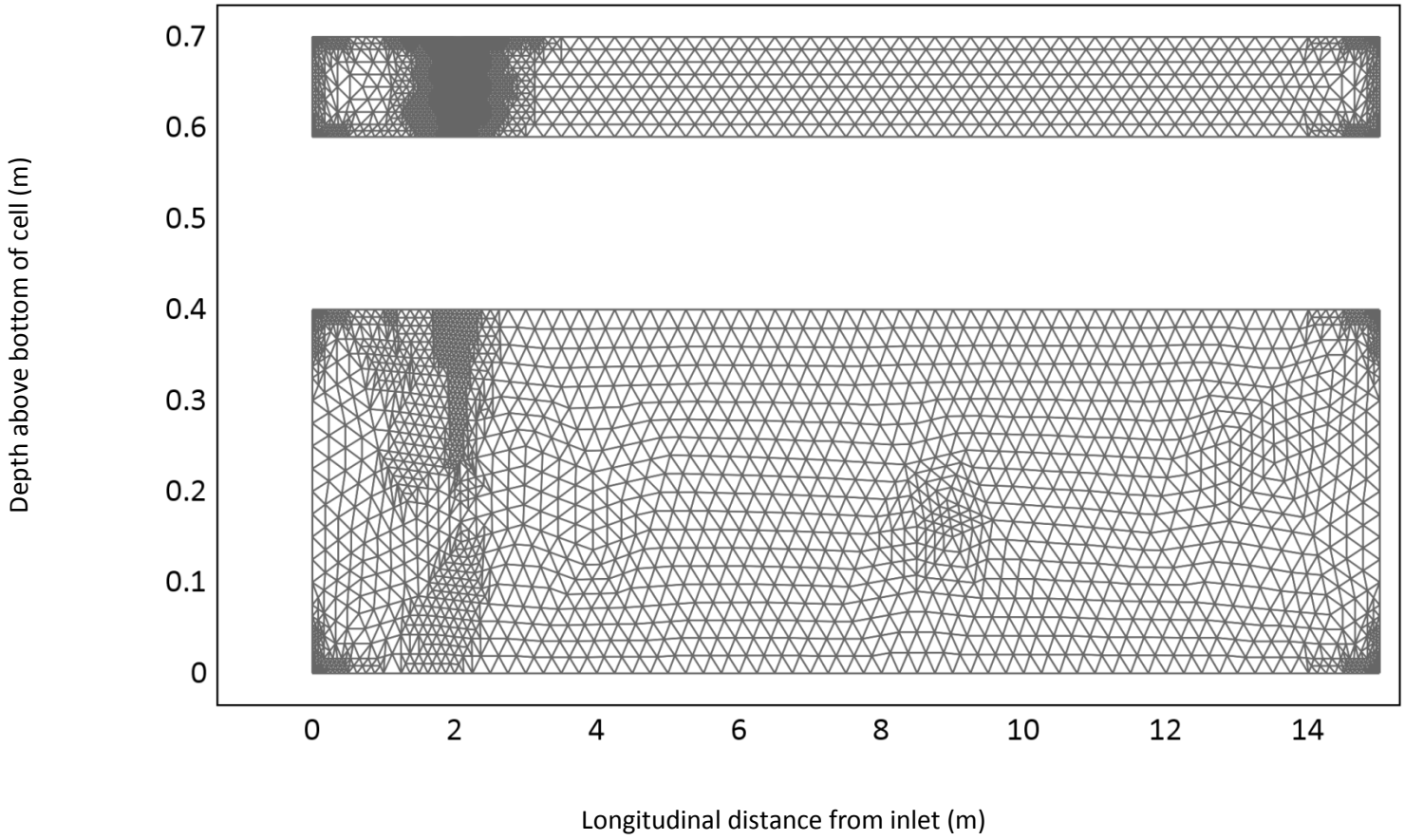

Appendix D.2: FEA Modelling Results – CF_T = 0.60, Hydraulic Head

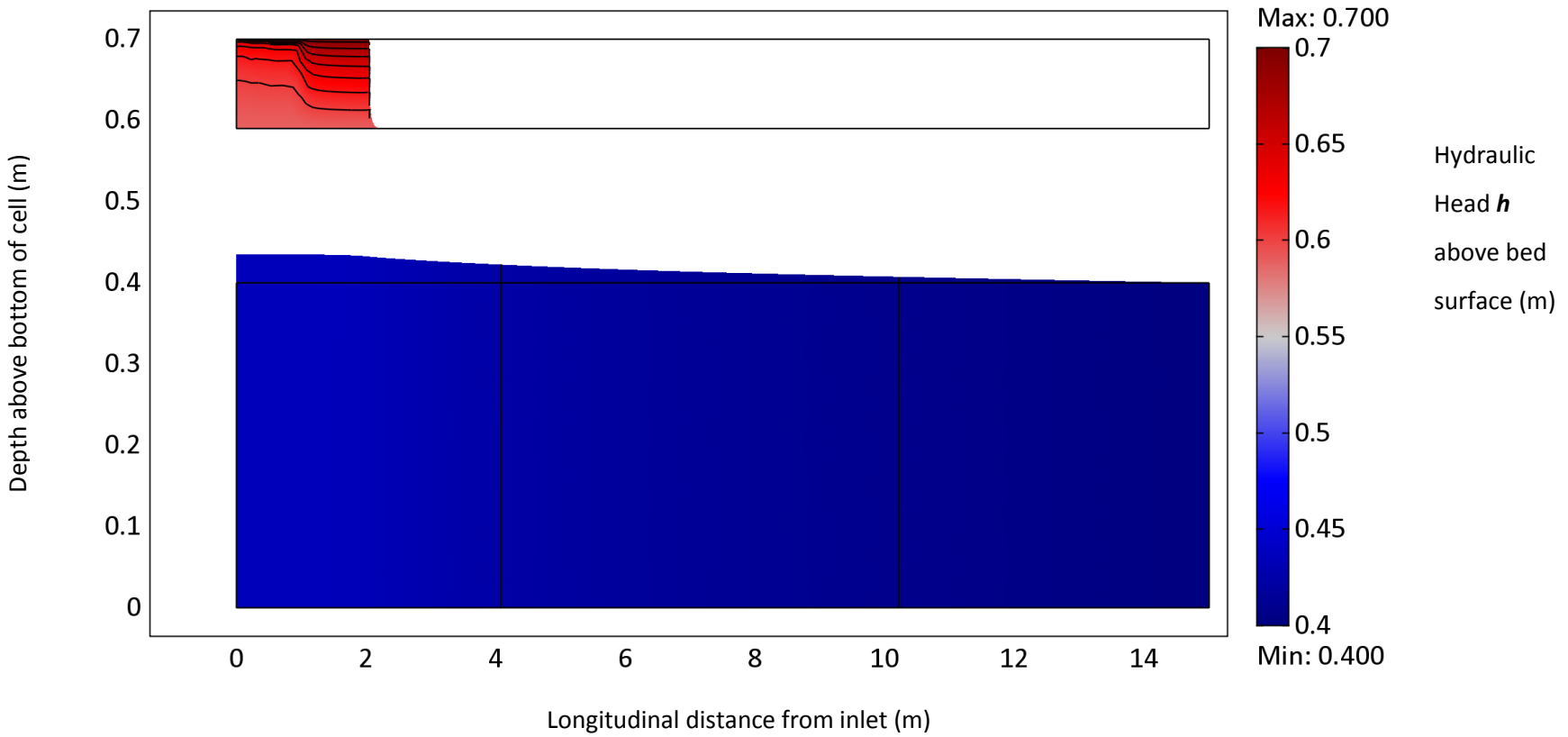

Appendix D.3: FEA Modelling Results – CF_T = 0.65, Hydraulic Conductivity Profile

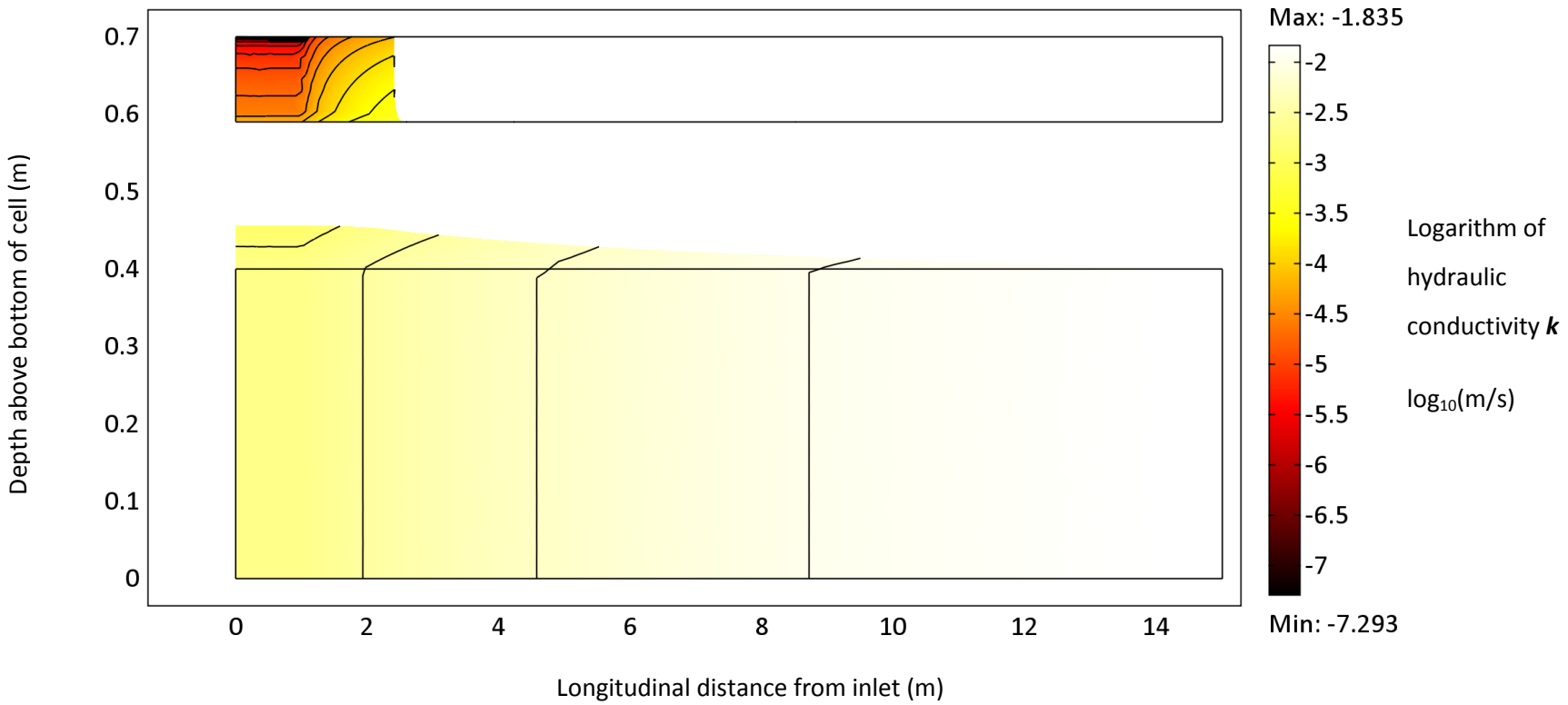

Appendix D.3: FEA Modelling Results – CF_T = 0.65, Adaptive Mesh

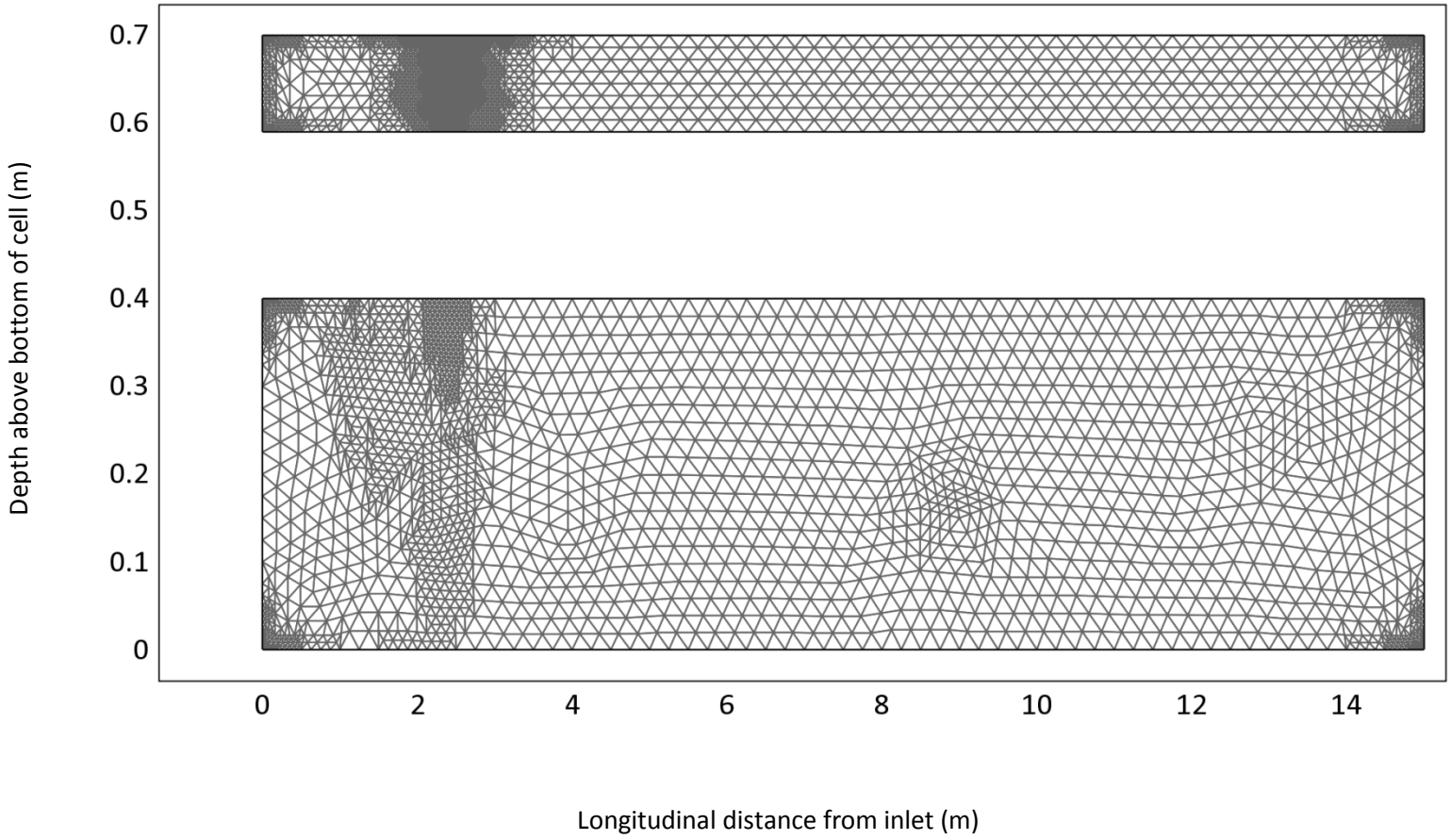

Appendix D.3: FEA Modelling Results – CF_T = 0.65, Hydraulic Head

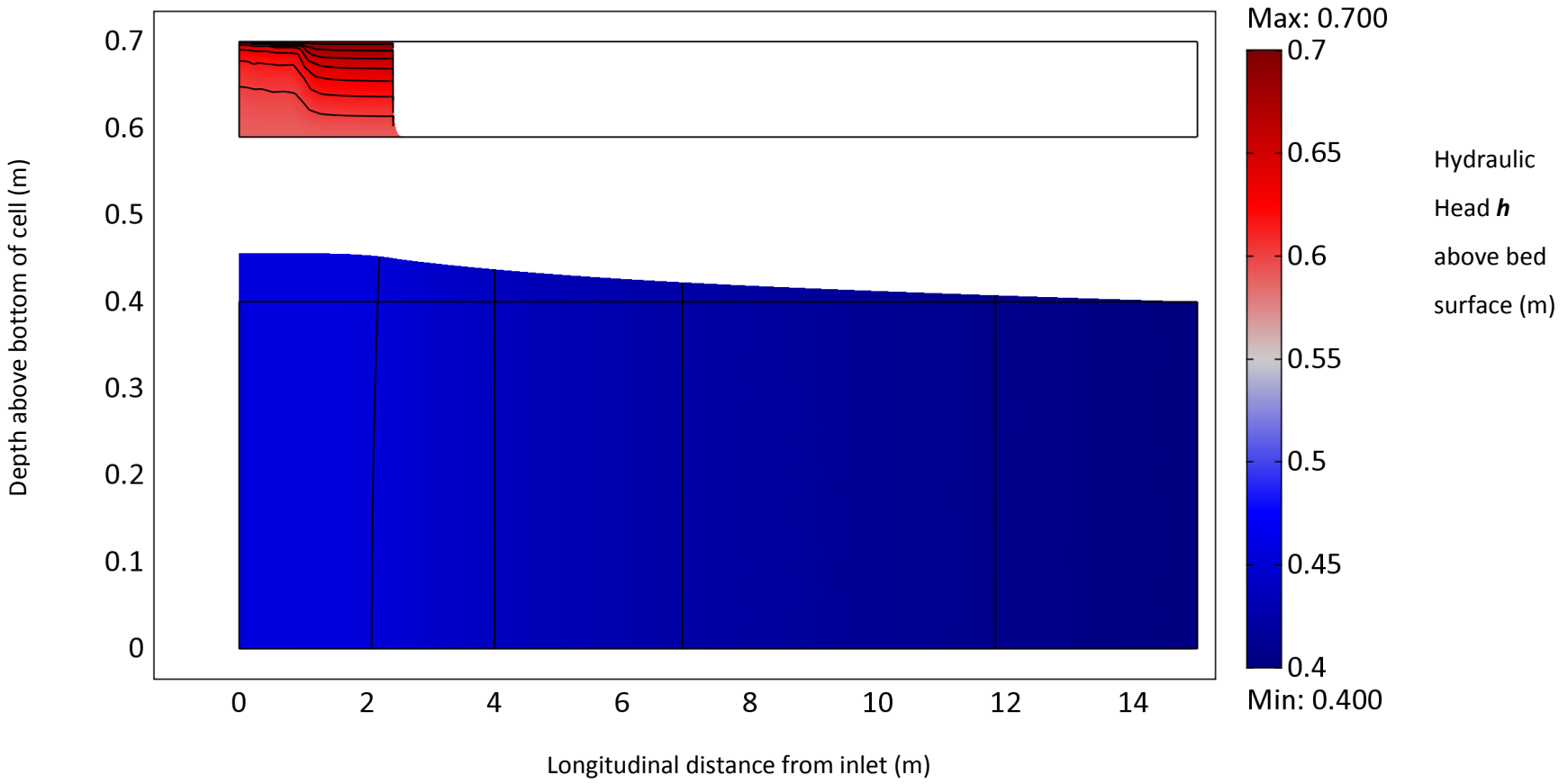

Appendix D.4: FEA Modelling Results – CF_T = 0.70, Hydraulic Conductivity Profile

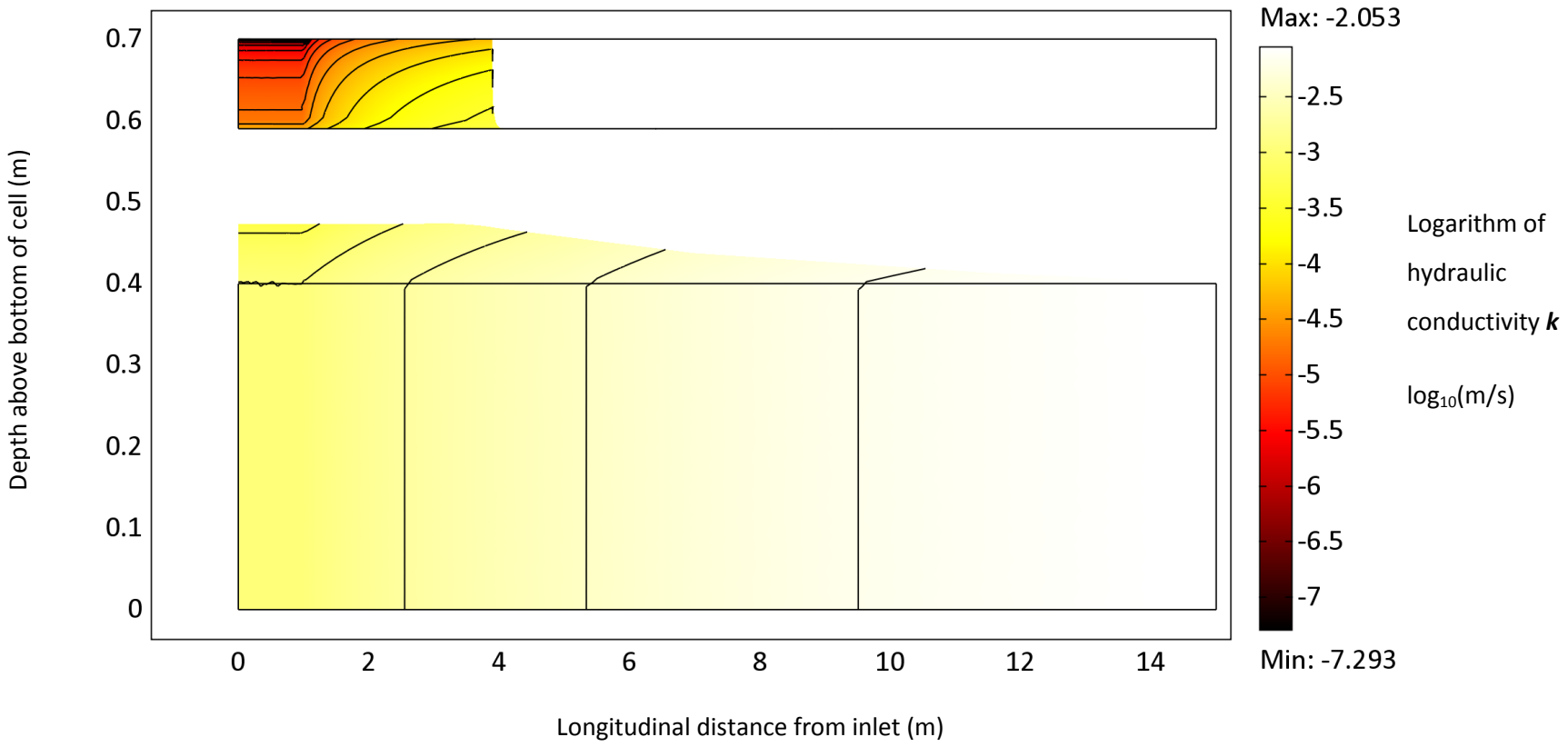

Appendix D.4: FEA Modelling Results – CF_T = 0.70, Adaptive Mesh

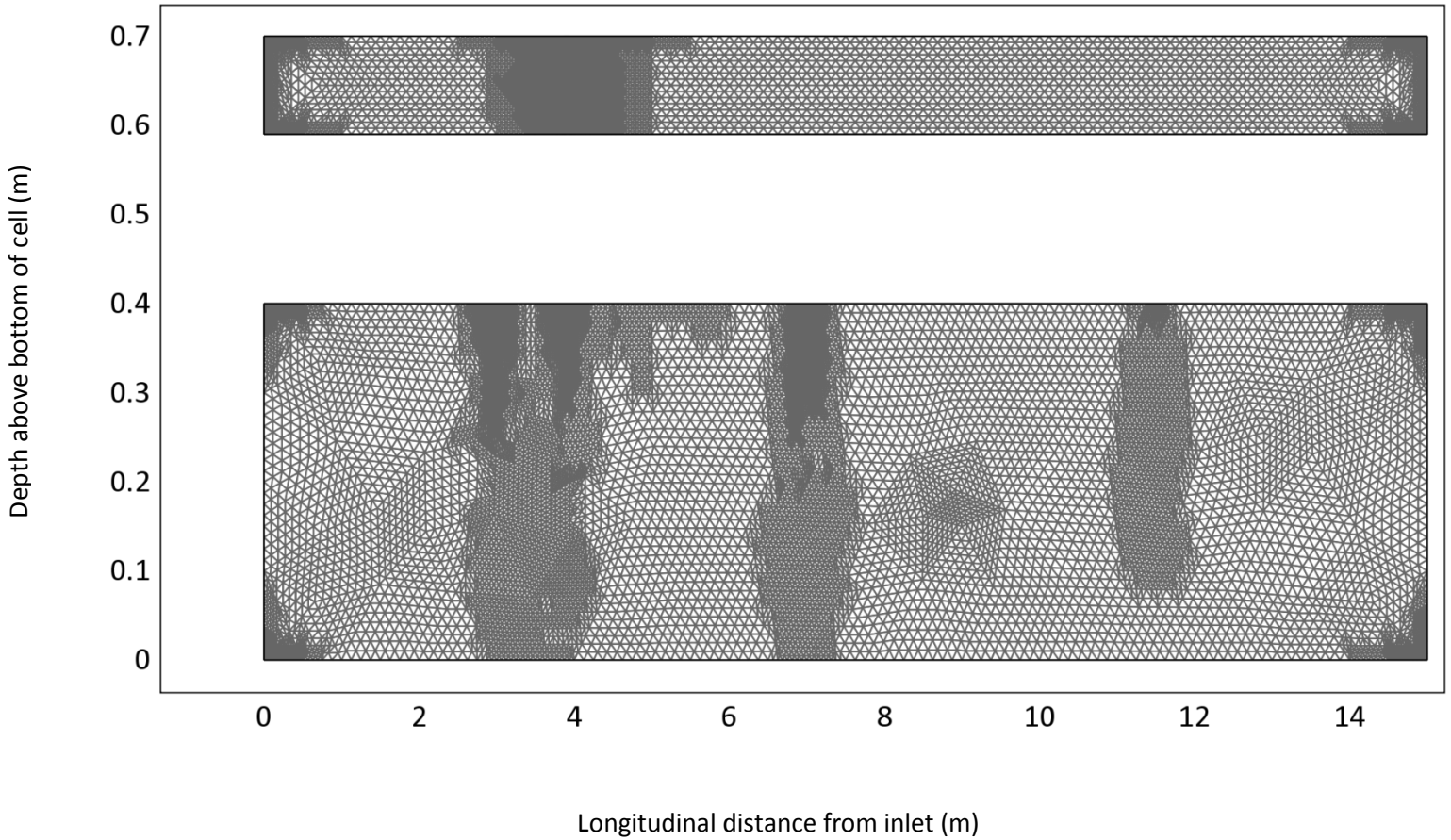

Appendix D.4: FEA Modelling Results – CF_T = 0.70, Hydraulic Head

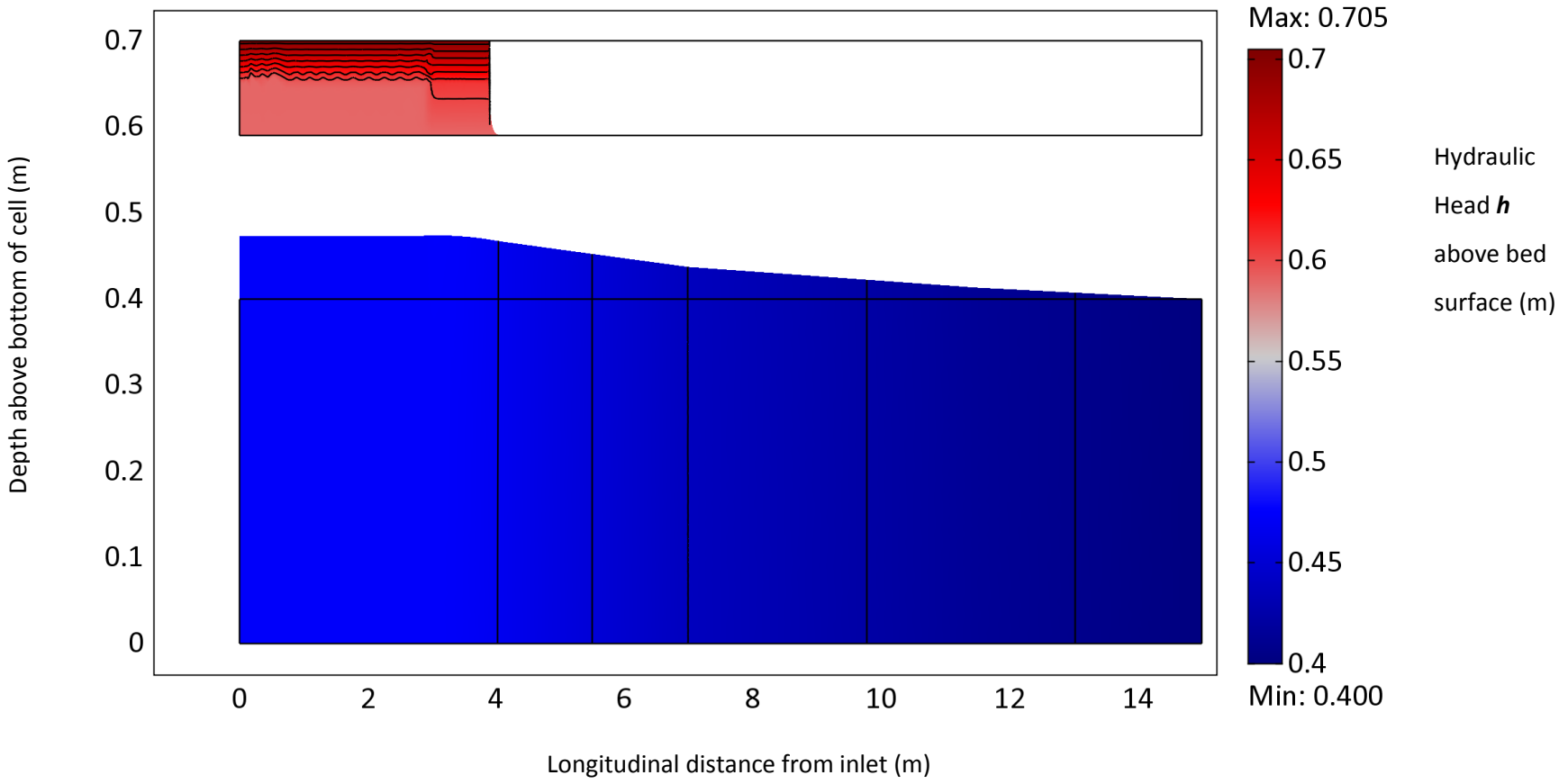

Appendix D.5: FEA Modelling Results – CF_T = 0.75, Hydraulic Conductivity Profile

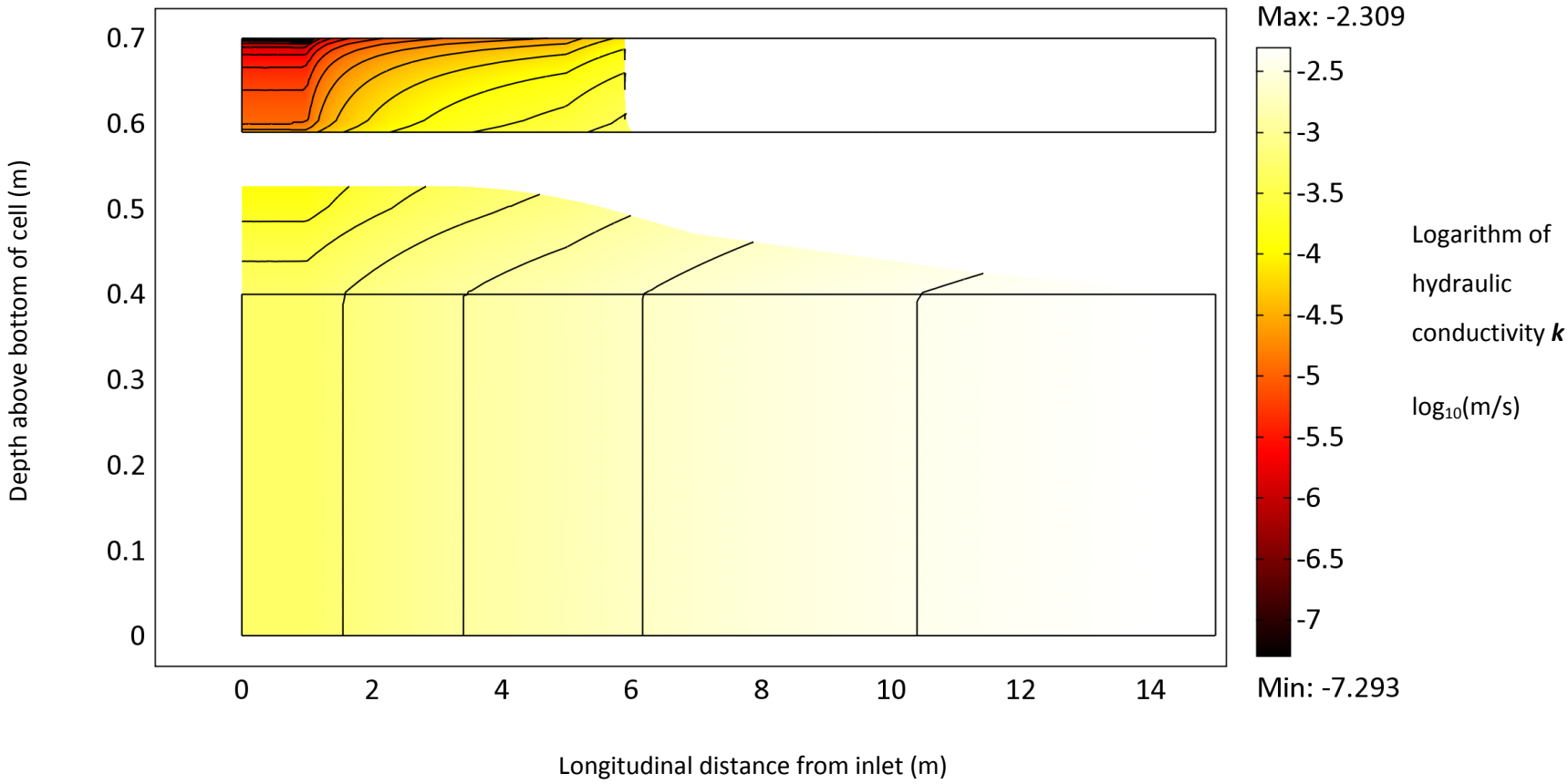

Appendix D.5: FEA Modelling Results – CF_T = 0.75, Adaptive Mesh

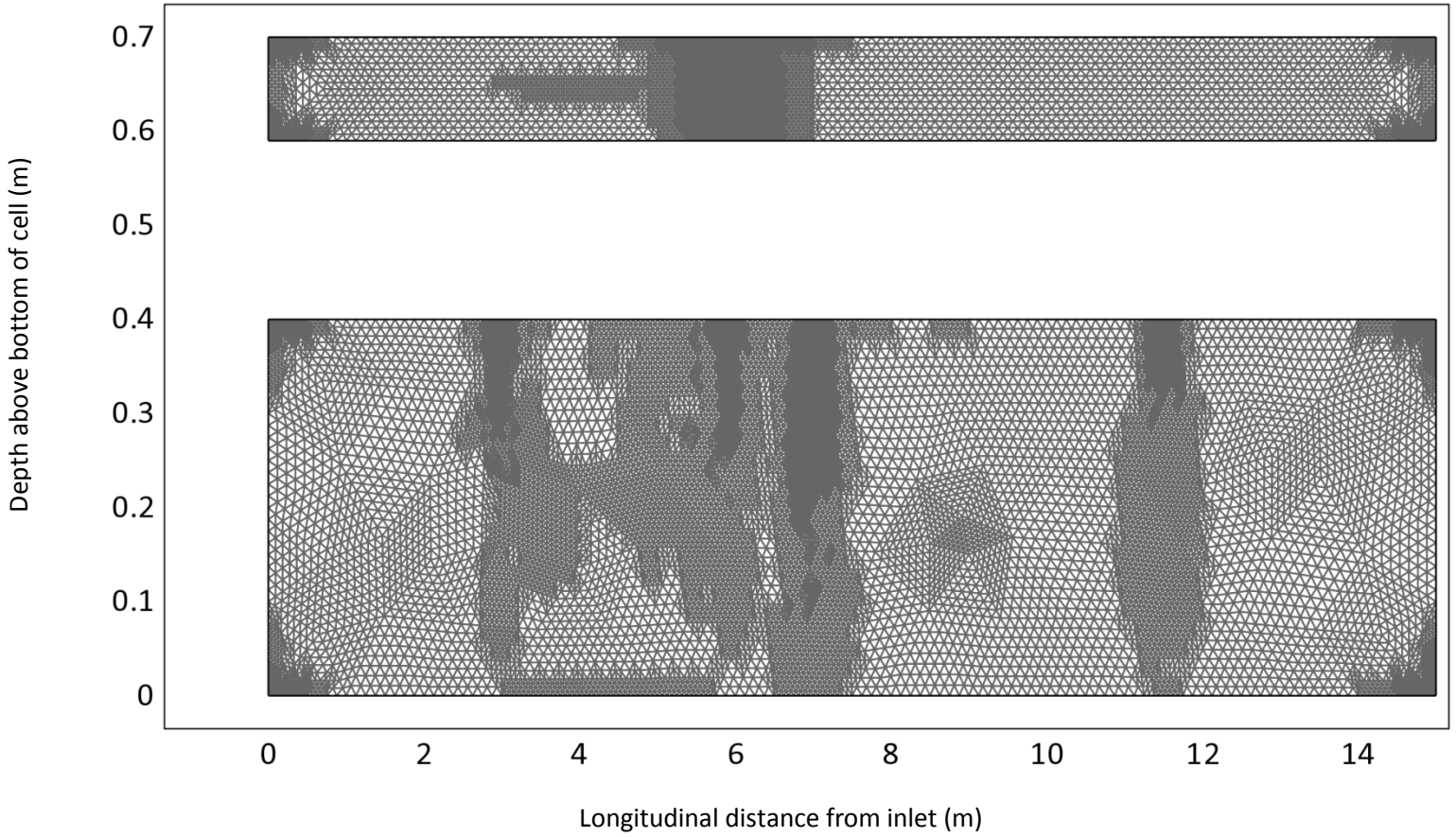

Appendix D.5: FEA Modelling Results – CF_T = 0.75, Hydraulic Head

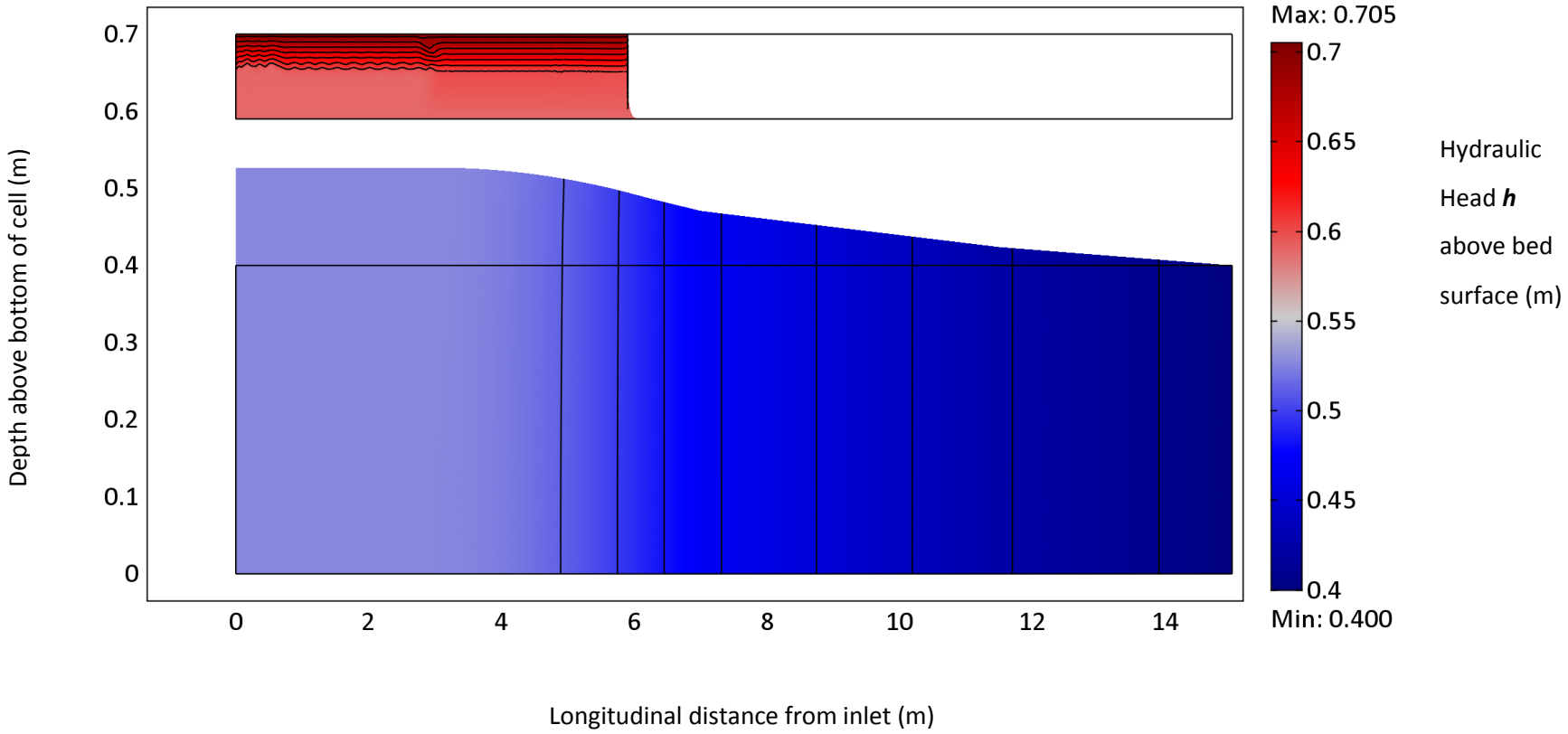

Appendix D.6: FEA Modelling Results – CF_T = 0.80, Hydraulic Conductivity Profile

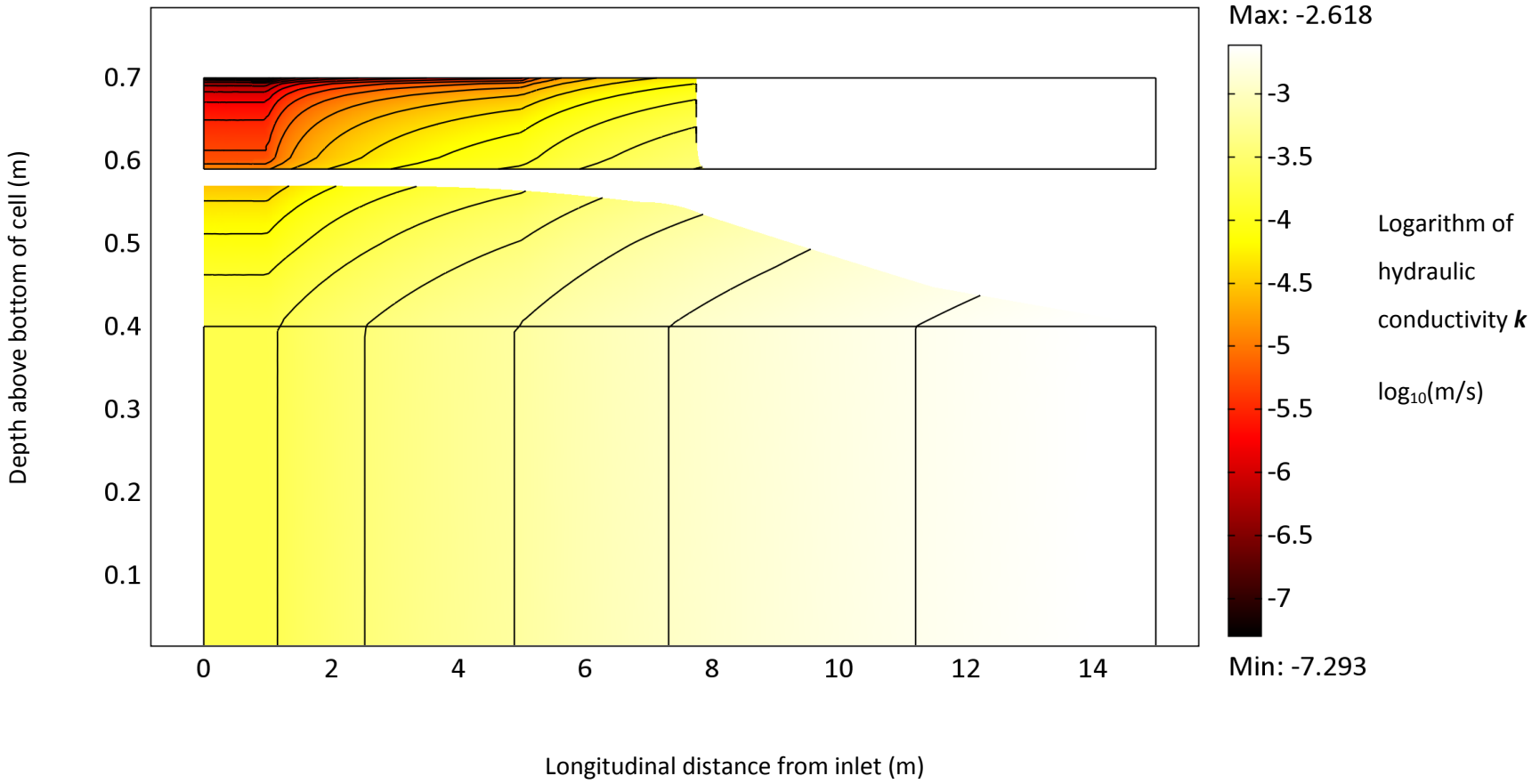

Appendix D.6: FEA Modelling Results – CF_T = 0.80, Adaptive Mesh

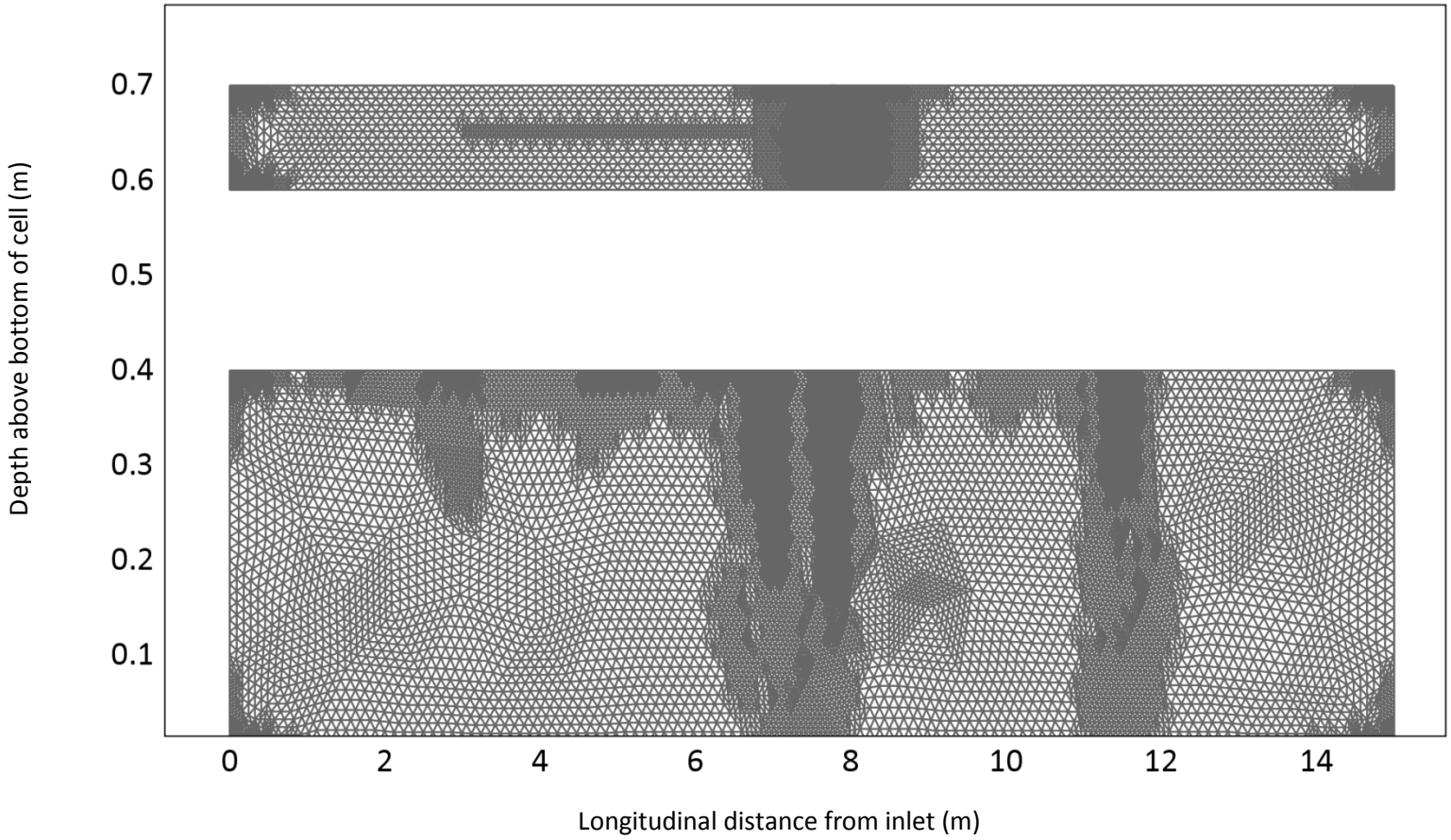

Appendix D.6: FEA Modelling Results – CF_T = 0.80, Hydraulic Head

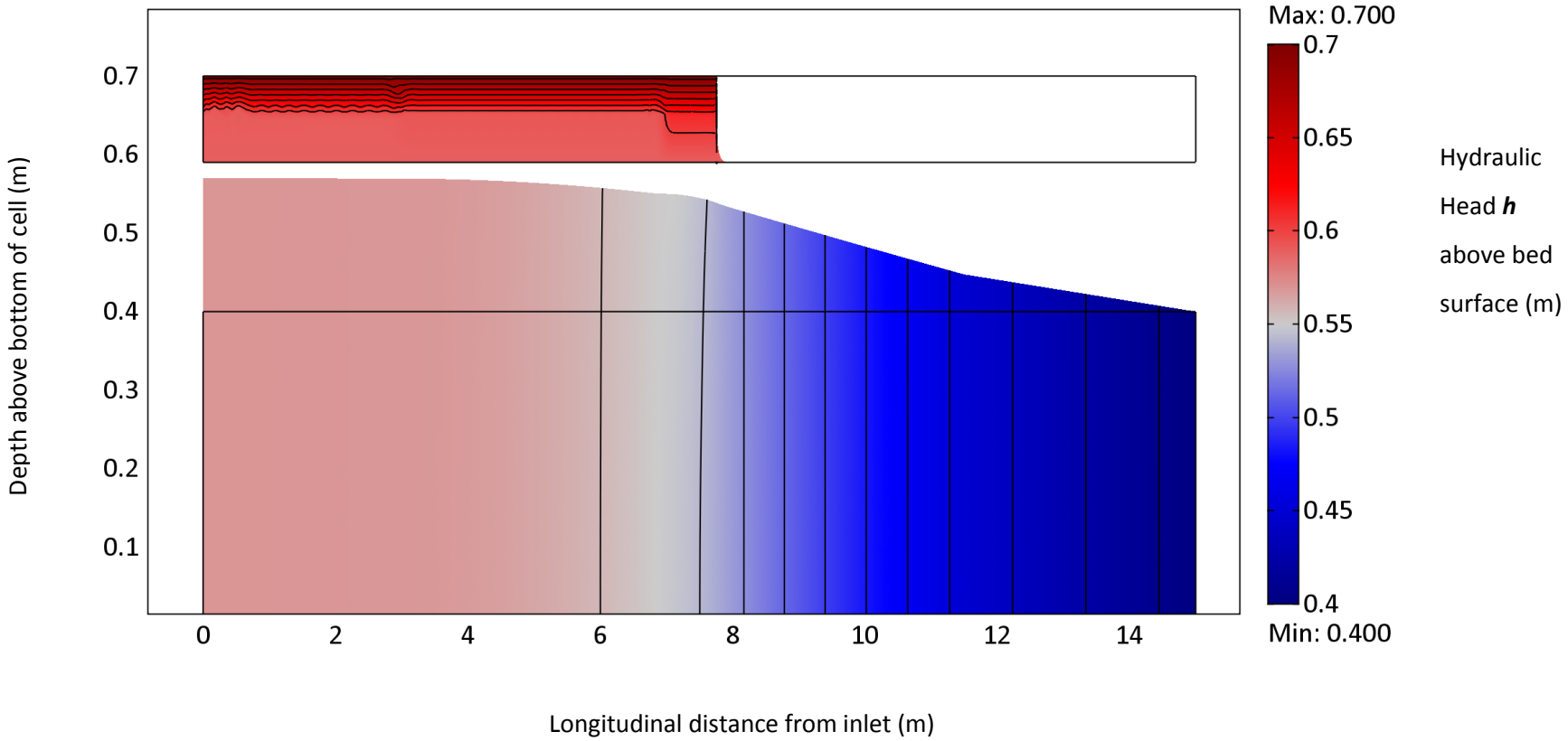

Appendix D.7: FEA Modelling Results – CF_T = 0.85, Hydraulic Conductivity Profile

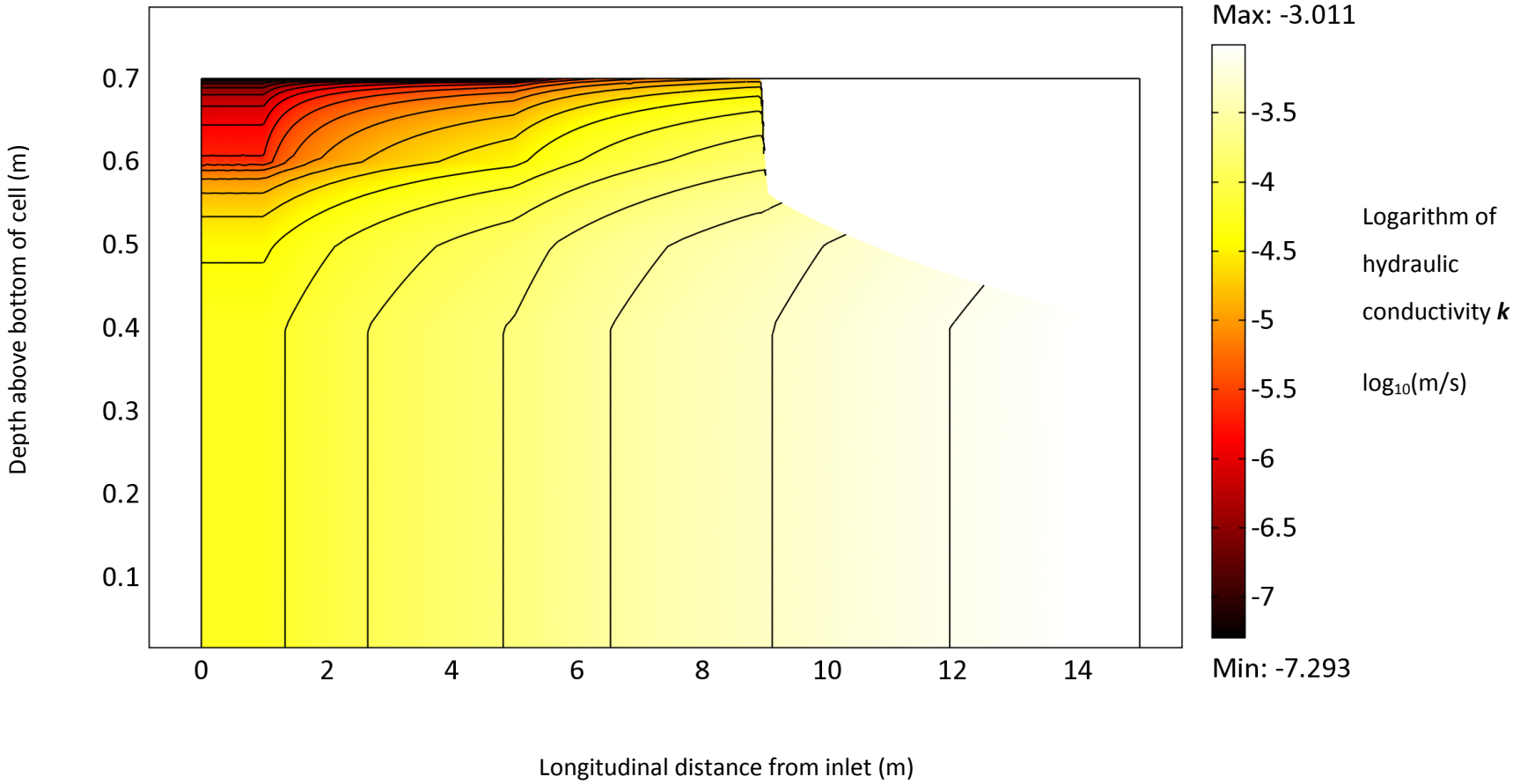

Appendix D.7: FEA Modelling Results – CF_T = 0.85, Adaptive Mesh

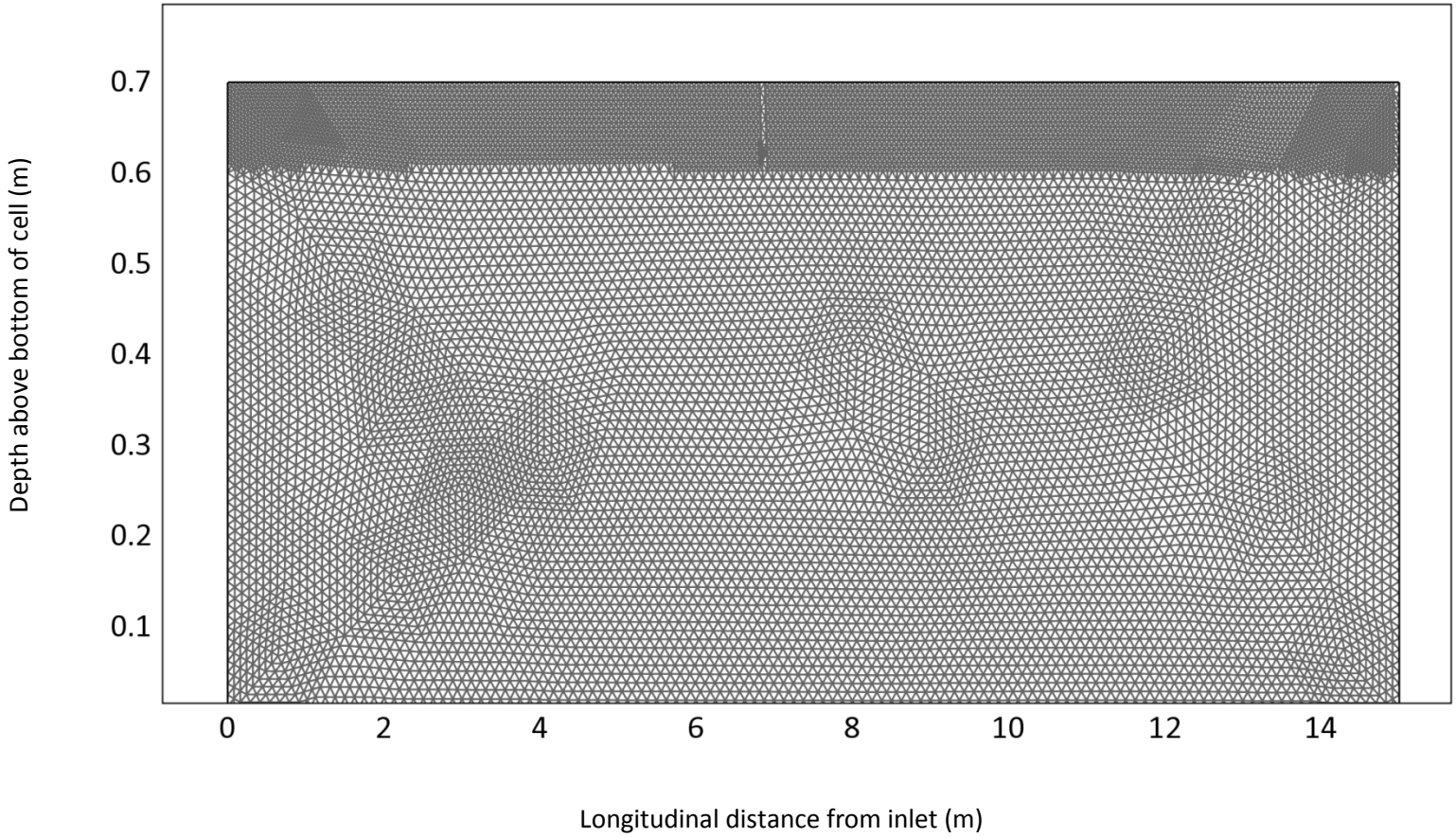

Appendix D.7: FEA Modelling Results – CF_T = 0.85, Hydraulic Head

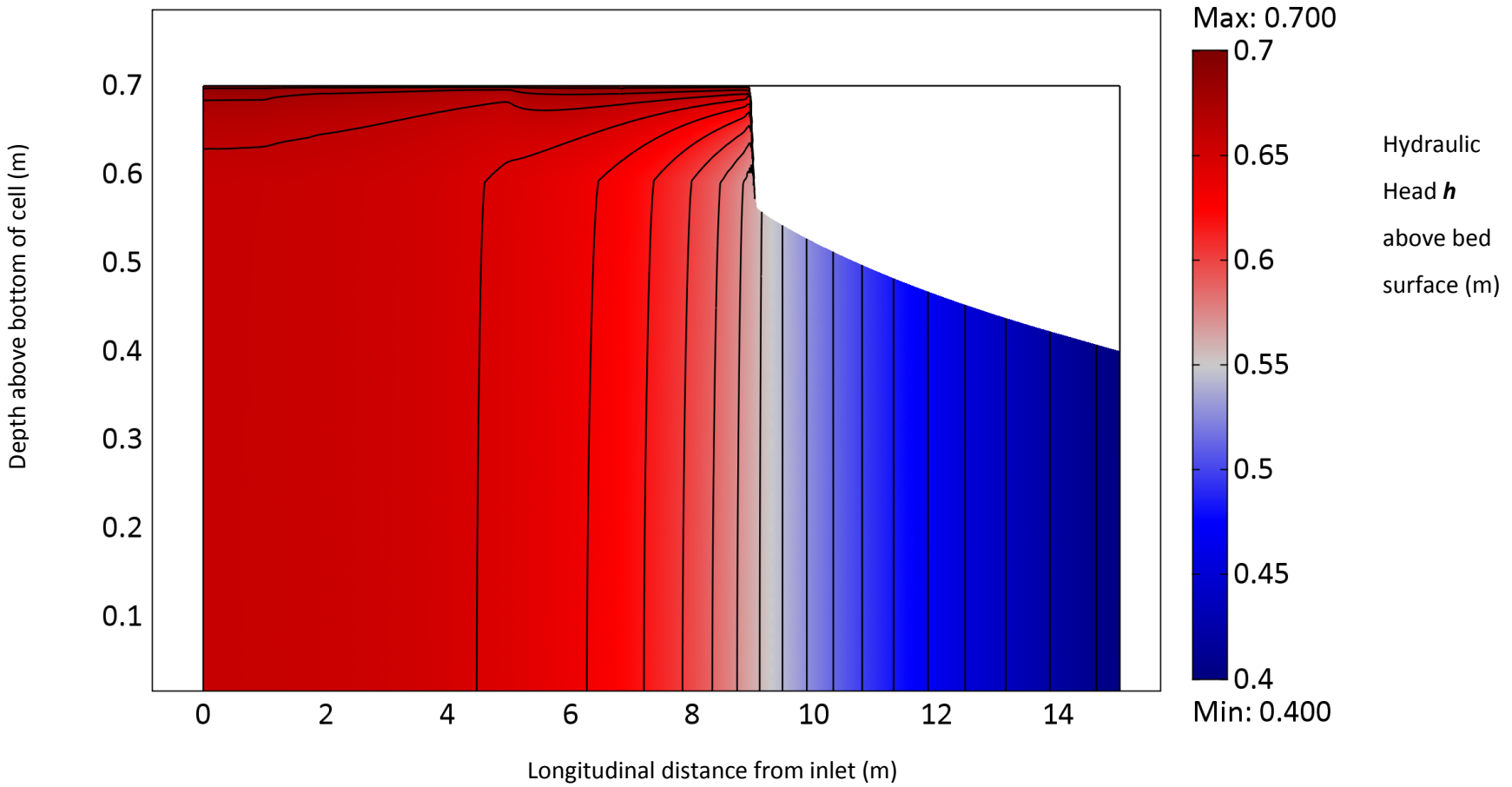

Appendix D.8: FEA Modelling Results – CF_T = 0.90, Hydraulic Conductivity Profile

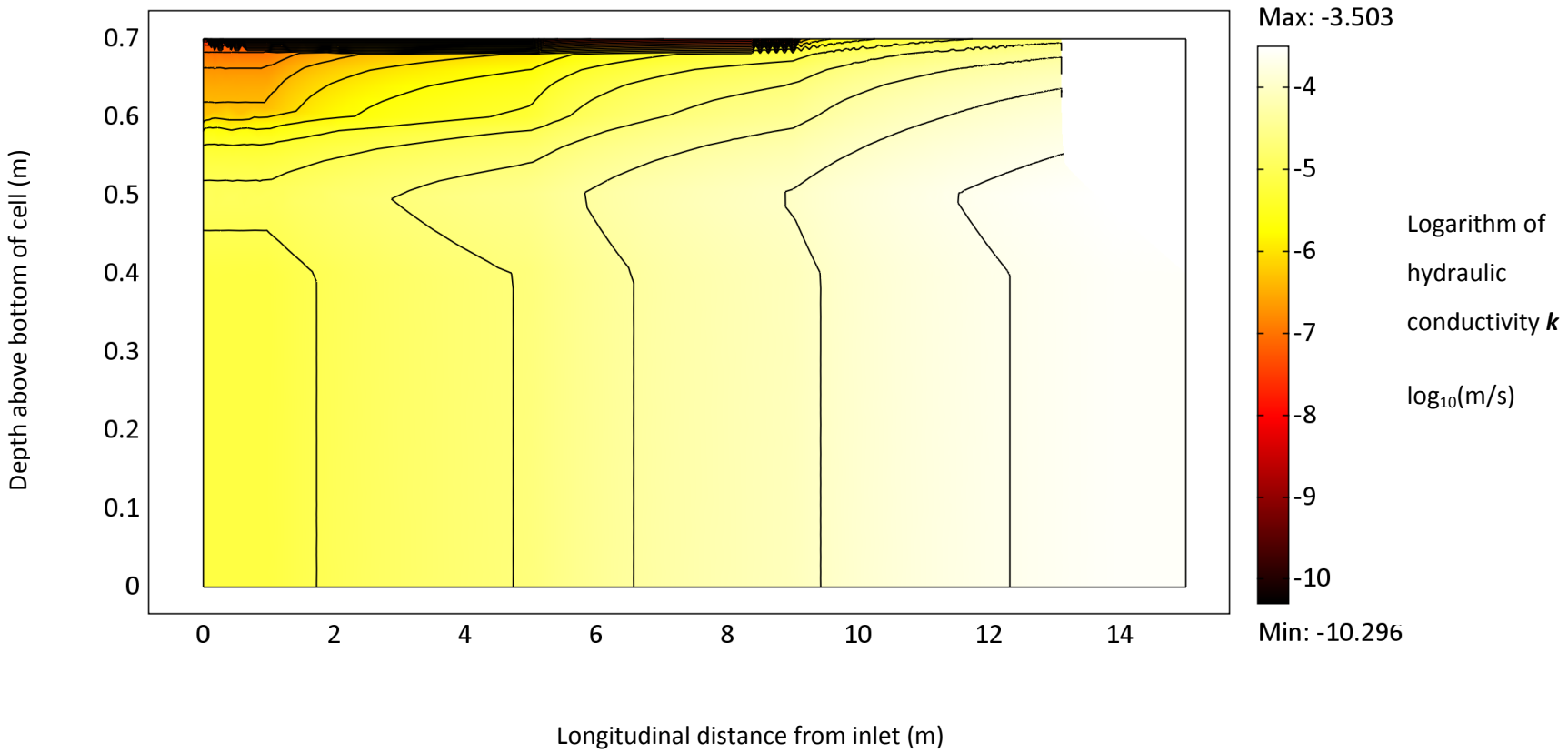

Appendix D.8: FEA Modelling Results – $CF_T = 0.90$, Adaptive Mesh

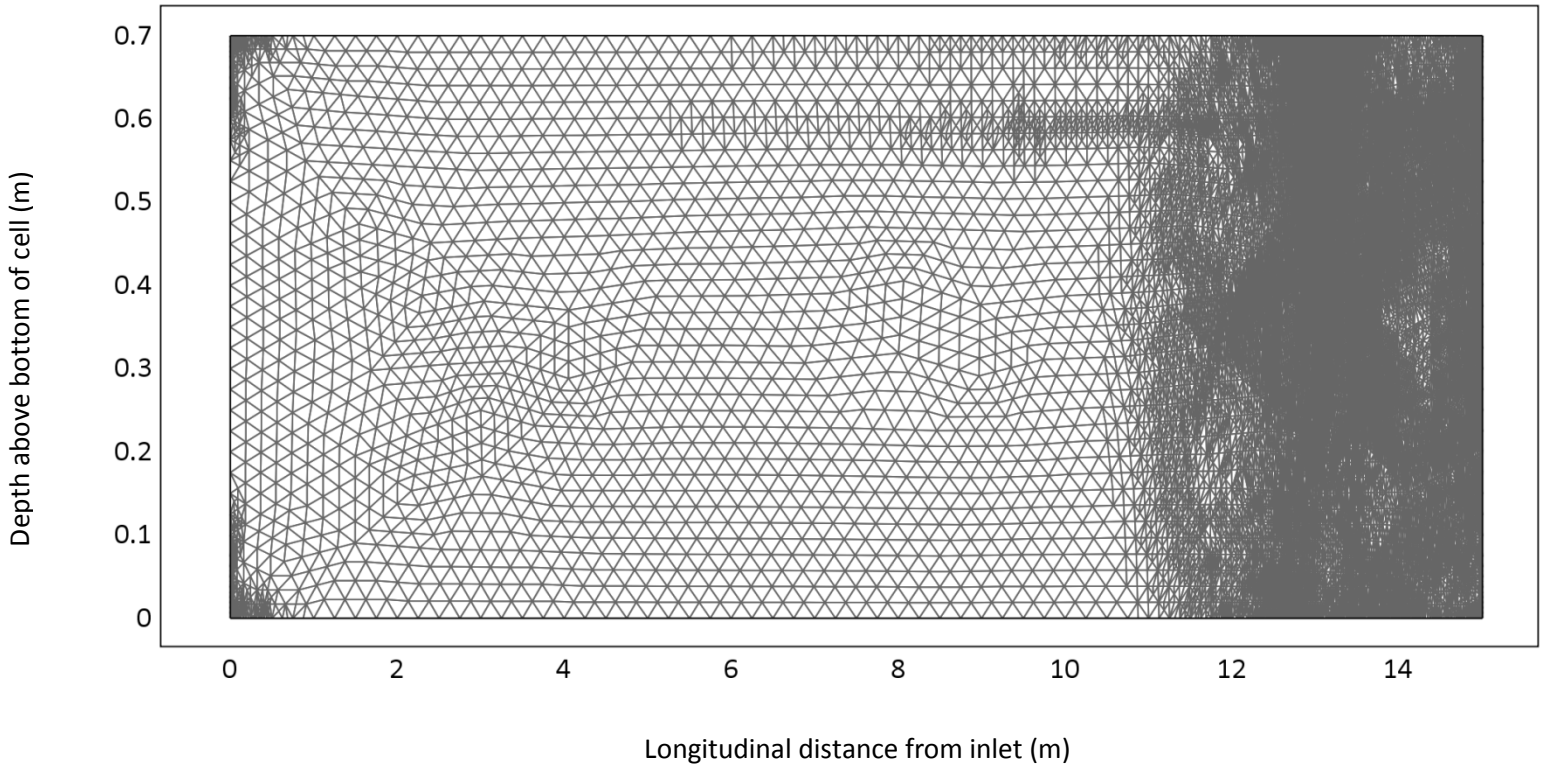

Appendix D.8: FEA Modelling Results – CF_T = 0.90, Hydraulic Head

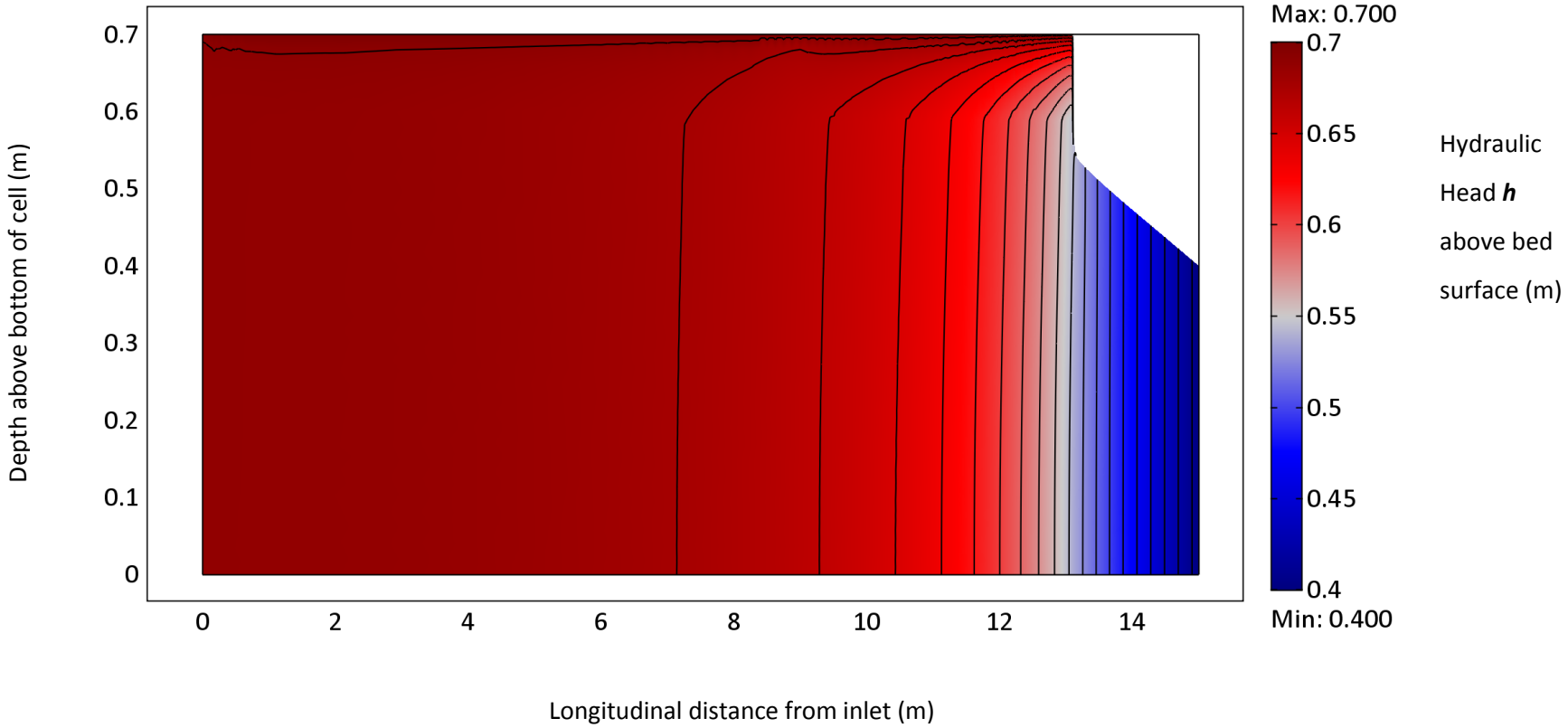

Appendix E: Design and fabrication of a multi-channel fluorimeter

It was decided to perform tracer studies to explore the hydrodynamic response of HSSF TWs to clogging, and monitor tracer both at the outlet and at numerous points inside the bed to develop a full picture of hydrodynamic behaviour. To accurately characterise the internal behaviour of the bed it was desired to have numerous tracer concentration detectors at different locations, sampling the flow automatically and at regular intervals. This minimises the errors introduced through manual collection of samples and will increase the number of samples obtainable. In response to there being no affordable proprietary tracer detector for synchronous measurement from a matrix of sampling points, a novel multi-channel tracer detector was created.

The type of tracer detector used depends on the type of water tracer used. The available families of water tracer are summarised in **Table App.F.1**. The two tracer materials that have been used predominantly in previous wetland studies are bromide salts and Rhodamine Water Tracer (RWT), although each noted to have certain limitations (Flury and Wai, 2003). It was decided that RWT would be the most suitable candidate as it is easily measured *in-situ* with relatively inexpensive equipment, and is highly specific so background interference is usually minimal. This has made it the choice for many previous TW hydraulics studies (Bhattarai and Griffin Jr, 1999, Holland et al., 2004, Shilton and Prasad, 1996, Simi and Mitchell, 1999). However, concerns regarding the conservatism of RWT have been raised, as it can be biologically and photochemically degraded and may also be adsorbed by sediments (Kadlec and Wallace, 2010). Such effects are said to be negligible if the TW is small, shallow (less than 0.6m) and with a HRT of less that one week (Lin et al., 2003). An experiment was conducted to assess the conservative nature of RWT and it was noted that the biggest source of losses is through biological degradation, although it took 10 days for the effect to become notable. The design guidelines that were applied during the construction of the majority of Severn Trent HSSF TWs suggest a HRT of approximately one day (Green and Upton, 1995), and as such RWT was approved for pilot experiments. Additionally, RWT has obvious advantages over more conservative tracers, such as radioactive or biologically based alternatives, in that it has low eco-toxicity and will eventually photochemically destabilise, making it a good choice for ecological applications.

Table App.F.1 Types of tracer used in fluid dynamics studies with notes regarding their appropriateness to this study- need to quote this happy

Tracer family	Notes
Biological tracers (bacteriophages, spores, pollution sediments)	Not permitted by regulators as requirements for a conservative tracer and polished final effluent are conflicting
Radioactive tracers	Require a great level of user expertise and expensive measuring equipment
Inorganic salts (bromide, chloride, lithium ion)	Large quantities required depending on background concentrations. Susceptible to gravitational forces because of buoyancy differences with water – Sanford etc.
Fluorescent dyes (Rhodamine WT, Fluorescene)	Less conservative than inorganic salts: suffer photochemical, biological degradation and sorptive losses.

Measurement of RWT concentration is done using Fluorimeters, which utilise the optical characteristics of fluorescing dyes (such as RWT) to produce a measureable analogue voltage. Fluorimeters produce light close to the excitation wavelength of the dye, and detect light close to the emission wavelength. The intensity of emitted light is linearly proportional to the concentration of RWT in solution up to about 1000 parts per billion (ppb) of RWT in water (hereafter assumed), after which self-quenching effects influence the optical output of the sample. The RWT breakthrough curve was measured at the outlet using a Cyclops 7 submersible fluorimeter (Turner Designs, USA), which has a detection resolution of 0.01 ppb across the range 0-500 ppb **(Figure App.F.1)**.

The multi-flurotimeter was designed to respond to the excitation and emission wavelenghs of the RWT used in this study (Tolbest, Warrington UK), which has excitation and emission wavelengths at 556 and 580 nm respectively. An optical arrangement was therefore proposed, using a Schott OG 570nm high pass filter (UQG Optics, Cambridge UK) and a VTB8440BH photodiode with peak sensitivity at 580 nm (PerkinElmer, Canada). Three candidate Light Emitting Diodes (LEDs) with relatively high intensity at 556 nm but low intensity above 570 nm (so interference at the detection wavelength is minimised) were compared using a USB2000+ light spectrophotometer (OceanOptics, Florida): HLMP-K640 (Hewlett Packard, USA); AGI-5N3-CUPG-A (Agilight, China); and L-7113VGC-H (Kingbright,

China). Across the bandwidth of interest, the Kingbright LED was superior to the other two LEDs (**Figure App.F.2**), having higher excitation intensity and lower intensities near the detection range. Relative to the intensity at the peak wavelength of 525 nm, the intensity at the wavelengths of 556 nm, 570 nm and 580 nm are 7 %, 0.5 % and 0 % respectively (at the operating voltage of 3.7 V). However, the Kingbright has as intensity of 18000 mCd (very bright in comparison to most commercial LEDs) which is why it is able to outperform the alternative LEDs despite seemingly low relative intensities at the design wavelengths.

The spectral output of the Kingbright LED and Turner Cyclops 7 light source were compared. At equivalent intensity the Kingbright LED produces more light in the excitation range than the Cyclops, but more interference in the detection range (**Figure App.F.3**).

Figure App.F.1 Cyclops 7 submersible portable fluorimeter (Turner Instruments, California USA) used for measuring the concentration of Rhodamine Water Tracer at the outlet of the HSSF TWs

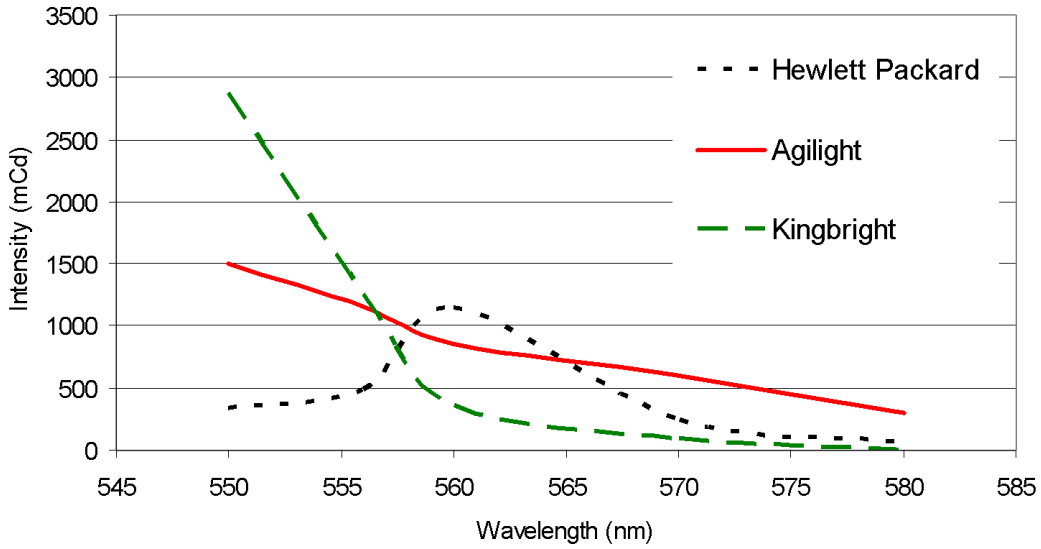

Figure App.F.2 Comparison of three commercially available LEDs across the 550 – 580nm spectrum using USB2000+ light spectrophotometer (OceanOptics, Florida). HLMP-K640 (Hewlett Packard, USA), AGI-5N3-CUPG-A (Agilight, China) and L-7113VGC-H (Kingbright, China).

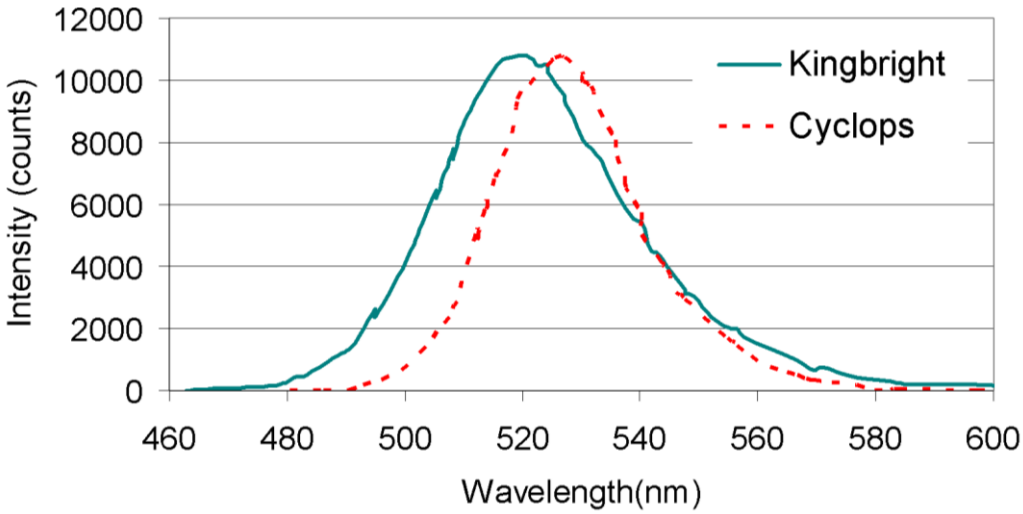

Figure App.F.3 Comparison of the light output from a L-7113VGC-H LED (Kingbright, China) and the light source inside the Cyclops 7 (Turner Instruments, California), across the 550 – 580 nm spectrum using the USB2000+ light spectrophotometer (OceanOptics, Florida).

It was not possible to find an LED that matched or exceeded the performance of the Cyclops for both excitation and detection; however, this was compensated for through the design of the opto-electronics arrangement. Firstly, the light source and detector are arranged around the sample cuvette at right angles, which means that more diffuse than incident light is detected. Most of the diffuse light will consist of the higher wavelength emissions from the fluorescing dye, so that the detected stray light from the LED will be minimal. Secondly, background detection readings can be adjusted for via the electronics module. The inverting amplifier stage is fitted with two 100k potentiometers, one of which is connected between the negative -5 V supply and op-amp PIN 1 and will allow the background detection to be reduced to 0 V. The second potentiometer controls the magnitude of the negative feedback loop, attenuating the sensitivity of the machine and allowing the range of detectable concentrations to be altered. Photodiode amplifier circuits are susceptible to a large amount of noise, such as electronic interference and mains hum. The capacitor input filter module compensates for this by smoothing the signal over time so that the effects of noise on the recorded reading are minimised. The arrangements of components used to make the four sub-circuits that comprise the opto-electronic module are shown in **Figure App.F.4.**

The linearity of the optoelectronic circuit was analysed over a range of Rhodamine WT concentrations and it was found linearity decreases as the sensitivity of the circuit is increased. The practical resolution of the machine would allow a useful detection range of 0-100ppb across 4.5V, compared to the Turner Cyclops minimum detection range of 0-10ppb across 4.5V (**Figure App.F.5**). The circuit was replicated 20 times and fitted around a custom built cuvette tray, which allows the monitoring of flow through samples. The sample fluid is drawn from different points within the TW aquatic environment using a 20 channel peristaltic pump (Watson-Marlow, Falmouth); each channel connected to a different opto-electronic module. The channel voltages are logged every 10 minutes using a CR800 Datalogger and AM16/32A Relay Analogue Multiplexer (Campbell Scientific, Utah).

All of the aforementioned components are mounted in a modified IP66 rated, weatherproof enclosure (Sarel, Italy) that can be wheeled onto the site of interest and supplied by either 110 or 240 V onsite mains electricity. Lengths of 20 m silicon tubing with an ID of 3 mm (Fisher Scientific, UK) are attached between different sampling points (in all three planes) and the fluorimeter channels.

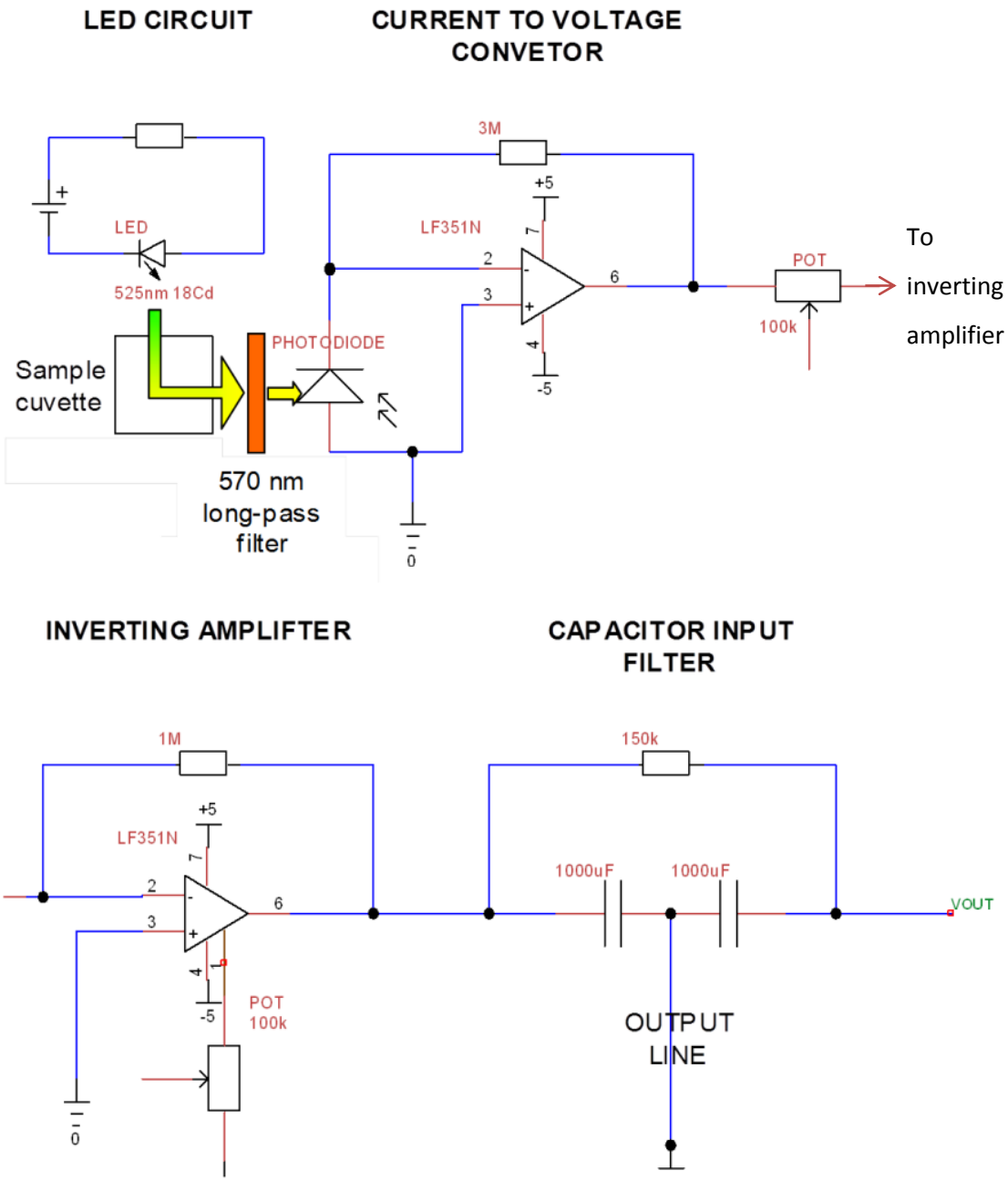

Figure App.F.4 The four electronic submodules that form the fluorimeter circuit used in the multi-channel fluorimeter.

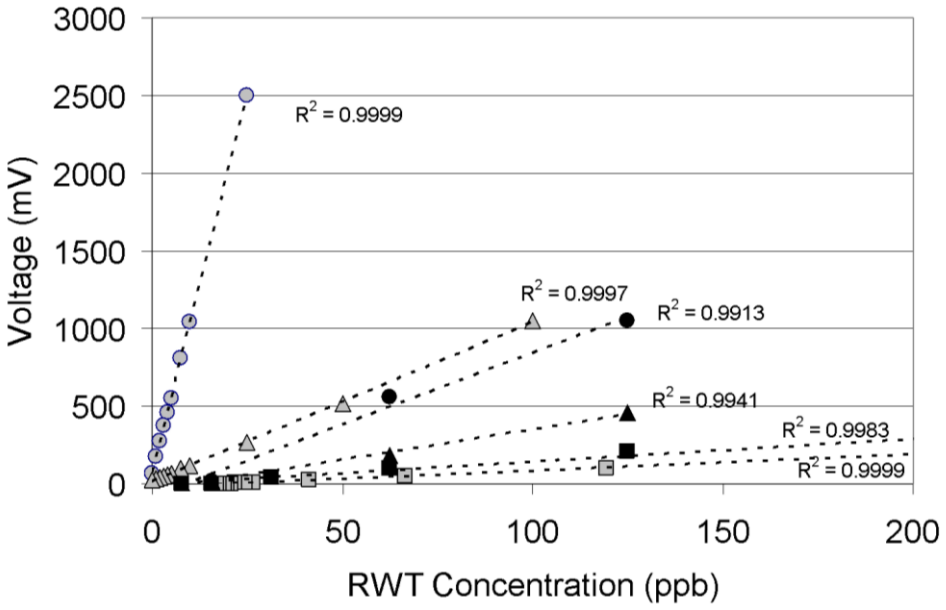

Figure App.F.5 RWT Concentration (ppb) versus analogue voltage output (mV) for the Cyclops 7 (Turner Designs, California) (grey shading) and bespoke Fluorimeter device (black shading). Linearity is shown for three sensitivity settings on each device; high (circles), medium (triangles) and low (squares). Good linearity is achieved in all cases, although the Cyclops is a superior instrument to the developed device, with approximately 25 times superior resolution at high sensitivity

RWT was typically does to the system as a 5-10 ml single-shot impulse of neat solution that was added to the inlet manifold, upstream of the wetland cell. The experiment was left to run for 3-4 days to ensure dye that remained in the system longer than the average HRT was accounted for. The peristaltic pump rotation was set to 50 rpm (about 55 % of maximum drive), which corresponds to a flowrate of 0.2 ml/s through each channel. This was considered a compromise between minimising sample transfer time from bed to fluorimeter (about 12 minutes) and preventing the machine from malfunctioning mid-experiment because of excessive ware on peristaltic pump parts at high drive-rates. The analysed sample is discharged directly onto the centre of the bed surface as it is considered the total discharge (0.003 l/s) is significantly small compared with average flow though these systems (2 l/s), to have negligible impact on downstream fluorescence measurements. A schematic representation of the operation of one channel is given in **Figure App.F.6** and **Figure App.F.7** shows a photograph of the interior of the multichannel fluorimeter at a TW in South Warwickshire.

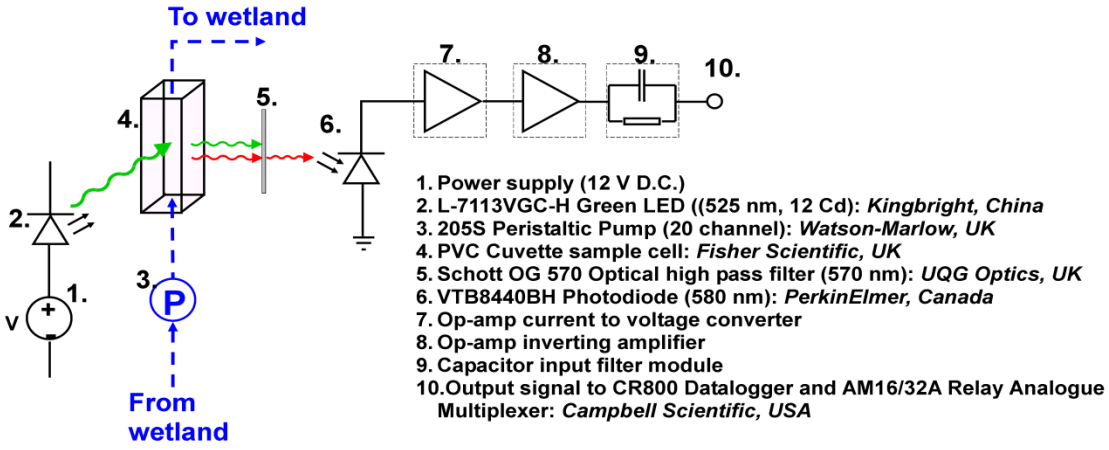

Figure App.F.6 Schematic representation of one channel from the portable, multichannel fluorimeter, showing the major opto-electronic and hydraulic modules involved in the design. Reproduced from Knowles et al. (2010).

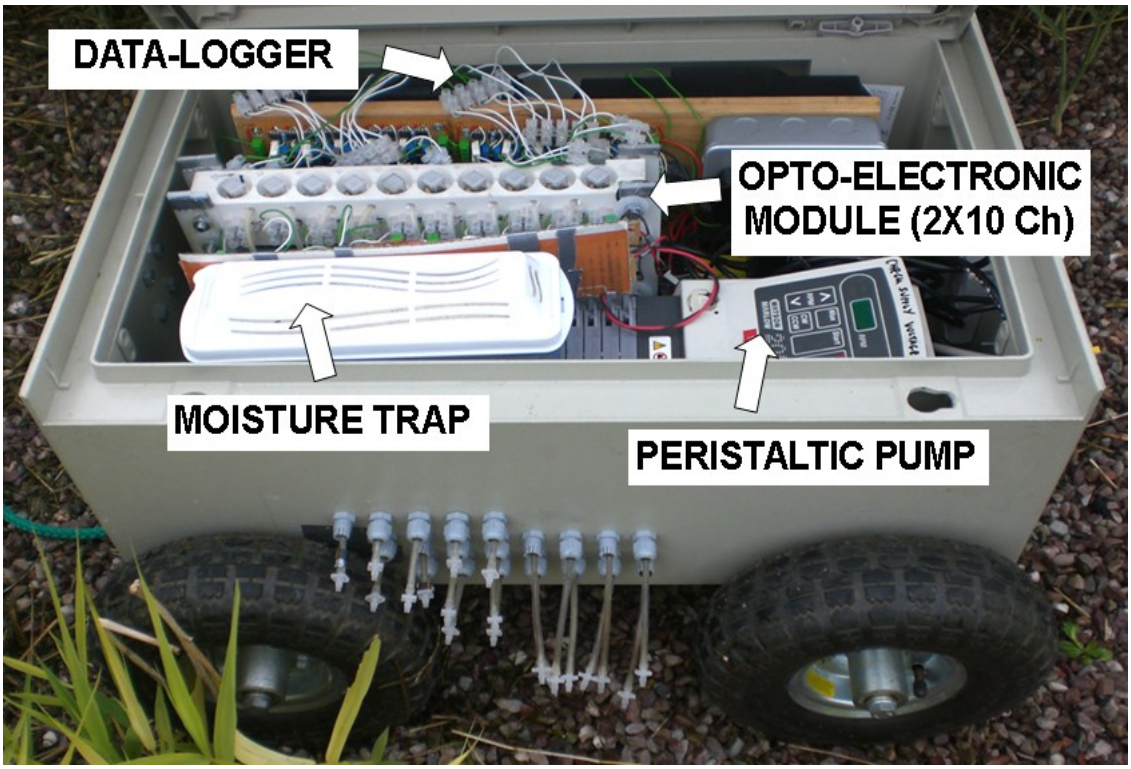

Figure App.F.7 The multi-channel, in-situ fluorimeter installed at a HSSF TW in the UK showing the arrangement of components in the weather-proof enclosure. Reproduced from Knowles et al. (2010).

Appendix F: Results of FEA tracer test and fit using analytical equation

	CF_T = 0.55			CF_T = 0.60		
x (m)	FEA Solution (m)	Analytical Fit (m)	Square Error	FEA Solution (m)	Analytical Fit (m)	Square Error
0.0	0.423	0.423	4.0E-08	0.435	0.435	3.1E-22
0.5	0.423	0.422	2.4E-07	0.435	0.434	3.5E-07
1.0	0.423	0.422	5.4E-07	0.435	0.434	1.4E-06
1.5	0.422	0.422	4.2E-07	0.434	0.433	1.7E-06
2.0	0.421	0.421	3.8E-08	0.432	0.432	6.5E-08
2.5	0.419	0.419	3.1E-10	0.430	0.430	3.6E-07
3.0	0.418	0.418	2.5E-08	0.427	0.428	1.1E-06
3.5	0.416	0.416	1.5E-07	0.425	0.426	1.9E-06
4.0	0.415	0.414	3.9E-07	0.423	0.424	2.4E-06
4.5	0.414	0.413	6.8E-07	0.421	0.423	2.5E-06
5.0	0.413	0.412	1.1E-06	0.419	0.421	2.5E-06
5.5	0.412	0.411	1.5E-06	0.418	0.420	2.4E-06
6.0	0.411	0.410	1.9E-06	0.416	0.418	2.0E-06
6.5	0.410	0.409	2.3E-06	0.415	0.416	1.6E-06
7.0	0.409	0.408	2.7E-06	0.414	0.415	1.3E-06
7.5	0.409	0.407	3.0E-06	0.413	0.414	8.6E-07
8.0	0.408	0.406	3.2E-06	0.412	0.412	5.4E-07
8.5	0.407	0.405	3.4E-06	0.411	0.411	3.2E-07
9.0	0.407	0.405	3.4E-06	0.410	0.410	1.3E-07
9.5	0.406	0.404	3.4E-06	0.409	0.409	3.5E-08
10.0	0.405	0.404	3.3E-06	0.408	0.408	3.5E-09
10.5	0.405	0.403	3.0E-06	0.407	0.407	3.8E-09
11.0	0.404	0.403	2.7E-06	0.406	0.406	2.0E-08
11.5	0.404	0.402	2.2E-06	0.405	0.405	4.3E-08
12.0	0.403	0.402	1.8E-06	0.405	0.404	6.2E-08
12.5	0.403	0.401	1.4E-06	0.404	0.404	6.9E-08
13.0	0.402	0.401	9.4E-07	0.403	0.403	6.6E-08
13.5	0.402	0.401	5.6E-07	0.402	0.402	5.2E-08
14.0	0.401	0.401	2.9E-07	0.402	0.401	3.5E-08
14.5	0.401	0.400	7.9E-08	0.401	0.401	1.2E-08
15.0	0.400	0.400	0.0E+00	0.400	0.400	0.0E+00

	CF_T = 0.65			CF_T = 0.70		
x (m)	FEA Solution (m)	Analytical Fit (m)	Square Error	FEA Solution (m)	Analytical Fit (m)	Square Error
0.0	0.456	0.456	2.0E-18	0.474	0.483	8.5E-05
0.5	0.456	0.455	9.6E-07	0.474	0.481	5.9E-05
1.0	0.456	0.454	3.8E-06	0.474	0.479	3.4E-05
1.5	0.455	0.453	5.8E-06	0.474	0.478	1.9E-05
2.0	0.453	0.452	2.7E-06	0.474	0.476	6.2E-06
2.5	0.449	0.450	8.8E-07	0.474	0.474	4.5E-07
3.0	0.445	0.448	7.6E-06	0.473	0.473	5.8E-07
3.5	0.441	0.446	2.0E-05	0.472	0.471	1.5E-06
4.0	0.438	0.443	3.3E-05	0.468	0.465	5.3E-06
4.5	0.435	0.441	4.3E-05	0.463	0.463	1.0E-07
5.0	0.432	0.439	5.3E-05	0.458	0.460	4.2E-06
5.5	0.429	0.437	5.9E-05	0.453	0.457	1.6E-05
6.0	0.427	0.435	6.3E-05	0.448	0.454	4.0E-05
6.5	0.424	0.432	6.4E-05	0.443	0.451	7.4E-05
7.0	0.423	0.430	6.3E-05	0.438	0.449	1.1E-04
7.5	0.421	0.428	6.0E-05	0.435	0.445	1.1E-04
8.0	0.419	0.426	5.5E-05	0.432	0.442	1.1E-04
8.5	0.417	0.424	5.0E-05	0.430	0.440	1.0E-04
9.0	0.415	0.422	4.4E-05	0.427	0.437	9.5E-05
9.5	0.414	0.420	3.8E-05	0.424	0.433	8.9E-05
10.0	0.413	0.418	3.2E-05	0.422	0.431	8.4E-05
10.5	0.411	0.416	2.6E-05	0.419	0.428	7.8E-05
11.0	0.410	0.415	2.2E-05	0.416	0.425	7.3E-05
11.5	0.408	0.413	1.7E-05	0.414	0.422	6.7E-05
12.0	0.407	0.411	1.2E-05	0.411	0.419	5.0E-05
12.5	0.406	0.409	8.8E-06	0.410	0.416	3.6E-05
13.0	0.405	0.407	5.6E-06	0.408	0.413	2.3E-05
13.5	0.403	0.405	3.0E-06	0.406	0.409	1.3E-05
14.0	0.402	0.404	1.5E-06	0.404	0.407	6.4E-06
14.5	0.401	0.402	3.5E-07	0.402	0.403	1.6E-06
15.0	0.400	0.400	0.0E+00	0.400	0.400	0.0E+00

	CF_T = 0.75			CF_T = 0.80		
x (m)	FEA Solution (m)	Analytical Fit (m)	Square Error	FEA Solution (m)	Analytical Fit (m)	Square Error
0.0	0.527	0.530	8.3E-06	0.570	0.580	1.0E-04
0.5	0.527	0.528	1.4E-06	0.570	0.578	6.7E-05
1.0	0.527	0.526	6.4E-07	0.570	0.576	3.5E-05
1.5	0.527	0.524	6.2E-06	0.570	0.574	1.7E-05
2.0	0.527	0.522	2.0E-05	0.570	0.572	3.7E-06
2.5	0.527	0.520	4.1E-05	0.570	0.569	3.3E-08
3.0	0.526	0.518	6.4E-05	0.569	0.567	3.8E-06
3.5	0.525	0.516	8.2E-05	0.569	0.565	1.5E-05
4.0	0.522	0.514	6.6E-05	0.568	0.563	2.7E-05
4.5	0.518	0.513	3.2E-05	0.566	0.561	3.3E-05
5.0	0.511	0.510	6.2E-07	0.564	0.558	3.3E-05
5.5	0.504	0.504	3.6E-08	0.561	0.556	2.7E-05
6.0	0.493	0.496	8.9E-06	0.558	0.554	1.6E-05
6.5	0.482	0.489	4.7E-05	0.554	0.552	4.4E-06
7.0	0.472	0.482	1.1E-04	0.549	0.549	8.8E-08
7.5	0.466	0.475	9.0E-05	0.543	0.532	1.2E-04
8.0	0.460	0.469	6.9E-05	0.532	0.524	6.3E-05
8.5	0.456	0.463	5.5E-05	0.521	0.517	1.6E-05
9.0	0.450	0.457	4.4E-05	0.508	0.508	2.8E-07
9.5	0.445	0.451	3.7E-05	0.495	0.500	2.3E-05
10.0	0.440	0.446	3.4E-05	0.484	0.492	6.8E-05
10.5	0.434	0.440	3.2E-05	0.472	0.484	1.4E-04
11.0	0.430	0.435	3.3E-05	0.461	0.476	2.3E-04
11.5	0.424	0.430	3.5E-05	0.448	0.467	3.4E-04
12.0	0.421	0.425	2.2E-05	0.441	0.457	2.7E-04
12.5	0.417	0.421	1.3E-05	0.435	0.449	2.1E-04
13.0	0.414	0.416	6.2E-06	0.428	0.440	1.4E-04
13.5	0.410	0.412	2.5E-06	0.420	0.430	8.5E-05
14.0	0.407	0.408	9.3E-07	0.414	0.421	4.4E-05
14.5	0.404	0.404	1.6E-07	0.407	0.411	1.2E-05
15.0	0.400	0.400	0.0E+00	0.400	0.400	0.0E+00

	CF_T = 0.85			CF_T = 0.90		
x (m)	FEA Solution (m)	Analytical Fit (m)	Square Error	FEA Solution (m)	Analytical Fit (m)	Square Error
0.0	0.658	0.652	4.0E-05	0.689	0.689	2.3E-17
0.5	0.658	0.649	7.3E-05	0.689	0.687	4.0E-06
1.0	0.658	0.647	1.2E-04	0.689	0.685	1.9E-05
1.5	0.657	0.644	1.6E-04	0.689	0.683	3.9E-05
2.0	0.656	0.642	2.2E-04	0.689	0.680	7.1E-05
2.5	0.655	0.639	2.7E-04	0.688	0.678	1.1E-04
3.0	0.654	0.637	3.1E-04	0.688	0.676	1.5E-04
3.5	0.652	0.634	3.5E-04	0.687	0.673	1.9E-04
4.0	0.650	0.631	3.6E-04	0.686	0.671	2.4E-04
4.5	0.648	0.629	3.6E-04	0.686	0.669	2.8E-04
5.0	0.644	0.626	3.5E-04	0.684	0.666	3.3E-04
5.5	0.641	0.623	3.1E-04	0.683	0.664	3.7E-04
6.0	0.636	0.621	2.5E-04	0.682	0.662	4.1E-04
6.5	0.630	0.618	1.5E-04	0.680	0.659	4.4E-04
7.0	0.623	0.615	5.7E-05	0.678	0.657	4.6E-04
7.5	0.612	0.612	4.2E-08	0.676	0.654	4.6E-04
8.0	0.598	0.582	2.8E-04	0.673	0.652	4.4E-04
8.5	0.584	0.572	1.5E-04	0.670	0.650	4.0E-04
9.0	0.563	0.560	1.2E-05	0.666	0.647	3.3E-04
9.5	0.542	0.548	3.4E-05	0.660	0.645	2.4E-04
10.0	0.525	0.537	1.5E-04	0.655	0.643	1.6E-04
10.5	0.507	0.524	3.0E-04	0.647	0.640	4.6E-05
11.0	0.493	0.513	4.0E-04	0.637	0.638	1.2E-07
11.5	0.478	0.500	4.8E-04	0.623	0.615	7.1E-05
12.0	0.464	0.486	4.9E-04	0.603	0.587	2.6E-04
12.5	0.453	0.474	4.5E-04	0.581	0.563	3.4E-04
13.0	0.441	0.460	3.6E-04	0.548	0.533	2.3E-04
13.5	0.430	0.445	2.4E-04	0.510	0.502	6.3E-05
14.0	0.421	0.432	1.3E-04	0.476	0.473	8.8E-06
14.5	0.410	0.416	3.6E-05	0.438	0.438	2.4E-08
15.0	0.400	0.400	0.0E+00	0.400	0.400	0.0E+00

Appendix G: Results of FEA tracer test and fit using analytical equation

	mg/L of tracer by CF_T					
	0.55		0.60		0.65	
t (d)	**n-TIS**	**FEA**	**n-TIS**	**FEA**	**n-TIS**	**FEA**
0.00	0.00E+00	0.00E+00	0.00E+00	0.00E+00	0.00E+00	4.38E-21
0.05	5.54E-08	9.30E-09	6.95E-08	9.90E-09	1.08E-07	4.32E-08
0.10	2.29E-07	2.39E-07	2.47E-07	2.46E-07	2.97E-07	2.90E-07
0.15	3.03E-07	3.10E-07	3.03E-07	3.11E-07	3.17E-07	3.17E-07
0.20	2.31E-07	1.91E-07	2.17E-07	1.90E-07	2.04E-07	1.68E-07
0.25	1.42E-07	1.14E-07	1.30E-07	1.12E-07	1.14E-07	8.01E-08
0.30	7.55E-08	6.05E-08	6.77E-08	6.12E-08	5.69E-08	4.22E-08
0.35	2.98E-08	2.52E-08	2.63E-08	2.48E-08	2.11E-08	2.25E-08
0.40	1.30E-08	1.80E-08	1.14E-08	1.87E-08	8.92E-09	1.49E-08
0.45	5.41E-09	1.24E-08	4.71E-09	1.27E-08	3.60E-09	7.61E-09
0.50	1.69E-09	6.12E-09	1.47E-09	6.48E-09	1.10E-09	5.62E-09
0.55	6.42E-10	4.87E-09	5.60E-10	5.18E-09	4.13E-10	4.02E-09
0.60	2.37E-10	3.63E-09	2.07E-10	3.88E-09	1.51E-10	2.75E-09
0.65	6.58E-11	2.44E-09	5.79E-11	2.74E-09	4.19E-11	2.15E-09
0.70	2.31E-11	2.02E-09	2.04E-11	2.32E-09	1.47E-11	1.67E-09
0.75	7.96E-12	1.61E-09	7.10E-12	1.90E-09	5.09E-12	1.32E-09
0.80	2.06E-12	1.24E-09	1.85E-12	1.54E-09	1.33E-12	1.03E-09
0.85	6.87E-13	1.05E-09	6.25E-13	1.33E-09	4.47E-13	8.03E-10
0.90	2.27E-13	8.51E-10	2.08E-13	1.12E-09	1.49E-13	6.64E-10
0.95	5.58E-14	6.87E-10	5.19E-14	9.48E-10	3.74E-14	5.19E-10
1.00	1.80E-14	5.79E-10	1.69E-14	8.21E-10	1.22E-14	4.06E-10
1.05	5.75E-15	4.70E-10	5.48E-15	6.97E-10	3.97E-15	3.45E-10
1.10	1.37E-15	3.64E-10	1.32E-15	5.96E-10	9.66E-16	2.68E-10
1.15	4.30E-16	2.93E-10	4.22E-16	5.16E-10	3.10E-16	2.15E-10
1.20	1.34E-16	2.34E-10	1.34E-16	4.38E-10	9.87E-17	1.81E-10
1.25	3.11E-17	1.73E-10	3.15E-17	3.58E-10	2.35E-17	1.40E-10
1.30	9.59E-18	1.35E-10	9.85E-18	3.02E-10	7.40E-18	1.13E-10

	mg/L of tracer by CF_T					
	0.70		0.75		0.80	
t (d)	**n-TIS**	**FEA**	**n-TIS**	**FEA**	**n-TIS**	**FEA**
0.00	0.00E+00	0.00E+00	0.00E+00	0.00E+00	0.00E+00	0.00E+00
0.05	9.59E-08	1.57E-08	1.00E-07	9.31E-09	2.41E-07	2.14E-07
0.10	3.62E-07	3.55E-07	3.90E-07	4.12E-07	4.30E-07	4.19E-07
0.15	3.38E-07	3.17E-07	4.16E-07	3.63E-07	1.54E-07	1.52E-07
0.20	1.44E-07	1.21E-07	2.21E-07	1.76E-07	1.75E-08	5.59E-08
0.25	5.23E-08	4.76E-08	9.84E-08	8.70E-08	2.10E-09	3.41E-08
0.30	1.59E-08	2.14E-08	3.71E-08	4.09E-08	2.06E-10	2.62E-08
0.35	3.03E-09	8.83E-09	9.34E-09	2.52E-08	9.25E-12	2.18E-08
0.40	7.27E-10	4.50E-09	2.82E-09	1.28E-08	6.87E-13	1.86E-08
0.45	1.63E-10	2.97E-09	8.01E-10	8.37E-09	4.73E-14	1.65E-08
0.50	2.33E-11	1.06E-09	1.55E-10	5.14E-09	1.53E-15	1.39E-08
0.55	4.70E-12	9.01E-10	3.97E-11	2.69E-09	9.27E-17	1.20E-08
0.60	9.12E-13	8.55E-10	9.87E-12	2.18E-09	5.40E-18	1.06E-08
0.65	1.13E-13	7.71E-10	1.67E-12	1.53E-09	1.47E-19	8.70E-09
0.70	2.06E-14	5.76E-10	3.91E-13	1.11E-09	8.00E-21	7.55E-09
0.75	3.68E-15	3.80E-10	9.00E-14	8.86E-10	4.23E-22	6.54E-09
0.80	4.17E-16	2.14E-10	1.40E-14	6.09E-10	1.04E-23	5.26E-09
0.85	7.17E-17	2.02E-10	3.10E-15	4.69E-10	5.27E-25	4.43E-09
0.90	1.21E-17	1.90E-10	6.78E-16	3.91E-10	2.62E-26	3.69E-09
0.95	1.29E-18	1.62E-10	9.97E-17	2.94E-10	6.03E-28	2.90E-09
1.00	2.13E-19	1.32E-10	2.13E-17	2.50E-10	2.90E-29	2.36E-09
1.05	3.47E-20	1.01E-10	4.49E-18	2.14E-10	1.38E-30	1.91E-09
1.10	3.55E-21	8.47E-11	6.34E-19	1.70E-10	3.02E-32	1.45E-09
1.15	5.66E-22	7.75E-11	1.31E-19	1.52E-10	1.40E-33	1.15E-09
1.20	8.97E-23	7.03E-11	2.70E-20	1.33E-10	6.47E-35	9.08E-10
1.25	8.87E-24	6.17E-11	3.70E-21	1.12E-10	1.36E-36	6.69E-10
1.30	1.38E-24	5.49E-11	7.51E-22	1.02E-10	6.16E-38	5.15E-10

	mg/L of tracer by CF_T			
	0.85		0.90	
t (d)	**n-TIS**	**FEA**	**n-TIS**	**FEA**
0.00	0.00E+00	-2.80E-28	0.00E+00	0.00E+00
0.05	2.97E-07	2.37E-07	5.44E-07	2.70E-07
0.10	4.48E-07	4.36E-07	5.21E-07	3.25E-07
0.15	1.24E-07	1.41E-07	6.02E-08	1.03E-07
0.20	9.70E-09	5.06E-08	1.26E-09	5.12E-08
0.25	8.51E-10	3.01E-08	3.50E-11	3.20E-08
0.30	6.01E-11	2.31E-08	7.40E-13	2.16E-08
0.35	1.77E-12	1.95E-08	4.59E-15	1.54E-08
0.40	9.34E-14	1.67E-08	6.76E-17	1.05E-08
0.45	4.54E-15	1.48E-08	8.98E-19	8.73E-09
0.50	9.47E-17	1.25E-08	3.62E-21	6.52E-09
0.55	4.04E-18	1.08E-08	4.08E-23	5.02E-09
0.60	1.65E-19	9.48E-09	4.36E-25	4.28E-09
0.65	2.88E-21	7.89E-09	1.41E-27	3.35E-09
0.70	1.09E-22	6.77E-09	1.37E-29	2.79E-09
0.75	4.02E-24	5.91E-09	1.29E-31	2.41E-09
0.80	6.31E-26	4.83E-09	3.65E-34	1.94E-09
0.85	2.22E-27	4.16E-09	3.24E-36	1.69E-09
0.90	7.66E-29	3.60E-09	2.81E-38	1.48E-09
0.95	1.12E-30	2.90E-09	7.26E-41	1.22E-09
1.00	3.73E-32	2.53E-09	6.04E-43	1.10E-09
1.05	1.23E-33	2.17E-09	4.95E-45	9.77E-10
1.10	1.70E-35	1.75E-09	1.20E-47	8.35E-10
1.15	5.47E-37	1.53E-09	9.50E-50	7.58E-10
1.20	1.74E-38	1.31E-09	7.46E-52	6.82E-10
1.25	2.32E-40	1.07E-09	1.72E-54	5.99E-10
1.30	7.25E-42	9.35E-10	1.32E-56	5.49E-10